

AD-A213 378

WRDC-TR-89-3076
VOLUME II



ADVANCED ACTUATION SYSTEMS DEVELOPMENT

Gavin D. Jenney
Harry W. Schreadley
John A. Anderson
William G. Talley
Carl A. Allbright

DTIC
ELECTE
OCT 17 1989
S D & D

DYNAMIC CONTROLS, INC.
DAYTON, OHIO 45424-2929

August 1989

Final Report for Period May 1983 - January 1987

APPROVED FOR PUBLIC RELEASE; DISTRIBUTION UNLIMITED

FLIGHT DYNAMICS LABORATORY
WRIGHT RESEARCH DEVELOPMENT CENTER
AIR FORCE SYSTEMS COMMAND
WRIGHT-PATTERSON AIR FORCE BASE, OHIO 45433-6553

89 10 17 002

UNCLASSIFIED

SECURITY CLASSIFICATION OF THIS PAGE

REPORT DOCUMENTATION PAGE

Form Approved
OMB No 0704-0188

1a. REPORT SECURITY CLASSIFICATION UNCLASSIFIED			1b. RESTRICTIVE MARKINGS NONE	
2a. SECURITY CLASSIFICATION AUTHORITY N/A			3. DISTRIBUTION/AVAILABILITY OF REPORT Approved for Public Release: distribution unlimited.	
2b. DECLASSIFICATION/DOWNGRADING SCHEDULE N/A				
4. PERFORMING ORGANIZATION REPORT NUMBER(S)			5. MONITORING ORGANIZATION REPORT NUMBER(S) WRDC-TR-89-3076, Volume II	
6a. NAME OF PERFORMING ORGANIZATION Dynamic Controls, Inc.		6b. OFFICE SYMBOL (if applicable)	7a. NAME OF MONITORING ORGANIZATION Flight Dynamics Laboratory (WRDC/FIGL) Wright Research and Development Center	
6c. ADDRESS (City, State, and ZIP Code) 7060 Cliffwood Place Dayton, OH 45424-2929			7b. ADDRESS (City, State, and ZIP Code) Wright-Patterson AFB, OH 45433-6553	
8a. NAME OF FUNDING/SPONSORING ORGANIZATION		8b. OFFICE SYMBOL (if applicable)	9. PROCUREMENT INSTRUMENT IDENTIFICATION NUMBER F33615-S3-C-3600	
8c. ADDRESS (City, State, and ZIP Code)			10. SOURCE OF FUNDING NUMBERS	
			PROGRAM ELEMENT NO 62210F	PROJECT NO 2403
			TASK NO 02	WORK UNIT ACCESSION NO 91
11. TITLE (Include Security Classification) ADVANCED ACTUATION SYSTEMS DEVELOPMENT - Volume II				
12. PERSONAL AUTHOR(S) John A. Anderson, Carl A. Allbright, Gavin D. Jenney, Harry W. Schreadley, William G. Talley				
13a. TYPE OF REPORT Final	13b. TIME COVERED FROM 5/83 TO 1/87	14. DATE OF REPORT (Year, Month, Day) 1989 August	15. PAGE COUNT 366	
16. SUPPLEMENTARY NOTATION None				
17. COSATI CODES			18. SUBJECT TERMS (Continue on reverse if necessary and identify by block number) Sealing Systems, Digital Servo Valve, Direct Drive Flap, Flutter Suppression, Flight Control Actuator	
FIELD	GROUP	SUB-GROUP		
01	03			
19. ABSTRACT (Continue on reverse if necessary and identify by block number)				
<p>1. This report describes six different research and development activities in flight control actuation. The activities are: (1) the development and test of a unique linear actuator sealing system for high-pressure systems, (2) the development and test of a digital servo valve using piezo-controlled high-speed solenoid valves, (3) the performance evaluation of an F-15 rudder actuator under applied loads, (4) the performance evaluation of a Mission Adaptive Wing section under different load conditions, (5) the evaluation of output impedance modification of an electrohydraulic actuator for flutter suppression, and (6) the development and test of a direct drive valve and electronics (analog and digital) for an F-16 Horizontal Tail/Flaperon actuator. Volume I of the report presents activities 1, 2, and 3. Volume II presents activities 4, 5 and 6.</p> <p>2. The sealing system was based upon using two-stage sealing for the piston rod seals and a pressure-activated backup ring configuration for the piston seals. The system eliminated the use of elastomeric dynamic seals. The piston rod first-stage seal was a laminar pressure-drop design which also served as a rod-support bearing. The piston rod seal used commercial non-elastomeric seals. The design was tested in actuators with thin wall cylinders at 8000 psi. Both MIL-H-83282 and CTFE hydraulic fluid systems were used for the testing. The system was tested with 500,000 impulse-loading cycles without any seal degradation.</p>				
20. DISTRIBUTION/AVAILABILITY OF ABSTRACT <input checked="" type="checkbox"/> UNCLASSIFIED/UNLIMITED <input type="checkbox"/> SAME AS RPT <input type="checkbox"/> DTIC USERS			21. ABSTRACT SECURITY CLASSIFICATION UNCLASSIFIED	
22a. NAME OF RESPONSIBLE INDIVIDUAL Mr. Gregory Cecere			22b. TELEPHONE (Include Area Code) 513-255-2831	22c. OFFICE SYMBOL AFWAL/FIGL

ABSTRACT (continued)

3. The digital servovalve was constructed with discrete high-speed solenoid valves to control the flow to a control actuator. The solenoid valves were a poppet design using a piezoelectric stack and a hydraulic motion amplifier. The valves activated in less than one millisecond. A microprocessor was used to control the valve and close the control loop. The servovalve worked successfully. Since the output flow of the solenoid valves is low, the approach is suitable primarily for small actuators.
4. The performance of an F-15 rudder actuator was evaluated in a loading test stand. The evaluation was limited to the electrical command mode with the manual input grounded. The input/output performance characteristics in both unloaded and loaded operation were documented and analyzed. The actuator is a rotary vane actuator. The performance characteristics were similar to those of a linear actuator with the exception of characteristics directly affected by the vane sealing method.
5. The Mission Adaptive Wing evaluation was a measurement of the loaded and unloaded performance characteristics of a test specimen produced by General Dynamics Corporation as a feasibility model. The actuation system for changing the camber of the test specimen is unique and was evaluated with a series of input/output measurements. The testing verified the general concept and revealed two design areas requiring additional development effort before flight test evaluation.
6. The impedance modification investigation used electronic load pressure sensing to change the output impedance of an actuator over a selected frequency band. Changing the output impedance of an actuator potentially can be used to suppress classical slab-surface flutter. A demonstration actuator was sized to evaluate the impedance change capability. The test results indicated that the output impedance of an electrohydraulic actuator can be modified over a useful but limited frequency range using electronic pressure sensing and the control servovalve for the actuator. The limitation in the range of the impedance modification is primarily determined by the frequency response characteristics of the servovalve used to control the actuator.
7. The F-16 Direct Drive Actuator development effort produced a direct drive control valve package which replaces the normal control valve and secondary actuator mounted on the actuator body of an F-16 Horizontal Tail/Flaperon ISA. The design maintains the failure-mode characteristics of the normal F-16 ISA including the centering mode as the final failure mode. The measured performance was equivalent to or better than that of the normal F-16 ISA. As part of the evaluation, a microprocessor-controlled initial checkout, failure monitor, and failure switching unit was evaluated with the test actuator.

FOREWORD

The effort described in this document was performed by Dynamic Controls, Inc., (DCI) of Dayton, Ohio, under Air Force Contract F33615-83-C-3600. The contract was performed under Project Number 2403, Task 02. The work under the contract was carried out in the Air Force Flight Dynamics Laboratory, Wright-Patterson Air Force Base, Ohio. The work was administered by Mr. Gregory Cecere, AFFDL/FIGL Program Manager.

This report covers work performed between May 1983 and January 1987. The technical report was submitted in September 1988.

The authors wish to express their appreciation to DCI technicians Steve Murphy, Connie Graham, and Julie Minch for their contributions in implementing designs, testing, and engineering support for the efforts described in the report. Appreciation is also expressed to Linda Pytosh and Lynda Gopinath for their efforts in preparation of the data and text which make up the report.



Accession For	
NTIS CRA&I	<input checked="" type="checkbox"/>
DTIC TAB	<input type="checkbox"/>
Unannounced	<input type="checkbox"/>
Justification	
By	
Distribution /	
Availability Codes	
Dist	Avail and/or Special
A-1	

VOLUME II

TABLE OF CONTENTS

SECTION IV - MISSION ADAPTIVE WING EVALUATION

Section IV - Page No.

I.	INTRODUCTION AND SUMMARY	1
II.	TECHINICAL APPROACH	2
	MAW Test Section Description	2
	MAWS General Test Procedure	6
	General Performance Measurements	10
	Test Configuration	10
	Specific Test Procedure - Unloaded Leading Edge	12
	Linearity	12
	Hysteresis	12
	Frequency Response	12
	Static Threshold	14
	Dynamic Threshold	14
	Saturation Velocity	14
	Transient Response	14
	Specific Test Procedure - Unloaded Trailing Edge	14
	Linearity	17
	Hysteresis	18
	Frequency Response	18
	Static Threshold	18
	Dynamic Threshold	19
	Saturation Velocity	19
	Transient Response	19
	Loaded Testing	19
	General	19
	Loaded Leading-Edge Tests	22
	Loaded Trailing-Edge Tests	22
III.	TEST RESULTS	26
	Unloaded Leading-Edge Test Results	26
	General	26
	Static Threshold	27
	Dynamic Threshold	27
	Frequency Response	32
	Saturation Velocity	46
	Transient Response	49
	Unloaded Trailing-Edge Test Results	53
	General	53
	Static Threshold	54
	Dynamic Threshold	63
	Linearity & Large Amplitude Hysteresis	63
	Hysteresis - Small Amplitude	72
	Frequency Response	82
	Step Response	92
	Saturation Velocity	95
	Loaded Leading-Edge Test Results	101
	General	101
	Loaded Leading-Edge Hysteresis	101
	Loaded Leading-Edge Frequency Response	106
	Loaded Leading-Edge Transient Response	116

VOLUME II

Loaded Trailing-Edge Test Results	120
General	120
Loaded Trailing-Edge Static Threshold	120
Loaded Trailing-Edge Dynamic Threshold	129
Loaded Trailing-Edge Hysteresis	137
Loaded Trailing-Edge Frequency Response	145
Loaded Trailing-Edge Step Response	150

Section IV - Page No.

IV.	CONSIDERATIONS AND ANOMALIES	155
	General	155
	Gear-Box Load Capacity Limitation	156
	Universal Joint Failure and Correction	155
V.	CONCLUSIONS AND RECOMMENDATIONS	161

SECTION V - FLUTTER SUPPRESSION - PHASE III

Section V - Page No.

I.	INTRODUCTION AND SUMMARY	1
II.	TECHNICAL APPROACH	2
	General Technical Approach	2
	Specific Technical Approach	3
III.	TEST PROCEDURE	12
IV.	TEST RESULTS AND ANALYSIS	16
V.	CONCLUSIONS AND RECOMMENDATIONS	41

SECTION VI - DIRECT DRIVE F-16 ACTUATOR

Section VI - Page No.

I.	INTRODUCTION AND SUMMARY	1
II.	TECHNICAL APPROACH	2
	General	2
	F-16 ISA Description	3
	Direct Drive System Description	6
	General	6
	Control System Description	10
	Control Valve Description	12
	Feedback Design Description	16
	Control Electronics Description	23
	General	23
	Control Electronic Circuits	23
	Power Supply Description	32
	Pilot Monitor Box	32

VOLUME II

Microprocessor Description	36
General	36
Analog System Modification	38
Hardware	38
General	38
Components	38
Logic Description	41
General	41
Self-Test	43
Continuous Monitor	44

Section VI - Page No.

III. GENERAL TEST PROCEDURE	49
Performance Measurements	49
Static Threshold	49
Dynamic Threshold	49
Frequency Response	50
Linearity	50
Hysteresis	50
Time Response	51
Saturation Velocity	51
Step Response	51
Failure Effects On Performance	51
Failure Effect	51
Failure Transients	51
Electrical Failure Transients	51
Hydraulic Failure Transients	52
Failure Logic Detection Characteristics	52
Logic Detection Characteristics	52
IV. SPECIFIC TEST PROCEDURES	54
System Setup	54
Specific Test Conditions	54
Deviations And/Or Additions To The General Test Procedure	57
Test Hardware Setup	57
V. TEST RESULTS	61
Dynamic Threshold Results	63
Hysteresis Test Results - 1 Percent Command	63
Hysteresis Test Results - 10 Percent Command	68
Linearity Test Results	68
Frequency Response Test Results	68
Hardover Failure Transients - Analog Monitor	91
Slowover Failure Transients - Analog Monitor	96
Static Failure Detection - Analog Monitor	96
Dynamic Hardover Failure Transient - Analog Monitor	96
Pressure Failure Transients - Analog Monitor	102
Hardover Failure Transient - Logic Processor	106
Static Failure Detection - Logic Processor	111
Dynamic Hardover Failure Transients - Logic Processor	111
Pressure Failure Transients	115
Current Failure Transients - Logic Processor	121
Dynamic Failure Detection - Logic Processor	124

VOLUME II

VI. CONCLUSIONS AND RECOMMENDATIONS	126
APPENDIX A2 - PARTS LIST FOR F-16 DIRECT DRIVE	A2-1
APPENDIX A3 - LOGIC PROCESSOR PROGRAM	A3-1
BIBLIOGRAPHY FOR VOLUME II	B2-1
LIST OF ACRONYMS	B2-2

VOLUME II

LIST OF FIGURES

SECTION IV - MISSION ADAPTIVE WING EVALUATION

Section IV - Page No.

Figure IV-1.	MAW in <i>up</i> position.	3
Figure IV-2.	MAW in <i>down</i> position.	4
Figure IV-3.	MAW control electronics and leading-edge actuator.	5
Figure IV-4.	MAW installed in MASTR.	7
Figure IV-5.	Control valve mounting in MASTR.	8
Figure IV-6.	MAW control electronics installed in MASTR.	9
Figure IV-7.	Instrumentation block diagram.	11
Figure IV-8.	Leading-edge position transducer attachment.	13
Figure IV-9.	Surface position transducer and load actuator attachment points.	15
Figure IV-10.	Surface position transducer and load actuator attachment points.	16
Figure IV-11.	Loading system installation, right-side view.	20
Figure IV-12.	Loading system installation, left-side view.	21
Figure IV-13.	Leading-edge loading system.	23
Figure IV-14.	Trailing-edge loading system.	24
Figure IV-15.	Static threshold - leading edge - data 1.	28
Figure IV-16.	Static threshold - leading edge - data 2.	29
Figure IV-17.	Dynamic threshold - leading edge - data 1.	30
Figure IV-18.	Dynamic threshold - leading edge - data 2.	31
Figure IV-19.	Leading-edge actuator - position 2.	33
Figure IV-20.	Leading edge actuator - position 2.	34
Figure IV-21.	Leading-edge actuator - position 2.	35
Figure IV-22.	Leading-edge actuator - position 2.	36
Figure IV-23.	Linearity - motion point P_1	38
Figure IV-24.	Linearity - motion point P_2	39
Figure IV-25.	Linearity - motion point X_5	40
Figure IV-26.	Linearity - motion point X_6	41
Figure IV-27.	Hysteresis at 10-percent input - motion point P_1	42
Figure IV-28.	Hysteresis at 1-percent input - motion point P_1	43
Figure IV-29.	Hysteresis at 10-percent input - motion point X_5	44
Figure IV-30.	Hysteresis at 1-percent input - motion point X_5	45
Figure IV-31.	Surface <i>up</i> - saturation velocity.	47
Figure IV-32.	Surface <i>down</i> - saturation velocity.	48
Figure IV-33.	Surface <i>up</i> - step response.	50
Figure IV-34.	Surface <i>down</i> - step response.	51
Figure IV-35.	Linearity of right secondary actuator.	55
Figure IV-36.	Linearity of left secondary actuator.	56
Figure IV-37.	Static threshold - trailing edge - rotary motion.	57
Figure IV-38.	Static threshold - trailing edge - X_2 motion.	58
Figure IV-39.	Static threshold - trailing edge - X_4 motion.	59
Figure IV-40.	Static threshold - trailing edge - X_1 motion.	60
Figure IV-41.	Static threshold - trailing edge - X_3 motion.	61
Figure IV-42.	Dynamic threshold - trailing edge - rotary motion.	64
Figure IV-43.	Dynamic threshold - trailing edge - X_1, X_2 motion.	65
Figure IV-44.	Dynamic threshold - trailing edge - X_4 motion.	66
Figure IV-45.	Dynamic threshold - trailing edge - X_3 motion.	67
Figure IV-46.	Linearity - trailing edge - left rotary - X_1 motion.	68
Figure IV-47.	Linearity - trailing edge - left rotary - X_3 motion.	69
Figure IV-48.	Linearity - trailing edge - right rotary - X_2 motion.	70
Figure IV-49.	Linearity - trailing edge - right rotary - X_4 motion.	71

VOLUME II

Section IV - Page No.

Figure IV-50.	Hysteresis - 3-percent command - trailing edge - left rotary - X_3	73
Figure IV-51.	Hysteresis - 3-percent command - trailing edge - right rotary - X_4 motion.	74
Figure IV-52.	Hysteresis - 3-percent command - trailing edge - left rotary - X_1 motion.	75
Figure IV-53.	Hysteresis - 3-percent command - trailing edge - right rotary - X_2 motion.	76
Figure IV-54.	Hysteresis - 3-percent command - trailing edge - left rotary - X_1 motion.	77
Figure IV-55.	Hysteresis - 10-percent command - trailing edge - left rotary - X_3 motion.	78
Figure IV-56.	Hysteresis - 10-percent command - trailing edge - right rotary - X_2 motion.	79
Figure IV-57.	Hysteresis - 10-percent command - trailing edge - right rotary - X_4 motion.	80
Figure IV-58.	Amplitude response - 5-percent command - left rotary potentiometer - unloaded trailing edge.	83
Figure IV-59.	Phase response - 5-percent command - left rotary potentiometer - unloaded trailing edge.	84
Figure IV-60.	Amplitude response - 5-percent command - right rotary potentiometer - unloaded trailing edge.	85
Figure IV-61.	Phase response - 5-percent command - right rotary potentiometer - unloaded trailing edge.	86
Figure IV-62.	Amplitude response - 10-percent command - left rotary potentiometer - unloaded trailing edge.	87
Figure IV-63.	Phase response - 10-percent command - left rotary potentiometer - unloaded trailing edge.	88
Figure IV-64.	Amplitude response - 10-percent command - right rotary potentiometer - unloaded trailing edge.	89
Figure IV-65.	Phase response - 10-percent command - right rotary potentiometer - unloaded trailing edge.	90
Figure IV-66.	Step response - X_1, X_3	93
Figure IV-67.	Step response - X_2, X_4	94
Figure IV-68.	Saturation velocity - rotary potentiometer, X_1	97
Figure IV-69.	Saturation velocity - X_2, X_3, X_4	98
Figure IV-70.	Saturation velocity - X_2, X_3, X_4	99
Figure IV-71.	Saturation velocity - rotary potentiometer - X_1	100
Figure IV-72.	Hysteresis at 1-percent input - 1-psi load - motion point X_5	102
Figure IV-73.	Hysteresis at 1-percent input - 1-psi load - motion point X_6	103
Figure IV-74.	Hysteresis at 1-percent input - 2-psi load - motion point X_5	104
Figure IV-75.	Hysteresis at 1-percent input - 2-psi load - motion point X_6	105
Figure IV-76.	Leading-edge actuator - 1-psi load - position P_2	107
Figure IV-77.	Leading-edge actuator - 1-psi load - position P_2	108
Figure IV-78.	Leading-edge actuator - 1-psi load - position X_6	109
Figure IV-79.	Leading-edge actuator - 1-psi load - position X_6	110
Figure IV-80.	Leading-edge actuator - 1-psi load - position P_2	111
Figure IV-81.	Leading-edge actuator - 1-psi load - position P_2	112
Figure IV-82.	Leading-edge actuator - 1-psi load - position X_6	113
Figure IV-83.	Leading-edge actuator - 1-psi load - position X_6	114
Figure IV-84.	Step response - 10-percent - 1-psi load - X_6	117
Figure IV-85.	Step response - 10-percent - 2-psi load - X_6	118

VOLUME II

Section IV - Page No.

Figure IV-86.	Loaded trailing-edge static threshold - 1-psi load - left and right rotary motion.	121
Figure IV-87.	Loaded trailing-edge static threshold - 1-psi load - left and right rotary - X_1 and X_2 motion.	122
Figure IV-88.	Loaded trailing-edge static threshold - 1-psi load - left and right rotary - X_1 , X_2 , X_3 , and X_4 motion.	123
Figure IV-89.	Loaded trailing-edge static threshold - 3-psi load - left and right rotary motion.	124
Figure IV-90.	Loaded trailing-edge static threshold - 3-psi load - X_1 motion.	125
Figure IV-91.	Loaded trailing-edge static threshold - 3-psi load - X_2 motion.	126
Figure IV-92.	Loaded trailing-edge static threshold - 3-psi load - X_3 , X_4 motion.	127
Figure IV-93.	Loaded trailing-edge dynamic threshold - 1-psi load - left and right rotary motion.	130
Figure IV-94.	Loaded trailing-edge dynamic threshold - 1-psi load - X_1 , X_2 motion.	131
Figure IV-95.	Loaded trailing-edge dynamic threshold - 1-psi load - X_1 , X_2 , X_3 , X_4 motion.	132
Figure IV-96.	Loaded trailing-edge dynamic threshold - 3-psi load - left and right rotary motion.	133
Figure IV-97.	Loaded trailing-edge dynamic threshold - 3-psi load - left and right rotary motion.	134
Figure IV-98.	Loaded trailing-edge dynamic threshold - 3-psi load - X_3 and X_4 motion.	135
Figure IV-99.	Loaded trailing-edge hysteresis - 2-psi load - left rotary motion.	138
Figure IV-100.	Loaded trailing-edge hysteresis - 2-psi load - right rotary motion.	139
Figure IV-101.	Loaded trailing-edge hysteresis - 2-psi load - X_1 motion.	140
Figure IV-102.	Loaded trailing-edge hysteresis - 2-psi load - X_2 motion.	141
Figure IV-103.	Loaded trailing-edge hysteresis - 2-psi load - X_3 motion.	142
Figure IV-104.	Loaded trailing-edge hysteresis - 2-psi load - X_4 motion.	143
Figure IV-105.	Trailing-edge actuator - 1-psi load - position X_2	146
Figure IV-106.	Trailing-edge actuator - 1-psi load - position X_2	147
Figure IV-107.	Trailing-edge actuator - 1-psi load - position X_4	148
Figure IV-108.	Trailing-edge actuator - 1-psi load - position X_4	149
Figure IV-109.	Step response - X_1 , X_3	151
Figure IV-110.	Step response - X_2 , X_4	152
Figure IV-111.	Loaded trailing-edge hysteresis - 5-psi load - left rotary motion - 10-percent input.	156
Figure IV-112.	Loaded trailing-edge hysteresis - 5-psi load - right rotary motion - 10-percent input.	157
Figure IV-113.	Original U-joint design.	159
Figure IV-114.	Modified U-joint design.	160

SECTION V - FLUTTER SUPPRESSION - PHASE III

Section V - Page No.

Figure V-1.	Test actuator.	4
Figure V-2.	Left side of test actuator.	7
Figure V-3.	Front panel of flutter suppression controller.	9
Figure V-4.	Rear panel of flutter suppression controller.	11
Figure V-5.	Block diagram.	13
Figure V-6.	Flutter actuator test configuration.	14

VOLUME II

Section V - Page No.

Figure V-7.	Close-up view of test configuration.	17
Figure V-8.	Position response - magnitude - 50 Hz.	18
Figure V-9.	Position response - phase - 50 Hz.	19
Figure V-10.	Position response - magnitude - 12 Hz.	20
Figure V-11.	Position response - phase - 12 Hz.	21
Figure V-12.	Load force response - magnitude - 50 Hz.	23
Figure V-13.	Load force response - phase - 50 Hz.	24
Figure V-14.	Position response - zero load - magnitude.	25
Figure V-15.	Position response - zero load - phase.	26
Figure V-16.	Frequency response - pressure signal.	28
Figure V-17.	Stiffness response - magnitude.	29
Figure V-18.	Stiffness response - phase.	30
Figure V-19.	F/X with load pressure feedback.	31
Figure V-20.	Response - bandpass filter.	34
Figure V-21.	F/X at 0.2 gain.	35
Figure V-22.	F/X at 0.4 gain.	36
Figure V-23.	F/X at 0.8 gain.	37
Figure V-24.	Damping flow gain response.	40

SECTION VI - F-16 DIRECT DRIVE ACTUATOR

Section VI - Page No.

Figure VI-1.	F-16 integrated servoactuator (ISA).	4
Figure VI-2.	Integrated servoactuator schematic diagram.	5
Figure VI-3.	Single fail-operate direct drive valve (DDV) system.	7
Figure VI-4.	F-4 direct drive valve (DDV) aileron and F-16 integrated servo-actuator (ISA).	8
Figure VI-5.	F-16 direct drive valve (DDV) actuator schematic.	11
Figure VI-6.	Direct drive valve (DDV) coil and suspension.	13
Figure VI-7.	DDV coil force motor.	14
Figure VI-8.	DDV control spool and sleeves.	15
Figure VI-9.	Centering sleeve, link, and shaft.	17
Figure VI-10.	DDV body and force motors.	18
Figure VI-11.	Feedback hardware.	19
Figure VI-12.	Manifold plate.	20
Figure VI-13.	Control package assembly.	21
Figure VI-14.	Direct drive F-16 actuator.	22
Figure VI-15.	Control electronics chassis.	24
Figure VI-16.	Open control chassis.	25
Figure VI-17.	Single channel schematic.	26
Figure VI-18.	PWM schematic.	28
Figure VI-19.	Summing circuit.	29
Figure VI-20.	Solenoid driver schematic.	30
Figure VI-21.	Power supply.	33
Figure VI-22.	Power supply without cover.	34
Figure VI-23.	Pilot monitor.	35
Figure VI-24.	F-16 Logic Processor.	37
Figure VI-25.	Logic Processor construction.	39
Figure VI-26.	F-16 Logic Processor hardware and interface schematic.	42
Figure VI-27.	Structure chart.	45
Figure VI-28.	F-16 direct drive test installation.	58

VOLUME II

Section VI - Page No.

Figure VI-29.	F-16 direct drive actuator.	59
Figure VI-30.	Direct drive test electronics.	60
Figure VI-31.	Dynamic threshold - condition 1.	64
Figure VI-32.	Hysteresis - 1 percent command - condition 1.	66
Figure VI-33.	Hysteresis - 1 percent command - condition 5.	67
Figure VI-34.	Hysteresis - 10 percent command - condition 1.	70
Figure VI-35.	Linearity - 110 percent command - condition 1.	71
Figure VI-36.	Amplitude ratio response - 3 percent input - condition 1.	72
Figure VI-37.	Phase response - 3 percent input - condition 1.	73
Figure VI-38.	Amplitude ratio response - 3 percent input - condition 4.	75
Figure VI-39.	Phase response - 3 percent input - condition 4.	76
Figure VI-40.	Amplitude response - 10 percent input - condition 1.	78
Figure VI-41.	Phase response - 10 percent input - condition 1.	79
Figure VI-42.	Amplitude ratio response - 10 percent input - condition 4.	80
Figure VI-43.	Amplitude response - 10 percent input - condition 4.	81
Figure VI-44.	Step response - condition 1.	83
Figure VI-45.	Step response - condition 2.	84
Figure VI-46.	Step response - condition 3.	85
Figure VI-47.	Step response - condition 4.	86
Figure VI-48.	Step response - condition 5.	87
Figure VI-49.	Saturation velocity - condition 1.	89
Figure VI-50.	Hardover failures - condition 6.	92
Figure VI-51.	Hardover failures - condition 7 - channel 1.	93
Figure VI-52.	Hardover failures - condition 7 - channel 2.	94
Figure VI-53.	Hardover failures - condition 7 - channel 3.	95
Figure VI-54.	Slowover failure transients - condition 10.	97
Figure VI-55.	Slowover failure transients - condition 11.	98
Figure VI-56.	Slowover failure transients - condition 12.	99
Figure VI-57.	Slowover failure transients - condition 16.	100
Figure VI-58.	Slowover failure transients - condition 17.	101
Figure VI-59.	Slowover failure transients - condition 18.	103
Figure VI-60.	Slowover failure transients - condition 19.	104
Figure VI-61.	Pressure failure transients - condition 20.	105
Figure VI-62.	Hardover failure transients - condition 6.	107
Figure VI-63.	Hardover failure transients - condition 8.	108
Figure VI-64.	Hardover failure transients - condition 9.	109
Figure VI-65.	Slowover failure transients - condition 13.	110
Figure VI-66.	Slowover failure transients - condition 14.	112
Figure VI-67.	Slowover failure transients - condition 15.	113
Figure VI-68.	Dynamic failure transients - condition 16.	114
Figure VI-69.	Dynamic failure transients - condition 17.	116
Figure VI-70.	Dynamic failure transients - condition 18.	117
Figure VI-71.	Dynamic failure transients - condition 19.	118
Figure VI-72.	Slowover failure transients - condition 21.	119
Figure VI-73.	Slowover failure transients - condition 22.	120
Figure VI-74.	Current failure transients - condition 23.	122
Figure VI-75.	Current failure transients - condition 25.	123
Figure VI-76.	Dynamic failure detection - Logic Processor.	125

VOLUME II

LIST OF TABLES

SECTION IV - MISSION ADAPTIVE WING EVALUATION

Section IV - Page No.

Table IV-1.	Calibration factors for leading-edge instrumentation.	26
Table IV-2.	Static threshold results.	27
Table IV-3.	Dynamic threshold results.	32
Table IV-4.	Frequency response - 3-percent input.	32
Table IV-5.	Frequency response - 3-percent input.	37
Table IV-6.	Hysteresis for a 10-percent input.	46
Table IV-7.	Hysteresis for a 1-percent input.	46
Table IV-8.	Saturation rate.	49
Table IV-9.	Step response.	49
Table IV-9.	Step response (continued).	52
Table IV-10.	Calibration factors - trailing-edge transducers.	53
Table IV-11.	Calibration factors - rotary potentiometers.	53
Table IV-12.	Static threshold - unloaded trailing edge.	62
Table IV-13.	Dynamic threshold - unloaded trailing edge.	63
Table IV-14.	Large amplitude hysteresis - unloaded trailing edge.	72
Table IV-15.	Small amplitude hysteresis - 3-percent input - unloaded trailing edge.	81
Table IV-16.	Small amplitude hysteresis - 10-percent input - unloaded trailing edge.	82
Table IV-17.	Frequency response - unloaded trailing edge.	91
Table IV-18.	Frequency response - unloaded trailing edge.	92
Table IV-19.	Step response - unloaded trailing edge.	95
Table IV-20.	Trailing-edge maximum velocity - unloaded.	96
Table IV-21.	One-psi loaded leading-edge hysteresis for a 1-percent input.	106
Table IV-22.	Two-psi loaded leading-edge hysteresis for a 1-percent input.	106
Table IV-23.	Loaded leading-edge frequency response - 1 psi load.	115
Table IV-24.	Leading-edge loaded frequency response - 2 psi load.	115
Table IV-25.	Loaded leading-edge transient step response.	119
Table IV-26.	Static threshold - loaded trailing-edge.	128
Table IV-27.	Dynamic threshold - loaded trailing edge.	136
Table IV-28.	Trailing-edge hysteresis - 3-percent command.	137
Table IV-29.	Trailing-edge hysteresis - 5-percent command.	144
Table IV-30.	Trailing-edge hysteresis - 10-percent command.	144
Table IV-31.	Loaded trailing-edge frequency response at 5-percent command.	145
Table IV-32.	Loaded trailing-edge frequency response at 10-percent command.	150
Table IV-33.	Loaded trailing-edge step response.	153

SECTION VI - DIRECT DRIVE F-16 ACTUATOR

Section VI - Page No.

Table VI-1.	F-16 program descriptive table of contents.	46
Table VI-2.	Test conditions for the F-16 Direct Drive Actuator.	55
Table VI-3.	Dynamic threshold.	65
Table VI-4.	Hysteresis - 1 percent command.	69
Table VI-5.	Hysteresis - 10 percent command.	69
Table VI-6.	Frequency response - 3 percent input.	77
Table VI-7.	Frequency response - 10 percent input.	77
Table VI-8.	Saturation rates.	90

SUMMARY

This report describes six different research and development activities in flight control actuation. The activities are: (1) the development and test of a unique linear actuator sealing system for high-pressure systems, (2) the development and test of a digital servovalve using piezo-controlled high-speed solenoid valves, (3) the performance evaluation of an F-15 rudder actuator under applied loads, (4) the performance evaluation of a Mission Adaptive Wing section under different load conditions, (5) the evaluation of output impedance modification of an electrohydraulic actuator for flutter suppression, and (6) the development and test of a direct drive valve and electronics (analog and digital) for an F-16 Horizontal Tail/Flaperon actuator. Volume I of the report presents activities 1, 2, and 3. Volume II presents activities 4, 5, and 6. *2211 47*

The sealing system was based upon using two-stage sealing for the piston rod seals and a pressure-activated backup ring configuration for the piston seals. The system eliminated the use of elastomeric dynamic seals. The piston rod first-stage seal was a laminar pressure-drop design which also served as a rod-support bearing. The piston rod seal used commercial non-elastomeric seals. The design was tested in actuators with thin wall cylinders at 8000 psi. Both MIL-H-83282 and CTFE hydraulic fluid systems were used for the testing. The system was tested with 500,000 impulse-loading cycles without any seal degradation.

The digital servovalve was constructed with discrete high-speed solenoid valves to control the flow to a control actuator. The solenoid valves were a poppet design using a piezoelectric stack and a hydraulic motion amplifier. The valves activated in less than one millisecond. A microprocessor was used to control the valve and close the control loop. The servovalve worked successfully. Since the output flow of the solenoid valves is low, the approach is suitable primarily for small actuators.

The performance of an F-15 rudder actuator was evaluated in a loading test stand. The evaluation was limited to the electrical command mode with the manual input grounded. The input/output performance characteristics in both unloaded and loaded operation were documented and analyzed. The actuator is a rotary vane actuator. The performance characteristics were similar to those of a linear actuator with the exception of characteristics directly affected by the vane sealing method.

The Mission Adaptive Wing evaluation was a measurement of the loaded and unloaded performance characteristics of a test specimen produced by General Dynamics Corporation as a feasibility model. The actuation system for changing the camber of the test specimen is unique and was evaluated with a series of input/output measurements. The testing verified the general concept and revealed two design areas requiring additional development effort before flight test evaluation.

The impedance modification investigation used electronic load pressure sensing to change the output impedance of an actuator over a selected frequency band. Changing the output impedance of an actuator potentially can be used to suppress classical slab-surface flutter. A demonstration actuator was sized to evaluate the impedance change capability. The test results indicated that the output impedance of an electrohydraulic actuator can be modified over a useful but limited frequency range using electronic pressure sensing and the control servovalve for the actuator. The limitation in the range of the impedance modification is primarily determined by the frequency response characteristics of the servovalve used to control the actuator.

The F-16 Direct Drive Actuator development effort produced a direct drive control valve package which replaces the normal control valve and secondary actuator mounted on the actuator body of an F-16 Horizontal Tail/Flaperon ISA. The design maintains the failure-mode characteristics of the normal F-16 ISA including the centering mode as the final failure mode. The measured performance was equivalent to or better than that of the normal F-16 ISA. As part of the evaluation, a microprocessor-controlled initial checkout, failure monitor, and failure switching unit was evaluated with the test actuator.

SECTION IV MISSION ADAPTIVE WING EVALUATION

I. INTRODUCTION AND SUMMARY

This report section describes the evaluation of a Mission Adaptive Wing (MAW) test section designed and manufactured by General Dynamics (GD), Fort Worth Division, Fort Worth, Texas. The MAW test section was a 42-inch span of an F-111 wing with full chord, leading edge to trailing edge. This test section is located just inboard of the F-111 wing tip (F-111 wing station 286.0). The test section was designed and constructed full-scale by GD to realistic flight loads, material properties and safety requirements. A description of a Mission Adaptive Wing System and the test specimen appears in the Journal of Aircraft, Volume 18, No. 7, July 1981 in an article by William W. Gilbert. The test section was transferred by General Dynamics to the Air Force Flight Dynamics Laboratory at Wright-Patterson Air Force Base, Ohio.

The purpose of testing the MAW section was to evaluate the performance characteristics of the section, particularly under loaded conditions. The mechanization of the test section was sufficiently unique, from a control surface actuation approach, to warrant evaluation. Although the MAW test section was designed to operate with two hydraulic systems, the redundancy characteristics of the test section were not evaluated in the investigation. All testing was conducted with the test section operating in a *no failure* condition. The evaluation was based upon measuring the input/output characteristics of the test section in an unloaded and loaded condition. The test section was modified by installing of load attachment pads to the lower surface of the leading and trailing edges. The test section was installed in the Multipurpose Actuation System Test Rig (MASTR) in the Actuation Laboratory in Building 145, Area B, Wright-Patterson Air Force Base, Ohio for both the unloaded and loaded performance testing.

The test section operated satisfactorily unloaded and with applied loads corresponding to surface loads 1, 2 and 3 psi. The input/output characteristics, particularly with the surface loaded, appeared consistent with more conventional surface actuation techniques. Two areas of further development were indicated by the results of the loaded testing, both in a detail design area of the mechanization. One development area was the design of the universal joints used in the trailing-edge mechanization. During the loaded testing, failure of the universal joints occurred (an alternate design was designed and installed by DCI). The second development area was the planetary gear box design. For surface loads of 5 psi, gear separation occurs, indicating that the gear box would require some redesign to operate with the large torque input capability of the hydraulic motors.

II. TECHNICAL APPROACH

MAW Test Section Description

The test section incorporated two different actuation mechanizations, one for the leading edge and one for the trailing edge. Figure IV-1 shows the test section mounted on a supporting table with the leading and trailing edges commanded to maximum *up* deflection. Figure IV-2 shows the test section with the leading and trailing edges commanded to the maximum *down* deflection. The leading edge deflects from -5° to $+30^{\circ}$ (down). The trailing edge deflects from -70° to $+25^{\circ}$ (down).

The leading-edge control system uses a linear actuator and linkages to control the leading-edge surface shape. The control linkage consists of a main drive bellcrank and two control links. The linkage supports a rigid aluminum nose cap and the upper and lower flexible skins. The fiberglass skin is designed provide a smooth contour over the deflection range of the leading edge. No sliding joints exist on the leading nose or upper surface. A sliding joint (faired) is used on the lower surface (in a region with positive pressure). The control actuator is a tandem design and uses two servovalve control modules with monitoring provisions for failure detection.

The variable camber trailing-edge mechanization is based on a variable-geometry, three-section truss. Each truss is joined with a three section acme screw and nut and slide. Each acme section uses a different thread pitch to produce the desired airfoil camber with deflection. The three acme thread sections are connected by universal joints so the thread sections drive in series. The upper and lower skins are independent, attached at the forward edge to the wing box, and use a slip joint at the trailing edge. The skins are supported by beams (oriented spanwise). The beams are attached to the skin and are supported at each end by a pivoting slide blocks running in grooves in the truss members. The support system allows the skin to pick up only the normal air loads and transfer them from the support beams to the trusses. A motor-gearbox is used to drive the acme threads of each truss. Two hydraulic motors are used for each gearbox (each supplied by a different hydraulic supply). The motors are driven by manual input tandem valves positioned by F-111 damper servo packages. The tandem control valves and the damper servo packages are located below the test section as shown in Figures IV-1 and IV-2.

The control electronics for the test system were constructed to allow manual or remote electrical operation of the leading and trailing edge. The electronics consisted of the driving electronics for the leading- and trailing-edge servovalves and included failure detection logic and reset provisions. Figure IV-3 shows the control electronics (including power supplies) and the linear actuator controlling the leading edge.

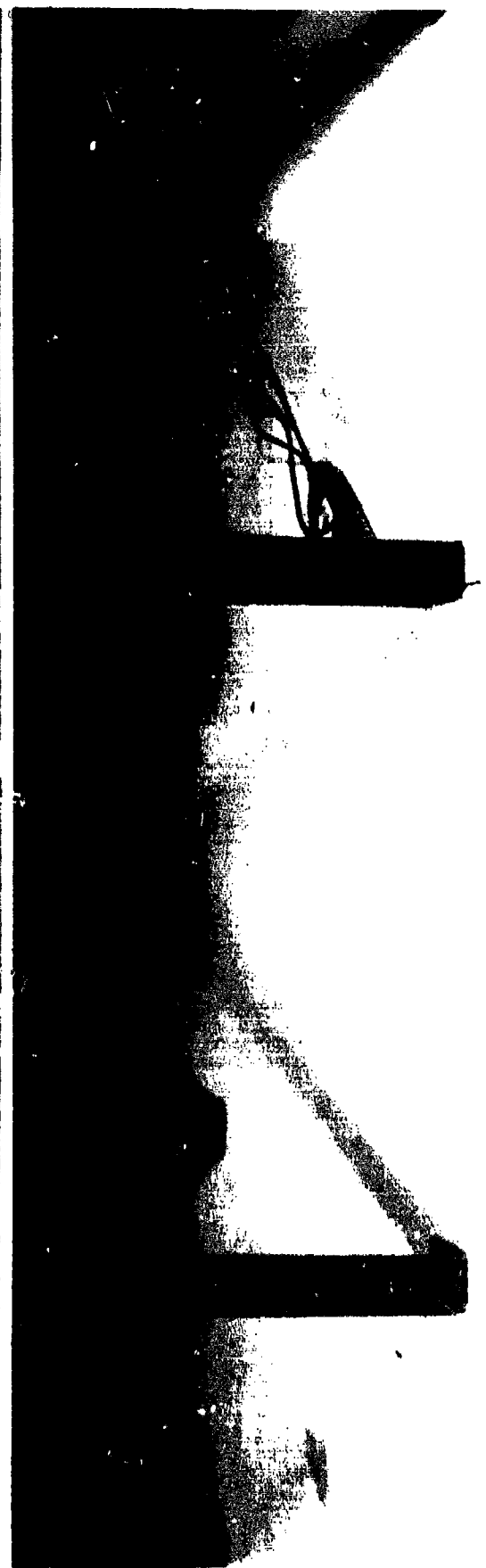
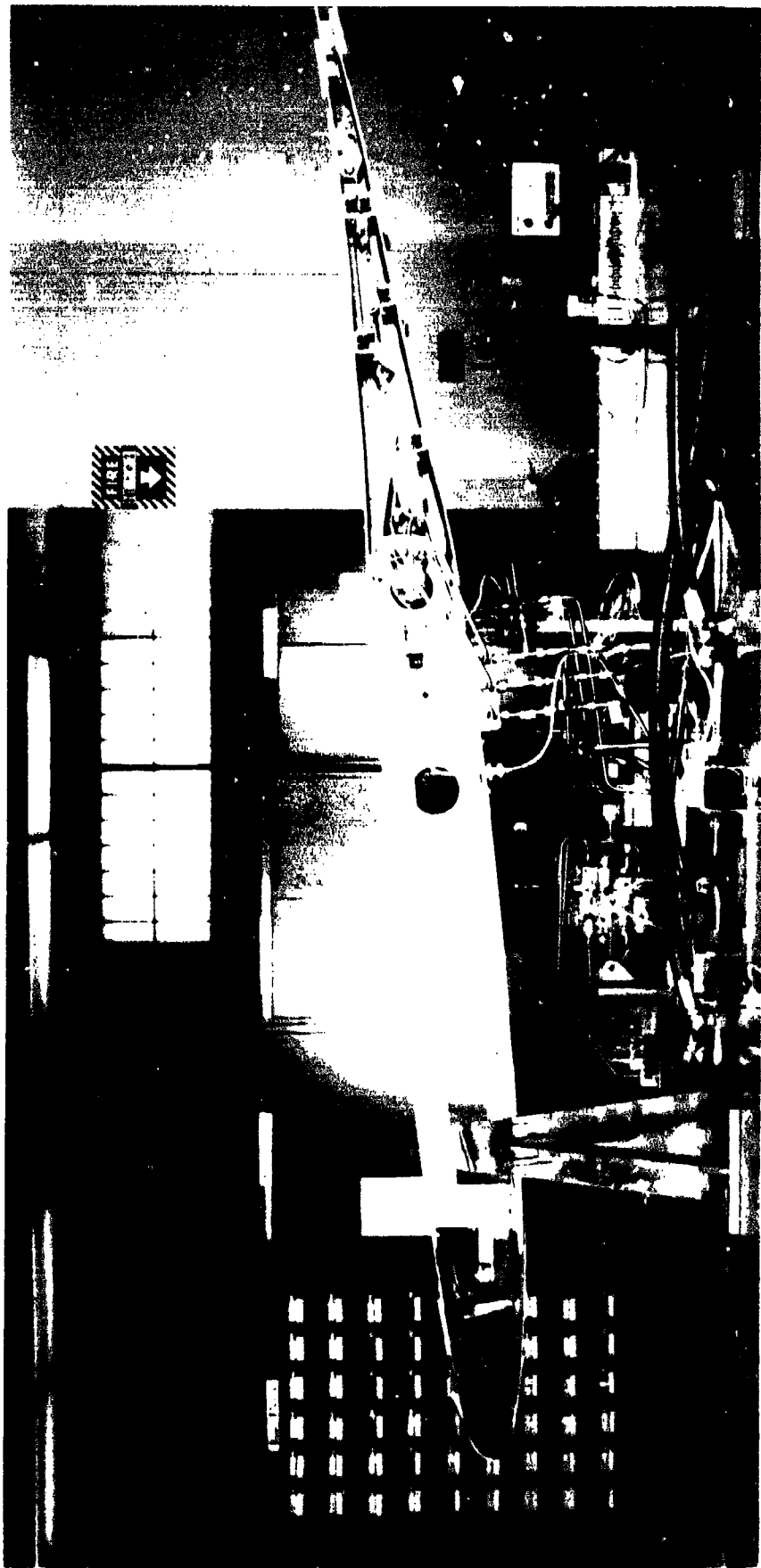


Figure IV-1. MAW in *up* position.

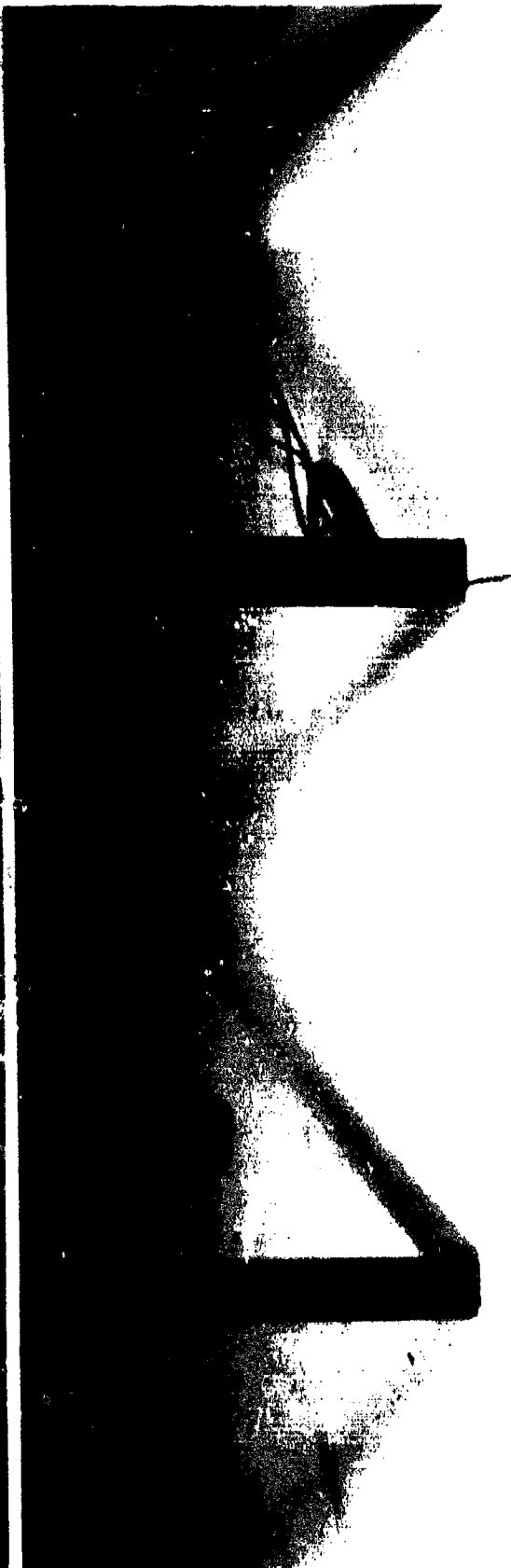
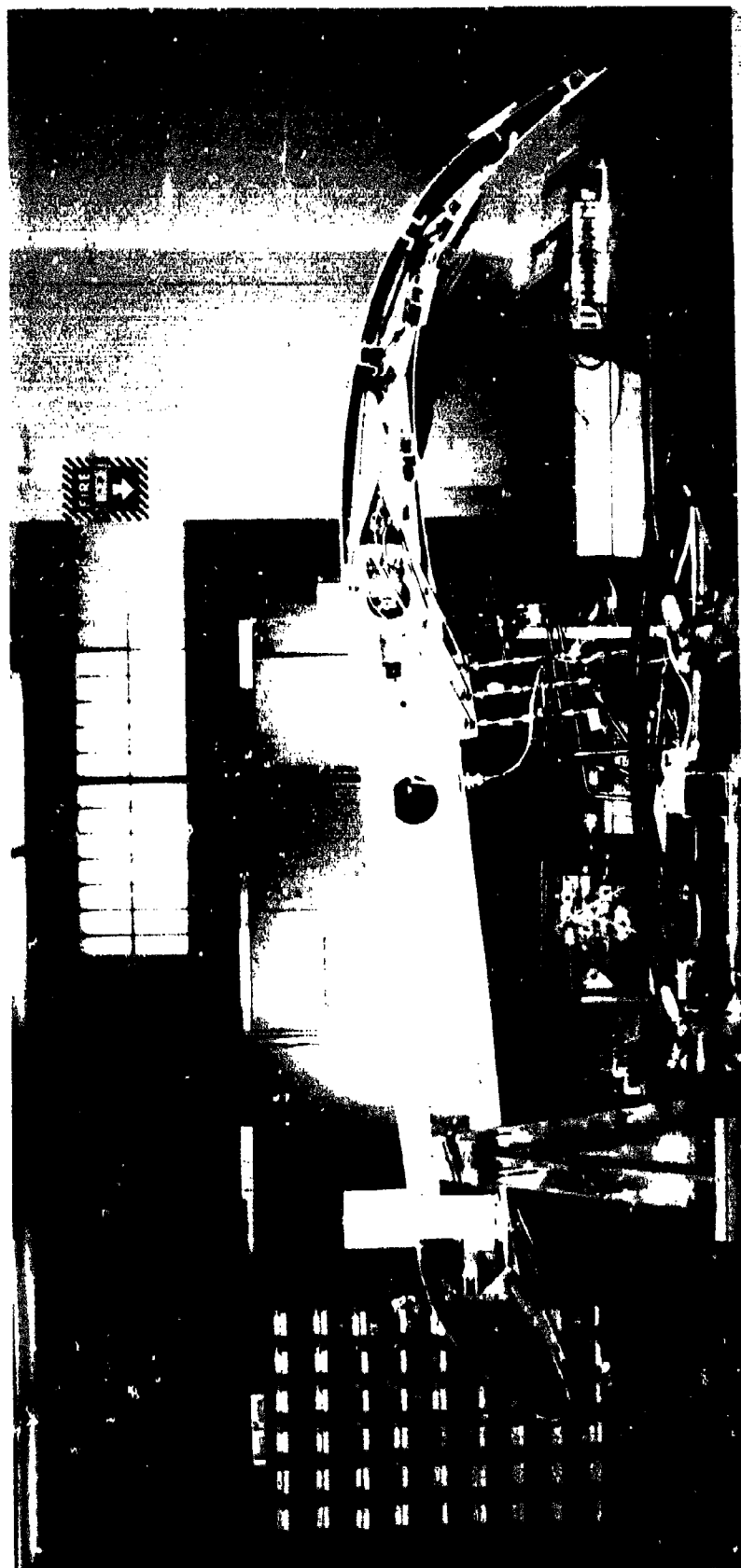


Figure IV-2. MAW in *down* position.

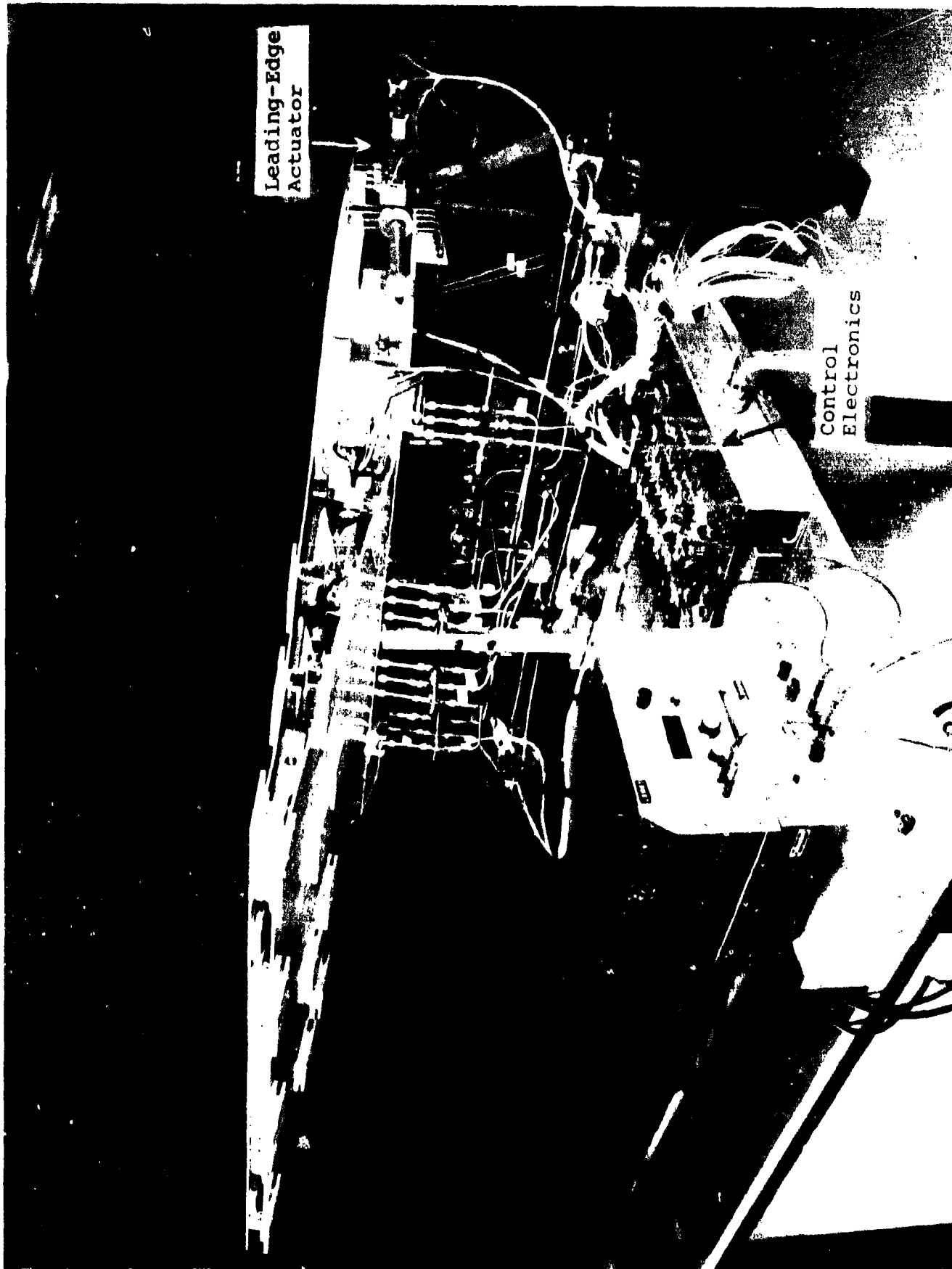


Figure IV-3. MAW control electronics and leading-edge actuator.

MAWS General Test Procedure

The MAW test section was mounted in the Multipurpose Actuation System Test Rig (MASTR) in Building 145, Area B, Wright-Patterson Air Force Base, Ohio. The MASTR provided a mounting table for the wing box of the test section. The wing box was clamped to the table using wood supports (cut to the contour of the wing box) and a clamping plate. The leading and trailing edges of the test section extended over the edge of the table. Figure IV-4 shows the section mounted in the MASTR. Note the mounting pads on the lower surface of the leading and trailing edges. For the loaded testing, the pads were used (with adapters) to attach the load actuators to the test section. The control valving and series damper-actuators assembly was mounted on the mounting table at the side of the test section as shown in Figure IV-5. The control electronics were positioned on the opposite side of the test section on the mounting table as shown in Figure IV-6.

The test section was subjected to a series of input/output tests defining the performance characteristics of the test section. The measurements are based on a series of input/output tests used by Dynamic Controls, Incorporated (DCI) for testing other actuation systems for the Flight Dynamics Laboratory at Wright-Patterson Air Force Base, Ohio. Input commands for the measurements were based upon 100-percent full stroke for the leading-edge actuator (since the actuator stroke provided the deflection limits for the leading-edge surface). For the trailing-edge commands, the full-stroke inputs were established at 90 percent of the input which would cause the surface to deflect enough for safety microswitches to fail the control system. The microswitches were used as deflection-limiting safety devices to prevent overstroking the trailing-edge drive system and running the acme screws in the variable-geometry trusses out of their operating range.

Due to the complexity of the MAW test section the testing was conducted in four steps as follows:

- (1) Leading-edge tests - unloaded
- (2) Trailing-edge tests - unloaded
- (3) Leading-edge tests - loaded
- (4) Trailing-edge tests - loaded

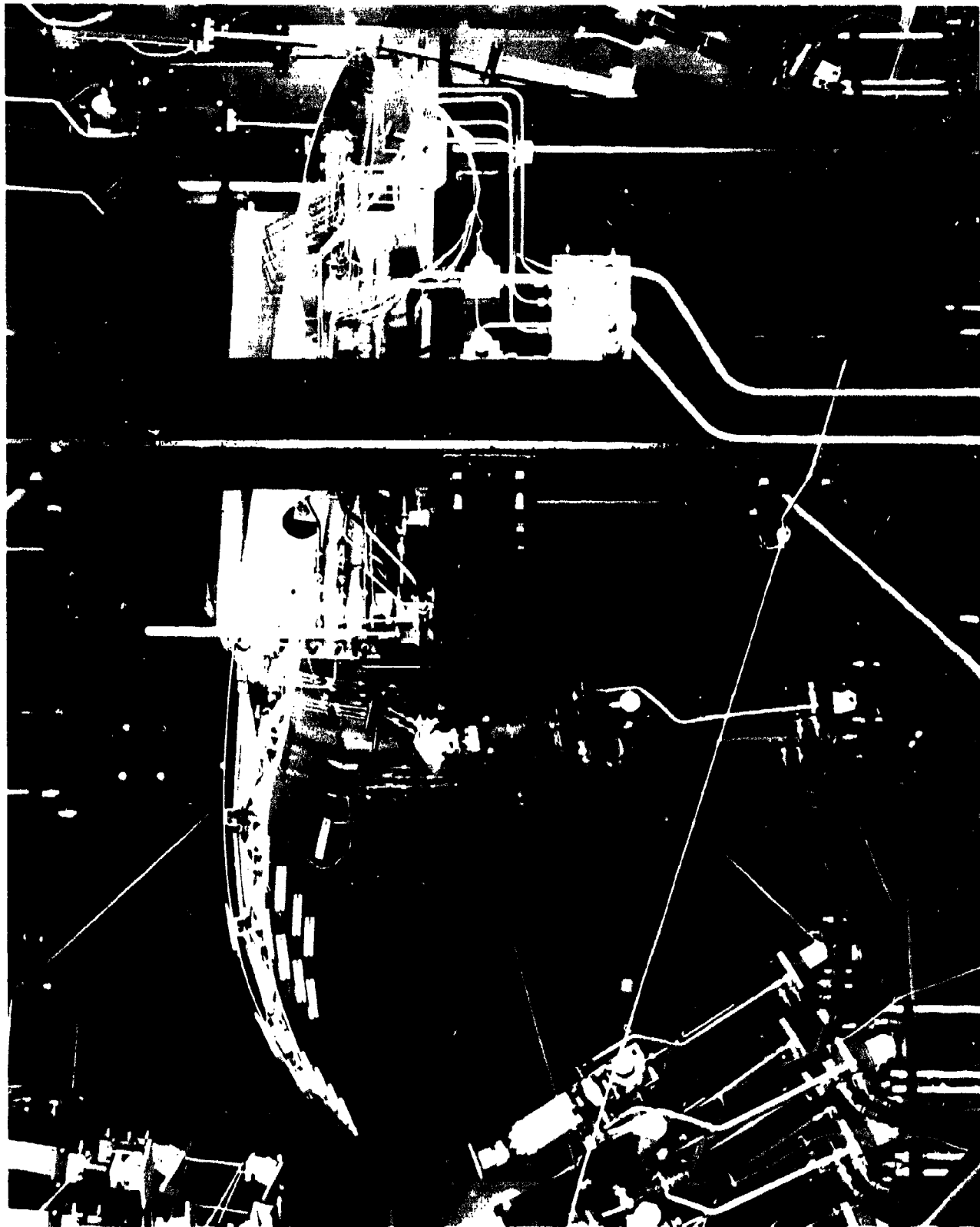


Figure IV-4. MAW installed in MASTR.

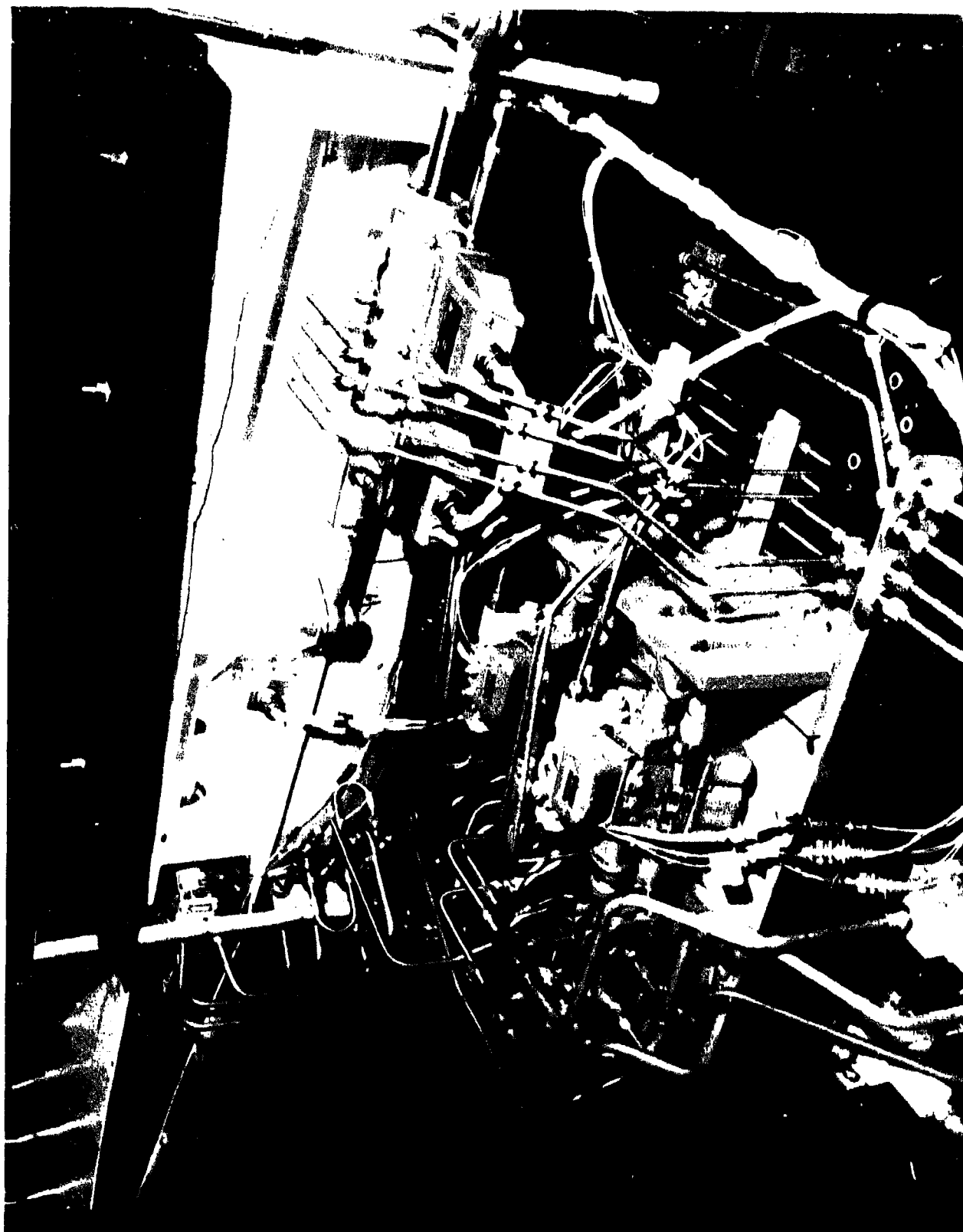


Figure IV-5. Control valve mounting in MASTR.

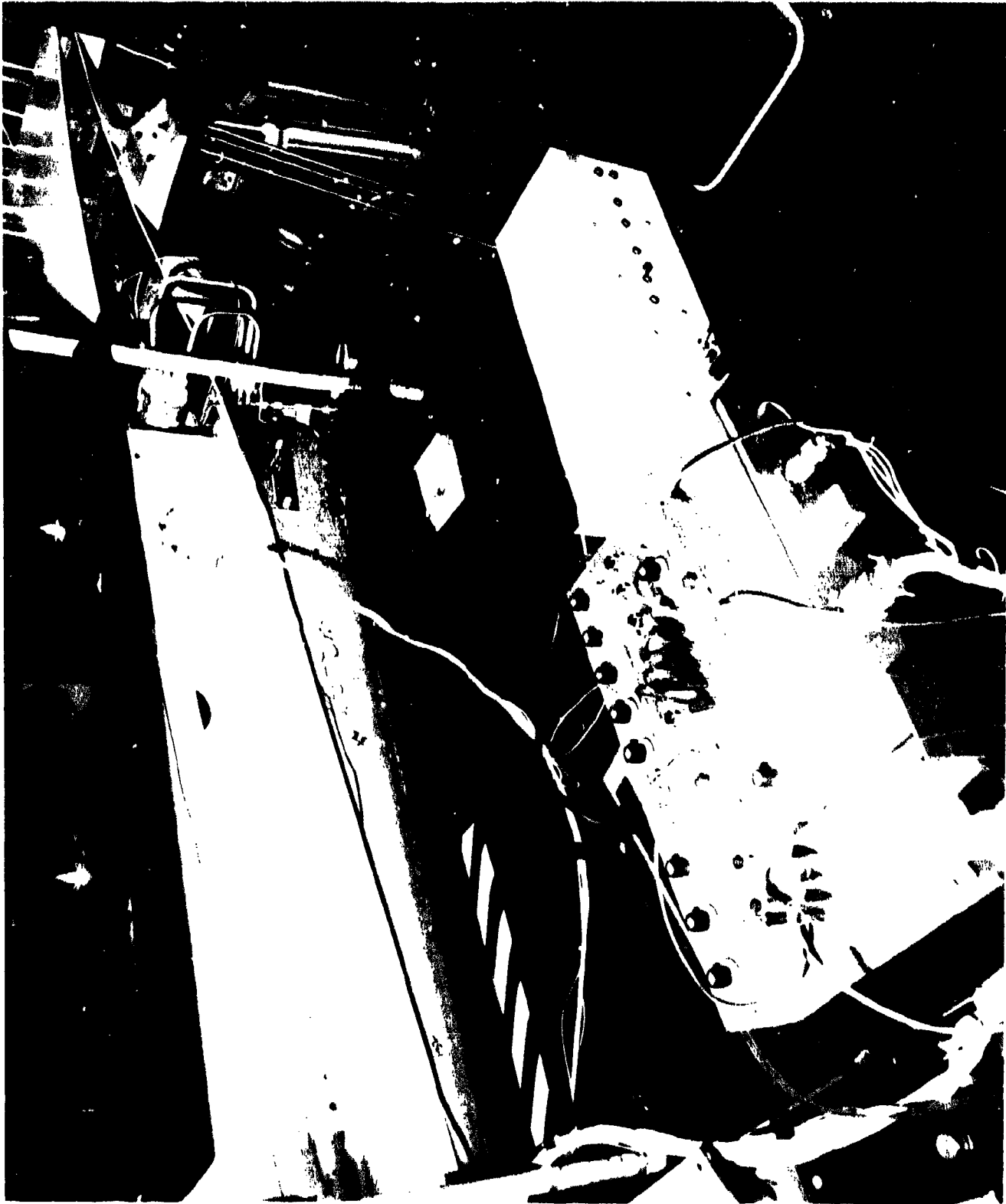


Figure IV-6. MAW control electronics installed in MASTR.

General Performance Measurements

The following input/output measurements were performed on the MAW specimen. The same measurements were conducted for both loaded and unloaded tests (with the exception of the *saturation velocity* measurement which was performed only in the unloaded tests).

<u>Measurement</u>	<u>Definition</u>
Linearity	<i>The deviation of output-versus-input from a straight-line relationship.</i>
Hysteresis	<i>The non-coincidence of loading and unloading curves at large and small input command levels.</i>
Frequency Response	<i>For a sinusoidal actuator input, the frequency response of the actuator is the relationship of the output to input expressed as an amplitude ratio and phase shift as a function of frequency.</i>
Static Threshold	<i>The minimum change from zero level which causes a measurable output change.</i>
Dynamic Threshold	<i>The input level a frequency of 50 percent of the actuator's bandpass required to cause a measurable output level.</i>
Saturation Velocity	<i>The maximum velocity at which the actuator is capable of moving in each direction.</i>
Transient Response	<i>The time response of the actuator output to an applied step input whose amplitude minimizes the nonlinear distortions of threshold and hysteresis, yet avoids velocity saturation.</i>

Test Configuration

Figure IV-7 is a block diagram of the instrumentation, command, and power connections used during the evaluation of the General Dynamics's MAW system. As shown in the diagram, a Hewlett Packard 5423A structural dynamic analyzer with a Hewlett Packard 9872A digital plotter was used for frequency response measurements.

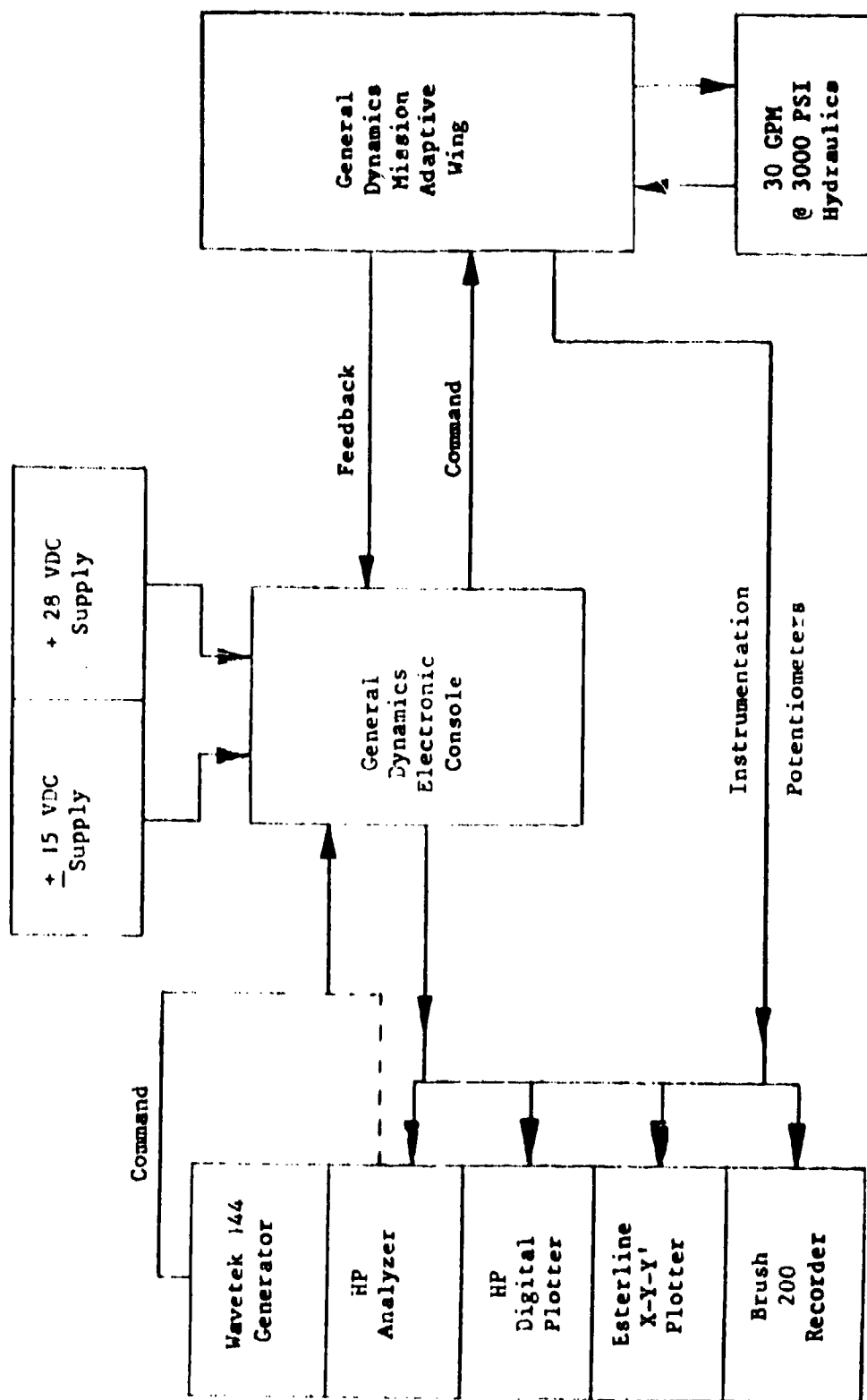


Figure IV-7. Instrumentation block diagram.

A Wavetek sweep generator and an Esterline Angus 540 X-Y-Y' plotter was used to record linearity and hysteresis measurements. A Brush 200 pen recorder was used for recording the threshold, transient response, and saturation velocity measurements. Both the 28 VDC and ± 15 VDC electrical supply requirements for the MAW control electronics were met with laboratory power supplies. The MAW was supplied with 3000 psi with a 30-gpm hydraulic pumping system. Six Waters linear potentiometers were installed to measure the surface motion of the test section.

Specific Test Procedure - Unloaded Leading Edge

The motion of the leading edge was measured with two linear position transducers (precision film potentiometers) attached between the inboard and outboard loading pads mounted on the leading-edge lower surface and the frame of the MASTR. Figure IV-8 shows the leading-edge position transducer attachment point at 11.75 inches forward of the actuator bellcrank pivot point. The motion of the actuator driving the leading edge was measured by using the demodulated outputs of the two-section LVDT incorporated as part of the actuator for actuator-position feedback. The following is summary presentation of the procedure used to make the input/output measurements with the test configuration (shown in Figure IV-7).

Linearity

The sweep generator is used to drive the control actuator to positive and negative position limits using a triangular waveform at 0.1 Hz. The plotter is used to record the output of each leading-edge position potentiometer and the actuator position LVDT (on the Y axis) versus the input (on the X axis).

Hysteresis

The sweep generator is used to drive the control actuator with a 0.1 Hz sine wave at amplitudes of 1.0 and 10 percent of the maximum input voltage. The output of each leading-edge position transducer and the output of the actuator LVDT are recorded by the plotter (on the Y axis) versus the input command input (on the X axis).

Frequency Response

The HP 5423A analyzer is used to drive the control actuator with a band limited (0 to 50 Hz) white noise input signal having a peak amplitude of ± 3 percent of the maximum input signal

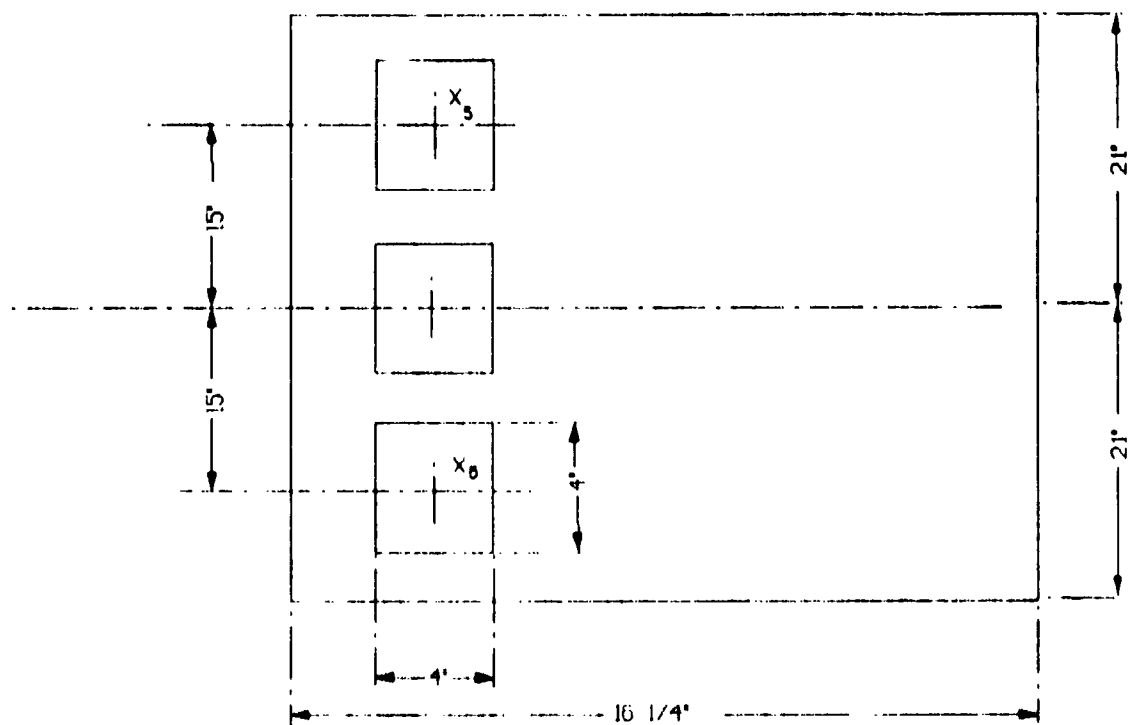
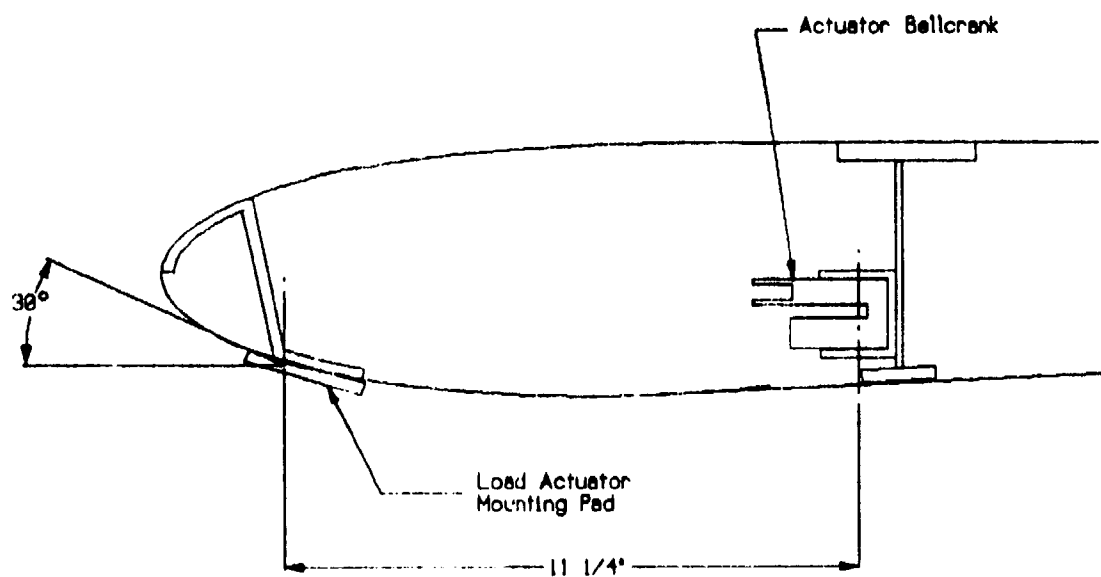


Figure IV-8. Leading-edge position transducer attachment.

(for small signal response) or ± 10 percent of the maximum input signal (for large signal response). The HP digital plotter is used to record the analyzer's output of amplitude ratio and phase angle of the actuator motion and surface position versus input.

Static Threshold

The sweep generator is used to drive the input of the leading-edge control system at 0.3 Hz with a triangular waveform. The initial input amplitude is started at zero and gradually increased until a measurable output is recorded. The input, the actuator position, and surface positions are recorded using the Brush 200 recorder.

Dynamic Threshold

The sweep generator is used to drive the input of the leading-edge control system with a sinusoid at 5 Hz (a frequency equal to one-half of the leading-edge bandpass frequency). Starting at zero, the amplitude of the input is gradually increased until a measurable output is recorded for the actuator and for the surface position outputs. The inputs, the actuator position, and surface position are recorded using the Brush 200 recorder.

Saturation Velocity

The sweep generator is used to drive the input of the leading-edge control system with a square wave having an amplitude sufficient to drive the actuator to full stroke. The input, the actuator position, and surface positions are recorded using the Brush 200 recorder.

Transient Response

The input is commanded with a step input having an amplitude equal to 10 percent of maximum command input. The input, the actuator position, and surface positions are recorded using the Brush 200 recorder.

Specific Test Procedure - Unloaded Trailing Edge

The motion of the trailing edge was measured by attaching the four position transducers (linear precision potentiometers) to load attachment beams as shown on Figures IV-9 and IV-10. As shown in these two figures, the load actuator attachment beams were mounted to the loading pads and the

Note: Beams in rows 2 and 4 were also used to monitor position

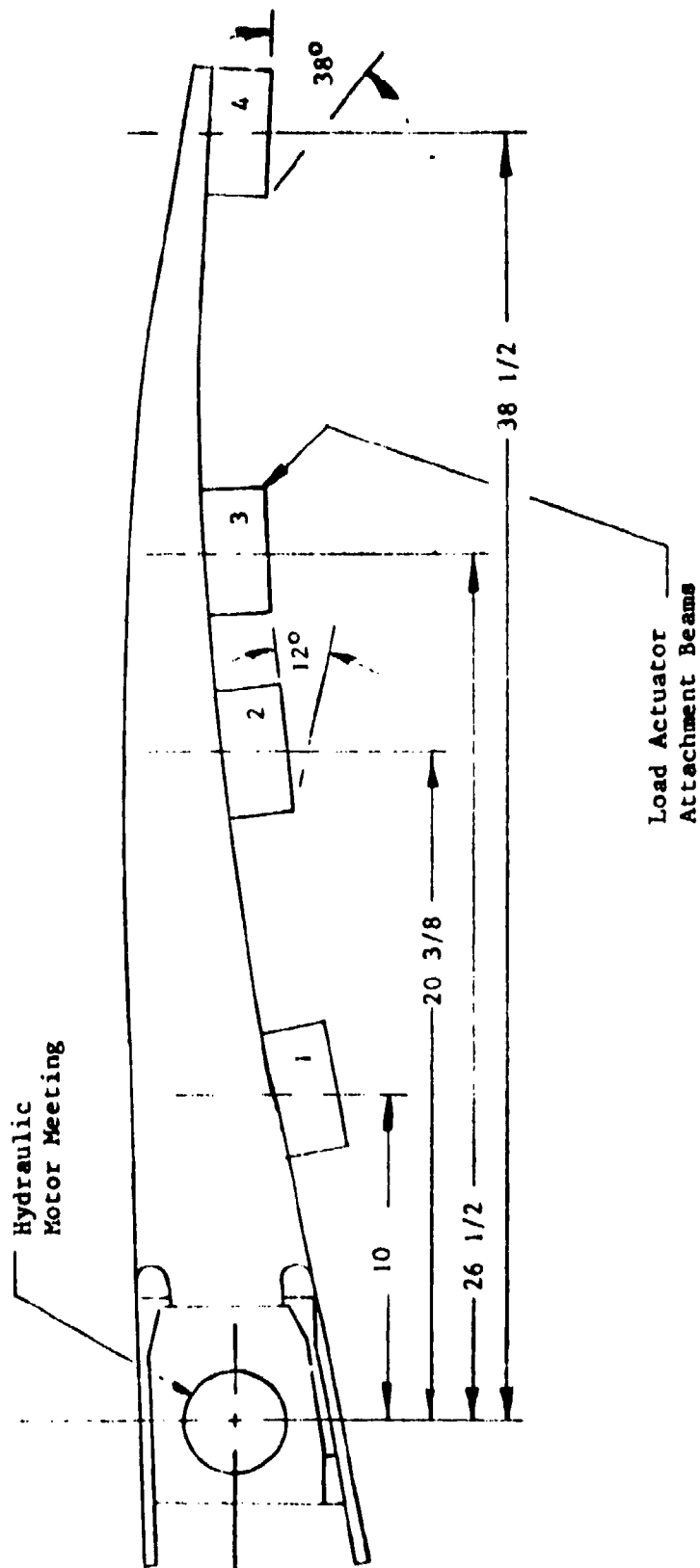


Figure IV-9. Surface position transducer and load actuator attachment points.

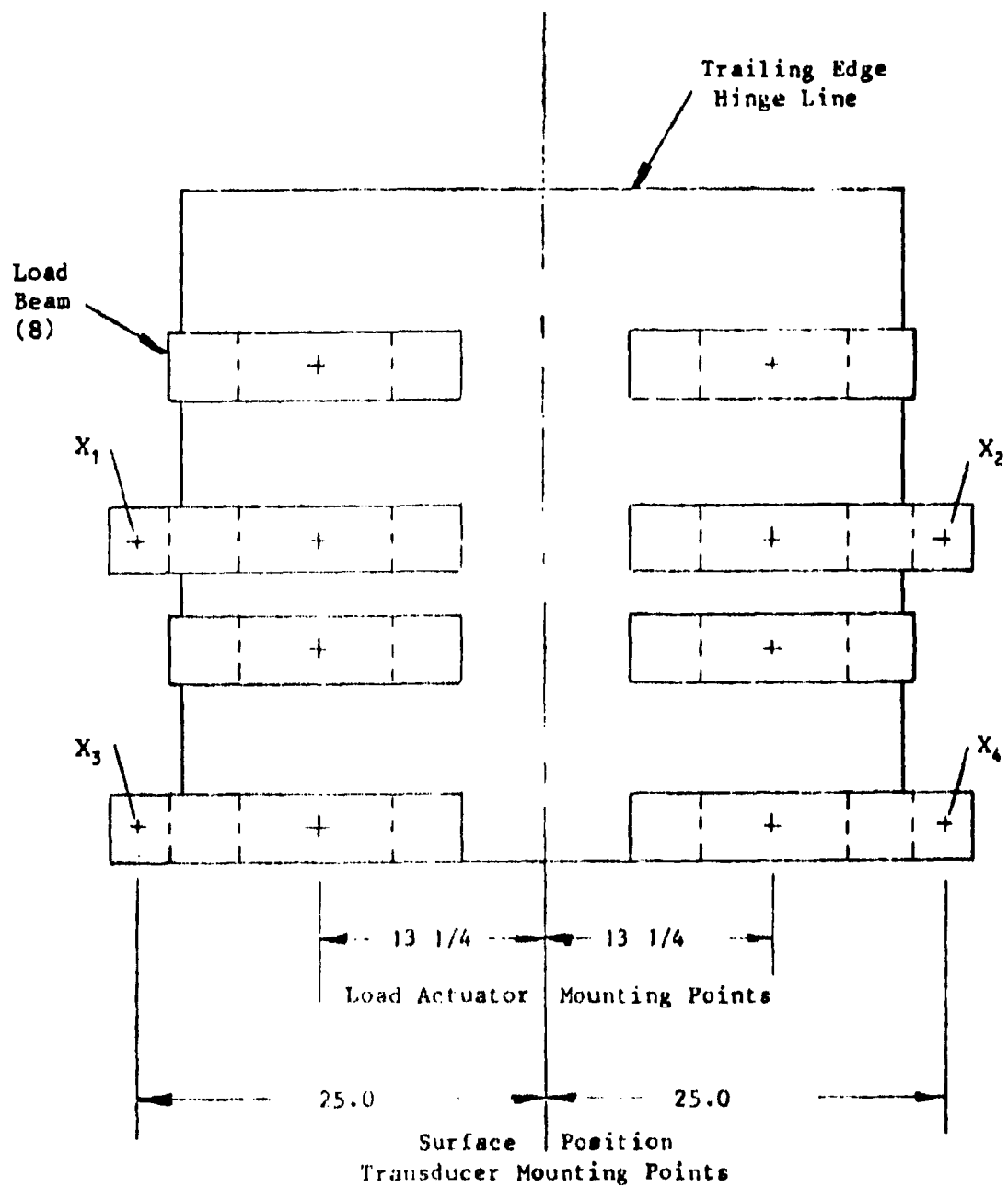


Figure IV-10. Surface position transducer and load actuator attachment points.

position transducers were attached to the attachment beams. The position transducers and the rotary potentiometers incorporated in the design of the test section (to feedback the output shaft position of the differential gear boxes) were used to measure the performance the surface shaping mechanism.

In order to gauge the performance of the variable-geometry truss mechanization, recordings of the rotary gear-box output motion and the surface position transducers versus input were made wherever possible. A comparison of the surface position transducer outputs and the rotary gear box output indicated the motion coupling characteristics of the variable-geometry truss design.

Linearity

The sweep generator is used to drive the control actuator to positive and negative position limits using a triangular waveform at 0.1 Hz. The X-Y-Y' plotter is used to record the output of each trailing-edge position potentiometer and the rotary gear-box position transducer in the following combinations:

- a. X axis - input command voltage
 Y axis - rotary potentiometer output (left side)
 Y'axis - #1 position potentiometer output
- b. X axis - input command voltage
 Y axis - rotary potentiometer output (left side)
 Y'axis - #3 position potentiometer output
- c. X axis - input voltage
 Y axis - #1 position potentiometer output
 Y'axis - #3 position potentiometer output

The sequence is repeated for the right side with position potentiometer #2 and #4 in place of #1 and #3 respectively and the right side's rotary potentiometer output in place of the left side's rotary potentiometer.

Hysteresis

The sweep generator is used to drive the control actuator with a 0.1 Hz sine wave at amplitudes of 3.0 and 10 percent of the maximum input voltage. The X-Y-Y' plotter is used to record the output of each trailing-edge position potentiometer and the gear box rotary position transducer in the following combinations:

- a. X axis - input command voltage
Y axis - rotary potentiometer output (left side)
Y'axis - #1 position potentiometer output
- b. X axis - input command voltage
Y axis - rotary potentiometer output (left side)
Y'axis - #3 position potentiometer output

The sequence is repeated for the right side with position potentiometer #2 and #4 in place of #1 and #3 respectively and the right side's rotary potentiometer output in place of the left side's rotary potentiometer.

Frequency Response

The HP 5423A analyzer is used to drive the control actuator with a band limited (0 to 25 Hz) white noise input signal having a peak amplitude of ± 5 percent of the maximum input signal (for small signal response) or ± 10 percent of the maximum input signal (for large signal response). The HP digital plotter is used to record the analyzer's output of amplitude ratio and phase angle of the actuator motion and surface position versus input. The output motion of the left and right potentiometers, and surface position transducers 1, 2, 3 and 4 versus the command input are recorded for both the 5 percent and 10 percent input level. The 5 percent input (rather than 3 percent) was required to minimize the effects of threshold and hysteresis on the measured frequency response.

Static Threshold

The sweep generator is used to drive the input of the leading-edge control system at 0.3 Hz to 0.6 Hz with a triangular waveform. The initial input amplitude is started at zero and gradually increased until a measurable output is recorded. The input, the outputs of the rotary potentiometers and the outputs of the four surface position transducers are recorded using the Brush 200 recorder.

Dynamic Threshold

The sweep generator is used to drive the input of the leading-edge control system with a sinusoid at 1.5 Hz (a frequency equal to one-half of the nominal bandpass frequency of the trailing edge. Starting at zero, the amplitude of the input is gradually increased until the measurable output is recorded. The input, the outputs of the rotary potentiometers and the outputs of the 4 surface position transducers are recorded using the Brush 200 recorder.

Saturation Velocity

The sweep generator is used to drive the input of the leading-edge control system with a square wave having an amplitude equal to 80 percent of the maximum command input. The input, the outputs of the rotary potentiometers and the outputs of the 4 surface position transducers are recorded using the Brush 200 recorder.

Transient Response

The input is commanded with a step input having an amplitude equal to 10 percent of maximum command input. The input, the outputs of the rotary potentiometers and the outputs of the 4 surface position transducers are recorded using the Brush 200 recorder.

Loaded Testing

General

The general approach for loaded testing of both the leading- and trailing-edge surfaces of the MAW specimen was to attach loading actuators only to the lower surfaces of both the leading and trailing edges. The rationale in loading only the lower surface with a compressive load was that type of loading was sufficient to apply the desired net load to the actuation mechanism within each edge (without incurring the complexity of running another set of load actuators, operating in tension, on the top of the surfaces). Three load actuators were used for the leading edge and eight actuators were used for the trailing edge. Figure IV-10 shows the load actuator installation from the right side of the MASTR. Figure IV-11 shows the loading systems installation from the left side of the MASTR. Each load actuator incorporated a load cell in its base and was driven by a single load control channel. The maximum output force capability of each load actuator is 3000 pounds with a supply pressure of 3000 psi. The actuators were commanded to a constant force output which created equivalent

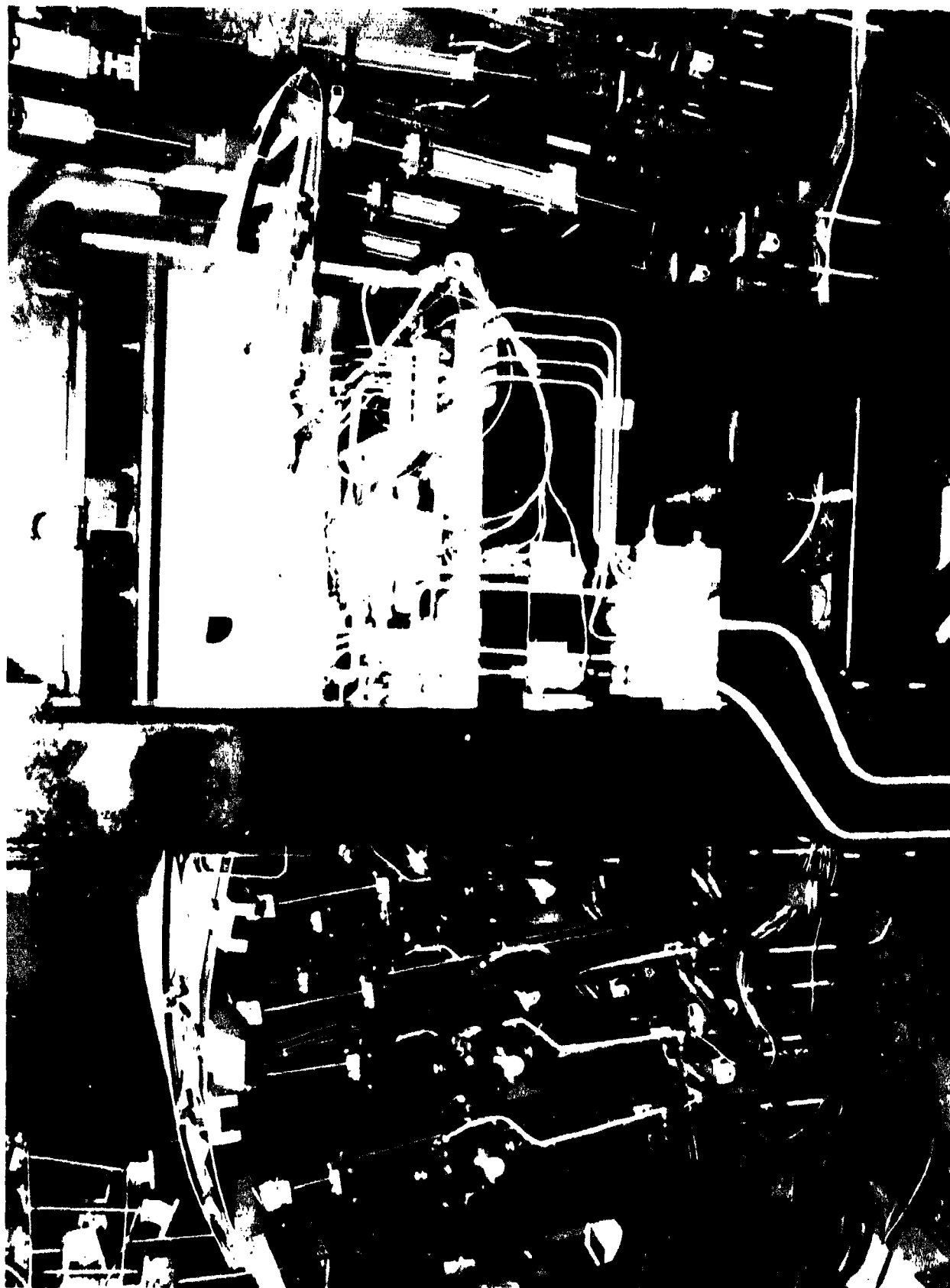


Figure IV-11. Loading system installation, right-side view.

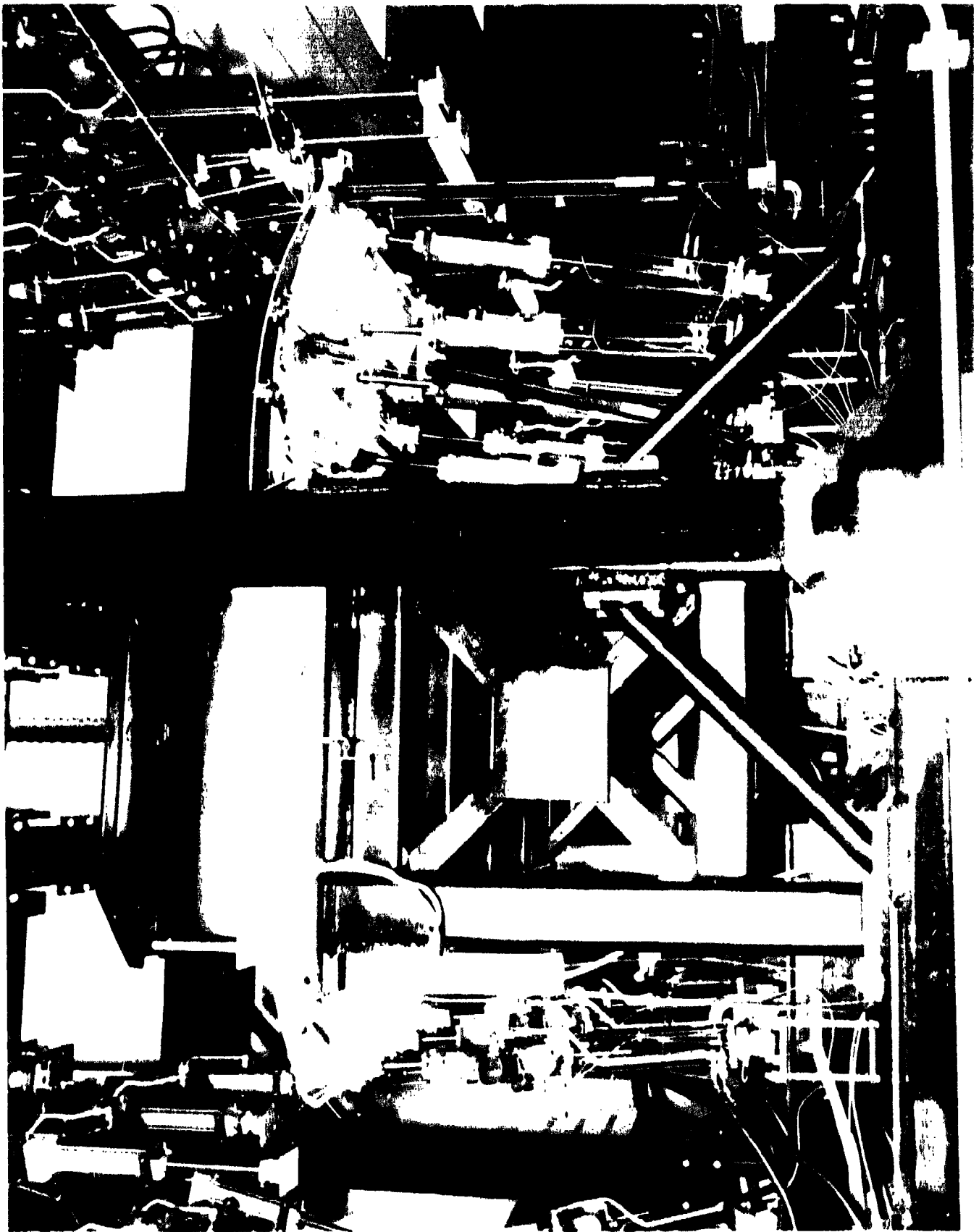


Figure IV-12. Loading system installation, left-side view.

surface loading corresponding to pressure loadings of 1 and 2 psi on the leading edge and up to 5 psi on the trailing edge. The load distribution assigned to the loading actuators was based upon an area weighting according to the attach points of the actuators. The position of the surfaces were measured with the same linear position transducers used for the unloaded testing.

Loaded Leading-Edge Tests

Figure IV-13 is a closeup view of the leading-edge loading system as viewed from the right side. The load actuators were attached to three pads located 15 inches apart on the forward lower edge of the surface. The loading pads were located *on center* with the three internal control linkages of the forward edge. As shown in Figure IV-13, the position transducer to the left of the figure (along side the closest load actuator) is position transducer X_6 . The position transducer measuring the surface deflection along side the farthest load actuator is position transducer X_5 . X_6 is the surface location closest to the leading-edge linear actuator.

The leading-edge control surface had a nominal surface area of 682 square inches (42 inches \times 16.25 inches). The total surface load for 1 psi aerodynamic load therefore totaled 682 pounds. Using the area weighting criteria, the center loading actuator was used to apply a *load force per psi of aerodynamic load* of 243 pounds and the two outboard actuators were used to provide a *load force per psi of aerodynamic load* of 219 pounds.

Hysteresis, frequency response, and step response measurements were made for surface loads equivalent to 1 and 2 psi for the loaded leading-edge testing. The procedure used for these input/output tests was identical to that used for the same measurement with an unloaded surface.

Loaded Trailing-Edge Tests

Figure IV-14 is a closeup view of the trailing-edge loading system. Note that the mounting of the load actuators is at an angle in order to provide a load force perpendicular to the lower surface with the trailing edge deflected nominally 6 degrees down. The trailing-edge surface area was 1680 square inches (40 inches \times 42 inches), or 2.46 times the leading-edge surface area. As with the leading-edge loads, each load actuator was assigned a percentage of the total load based upon a division of the total surface area between the actuators according to the actuator mounting location as previously shown in Figures IV-9 and IV-10. All the load actuators were attached along a line 13.25 inches either side of the centerline of the trailing edge. This placed the load application points over the center of the two trailing-edge variable truss structures. The force output of the load

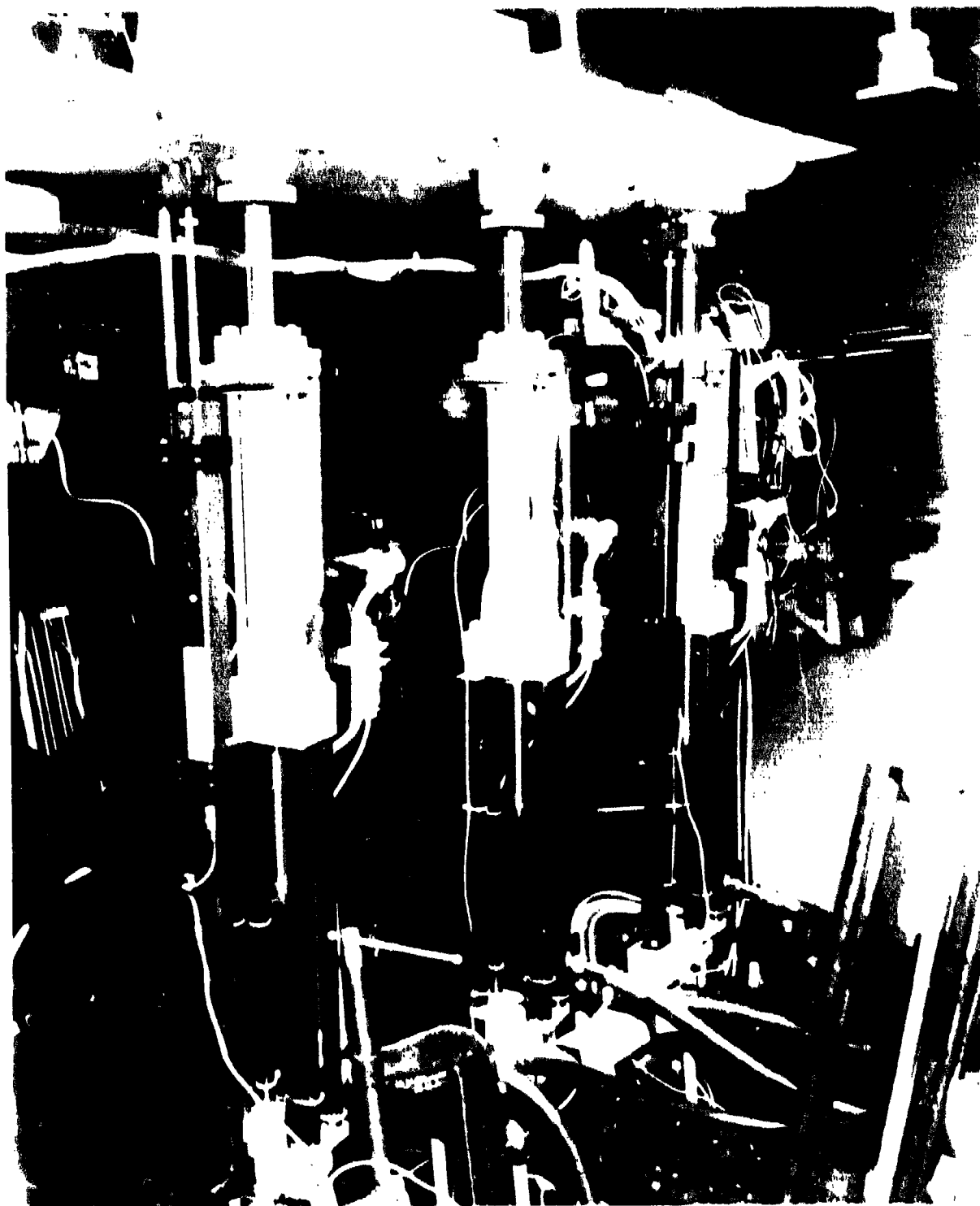


Figure IV-13. Leading-edge loading system.



Figure IV-14. Trailing-edge loading system.

actuators were established to give loads equivalent to 1-, 2-, 3-, and 5-psi surface loading. The input/output performance measurements as previously described for the unloaded tests were repeated for each load condition. Only the saturated rate tests were not used for the loaded trailing-edge performance tests because of load actuator total-stroke limitations.

III. TEST RESULTS

Unloaded Leading-Edge Test Results

General

The motion of the leading edge was instrumented at two points on the surface (X_5 and X_6 as shown previously on Figure IV-8). The output of the leading-edge actuator as measured by the actuator's integral dual channel LVDT. For most of the data, both outputs of the LVDT were recorded for reference purposes. The small difference between the recorded outputs of the two channels reflects the linearity differences between the channels and/or the accuracy of reading the outputs.

In order to relate the recorded data to the actuator output and/or command input, the surface deflection in terms of local surface slope in degrees (0° being equal to 0 slope) was measured at each instrumentation potentiometer attach point (X_5 and X_6). An inclinometer was attached to the leading-edge mounting pad to measure the leading-edge angle at the mounting pad. Table IV-1 lists the calibration factors for the leading-edge instrumentation. The first calibration factor column is the direct linear output gain of the LVDT and position transducers. The second column relates the output voltage change of the transducers to the surface deflection change with the leading edge operating around the 0° deflection point. Note that because of the linkage geometry, the output voltage/deflection gain did not remain constant over the entire deflection range. However, the operating position for the input/output tests was maintained at 0° nominal when allowed by the particular test procedure. Note also that the output of the LVDTs does not indicate the driving voltage for the actuator, only the direct demodulated output of the actuator's position feedback transducer.

Table IV-1. Calibration factors for leading-edge instrumentation.

Transducer	Calibration Factors	
Position 1 (Pos 1)	4.71 V/in	0.242 V/deg
Position 2 (Pos 2)	4.71 V/in	0.243 V/deg
Surface Position X_5	0.40 V/in	.0423 V/deg
Surface Position X_6	0.40 V/in	.0423 V/deg

Static Threshold

Figures IV-15 and IV-16 show the result of the static threshold on the leading edge. Note that as shown in Figure IV-15, the linear actuator (Pos 1 and 2) shows output motion and an input voltage of $\pm .002$ volts. However, the leading-edge surface does not show corresponding motion. This is because of the play in the control linkage connecting the output of the linear actuator to the control surface. There are five linkage joints between the output shaft of the linear actuator and the leading-edge control surface. The leading edge (as indicated by X_5 and X_6) does not move until the input command reaches $\pm .040$ volts as shown in Figure IV-16. The high-frequency noise shown on all the traces of the two figures is feed-through from the demodulated LVDT outputs and appears in most of the strip chart and X-Y data recorded for the leading edge. Table IV-2 lists the results of the static threshold in terms of a percentage of the maximum command input of ± 11.7 volts.

Table IV-2. Static threshold results.

Motion Point	Peak Input Volts	% of Maximum Input
Pos 1,2	0.002	0.017
X_5, X_6	0.040	0.34

Dynamic Threshold

Figures IV-17 and IV-18 show the dynamic threshold data for the unloaded leading-edge measurements. As with the static threshold, the linear actuator starts moving (as shown in Figure IV-17) before the leading-edge surface. In addition, X_6 (closest to the linear actuator in the driving mechanization) moves before X_5 (as shown in Figure IV-18). This characteristic is due to the linkage which couples the linear actuator to the control surface. Table IV-3 lists the threshold measured with the gradually increasing 5-Hz command input.

Test Item - General Dynamics
Mission Adaptive Wing

Date
Prepared: 6/3/85

Test - Static Threshold
Surface - Leading Edge
Load - Zero Load

Input Command
1 mv/div

Actuator
Position 1
1 mv/div

Actuator
Position 1
1 mv/div

Surface
Position X₅
2 mv/div

Surface
Position X₆
2 mv/div

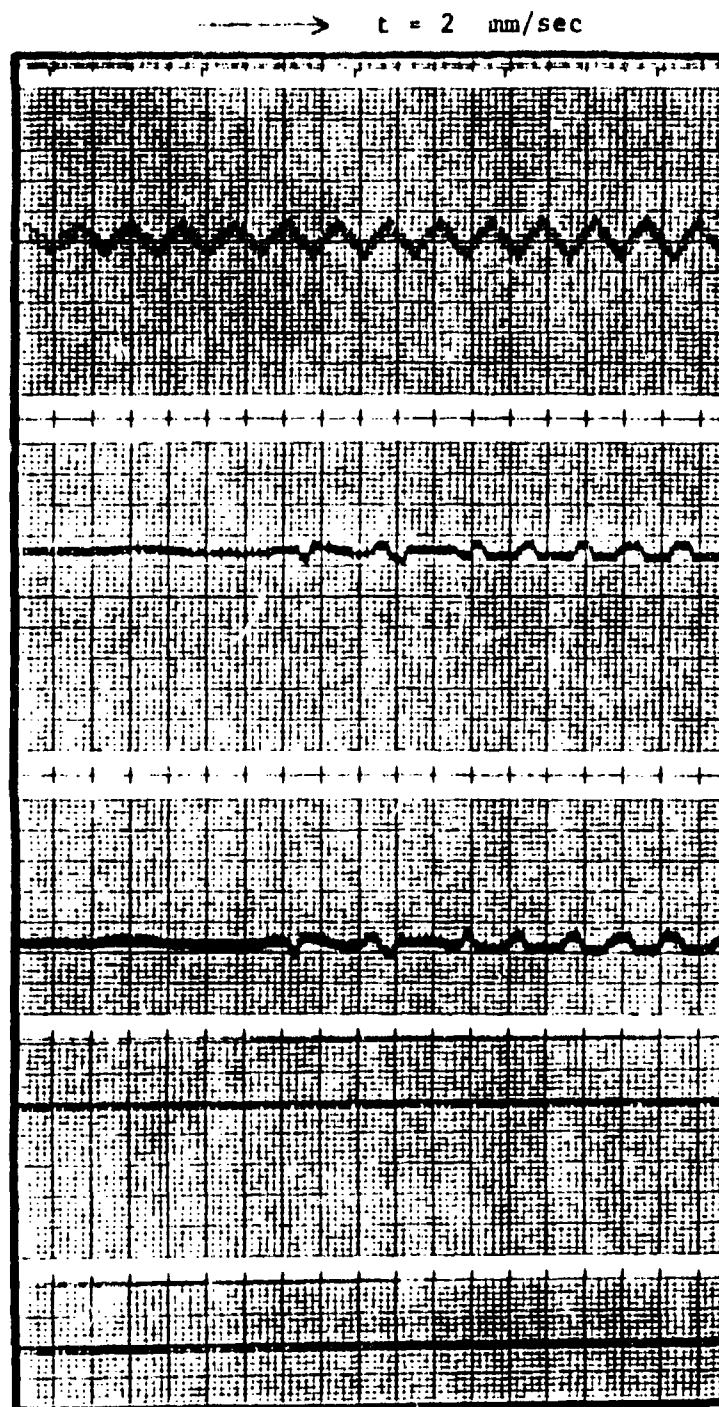


Figure IV-15. Static threshold - leading edge - data 1.

Test Item - General Dynamics
Mission Adaptive Wing

Date
Prepared: 6/3/85

Test - Static Threshold
Surface - Leading Edge
Load - Zero Load

→ $t = 2$ min/sec

Input Command
5 mv/div

Actuator
Position 1
.0012 in/div

Actuator
Position 2
.0012 in/div

Surface
Position X_5
2 mv/div

Surface
Position X_6
2 mv/div

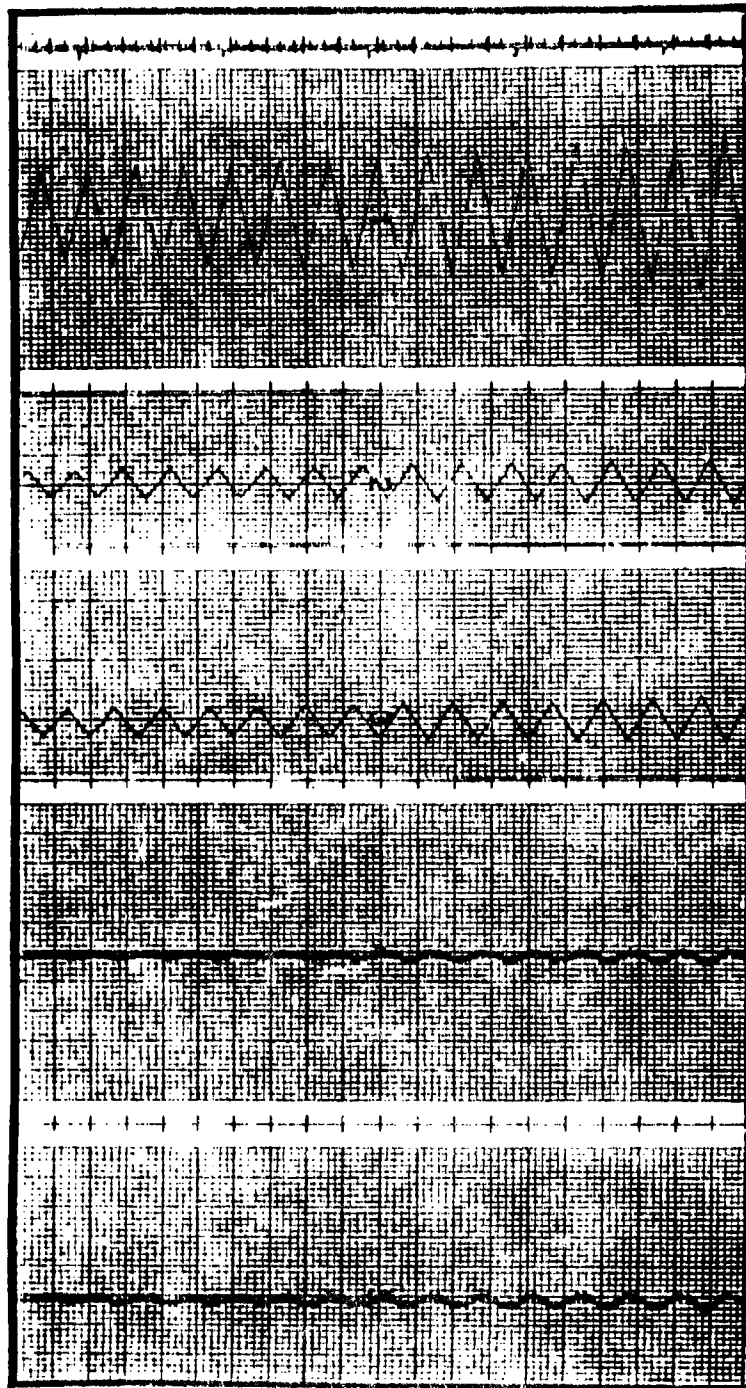


Figure IV-16. Static threshold leading edge - data 2.

Test Item - General Dynamics
Mission Adaptive Wing

Date
Prepared: 6/5/85

Test - Dynamic Threshold
Surface - Leading Edge
Load - Zero Load

Input Command
1 mv/div

Actuator
Position 1
1 mv/div

Actuator
Position 2
1 mv/div

Surface
Position X_5
1 mv/div

Surface
Position X_6
1 mv/div

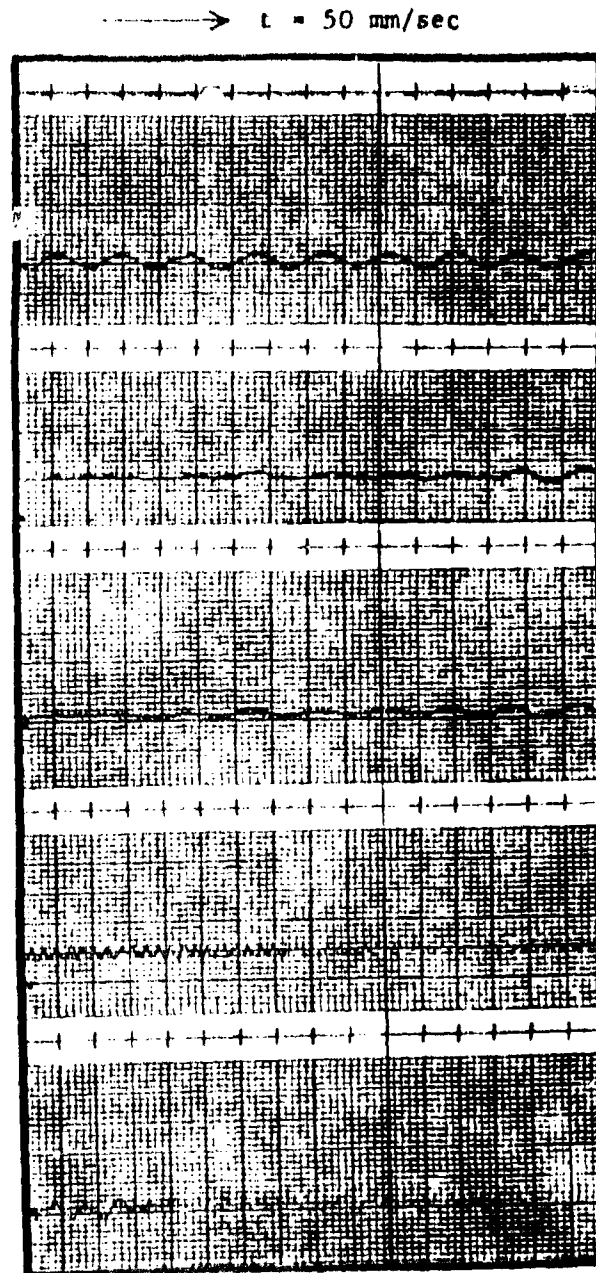


Figure IV-17. Dynamic threshold - leading edge - data 1.

Test Item - General Dynamics
Mission Adaptive Wing

Date
Prepared: 6/5/85

Test - Dynamic Threshold
Surface - Leading Edge
Load - Zero Load

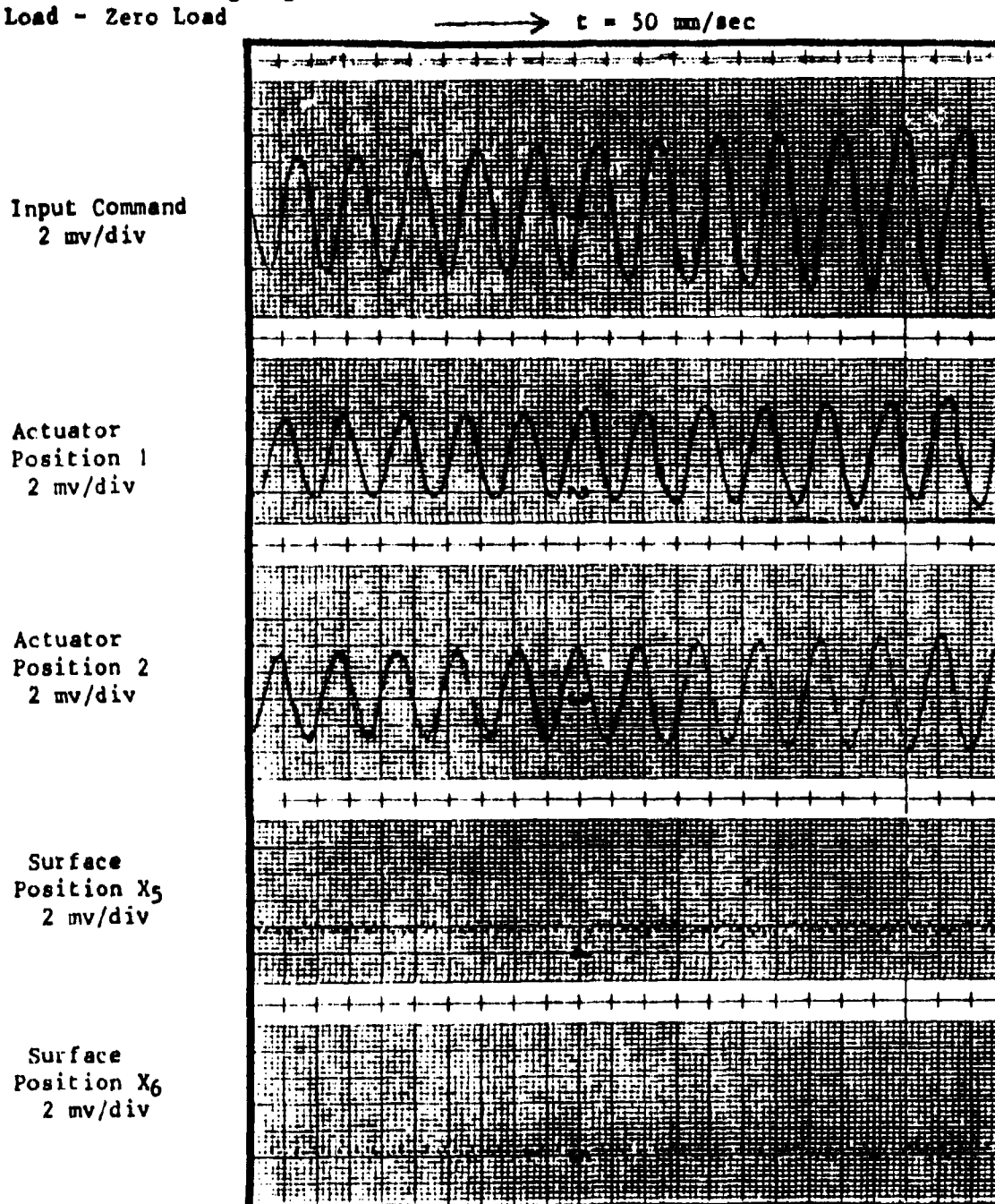


Figure IV-18. Dynamic threshold - leading edge - data 2.

Table IV-3. Dynamic threshold results.

Motion Point	Peak Input Volts	% of Maximum Input
Pos 1,2	.0015	.013
X ₅	.0220	0.188
X ₆	.030	0.256

The dynamic threshold for all the motion points is lower than the static threshold.

Frequency Response

Figures IV-19 and IV-20 show the frequency response of the linear actuator output Position 2 (Pos 2) with a 3-percent command input. Figures IV-21 and IV-22 show the frequency response of Position 2 with a 10-percent command input. This data is representative of the data recorded at positions X₅ and X₆ (with a smooth roll-off of the response and no amplitude peaking). Table IV-4 lists the frequency response of all the measurement points for the 3-percent input in terms of the frequency at which - 3 dB amplitude ratio and - 90° phase angle occurs. Table IV-5 lists the data for a 10-percent command input amplitude.

Table IV-4. Frequency response - 3-percent input.

Motion Point	- 3 dB Frequency	- 90° Frequency
Position 1	12.81	10.14
Position 2	12.06	9.92
X ₅	12.26	9.99
X ₆	13.91	11.08

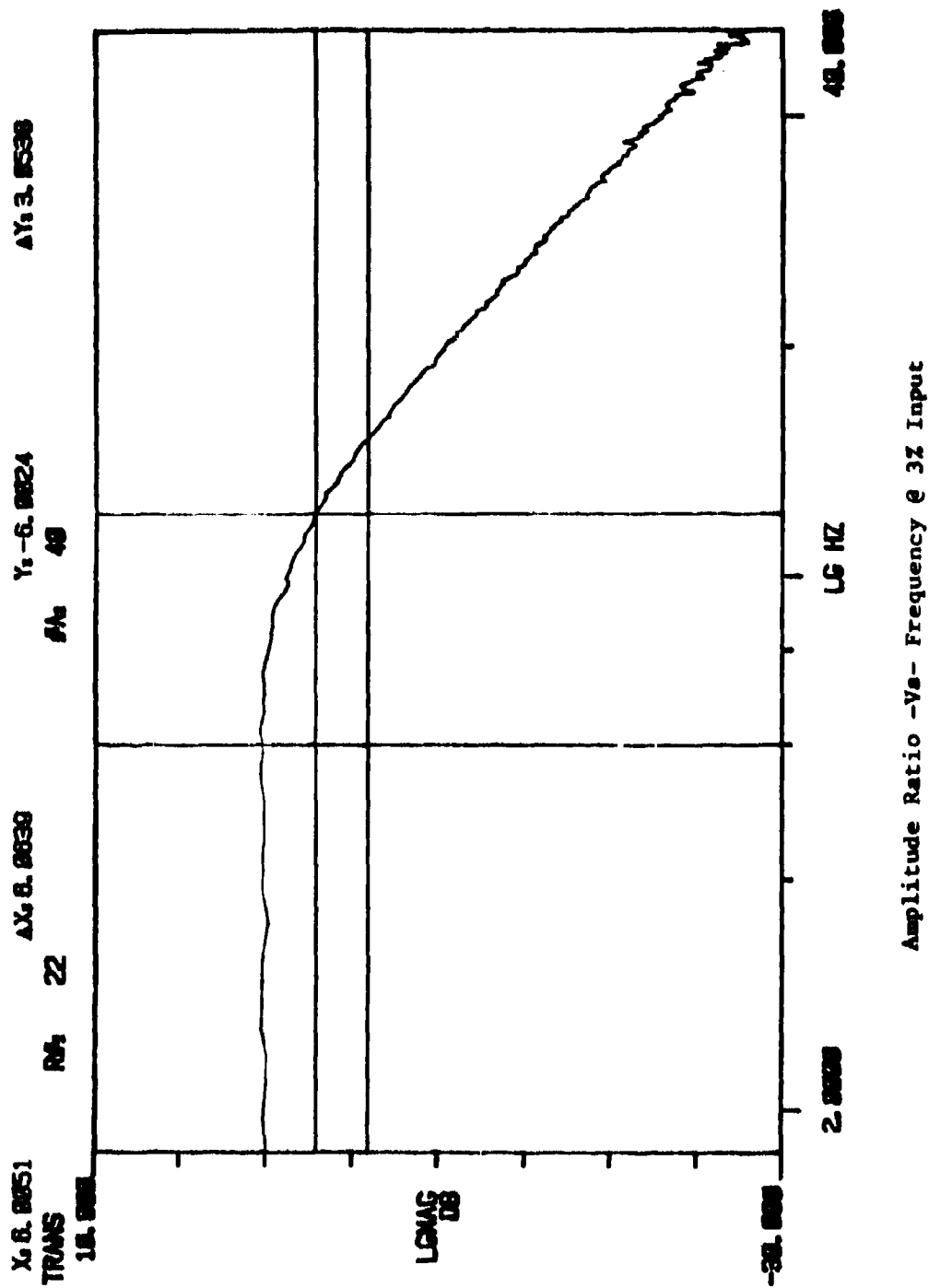


Figure IV-19. Leading-edge actuator - position 2.

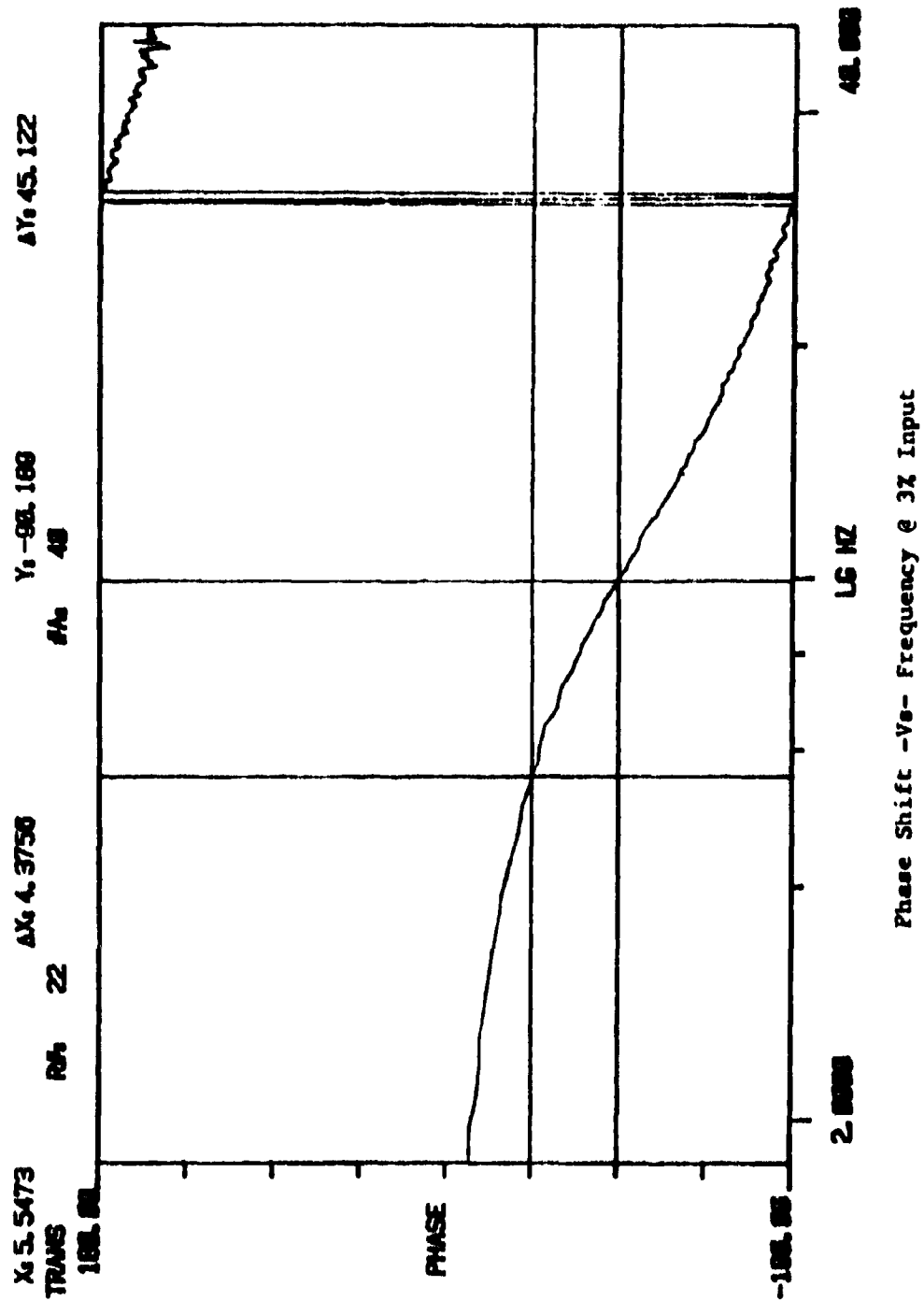
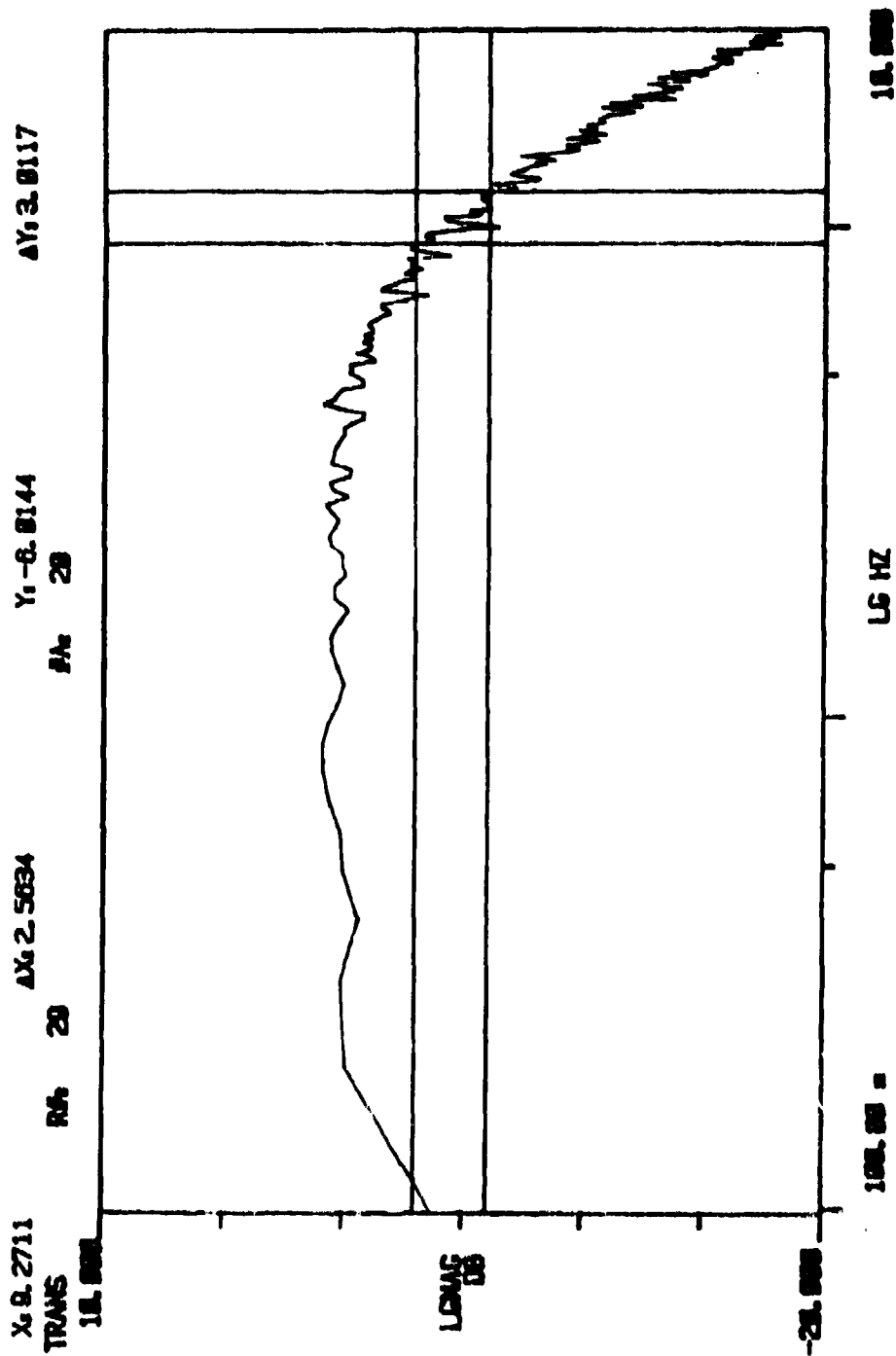


Figure IV-20. Leading edge actuator - position 2.



Amplitude Ratio -Vs- Frequency @ 10% Input

Figure IV-21. Leading-edge actuator - position 2.

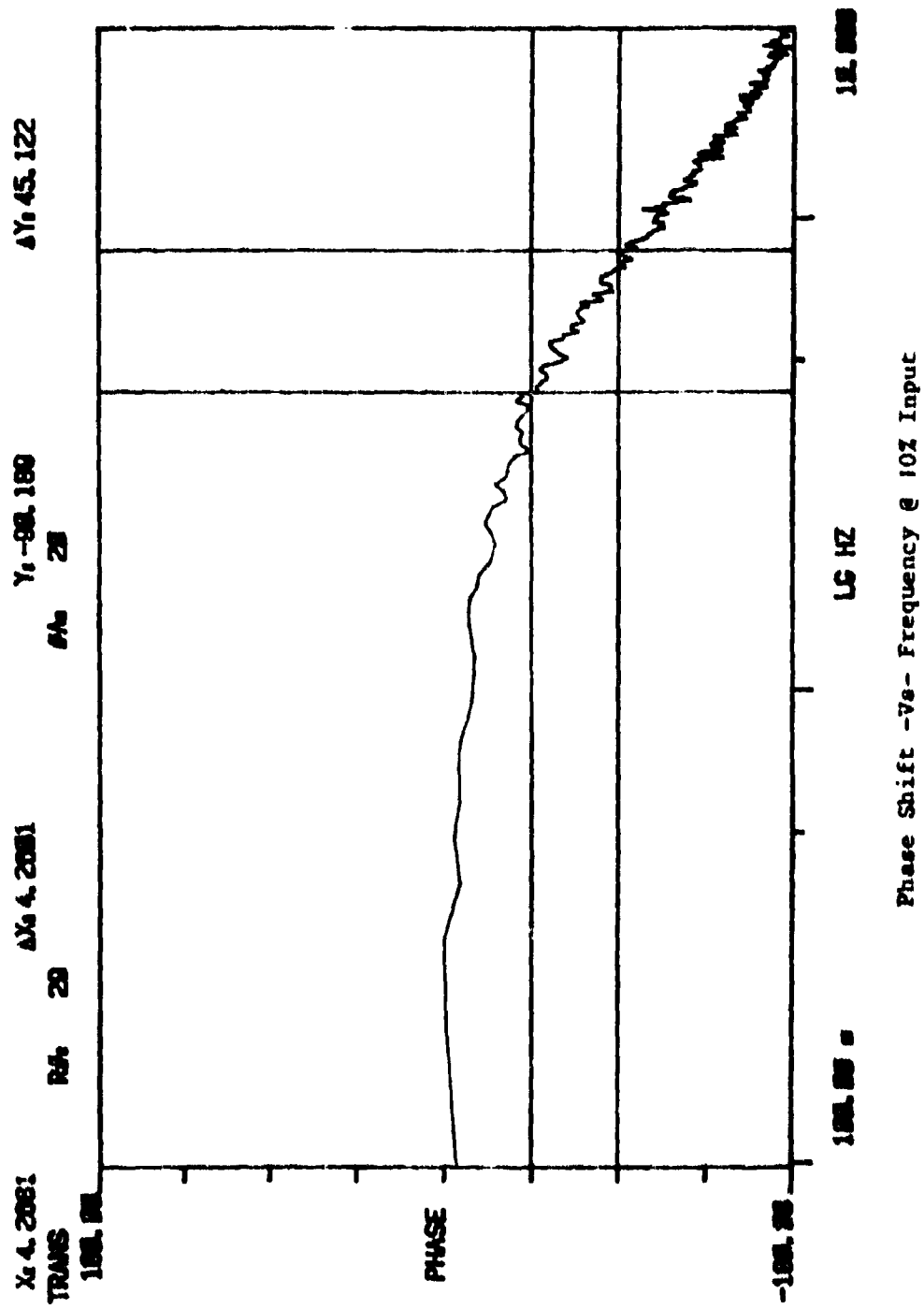


Figure IV-22. Leading-edge actuator - position 2.

Table IV-5. Frequency response - 3-percent input.

Motion Point	- 3 dB Frequency	- 90° Frequency
Position 1	9.14	8.65
Position 2	9.27	8.52
X ₅	11.15	10.06
X ₆	10.77	10.06

Note that the frequency response with the 10-percent input is not substantially reduced from the smaller input signal of 3 percent of maximum command and the actuator response is well above the 20 radian per second (gain bandwidth) minimum design value (given by William W. Gilbert of General Dynamics in paper AIAA 80-1886R). The slightly extended frequency response of points X₅ and X₆ indicate that there may be a well-damped resonance at 10 Hz. The unloaded response of the leading-edge shows that the mechanization can easily meet and or exceed the desired response for the control surface under low load conditions.

Linearity

Figures IV-23 through IV-26 show the linearity of the linear actuator and the two surface motion points. As should occur, the linearity plots of Position 1 and Position 2 (Figures IV-23 and IV-24) agree with each other and show little nonlinearity and hysteresis. Positions X₅ and X₆ show the combined nonlinearity effect of the drive linkage and the motion of the position transducers (the ends of which move through an arc as the surface deflects). There is a slight increase in the hysteresis at positions X₅ and X₆ compared to the linear actuator motion. Note also that the Position X₅ and X₆ includes the hysteresis and nonlinearity of the linear actuator in their motion.

Hysteresis

Figures IV-27 through IV-30 are representative of the data recorded to determine the hysteresis of the leading edge. Figures IV-27 and IV-28 show the hysteresis of the linear actuator at 10- and 1-percent inputs as measured by the Position 1 output. Figures IV-29 and IV-30 show the hysteresis characteristic of Position X₅ at 10- and 1-percent command inputs. Table IV-6 lists the hysteresis for the leading edge with a 10-percent input command. Notice that the surface positions X₅ and X₆ (which include the hysteresis of the actuator) exhibit 6.27 times the hysteresis of the actuator by itself. Table IV-7 lists the hysteresis for the leading edge with a 1 percent command input. The

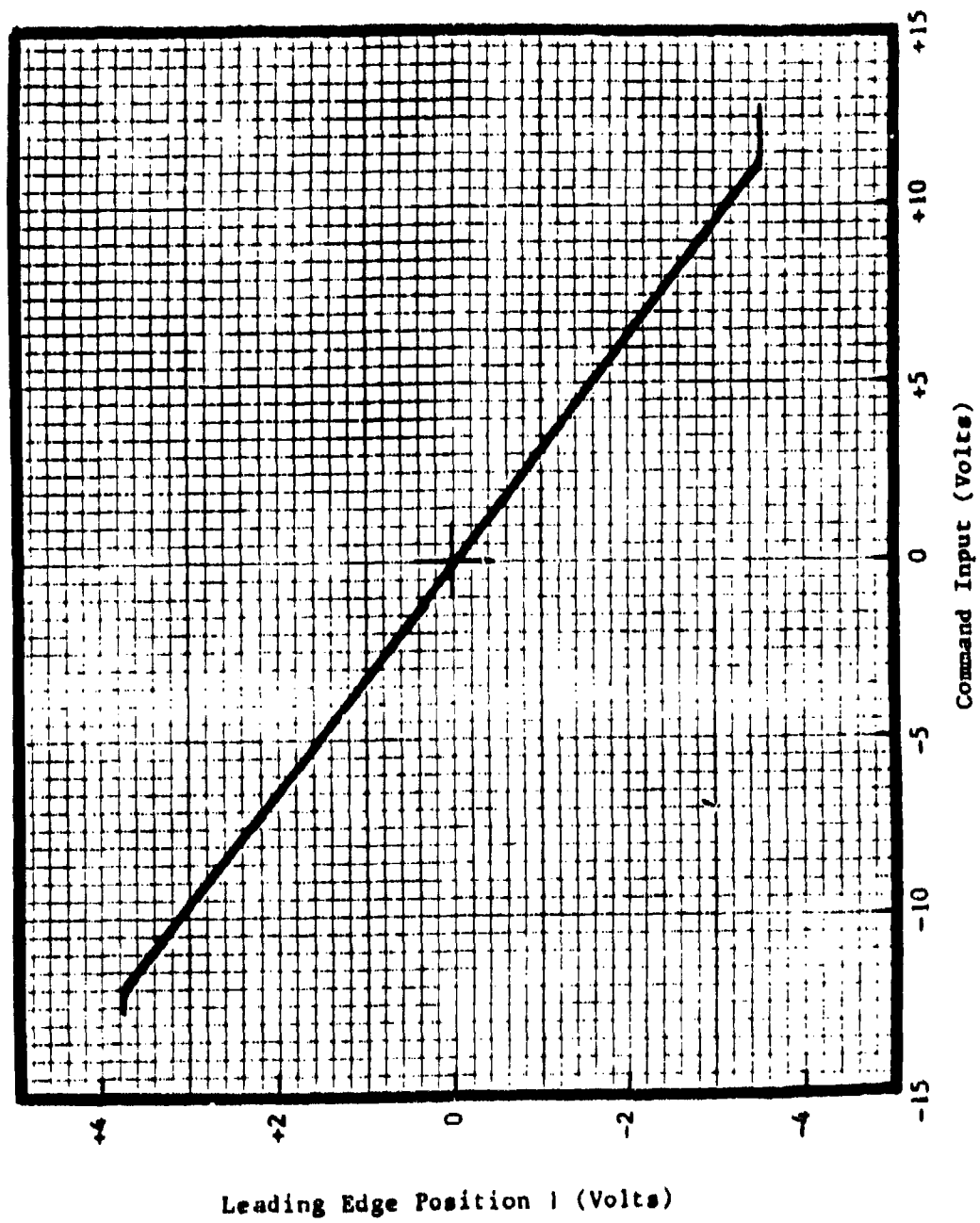


Figure IV-23. Linearity - motion point P_1 .

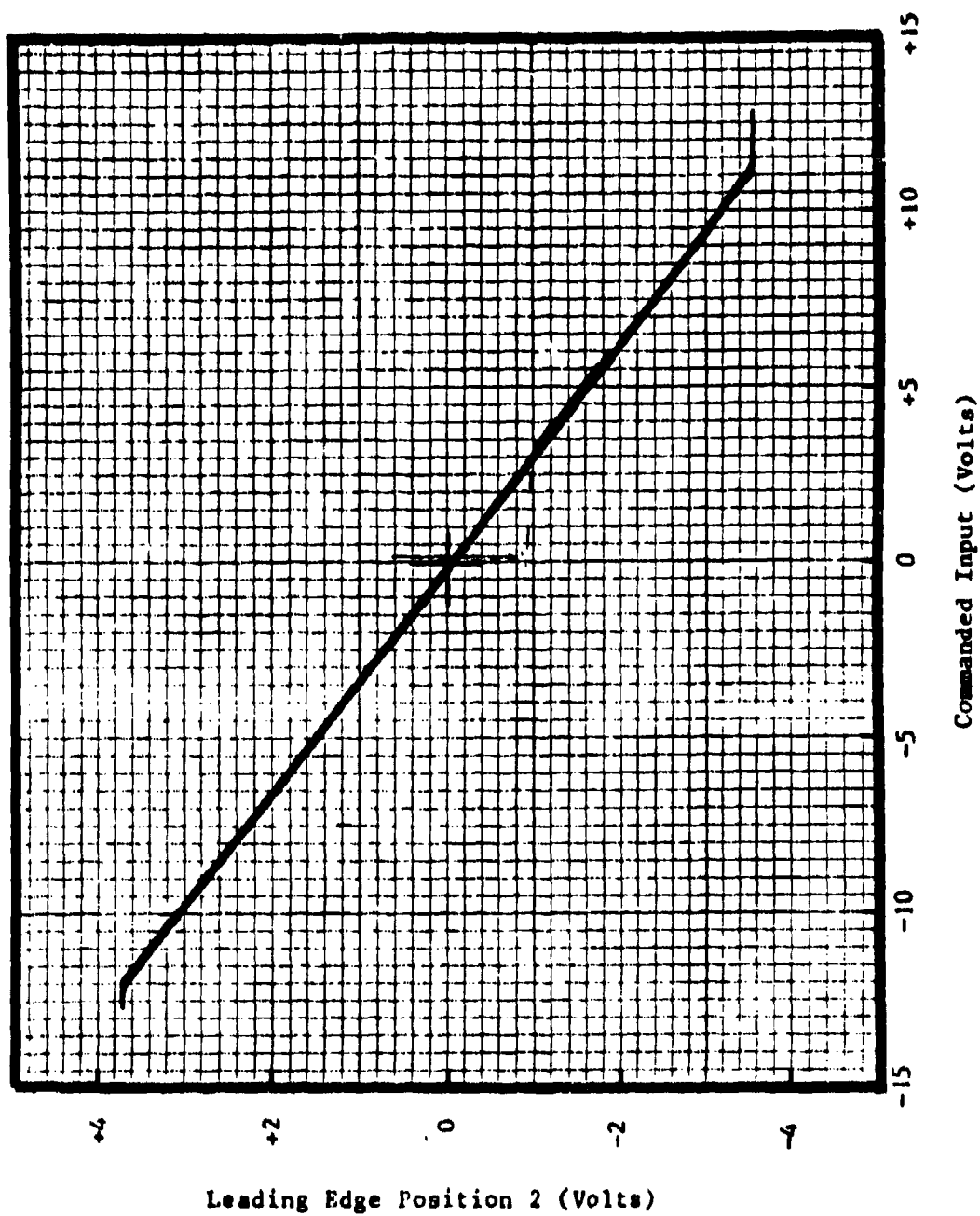


Figure IV-24. Linearity - motion point P_2 .

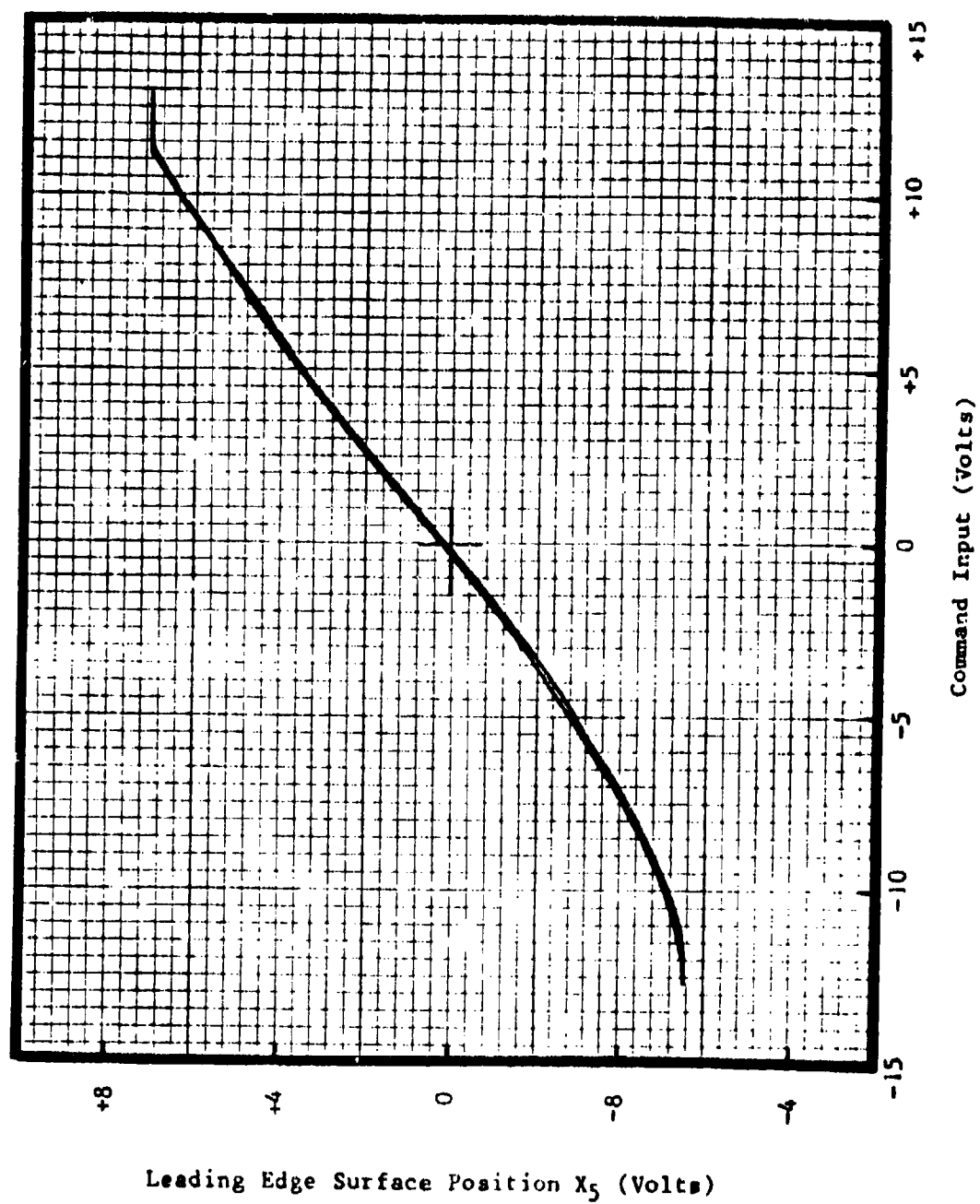


Figure IV-25. Linearity - motion point X_5 .

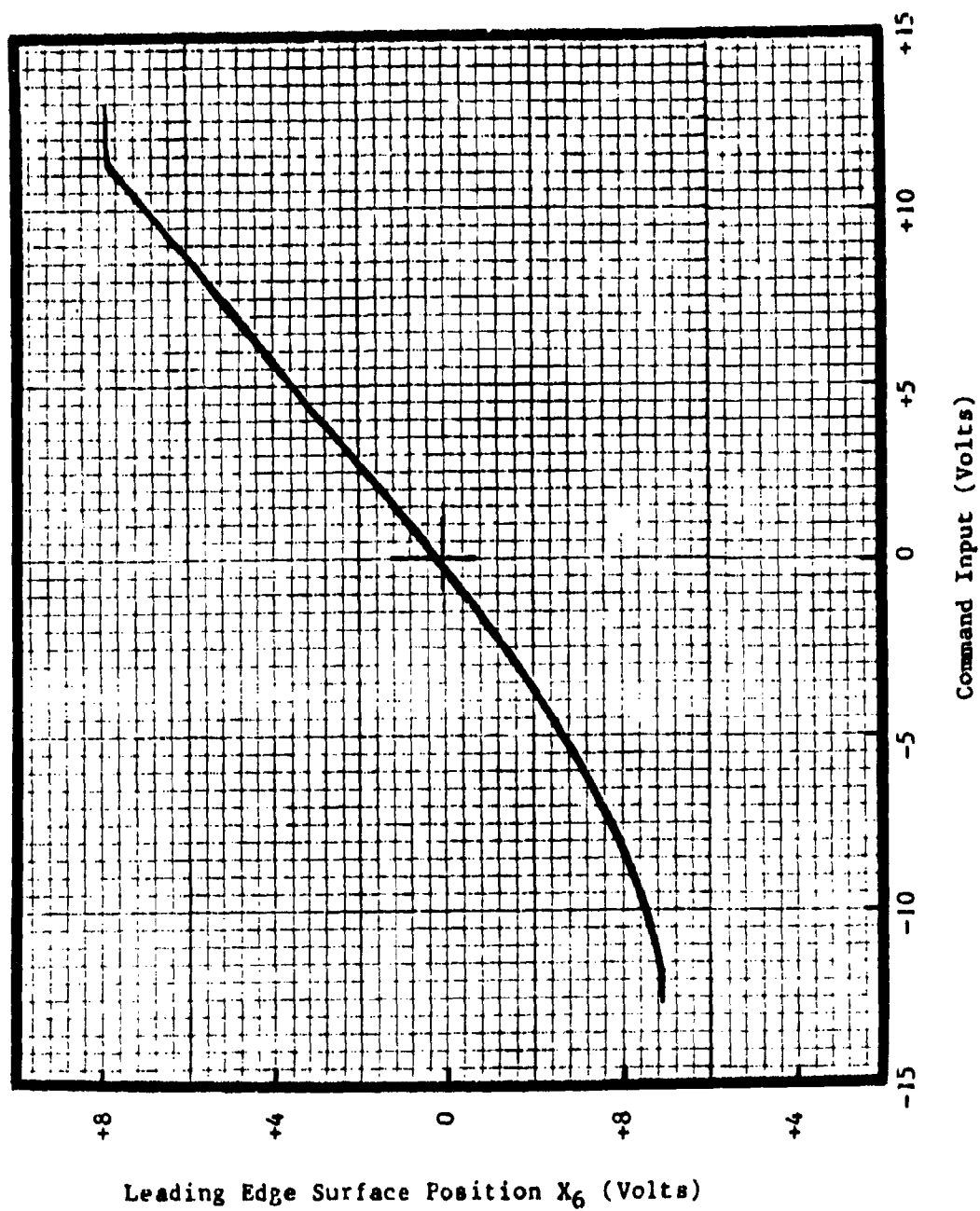


Figure IV-26. Linearity - motion point X_6 .

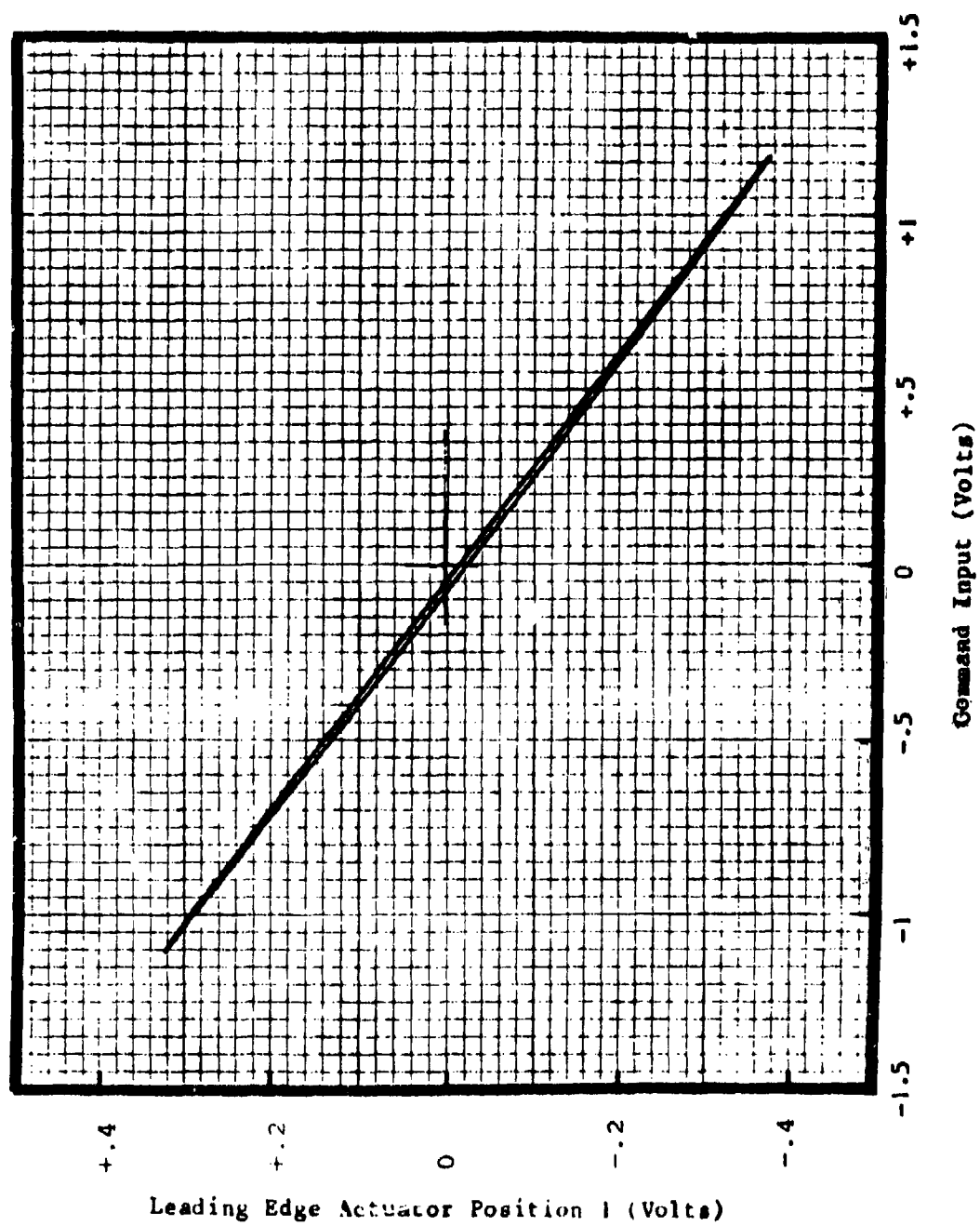


Figure IV-27. Hysteresis at 10-percent input - motion point P_1 .

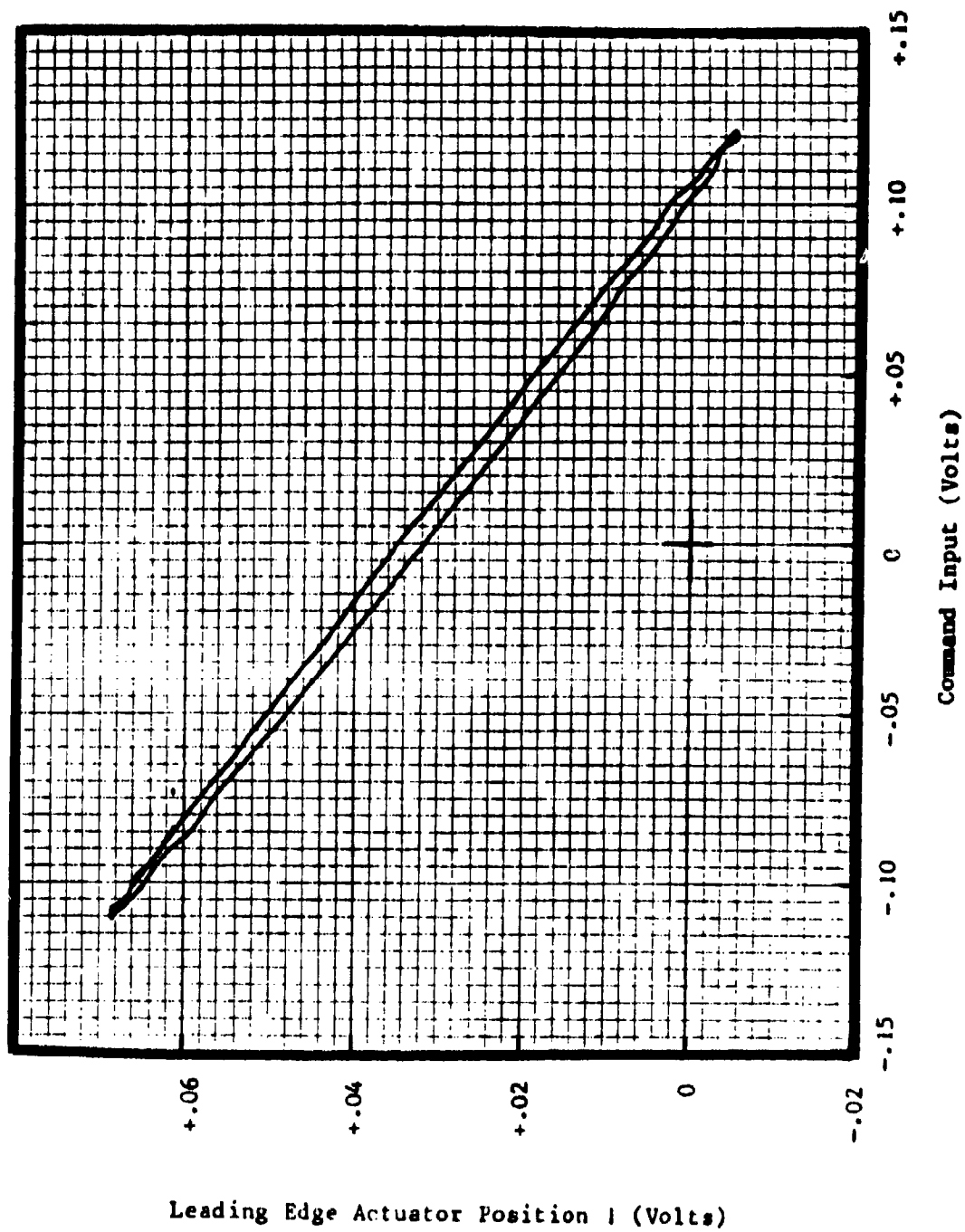


Figure IV-28. Hysteresis at 1-percent input - motion point P_1 .

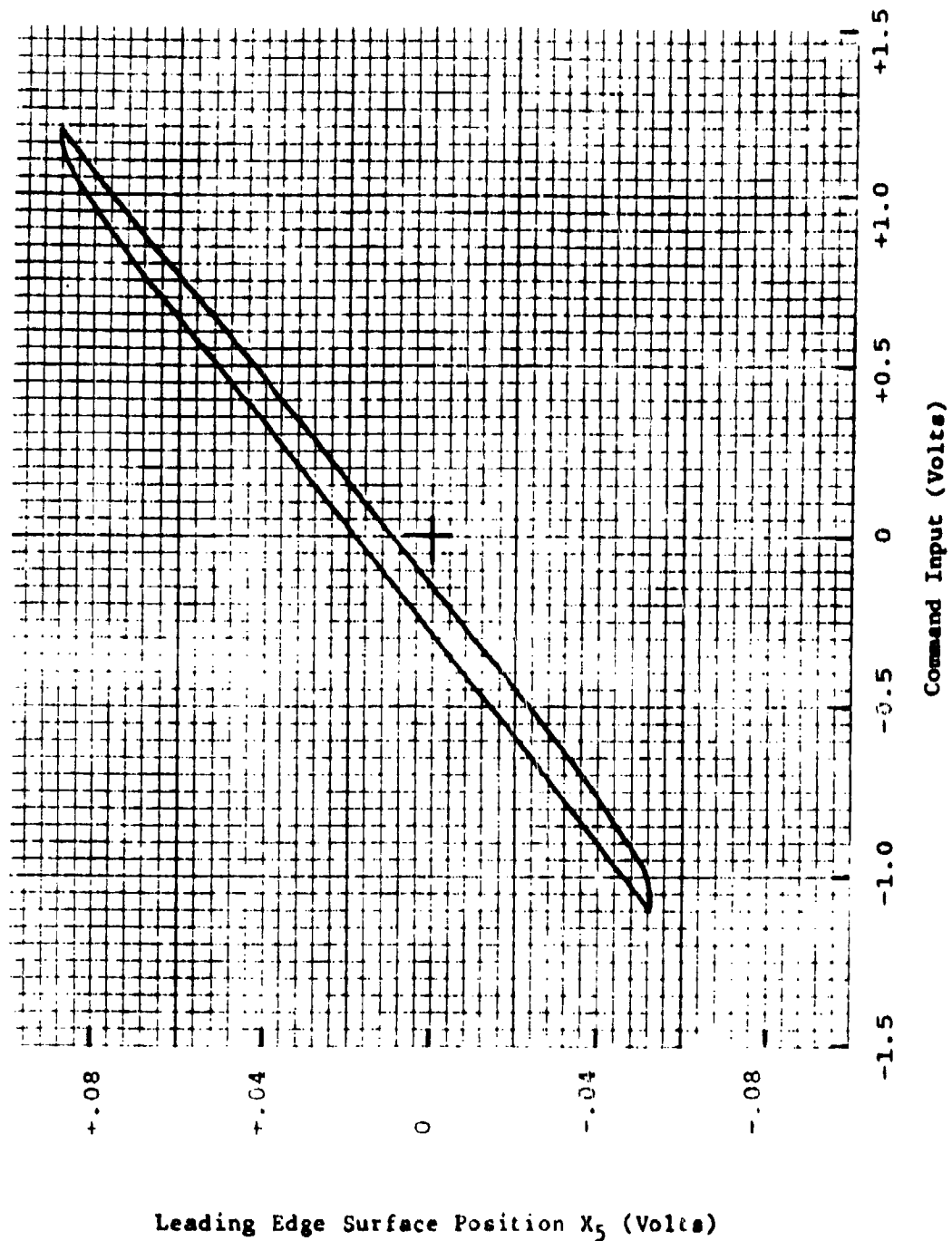


Figure IV-29. Hysteresis at 10-percent input - motion point X_5 .

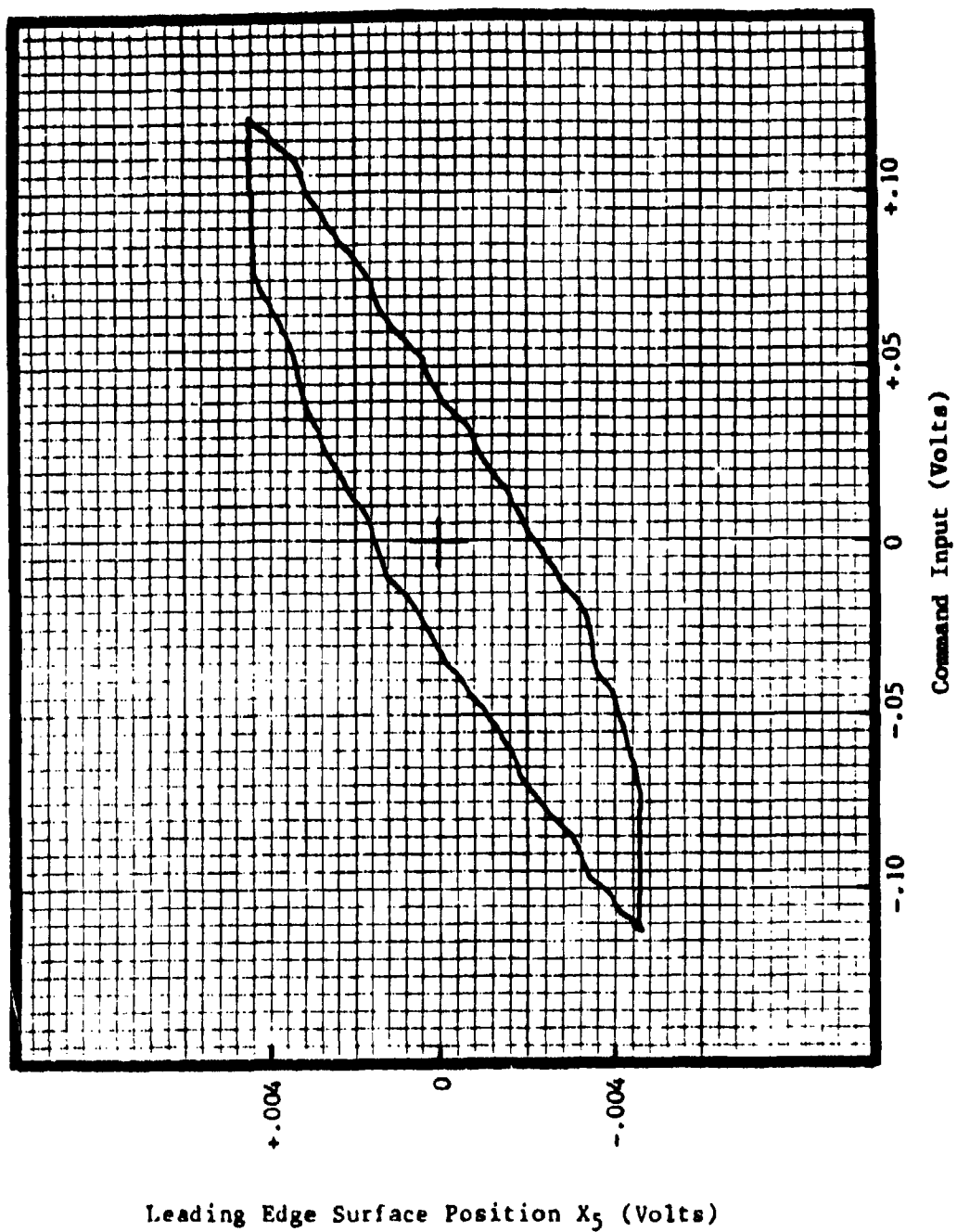


Figure IV-30. Hysteresis at 1-percent input - motion point X_5 .

hysteresis as a percent of the full-scale command has decreased compare to the 10-percent input. This indicates that the hysteresis is amplitude dependent. Note that in both tables, the hysteresis for motions at X_5 and X_6 is the same, indicating that the additional hysteresis caused by the coupling linkage is due to the linkage between the actuator and X_6 , not between positions X_5 and X_6 .

Table IV-6. Hysteresis for a 10-percent input.

Motion Point	% of Full Command	% of 10% Command
Position 1	0.102	1.02
Position 2	0.102	1.02
X_5	0.64	6.4
X_6	0.64	6.4

Table IV-7. Hysteresis for a 1-percent input.

Motion Point	% of Full Command	% of 1% Command
Position 1	.042	4.2
Position 2	.042	4.2
X_5	0.30	30.0
X_6	0.30	30.0

Saturation Velocity

Figures IV-31 and IV-32 show representative data recorded to establish the unloaded saturation velocity for the leading edge. Note that *surface down* corresponds to retraction of the linear actuator. Table IV-8 lists the saturated velocity as measured at each motion point.

Test Item - General Dynamics
Mission Adaptive Wing

Date
Prepared: 6/17/85

Test - Saturation Velocity
Surface - Leading Edge
Load - Zero Load

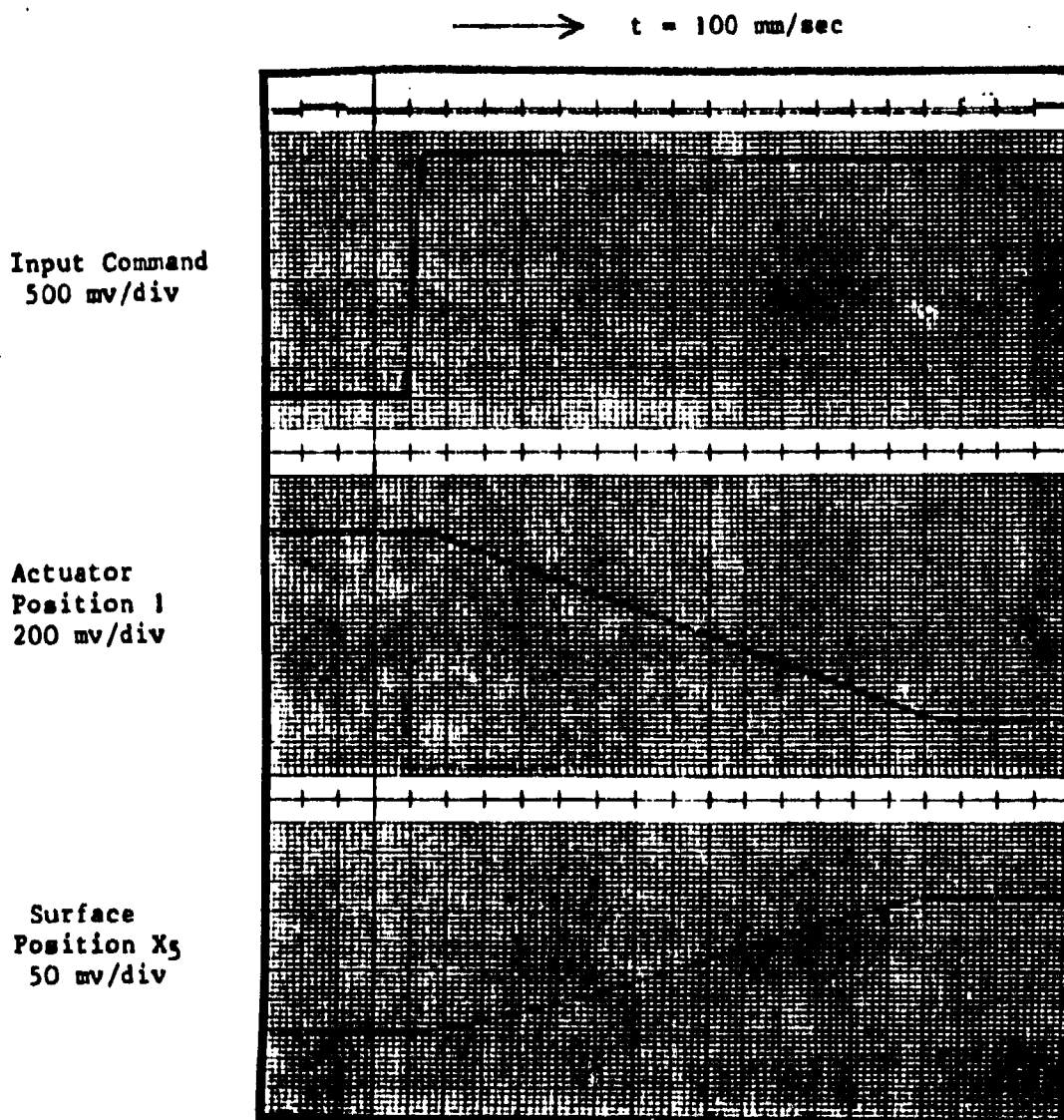


Figure IV-31. Surface up - saturation velocity.

Test Item - General Dynamics
Mission Adaptive Wing

Date
Prepared: 6/17/85

Test - Saturation Velocity
Surface - Leading Edge
Load - Zero Load

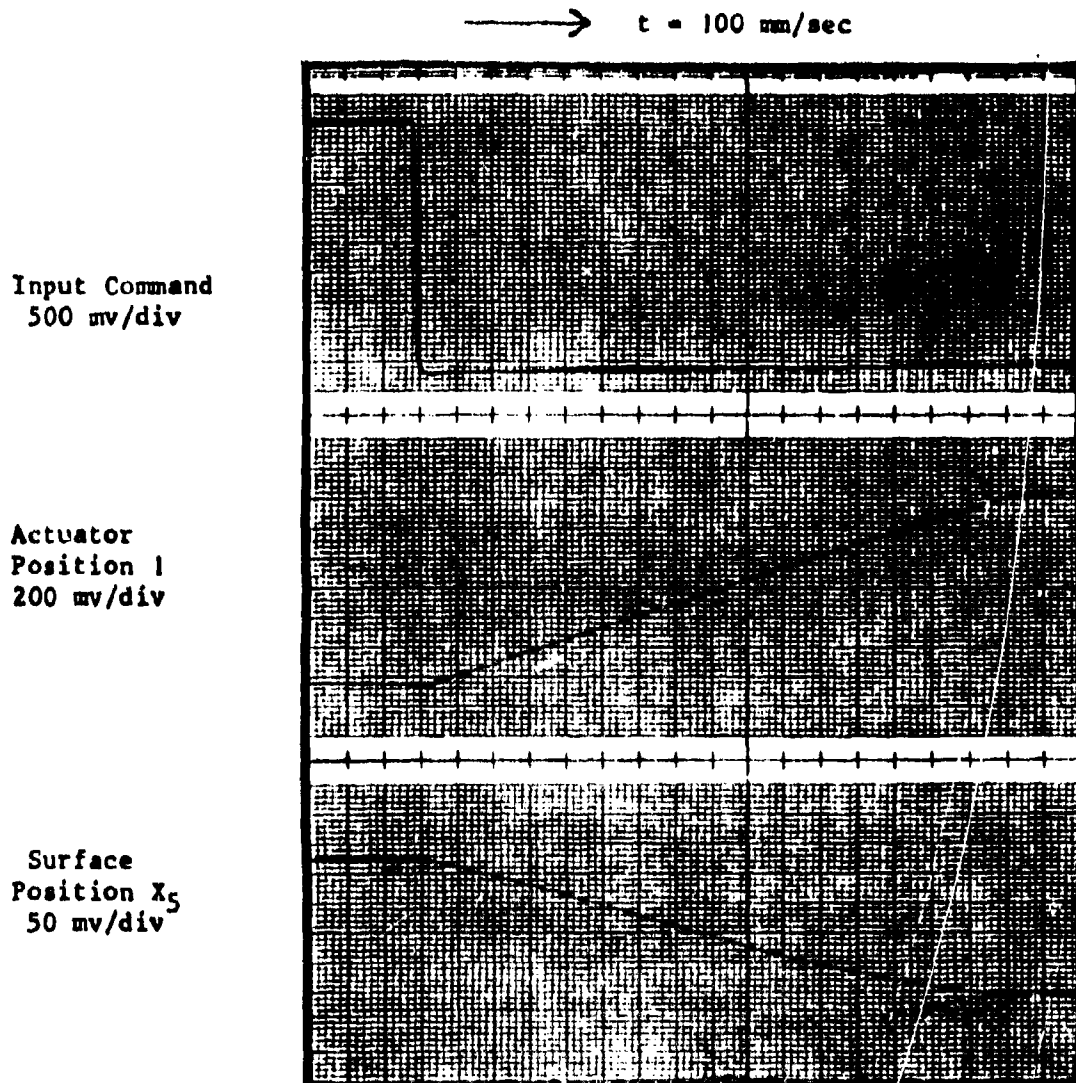


Figure IV-32. Surface down saturation velocity.

Table IV-8. Saturation rate.

Motion Point	Linear Actuator (in/sec)		Surface (deg/sec)	
	Extend	Retract	Up	Down
Position 1	2.02	1.64	----	----
Position 2	2.02	1.64	----	----
Surface X ₅	----	----	41.5	34.0
Surface X ₆	----	----	41.0	33.9

Note that the surface rate (maximum) is sufficient to achieve full deflection (-5° to +30°) in nominally 1 second.

Transient Response

Figures IV-33 and IV-34 show the large amplitude step response of the leading-edge control system. Note that the input voltage is a 4.6-volt step, creating an output change of 20 percent of the maximum output. There is a short time delay (associated with the response of the linear actuator) before the actuator and leading-edge surface move. Note, as shown in the figures, the step input is large enough to cause rate saturation of the linear actuator. Note also that there is no overshoot or ringing of the motion points. Table IV-9 lists the time response for the motion points of the leading edge for both the *surface up* and *surface down* motions.

Table IV-9. Step response.

Surface Up			
Motion Point	Time to Start Motion (sec)	Time to 63% of Travel (sec)	Time to 100% of Travel (sec)
Position 1	.015	0.100	0.170
Position 2	.015	0.100	0.170
Surface X ₅	.015	.095	0.172
Surface X ₆	.015	.095	0.175

Test Item - General Dynamics
Mission Adaptive Wing

Date
Prepared: 6/17/85

Test - Transient Response
Surface - Leading Edge
Load - Zero Load

Input Command
100 mv/div

Actuator
Position 1
50 mv/div

Surface
Position X_5
10 mv/div

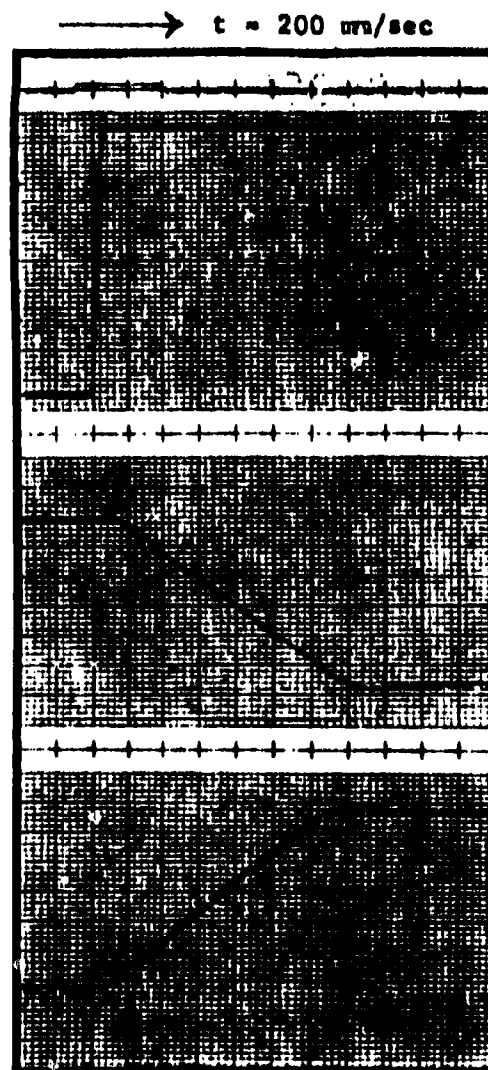


Figure IV-33. Surface *up* - step response.

Test Item - General Dynamics
Mission Adaptive Wing

Date
Prepared: 6/17/85

Test - Transient Response
Surface - Leading Edge
Load - Zero Load

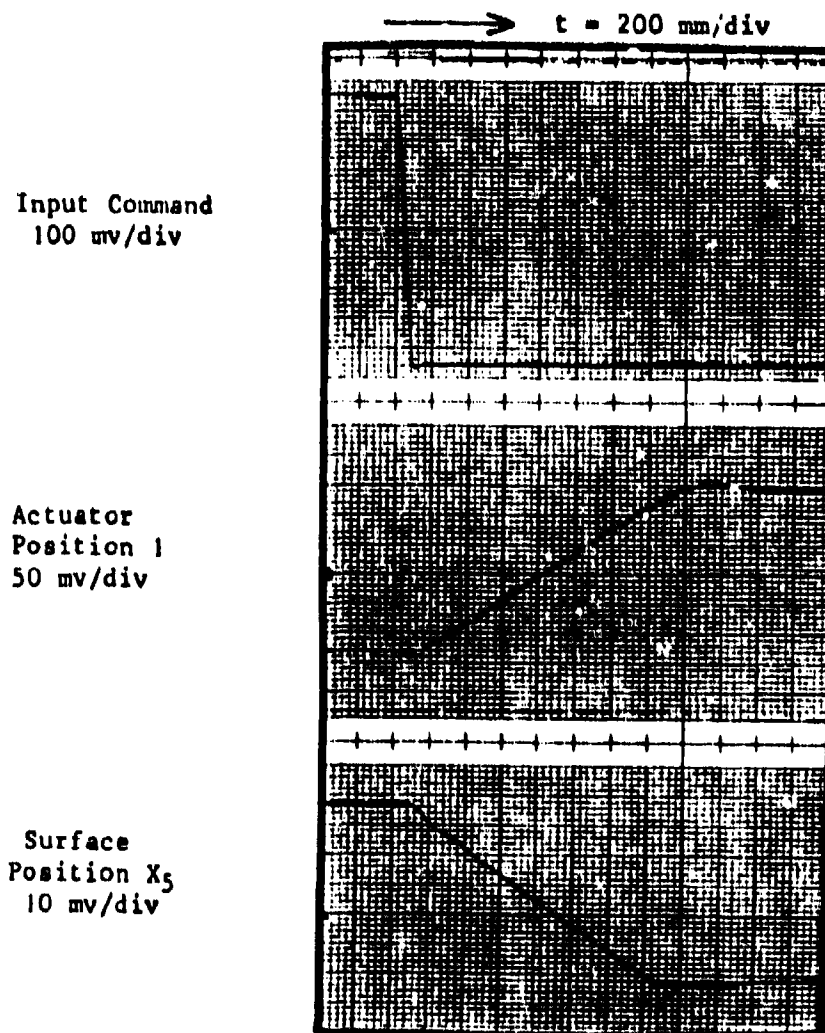


Figure IV-34. Surface *down* - step response.

Table IV-9. Step response (continued).

Motion Point	Surface Down		
	Time to Start Motion (sec)	Time to 63% of Travel (sec)	Time to 100% of Travel (sec)
Position 1	0.017	0.115	0.190
Position 2	0.017	0.115	0.190
Surface X ₅	0.017	0.115	0.190
Surface X ₆	0.017	0.115	0.185

The time response shown in the tables indicates a slight difference between the direction of motions. This is consistent with the requirement for the force to bend the fiberglass top skin, thus aiding the actuator in one direction of motion and opposing in the other direction of motion.

Unloaded Trailing-Edge Test Results

General

The motion of the trailing edge was instrumented at four points on the surface (X_1 , X_2 , X_3 and X_4 as shown previously on Figures IV-9 and IV-10). These points on the trailing-edge surface and rotary potentiometers which measured the output shaft position of the differential gear boxes were used to document the performance of the trailing-edge mechanization.

Tables IV-10 and IV-11 list the calibration factors for the instrumentation potentiometers used with the trailing edge. Table IV-10 lists the calibration factors for the surface potentiometers. Both the linear output/inch of deflection and the output/degree of local angular motion of the surface at each mounting point is listed in the table. Table IV-11 lists the calibration factors for the left and right rotary potentiometers in terms of the surface position motion. The V/inch and V/degree indicate the output change of the appropriate rotary potentiometer for a corresponding position change of the trailing-edge surface at positions X_1 , X_2 , X_3 and X_4 .

Table IV-10. Calibration factors - trailing-edge transducers.

Motion Point	V/in	V/Deg
X_1	1.00	0.275
X_2	1.00	0.276
X_3	1.00	0.183
X_4	1.00	0.173

Table IV-11. Calibration factors - rotary potentiometers.

Motion Point	<u>Left Rotary Potentiometer</u>		<u>Right Rotary Potentiometer</u>	
	V/in	V/deg	V/in	V/deg
X_1	0.665	0.183	----	----
X_2	----	----	0.672	0.186
X_3	3.166	0.58	----	----
X_4	----	----	2.974	0.516

Linearity data was also obtained on the secondary actuator (F-111 damper actuators) which commanded the flow control valves for the hydraulic motors used with the rotary gearboxes. Figures IV-35 and IV-36 show the output/input linearity for these actuators. The output motion of the actuator was measured with the position transducers incorporated in the secondary actuators with outputs provided in the control electronics for the system. For this measurement, the flow to the hydraulic motors was disabled so that the input to the system drove only the secondary actuators. The linearity data both shows the input voltage for maximum actuator stroke (± 2.3 volts). This is the input for maximum surface rate, since the actuators drive (through a motion reduction linkage) the flow control valves for the trailing-edge hydraulic motors. Note that both actuators exhibit good linearity and some hysteresis. The hysteresis for the right actuator is 1.0 percent of maximum actuator command while the left actuator is higher at 2.2 percent of maximum actuator input command.

Static Threshold

Figures IV-37 and IV-38 show data taken during static threshold test. Note that as shown in Figure IV-37, both the left and right rotary potentiometers sense motion of their respective gear boxes at the same input level. Figure IV-38 shows the first recorded motion of the surface at X_2 , the right center of the trailing edge. Figure IV-39 shows the motion at X_4 , the right tip of the surface. The difference between the static thresholds of these two points is due to lost motion in variable-geometry truss drive between these two points. Figure IV-40 shows the first recorded motion of the surface at X_1 , the left center motion point. Figure IV-41 show the motion at X_3 , the left tip. Note that the static threshold for the left arm is greater than the right arm. This is due to the free-play difference between the two trusses since as noted above, both differential gear boxes operated simultaneously during this test.

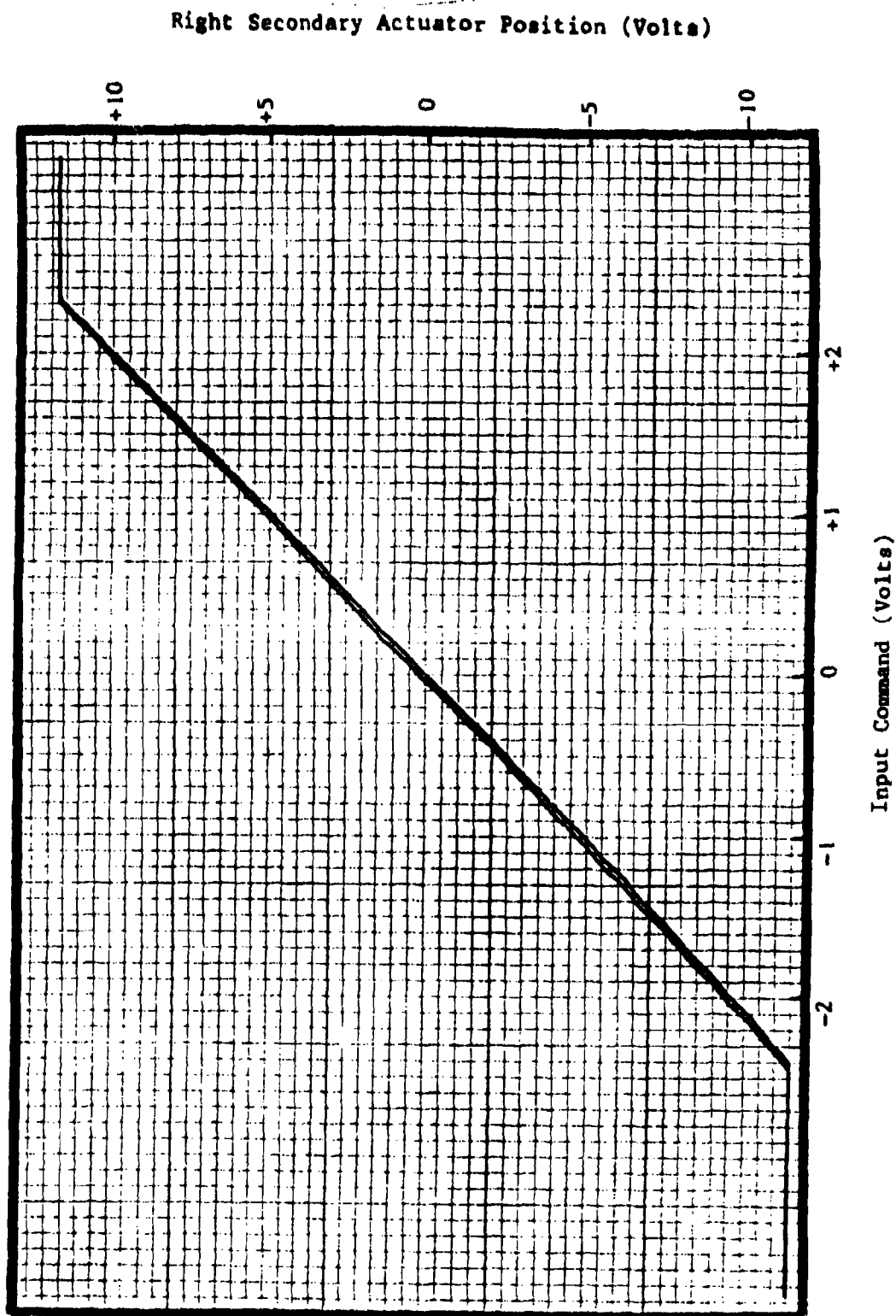


Figure IV-35. Linearity of right secondary actuator.

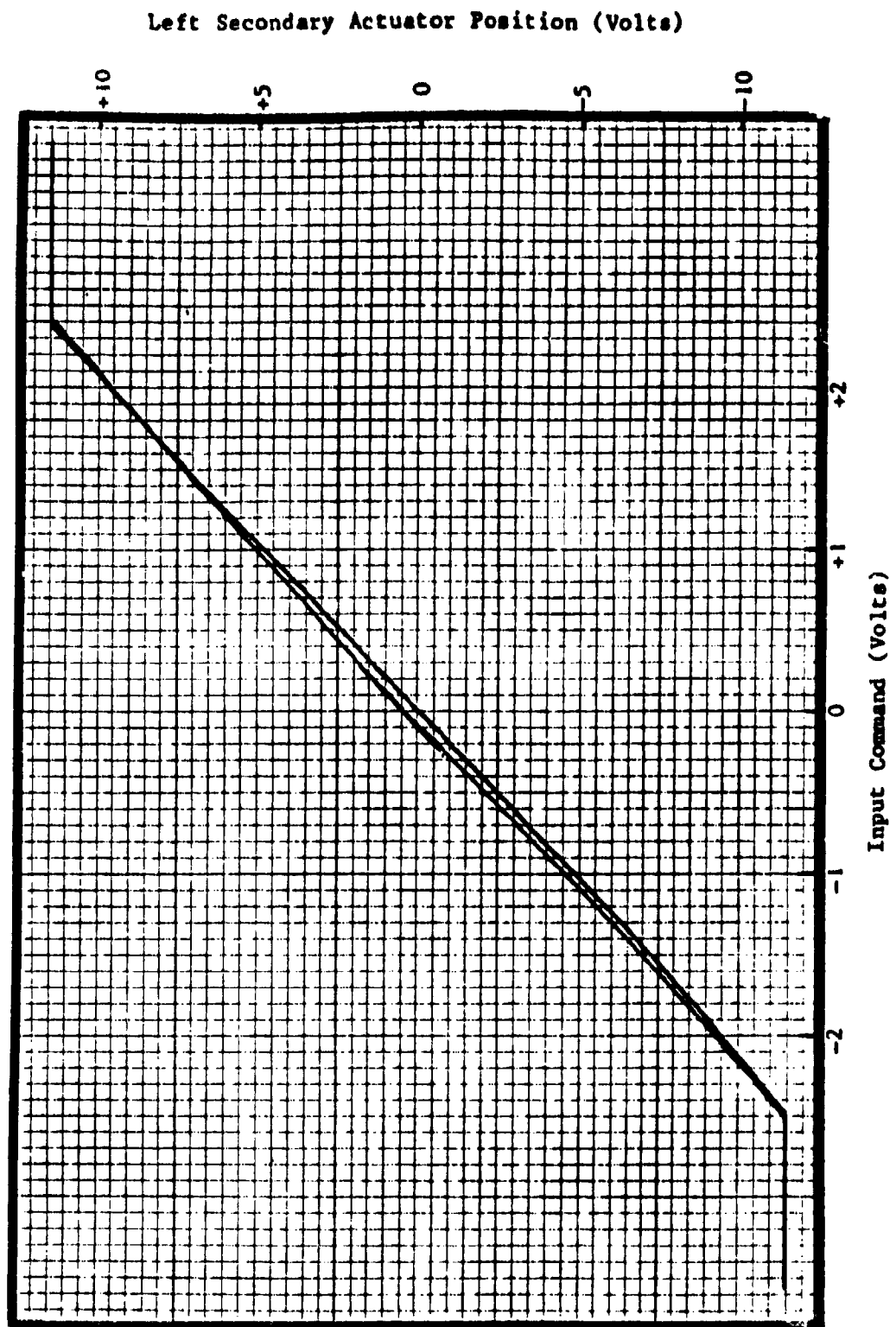


Figure IV-36. Linearity of left secondary actuator.

Test Item - General Dynamics
Mission Adaptive Wing

Date
Prepared: 7/22/85

Test - Static Threshold
Surface - Trailing Edge
Load - Zero Load

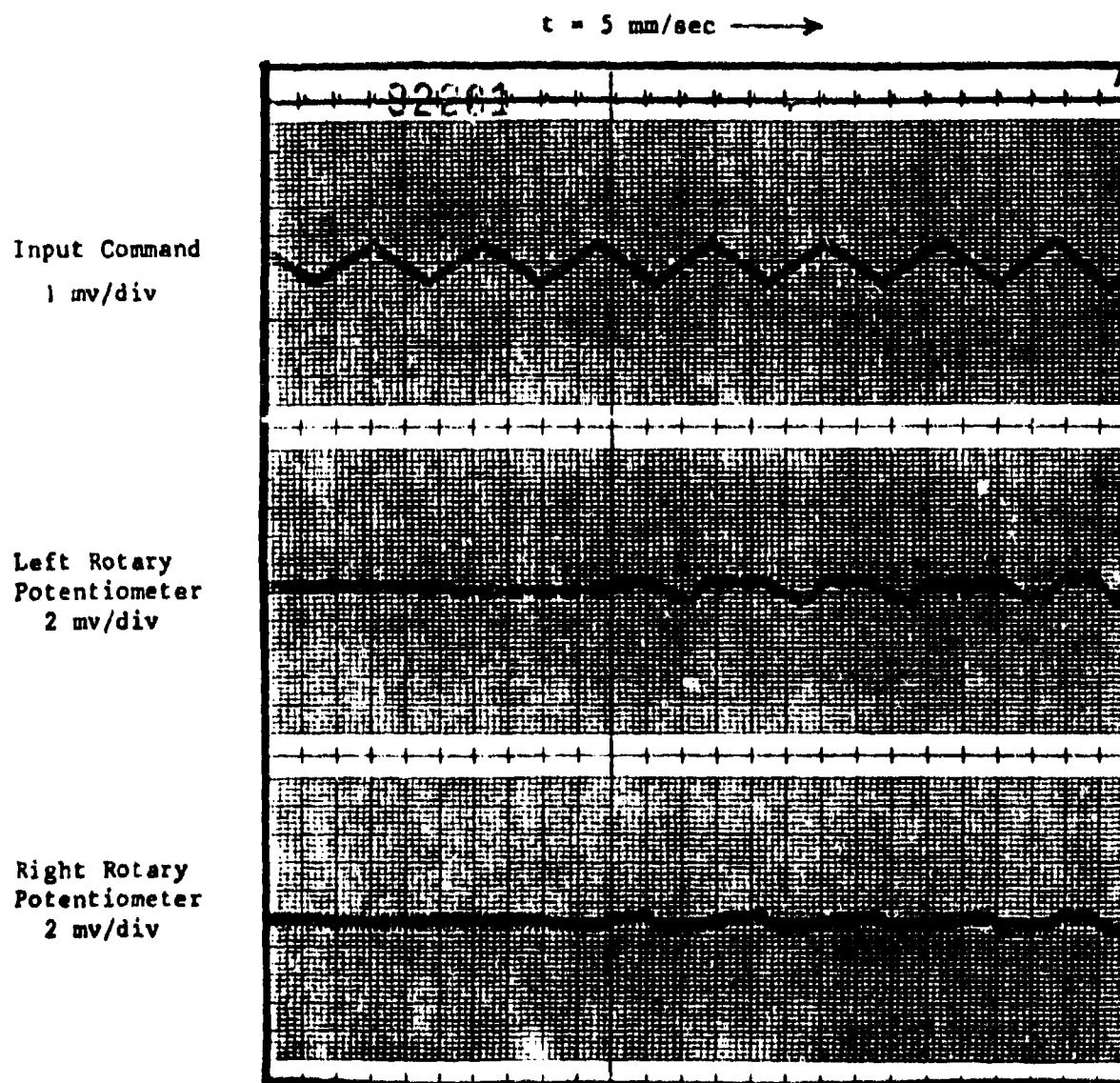


Figure IV-37. Static threshold - trailing edge - rotary motion.

Test Item - General Dynamics
Mission Adaptive Wing

Date
Prepared: 7/23/85

Test - Static Threshold
Surface - Trailing Edge
Load - Zero Load

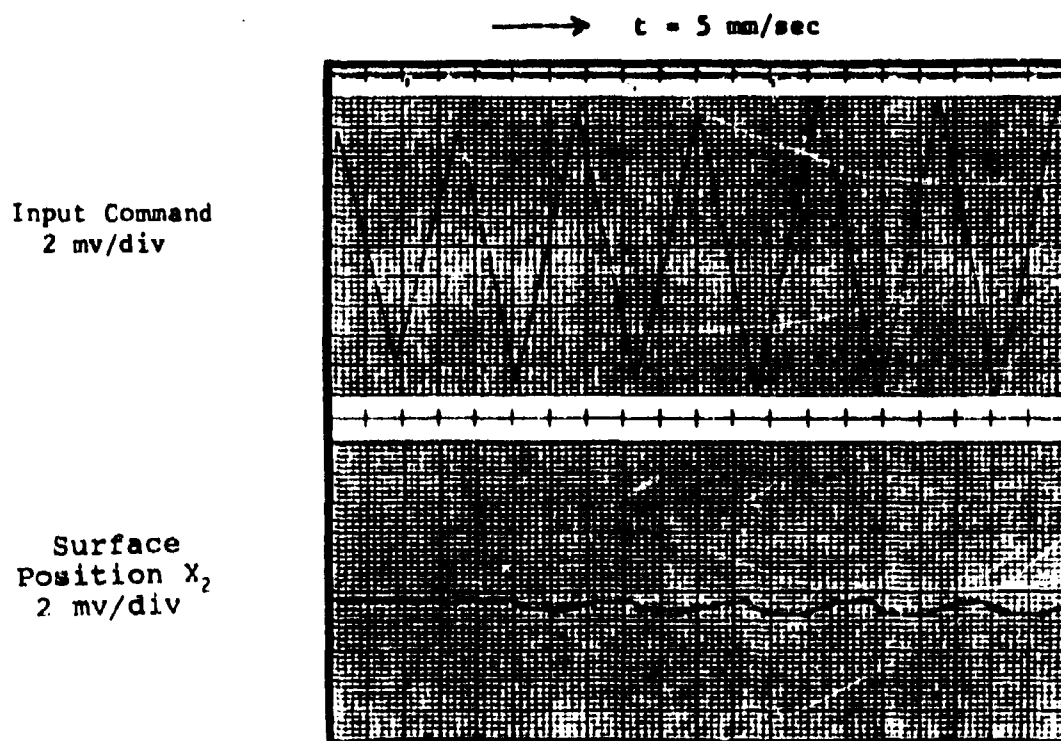


Figure IV-38. Static threshold - trailing edge - X_2 motion.

Test Item - General Dynamics
Mission Adaptive Wing

Date
Prepared: 7/23/85

Test - Static Threshold
Surface - Trailing Edge
Load - Zero Load

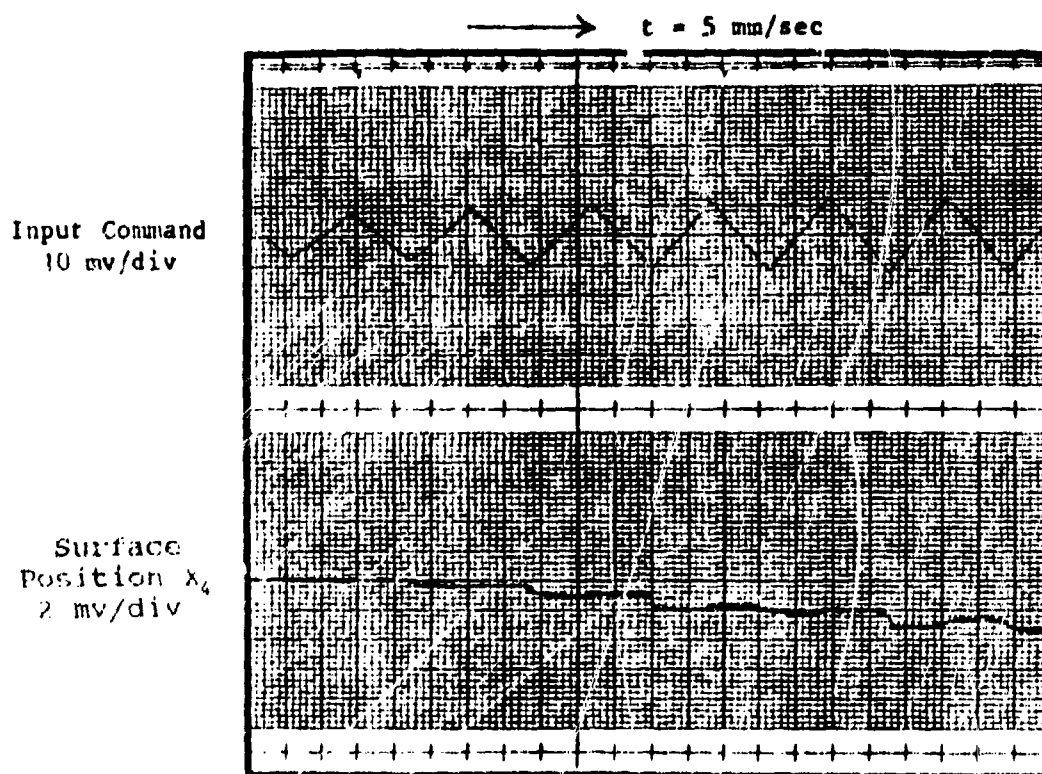


Figure IV-39. Static threshold - trailing edge - x_4 motion.

Test Item - General Dynamics
Mission Adaptive Wing

Date
Prepared: 7/23/85

Test - Static Threshold
Surface - Trailing Edge
Load - Zero Load

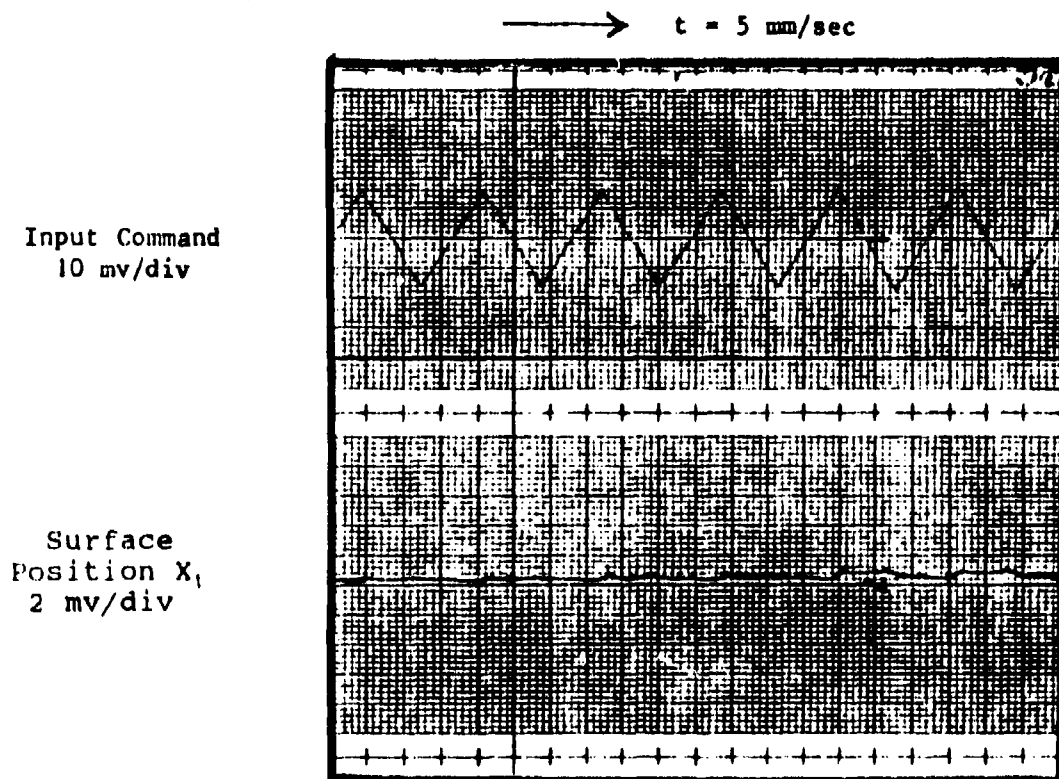


Figure IV-40. Static threshold - trailing edge - X_1 motion.

Test Item - General Dynamics
Mission Adaptive Wing

Date
Prepared: 7/23/85

Test - Static Threshold
Surface - Trailing Edge
Load - Zero Load

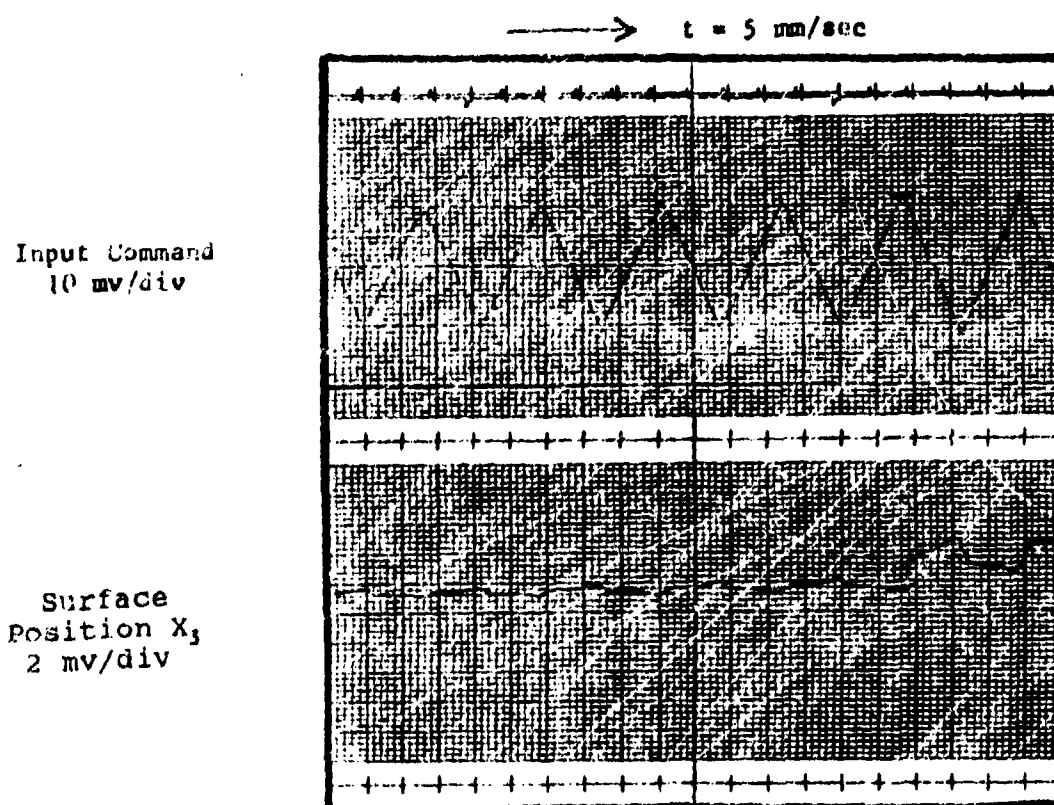


Figure IV-41. Static threshold - trailing edge - X_3 motion.

Table IV-12 summarizes the threshold of the motion points in terms of the maximum command input of ± 11.7 volts. The threshold for the left variable-geometry truss (measurement points X_1, X_3) is greater than the right (measurement points X_2, X_4) by nominally 100 percent. This is probably due to the wear in the actuating mechanism (since both the left and right gear boxes move at the same input level).

Note that for the trailing edge, a command voltage of ± 5.61 volts produced full surface deflection. This voltage was used to calculate the *percentage of maximum position command* for the performance measurements. For the description of the test results in terms of the command to produce maximum surface rate, the maximum command voltage of ± 2.35 volts for the series actuator was used.

Table IV-12. Static threshold - unloaded trailing edge.

Motion Point	Threshold (peak volts)	% Max Rate Command	% Max Position Command
Left Rotary Potentiometer	0.004	0.170	0.071
X_1	0.090	3.45	1.604
X_3	0.120	5.11	2.138
Right Rotary Potentiometer	0.004	0.170	0.071
X_2	0.038	1.62	0.677
X_4	0.045	1.92	0.802

Dynamic Threshold

Figures IV-42 through IV-45 show the data recorded for dynamic threshold tests on the unloaded trailing edge. The test used an input frequency of nominally 1.0 Hz for exciting the surface. Note that the rotary potentiometer for the left arm requires slightly lower input to start moving than the right arm. However, the tip of the left truss is also the last point to show motion with an increasing input. Table IV-13 lists the dynamic thresholds of the motion points on the trailing edge with the motion points of each variable-geometry truss grouped together. The threshold values are listed both in terms of maximum command input and the input required to cause maximum position of the damping actuators used to drive the control valve for flow to the hydraulic motors. This input command corresponds to the maximum error voltage required for maximum surface rate.

Table IV-13. Dynamic threshold - unloaded trailing edge.

Motion Point	Threshold (pk volts)	% Max Rate Command	% Max Position Command
Left Rotary Potentiometer	0.006	0.268	0.106
X ₁	0.060	2.55	1.07
X ₃	0.090	3.82	1.60
Right Rotary Potentiometer	0.007	0.304	0.124
X ₂	0.055	2.34	0.980
X ₄	0.080	3.40	1.426

Linearity and Large Amplitude Hysteresis

Figure IV-46 through IV-48 show the linearity of motion as measured by the rotary potentiometers and the linear potentiometers attached to points X₁, X₂, X₃, and X₄. The input level used for the test was 90 percent of the maximum command level or ± 5.05 volts. Figures IV-46 and IV-47 show the linearity (and hysteresis) of the left truss while Figures IV-48 and IV-49 show the linearity and hysteresis of the right truss. Note that the output of the rotary potentiometers is very good while

Test Item - General Dynamics
Mission Adaptive Wing

Date
Prepared: 7/23/85

Test - Dynamic Threshold
Surface - Trailing Edge
Load - Zero Load

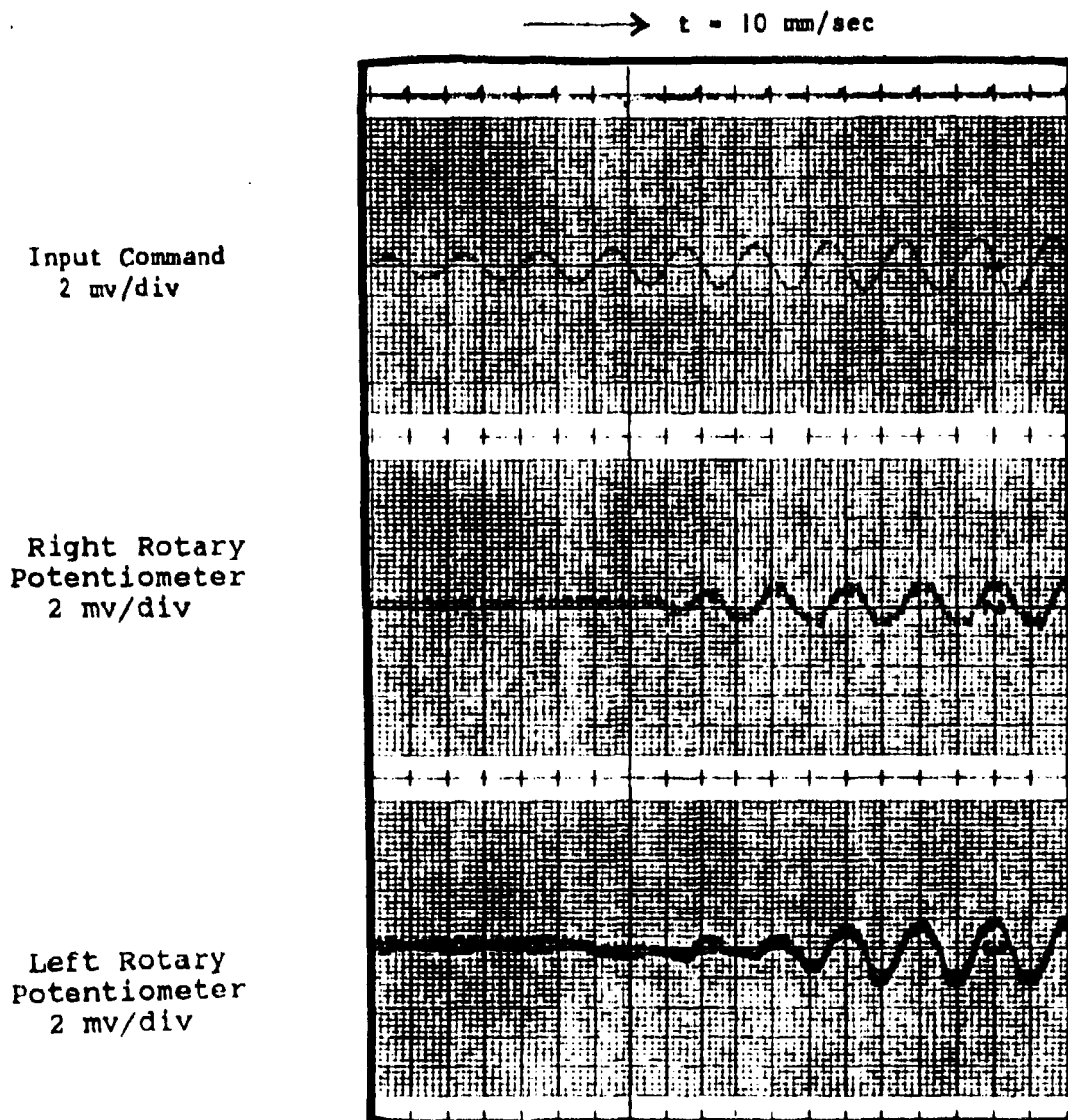


Figure IV-42. Dynamic threshold - trailing edge - rotary motion.

Test - Dynamic Threshold
Surface - Trailing Edge
Load - Zero Load

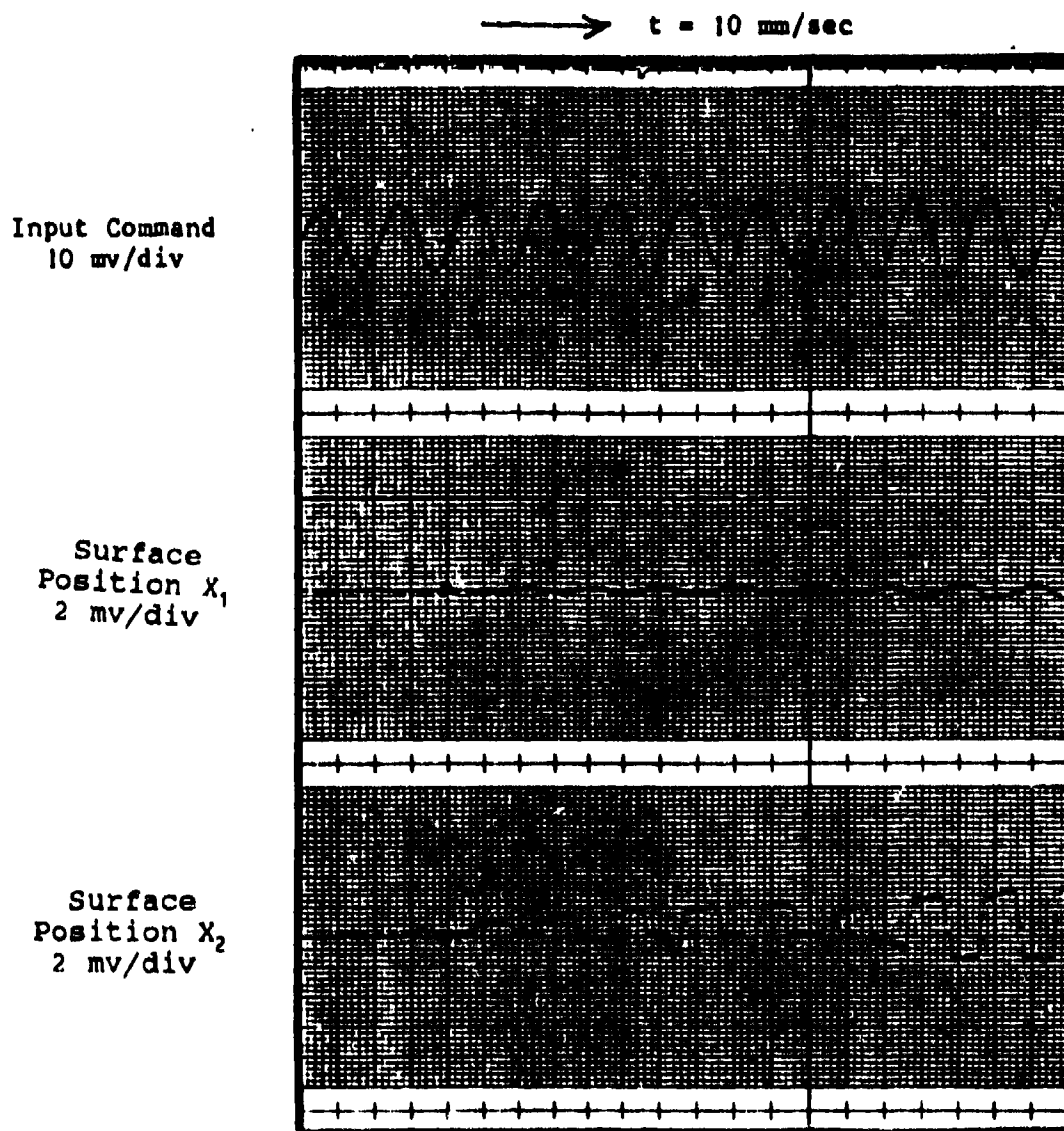


Figure IV-43. Dynamic threshold - trailing edge - X_1 , X_2 motion.

Test Item - General Dynamics
Mission Adaptive Wing

Date
Prepared: 7/29/85

Test - Dynamic Threshold
Surface - Trailing Edge
Load - Zero Load

Input Command
10 mv/div

Surface
Position X_4
2 mv/div

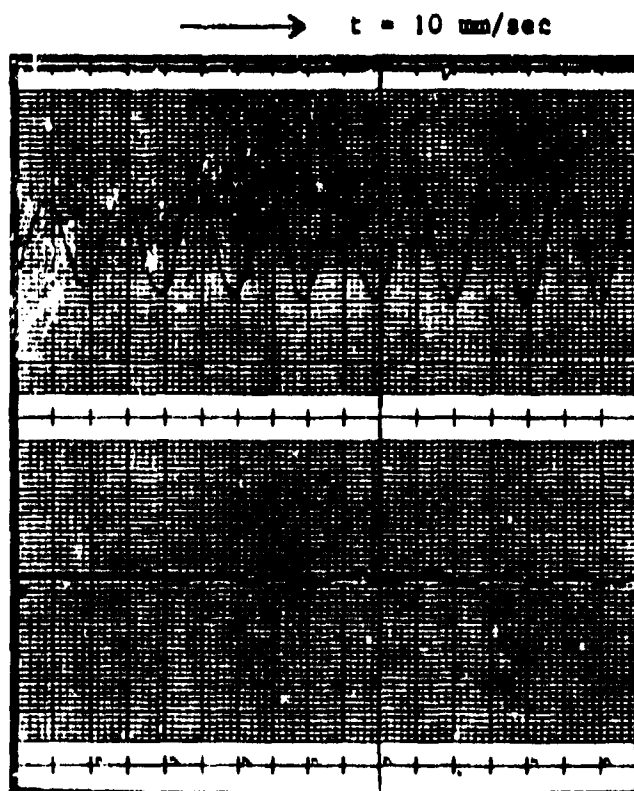


Figure IV-44. Dynamic threshold - trailing edge - X_4 motion.

Test Item - General Dynamics
Mission Adaptive Wing

Date
Prepared: 7/29/85

Test - Dynamic Threshold
Surface - Trailing Edge
Load - Zero Load

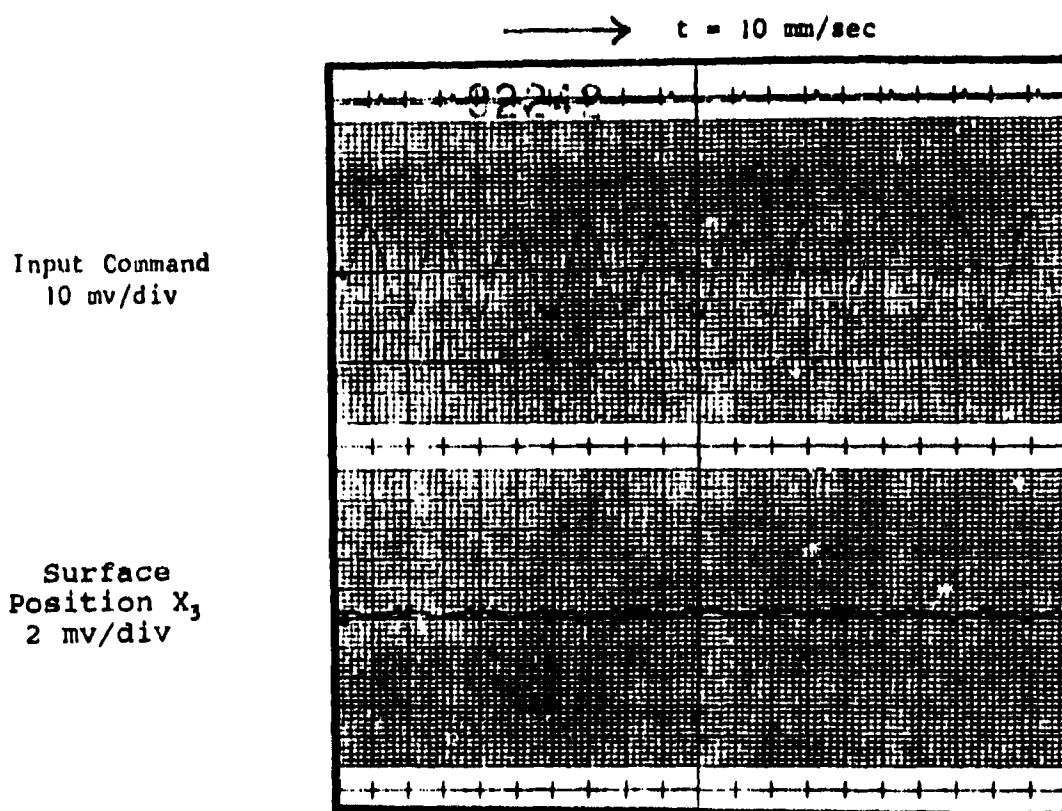


Figure IV-45. Dynamic threshold - trailing edge - X_3 motion.

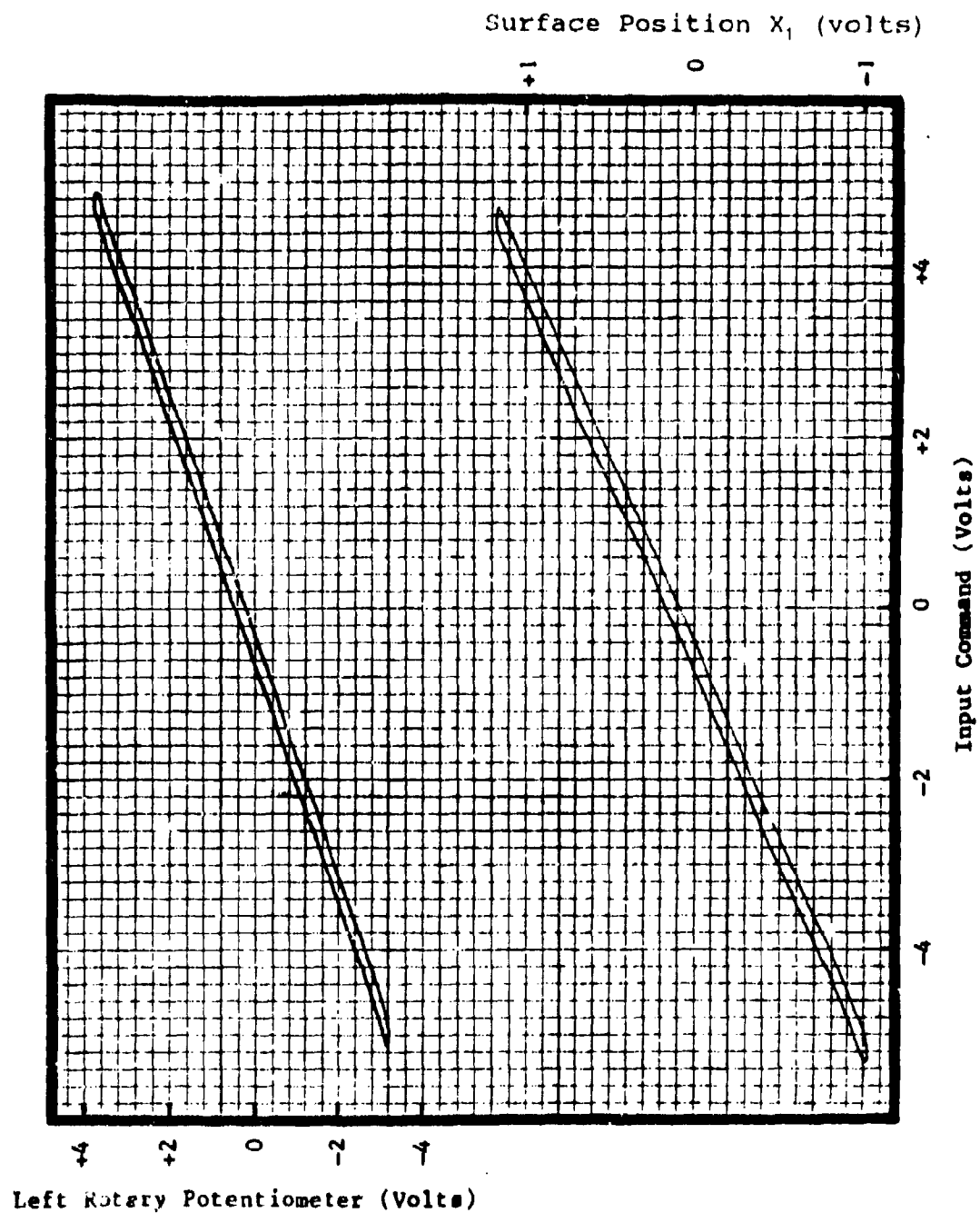


Figure IV-46. Linearity - trailing edge - left rotary - X_1 motion.

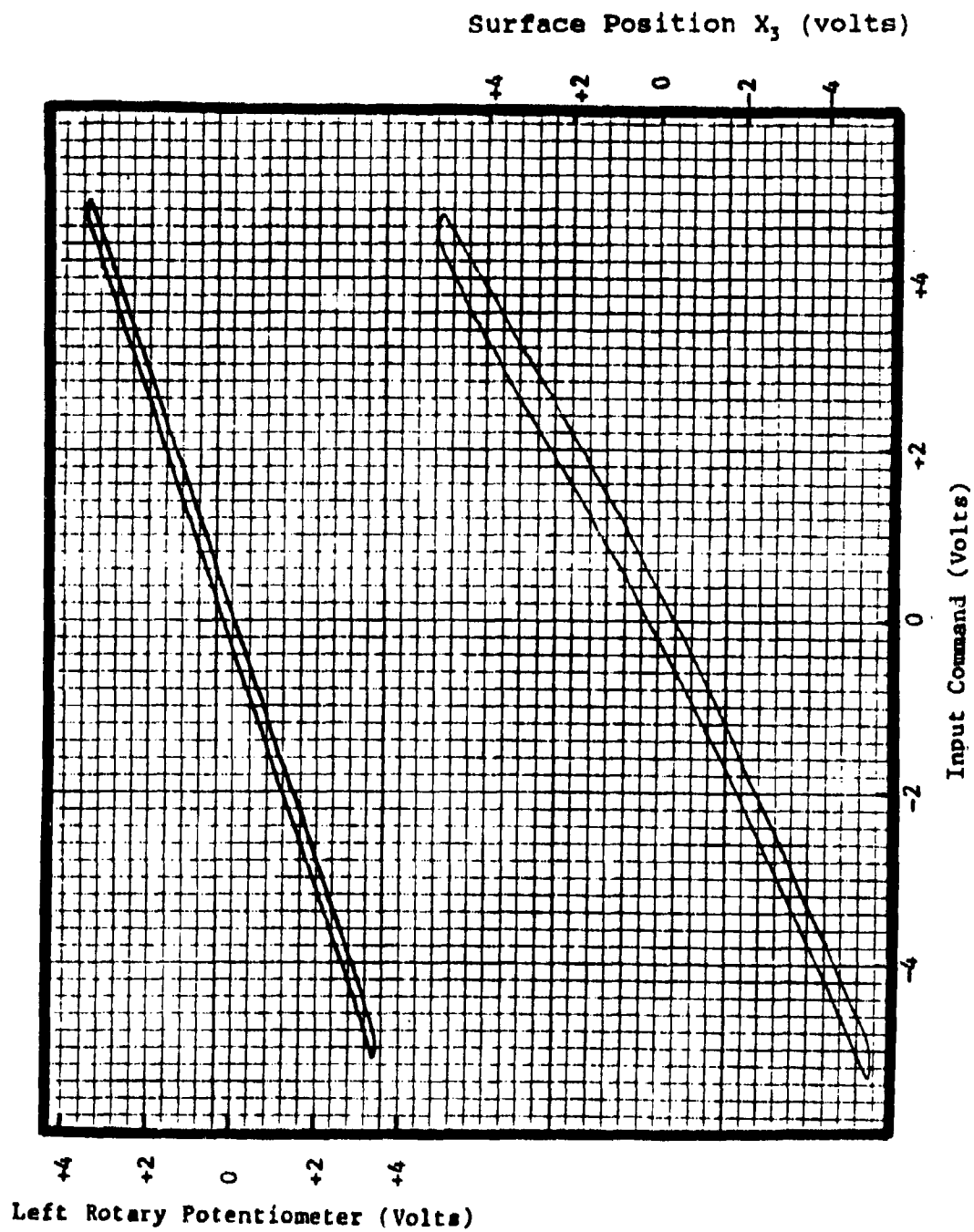


Figure IV-47. Linearity - trailing edge - left rotary - X_3 motion.

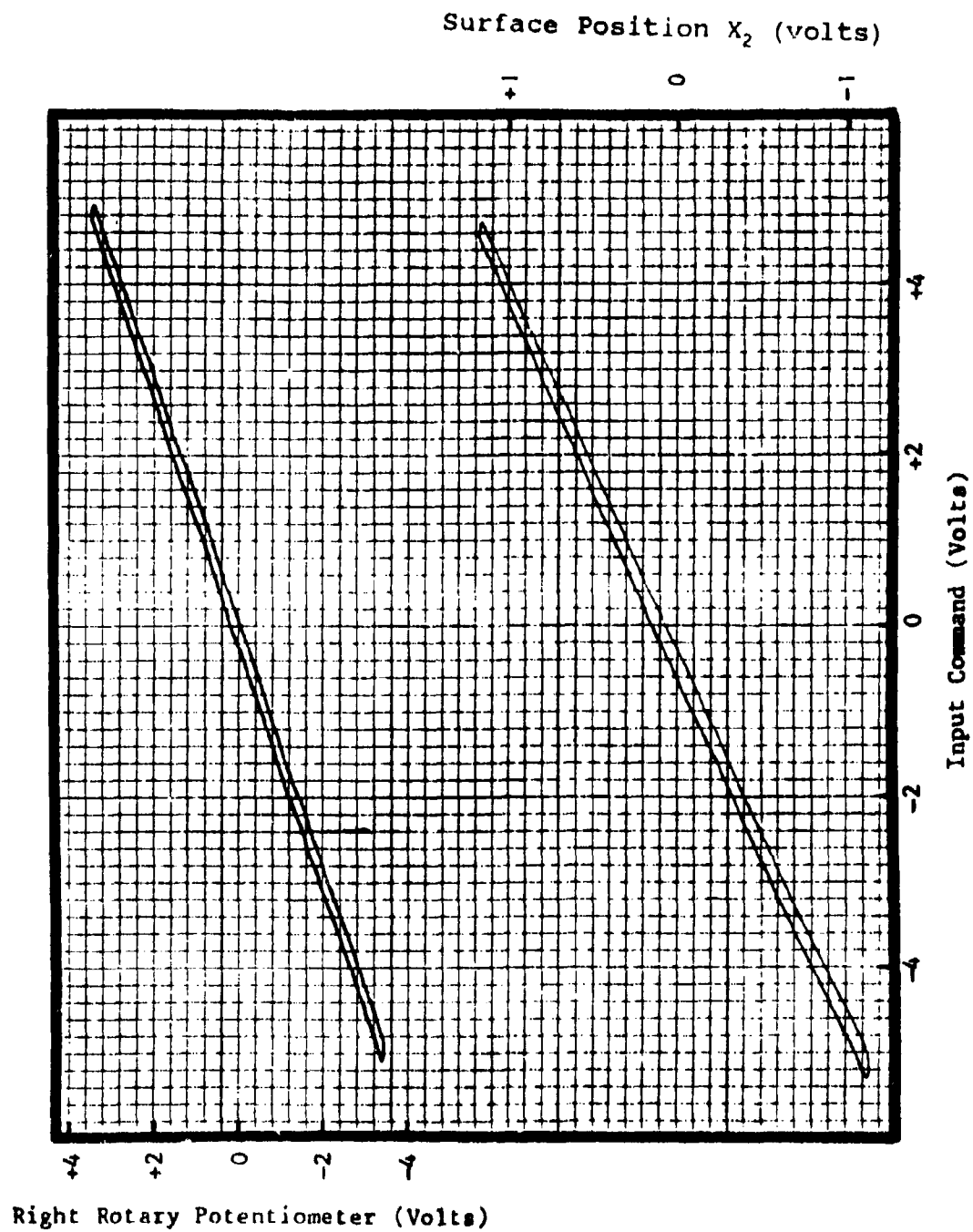


Figure IV-48. Linearity - trailing edge - right rotary - X_2 motion.

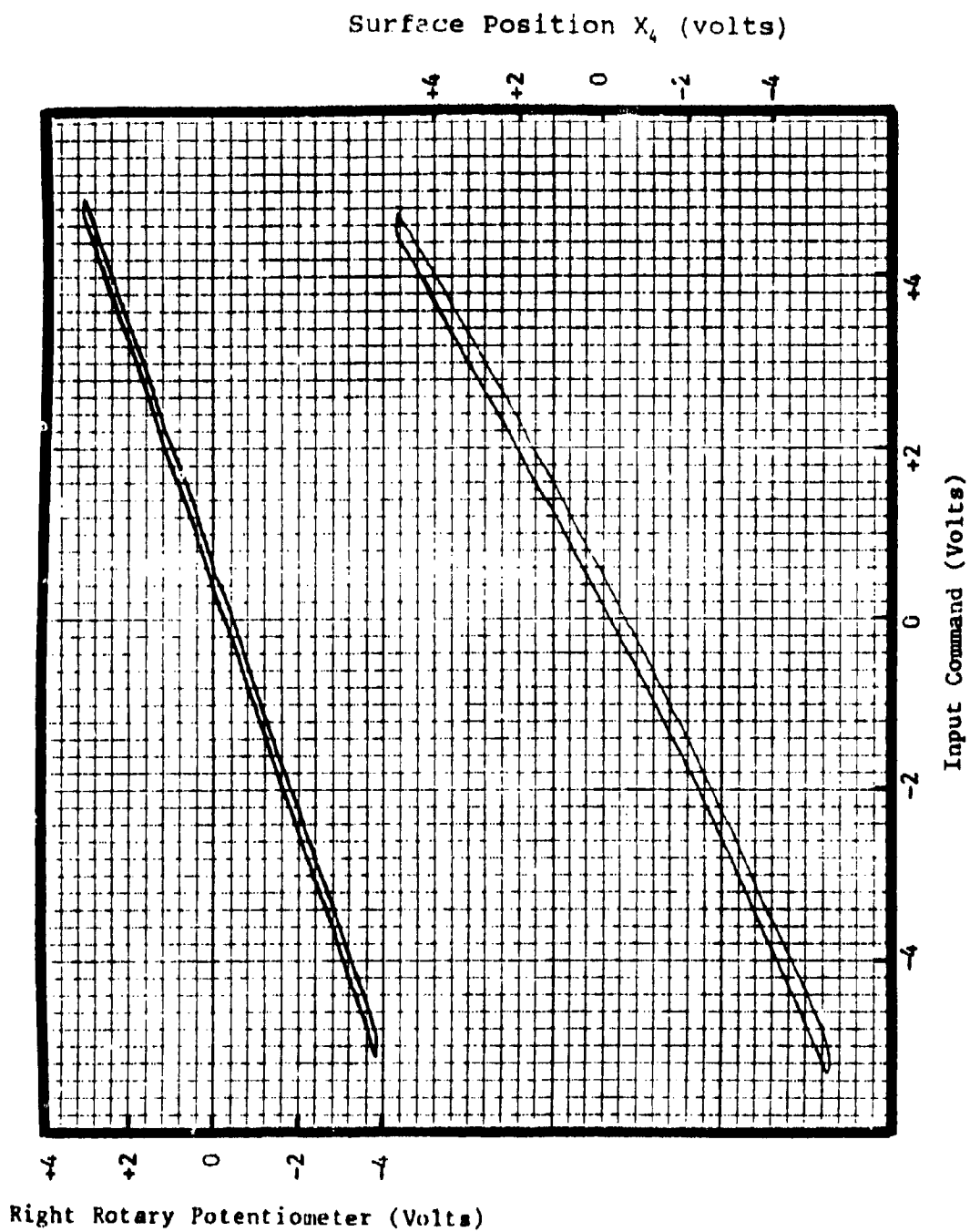


Figure IV-49. Linearity - trailing edge - right rotary, X_4 motion.

the surface position transducers show some nonlinearity. This is because of the surface position transducers necessarily must track an arc when the surface deflects. Note the increase in hysteresis from the rotary potentiometer output to the tip position transducers X_3 and X_4 . This is result of the accumulated free-play in the truss driving mechanization from the gear boxes to the tip of the trailing-edge surface and is expected.

Table IV-14 lists the hysteresis for the large (90 percent) input command in terms of a percentage of the 90-percent command voltage of ± 5.05 volts and in terms of the command voltage of ± 2.35 volts to produce 100-percent series actuator stroke.

Table IV-14. Large amplitude hysteresis - unloaded trailing edge.

Motion Point	% Full-Scale Hysteresis (Ref. to 90% Max Input)	% Full-Scale Hysteresis (Ref. to 100% Max Rate Input)
Left Rotary Potentiometer	2.35	5.05
X_1	3.49	7.50
X_3	5.82	12.51
Right Rotary Potentiometer	2.19	4.72
X_2	3.13	6.73
X_4	4.07	8.75

Hysteresis - Small Amplitude

Figures IV-50 through IV-57 show the data recorded at 3 percent (± 0.168 volts) and 10 percent (± 0.561 volts) of full-scale input level of ± 5.61 volts. Table IV-15 lists the hysteresis values for the 3 percent input in terms of the full-scale input and the 3-percent input.

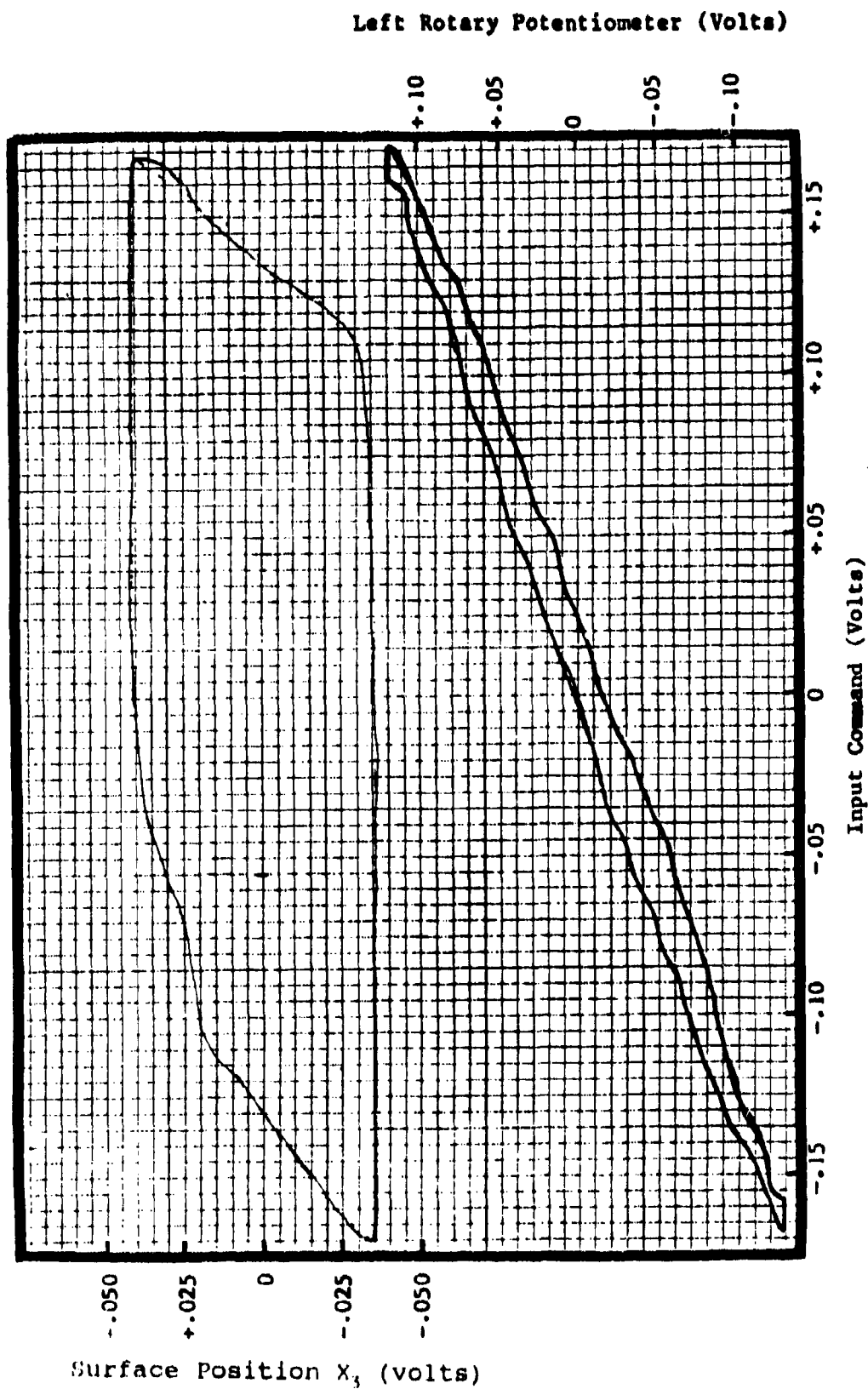


Figure IV -50. Hysteresis - 3-percent command - trailing edge - left rotary - X_3 motion.

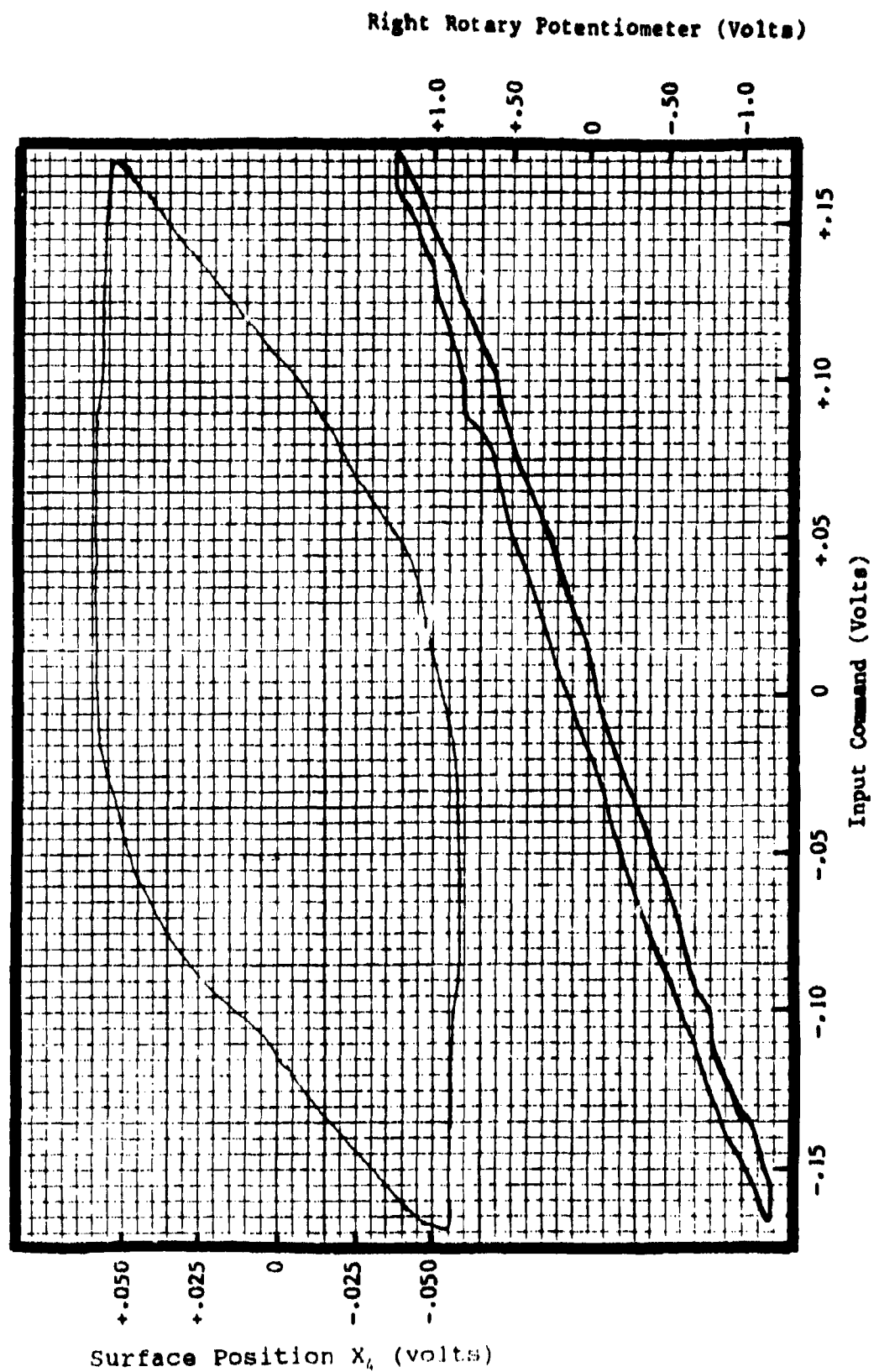


Figure IV-51. Hysteresis - 3-percent command - trailing edge - right rotary - X_4 motion.

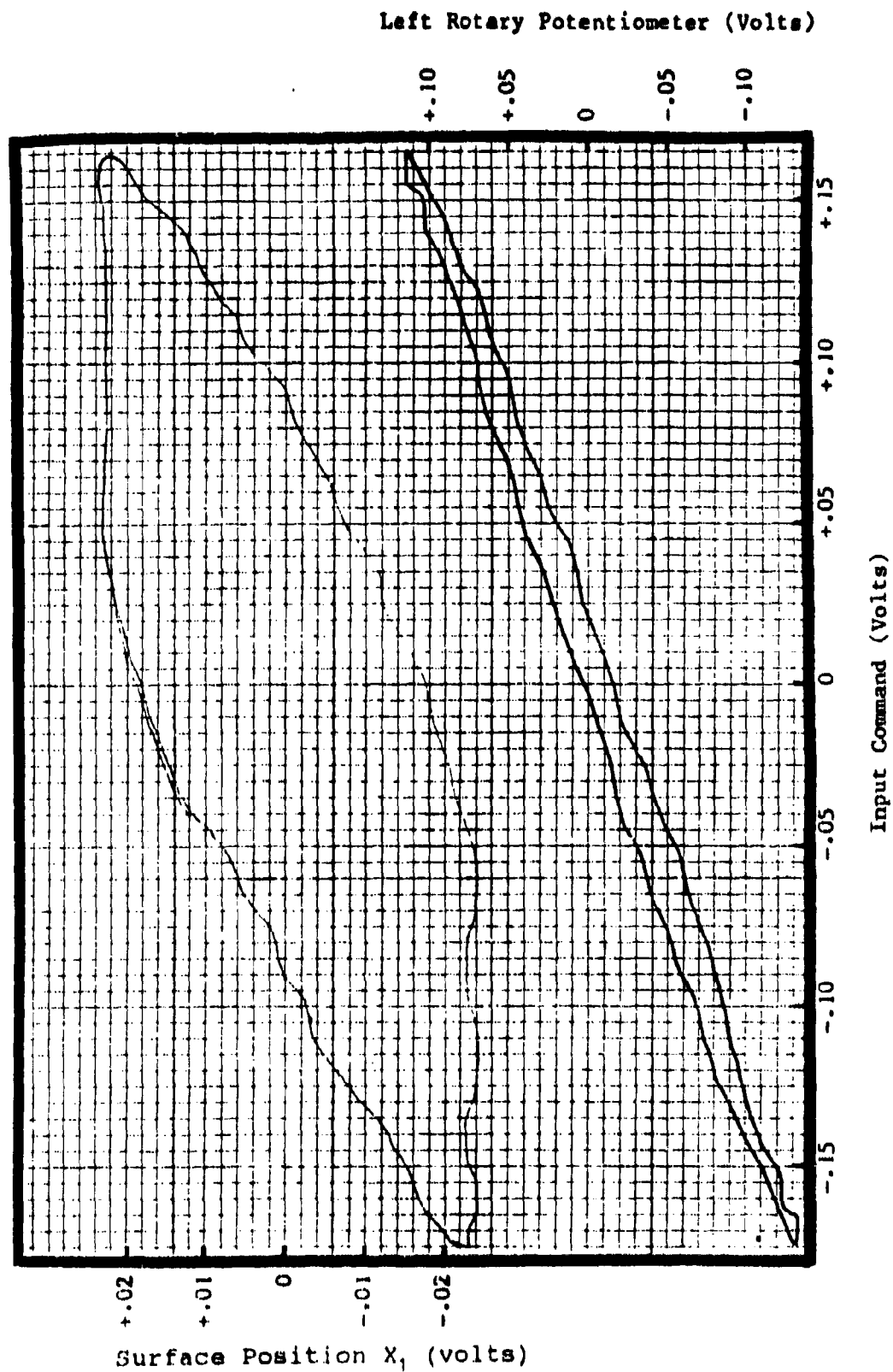


Figure IV-52. Hysteresis - 3-percent command - trailing edge - left rotary - X_1 motion.

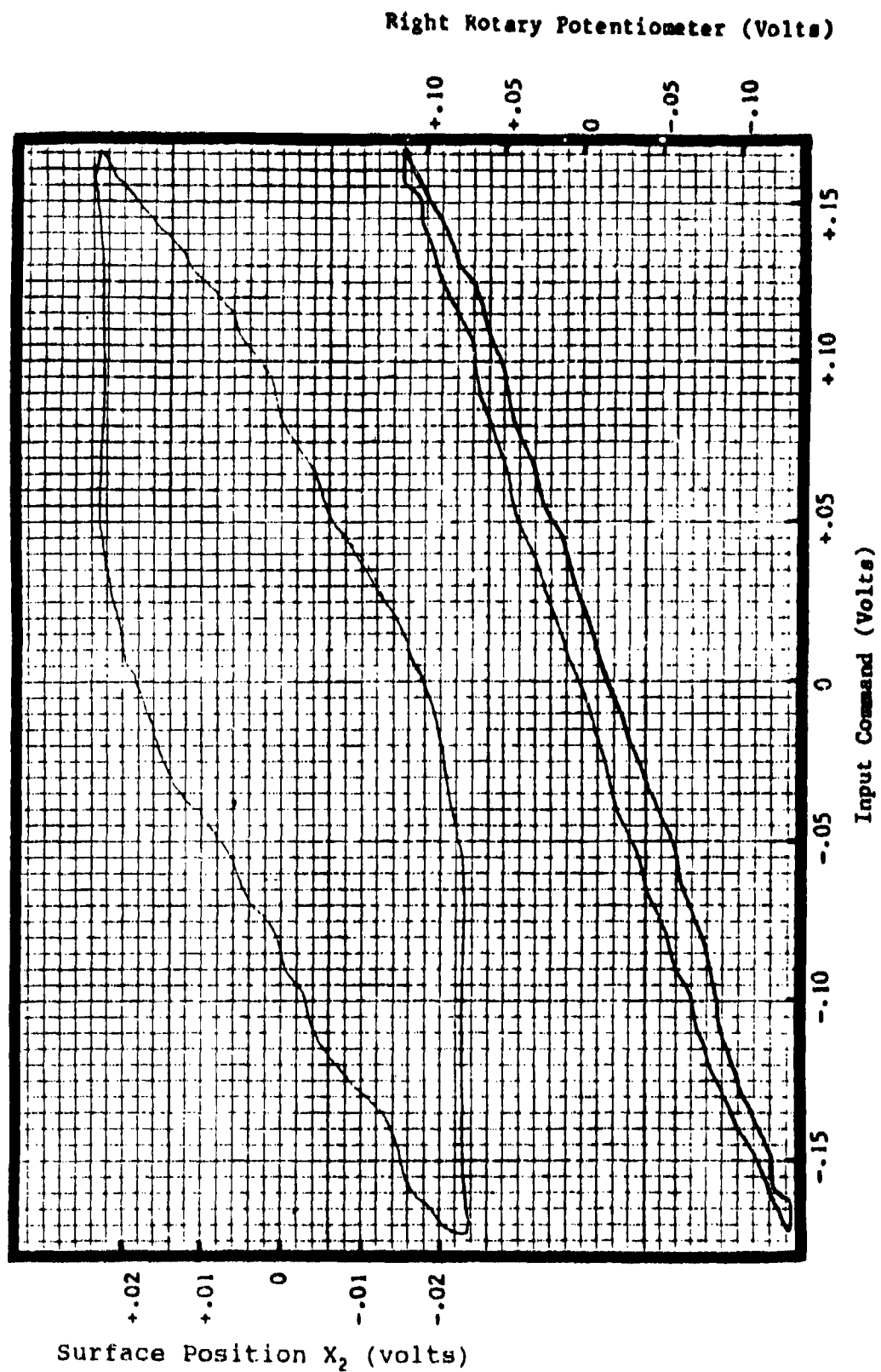


Figure IV-53. Hysteresis - 3-percent command - trailing edge - right rotary - X_2 motion.

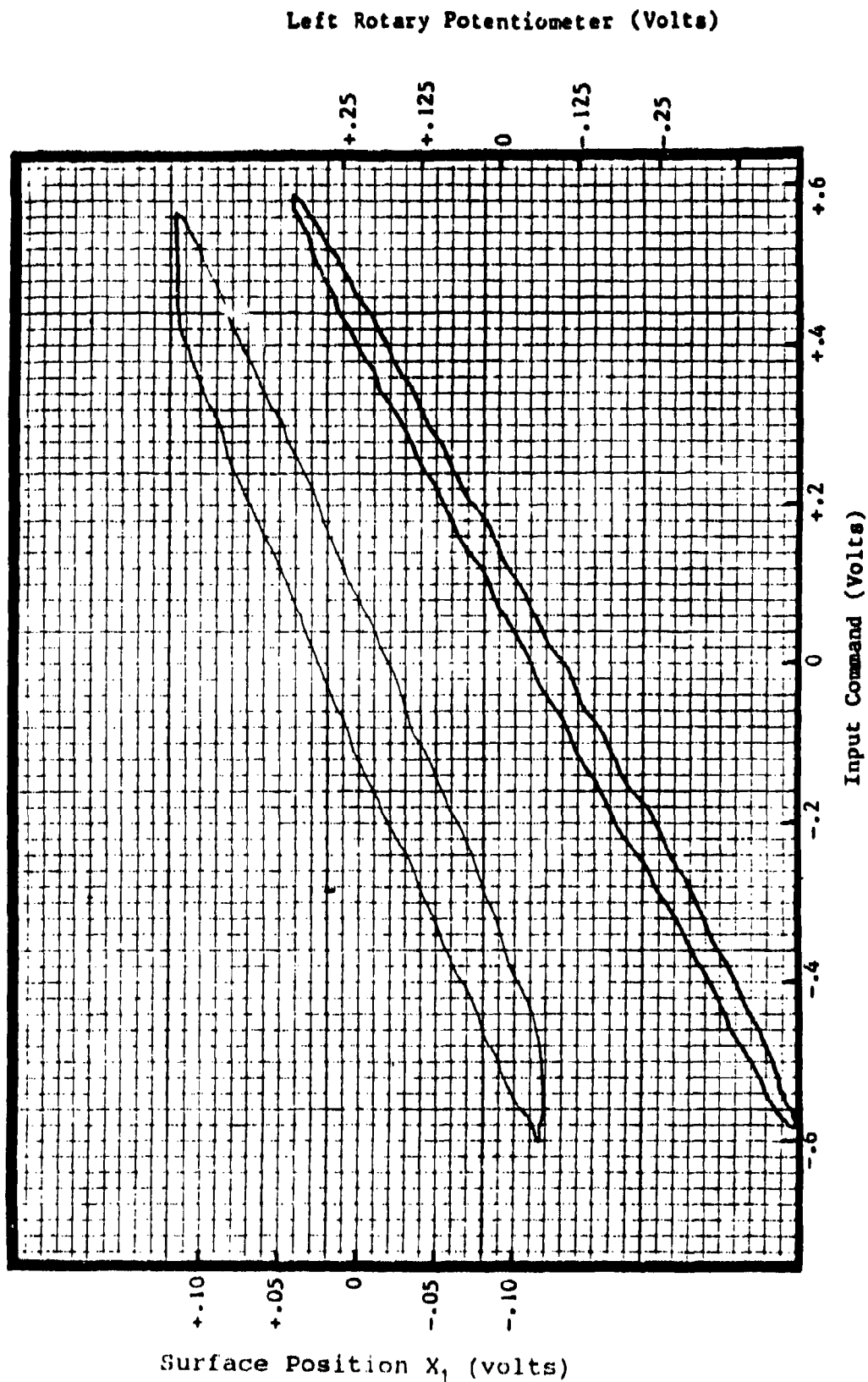


Figure IV-54. Hysteresis - 3-percent command - trailing edge - left rotary - X_1 motion.

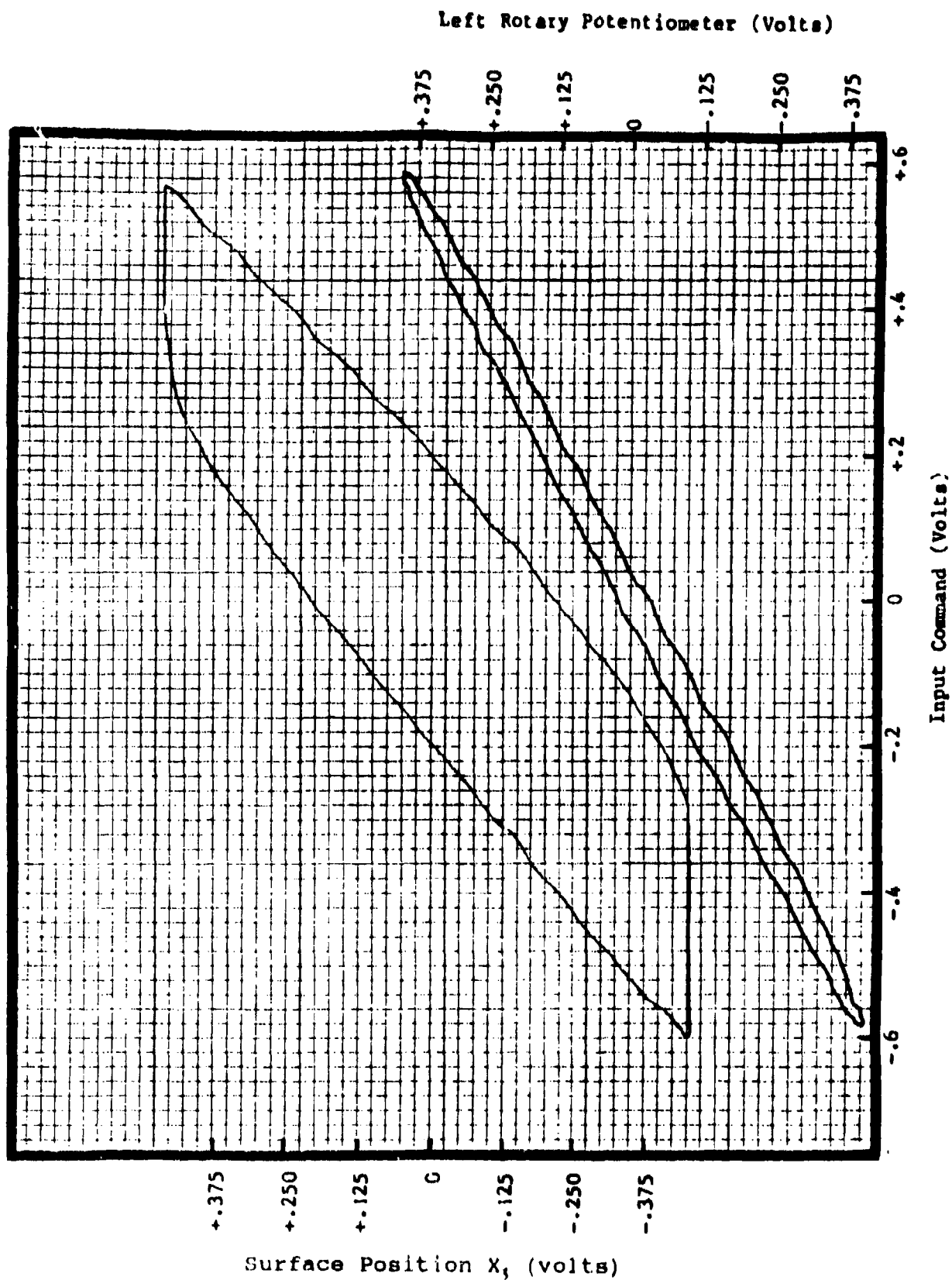


Figure IV-55. Hysteresis - 10-percent command - trailing edge - left rotary - X_3 motion.

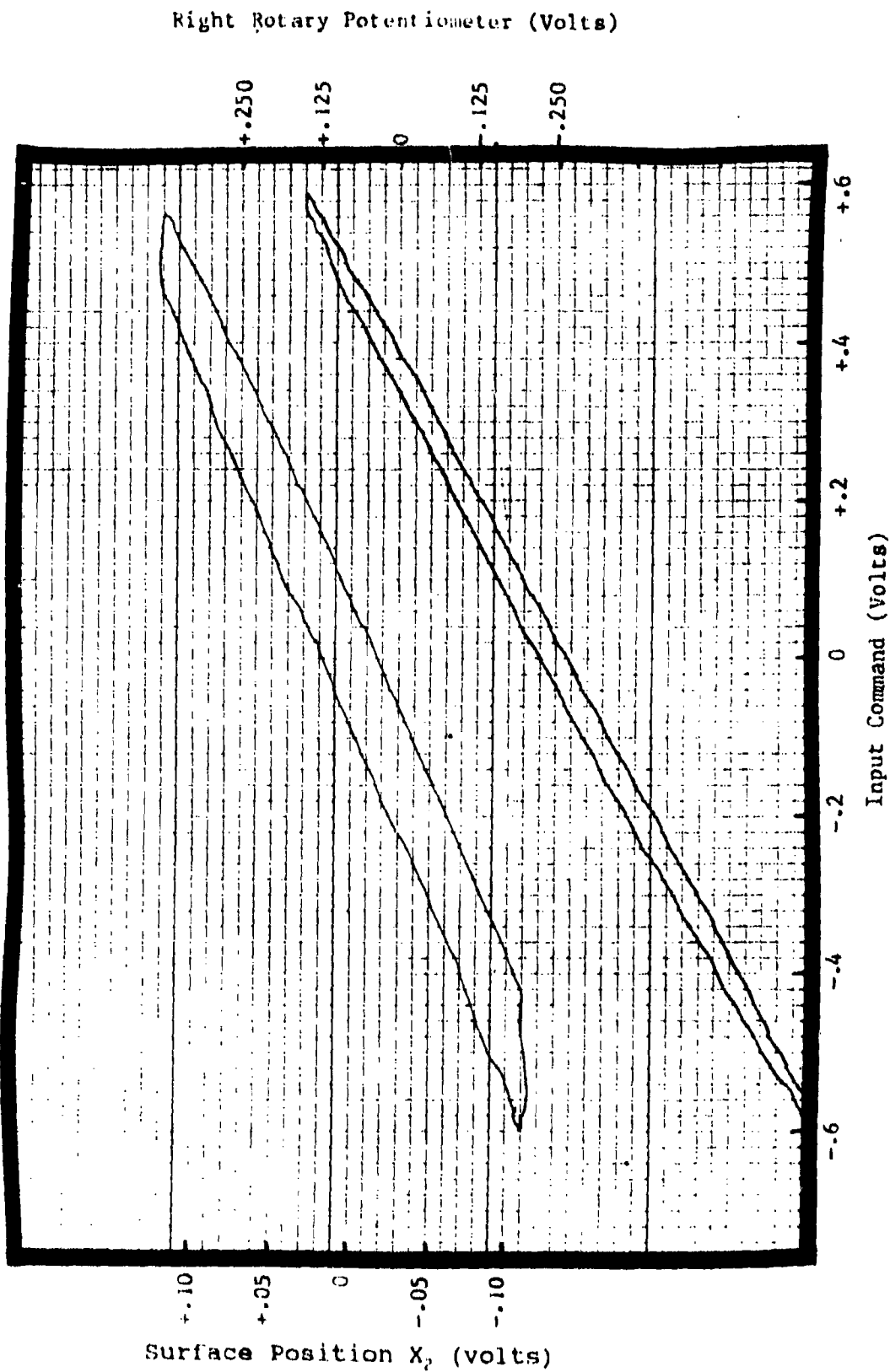


Figure IV-56. Hysteresis - 10 percent command - trailing edge - right rotary - X_2 motion.

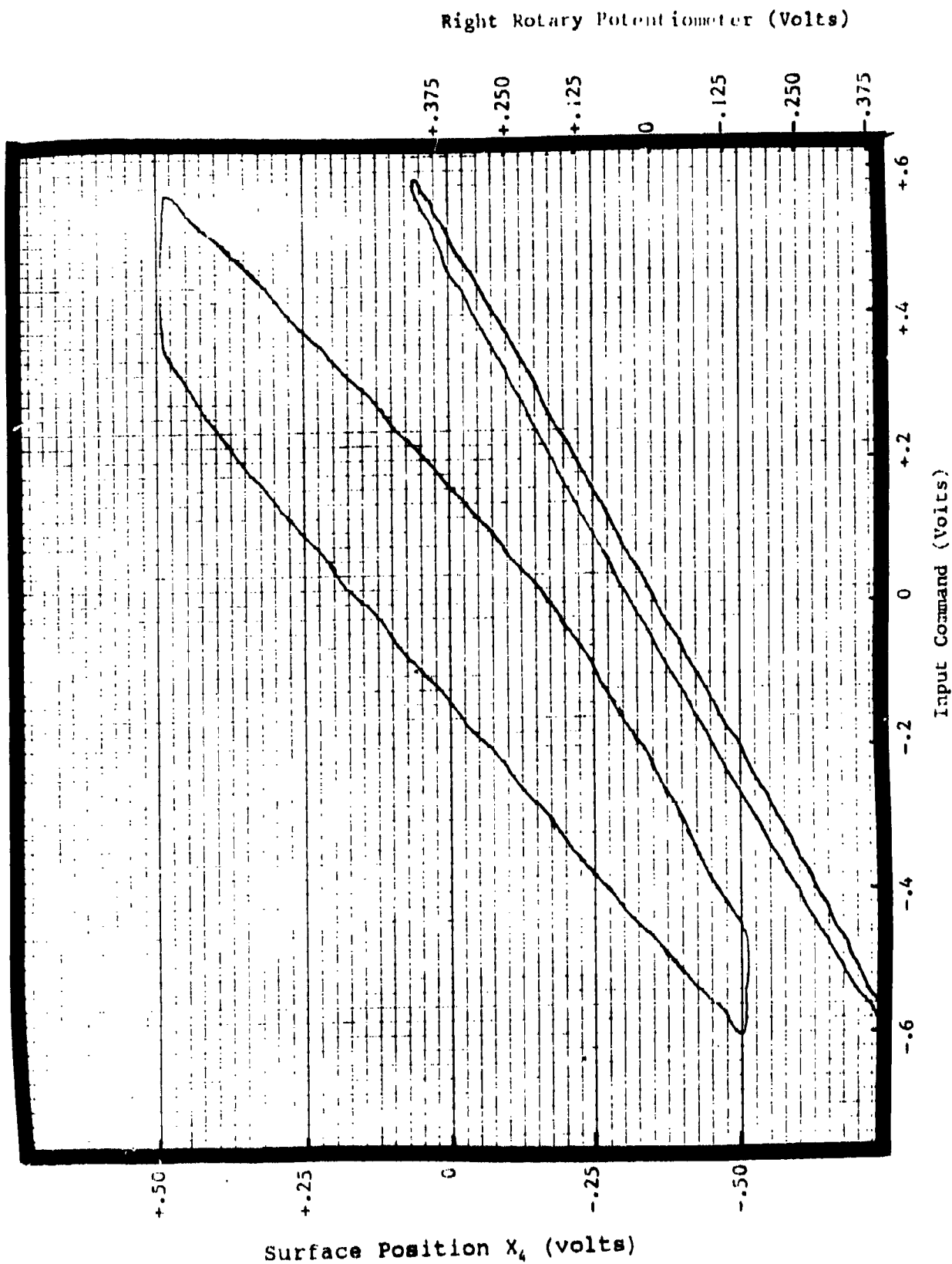


Figure IV-57. Hysteresis 10-percent command - trailing edge - right rotary - X_4 motion.

Table IV-15. Small amplitude hysteresis - 3-percent input - unloaded trailing edge.

Motion Point	Hysteresis Input (volts)	% Hysteresis (Ref. 3 % Input)	% Hysteresis (Ref. 100% Input)
Left Rotary Potentiometer	0.029	8.63	0.258
X ₁	0.178	52.97	1.58
X ₃	0.250	74.4	2.23
Right Rotary Potentiometer	0.034	10.1	0.304
X ₂	0.171	50.9	1.52
X ₄	0.228	67.9	2.03

Note that for this amplitude of input, the hysteresis contribution of the driving linkage for both the left and right trusses is 50 percent of the input (or greater).

Table IV-16 lists the hysteresis for an input of 10 percent in terms of the full-scale input and the 10-percent input.

Note that the higher input level exhibits hysteresis similar to the low-level inputs when expressed in terms of the maximum input. The readings at the midpoints of the surface (X₁ and X₂) unchanged by the higher input. The hysteresis at the tip of the surface (points X₃ and X₄) is above 2.5 percent of the maximum input, indicating that small signal response will be affected for light surface loads.

Table IV-16. Small amplitude hysteresis - 10-percent input - unloaded trailing edge.

Motion Point	Hysteresis Input (volts)	% Hysteresis (Ref. 10% Input)	% Hysteresis (Ref. 100% Input)
Left Rotary Potentiometer	0.072	6.42	0.64
X ₁	0.199	17.8	1.78
X ₃	0.374	33.4	3.34
Right Rotary Potentiometer	0.062	5.54	0.55
X ₂	0.156	13.9	1.39
X ₄	0.300	26.8	2.68

Frequency Response

Figures IV-58 through IV-65 show representative data recorded for the frequency response measurements. The figures show the response of the left and right gear boxes as measured by the rotary position potentiometers. Both input levels of 5- and 10-percent maximum command were used for the measurements and the results of both input levels is shown. For each potentiometer and input level, two response plots are shown: one of the amplitude response and one of the phase response. This was done to allow using cursor locations on the response plots to mark the - 3 dB amplitude point (or the - 45° and - 90° phase angles) and have the cursor locations print on the plot legend. The response of the other motion points of X₁, X₂, X₃ and X₄ resembled that of Figures IV-58 through IV-56 in terms of no peaking. Table IV-17 summarizes the response of the motion points for the 5-percent command input level. Table IV-18 lists the response of the motion points for the 10-percent command input level.

As shown in Tables IV-17 and IV-18, the frequency response of the motion points decreases from the rotary potentiometers (gear box motion) to the tip motion of the surface (points X₃ and X₄). The frequency response also improves with the higher input amplitude. Both of these characteristics reflect the effect of the free-play in the driving mechanization of the variable-geometry trusses.

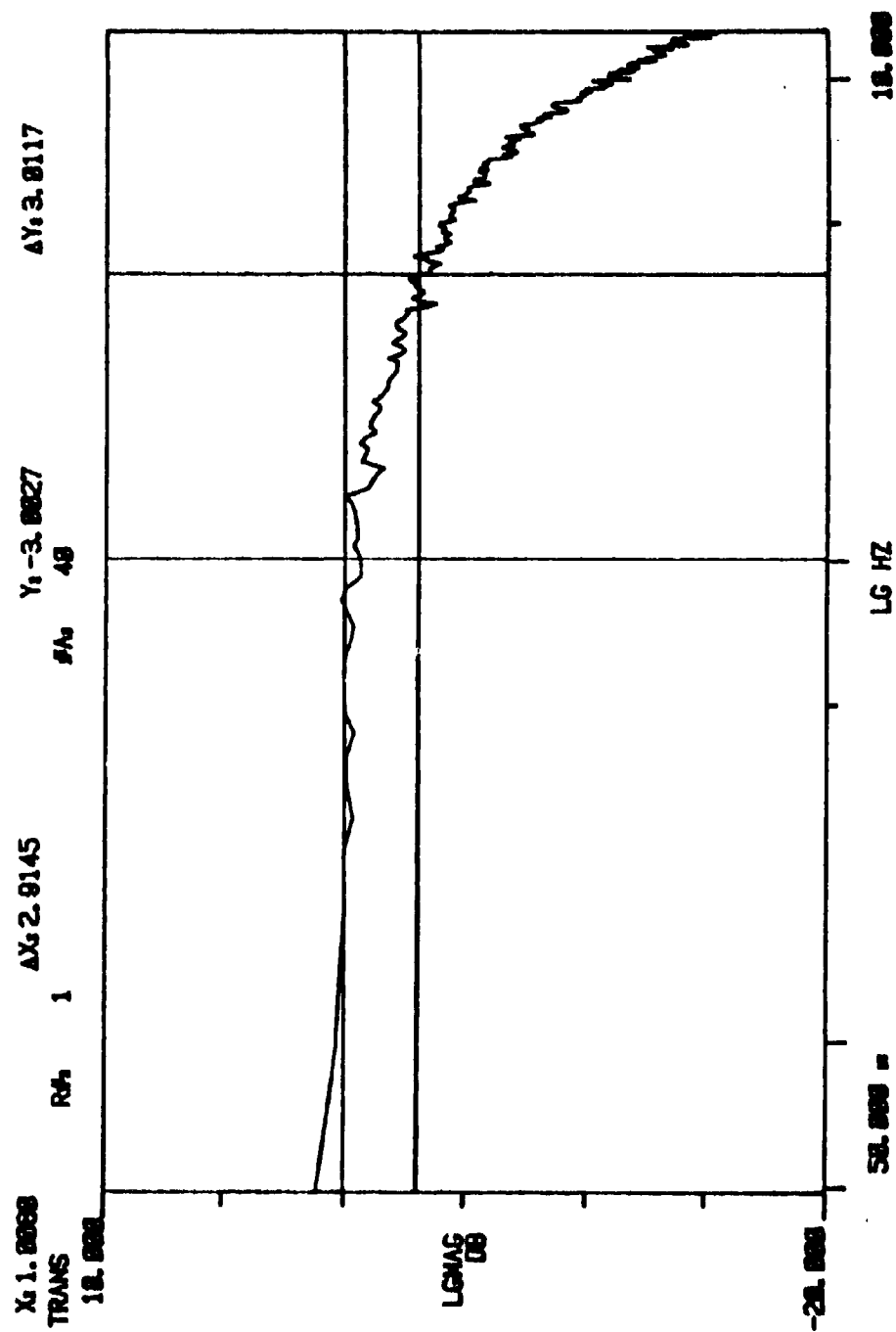


Figure IV-58. Amplitude response - 5-percent command - left rotary potentiometer - unloaded trailing edge.

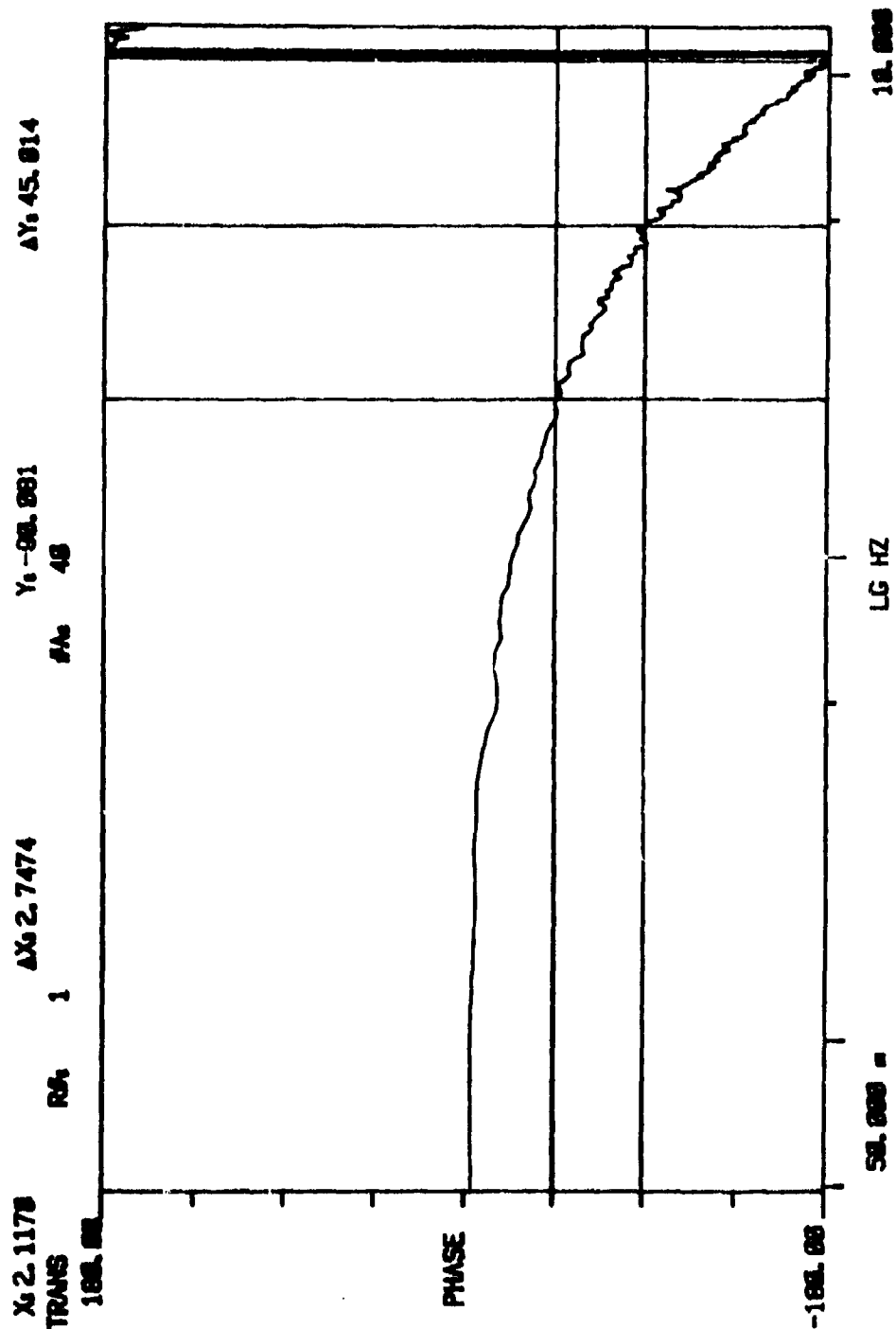


Figure IV-59. Phase response - 5-percent command - left rotary potentiometer - unloaded trailing edge.

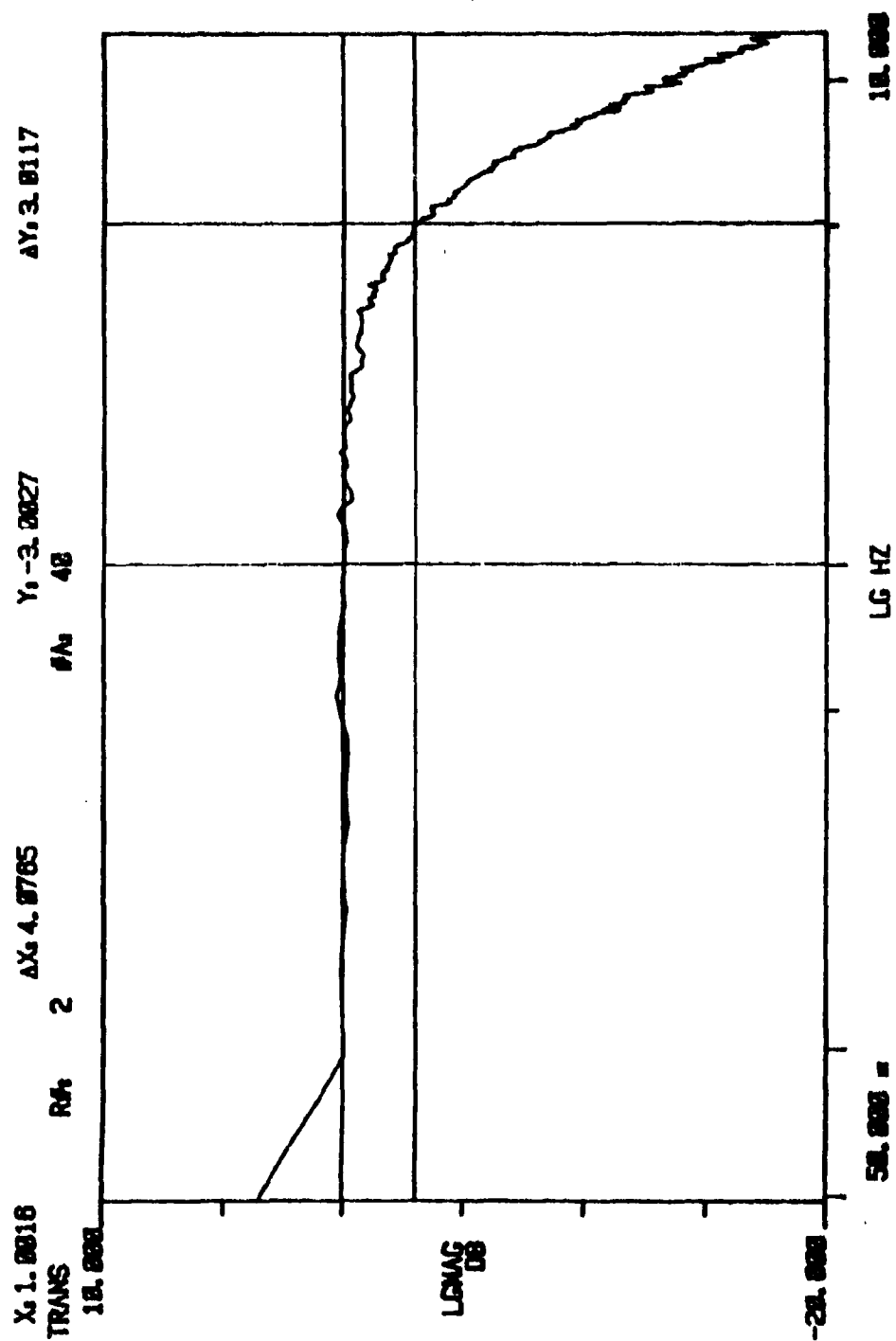


Figure IV-60. Amplitude response - 5-percent command - right rotary potentiometer - unloaded trailing edge.

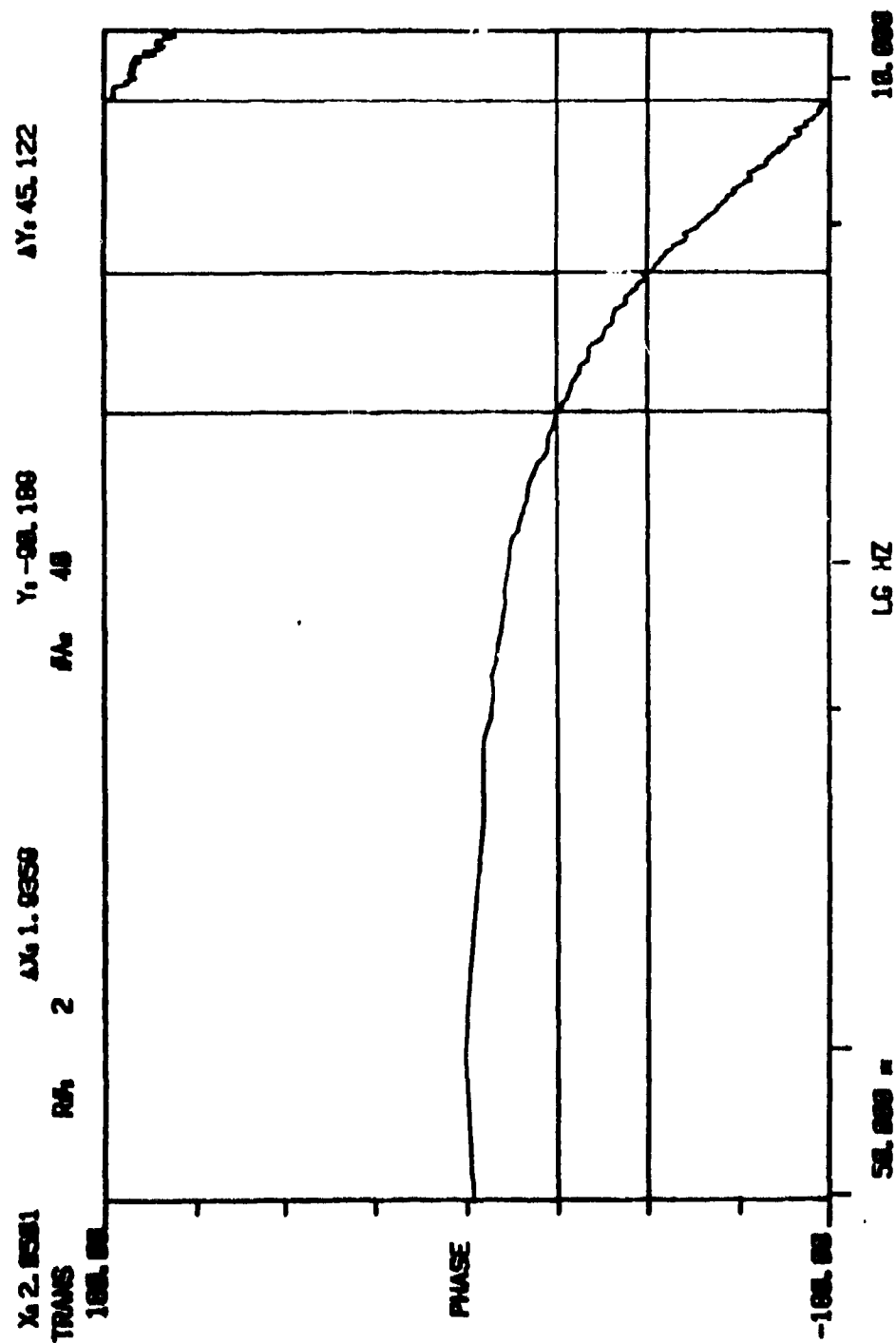


Figure IV-61. Phase response - 5-percent command - right rotary potentiometer - unloaded trailing edge.

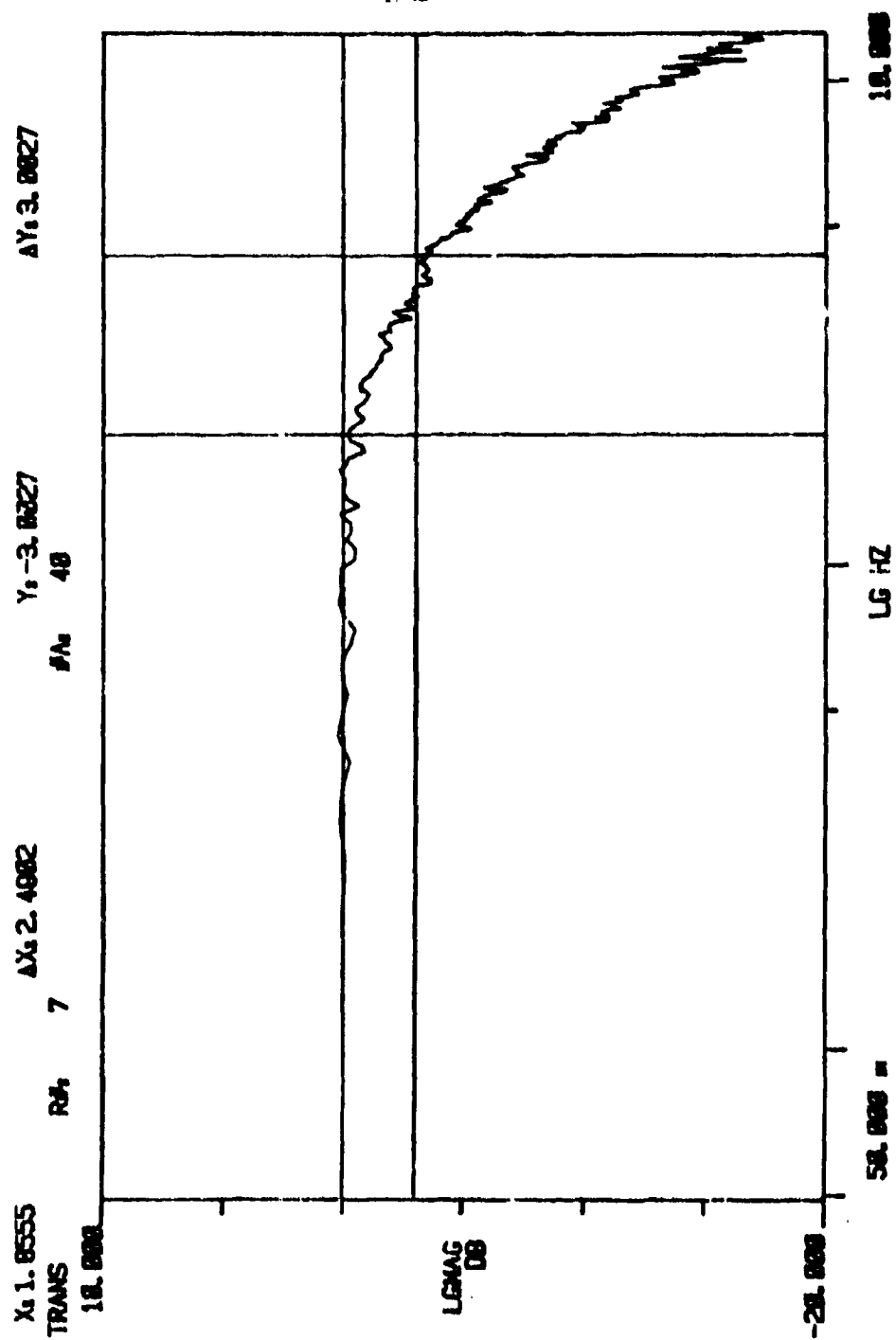


Figure IV-62. Amplitude response - 10-percent command - left rotary potentiometer - unloaded trailing edge.

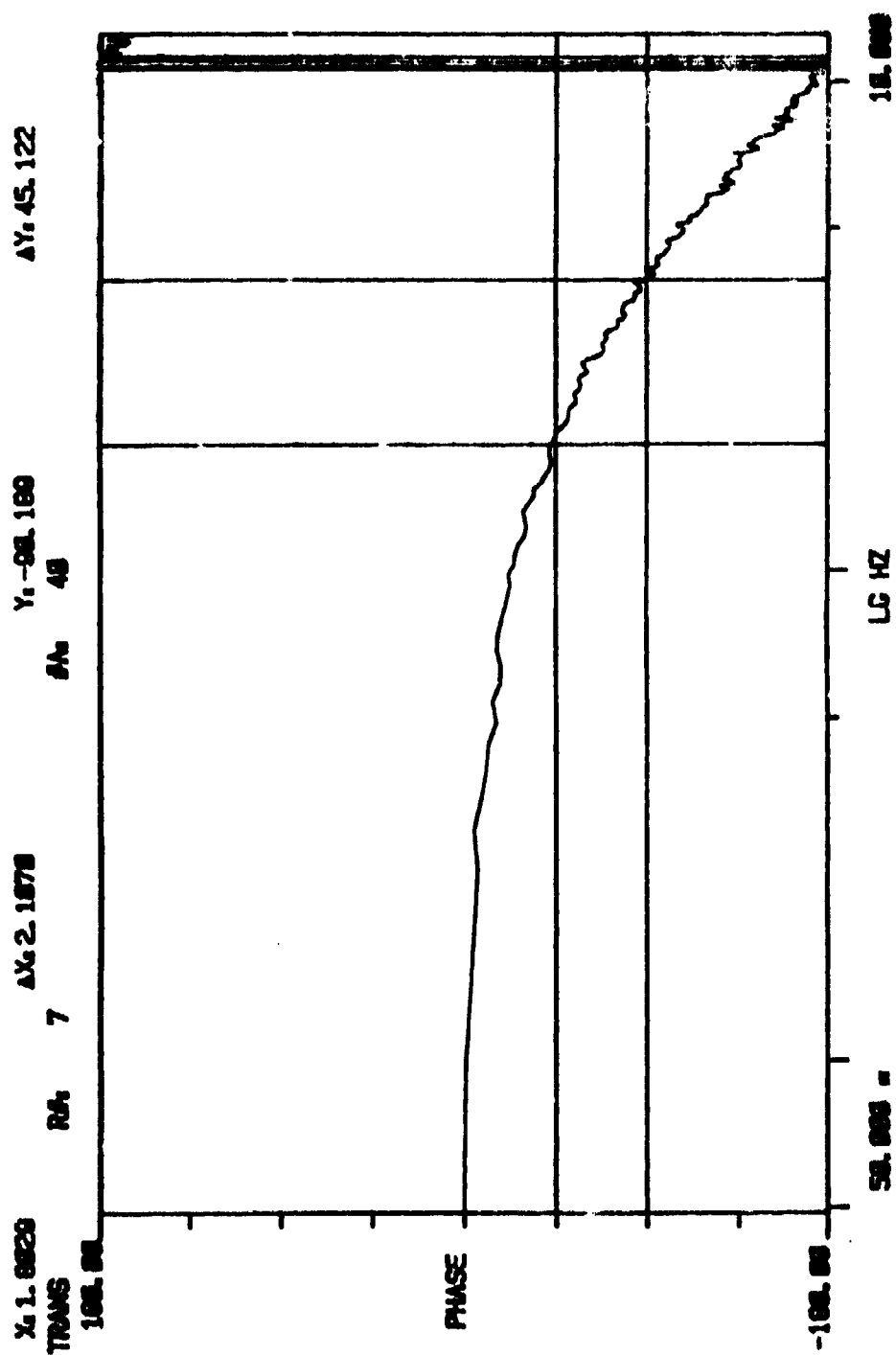
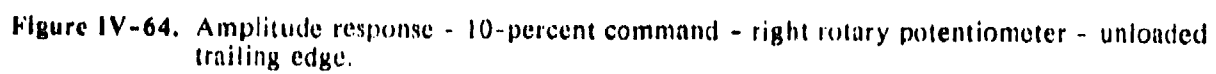


Figure IV-63. Phase response - 10-percent command - left rotary potentiometer - unloaded trailing edge.



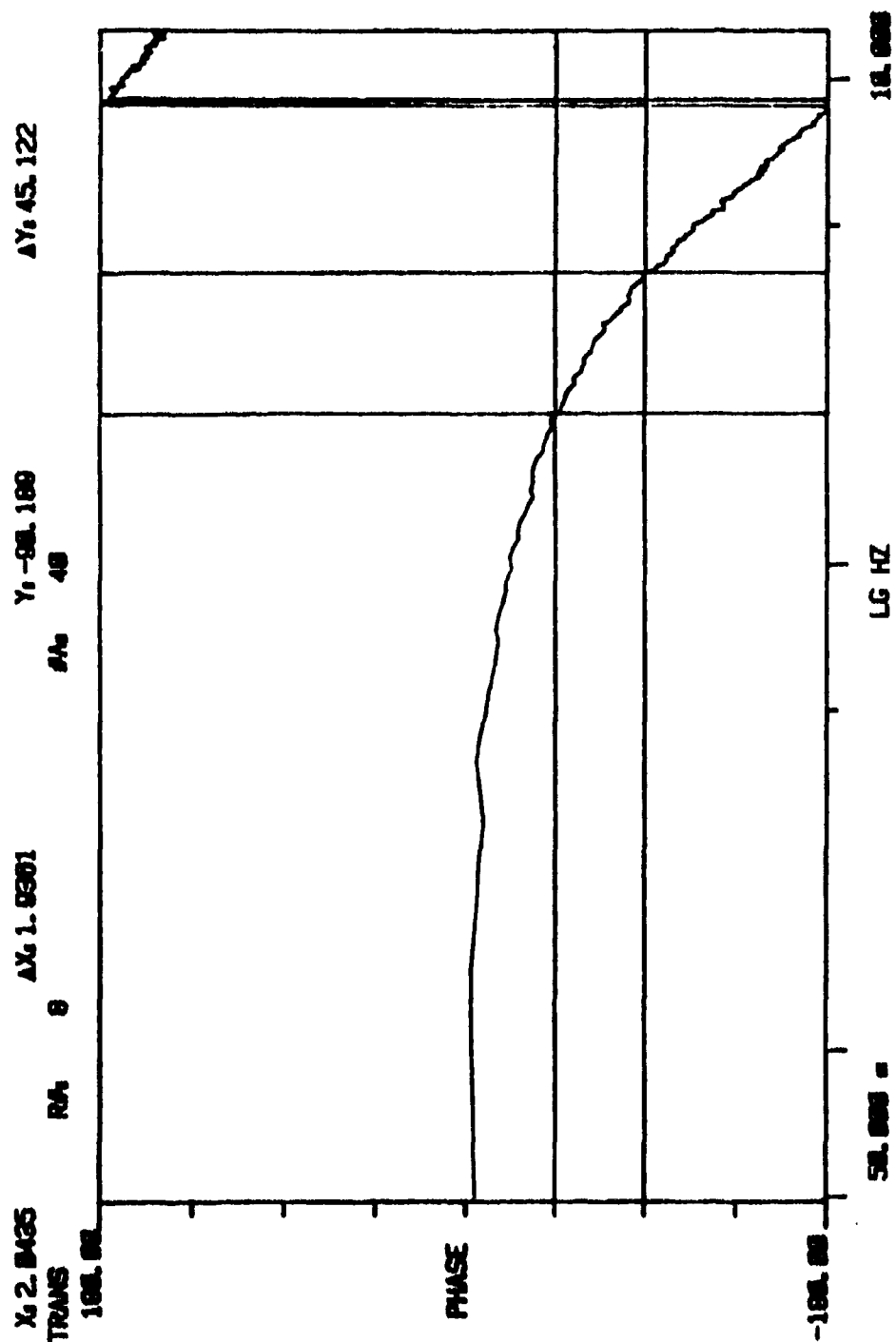


Figure IV-65. Phase response - 10-percent command - right rotary potentiometer - unloaded trailing edge.

Note also that the frequency response of the tip of the left truss is lower than the right truss. This is consistent with the difference in the measured hysteresis between the two trusses.

Table IV-17. Frequency response - unloaded trailing edge.

5-Percent Input Command

Motion Point	-3 dB Freq. (Hz)	-45° Phase Freq. (Hz)	-90° Phase Freq. (Hz)
Left Rotary Potentiometer	3.914	2.117	4.864
X ₁	3.054	1.298	2.193
X ₃	0.800	0.766	2.270
Right Rotary Potentiometer	5.077	2.050	3.986
X ₂	2.883	1.270	2.971
X ₄	1.487	0.674	2.257

Table IV-18. Frequency response - unloaded trailing edge.

10-Percent Input Command			
Motion Point (Hz)	-3 dB Freq. (Hz)	-45° Phase Freq. (Hz)	-90° Phase Freq.
Left Rotary Potentiometer	4.346	1.803	3.910
X ₁	2.497	1.494	3.034
X ₃	0.867	0.719	1.697
Right Rotary Potentiometer	4.904	2.044	3.980
X ₂	4.285	1.521	2.995
X ₄	3.573	1.337	2.783

Step Response

Figures IV-66 and IV-67 show the step response recorded for the left and right sections of the trailing edge. The amplitude of the step input was nominally 1.12 volts or 10 percent of the total ± 5.61 volt input. Figure IV-66 shows the test results for the left section. Note that on the surface down motion, the rotary potentiometer shows some overshoot of the final position. However, the overshoot motion does not feed through to positions X₁ and X₃. The movement into the final positions for both X₁ and X₃ show minor amplitude variations, indicating some free play in the mechanization.

Figure IV-67 shows the test results for the right section. Note that the for the *surface up* direction, the rotary potentiometer shows some overshoot without ringing. As with the left section's response, the surface positions show minor amplitude irregularities in settling into the final position.

Table IV-19 lists the measured response in terms of time to reach 63 percent of the final value (after start of motion) and the time delay to start motion after application of the step input. The difference in response times shows the effect of free play on the response of the variable-geometry trusses.

Test Item - General Dynamics
Mission Adaptive Wing

Date
Prepared: 8/1/85

Test - Step Response
Surface - Trailing Edge
Load - Zero Load

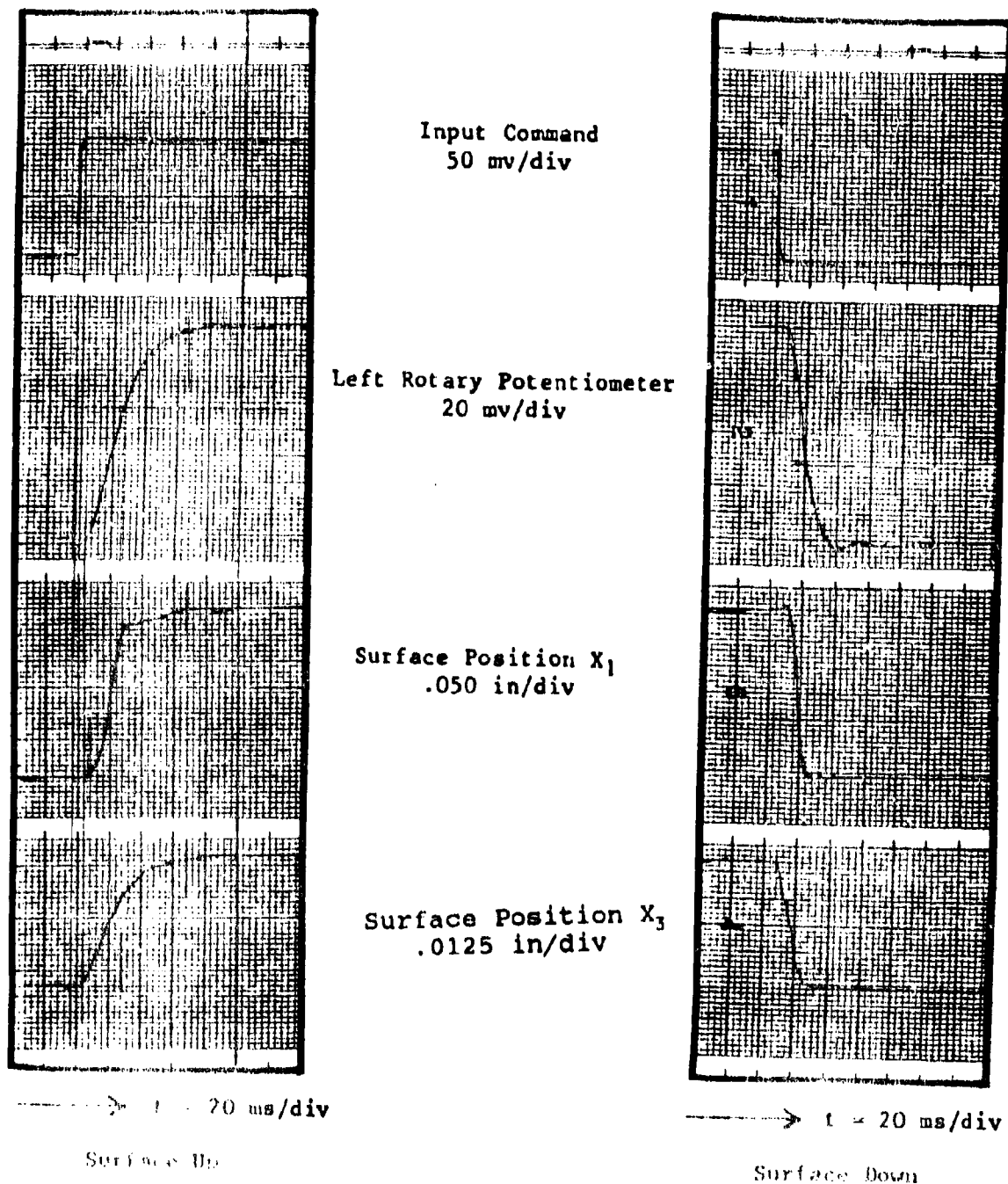
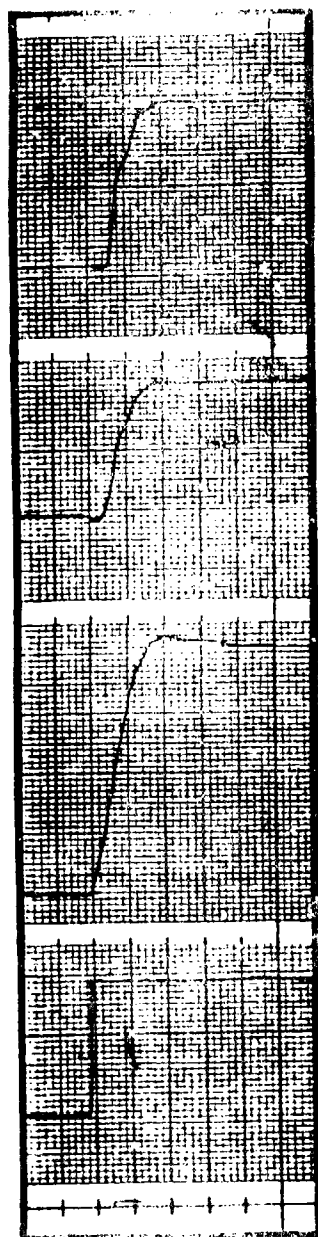


Figure IV-66. Step response - X_1 , X_3 .

Test - Step Response
Surface - Trailing Edge
Load - Zero Load



Surface Up

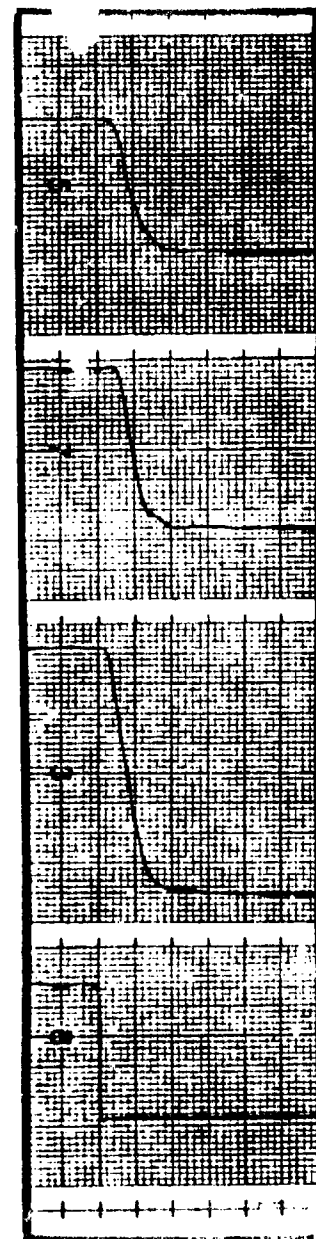
Surface Position X_4
.0125 in/div

Surface Position X_2
.050 in/div

Right Rotary Potentiometer
20 mv/div

Input Command
50 mv/div

20 ms/div



Surface Down

20 ms/div

Figure IV-67. Step response - X_2 , X_4 .

Table IV-19. Step response - unloaded trailing edge.

Motion Point	<u>Surface Up</u>		<u>Surface Down</u>	
	Time Delay (ms)	63% Time (ms)	Time Delay (ms)	63% Time (ms)
Left Rotary Pot.	40	125	40	70
X ₁	60	80	50	55
X ₃	40	130	40	95
Right Rotary Pot.	20	90	15	70
X ₂	50	40	50	45
X ₄	65	55	40	60

Saturation Velocity

Figures IV-68 through IV-71 show data recorded during the saturation velocity test. The input command amplitude step level was 4.5 volts (40 percent of the maximum command voltage). This was the maximum step input that the system would accept without tripping the failure-detection logic. The step was large enough to ensure that the control valves for the hydraulic motors traveled to their full excursions. Note that as shown in Figure IV-68 and IV-71, there is a difference in the velocities indicated by the rotary potentiometers. Table IV-20 summarizes the saturation rate for the motion points of the trailing-edge surface. Note that the X₂ and X₄ surface velocities exceed 20 degrees per second and that there is a difference between the velocities indicated by the rotary potentiometers.

Table IV-20. Trailing-edge maximum velocity - unloaded.

Motion Point	<u>Surface Up</u>		<u>Surface Down</u>	
	In/Sec.	Deg/Sec.	In/Sec.	Deg/Sec.
X₁	2.13	5.82	3.40	9.29
X₃	15.0	27.27	22.50	40.91
X₂	2.7	7.8	2.80	8.09
X₄	14.0	25.35	13.50	24.46

The differences in the rates for the surface down and surface up as well as the differences between the right side of the surface (X₂, X₄) and left side (X₁, X₃) were probably caused by a slight asymmetry in the flow from the two control valves. This could be easily eliminated if necessary by adjusting mechanical spool stops (or the driving-actuator-mounting position).

Test Item - General Dynamics
Mission Adaptive Wing

Date
Prepared: 8/6/85

Test - Saturation Velocity

Surface - Trailing Edge - Surface Down

Load - Zero Load

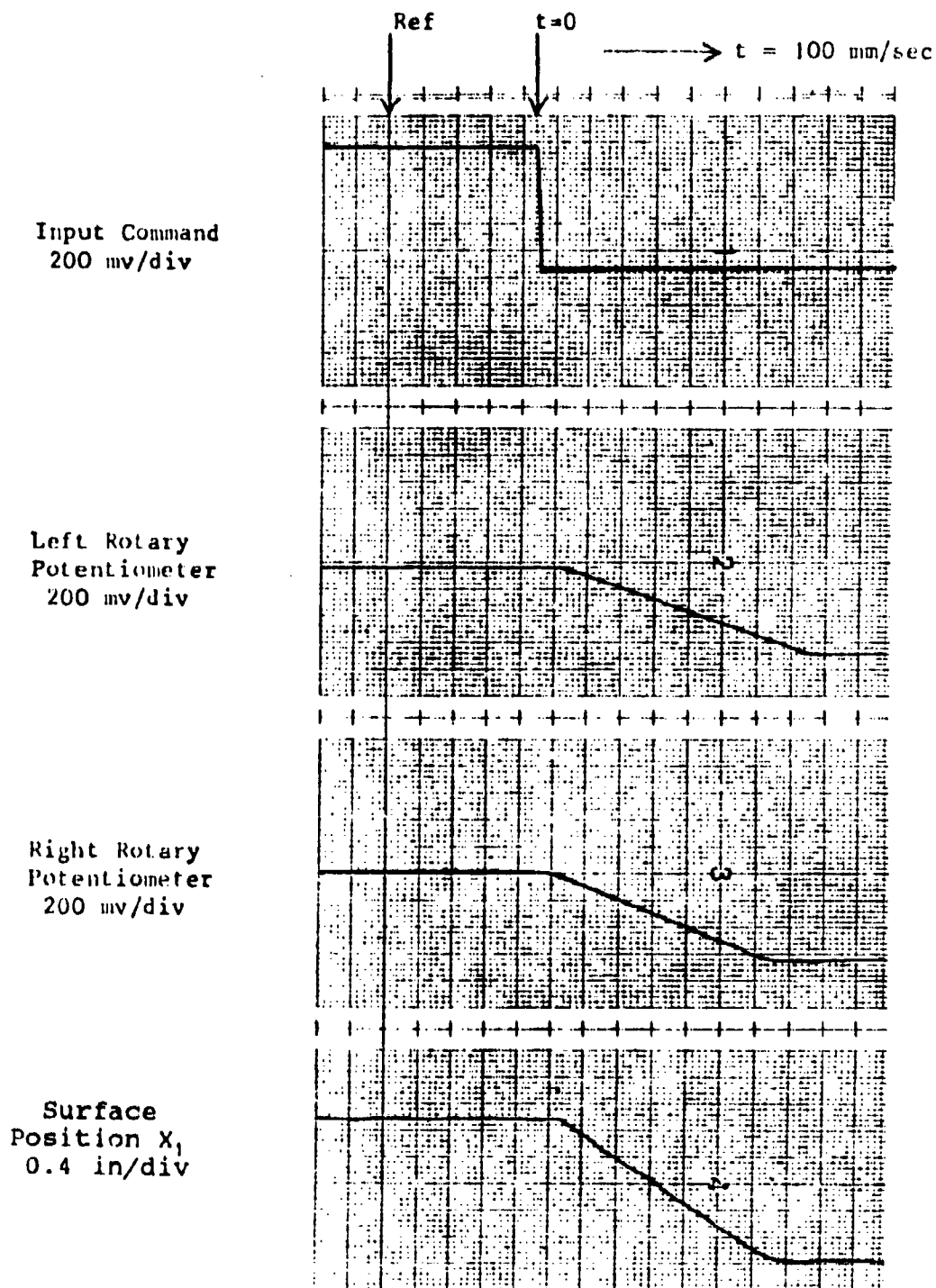


Figure IV-68. Saturation velocity - rotary potentiometer, X_1

Test Item - General Dynamics
Mission Adaptive Wing

Date
Prepared: 8/6/85

Test - Saturation Velocity
Surface - Trailing Edge - Surface Down
Load - Zero Load

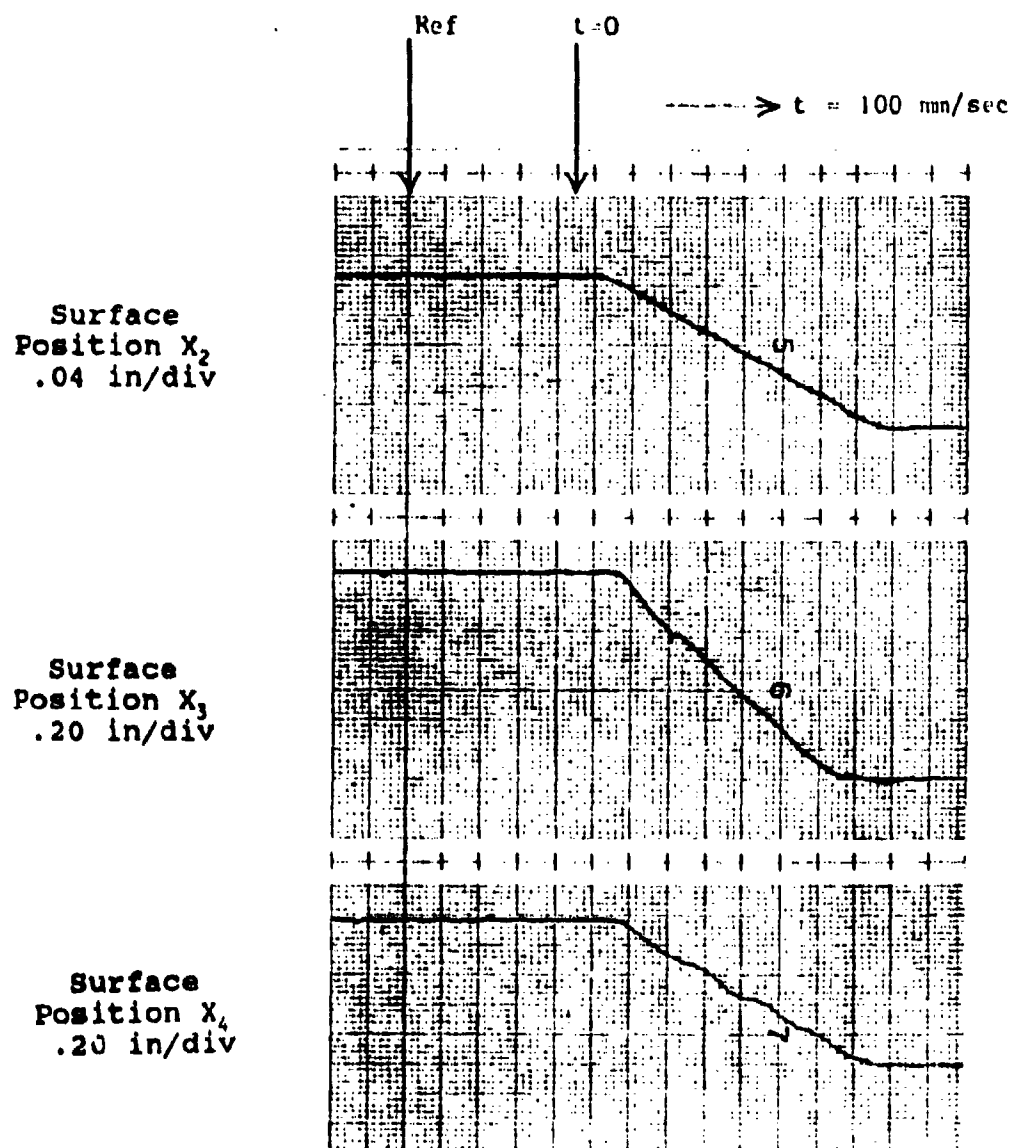


Figure IV-69. Saturation velocity - X_2 , X_3 , X_4 .

Test Item - General Dynamics
Mission Adaptive Wing

Date
Prepared: 8/6/85

Test - Saturation Velocity
Surface - Trailing Edge - Surface Up
Load - Zero Load

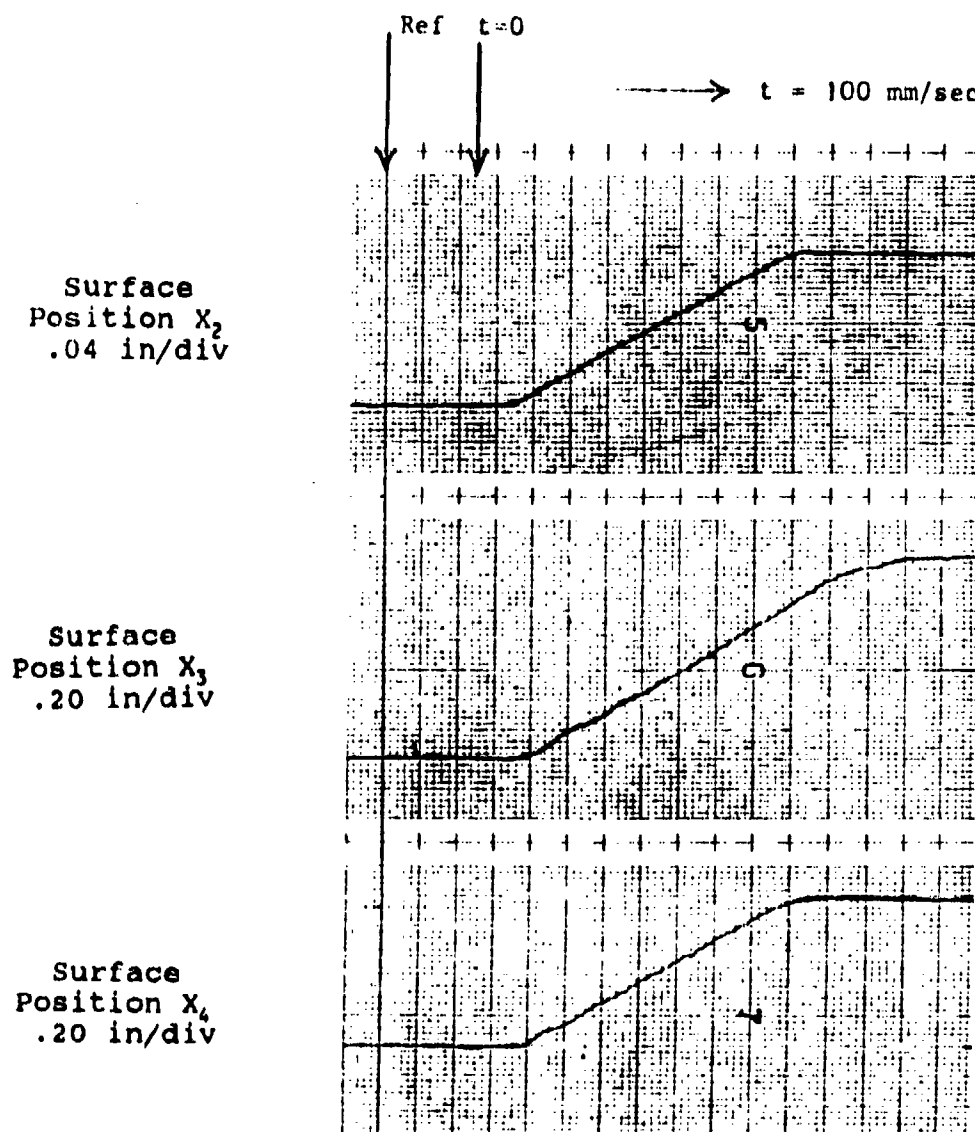


Figure IV-70. Saturation velocity - X_2 , X_3 , X_4 .

Test Item - General Dynamics
Mission Adaptive Wing

Date
Prepared: 8/6/85

Test - Saturation Velocity
Surface - Trailing Edge - Surface Up
Load - Zero Load

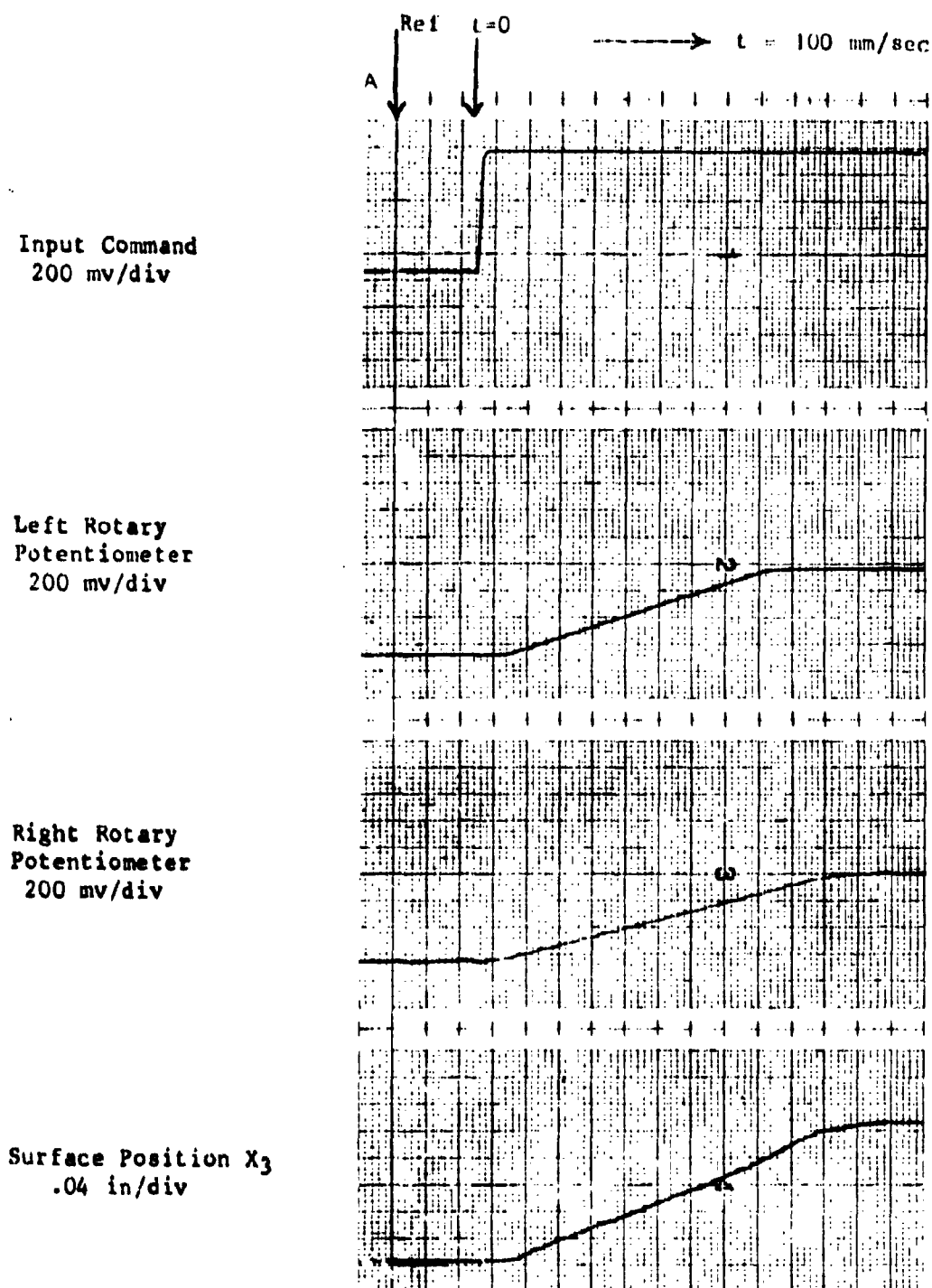


Figure IV-71. Saturation velocity - rotary potentiometer - X_1 .

Loaded Leading-Edge Test Results

General

For two reasons, only limited performance testing was performed on the leading-edge surface under loaded conditions. The first reason was because the surface loads for which the leading edge was designed were lower than the trailing edge (based upon the AIAA paper 80-1886R which stated that the hinge moments were assumed to not be in excess of one-third the trailing-edge hinge moments). Since 5-psi surface loading was used as the upper limit for the trailing-edge testing, a 2-psi maximum test load was used for the leading-edge testing. A lower load of 1 psi was also used as a test load for the leading edge, giving only two test load conditions.

The second reason was because the test results gave poor input-output characteristics. This was initially diagnosed as a problem with seal friction in the load actuators apparently dominating the applied load force characteristics of the load actuators and severely affecting the test results. Therefore, it was decided to truncate the loaded testing of the leading-edge surface and only limited test data was obtained. Subsequent analysis of the test data and test conditions (after completing all testing and removing the test section from the MASTR) determined that the test data obtained was not degraded by load-system characteristics. For example, three load actuators were used with the leading edge, each actuator loading one of the internal linkage assemblies. Each actuator was required to contribute 227 pounds of loading force for the 1-psi surface load and 454 pounds of loading force for the 2-psi surface load. The seal-friction force for the actuators (operating at 3000-psi supply pressure) varied from 15 to 35 pounds over the three actuators. This level of friction force was sufficiently low to not significantly affect the input-output performance measurements. In addition, the design vertical-load capability of the linkage (according analysis based upon data contained in AIAA paper 80-1886R) was 895 pounds at the load actuator attach points. The linkage design was therefore capable of easily overcoming load friction force levels of 15 to 35 pounds.

The loaded leading-edge test results in the following material are hysteresis, step, and frequency response measurements at surface loads of 1 and 2 psi. For the leading-edge linear actuator's response, only channel 2 of the actuator's LVDT was recorded.

Loaded Leading-Edge Hysteresis

Figures IV-72 through IV-75 show the 1-percent input hysteresis data taken on the leading edge under the 1- and 2-psi load conditions. Note that position X_3 , farthest away from the linear driving actuator, has only slight motion with the 1-psi load and essentially zero motion with the 2-psi load.

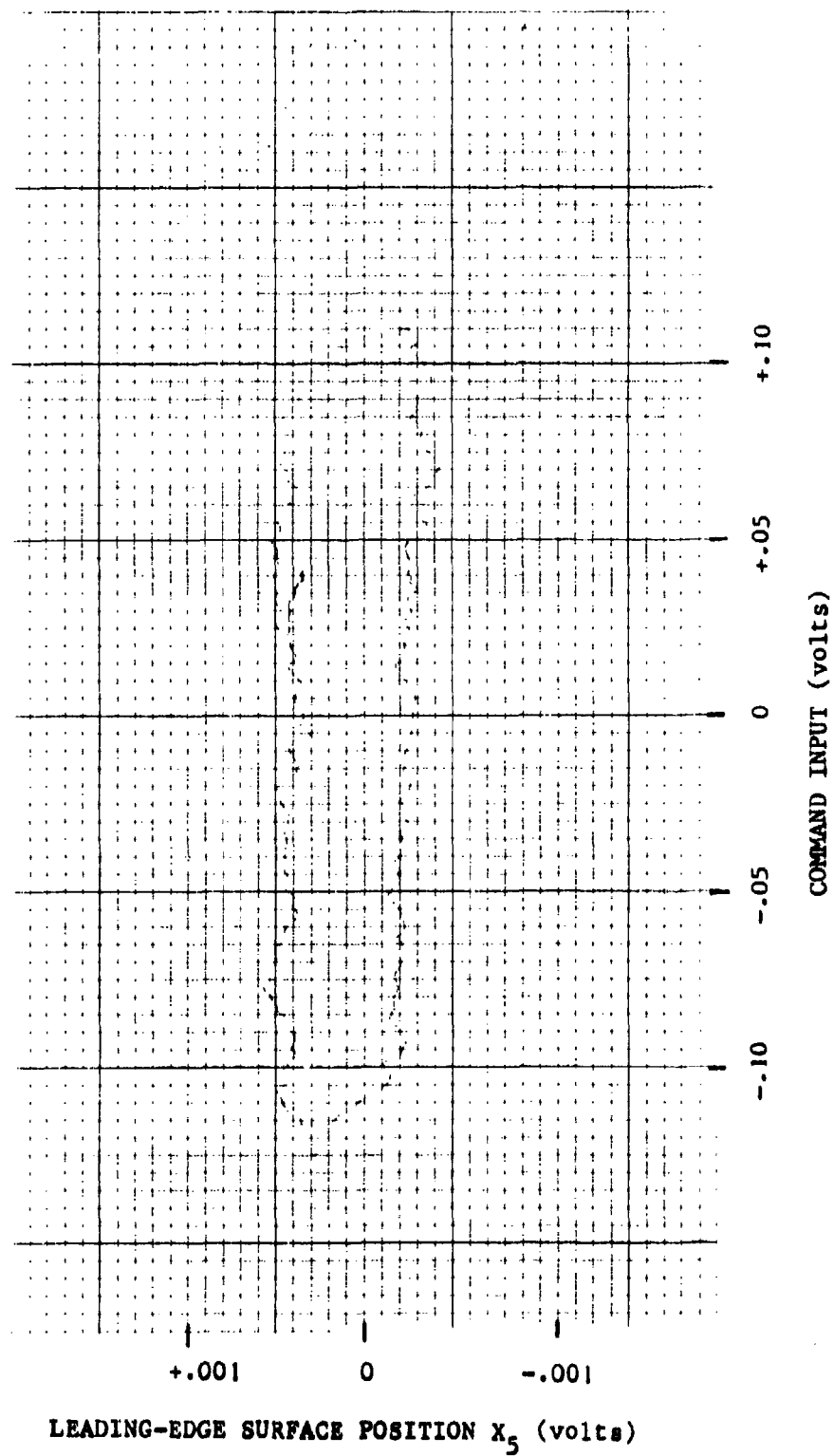


Figure IV-72. Hysteresis at 1-percent input - 1-psi load - motion point X_5 .

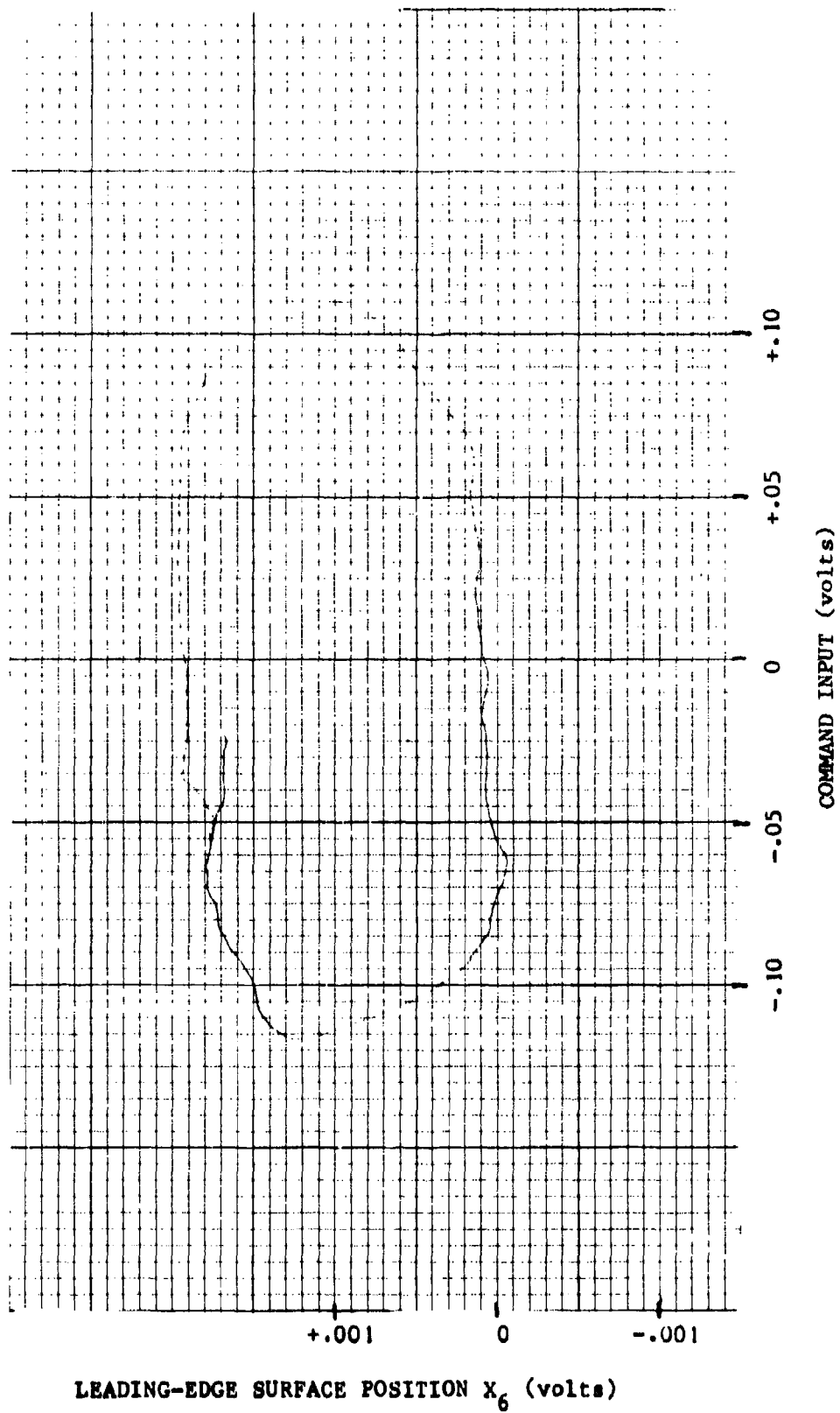


Figure IV-73. Hysteresis at 1-percent input - 1-psi load - motion point X_6 .

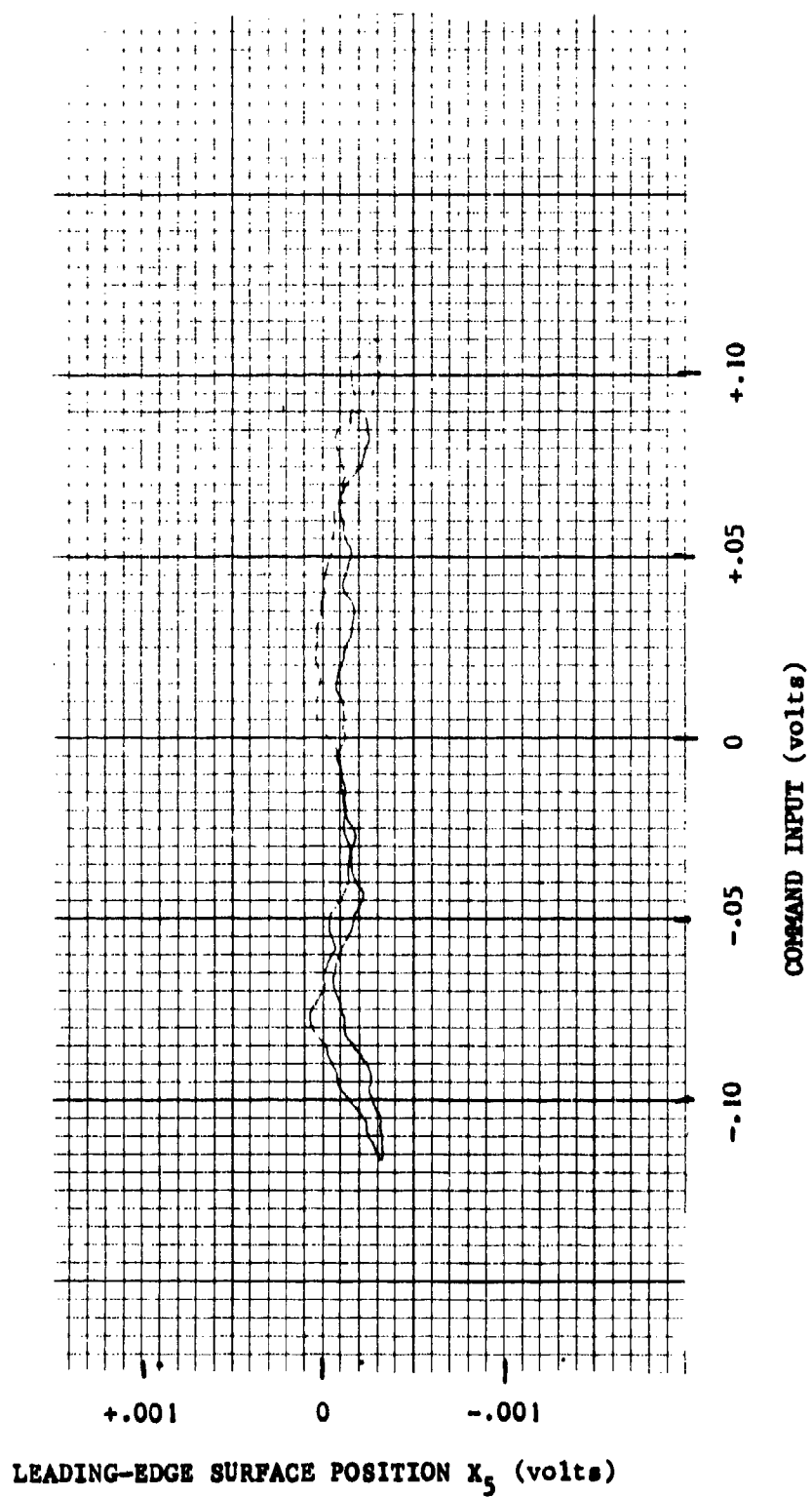


Figure IV-74. Hysteresis at 1-percent input - 2-psi load - motion point X_5 .

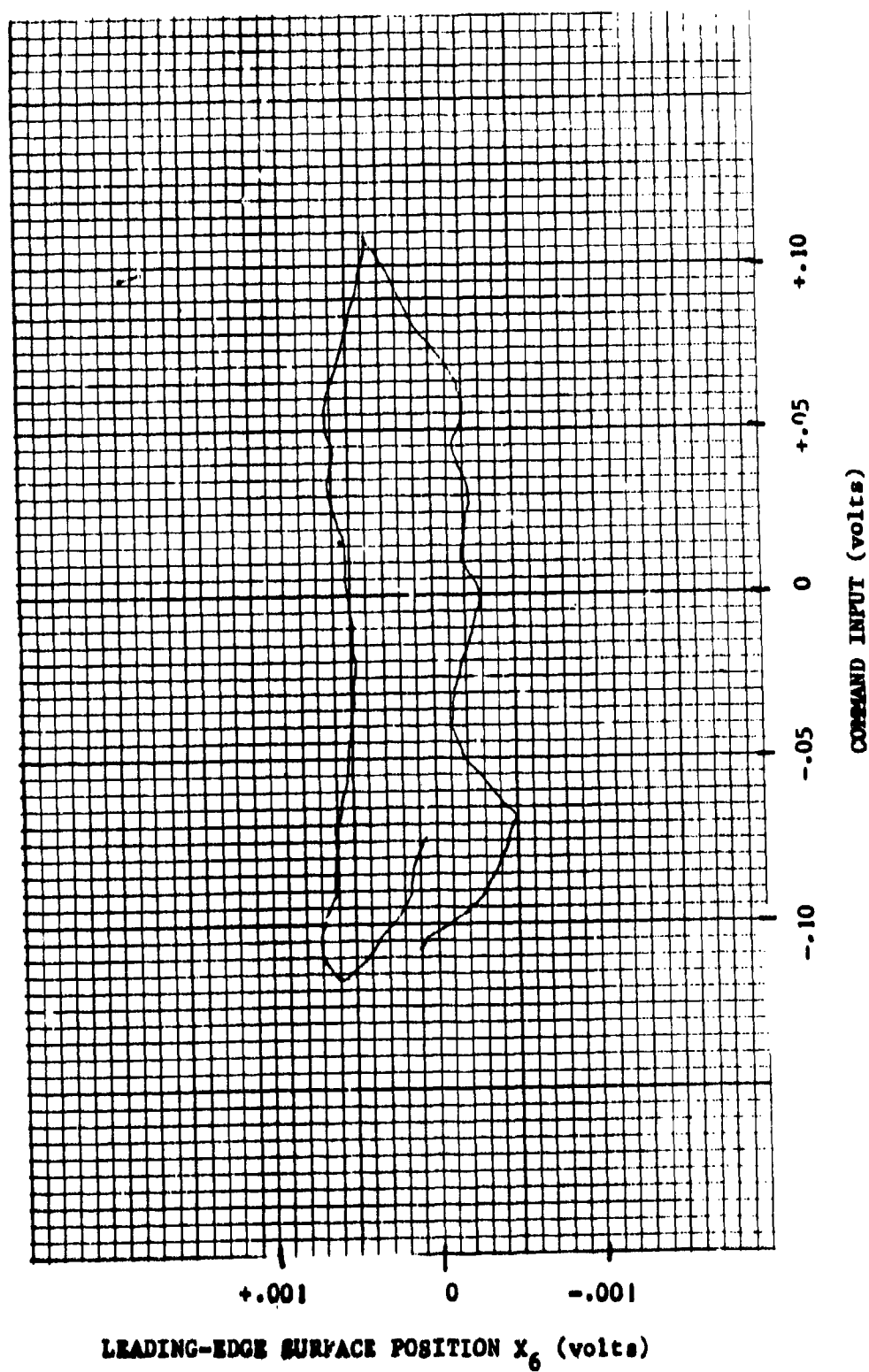


Figure IV-75. Hysteresis at 1-percent input - 2-psi load - motion point X_6 .

Position X_6 , closest to the linear driving actuator, exhibits less hysteresis and still maintains some motion with the 2-psi load condition. Tables IV-21 and IV-22 list the measured hysteresis for the two positions and the two load conditions. The test results indicate that the linkage operating characteristics do not transmit small amplitude motions under the load conditions used. Note that the hysteresis for each condition is similar, although X_6 moves more than X_5 . This is because of the hysteresis calculation being "the input change necessary to move a position point in one direction of motion to the same point in the other direction". For the 1-percent hysteresis loops, the motion points for the measurement calculation occurred only at direction reversal, giving very nearly 100-percent hysteresis for both loads and motion points.

Table IV-21. One-psi loaded leading-edge hysteresis for a 1-percent input.

Motion Point	% Full Command	% of 1% Command
X_5	0.98	98.0
X_6	0.97	97.0

Table IV-22. Two-psi loaded leading-edge hysteresis for a 1-percent input.

Motion Point	% Full Command	% of 1% Command
X_5	0.99	99.0
X_6	0.92	92.0

Loaded Leading-Edge Frequency Response

Frequency response of the loaded leading edge was measured with input levels of 3, 5, and 10 percent of the maximum command input. Figures IV-76 through IV-83 show some of the data recorded for the frequency response measurements. Data for motion points P_2 and X_6 are shown on the figures at input levels of 3 and 10 percent and for a surface load of 1 psi. This data is representative of that recorded for other input levels and surface loads. Tables IV-23 and IV-24 list the frequency response of motion points P_2 and X_6 for 1- and 2-psi loads respectively and the three input levels.

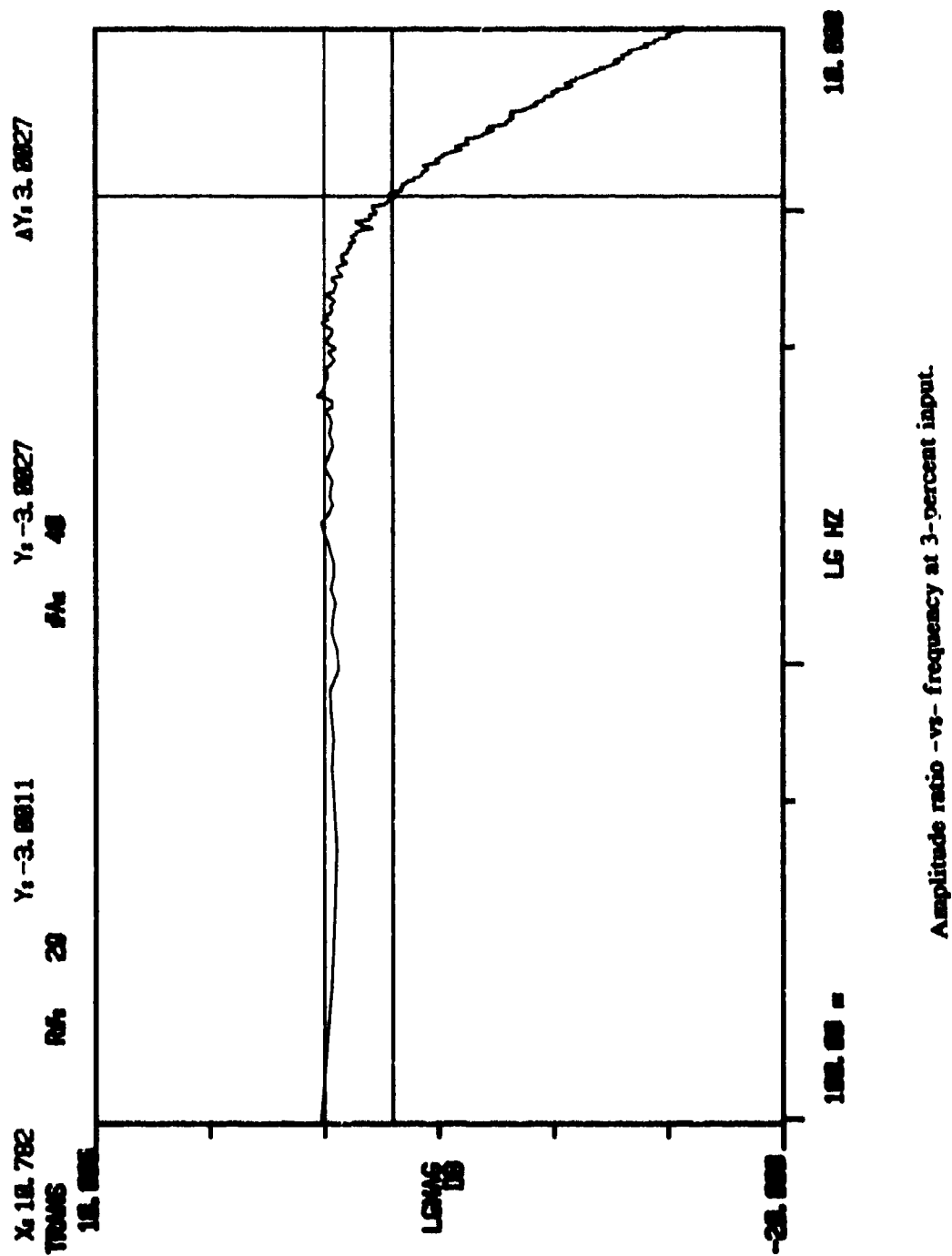


Figure IV-76. Leading-edge actuator - 1-psi load - position P₂.

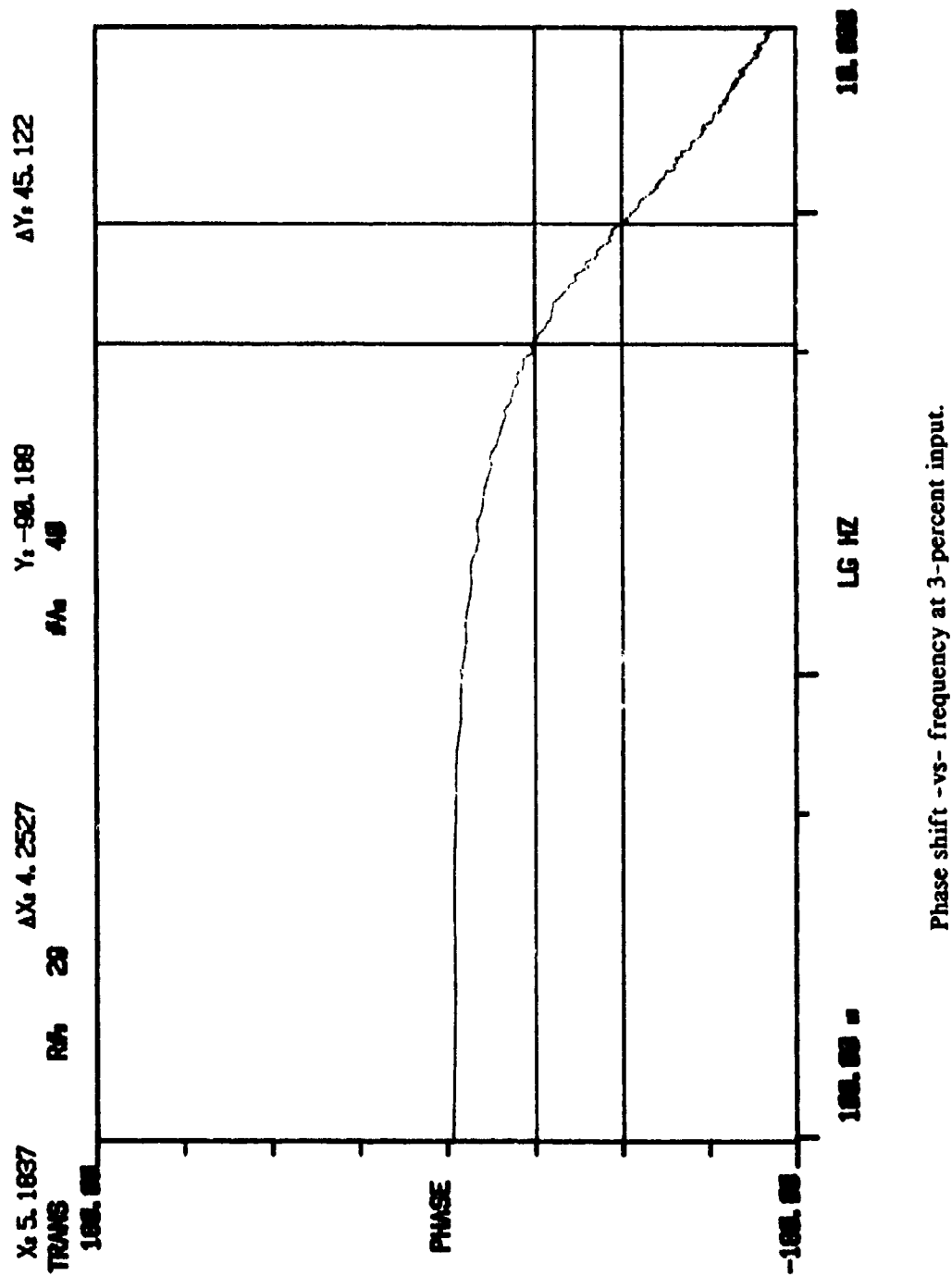
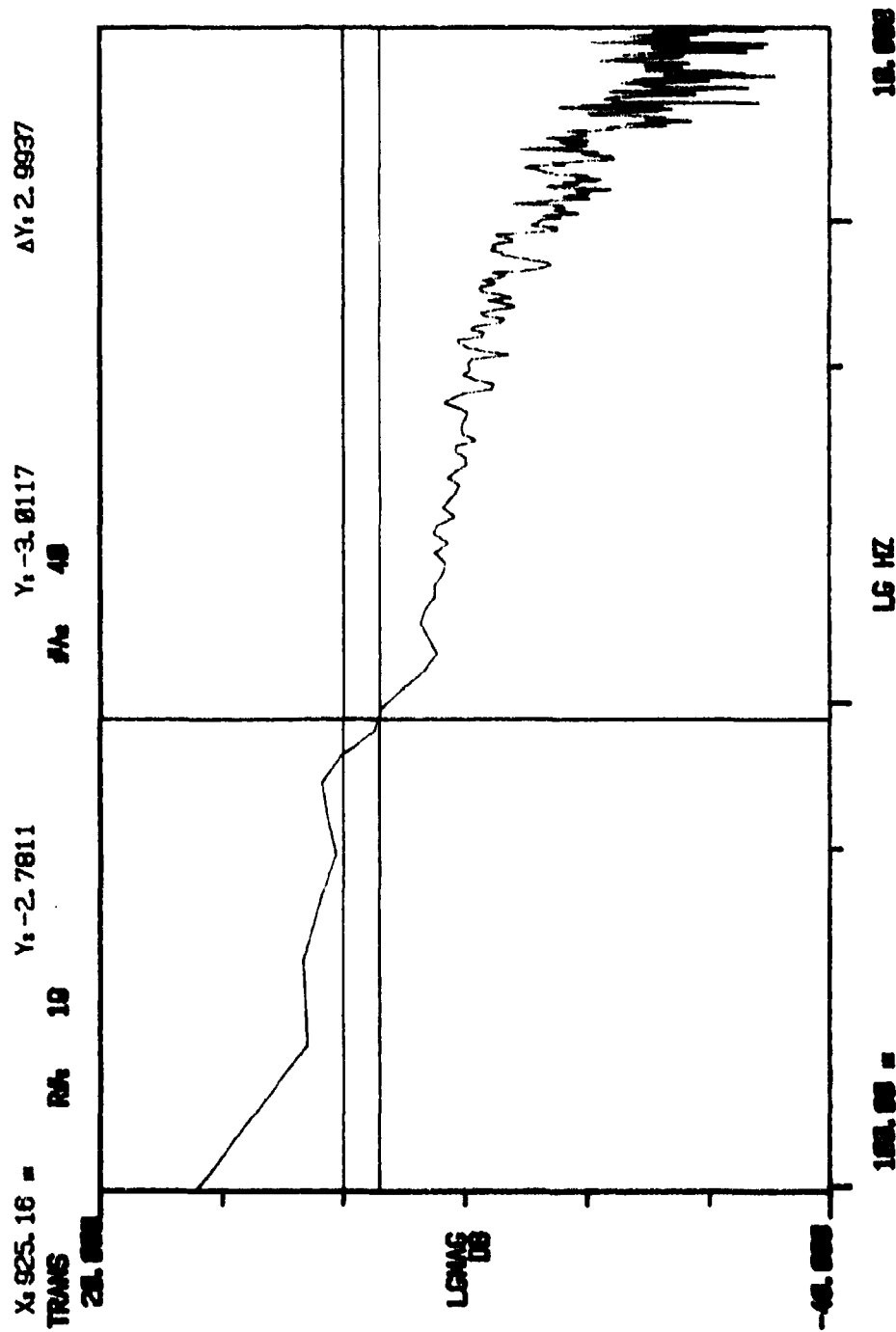


Figure IV-77. Leading-edge actuator - 1-psi load - position P_2 .



Amplitude ratio -vs- frequency at 3-percent input.

Figure IV-78. Leading-edge actuator - 1-psi load - position X_6 .

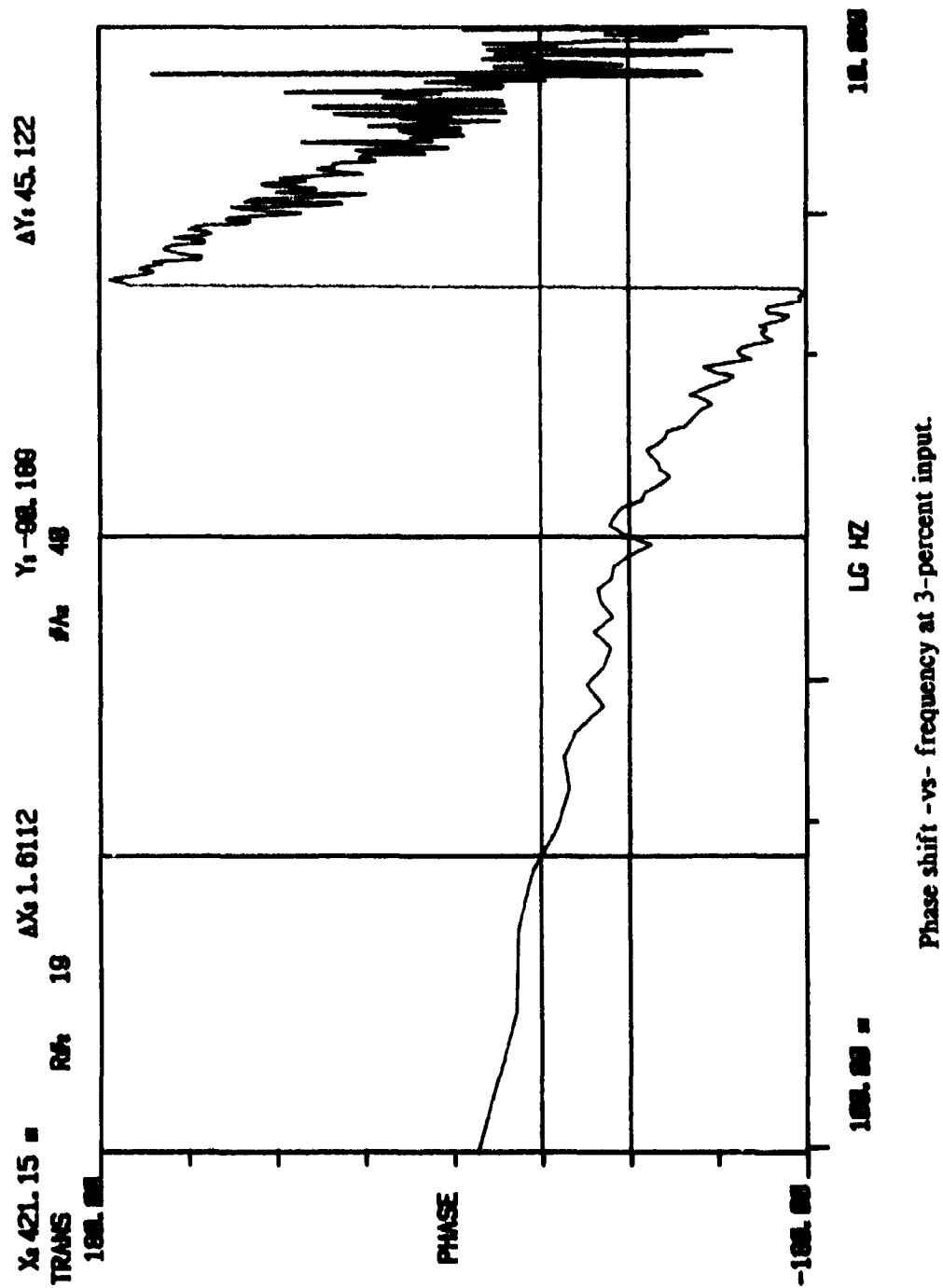


Figure IV-79. Leading-edge actuator - 1-psi load - position X_6 .

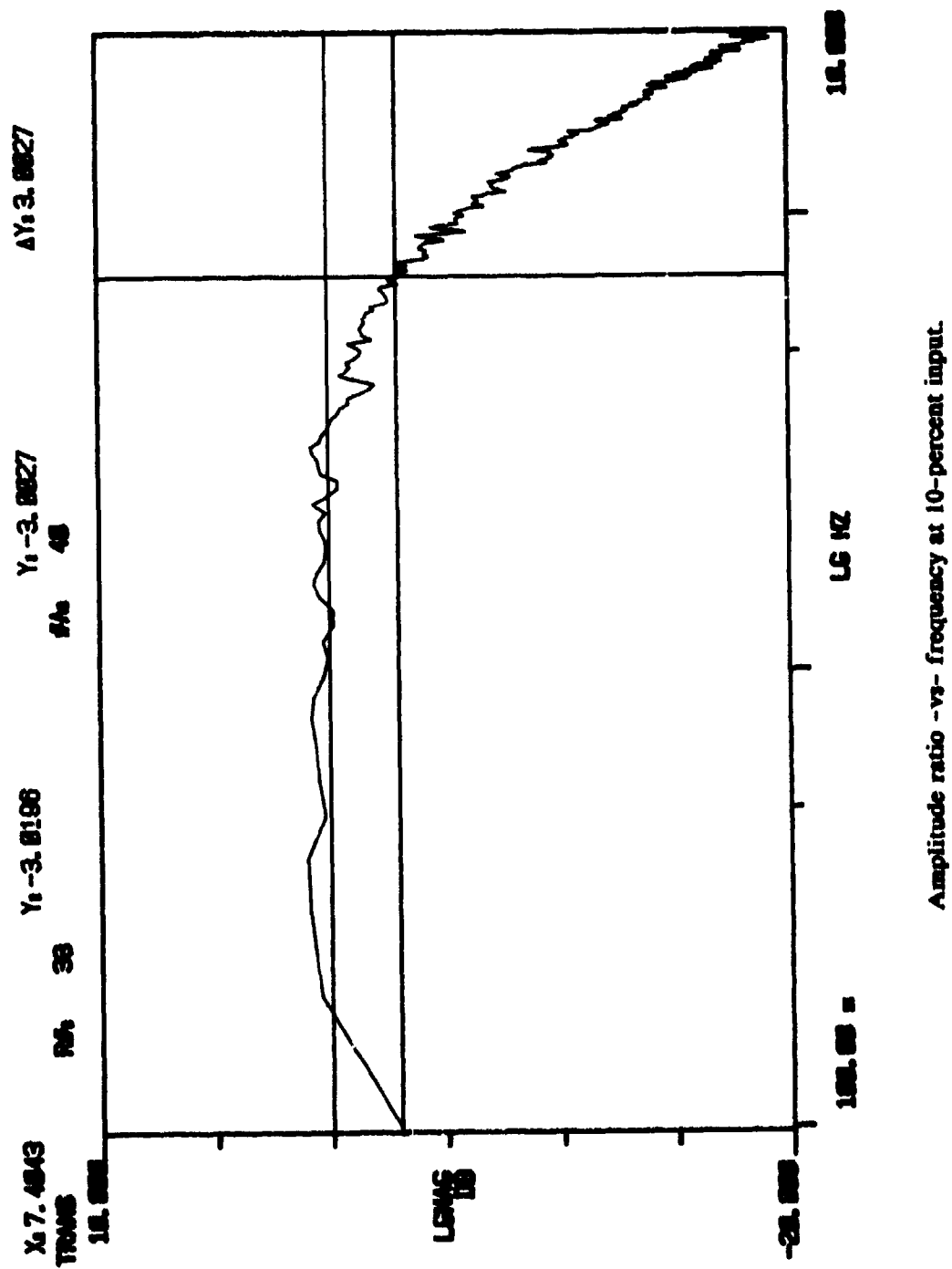


Figure IV-80. Leading-edge actuator - 1-psi load - position P₂.

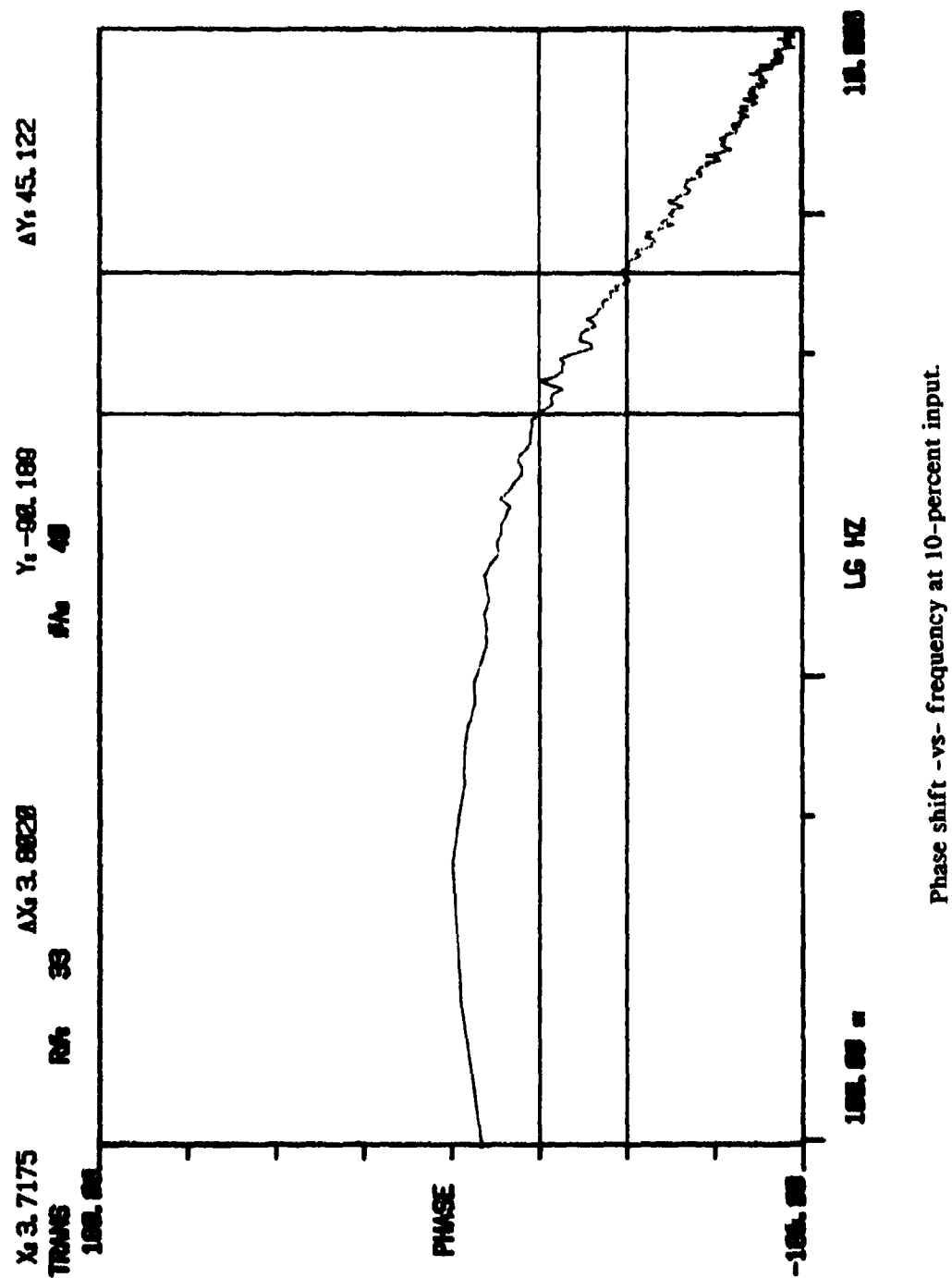


Figure IV-81. Leading-edge actuator - 1-psi load - position P_2 .

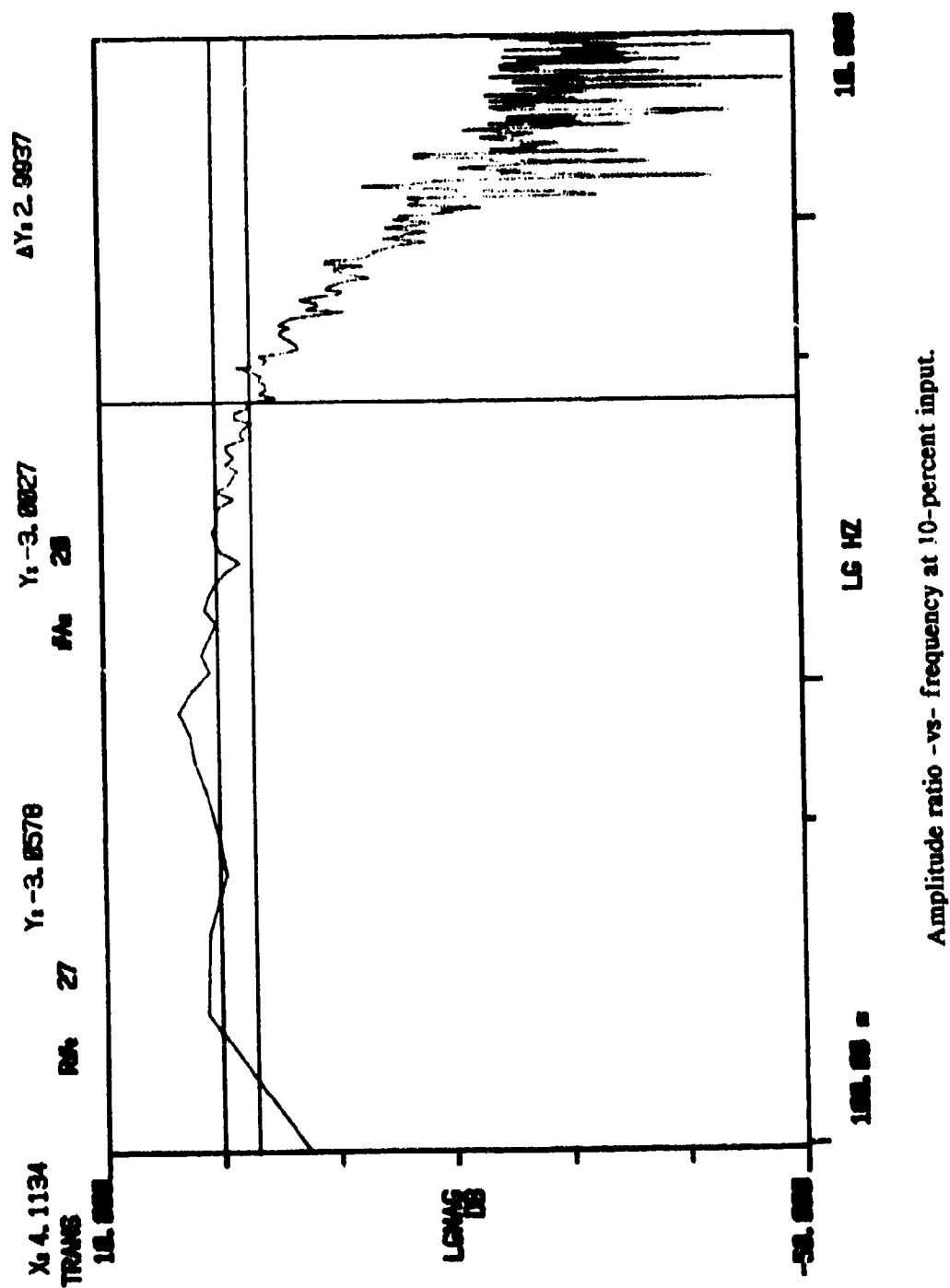
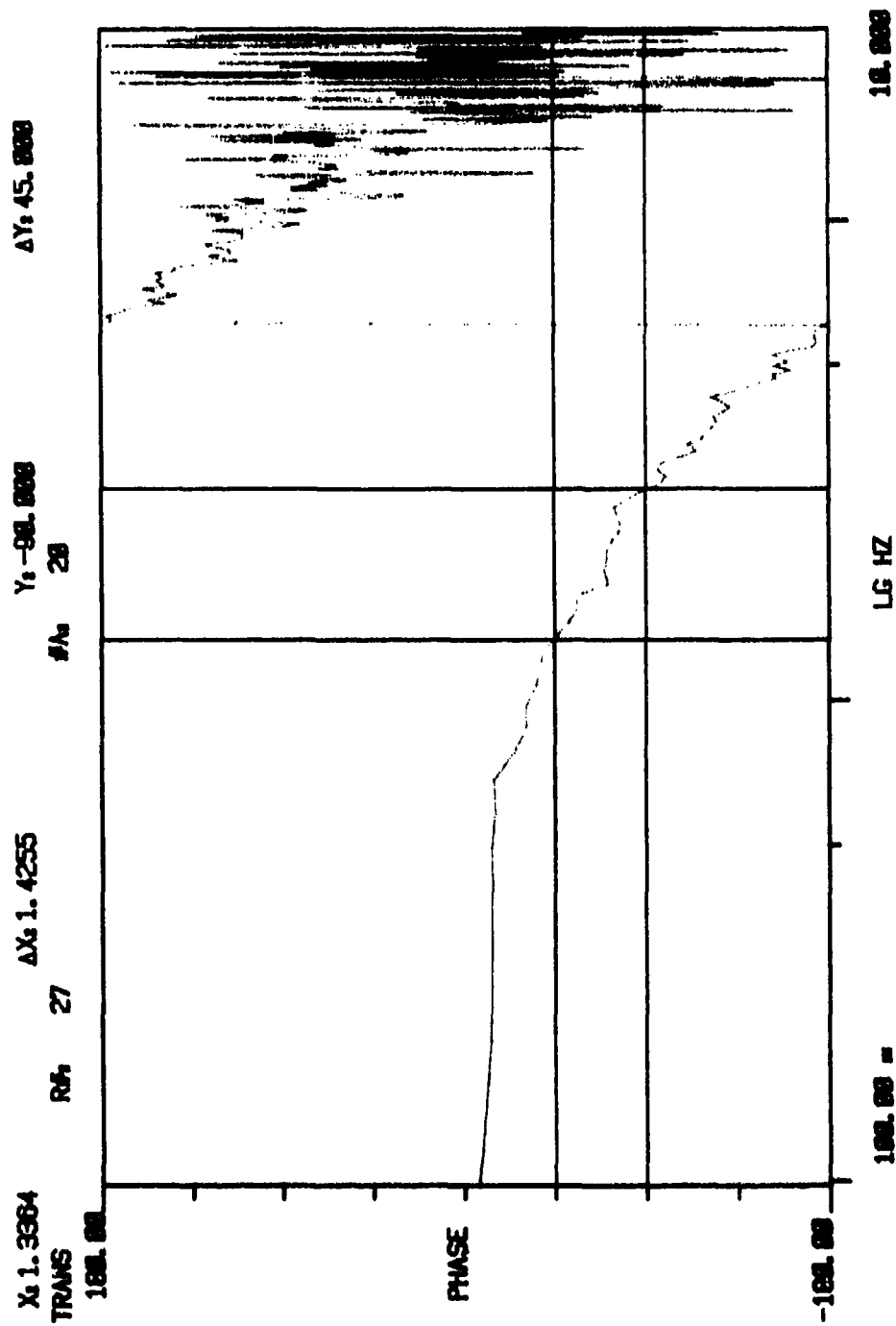


Figure IV-82. Leading-edge actuator - 1-psi load - position X_6 .



Phase shift -vs- frequency at 10-percent input.

Figure IV-83. Leading-edge actuator - 1-psi load - position X₆.

Table IV-23. Loaded leading-edge frequency response - 1 psi load.

Motion Point	Input Level (% Max. Com.)	-3 dB Freq. (Hz)	-45° Freq. (Hz)	-90° Freq. (Hz)
P ₂	3	10.8	5.2	9.5
X ₆	3	0.9	0.4	2.0
P ₂	5	10.4	5.0	9.6
X ₆	5	3.3	1.0	1.9
P ₂	10	7.4	3.7	7.5
X ₆	10	4.1	1.3	2.7

Table IV-24. Leading-edge loaded frequency response - 2 psi load.

Motion Point	Input Level (% Max. Com.)	-3 dB Freq. (Hz)	-45° Freq. (Hz)	-90° Freq. (Hz)
P ₂	5	9.8	5.1	9.5
X ₆	5	1.8	1.1	3.4
P ₂	10	7.1	3.7	7.3
X ₆	10	2.7	2.0	4.3

Note that as shown on Tables IV-23 and IV-24, changes in the load from 1 psi to 2 psi do not affect the response of the linear actuator (for the same input level). The degradation in response when the input level is increased to 10 percent of the maximum command from either 3 or 5 percent is to be expected. The degradation indicates that flow saturation of the control valve for the actuator is being reached at the higher frequencies of motion. Compared to the unloaded response measurements, the frequency response of the linear actuator was not changed by the 1- or 2- psi surface loads.

Note that for the 1-psi surface load, the frequency response of motion point X_6 (closest to the linear actuator) increases with each increase in input amplitude from 3 to 10 percent. This is consistent with the hysteresis measurements and indicates that the non-linearities of hysteresis (and threshold) effect the motion at low-level inputs. For the 2-psi surface load, as shown in Table IV-24, the frequency response of motion point X_6 is lower than that measured for a 1 psi surface load. The frequency response of motion point X_6 increases with an increase in input amplitude from 5 to 10 percent of maximum command.

The loaded frequency response measurements indicate that the leading-edge linkage mechanization did not transmit well the linear actuator's output motion to the surface position under load for low-amplitude (less than 10 percent) inputs and at high frequencies.

Loaded Leading-Edge Transient Response

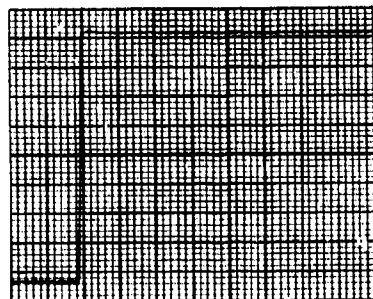
Figures IV-84 and IV-85 show the step response of position X_6 in response to the output of the linear actuator as measured by P_2 . The step response command to the actuator was 10 percent of the maximum command, or nominally 2.2 volts. As shown in these figures, the motion of X_6 shows some ratcheting in reaching the final position. Table IV-25 lists the values of transient response for the surface in terms of the time to start moving after the actuator output starts to move, the time to reach 63 percent of the final value after the surface point starts to move and the time to reach 100 percent of travel (after the actuator starts to move). The time for the start of motion for actuator outputs P_1 and P_2 is the time after application of the step input to the control system.

Test Item: General Dynamics
Mission Adaptive Wing

Date Prepared: 7/1/85

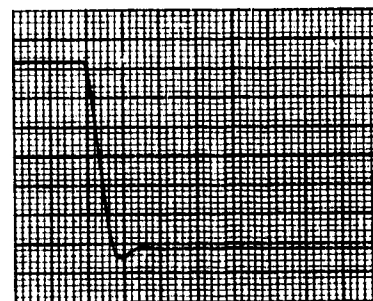
Test: Step Response - P_1 , X_5
Surface: Leading Edge
Load: 1-psi

Ad Inc. Cleveland, Ohio



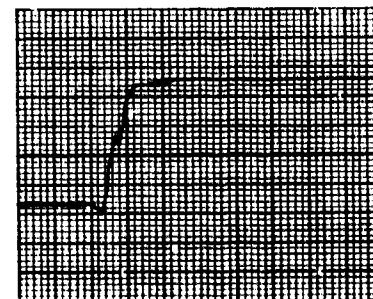
Input Command

50 mv/div



Position 1

.004 in/div

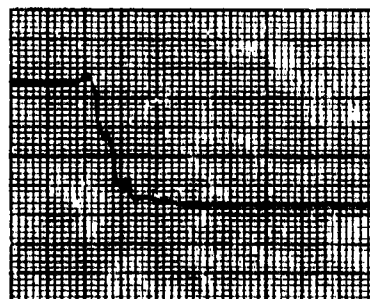
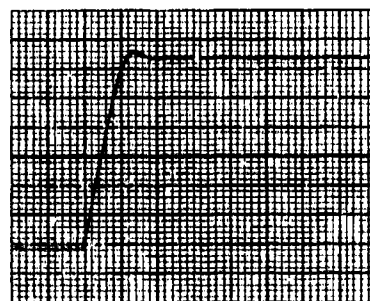
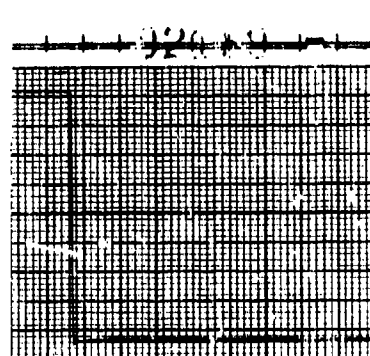


Position X_5

.025 in/div

----> t = 50 ms/div

SURFACE UP



----> t = 50 ms/div

SURFACE DOWN

Figure IV-84. Step response - 10-percent - 1-psi load - X_5 .

Test Item: General Dynamics
Mission Adaptive Wing

Date Prepared: 7/1/85

Test: Step Response - P_2 , X_6
Surface: Leading Edge
Load: 1-psi

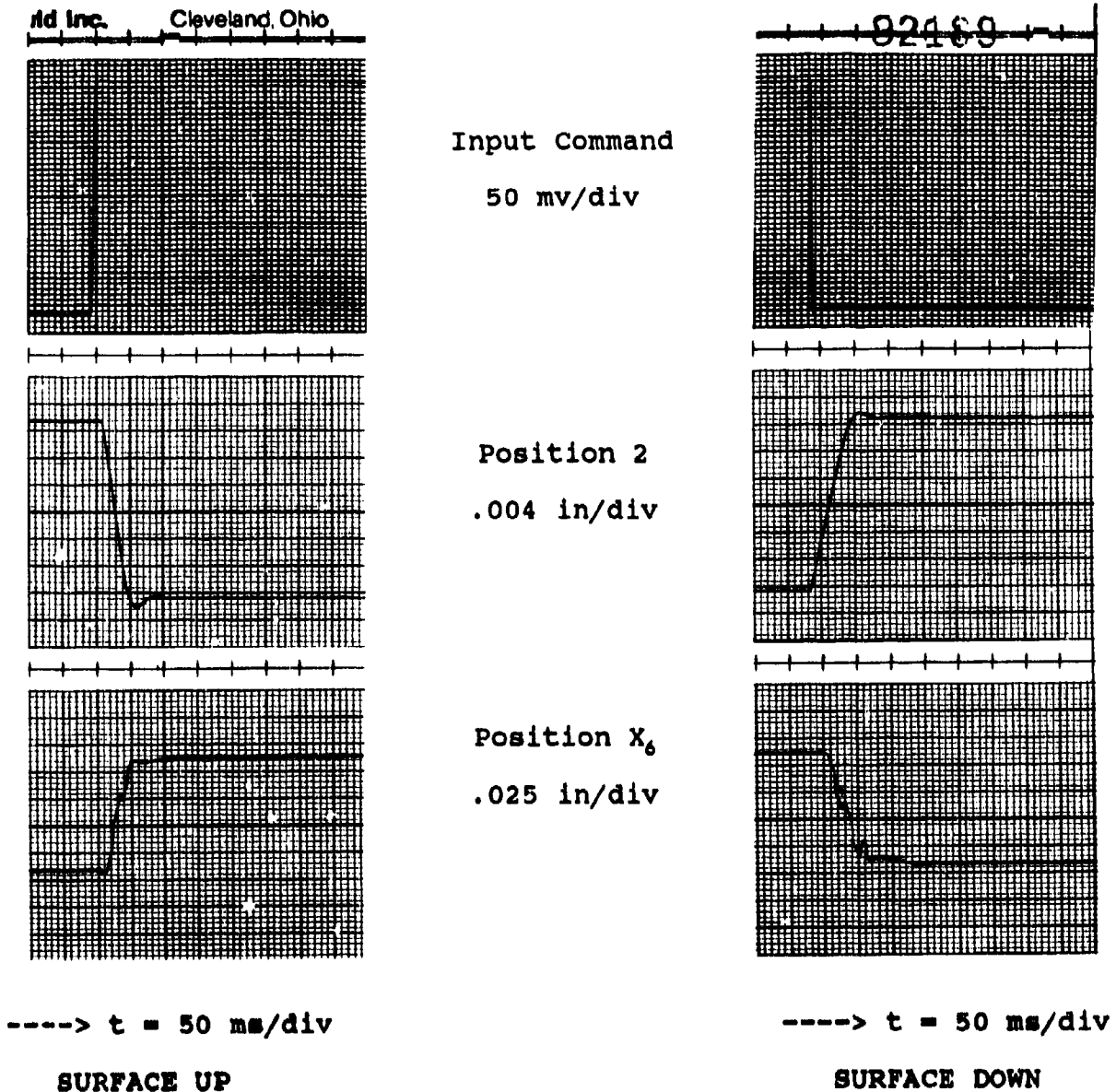


Figure IV-85. Step response - 10-percent - 2-psi load - X_6 .

Table IV-25. Loaded leading-edge transient step response.

Surface Up

Motion Point	Load (psi)	Time to Start Motion (sec)	Time to 63% of Travel (sec)	Time to 100% of Travel (sec)
P ₁	1	0.050	0.110	0.210
X ₅	1	0.040	0.140	0.300
P ₂	1	0.050	0.115	0.200
X ₆	1	0.060	0.150	0.250
P ₂	2	----	0.050	0.075
X ₆	2	0.035	0.033	0.090

Surface Down

Motion Point	Load (psi)	Time to Start Motion (sec)	Time to 63% of Travel (sec)	Time to 100% of Travel (sec)
P ₁	1	0.050	0.160	0.350
X ₅	1	0.020	0.250	0.500
P ₂	1	0.050	0.175	0.350
X ₆	1	0.050	0.250	0.510
P ₂	2	----	0.085	0.160
X ₆	2	0.048	0.055	0.105

Note that the time for the *surface down* motion is greater than the *surface up* motion because the load is opposing the *down* motion and *aiding* the up motion. Also note that the time for the actuator to reach its final position is longer than the time for the surface to reach its final position. This is due to the effect of the coupling linkage characteristics not transferring all of the driving actuator motion to surface motion.

Loaded Trailing-Edge Test Results

General

Performance measurements on the trailing-edge surface were recorded with applied loads of 1, 2 and 3 psi. Performance measurements with a 5-psi surface load were attempted. However, when making hysteresis measurements at that surface load, the output of the rotary potentiometer indicated that the gear-box load capacity had been reached. Therefore, testing with a 5-psi surface load was not conducted. No loaded linearity measurements were made because of stroke limitations on the loading actuators prevented operating the trailing edge over the full deflection range.

Loaded Trailing-Edge Static Threshold

Figures IV-86 through IV-88 show the data recorded for the 1-psi load threshold characteristics for the trailing edge. Note that on Figure IV-86, the left rotary potentiometer shows a periodic motion unrelated to the input command. This was caused by a low-amplitude limit cycle of the control system for the left truss. The limit cycle which developed during the test series evaluation occurred only at the 1-psi loading of the trailing edge. Figure IV-87 shows the start of the motion for mid-surface points X_1 and X_2 . Note that the left rotary potentiometer shows a mix of the input command and the limit cycle motion previously noted on Figure IV-86. Figure IV-88 shows the simultaneous motion of the rotary and surface points. Note that surface positions X_3 and X_4 are the last points to move.

Figures IV-89 through IV-92 show the data recorded for the 3-psi load threshold characteristics of the trailing edge. As shown in Figure IV-89, the left and right rotary potentiometers move with about the same input command level. Figures IV-90 and IV-91 show the mid-surface motions of X_1 and X_2 . Note that the limit cycle in the output of the left rotary potentiometer that was previously observed in the 1-psi data is gone. Figure IV-92 shows the edge-motion threshold of the surface. Note that the input level for start of motion is not much greater than for mid-position motion. This indicates that the effect of loading is to eliminate free-play in the trailing-edge truss mechanization.

Table IV-26 lists the static threshold values for the trailing edge. The threshold is grouped by the surface loads.

Test Item - General Dynamics
Mission Adaptive Wing

Date
Prepared: 4/30/87

Test - Static Threshold
Surface - Trailing Edge
Load - 1 lb/in²



Input Command
1 mv/div

Left Rotary Potentiometer
5 mv/div

Right Rotary Potentiometer
1 mv/div

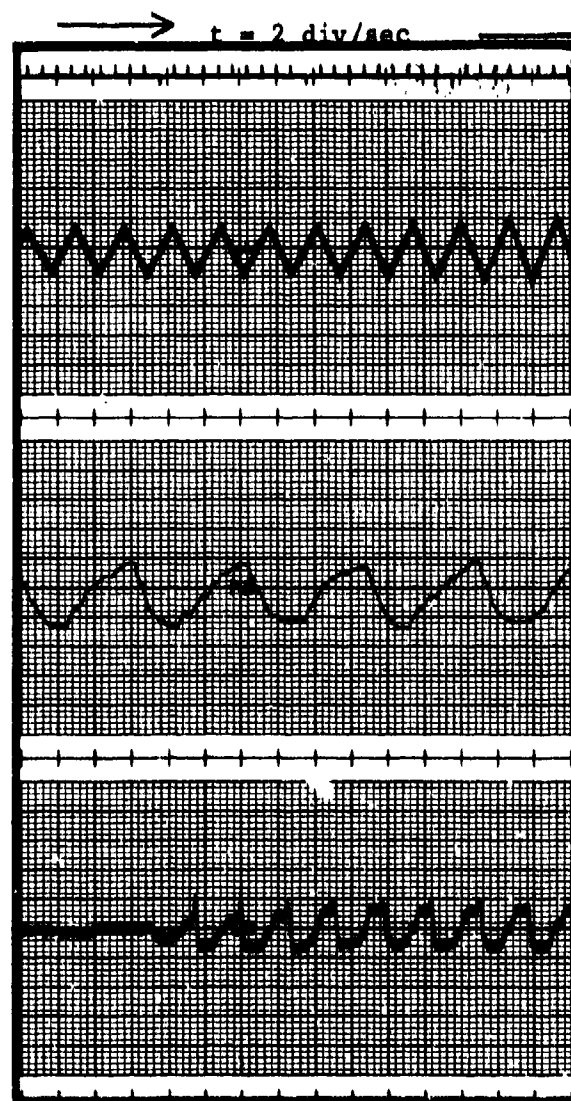


Figure IV-86. Loaded trailing-edge static threshold - 1-psi load - left and right rotary motion.

Test Item - General Dynamics
Mission Adaptive Wing

Date
Prepared: 4/30/87

Test - Static Threshold
Surface - Trailing Edge
Load - 1 lb/in²

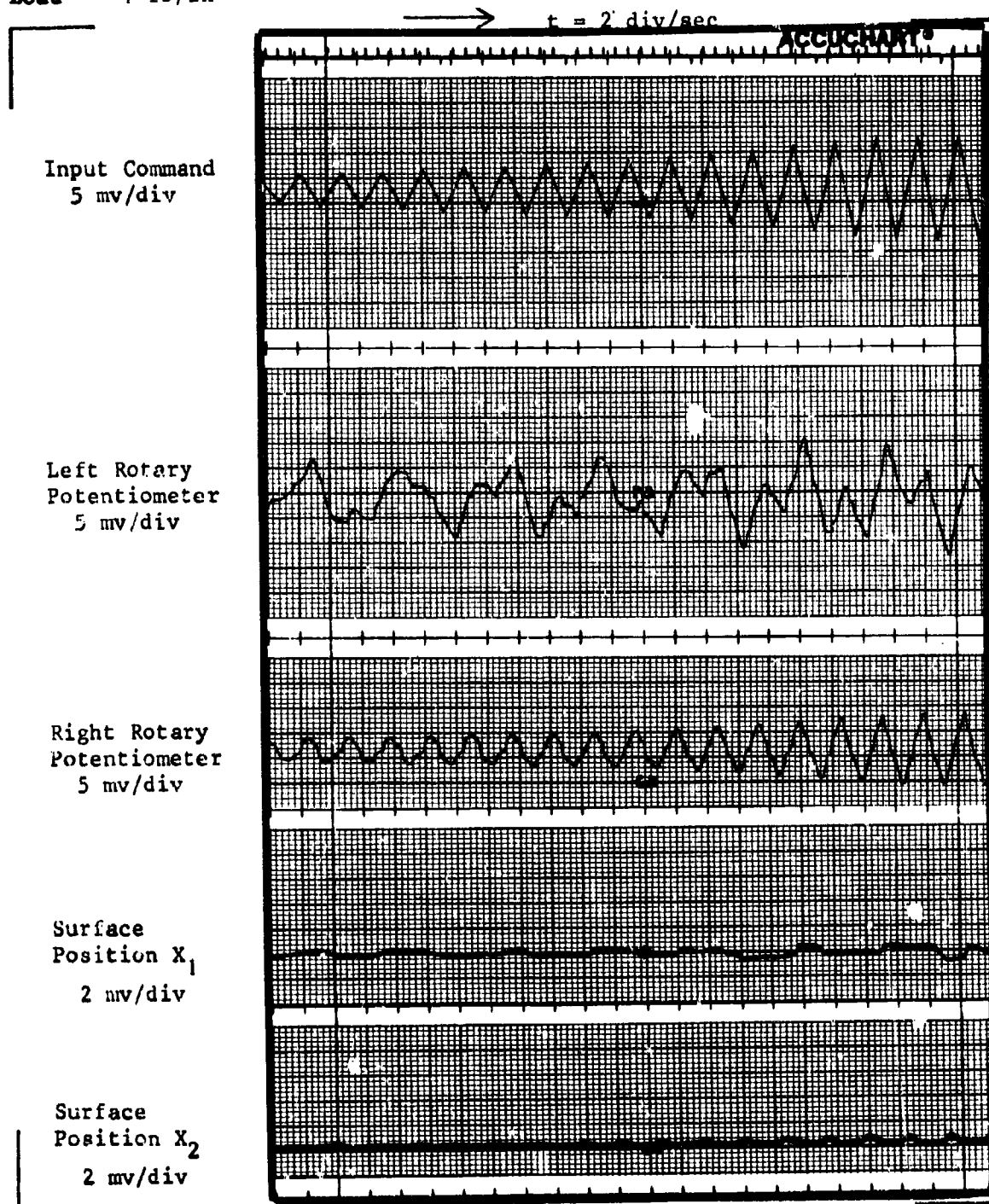


Figure IV-87. Loaded trailing-edge static threshold - 1-psi load - left and right rotary - X_1 and X_2 motion.

Test Item - General Dynamics
Mission Adaptive Wing

Date
Prepared: 5/1/87

Test - Static Threshold
Surface - Trailing Edge
Load - 1 lb/in²

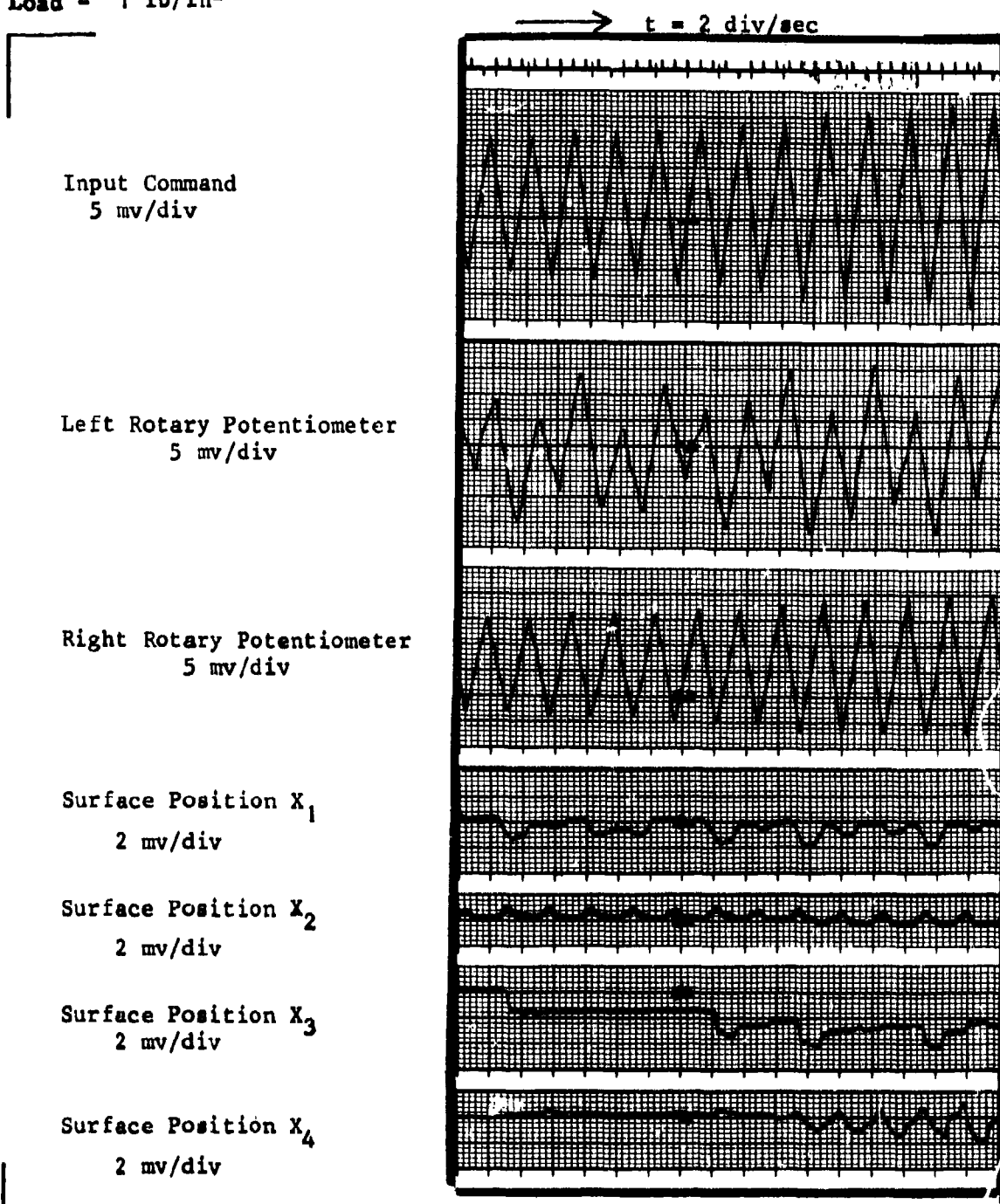


Figure IV-88. Loaded trailing-edge static threshold - 1-psi load - left and right rotary - X_1 , X_2 , X_3 , and X_4 motion.

Test Item - General Dynamics
Mission Adaptive Wing

Date
Prepared: 5/4/87

Test - Static Threshold
Surface - Trailing Edge
Load - 3 lb/in²

Input Command
1 mv/div

Left Rotary Potentiometer
2 mv/div

Right Rotary Potentiometer
2 mv/div

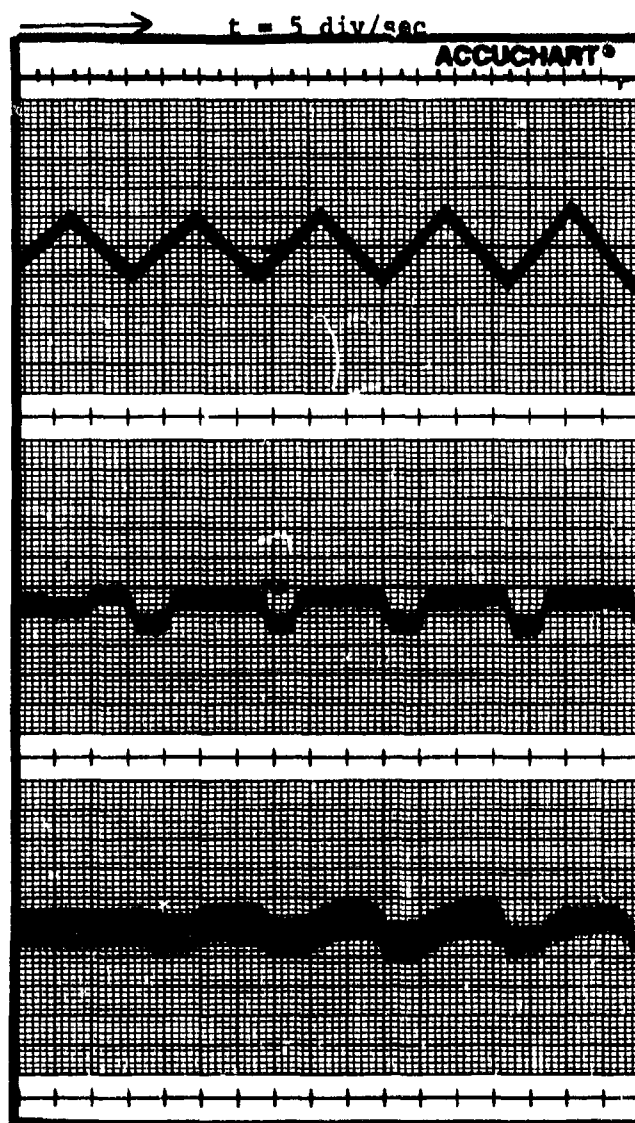


Figure IV-89. Loaded trailing-edge static threshold - 3-psi load - left and right rotary motion.

Test Item - General Dynamics
Mission Adaptive Wing

Date
Prepared: 5/4/87

Test -- Static Threshold
Surface - Trailing Edge
Load - 3 lb/in²

Input Command
5 mv/div

Left Rotary Potentiometer
10 mv/div

Right Rotary Potentiometer
10 mv/div

Surface Position X₁
2 mv/div

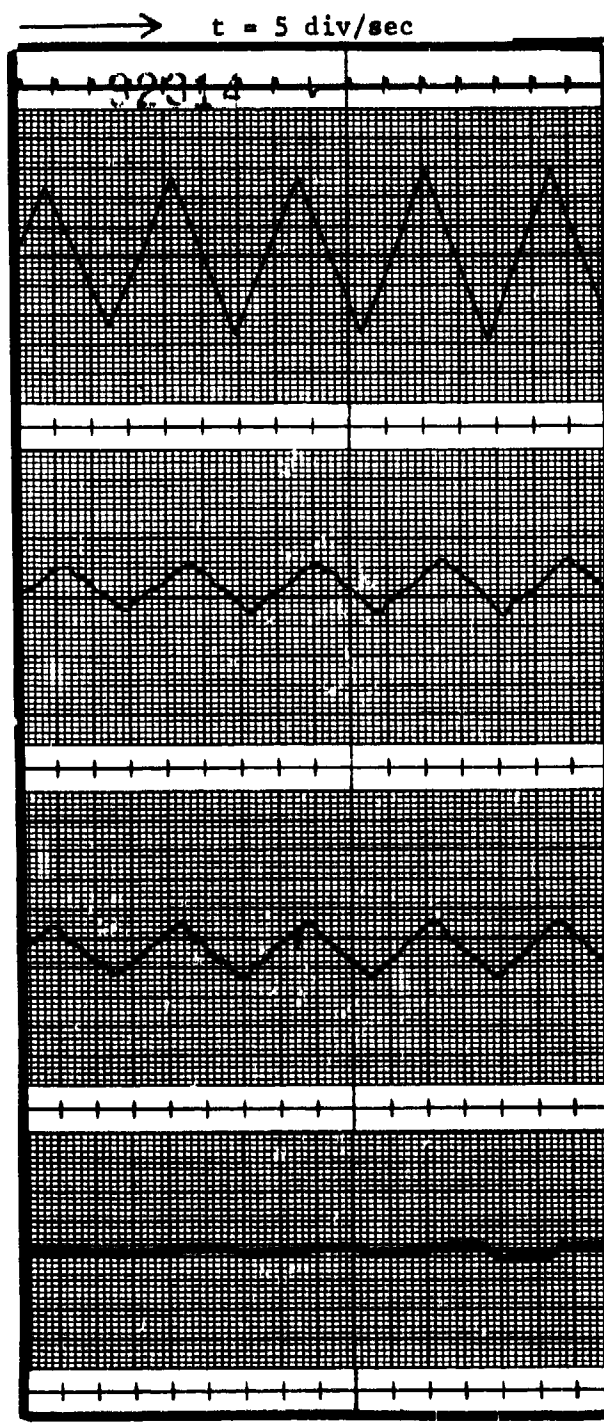


Figure IV-90. Loaded trailing-edge static threshold - 3-psi load - X₁ motion.

Test Item - General Dynamics
Mission Adaptive Wing

Date
Prepared: 5/4/87

Test - Static Threshold
Surface - Trailing Edge
Load - 3 lb/in²

Input Command
2 mv/div

Left Rotary Potentiometer
5 mv/div

Right Rotary Potentiometer
5 mv/div

Surface Position X_4
2 mv/div

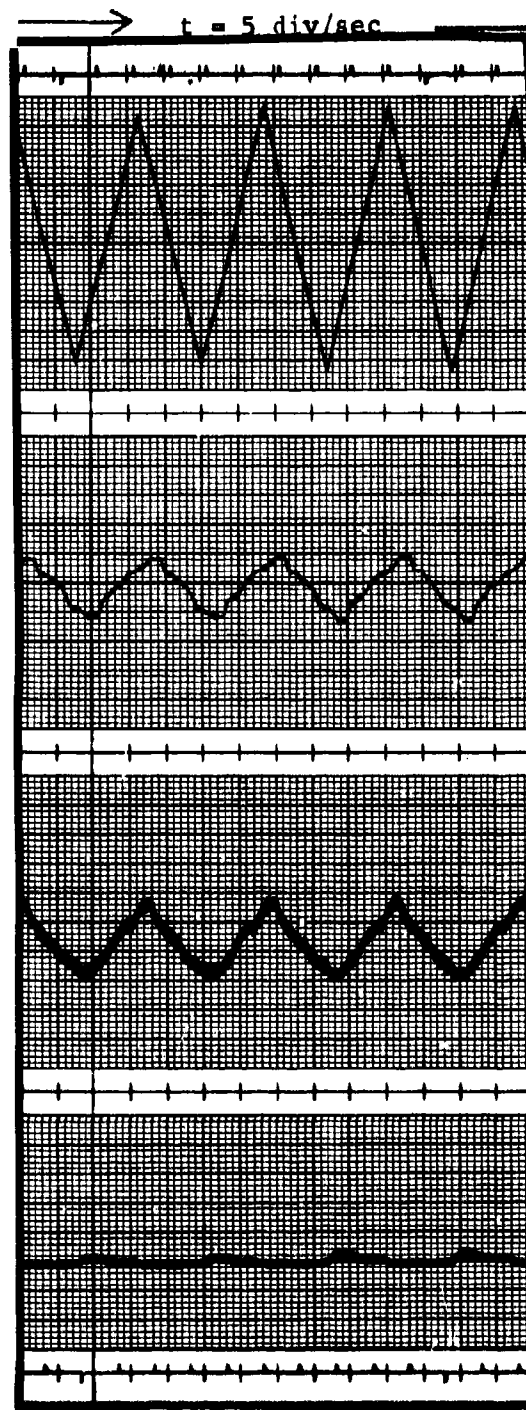


Figure IV-91. Loaded trailing-edge static threshold - 3-psi load - X_2 motion.

Test Item - General Dynamics
Mission Adaptive Wing

Date 5/4/87
Prepared: _____

Test - Static Threshold
Surface - Trailing Edge
Load - 3 lb/in²

Input Command
5 mv/div

Left Rotary Potentiometer
10 mv/div

Right Rotary Potentiometer
10 mv/div

Surface Position X_1
2 mv/div

Surface Position X_2
2 mv/div

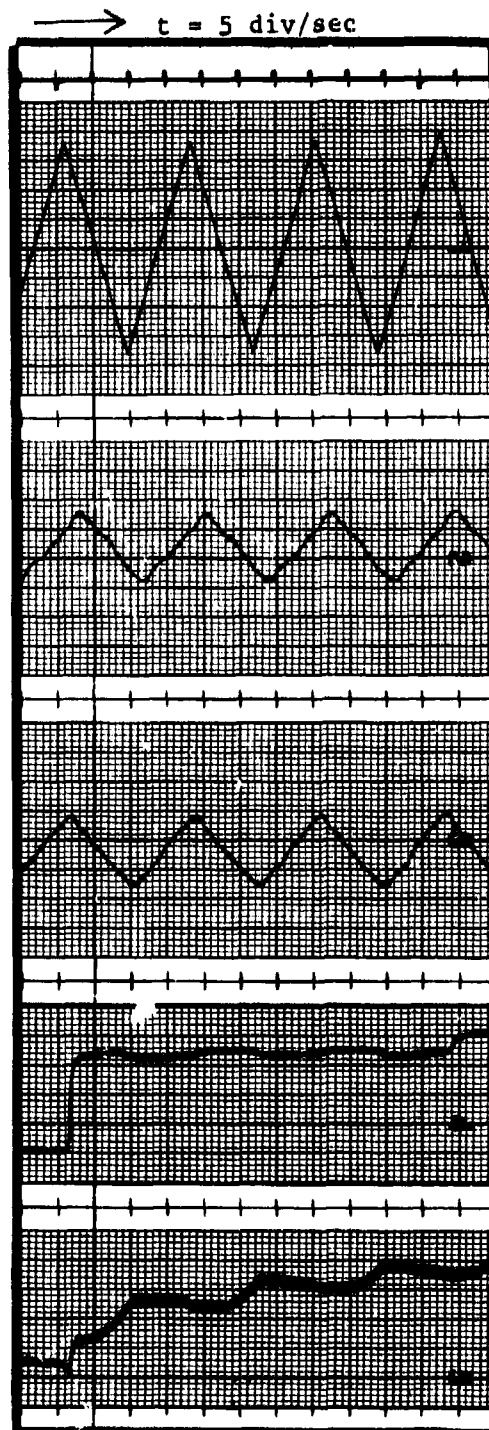


Figure IV-92. Loaded trailing-edge static threshold - 3-psi load - X_3 , X_4 motion.

Table IV-26. Static threshold - loaded trailing-edge.

Load (psi)	Motion Point	Threshold (pk volts)	% Max Rate Command	% Max Position Command
1.0	Left Rotary Potentiometer	0.023	0.983	0.403
	Right Rotary Potentiometer	0.005	0.198	0.081
	X₁	0.043	1.848	0.758
	X₂	0.038	1.629	0.668
	X₃	0.078	3.390	1.390
	X₄	0.078	3.390	1.390
2.0	Left Rotary Potentiometer	0.005	0.195	0.080
	Right Rotary Potentiometer	0.006	0.239	0.098
	X₁	0.050	2.173	0.891
	X₂	0.055	2.391	0.980
	X₃	0.075	3.261	1.337
	X₄	0.075	3.261	1.337
3.0	Left Rotary Potentiometer	0.004	0.173	0.071
	Right Rotary Potentiometer	0.004	0.173	0.071
	X₁	0.065	2.826	1.158
	X₂	0.041	1.783	0.731
	X₃	0.090	3.913	1.604
	X₄	0.090	3.913	1.604

Note that the static threshold as listed in the preceding tables, is not greatly changed with increasing surface load.

Loaded Trailing-Edge Dynamic Threshold

Figures IV-93 through IV-98 show the data recorded for the dynamic threshold measurements of the trailing edge with 1 psi and 3 psi surface loading. A sinusoidal input of 1.5 Hz was used for the dynamic threshold measurement and appears on each of the figures. Figure IV-93 for the 1 psi load, the left rotary potentiometer output shows the same limit cycle (at nominally 0.2 Hz) that existed with the same load and the static threshold measurements. The higher surface load of 3 psi eliminates the limit cycle of the left truss. Table IV-27 lists the dynamic threshold for each of the motion points and surface loads of 1, 2, and 3 psi.

Note that the dynamic thresholds of the surface positions X_1 , X_2 , X_3 and X_4 are lower for the 2-psi load than for either the 1- or 3-psi load. The surface-position dynamic thresholds are not greatly changed with increasing surface load. The dynamic threshold of the rotary potentiometers increases with increasing surface load. Any change in the dynamic threshold of the surface positions with load can be attributed to the friction loads in the truss which are associated with the surface load. As shown on Table IV-27, there is less surface threshold for the 3-psi surface loads than for the 1-psi loads. This indicates that the surface loading eliminates free-play from the truss mechanization and the internal friction forces are low enough to not effect the motion threshold of the truss.

Test Item - General Dynamics
Mission Adaptive Wing

Date
Prepared: 5/4/87

Test - Dynamic Threshold
Surface - Trailing Edge
Load - 1 lb/in²



Input Command
2 mv/div

Left Rotary Potentiometer
2 mv/div

Right Rotary Potentiometer
2 mv/div

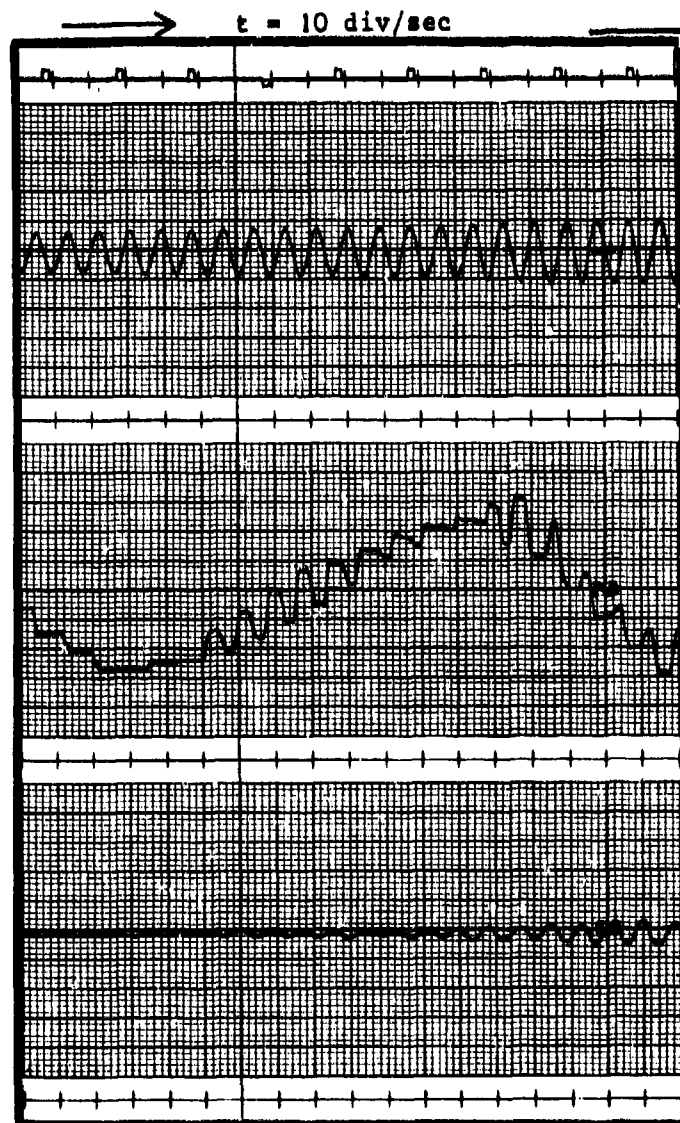


Figure IV-93. Loaded trailing-edge dynamic threshold - 1-psi load - left and right rotary motion.

Test Item - General Dynamics
Mission Adaptive Wing

Date
Prepared: 5/5/87

Test - Dynamic Threshold
Surface - Trailing Edge
Load - 1 lb/in²

Input Command
5 mv/div

Left Rotary Potentiometer
5 mv/div

Right Rotary Potentiometer
5 mv/div

Surface Position X_1
2 mv/div

Surface Position X_2
2 mv/div

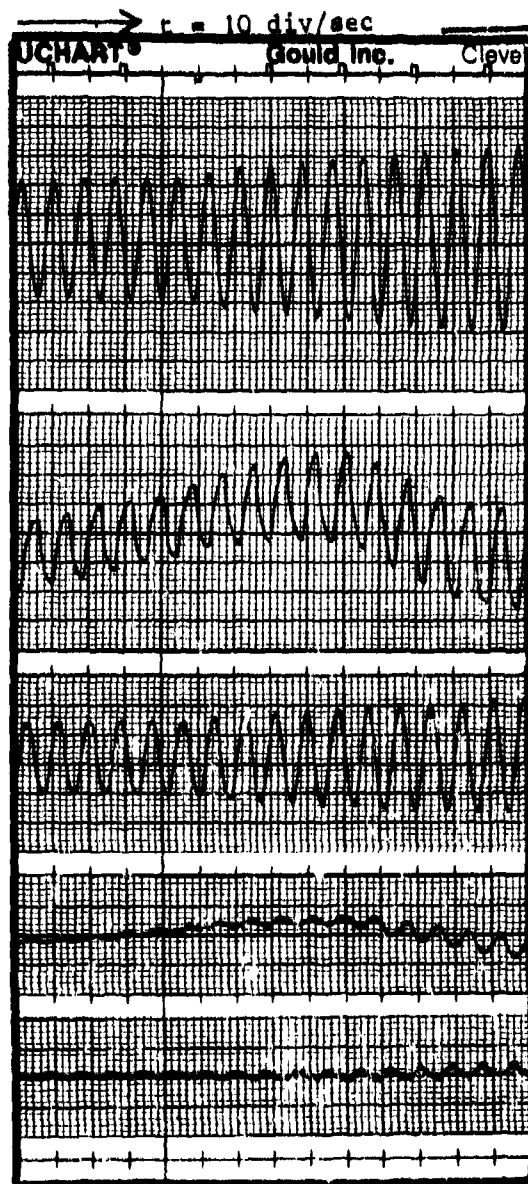


Figure IV-94. Loaded trailing-edge dynamic threshold - 1-psi load - X_1 , X_2 motion.

Test Item - General Dynamics
Mission Adaptive Wing

Date
Prepared: 5/5/87

Test - Dynamic Threshold
Surface - Trailing Edge
Load - 1 lb/in²

Input Command
10 mv/div

Left Rotary Potentiometer
10 mv/div

Right Rotary Potentiometer
10 mv/div

Surface Position X_1
2 mv/div

Surface Position X_2
2 mv/div

Surface Position X_3
2 mv/div

Surface Position X_4
2 mv/div

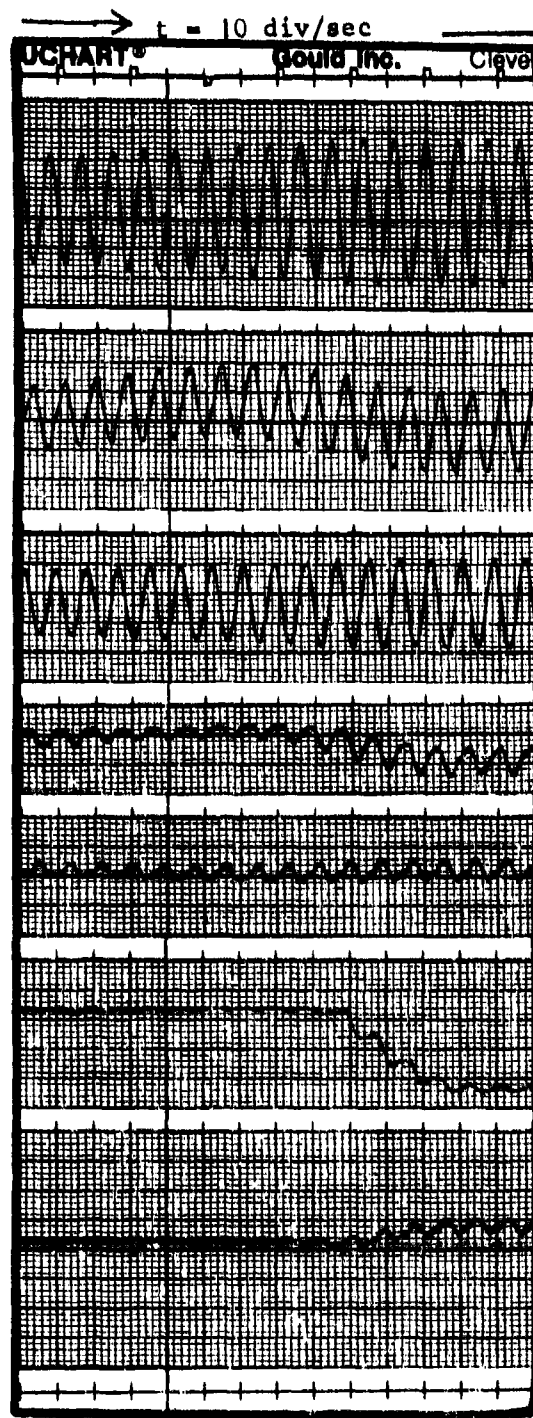


Figure IV-95. Loaded trailing-edge dynamic threshold - 1-psi load - X_1 , X_2 , X_3 , X_4 motion.

Test Item - General Dynamics
Mission Adaptive Wing

Date
Prepared: 5/6/87

Test - Dynamic Threshold
Surface - Trailing Edge
Load - 3 lb/in²

Input Command
2 mv/div

Left Rotary Potentiometer
2 mv/div

Right Rotary Potentiometer
2 mv/div

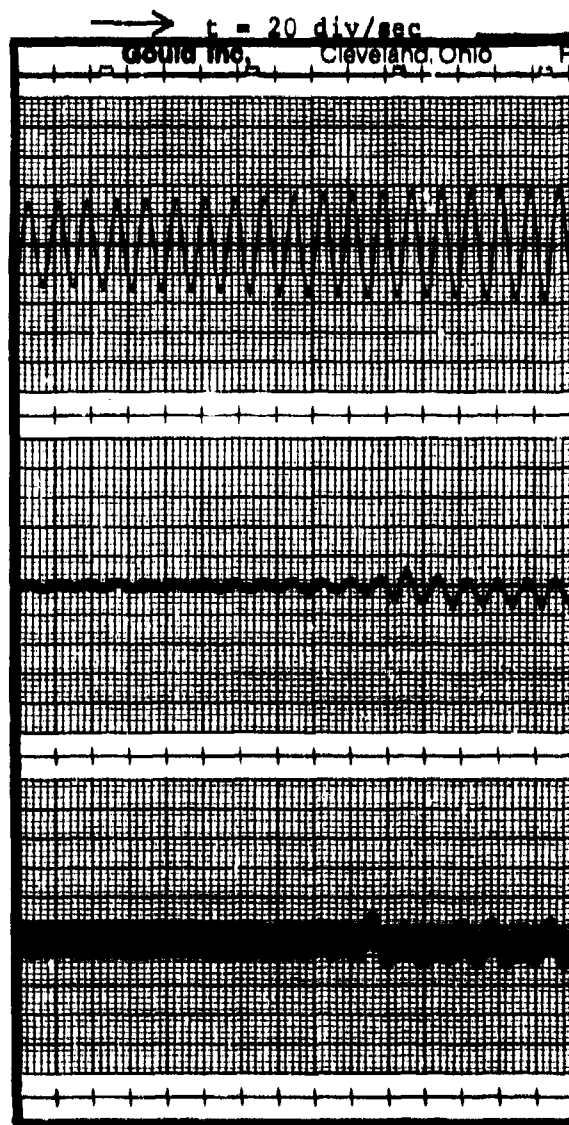


Figure IV-96. Loaded trailing-edge dynamic threshold - 3-psi load - left and right rotary motion.

Test Item - General Dynamics
Mission Adaptive Wing

Date
Prepared: 5/6/87

Test - Dynamic Threshold
Surface - Trailing Edge
Load - 3 lb/in²

Input Command
2 mv/div

Left Rotary Potentiometer
2 mv/div

Right Rotary Potentiometer
2 mv/div

Surface Position X_1
2 mv/div

Surface Position X_2
2 mv/div

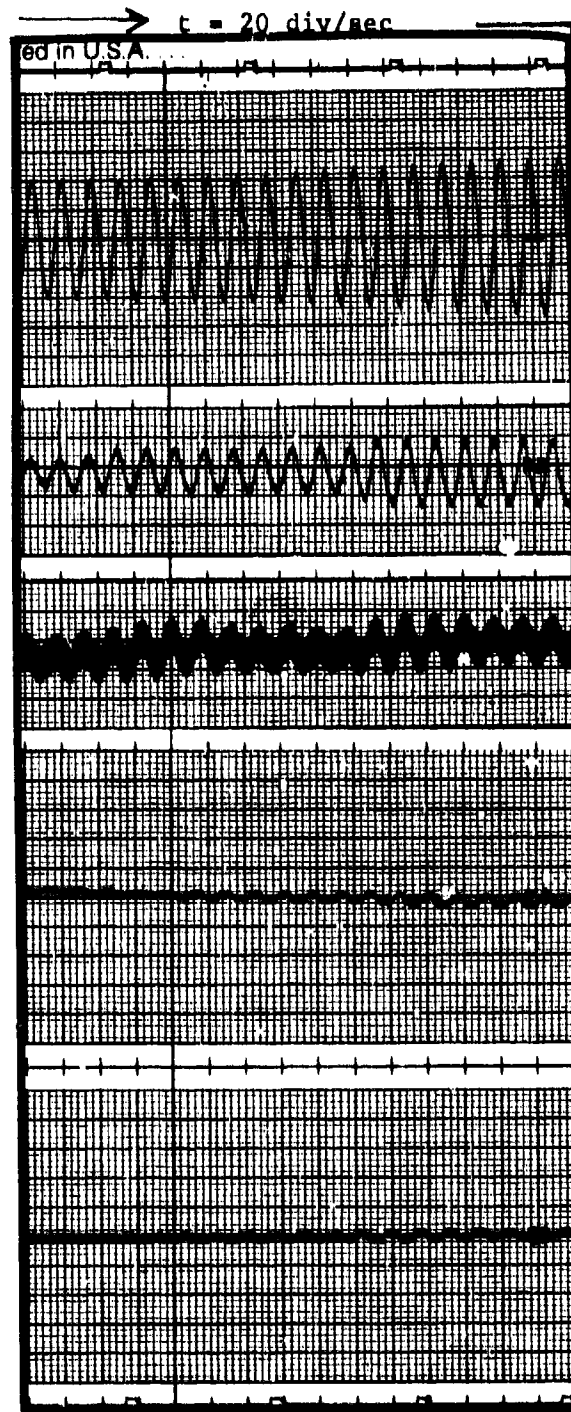


Figure IV-97. Loaded trailing-edge dynamic threshold - 3-psi load - X_1 , X_2 motion.

Test Item - General Dynamics
Mission Adaptive Wing

Date
Prepared: 5/6/87

Test - Dynamic Threshold
Surface - Trailing Edge
Load - 3 lb/in²

Input Command
5 mv/div

Left Rotary Potentiometer
10 mv/div

Right Rotary Potentiometer
10 mv/div

Surface Position X_3
2 mv/div

Surface Position X_4
2 mv/div

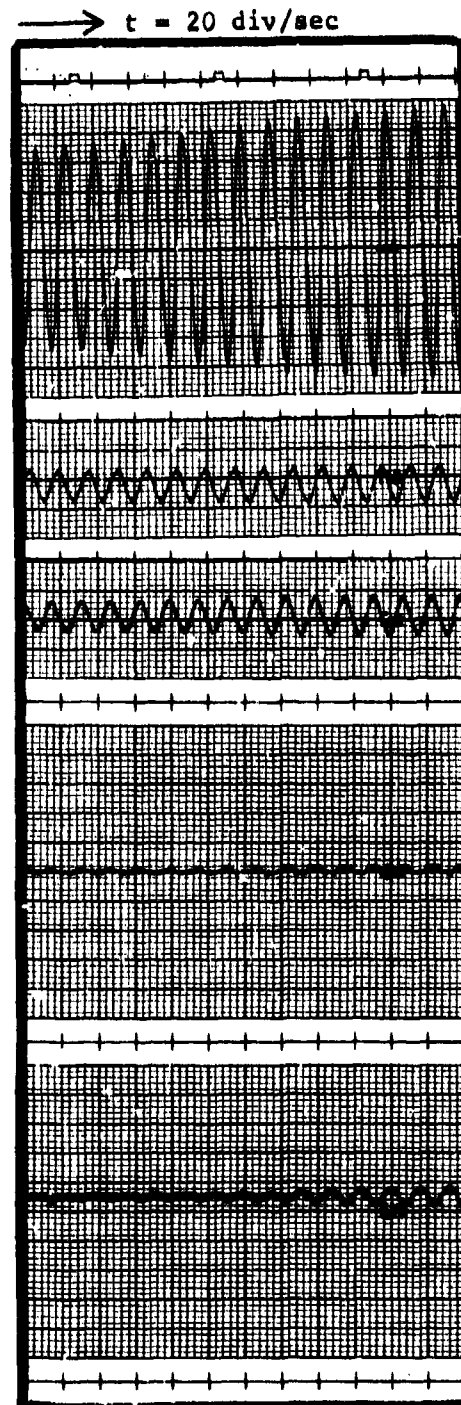


Figure IV-98. Loaded trailing-edge dynamic threshold - 3-psi load - X_3 and X_4 motion.

Table IV-27. Dynamic threshold - loaded trailing edge.

Load (psi)	Motion Point	Threshold (pk volts)	% Max Rate Command	% Max Position Command
1.0	Left Rotary Potentiometer	0.007	0.304	0.125
	Right Rotary Potentiometer	0.007	0.304	0.125
	X ₁	0.067	2.934	1.203
	X ₂	0.077	3.360	1.381
	X ₃	0.120	5.217	2.139
	X ₄	0.115	3.000	2.049
2.0	Left Rotary Potentiometer	0.008	0.369	0.152
	Right Rotary Potentiometer	0.012	0.503	0.206
	X ₁	0.009	0.414	0.170
	X ₂	0.015	0.654	0.268
	X ₃	0.043	1.853	0.760
	X ₄	0.048	2.073	0.850
3.0	Left Rotary Potentiometer	0.017	0.741	0.304
	Right Rotary Potentiometer	0.018	0.785	0.322
	X ₁	0.022	0.961	0.394
	X ₂	0.024	1.046	0.429
	X ₃	0.110	4.805	1.970
	X ₄	0.097	4.244	1.740

Loaded Trailing-Edge Hysteresis

Figures IV-99 through IV-98 show hysteresis data recorded on the trailing-edge surface loaded to 2 psi. This data is representative of the trailing-edge data at other input levels and loads. Tables IV-28 through IV-30 list the hysteresis measured on the trailing edge with different loads and at different input levels. Table IV-28 lists the hysteresis for 3-percent input command and loads of 2 and 3 psi. Table IV-29 lists the hysteresis with a 5-percent input and a surface load of 1 psi. Table IV-30 lists the hysteresis measured with 1- and 2-psi loads and a 10-percent input level.

Table IV-28. Trailing-edge hysteresis - 3-percent command input.

Load (psi)	Motion Point	Hysteresis (volts)	% Max Rate Command	% Max Position Command
2.0	Left Rotary Potentiometer	0.018	0.391	0.160
	Right Rotary Potentiometer	0.016	0.348	0.143
	X ₁	0.021	0.456	0.187
	X ₂	0.045	0.978	0.401
	X ₃	0.155	3.369	1.381
	X ₄	0.200	4.347	1.782
3.0	Left Rotary Potentiometer	0.013	0.286	0.115
	Right Rotary Potentiometer	0.008	0.173	0.071
	X ₁	0.013	0.282	0.115
	X ₂	0.030	0.652	0.267
	X ₃	0.020	0.434	0.178
	X ₄	0.054	1.174	0.481

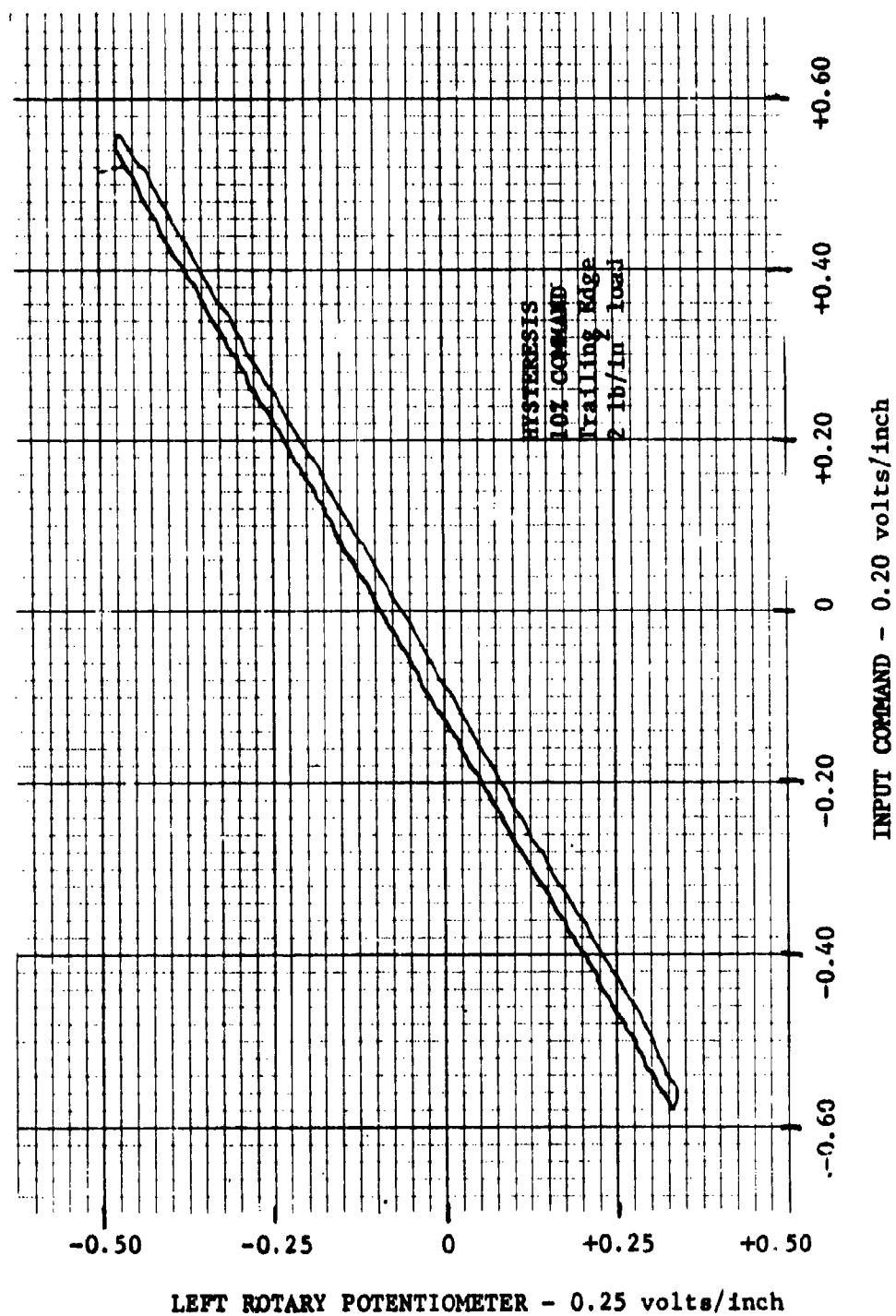


Figure IV-99. Loaded trailing-edge hysteresis - 2-psi load - left rotary motion.

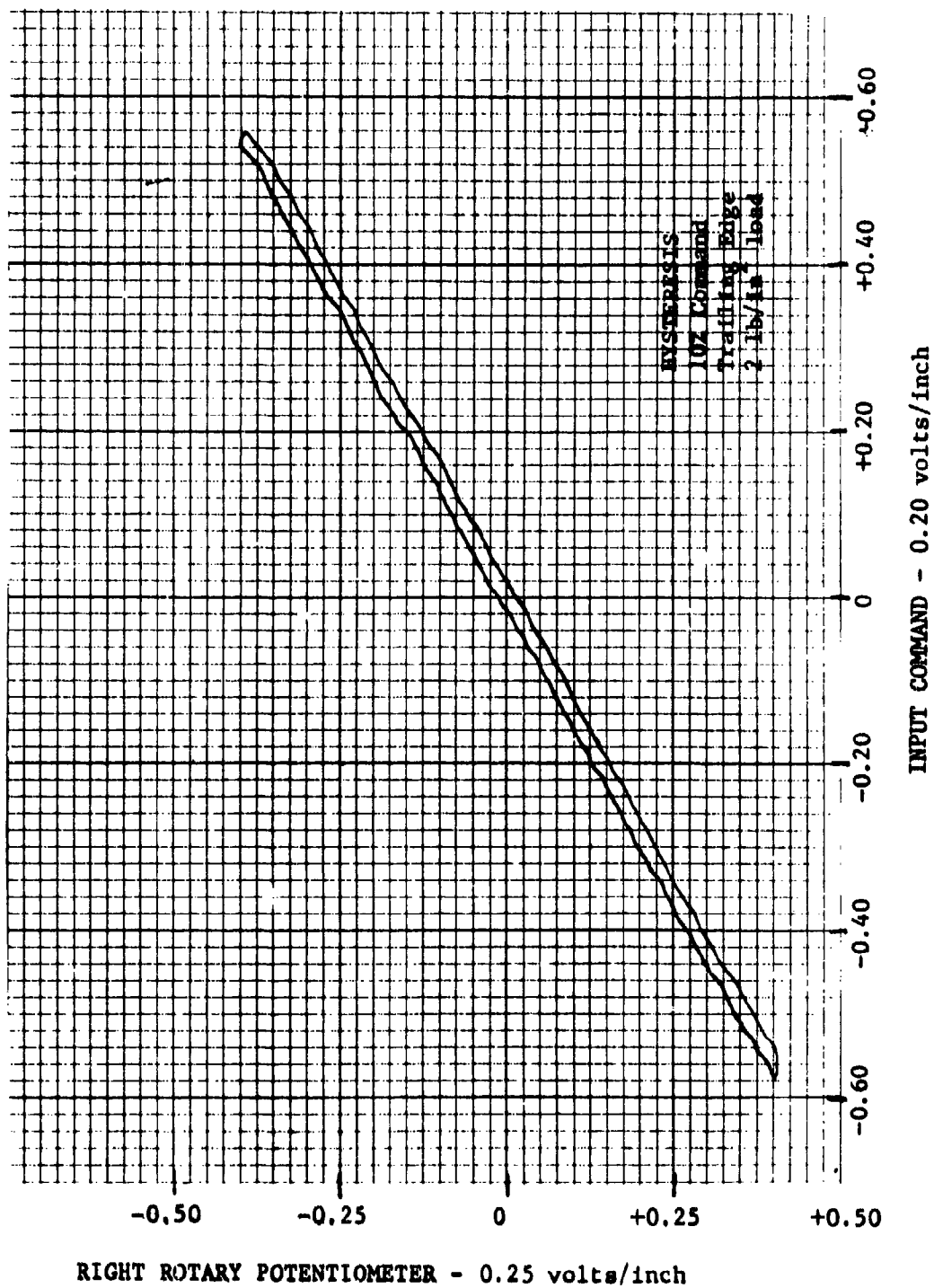


Figure IV-100. Loaded trailing-edge hysteresis - 2-psi load - right rotary motion.

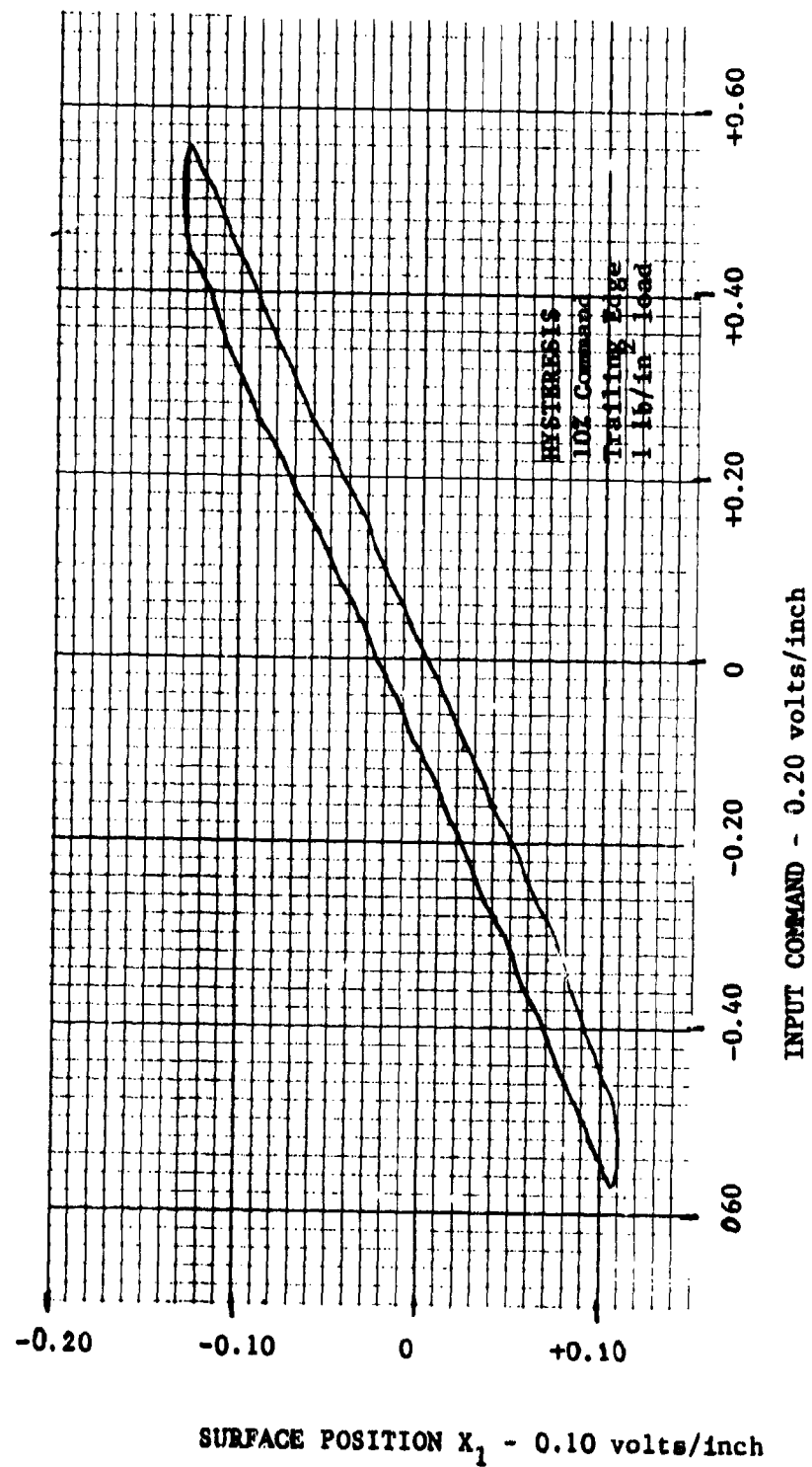


Figure IV-101. Loaded trailing-edge hysteresis - 2-psi load - X_1 motion.

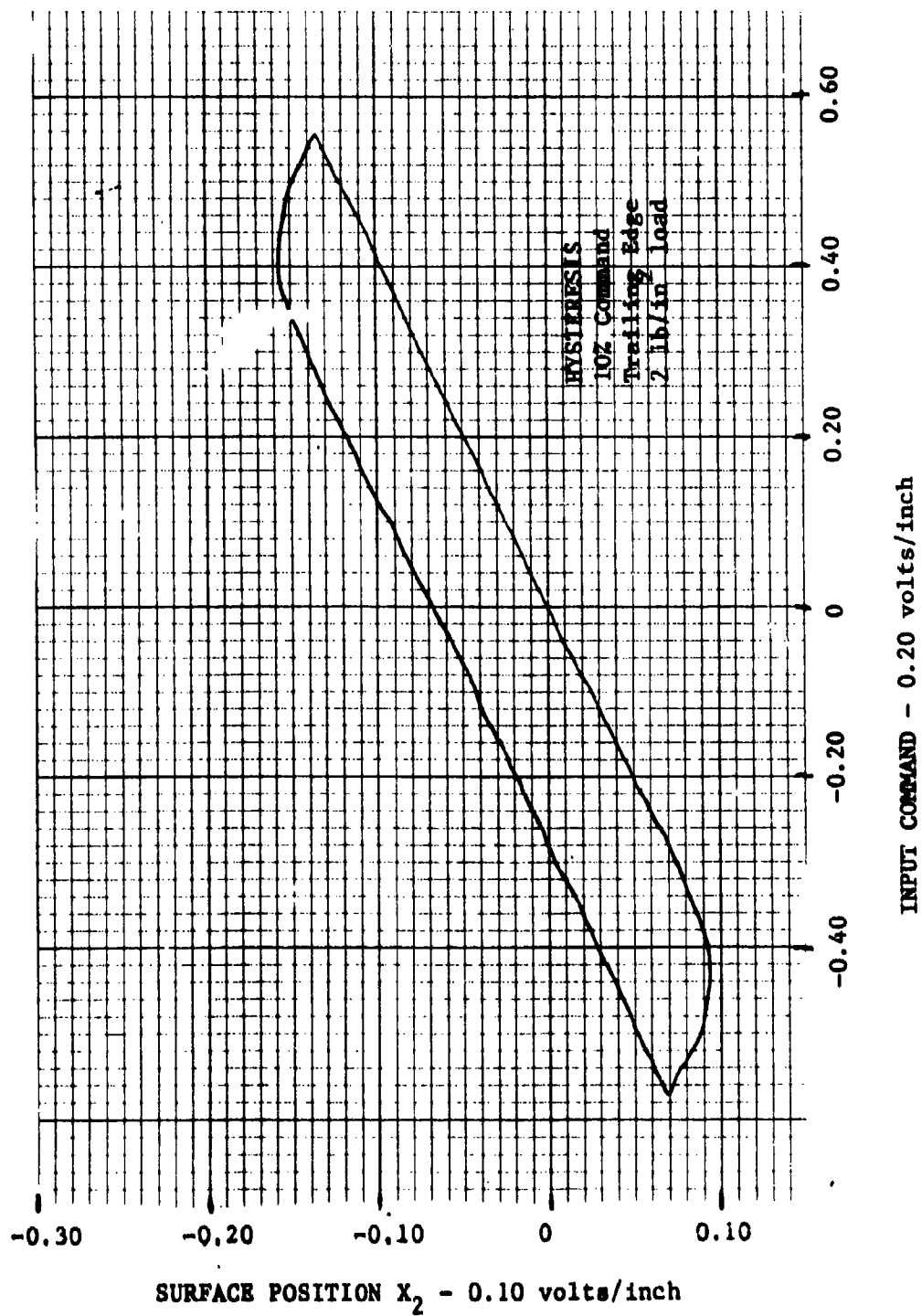


Figure IV-102. Loaded trailing-edge hysteresis - 2-psi load - X_2 motion.

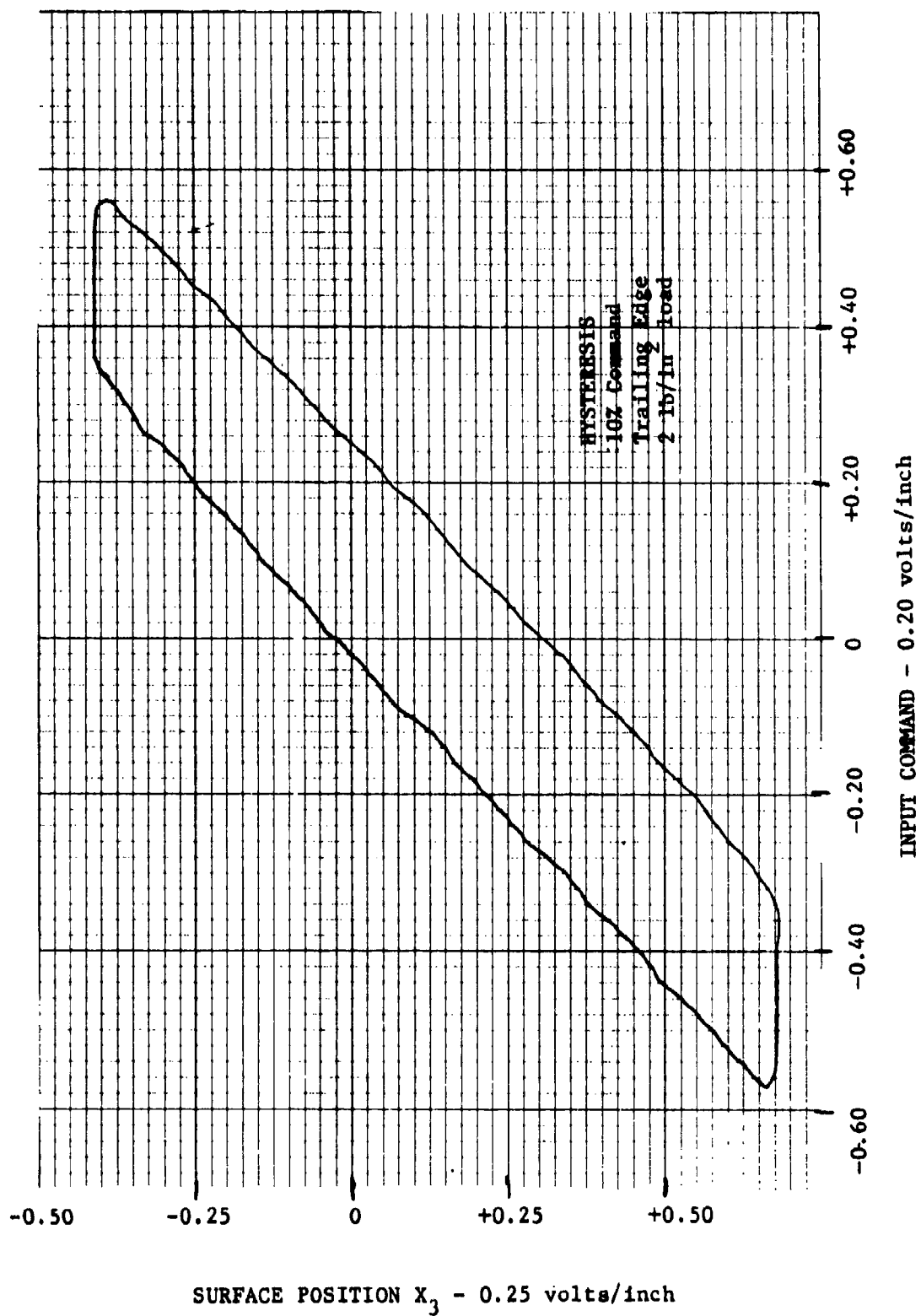


Figure IV-103. Loaded trailing-edge hysteresis - 2-psi load - X_3 motion.

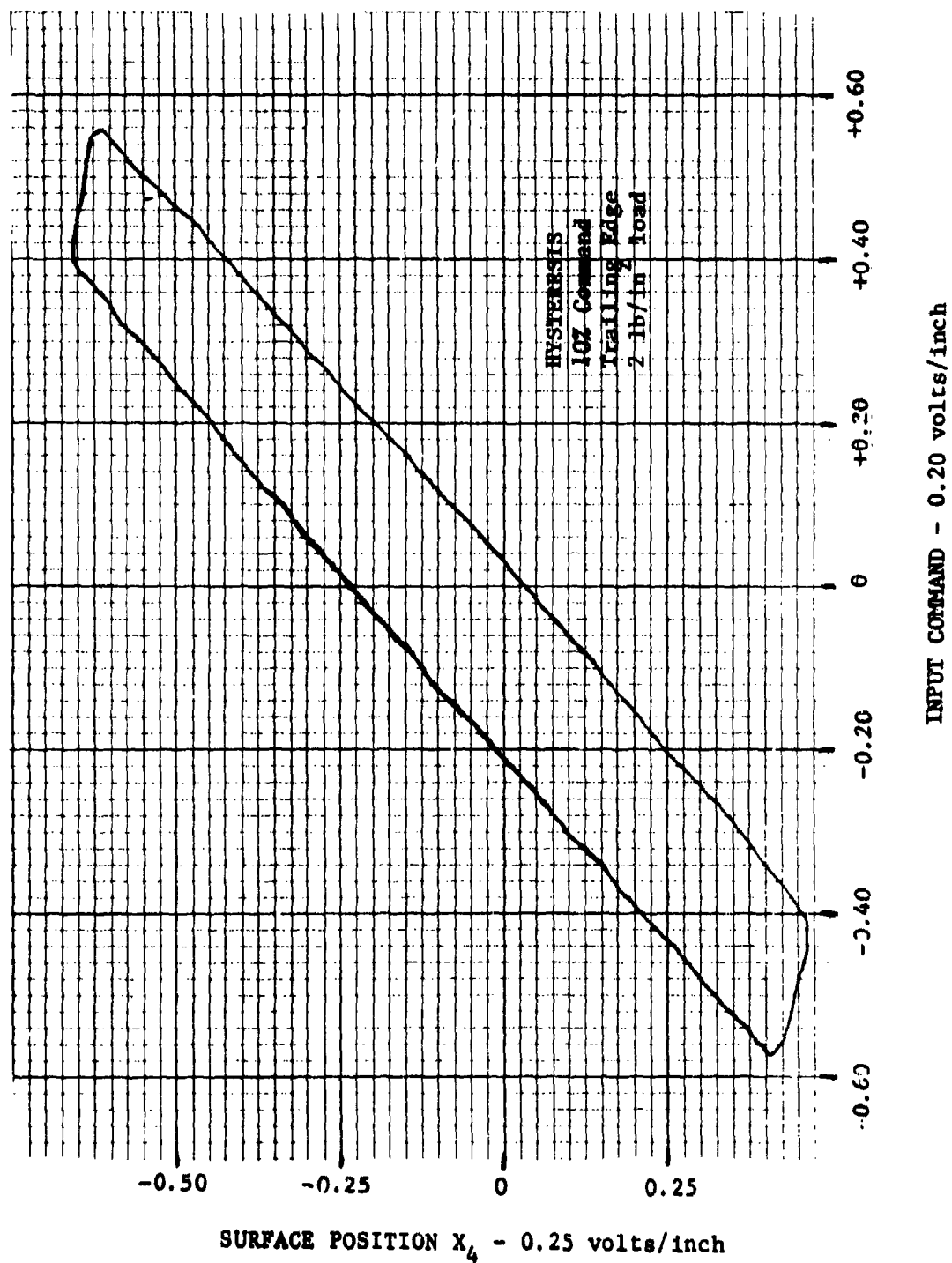


Figure IV-104. Loaded trailing-edge hysteresis - 2-psi load - X_3 motion.

Table IV-29. Trailing-edge hysteresis - 5-percent command.

Load (psi)	Motion Point	Hysteresis (volts)	% Max Rate Command	% Max Position Command
1.0	Left Rotary Potentiometer	0.081	1.761	0.722
	Right Rotary Potentiometer	0.020	0.434	0.178
	X ₁	0.044	0.956	0.392
	X ₂	0.038	0.826	0.388
	X ₃	0.155	3.369	1.382
	X ₄	0.172	3.739	1.533

Table IV-30. Trailing edge hysteresis, 10-percent command.

Load (psi)	Motion Point	Hysteresis (volts)	% Max Rate Command	% Max Position Command
1.0	Left Rotary Potentiometer	0.028	0.608	0.249
	Right Rotary Potentiometer	0.038	0.826	0.339
	X ₁	0.018	0.391	0.160
	X ₂	0.039	0.847	0.347
	X ₃	0.145	3.152	1.292
	X ₄	0.195	4.239	1.738
2.0	Left Rotary Potentiometer	0.033	0.717	0.294
	Right Rotary Potentiometer	0.035	0.761	0.312
	X ₁	0.056	1.217	0.499
	X ₂	0.068	1.478	0.606
	X ₃	0.338	7.348	3.012
	X ₄	0.275	5.978	2.451

Note that for small input commands of 3 percent and 2-psi load, the hysteresis at the tip of the trailing edge (motions X_3 and X_4) is over 45 percent of the input command. However, at 3-psi surface loading, the hysteresis decreases to less than 16 percent of the input command, indicating that increased loading improves the small signal motion transmission of the truss.

Loaded Trailing-Edge Frequency Response

Frequency response measurements were made at both 5- and 10-percent input command and loads of 1 and 2 psi. Figures IV-105 through IV-108 are representative samples of the data recorded for the loaded trailing-edge frequency response. Tables IV-31 and IV-32 list the frequency response in terms of the frequency at which - 3 dB occurs in the amplitude ratio and the frequencies at which - 45° and - 90° phase angles occur.

Table IV-31. Loaded trailing-edge frequency response at 5-percent command.

Load (psi)	Motion Point	-3 dB Freq. (Hz)	-45° Freq. (Hz)	-90° Freq. (Hz)
1.0	Left Rotary Potentiometer	3.00	1.95	4.50
	X_1	1.176	0.867	2.44
	X_3	0.822	0.682	1.688
	Right Rotary Potentiometer	4.49	1.95	3.90
	X_2	1.737	0.664	1.399
	X_4	1.412	0.589	1.299
2.0	Left Rotary Potentiometer	3.46	1.393	3.253
	X_1	2.00	1.061	2.777
	X_3	1.209	0.563	1.336
	Right Rotary Potentiometer	4.00	1.487	3.000
	X_2	2.743	0.734	1.597
	X_4	1.699	0.821	1.632

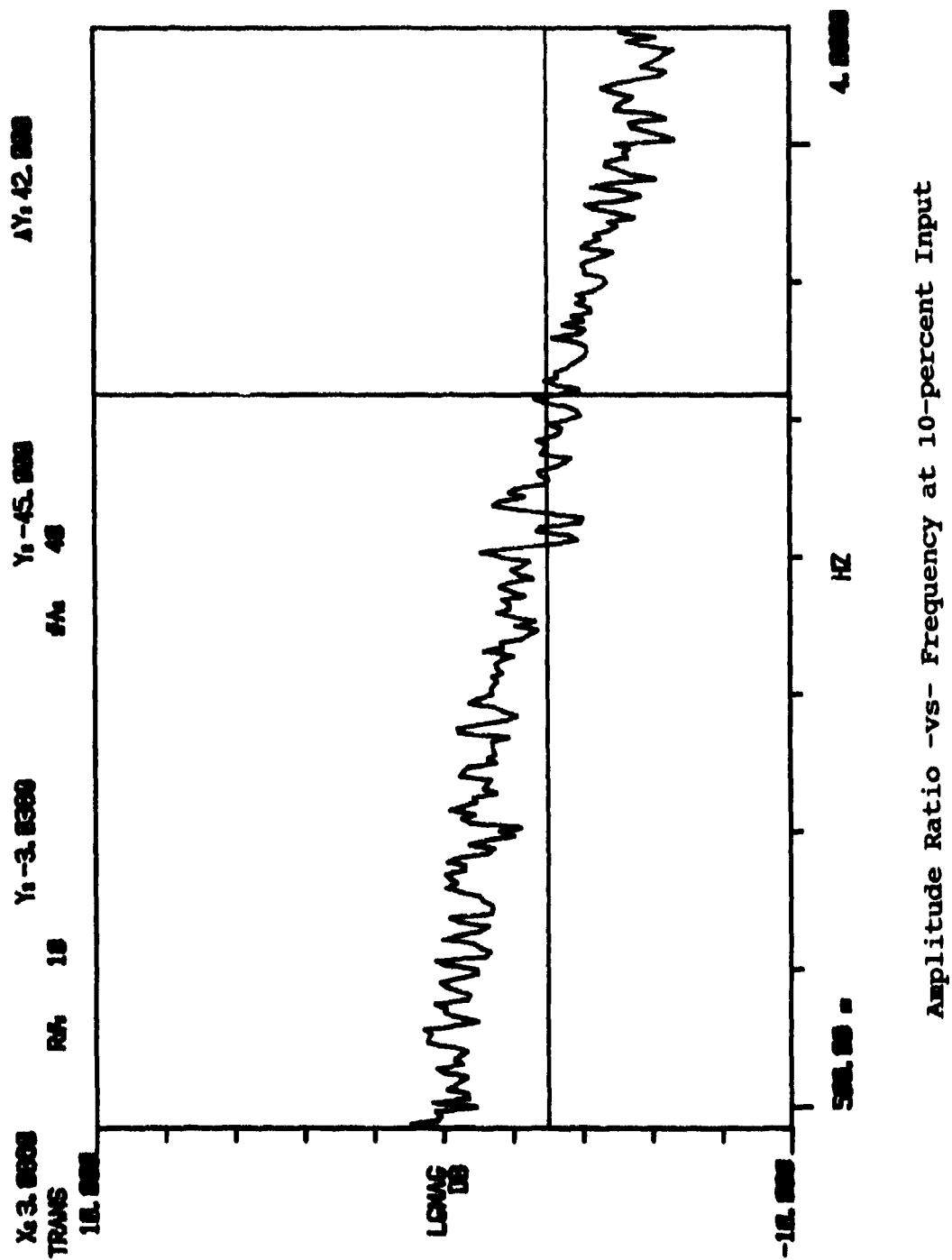
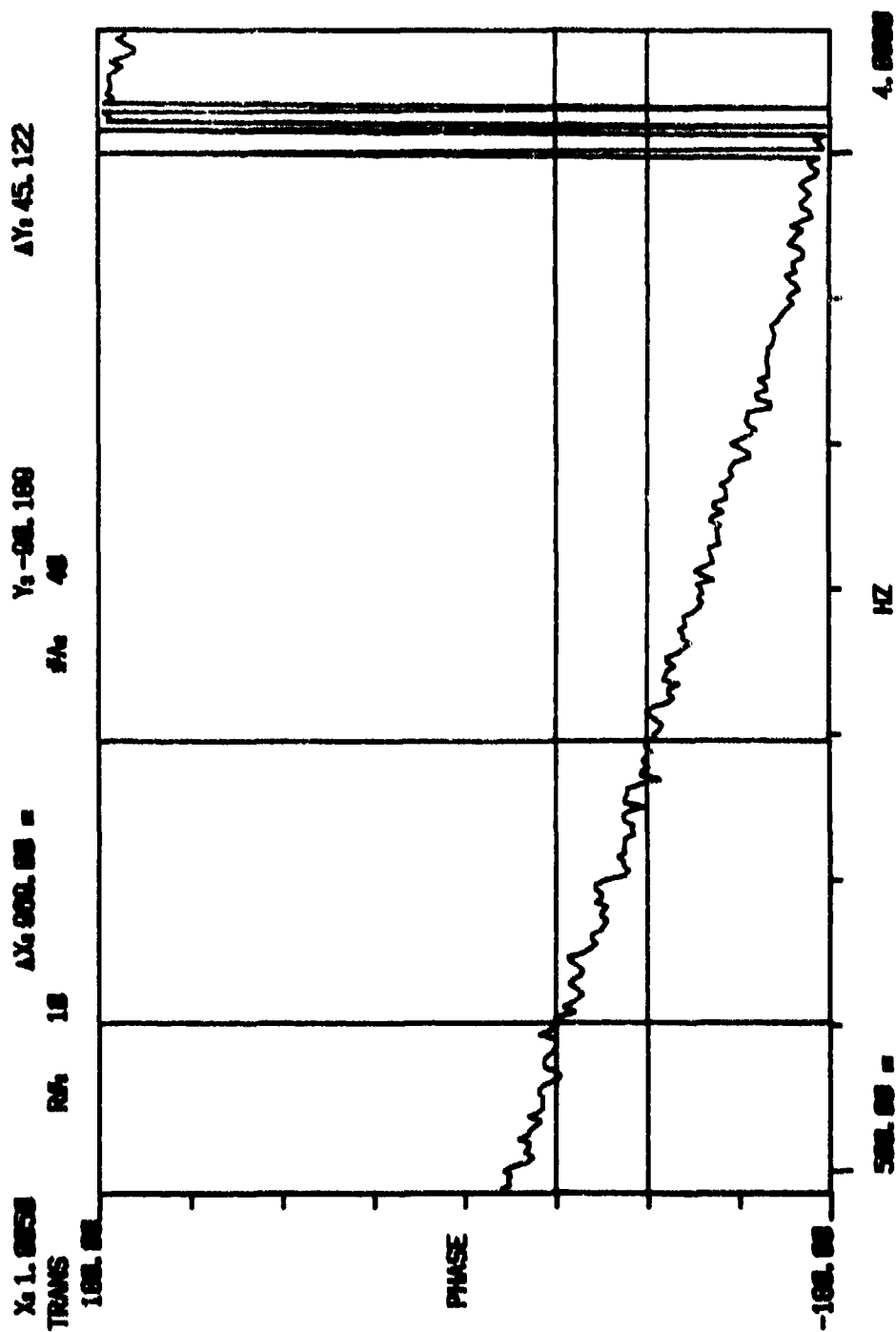
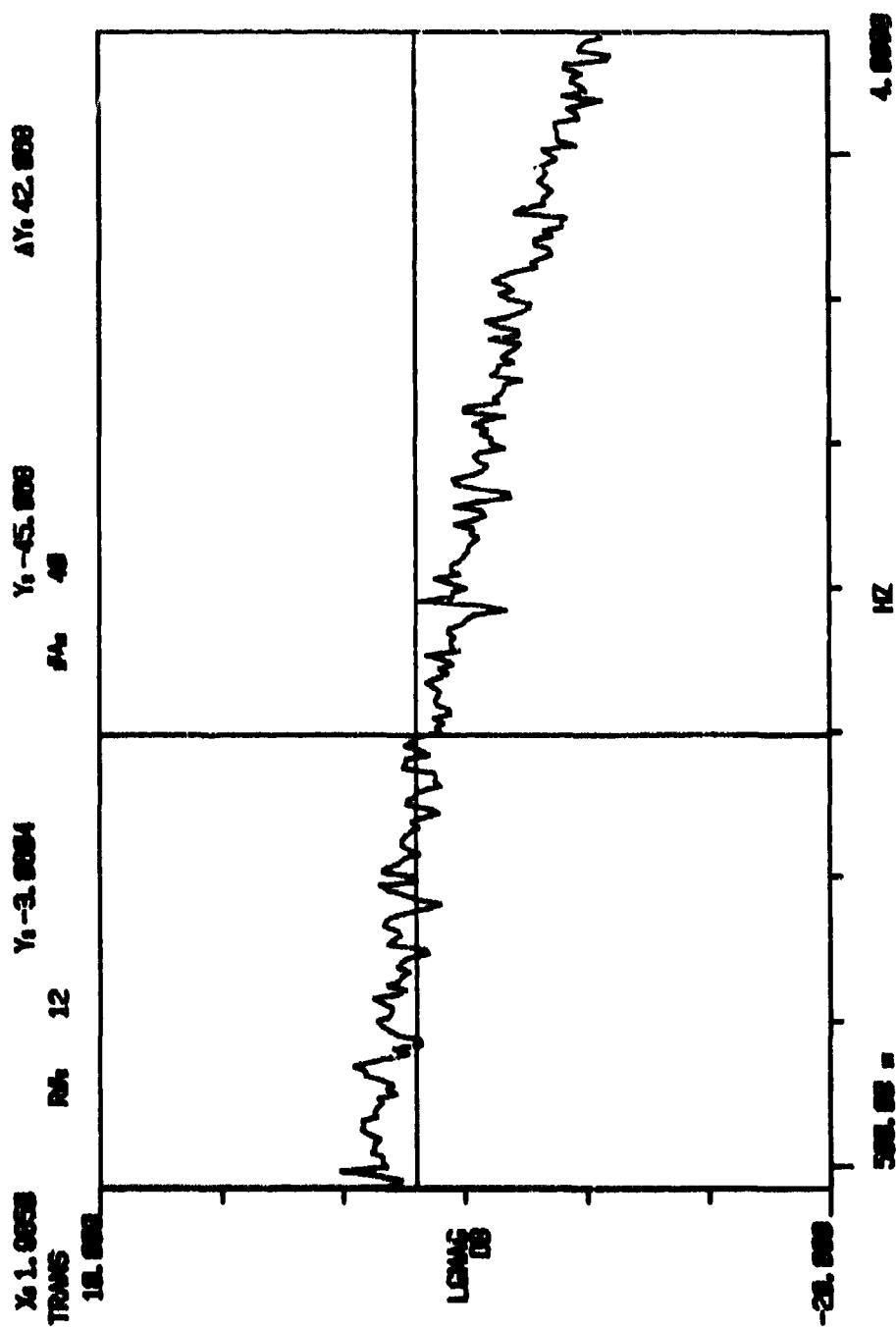


Figure IV-105. Trailing-edge actuator - 1-psi load - position X_2 .



Phase Response -vs- Frequency at 10-percent Input

Figure IV-106. Trailing-edge actuator - 1-psi load - position X_2 .



Amplitude Ratio -vs- Frequency at 10-percent Input

Figure IV-107. Trailing-edge actuator - 1-psi load - position X_A .

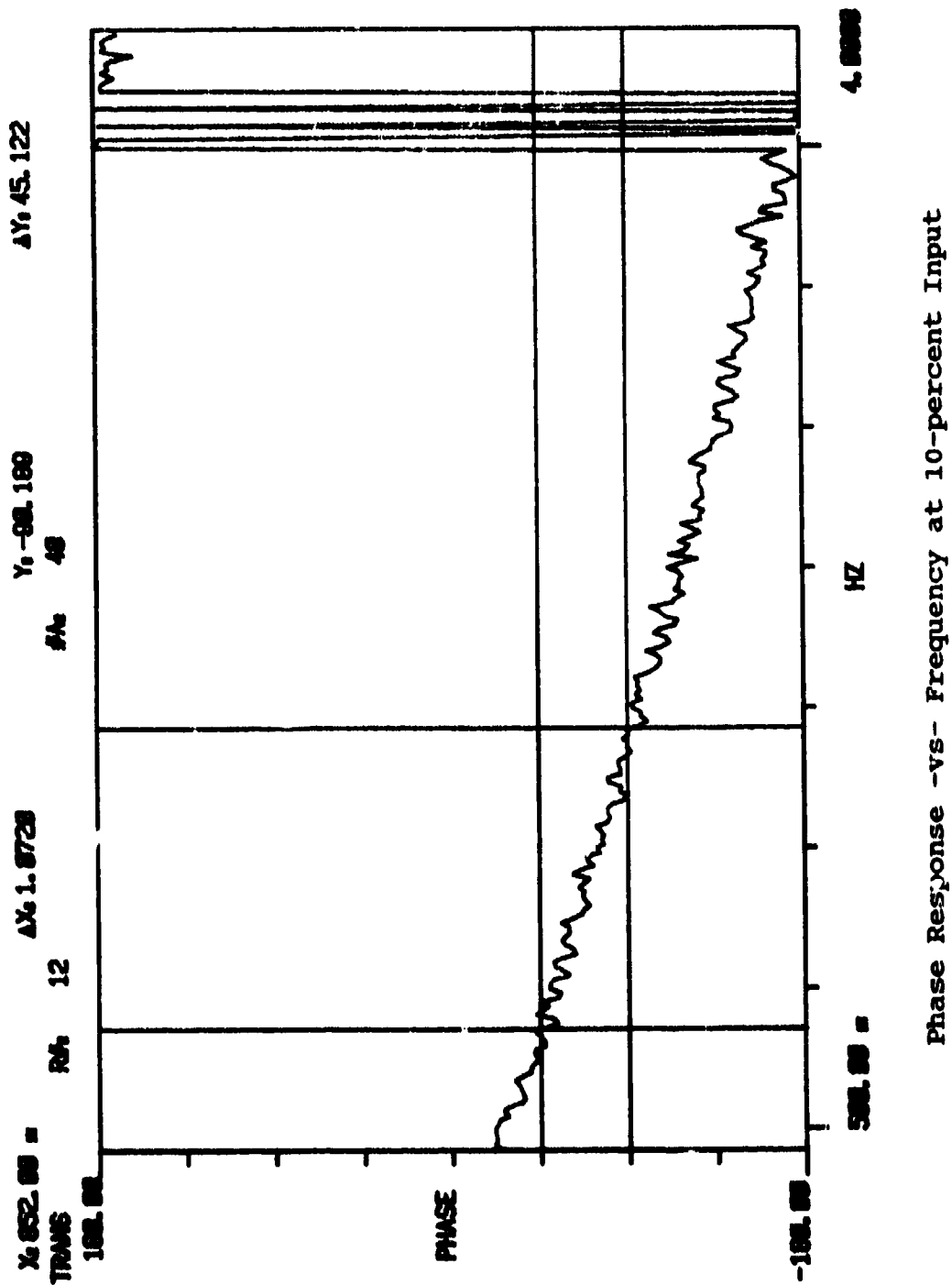


Figure IV-108. Trailing-edge actuator - 1-psi load - position X_4 .

Table IV-32. Loaded trailing-edge frequency response at 10-percent command.

Load (psi)	Motion Point	- 3 dB Freq. (Hz)	-45° Phase Freq. (Hz)	-90° Phase Freq. (Hz)
1.0	Left Rotary Potentiometer	3.717	1.742	3.751
	X ₁	2.535	1.117	2.266
	X ₃	1.883	0.851	1.941
	Right Rotary Potentiometer	4.500	1.905	3.611
	X ₂	3.086	1.005	1.974
	X ₄	1.985	0.852	1.924
2.0	Left Rotary Potentiometer	3.054	1.441	2.961
	X ₁	2.156	1.033	2.471
	X ₃	1.628	0.803	1.808
	Right Rotary Potentiometer	3.699	1.470	2.983
	X ₂	2.620	0.882	1.869
	X ₄	1.683	0.837	1.947

Loaded Trailing Edge Step Response

Table IV-33 is a listing of the results of the test response measurements on the loaded trailing-edge surface. A 10-percent-of-maximum-command input was used for the step amplitude. The three loads of 1, 2 and 3 psi were used for the surface loading. Figures IV-109 and IV-110 (showing the step response for the 1-psi load) are representative samples of the data recorded for the loaded trailing-edge. As listed in the table, two time values are used to describe the step response. The first time value is the time for movement of the particular motion point to start after application of the step response to the trailing-edge control system. This time delay includes the time delay of the series actuators used to control the valve for the trailing-edge hydraulic motors. The second time value is the time for the motion point to reach 63 percent of the final value after motion starts.

Test Item: General Dynamics
Mission Adaptive Wing

Date Prepared: 9/1/85

Test: Step Response - X_1 , X_3
Surface: Trailing Edge
Load: 1 lb/in²

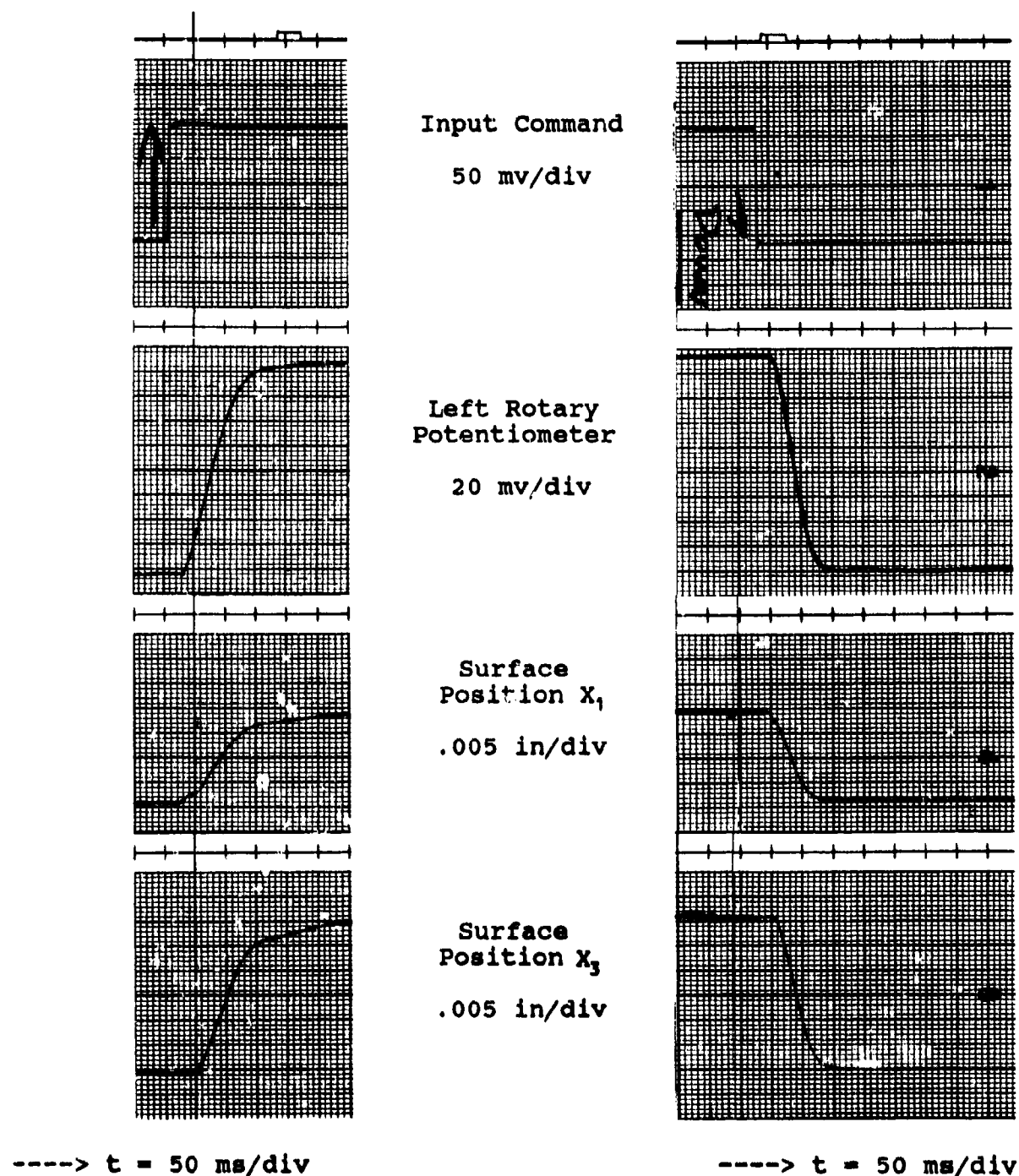


Figure IV-109. Step response - X_1 , X_3 .

Test Item: General Dynamics
Mission Adaptive Wing

Date Prepared: 9/1/85

Test: Step Response - X_2 , X_4
Surface: Trailing Edge
Load: 1 lb/in²

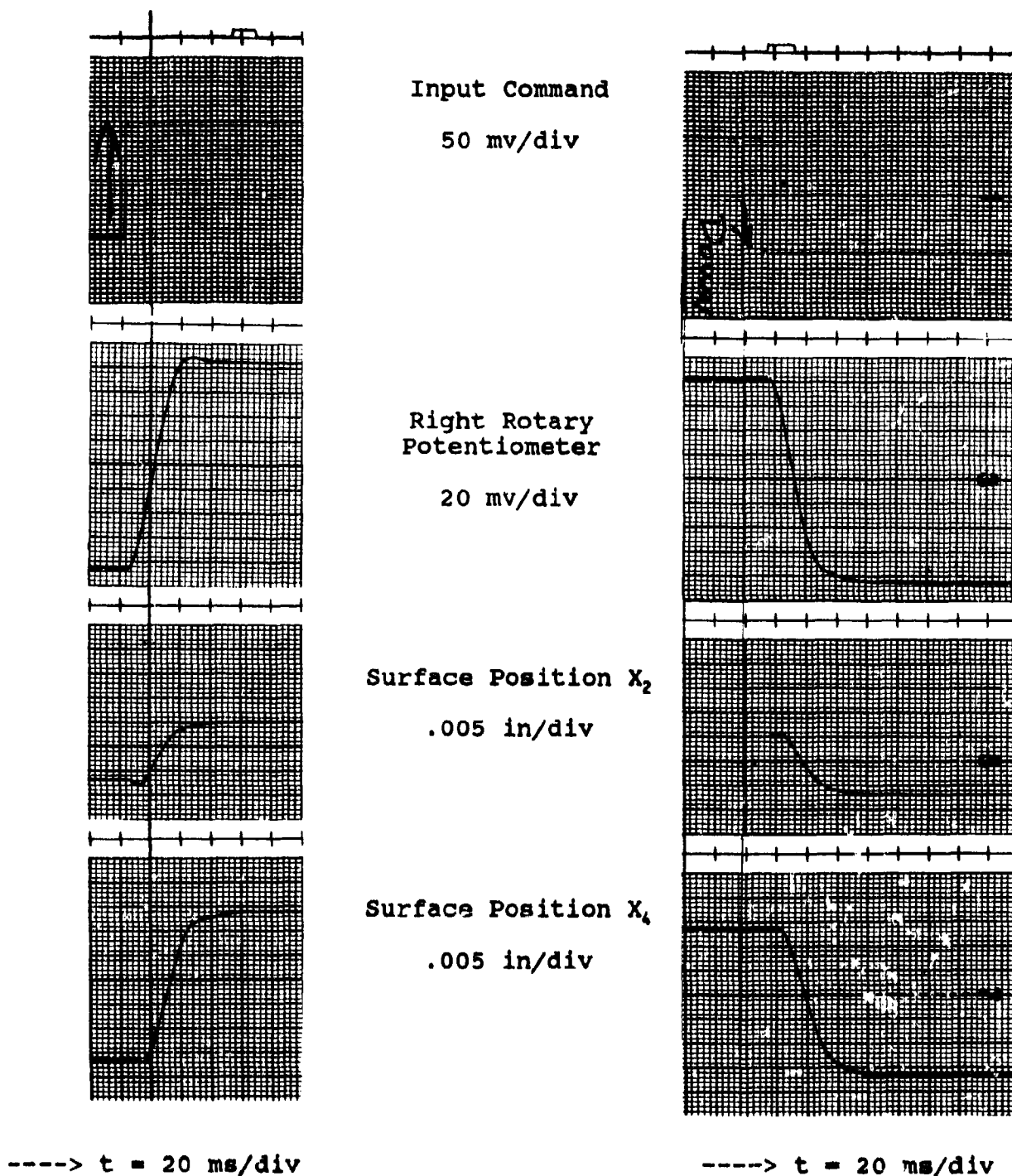


Figure IV-110. Step response - X_2 , X_4 .

Table IV-33. Loaded trailing-edge step response.

Load (psi)	Motion Point	<u>Surface Up</u>		<u>Surface Down</u>	
		Time Delay (ms)	63% Travel (ms)	Time Delay (ms)	63% Travel (ms)
1.0	Left Rotary Potentiometer	30	120	40	80
	X ₁	40	130	40	79
	X ₃	70	100	60	80
	Right Rotary Potentiometer	20	90	30	90
	X ₂	25	70	30	70
	X ₄	40	100	40	110
2.0	Left Rotary Potentiometer	30	180	40	145
	X ₁	30	200	70	170
	X ₃	160	160	120	160
	Right Rotary Potentiometer	35	140	60	175
	X ₂	40	110	70	140
	X ₄	50	110	90	180
3.0	Left Rotary Potentiometer	45	112	42	105
	X ₁	45	65	44	70
	X ₃	58	85	55	70
	Right Rotary Potentiometer	30	93	33	110
	X ₂	30	60	35	80
	X ₄	40	60	40	85

The general effect of the load on the step response of the trailing edge is to reduce the time delay and time to final position for *up* surface motion and to increase the times for *down* surface motion. However, the times are still similar to the unloaded trailing-edge surface response in magnitude, indicating that the surface load is well within the capability of the truss driving force. The effect of the 3-psi surface load was to decrease the step response times compared to the 2-psi surface load. This suggests that the 3-psi surface load eliminates any compliance associated with clearances in the truss better than the 2-psi surface load. The step response with 3-psi surface load is similar to the 1-psi surface load.

IV. CONSIDERATIONS AND ANOMALIES

General

As mentioned in the previous material, there were two apparent design deficiencies of the MAWS mechanization which were discovered during the evaluation of the test section. One was the load capacity of the gear boxes used to drive the trailing edge. The second was the design of the universal joints used in the trailing edge. Both deficiencies could be easily corrected on any future design using the mechanization.

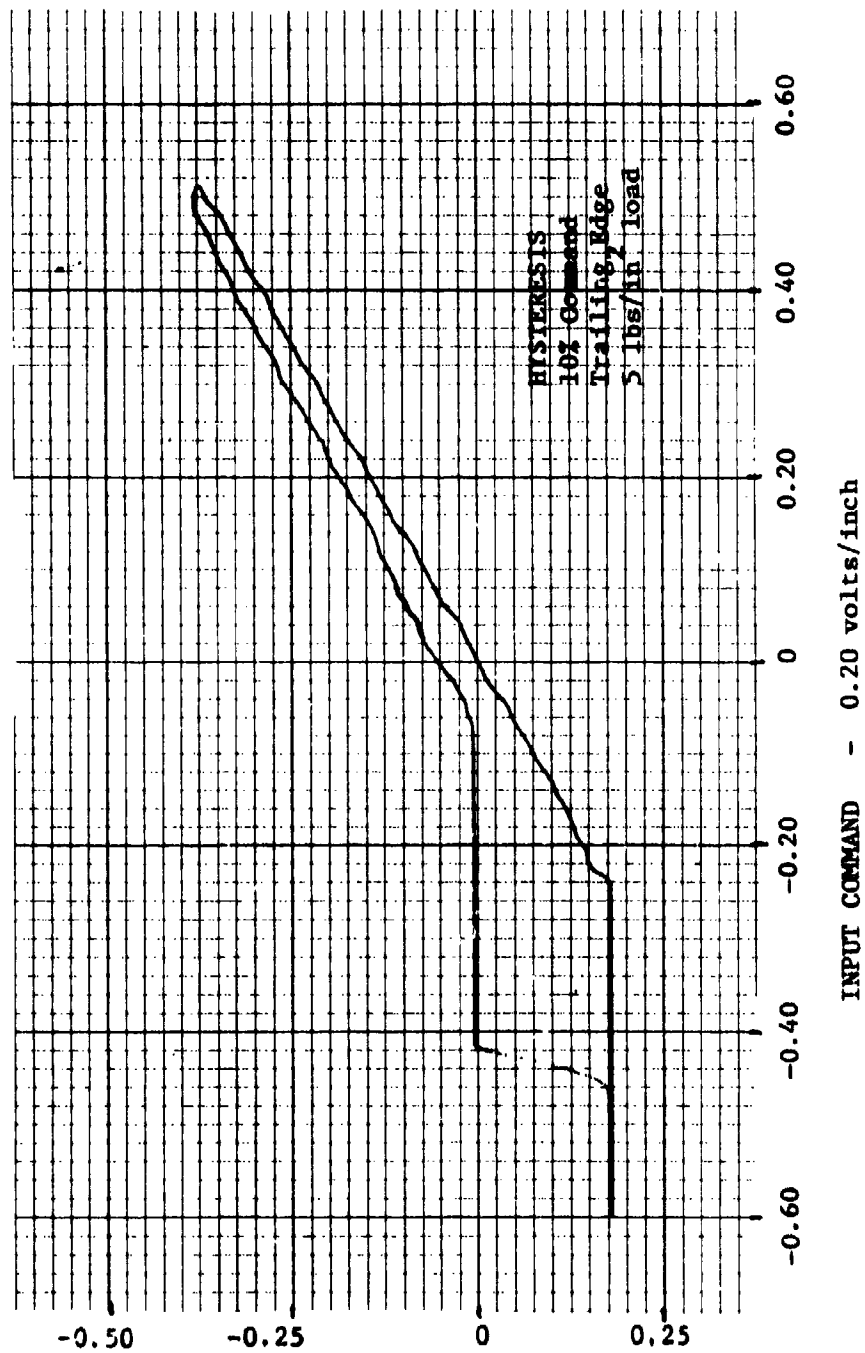
The gear-box load capacity limited the test load evaluation of the trailing edge. The universal joints failed during initial testing and were replaced by a DCI design for the test evaluation. After the universal joints in the trailing edge were replaced with a modified design, both unloaded and loaded testing of the test section were re-run.

Gear-Box Load Capacity Limitation

The load limitation of the gear boxes used to drive the trailing-edge variable-geometry trusses was discovered when hysteresis measurements were conducted on the trailing-edge surface with 5-psi loads. Figures IV-111 and IV-112 show two hysteresis measurements with a 10-percent input and 5-psi surface load. The hysteresis of the right and left rotary potentiometer outputs are shown on these figures. Note that on Figure IV-111, the output of the left rotary potentiometer shows the output shaft motion of the gear box stopping motion and then jumping to a new position. During testing, this jump produced a loud, snapping sound. As shown in Figure IV-112, the motion of the right gear exhibits a similar characteristics with the output shaft stopping movement with input command. Since the motion of the surface with a 10-percent input was only over a limited range and the output of the gear box moved over part of the input range against a constant load, it did not appear that a stall limit on the force output was causing the loss of output motion. It appeared the gear separation within the gear box was occurring, causing the loss of motion and the jump phenomena. If so, then a larger capacity gear box would solve the problem.

Universal Joint Failure and Correction

During initial testing of the test section in the MASTR with static load applications of 0 to 5 psi in increments of 1 psi to the trailing edge, it was observed that a pin of the left-arm Bay 1 U-joint had sheared (and fallen out). The left arm was disassembled and it was discovered that a pin had also



LEFT ROTARY POTENTIOMETER - 0.25 volts/inch

Figure IV-111. Loaded trailing-edge hysteresis - 5-psi load - left rotary motion - 10-percent input.

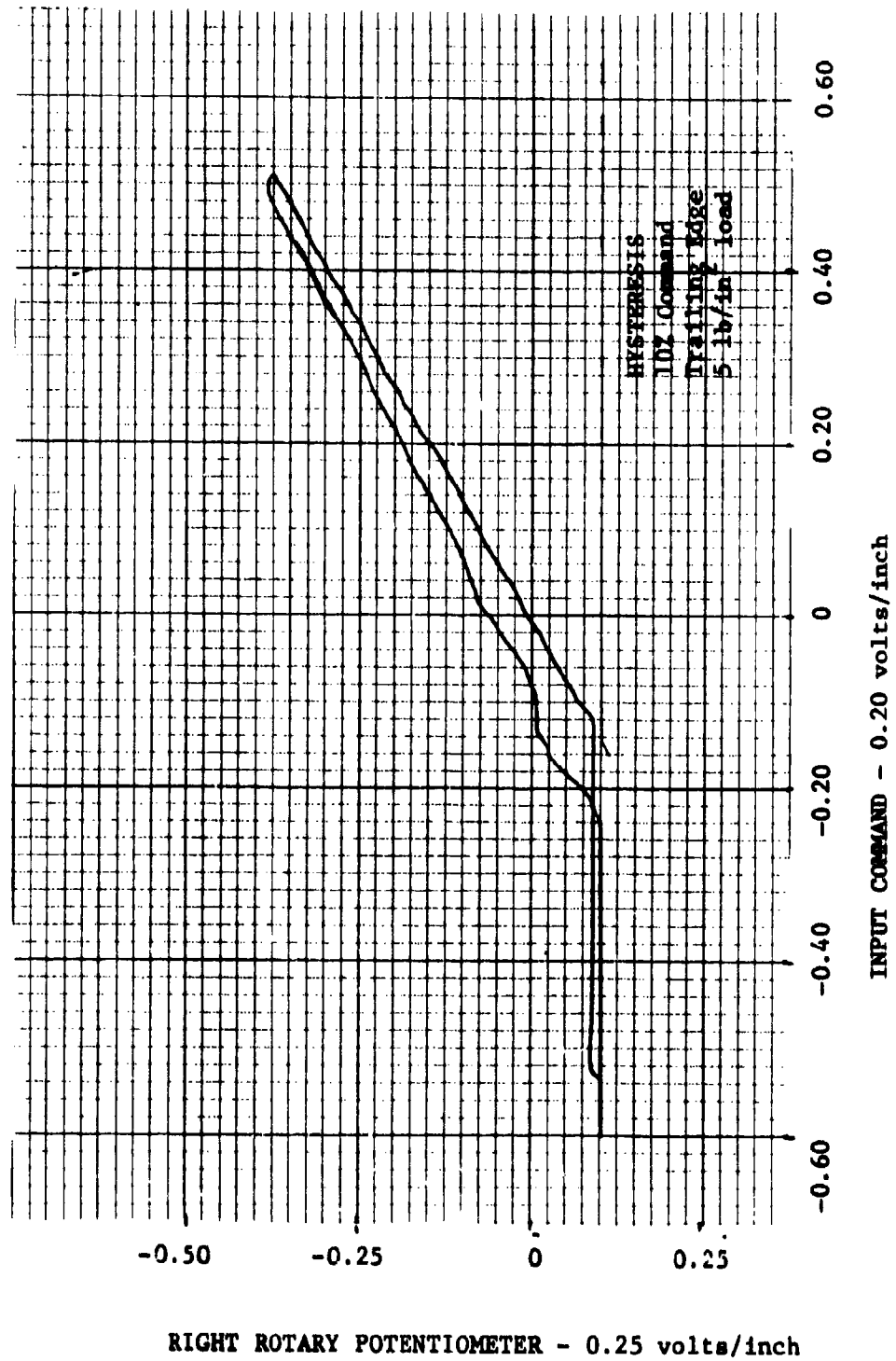


Figure IV-112.

Loaded trailing-edge hysteresis - 5-psi load - right rotary motion - 10-percent input.

sheared in the Bay-2-to-Bay-3 U-joint. Figure IV-113 show the U-joint design used in the MAWS test section. The pins for the cross are screwed into the center section of the cross. Examination of the design showed that the pins were not supported in the center section on the shoulder above the threads on the pin. The pins that broke failed at a point between the threaded section and the rest of the pin. This failure mode was consistent with pin operating as a cantilever and the thread acting as a stress riser. Also noted in the figure was the extrusion and wear of the bearing material which created increased clearances in the U-joint. Although the right arm had not failed, it was also disassembled and modified in order to reduce its free-play and prevent a future failure similar to that of the left truss.

To minimize free-play and eliminate further failure of the U-joints, a modified design, as shown in Figure IV-114, was used. As shown on this figure, the design of the new U-joints eliminated the screw threads entirely and the reduction in diameter for the threads. The material selected for the new U-joint pins and yoke was VascoMax C-300, a high-strength steel produced by Teledyne Vasco Company of Latrobe, Pennsylvania. The material has a yield strength of 290,000 psi and a fatigue strength (for 100 million cycles) of 125,000 psi after heat treating.

The fabric-lined bushings that the pins operated against were also replaced. The material used was Ampco 20, an aluminum-bronze material which has a high hardness and non-galling properties when used as a bearing material. Ampco 20 has a yield strength of 40,000 psi.

In order to minimize free-play and obtain good press-fit conditions for the new U-joints, the VascoMax C-300 pins were heat-treated and then centerless ground to a final dimension. The VascoMax C-300 yokes were heat-treated, surface ground (to obtain flat, square surfaces) and then jig ground for a medium press-fit of the pins. The Ampco 20 bushings were machined and pressed into the shell before a final reaming to a close clearance fit (within .001 in diametral clearance) with the pins.

To assemble the U-joints, the yokes were installed their respective mating parts and the pins pressed in through the bushings. As shown in Figure IV-114, two short pins and one long through-pin were used. After assembly, holes were drilled through the pins and yoke to install roll pins (in order to lock the assembly together).

No further problems with the U-joints were encountered and the free-play with the new bushings and pins was less than with the original U-joints.

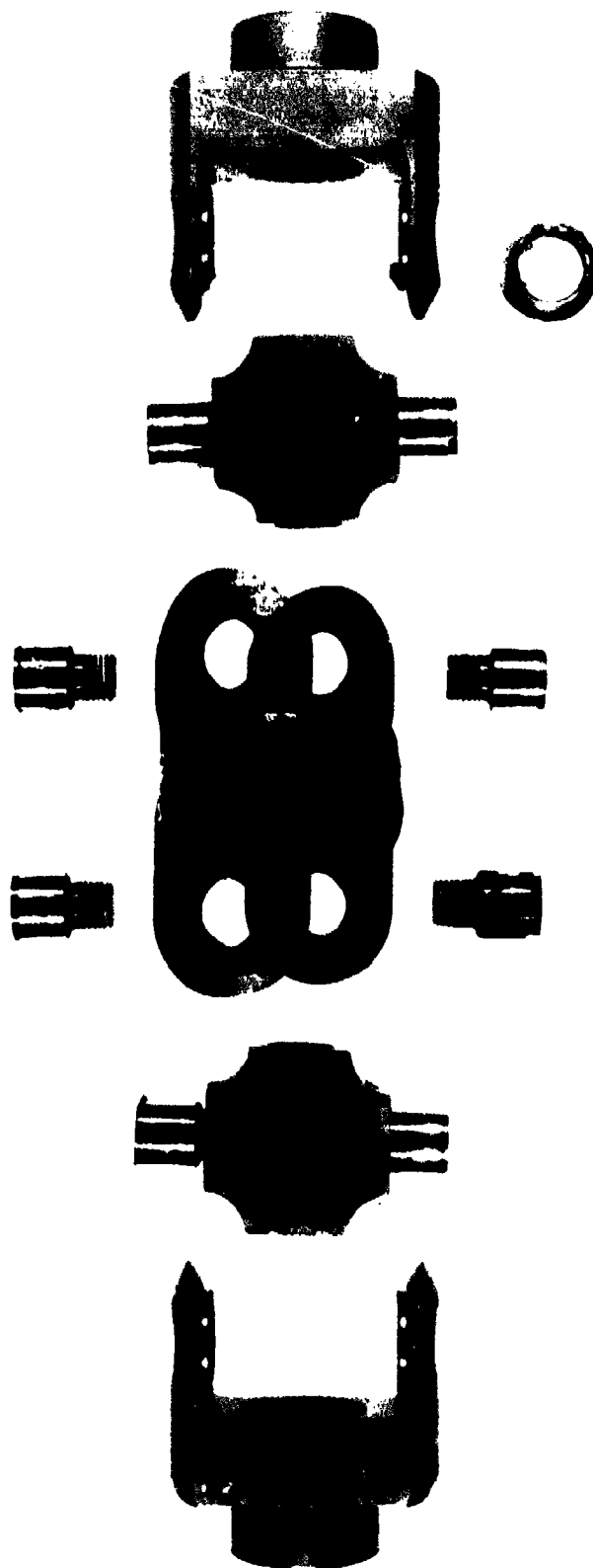


Figure IV-113. Original U-joint design.

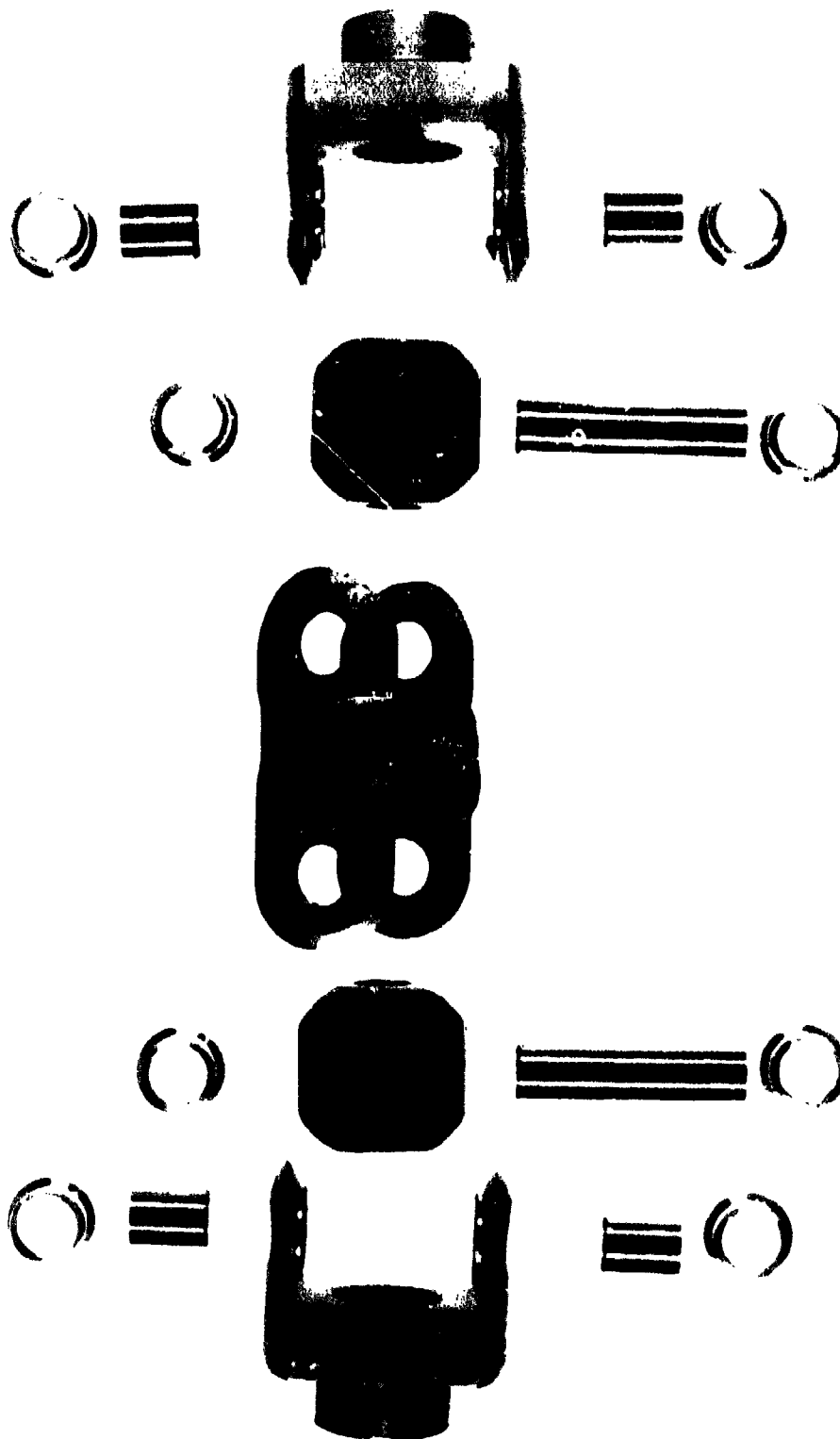


Figure IV-114. Modified U-joint design.

V. CONCLUSIONS AND RECOMMENDATIONS

The mechanization of the test section demonstrated that reshaping of a wing section with a flexible leading and trailing edge is practical. The linkage method for the leading and trailing edge introduced the effect of hysteresis and free-play into the surface motion characteristics. Loading the surface (as would normally occur with aerodynamic loads) minimized the free-play effects on the surface. The frequency response of both the leading and trailing edge met the nominal response requirement goals (both for loaded and unloaded test conditions).

The leading edge output to input performance characteristics degraded under the load conditions for small input-signal characteristics. This would appear to be an expected effect, since transmitting small motions through linkage over any distance is difficult, particularly under loads and with flight-weight hardware. If small amplitude-signal performance is critical, then the leading-edge linkage clearances and stiffness could be appropriately changed.

The anomalies encountered in the loaded testing indicate that some design improvement of the trailing edge gear boxes (for load capacity) and U-joints (for reliability) would be required before flight use.

The mechanizations for coupling the hydraulic actuator (or motors and gear box) are critical to the operation of the mechanization, both for performance and reliability. It is recommended that loaded testing be a requirement for evaluating any similar mechanization for reshaping a continuous aerodynamic surface. Unloaded testing can not adequately evaluate this type of control surface actuation concept.

SECTION V

FLUTTER SUPPRESSION - PHASE III

I. INTRODUCTION AND SUMMARY

The objective of this effort was to produce and evaluate an actuator which used electronic load-pressure sensing to change the output impedance of the actuator over a selected frequency band. Changing the output impedance of a hydraulic actuator potentially can be used to suppress classical slab-surface flutter. A demonstration actuator was sized to evaluate the impedance change capability over a frequency range wide enough to potentially meet current and future aircraft slab-surface flutter suppression requirements.

The phenomenon of slab control surface flutter is an aeroelastic, self-excited vibration in which airstream energy is absorbed by the lifting surface. The flutter motion consists of both bending and torsional components characterized by a unique frequency of simple harmonic oscillation. If either the bending or torsional component is suppressed, classical flutter will not occur. The slab surface's torsional motion is primarily determined by the spring rate of the actuator controlling the surface and the rotational inertia of the surface. Normally, the torsion resonant frequency is lightly damped. By changing the damping of the torsional mode to a damping ratio greater than critical, torsional motion at torsional resonance is suppressed. This damping can be accomplished by using load pressure feedback to change the impedance of the control actuator at the torsional resonant frequency.

The normal technique used for slab-surface flutter avoidance is to raise the torsional resonant frequency by increasing the stiffness of the control actuator. The stiffness increase is accomplished by increasing the actuator drive area, creating an actuator that has a higher output force (and flow demand) than that required by the aircraft for maneuvering.

There is a trend towards using higher system pressures in aircraft hydraulic systems. Higher system pressure allows using smaller actuators with smaller drive areas. This is in conflict with the using drive area increases for increasing actuator stiffness to avoid flutter. The impedance modification technique has a good potential payoff by allowing the use of slab surface control actuators sized for hinge moment requirements, rather than being oversized for flutter avoidance. By example, the *Tornado* aircraft uses a hydromechanical load-pressure feedback mechanization in its horizontal tail actuator for actuator output impedance modification.

The following material in this report section describes the design and test of a non-redundant, fly-by-wire actuator which incorporates electrical load pressure feedback to change the output impedance of the actuator. The recorded test data indicates that the output impedance of an actuator can be modified over a limited frequency range. The limitation in range of the modification is primarily due to the frequency response of the servovalve used to control the actuator.

II. TECHNICAL APPROACH

General Technical Approach

Dynamic Controls, Inc. during previous contract work for the US Air Force, constructed and tested a hydromechanical device that modified the impedance of an F-4 stabilator actuator. The technical reports for that contract work are AFFDL-TR-79-3117, Volume 1 and AFFDL-TR-75-29. The investigation described in this report was directed at evaluating whether electronic load pressure sensing and feedback would produce equivalent or better damping performance in a smaller and potentially less expensive package. For this investigation, the hardware of an F-4 stabilator actuator was not used directly. Application of electronic load feedback requires using a fly-by-wire actuator (commanded by electrical input signals). The F-4 stabilator actuator is a mechanical input actuator with limited-authority stability-augmentation and autopilot operation incorporated on the actuator. The F-4 actuator is also a tandem actuator with two actuator drive areas. The use of two drive areas requires synchronization of the control valving for the two sections in order to prevent a force fight. In converting an F-4 stabilator actuator to a fly-by-wire configuration, synchronization of the control valving for the tandem actuator would require using either a tandem power spool driven by a high response pilot-servovalve, a high response secondary actuator driving a tandem power pilot-spool, a high response direct-drive valve, or two high response servovalves with electronic force fight compensation. Incorporating these changes into an F-4 stabilator actuator in order to directly use it for the evaluation would have made the hardware more complicated and expensive while not aiding the purpose of the investigation. Therefore, a commercial actuator and control valve were used for the investigation. The single drive area actuator and servovalve eliminated the synchronization problem for the investigation hardware.

The drive area and stroke of the test actuator were selected to be similar to one section of the F-4 stabilator actuator. A high response servovalve (manufactured by DYVAL) was used. The servovalve had a nominal response at full amplitude of the 60 Hz (90° phase lag). A commercial actuator (manufactured by The Sheaffer Corporation) was modified to mount the high response valve on an adapter manifold and to use aerospace rod seals to reduce the actuator seal friction. The actuator

incorporated pressure-transducer mounting provisions so the pressures in the cylinder could be measured. The actuator incorporated rod-end bearings at both ends and was an equal area actuator. Position of the test actuator was measured by a precision position potentiometer (manufactured by the Waters Corporation) mounted parallel to the centerline of the actuator rod. Figure V-1 shows the test actuator, manifold, and servovalve assembly.

To use load-pressure feedback, the control electronics incorporated a variable bandpass filter in series with the load-pressure electrical signals. The control electronics incorporated a driving servoamplifier for the high-response valve and a position feedback summing amplifier for the position loop closure for the actuator. Signal conditioning for the pressure transducers used for feedback of the load-pressure was also incorporated into the control electronics.

Specific Technical Approach

The impedance characteristics necessary for flutter suppression were calculated from the equations for a second-order spring-mass system with damping. These calculations were made by DCI on prior programs and appear in the publication AFFDL-TR-75-29, pages 123 through 160.

The normal F-4 stabilator actuator (sized by flutter requirements) has a drive area of 6.0 square inches for each half of the tandem actuator. The drive area required by the stabilator for maneuvering the aircraft is 3.44 in^2 , or 57 percent of the area for the normal actuator. The torsional resonant frequency of the stabilator slab surface with both halves of the normal actuator operating is 23 Hz.^a

Test measurements of the normal actuator show that at frequencies above 1.5 Hz, the actuator stiffness is approximately 200,000 lbs/in.^b Test measurements for a modified stabilator actuator having 3.44 square inch drive areas and a half-stabilator surface (one half had been cut away, reducing the rotational inertia by nominally 50 percent) showed a torsional resonance frequency of nominally 20 Hz.^c This agreed fairly well with the 17.4 Hz frequency calculated by using the stiffness reduction of the modified actuator in combination with the inertia reduction corresponding

^aAFFDL-TR-71-20, Supplement 2, pages 217 and 218.

^bAFFDL-TR-72-13, page 190.

^cAFFDL-TR-79-3117, page 39.

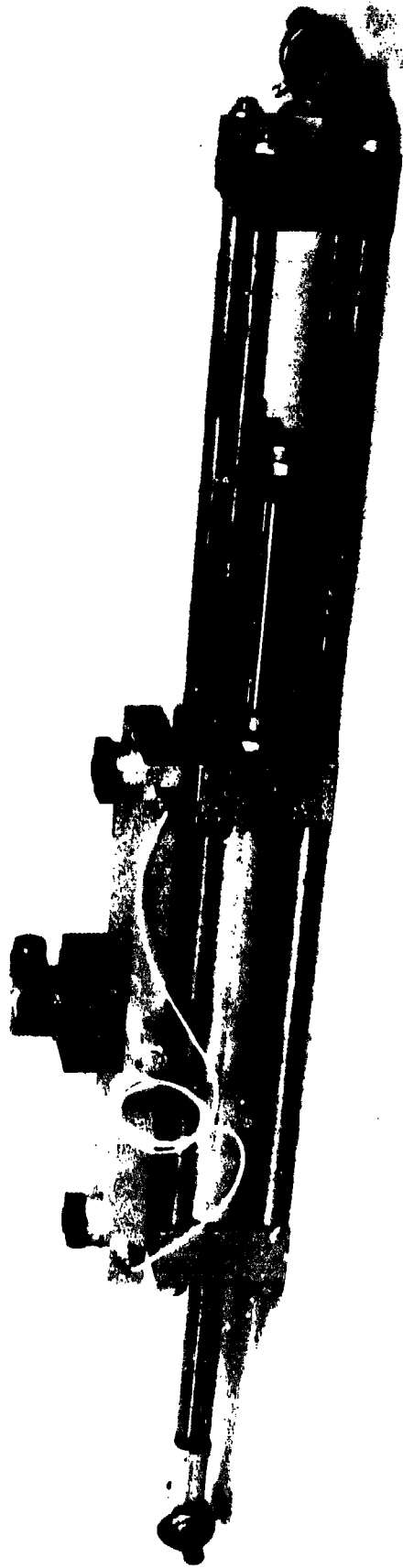


Figure V-1. Test actuator.

to a half-stabilator surface. The calculated torsional resonant frequency of a full stabilator surface when operating with one-half of the reduced drive area actuator is 12.3 Hz.^d

As described in AFFDL-TR-75-29, pages 142 and 143, providing an orifice across the actuator piston will suppress (damp) the amplitude of motion at the torsional resonant frequency. The inertia of the stabilator surface as presented to the actuator is nominally 19.15 lbs-sec²/in, based upon the measured stiffness of the normal F-4 stabilator actuator and the resonant frequency of 23 Hz.^e To provide a damping ratio of 1.0 (critical damping with no peaking) with a single 3.44 in² drive area actuator and the load inertia of 19.15 lbs-sec²/in, the load pressure feedback loop must provide a damping flow of 0.016 in³/sec/lb/in² at the resonant frequency of 12.3 Hz. Note that the damping flow required for critical damping decreases linearly with increasing frequency.

Using electronic feedback of the load pressure to change the impedance of a control actuator requires the servovalve controlling the actuator to have minimum phase shift and a flat amplitude response over the frequency range in which impedance modification is to be accomplished. For the F-4 stabilator example used for sizing the evaluation hardware, impedance modification in the range of 12 Hz to 25 Hz is desirable. The servovalve selected for the evaluation effort was a Model 12 DYVAL servovalve flow rated at 15 GPM with a pressure drop of 1000 psi. The valve was ordered with 80 ohm coils which required 75 ma for maximum flow (with the coils connected in series). According to the manufacturer's data sheet, the frequency response of the valve at maximum rated input current is attenuated by 3 dB at 50 Hz (relative to 0 dB at 1 Hz) and exhibits - 90° phase shift at 60 Hz. The frequency response of this valve (which has an output flow representative of a medium-flow aerospace valve) is representative of high response aerospace valves with similar flow ratings. The response is also rated at maximum input current, while many valves are response-rated at input levels of 10 to 25 percent of maximum and exhibit a reduced response at larger input levels.

The actuator used for the evaluation hardware was an "HH" series double-ended Sheaffer actuator rated for 3000 psi service. The actuator had a bore diameter of 2.5 inches, a rod diameter of 1.5 inches and a stroke of 11 inches. The bore and rod diameters defined a drive area of 4.12 in², slightly larger than the 3.44 in² required for F-4 stabilator maneuvering requirements with one half of the actuator operating. The stroke of the actuator, at 11 inches, was 0.5 inches longer than the stroke of a normal F-4 stabilator actuator. These deviations from the modified F-4 drive area and stroke previously used were made in order to use standard commercial hardware sizes wherever

^dAFFDL-TR-75-29, page 142.

^eAFFDL-TR-75-29, page 141.

possible and did not affect the results of the investigation. As shown in Figure V-1, four steel rods were used to construct a tail stock for the actuator. The rods, 3/4 inch diameter and 12 inches long, provided a tail stock stiffness of 3.64×10^6 lbs/in. The *oil column* stiffness of the actuator with an oil having a bulk modulus of 100,000 lbs/in² is 0.7×10^6 lbs/in, 4.24 percent of the tail stock stiffness. To minimize the seal friction in the actuator, the rod end seals received with the actuator were replaced with Shamban Delta seals.

The manifold used to connect the output ports of the servovalve to the cylinder mounted directly on the actuator, using two *screw-in* quills to attach the manifold to the actuator. The 3/8 inch diameter connecting passages between the servovalve and the ends of the cylinders were angle-drilled in the manifold to provide the shortest path for fluid flow. The manifold incorporated Kulite HKM-375-5000 SG pressure transducers mounted at the ends to monitor the cylinder port pressures of the actuator.

Figure V-2 shows the Waters 11-S-12/300-0-C position transducer mounted to the actuator body. The transducer was used to measure the actuator stroke. The output of the position transducer was used as a feedback signal for the actuator's position control loop and to measure the effect of load pressure feedback on actuator motion. Also shown in Figure V-2 is the coupling link from the actuator rod to the position transducer. A guide block mounted on the link was used to make the coupling link an anti-rotation device for the actuator rod.

Before the impedance modification evaluation of the complete actuator, the response of the DYVAL servovalve with three different driving configurations was evaluated. The valve was used to drive the test actuator at different input amplitudes and frequencies and the actuator response to driving signal recorded. Since the actuator was driven *open loop*, the actuator's integration of flow contributed 90° of phase lag. The difference between the measured phase lag and the 90° contributed by the actuator integration was the phase lag contribution of the servovalve. Two of the three configurations used a voltage driver and the valve coils connected in parallel or series. The third configuration used a current driver (with coil current being used as a feedback signal for the driver) and the coils connected in parallel. The following phase shift data (recorded for a input level to the valve driver of 10 percent) is representative of the servovalve phase response while driving the actuator.

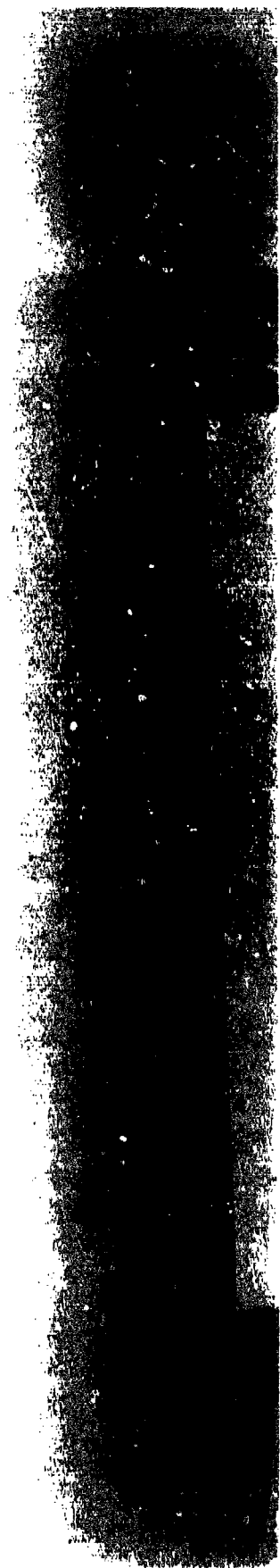
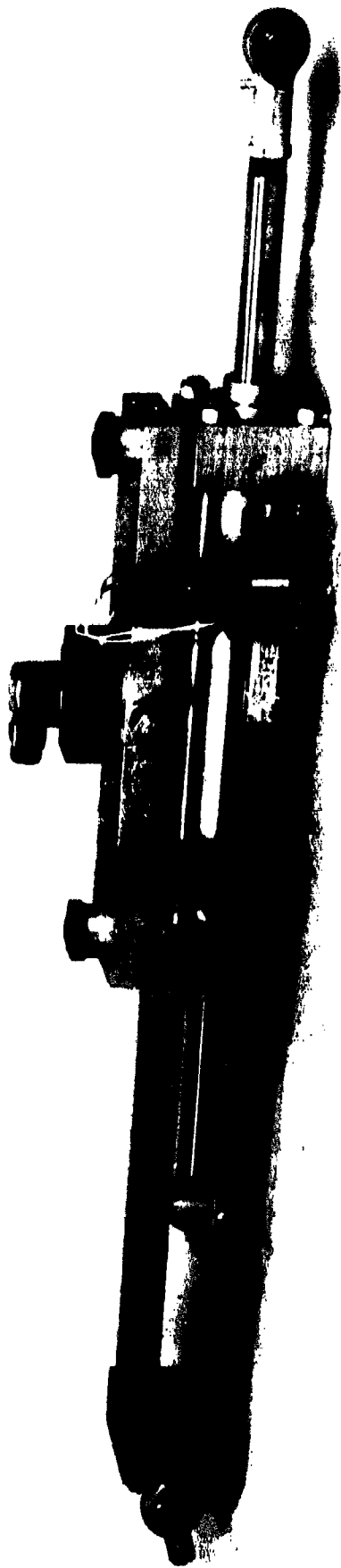


Figure V-2. Left side of test actuator.

Frequency In Hz	Phase Angle		
	Series Coil Voltage Driver	Parallel Coil Voltage Driver	Parallel Coil Current Driver
10	- 37.7°	-33.6°	-12.1°
30	- 93.5°	-82.9°	-30.8°
50	- 121.4°	-111.8°	-48.5°

The following observations can be made from this data:

1. Parallel coil operation gives slightly less phase shift than series operation.
2. The use of a current driver provides a significant reduction in the phase shift of the control valve.

A parallel-coil current driver for the servovalve was used in the control electronics for the impedance modification evaluation, since that driver gave the least phase shift.

Figure V-3 shows the front panel of the Flutter Suppression Controller used for the investigation. The control electronics incorporated ten-turn dial potentiometers and test jacks on the front panel. Four separate control sections were provided as follows:

1. Command
2. Position
3. Differential Pressure
4. Bandpass Filter

The four sections were designed to be connected together using the input and output jacks on the front panel. No internal interconnection between sections was provided.

The command section was constructed with four input jacks and a signal ground jack. Two potentiometers were used, one to apply a DC bias input voltage as a command and one to adjust the gain of the forward loop by attenuating the signal input to the servovalve current driver. A small

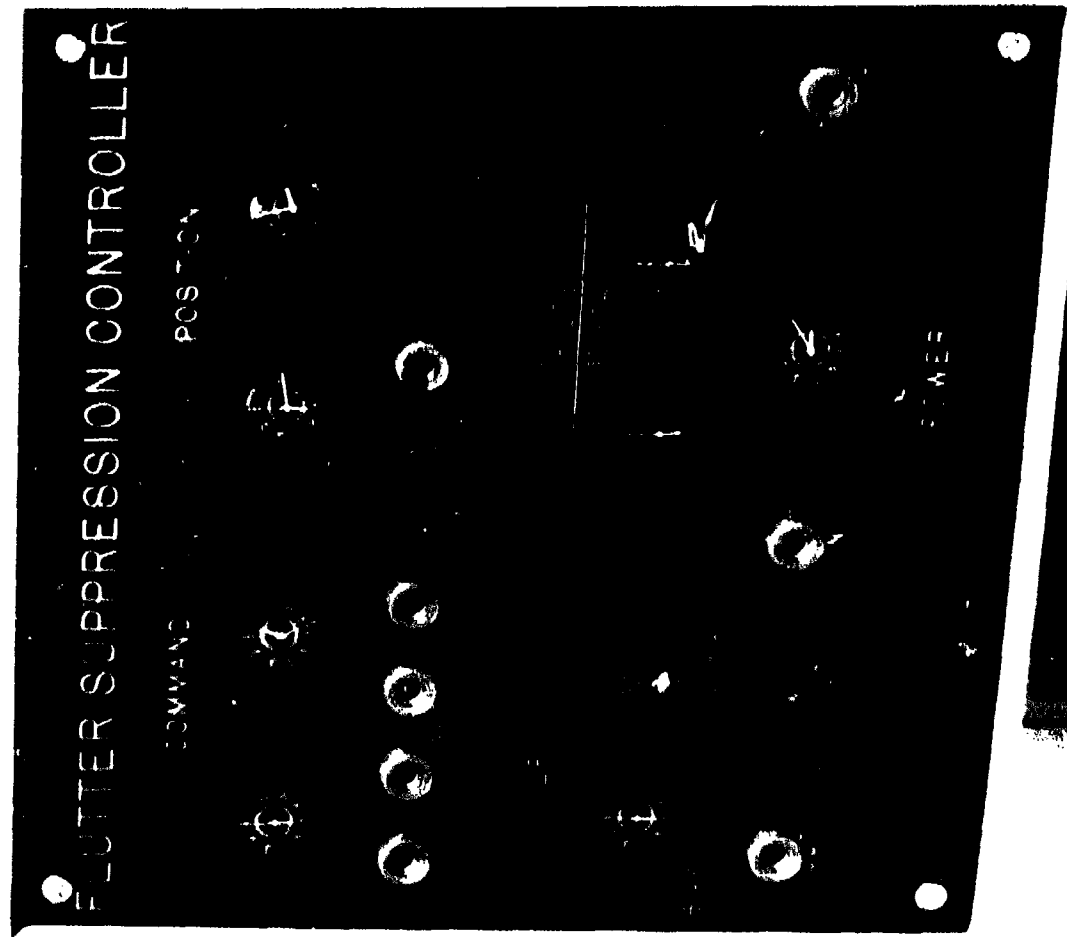


Figure V-3. Front panel of flutter suppression controller.

test jack to monitor the bias input voltage was provided on the front panel just below the bias potentiometer dial.

The position section was constructed with two output jacks and a signal ground jack. The two output jacks provided signals which were the complement of each other. Two potentiometers were used, one to provide a DC bias for the position output and the other to provide a variable gain between the input and output of the position section. A small test jack located just below the bias potentiometer dial was used to monitor the bias voltage.

The differential pressure section was constructed with a complementary pair of output jacks (for convenient signal polarity reversal) and a signal ground jack. The dial potentiometer was used to vary the gain of section. Two screwdriver adjustable panel potentiometers were located just below the differential pressure gain dial. These potentiometers were used to adjust the gain of the signal conditioning electronics for the individual pressure transducers used to create the differential pressure output signal. The small test jacks labeled *bias* and located immediately below the screwdriver adjustable panel potentiometers were used to monitor the output of individual pressure transducer electronics (before the outputs were summed to create a differential pressure output signal).

The bandpass filter section was designed with a single input and output jack. Filter slopes of 6 dB/octave were used for the test evaluation (although the internal design of the filter board allowed the option of using 12 db/octave slopes). Three front panel potentiometers allowed adjusting the two break frequencies of the bandpass filter and the gain of the filter section. A small test jack located between the two break frequency potentiometers provided a measurement point for the signal level between the low pass and high pass electronics of the filter section.

Figure V-4 shows the rear panel of the Flutter Suppression Controller. Three separate connectors were used for coupling the controller to the actuator. For the servovalve and position transducer a four pin connector was used. The position transducer required both a plus and minus voltage line and a wiper output line. The connector on the servovalve also used four pins, two for each of the torque motor armature coils. Parallel operation of the armature coils was implemented by interconnecting the coils at the controller connector. The differential pressure connector used ten pins. The Kulite pressure transducers were a bridge configuration, requiring four electrical connections for each transducer. The three unlabeled test jacks located above the connectors were connected to the positive, negative and ground connections of the controller's internal power supply.

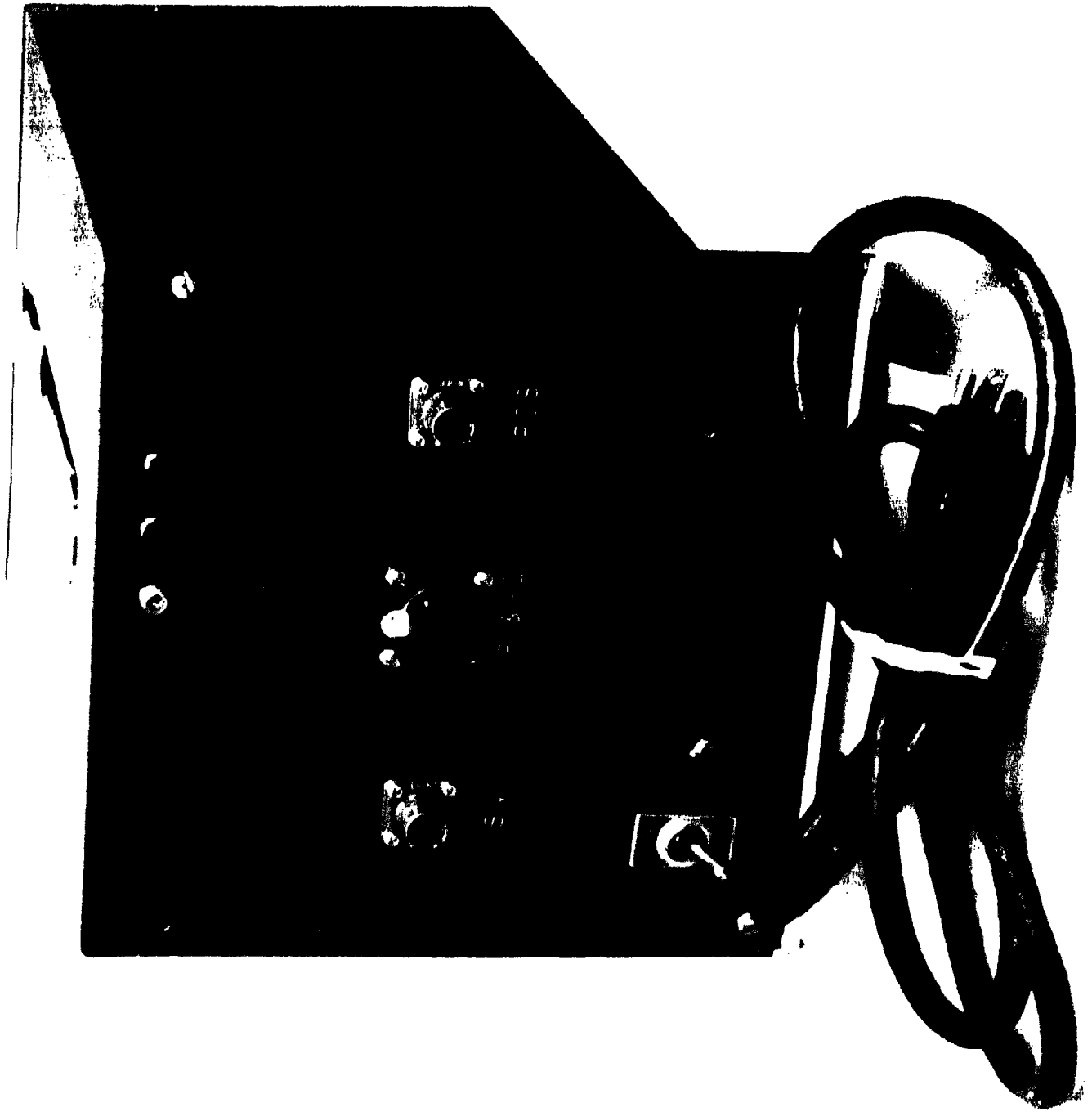


Figure V-4. Rear panel of flutter suppression controller.

The rear panel also incorporated the on-off switch and power line fuse for the controller. The *power on* indicator was mounted on the front panel of the controller.

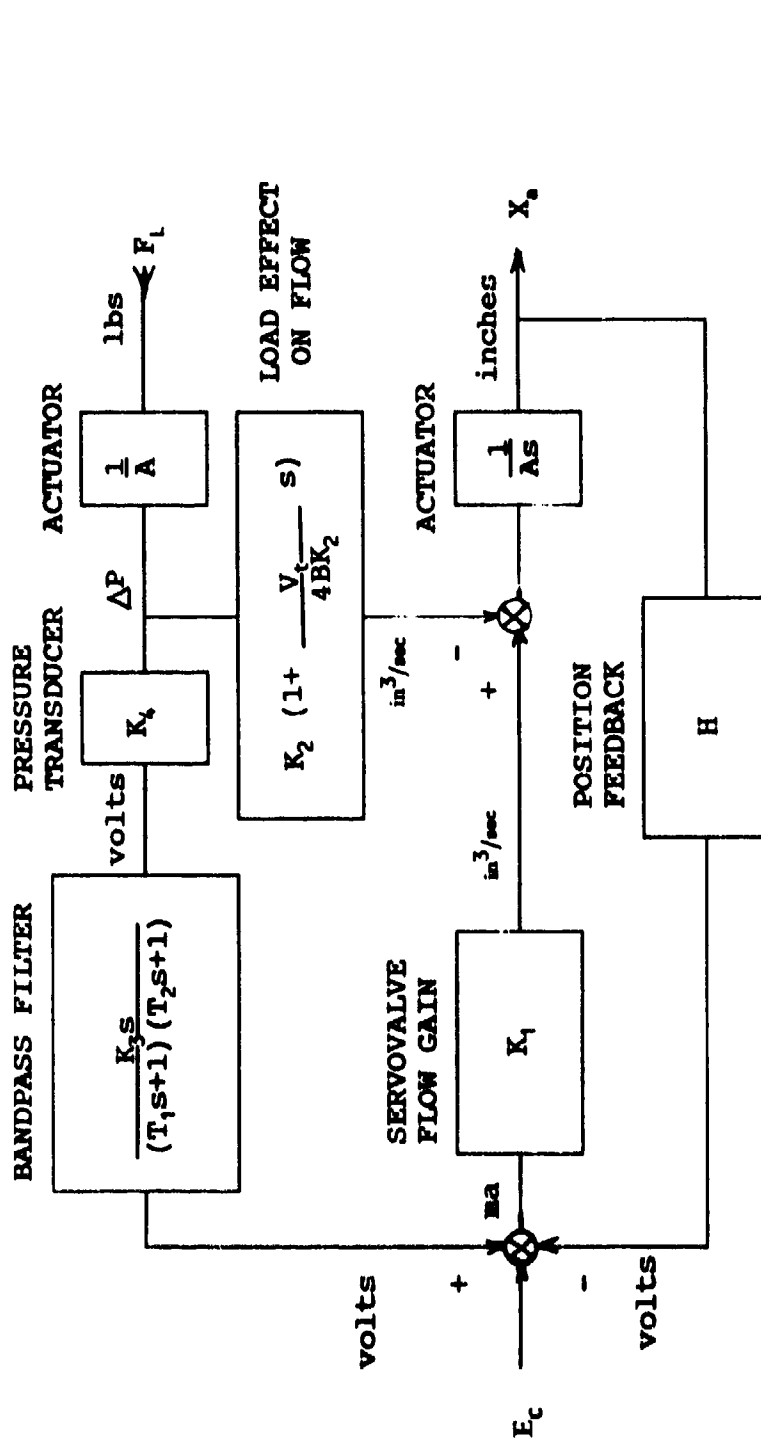
Figure V-5 is a simplified and linearized block diagram of the Flutter Suppression actuator. With no load force (F_L), the control loop is a conventional electrohydraulic position system. The effect of the load force is to reduce the flow to the integrating actuator from the servovalve. This reduction is both a steady state and dynamic effect. The steady state effect is a reduction of the flow to move the actuator because of leakage. This load pressure sensitivity is represented by the term K_2 . The effect of the load force reducing the differential pressure across the servovalve (which causes a reduction of the valve's output flow) is ignored in order to linearize the model. This assumption does not induce large errors if the differential load pressures are much less than the differential supply pressure across the servovalve (within the constraint of $P_L < 2/3 P_g$). The dynamic effect of the load pressure is due to the compliance of the fluid in the actuator and depends on the rate of change of the load pressure. The effect is to reduce the dynamic flow gain of the servovalve (particularly when the load is a function of the actuator motion).

The load pressure loop shown in Figure V-5 is a positive feedback loop. The bandpass filter in series with the differential pressure signal across the actuator's drive area is a *lead over a double lag* filter. This filter blocks the low frequency effects of feeding back load pressure so that the static stiffness and steady state position accuracy of the position control loop are not effected.

III. TEST PROCEDURE

To evaluate the operation of the test actuator and control electronics, the actuator was mounted in the General Purpose Actuator Test Rig (GPATR) located in the Actuation Laboratory, Area B, Building 145, WPAFB. The GPATR can generate a loading force of 82,000 lbs and has a maximum unloaded slew rate of 107 inches per second. For the tests conducted on the flutter suppression actuator, the load system was configured to generate a maximum force of 41,000 lbs. With this configuration, at 2/3 of the maximum force available force (with 2000 psi differential pressure across the load actuator drive area), the available slew rate was 62 inches/second. Figure V-6 shows the GPATR with flutter suppression actuator mounted in test actuator position and the Flutter Suppression Controller connected to the actuator.

Evaluation of the flutter suppression actuator was divided into eight separate tests. The first four tests were conducted to establish and document correct operation of the load system and test actuator combination. The last four tests were made to evaluate and document the effectiveness of using load



Where: E_c = input command (volts)
 T_1, T_2 = bandpass filter time constants (seconds)
 K_3 = bandpass filter gain (volts/volt)
 K_4 = differential pressure electronics gain (volts/psi)
 K_1 = servovalve flow gain (in\$^3\$/sec/ma)
 K_2 = servovalve flow gain (in\$^3\$/sec/psi)
 V_t = actuator fluid volume (in\$^3\$)
 B = adiabatic bulk modulus of fluid (lb/in\$^2\$)
 H = position feedback gain (volts/in)
 A = actuator drive area (in\$^2\$)
 S = Laplace operator

Figure V-5. Block diagram.

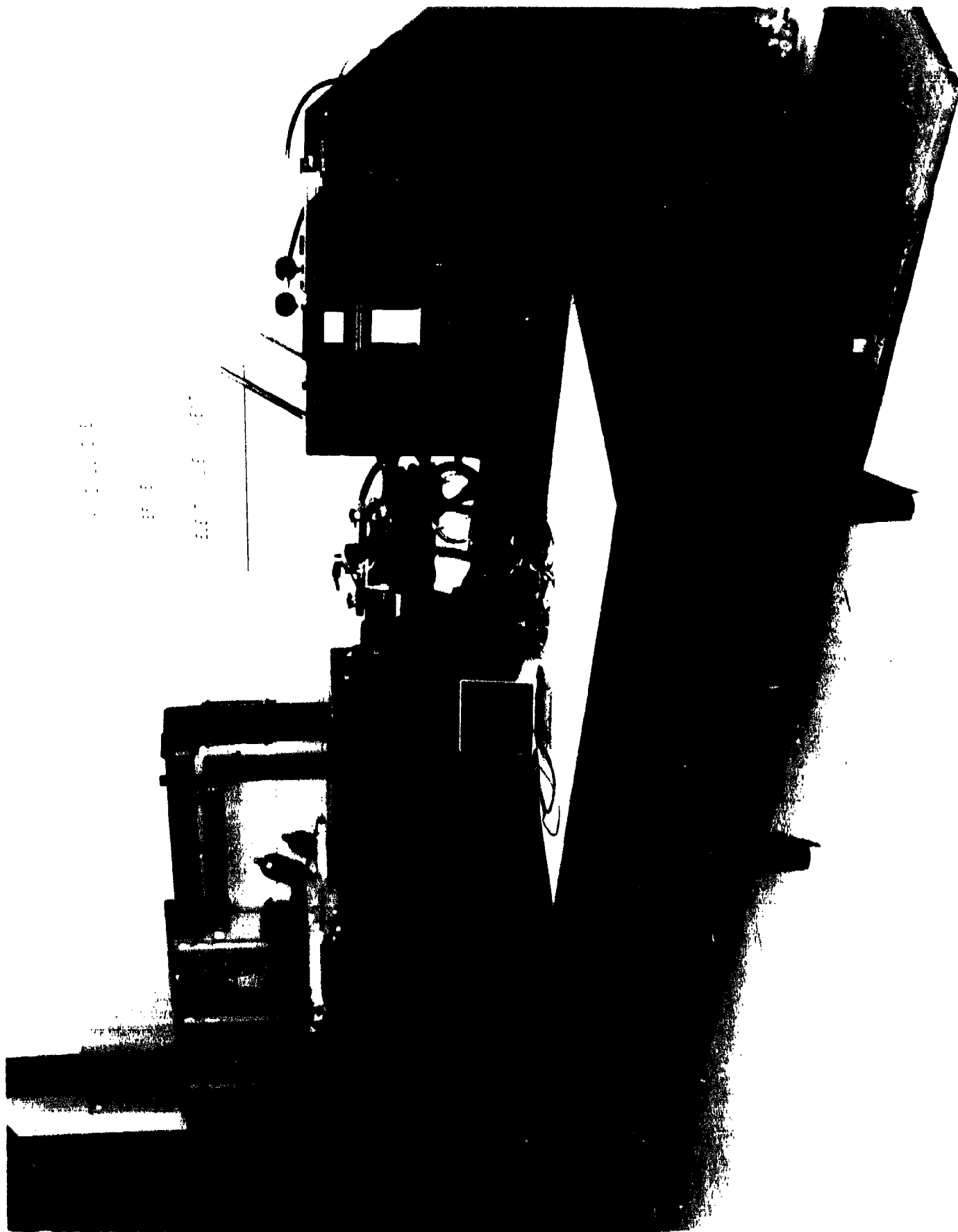


Figure V-6. Flutter actuator test configuration.

pressure feedback on the test actuator. For all tests, an HP 5423 Digital Response Analyzer was used to make response measurements. The seven tests run were the following:

<u>Test Sequence</u>	<u>Description</u>
A	Position frequency response of the flutter actuator coupled to the load actuator with the load actuator bypassed.
B	Force frequency response of the GPATR load actuator against the flutter actuator with the flutter actuator commanded to hold a steady state position.
C	Position frequency response of the flutter actuator coupled to the load actuator with the load actuator commanded to zero load.
D	Differential pressure/load force frequency response.
E	Flutter actuator stiffness with no load pressure feedback.
F	Flutter actuator stiffness with load pressure feedback without the bandpass filter.
G	Frequency response of bandpass filter - final settings.
H	Flutter actuator stiffness with load pressure feedback with the bandpass filter and different feedback gains.

Test A was run to establish the position response of the flutter actuator as adjusted for the test sequence. Two frequency ranges were used for the measurement. A 0-50 Hz frequency response measurement was made to document the actuator's position response capability over the frequency range in which the effect of load pressure feedback was expected to be effective. A 0-12 Hz frequency response measurement was also made to verify that the position loop gain of the test actuator had been set to match the nominal response of the F-4 stabilator actuator (-3 dB at 1.5 Hz).

Test B was run to document the load pressure response of the GPATR when applying a load to the flutter suppression actuator. For this test, the flutter suppression actuator was commanded to a mid-stroke position. The load actuator response at 12 percent of full scale (5000 lbs peak) was run over the 0-50 Hz frequency range. The purpose of this test was to verify that the GPATR load system could maintain a sufficiently large applied load over the frequency range of interest.

Test C was conducted to document the effect of the dynamic limitations of the loading system on the position response of the flutter actuator. For this test the load actuator was commanded to maintain zero load. The flutter actuator position response to a sinusoidal input was then recorded. Differences in the frequency response between this test and the results of Test A show the effect of the loading system dynamics on the flutter actuator response.

Test D was conducted to document the relationship between the load force applied to the flutter actuator and the output of the signal conditioning electronics used with the pressure transducers.

Test E measured the basic stiffness of the flutter suppression actuator without load pressure feedback. For this test, the flutter suppression actuator was commanded to hold a fixed position and the load actuator used to apply a force to the flutter suppression actuator. The ratio of force to deflection as a function of frequency was recorded over the frequency range of 0-50 Hz.

Test F measured the stiffness of the flutter suppression actuator with load pressure feedback and no bandpass filter. For this test, the pressure feedback gain was set considerably below where instability occurred. The purpose of this test was to evaluate the general effect of the load pressure feedback without the bandpass filter operating.

Test G was run to document the frequency response characteristics of the final configuration of the bandpass filter. The response of the filter from 0-50 Hz was recorded.

Tests H were run to document the performance of the complete configuration with load pressure feedback and the bandpass filter operating. The frequency range of 0-50 Hz was used for the response measurements. The force to deflection ratio was recorded over the 0-50 Hz range for three different feedback gain values. The highest gain used was as high as possible while maintaining stable operation of the actuator.

Figure V-7 is a closeup view of the flutter suppression actuator in the GPATR test rig. Note that the actuator was mounted as a moving body actuator in order to connect the rod end of the actuator to the sliding slug retained by a shear pin. If excess force were applied to the flutter actuator and the shear pin severed, any movement of the suppression actuator within the stroke limits of the load actuator would not damage the flutter suppression actuator.

IV. TEST RESULTS AND ANALYSIS

Figures V-8, V-9, V-10 and V-11 show the flutter actuator's position response for a 2-percent command input amplitude. Figure V-8 is a magnitude plot over the frequency range of 0 to 50 Hz and Figure V-9 is the corresponding phase angle plot. The cursors on Figure V-8 indicate that the magnitude is 3 dB down at 1.7 Hz. The cursors on Figure V-9 show that the phase angle of -90° occurs at 6.5 Hz. Note that the magnitude falls off smoothly above 1.7 Hz and the phase angle of the actuator approaches -180° at 50 Hz. Figures V-10 and V-11 present the same measurement over

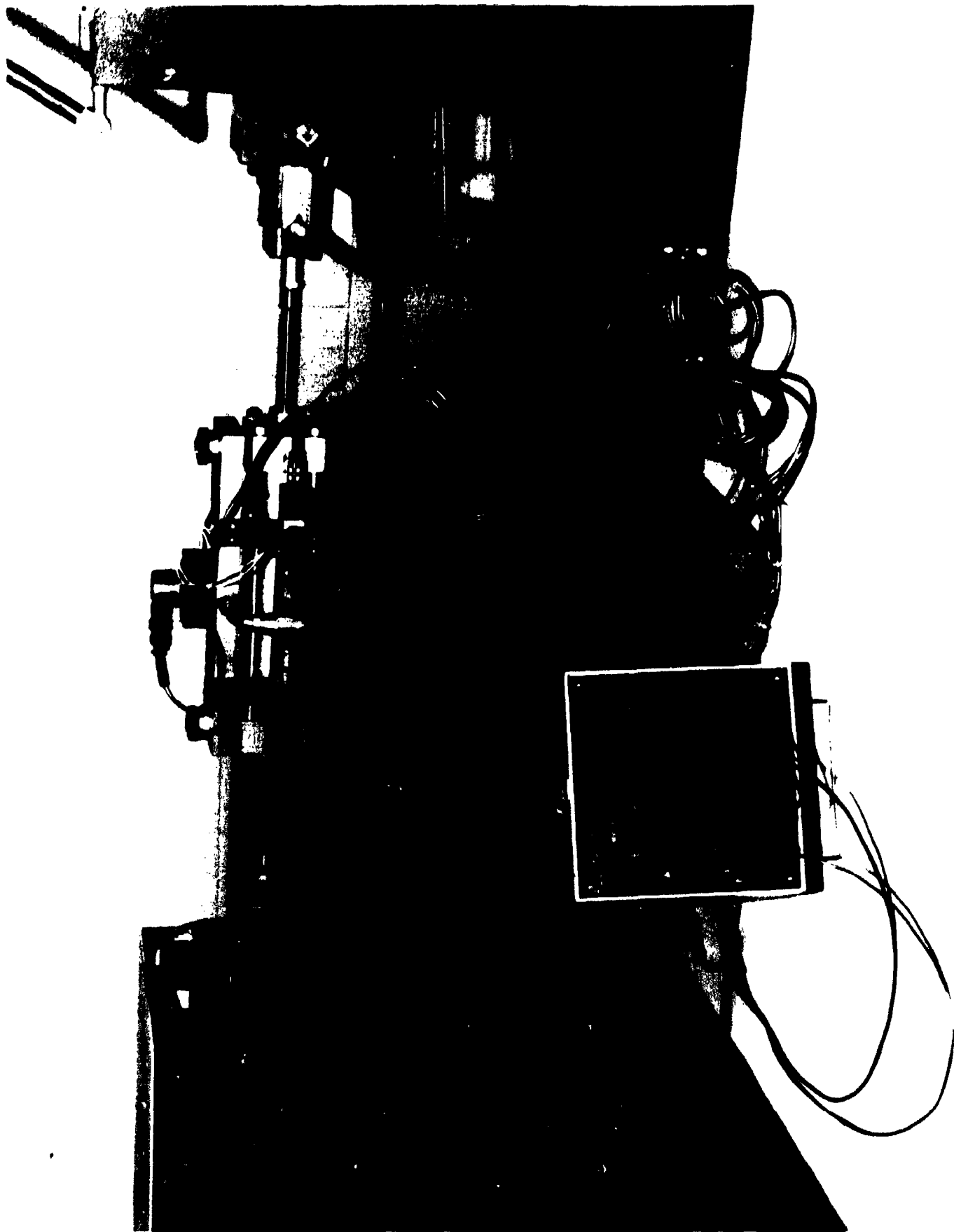


Figure V-7. Close-up view of test configuration.

TEST DATA

DATE: 10 APR 86

TEST ITEM: Flutter Suppression Actuator

CONFIGURATION: Position loop coupled to load actuator,
depressurized and bypassed

TEST: 2% FS - Frequency Response to 50 Hz

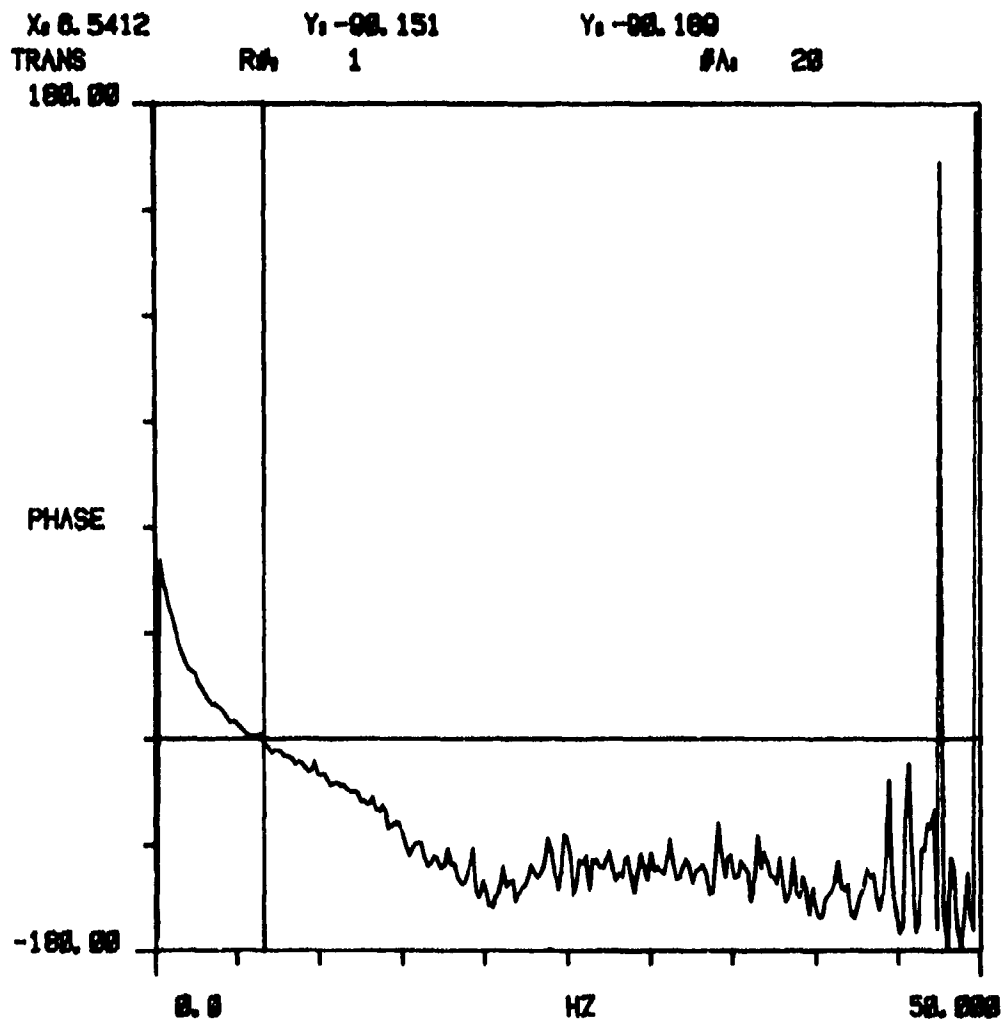


Figure V-9. Position response - phase - 50 Hz.

TEST DATA

DATE: 10 APR 86

TEST ITEM: Flutter Suppression Actuator

CONFIGURATION: Position loop coupled to load actuator,
depressurized and bypassed

TEST: 2% FS - Frequency Response to 12.5 Hz

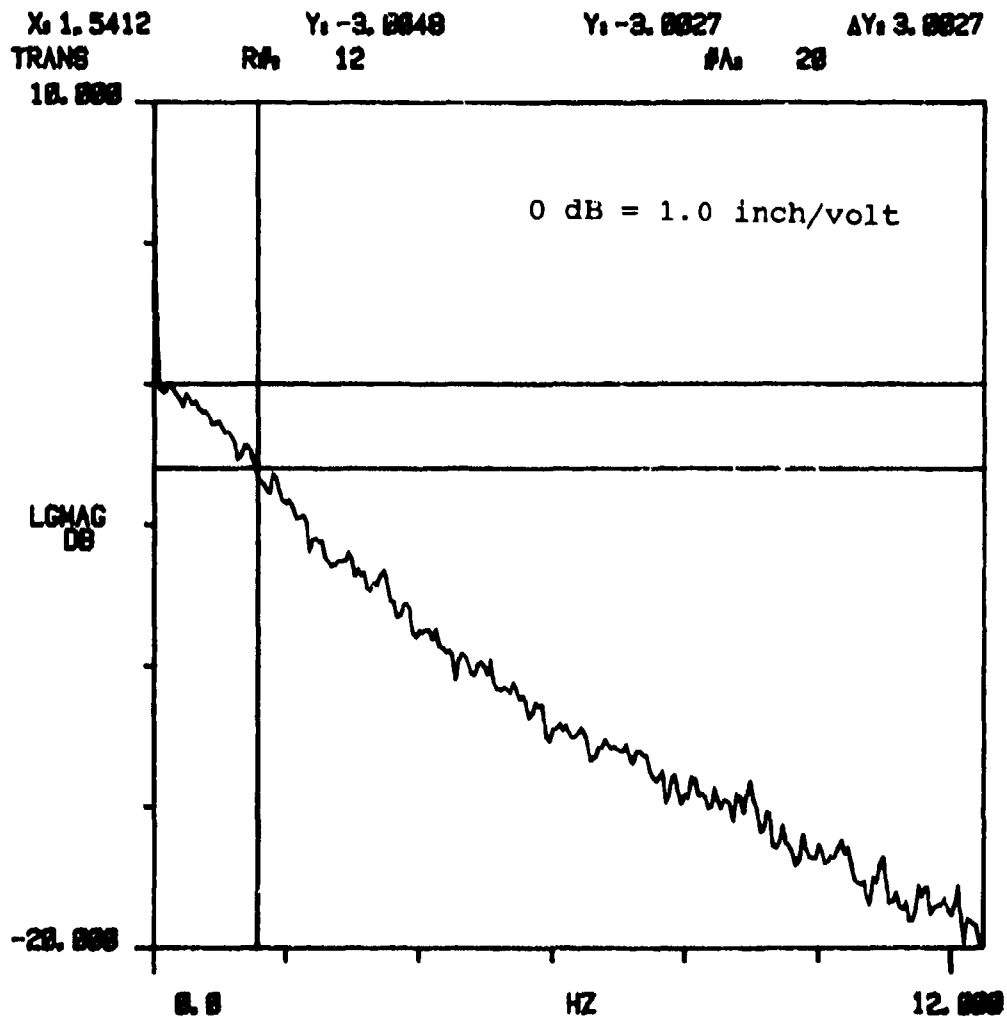


Figure V-10. Position response - magnitude - 12 Hz.

TEST DATA

DATE: 10 APR 86

TEST ITEM: GPATR Load Actuator

CONFIGURATION: Force loop, 5000 lbs compressive load bias

TEST: 2% FS - Frequency Response (\pm 5000 lbs)

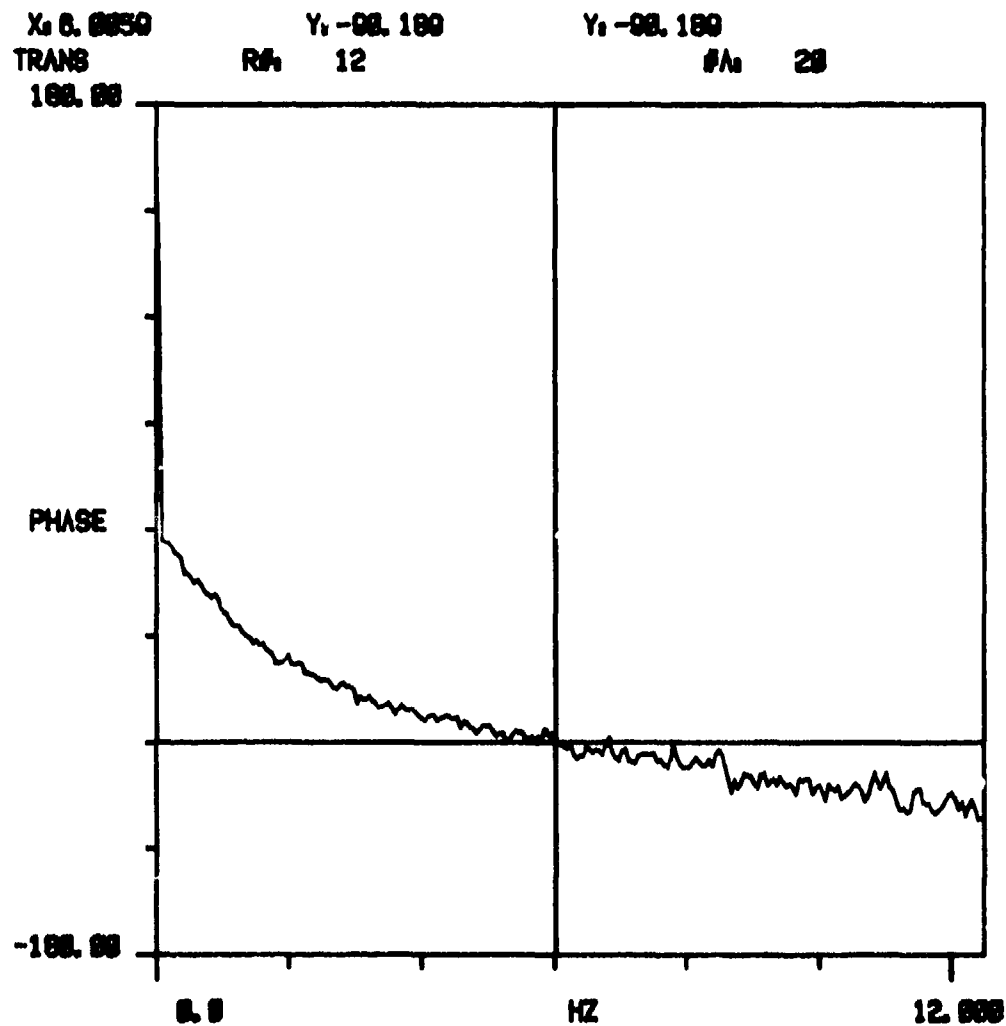


Figure V-11. Position response - phase - 12 Hz.

a more limited frequency range of 0 to 12 Hz for better resolution of the low frequency characteristics. The - 3 dB point on the magnitude curve of Figure V-10 occurs at 1.5 Hz and the - 90° phase angle of Figure V-11 occurs at 6.0 Hz. This frequency response compares well with the measured response of an F-4 actuator.^f

Figures V-12 and V-13 show the force response of the load actuator over frequency range of 0-50 Hz. A 5000 lb compressive load was maintained for this measurement (and for the actuator stiffness measurements run in the later tests). This steady state load was used to eliminate any effect from the bearing clearances of the rod end bearings used with the flutter suppression actuator. Therefore, 0 dB on Figure V-12 corresponds to 10,000 lb/volt (5000 lb compressive load \pm 5000 lb sinusoidal load). Note that the amplitude is attenuated by 3 dB at 26 Hz (to \pm 3535 lb) and 7.5 dB at 50 Hz (to \pm 2103 lbs). The phase angle of the applied load as shown in Figure V-13 corresponds to the gradual attenuation of the amplitude ratio over the 0-50 Hz frequency range. These results show that while driving the flutter actuator, the load system can generate sufficient force from 0-50 Hz to accurately measure the actuator stiffness. Note that for the force-to-deflection measurement, there is no requirement for a flat response from the loading system over the frequency range of interest (although it is desirable). The amplitude response only has to be adequate to load the test actuator enough to obtain some measurable deflection over the frequency range of interest.

Figures V-14 and V-15 are response plots of the flutter suppression actuator operating as a position actuator with the load actuator commanded to *zero* load. These plots, when compared to the unloaded plots taken in Test A, indicate whether the dynamic response of the load system is sufficient to ensure that the load system can *get-out-of-the-way* of the test actuator when the load system is commanded to *not-load* the test actuator. The test is a direct measurement of the quality of the load system. There is some level of load *error* required to command the load system to move in response to movement of the test actuator. If the load *error* is large enough to cause a significant change in the test actuator's position response, the load system has insufficient dynamic response for accurate load effect testing. Figures V-14 and V-15 show the position response of the flutter actuator from 0 to 12 Hz. The - 3 dB frequency is 1.53 Hz, which is the same as that of the unloaded actuator. The - 90° phase angle occurs at 4.1 Hz, slightly below the 6 Hz frequency measured by Test A. At 6 Hz, the effect of the load system to increase the phase lag by nominally 15°. From these test results, it was concluded that the load system operation had sufficient dynamic response for accurate load testing.

^f AFFDL-TR-72-13, page 204.

TEST DATA

DATE: 10 APR 86

TEST ITEM: GPATR Load Actuator

CONFIGURATION: Force loop, 5000 lbs compressive load bias

TEST: 2% FS - Frequency Response (\pm 5000 lbs)

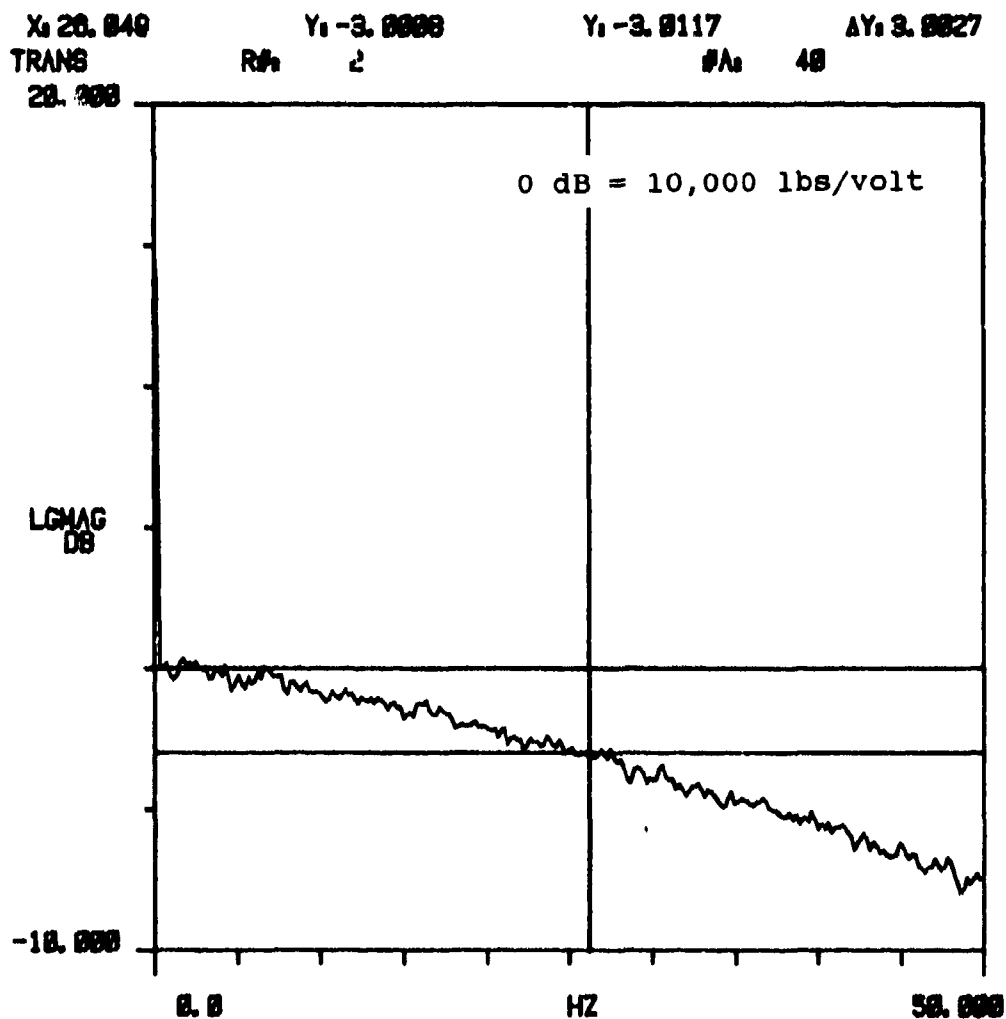


Figure V-12. Load force response - magnitude - 50 Hz.

TEST DATA

DATE: 10 APR 86
TEST ITEM: GPATR Load Actuator
CONFIGURATION: Force loop, 5000 lbs compressive load bias
TEST: 2% FS - Frequency Response to 12.5 Hz

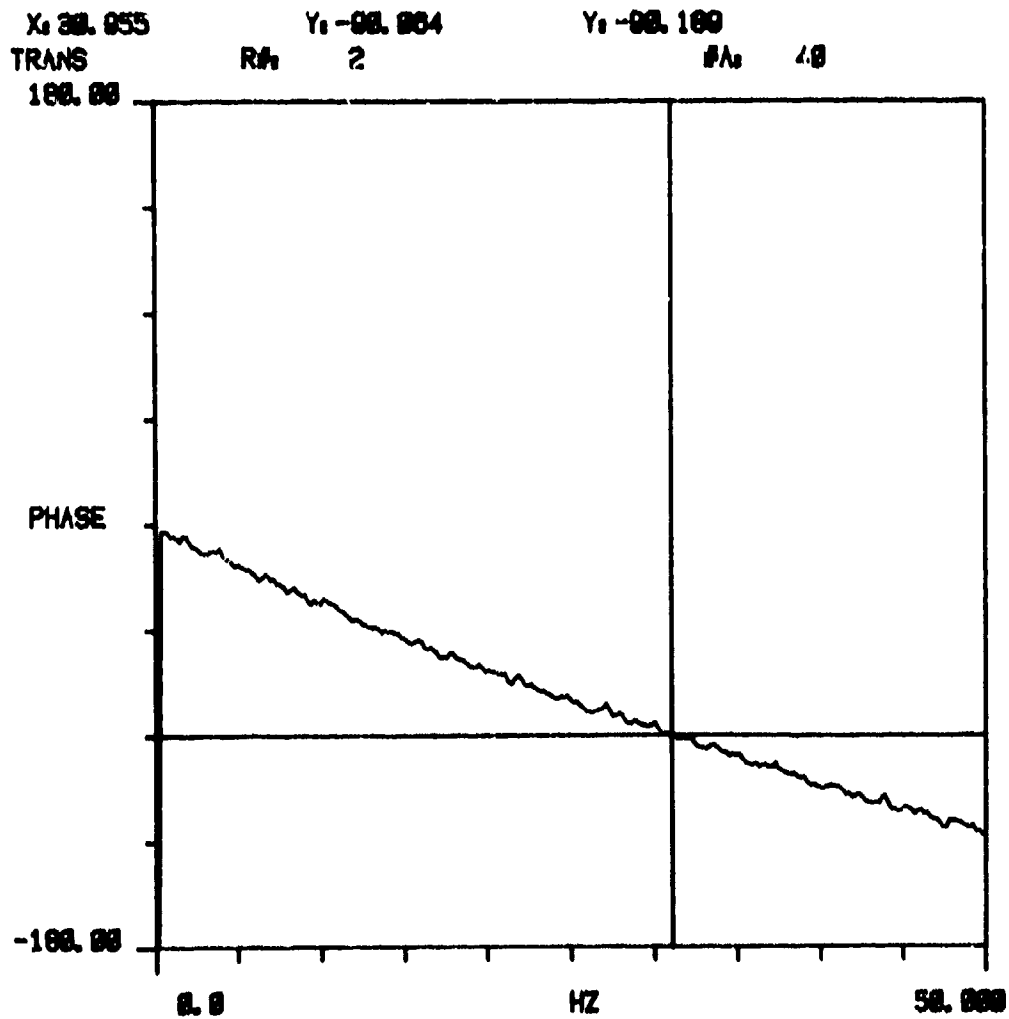


Figure V-13. Load force response - phase - 50 Hz.

TEST DATA

DATE: 10 APR 86

TEST ITEM: Flutter Suppression Actuator

CONFIGURATION: Position loop only, coupled to load actuator
Load actuator commanded to zero
5000 lbs compressive load bias

TEST: 2 $\frac{1}{2}$ FS - Frequency Response to 12.5 Hz

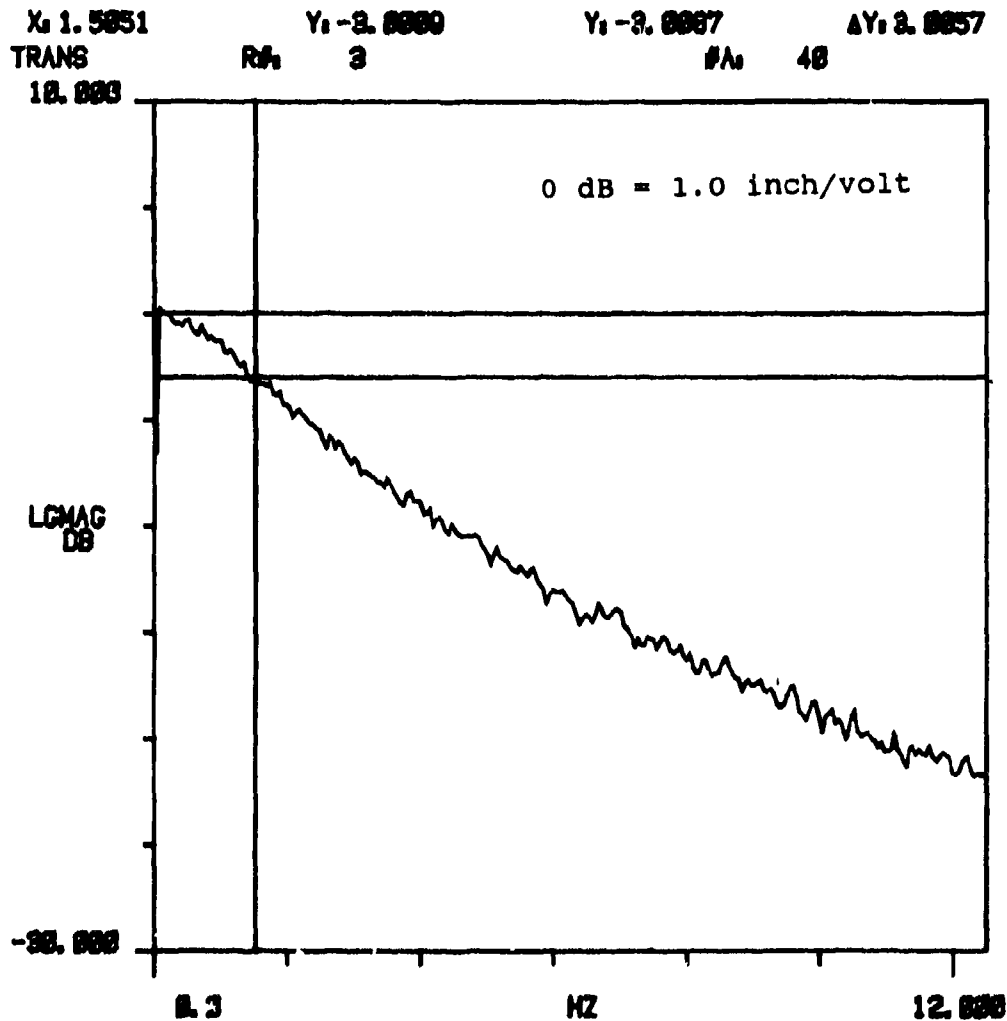


Figure V-14. Position response - zero load - magnitude.

TEST DATA

DATE: 10 APR 86

TEST ITEM: Flutter Suppression Actuator

CONFIGURATION: Position loop only, coupled to load actuator
Load actuator commanded to zero
5000 lbs compressive load bias

TEST: 2% FS - Frequency Response to 12.5 Hz

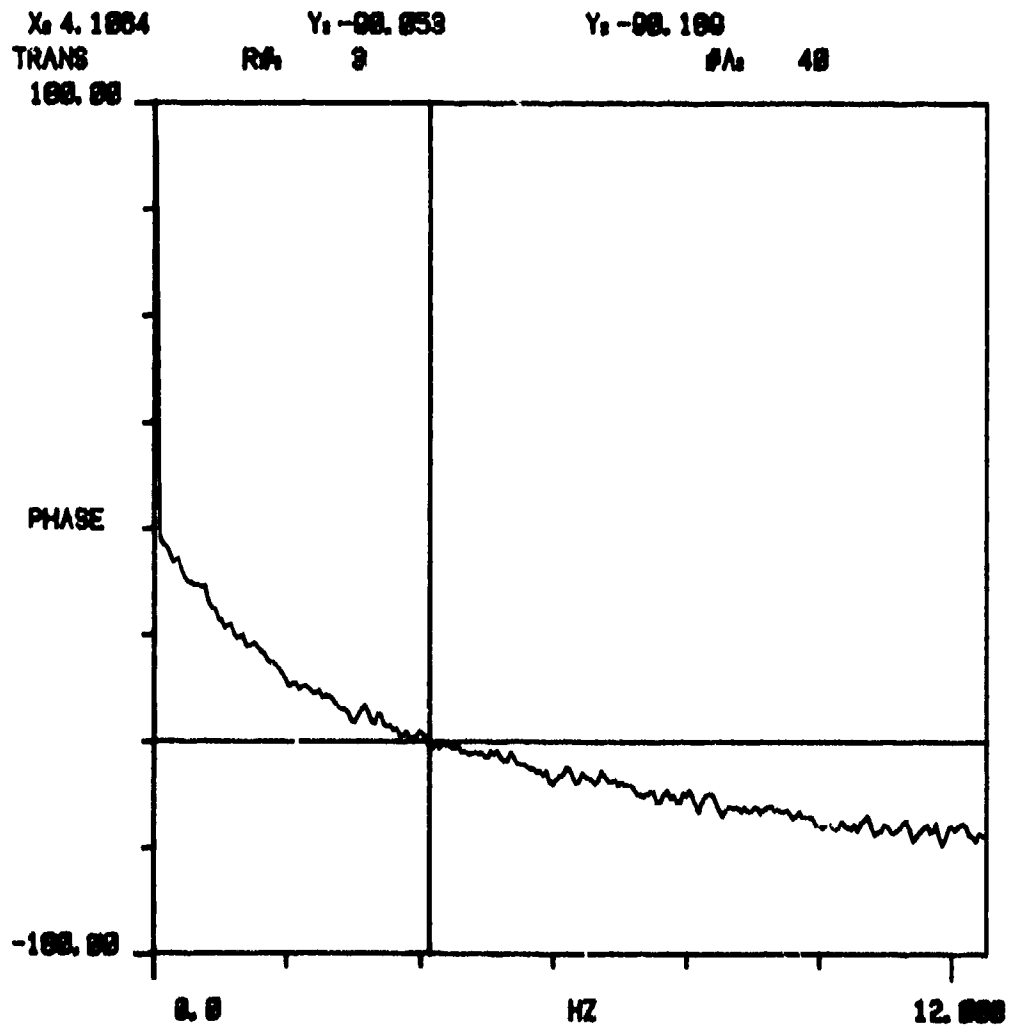


Figure V-15. Position response - zero load - phase.

Figure V-16 is a frequency response plot of the output of the differential pressure electronics versus the output of the load force transducer. For this measurement, a 5000 lb steady-state compressive-load-force was applied and a command voltage for a ± 5000 lb sinusoidal load was applied to the load system. The response plot shows that there is a slight amplitude attenuation of 2 dB over the measured frequency range of 0 to 50 Hz. There is also a slight phase angle change of nominally -5° over the same frequency range. The measured results demonstrate that the pressure transducer output provides an accurate measurement of the load force for use as a feedback signal over the frequency range of interest.

Figures V-17 and V-18 are stiffness (load force versus actuator deflection) response measurements of the flutter suppression actuator without load pressure feedback. The flutter suppression actuator's position command input is grounded. Note that on the amplitude plot of Figure V-17, the 27.8 dB amplitude corresponds to 245,000 lb/in. This stiffness is maintained from 0 to 25 Hz and then decreases gradually to 211,000 lb/in at 50 Hz. The measured stiffness of 245,000 lb/in is somewhat greater than the calculated value of 150,000 lb/in using oil with a bulk modulus of 100,000 lb/in². This implies that the bulk modulus of the oil was about 163,000 lb/in² for the response run. Figure V-18 shows the phase of the stiffness response. Except at very low frequencies (less than 2 Hz) where the position control system effects the phase angle, the force and deflection are in phase. This indicates that the actuator acts as a simple spring at frequencies above 2 Hz.

Figure V-19 is a response plot of the flutter suppression actuator's force-to-deflection ratio with load pressure feedback applied (without using the bandpass filter). The feedback gain of the pressure signal was set mid-value between 0 and a gain causing instability. Comparison of Figure V-19 with the stiffness plot of Figure V-17 is an indication of the effectiveness of load pressure feedback on modifying the stiffness of the flutter suppression actuator. Since no bandpass filter is used, Figure V-19 shows that the load pressure feedback degrades the static stiffness of the actuator. Note that the stiffness of the actuator is significantly reduced (compared to Figure V-17 without load pressure feedback) over the frequency range from 0 to 25 Hz. This is consistent with the physical operation of the actuator. Without load pressure feedback, actuator motion in response to an applied load is used entirely to compress the fluid contained in the actuator. With load pressure feedback, the actuator drive area has to push fluid *through the damping orifice* across the actuator piston in addition to compressing the fluid contained in the actuator. This additional motion for a given applied force results in a lower force-to-deflection ratio.

As shown in Figure V-19, the amplitude of the stiffness is lowest at nominally 0.5 Hz. The magnitude of the stiffness value is + 2.5 dB (13,300 lb/in) at this frequency. From 0.5 Hz to 25 Hz, the stiffness increases to + 28 dB (251,000 lb/in). From 25 Hz to 50 Hz the stiffness remains between 243,000 and 278,000 lb/in. Note that the phase of the stiffness is between $+45^\circ$ and $+75^\circ$

TEST DATA

DATE: 10 APR 86

TEST ITEM: Flutter Suppression Actuator

CONFIGURATION: Position loop
5000 lbs compressive load bias
± 5000 lbs load input (white noise)

TEST: Frequency Response ΔP vs Force

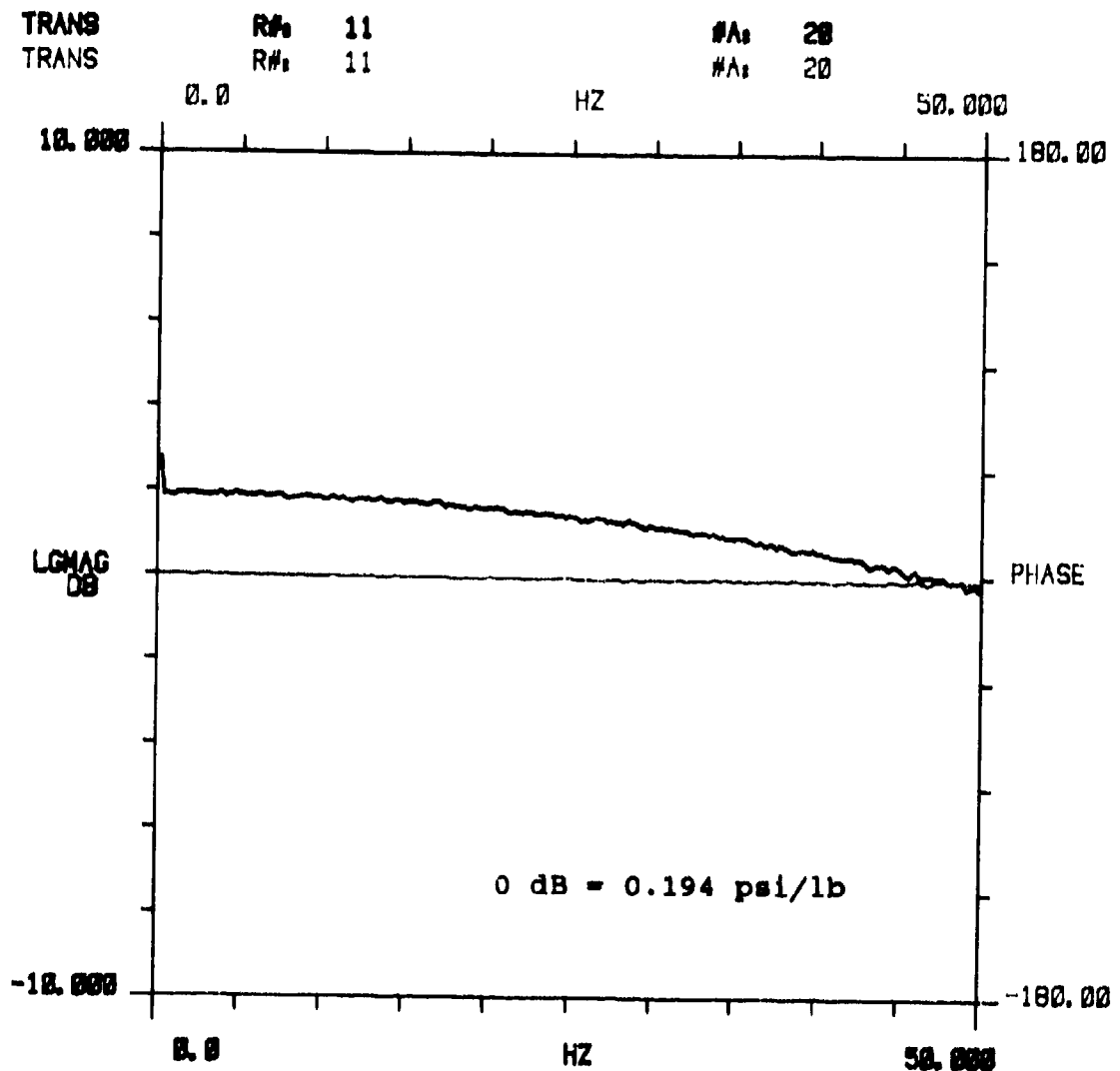


Figure V-16. Frequency response - pressure signal.

TEST DATA

DATE: 10 APR 86

TEST ITEM: Flutter Suppression Actuator

CONFIGURATION: Position loop
5000 lbs compressive load bias
± 5000 lbs load input (white noise)

TEST: Frequency Response - Force vs Deflection

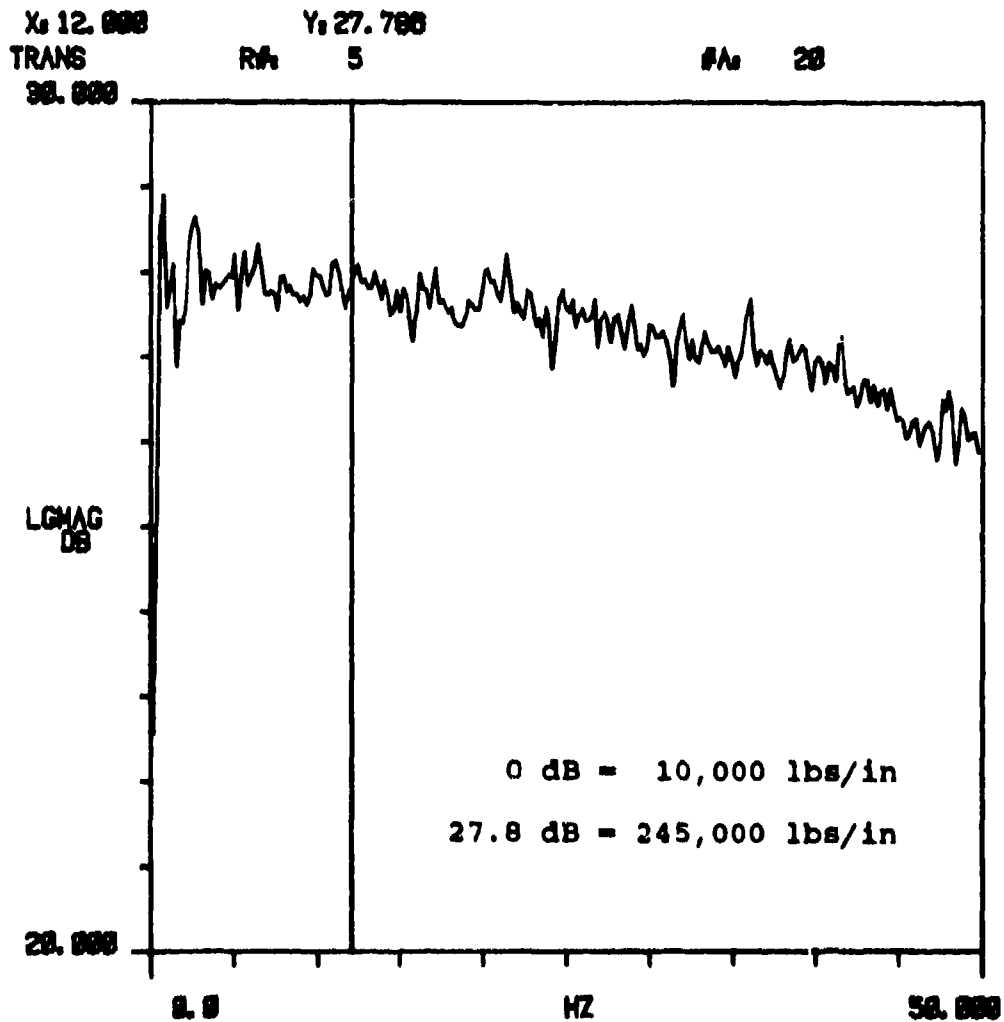


Figure V-17. Stiffness response - magnitude.

TEST DATA

DATE: 10 APR 86

TEST ITEM: Flutter Suppression Ac. ator

CONFIGURATION: Position loop
 5000 lbs compressive load bias
 \pm 5000 lbs load input (white noise)

TEST: Frequency Response - Force vs Deflection

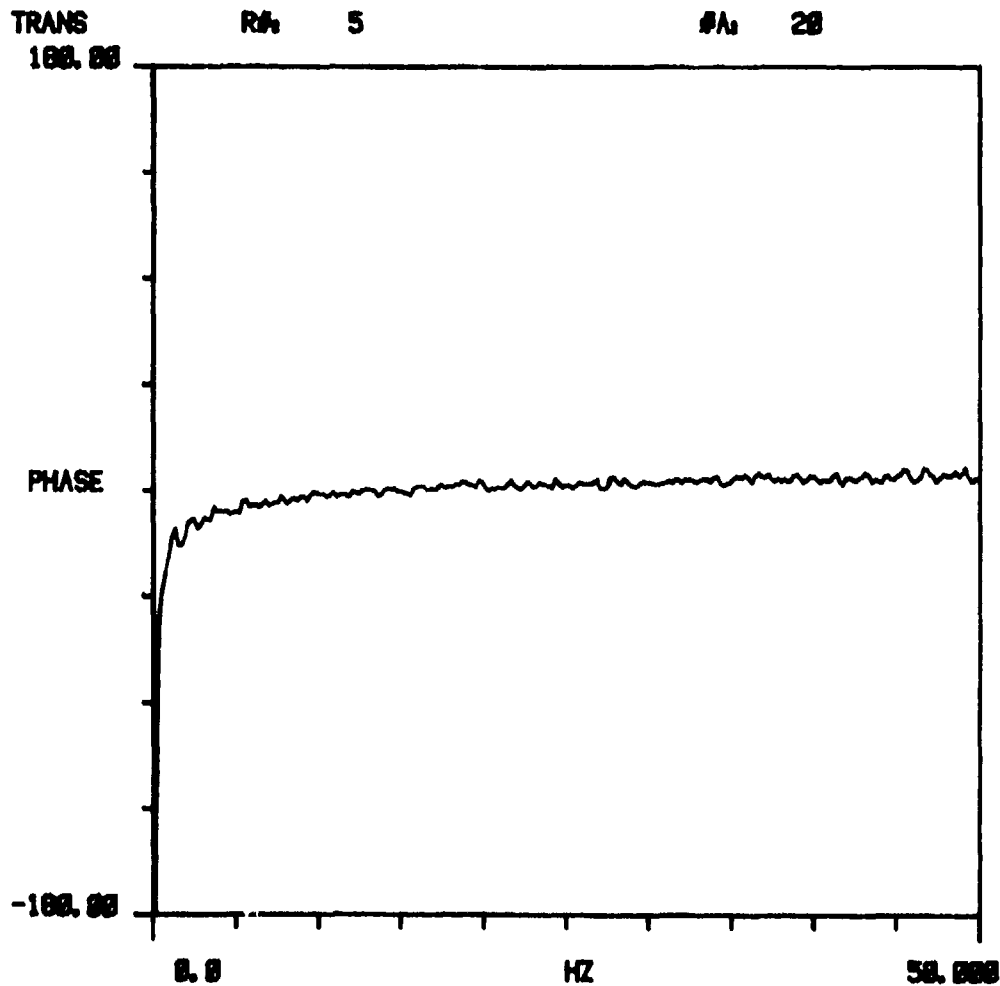


Figure V-18. Stiffness response - phase.

TEST DATA

DATE: 10 APR 86

TEST ITEM: Flutter Suppression Actuator

CONFIGURATION: Position loop + ΔP loop
5000 lbs compressive load bias
 ± 5000 lbs load input (white noise)

TEST: Frequency Response - Force vs Deflection

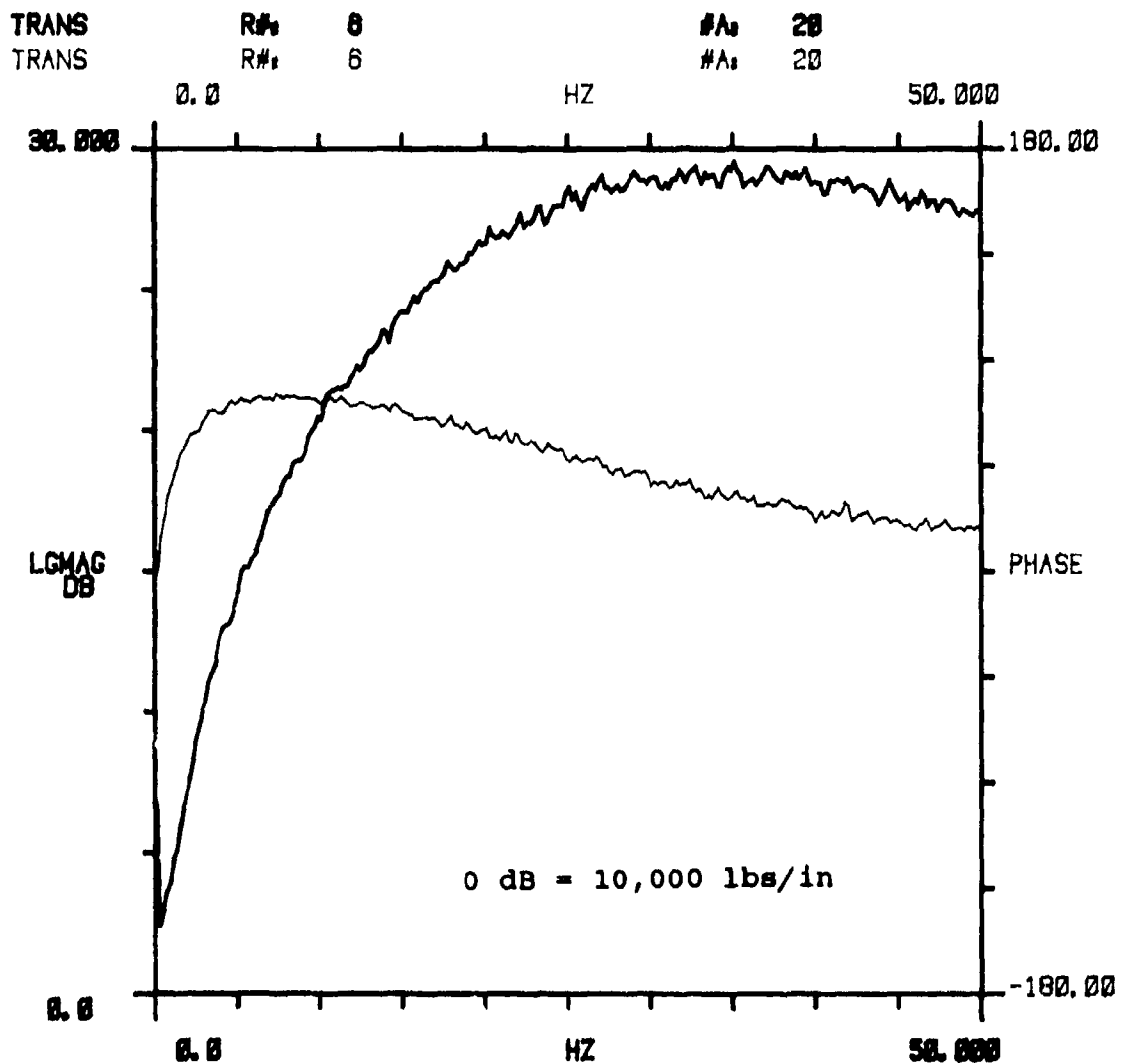


Figure V-19. F/X with load pressure feedback.

from 4 Hz to 25 Hz. The phase angle drops back from $+45^\circ$ to $+20^\circ$ as the frequency increases from 25 to 50 Hz. The actuator motion in response to the applied force is no longer a simple stiffness until the frequency of the applied force approaches 50 Hz. The phase lead effect of the load pressure feedback is consistent with providing motion damping or a force proportional to rate of motion of the actuator. This can be illustrated by considering the force and motion relationship of a spring operating in parallel with a damper as follows:

$$F = K_d dx/dt + K_s$$

Where: F is the applied force (lbs)
 K_d is the damping coefficient (lbs/in/sec)
 K_s is the spring coefficient (lbs/in)
 x is the free end motion of the damped-spring (in)
 t is time (seconds)

For zero initial conditions, taking the LaPlace Transform of the above equation gives:

$$F(s)/X(s) = K_d S + K_s$$

where S is the Laplace operator (seconds)

The damping coefficient of the force equation is represented by the $K_d S$ term which has a positive 90° phase angle and a magnitude which increases with frequency. The spring coefficient of the force equation is represented by K_s and has phase angle of 0° and a magnitude independent of frequency. The response plot of V-9 indicates that the load pressure feedback provides a damped spring characteristic over the response range measured. At frequencies approaching 50 Hz, the load pressure feedback becomes less effective and the phase angle between force and deflection approaches 0° . Below 25 Hz, the positive load pressure feedback reduces the magnitude of the force-to-deflection ratio as well as providing a leading phase angle corresponding to a damping force component.

Figure V-20 is a response plot of the bandpass filter used in series with the pressure feedback signal for the response measurements of Figures V-21 through V-23. The response plot is of the bandpass filter adjusted to its final setting. The purpose of the filter was to block the pressure feedback signal at steady state and low frequencies (and attenuate pressure feedback at high frequencies). Blocking the steady state and low frequency pressure feedback signal was required to prevent degradation of the actuator's stiffness and position accuracy under load in the position control response region. The

high frequency attenuation of the feedback signal was used to decrease noise sensitivity. The corner frequencies of the lag terms establishing the bandpass width were nominally 8 and 160 Hz. Note that the frequency response range for Figure V-20 is from 0 to 200 Hz. The filter provides a reasonably flat amplitude response (within 1 dB) from 15 to 50 Hz. The phase angle of the filter remains within 15° of 0° phase angle over the same frequency range (with 0° phase angle occurring at 30 Hz). The phase angle at 15 Hz is $+15^\circ$ and the phase angle of 50 Hz is -13° .

Figures V-21, V-22 and V-23 are force-to-deflection measurements of the flutter actuator with load pressure feedback and the bandpass filter operating. The feedback gain was increased by a factor of two from Figure V-21 to V-22 and again from Figure V-22 to Figure V-23. The feedback gain used for Figure V-23 was nearly as high as could be used without incurring instability. Note that the greatest change in the amplitude ratio and phase occurs for all three plots below 30 Hz.

For Figure V-21 with the lowest feedback gain, the maximum phase lead is $+45^\circ$ which occurs at 17 Hz. The magnitude of the force-to-deflection ratio is nominally 28 dB (251,000 lb/in) at all frequencies between 25 and 50 Hz. Note that the effect of the bandpass filter circuit is to retain a high steady state stiffness magnitude compared to operating with load pressure feedback and no bandpass filter (as shown on Figure V-19).

For Figure V-22 with twice the feedback gain as used for Figure V-21, the maximum phase lead is 72° at 20 Hz. The magnitude of the force-to-deflection ratio exceeds 30 dB from 35 to 45 Hz. Although the steady state stiffness is unchanged because the bandpass filter blocks any steady state pressure feedback, the increase in pressure feedback gain affects the amplitude response noticeably in the 2-5 Hz region. Figure V-23 with twice the feedback gain of Figure V-22 shows a maximum phase angle of $+99^\circ$. The magnitude of the force-to-deflection ratio is nominally 32 dB between 40 and 45 Hz. This magnitude is four to five dB greater than the magnitude without pressure feedback and indicates that the phasing of the pressure feedback at higher frequencies can be used to increase the apparent stiffness, if desired. As with Figure V-22, the magnitude of the force-to-deflection ratio from 2 to 5 Hz is reduced with the increased pressure gain.

The measured force-to-deflection ratio with pressure feedback can be used to calculate the damping flow. The calculation is based upon simple harmonic motion relationships and the force-to-deflection ratio of the damping component of the measured stiffness as follows:

TEST DATA

DATE: 10 APR 86

TEST ITEM: Flutter Suppression Controller

CONFIGURATION: Load pressure - filter #5
Electronics only

TEST: Frequency Response

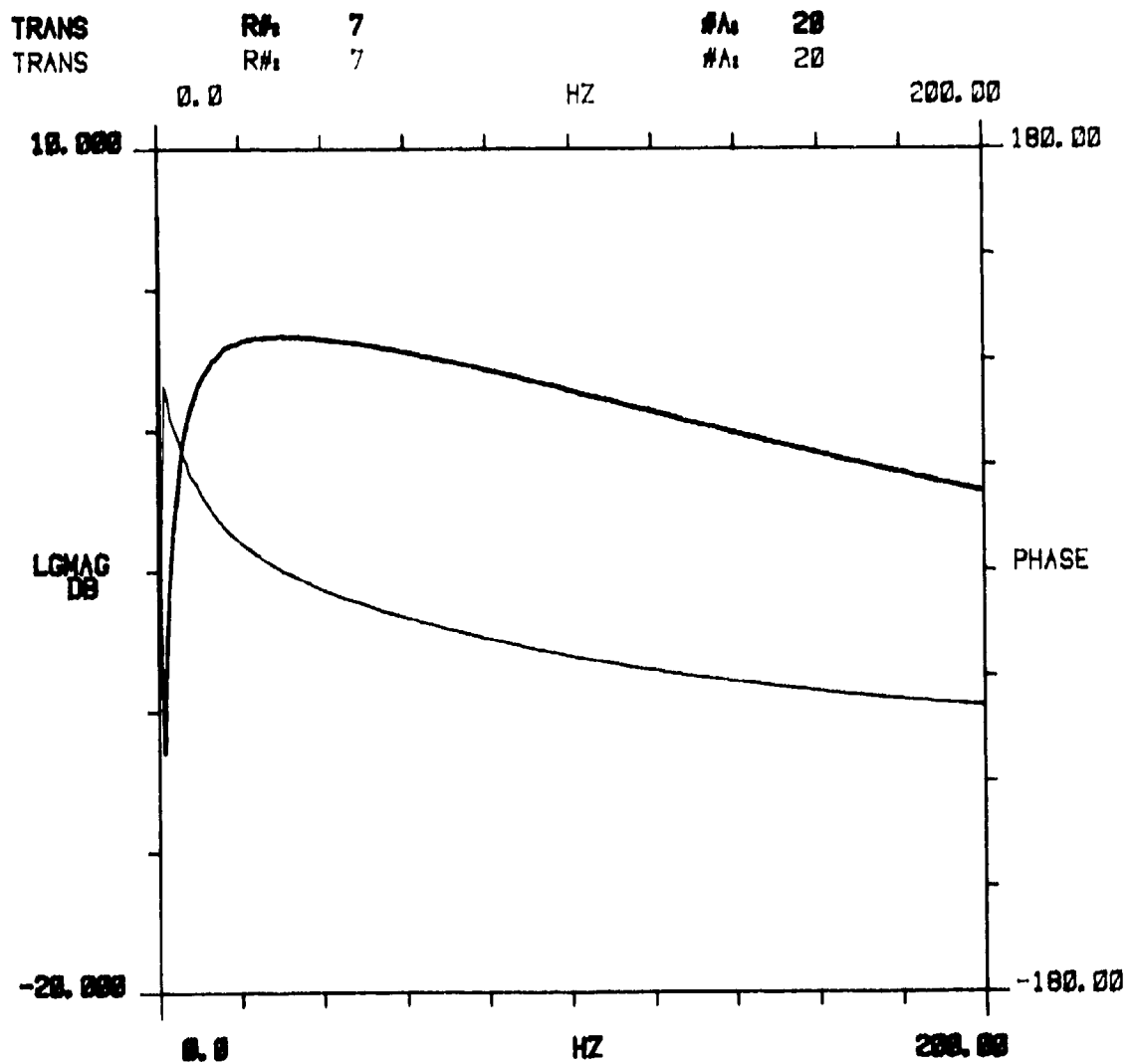


Figure V-20. Response - bandpass filter.

TEST DATA

DATE: 10 APR 86

TEST ITEM: Flutter Suppression Actuator

CONFIGURATION: Position + ΔP + Filter #6
5000 lbs compressive load bias
 \pm 5000 lbs load input (white noise)
Filter #6 gain at 0.2

TEST: Frequency Response - Force vs Deflection

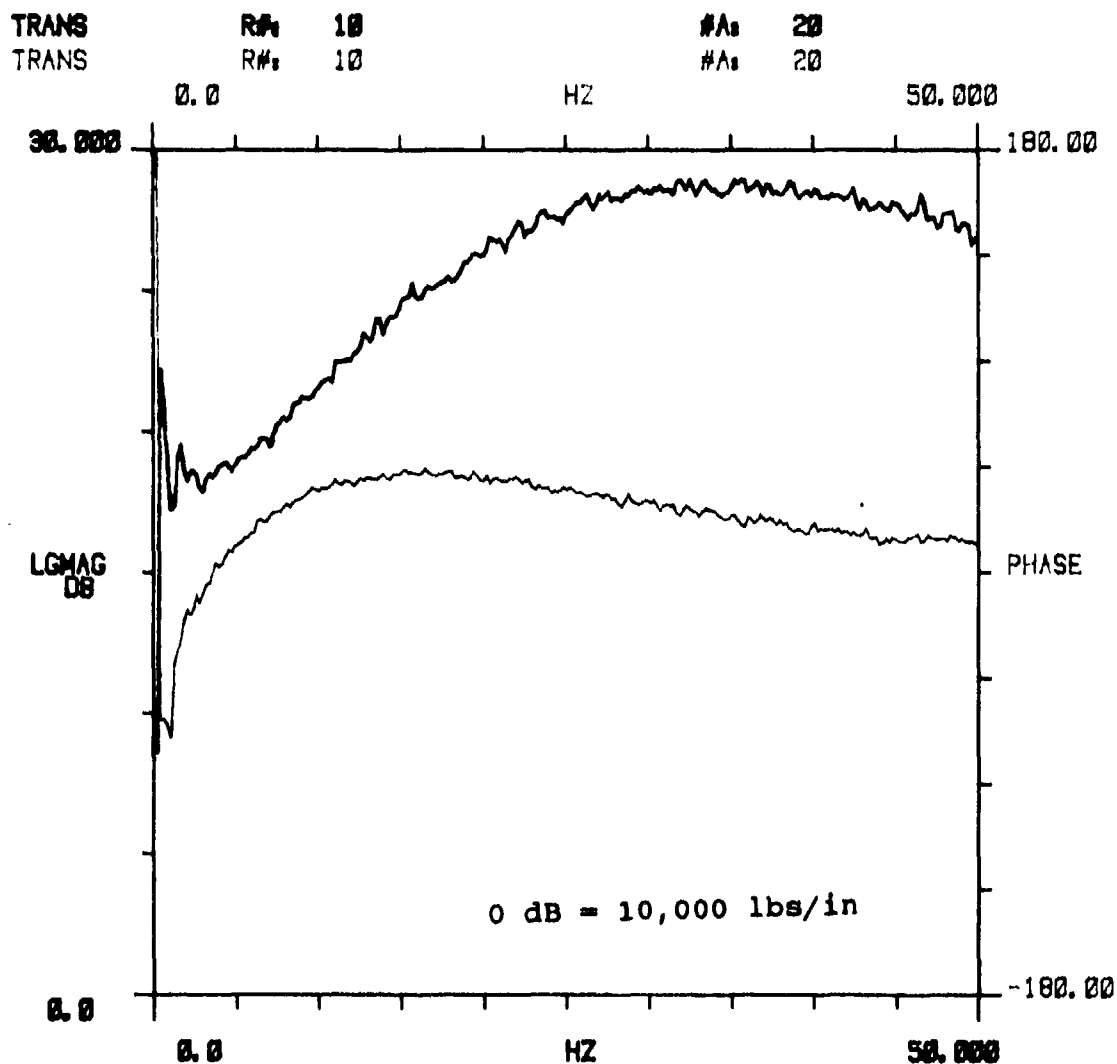


Figure V-21. F/X at 0.2 gain.

TEST DATA

DATE: 10 APR 86

TEST ITEM: Flutter Suppression Actuator

CONFIGURATION: Position + ΔP + Filter #6
5000 lbs compressive load bias
 ± 5000 lbs load input (white noise)
Filter #6 gain at 0.4

TEST: Frequency Response ΔP vs Force

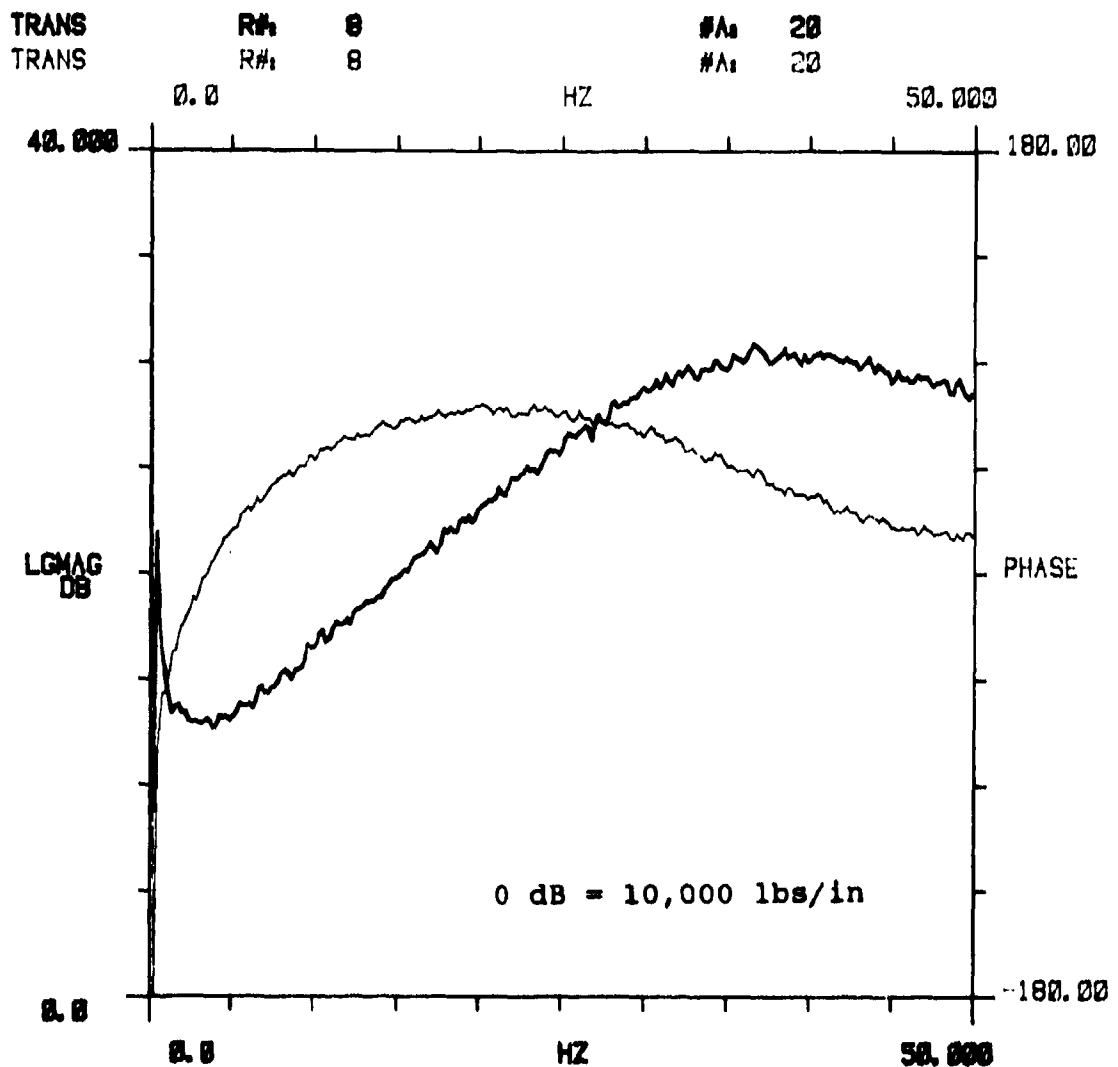


Figure V-22. F/X at 0.4 gain.

TEST DATA

DATE: 10 APR 86

TEST ITEM: Flutter Suppression Actuator

CONFIGURATION: Position + ΔP + Filter #6
5000 lbs compressive load bias
 ± 5000 lbs load input (white noise)
Filter #6 gain at 0.8

TEST: Frequency Response ΔP vs Force

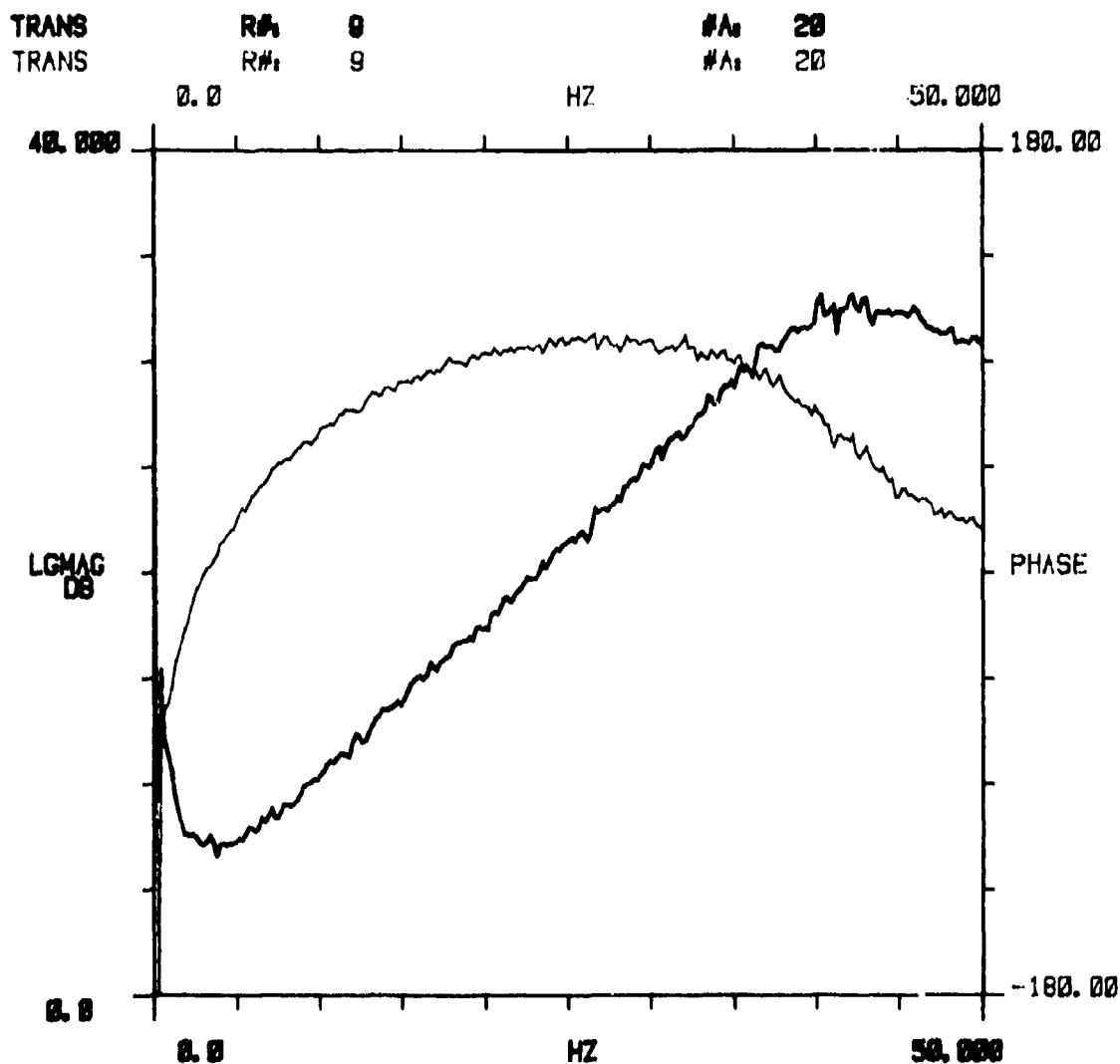


Figure V-23. F/X at 0.8 gain.

From Harmonic Motion:

$$\hat{Q} = \omega A \hat{x}$$

where: \hat{Q} is the peak flow (in³/second) or (cis)
 ω is the frequency (radians/second)
 \hat{x} is the peak stroke (in)
 A is the actuator drive area (in²)

From the definition of the ratio of damping force to deflection:

$$\frac{\hat{F}_d}{\hat{x}} = A \frac{\hat{P}}{\hat{x}}$$

where: \hat{P} is the peak pressure (lbs/in²) or (psi)
 \hat{x} is the peak stroke (in)
 \hat{F}_d is the peak force (lbs)

The response plots of Figures V-21, V-22, and V-23 can be used to determine the damping force-to-deflection ratio at each frequency by using the property that the force-to-deflection response consists of a magnitude and phase angle. The components of the force-to-deflection ratio which are in-phase correspond to the stiffness of the actuator. The components of the force-to-deflection ratio which are at + 90° correspond to the damping force of the actuator. It is assumed that the response is made up of only these two force-to-deflection components. These components at each frequency are then calculated from the measured response plots using the relationships:

$$F_s/X = |F/X| \cos \Theta$$

$$F_d/X = |F/X| \sin \Theta$$

Where: Θ is the measured phase angle (degrees), and
 $|F/X|$ is the magnitude of the response (lb/in).

Substituting the above into the ratio of in³/sec (cis) to psi:

$$\frac{\text{cis}}{\text{psi}} = \frac{\omega A^2 \hat{x}}{F_d}$$

$$\frac{\text{cis}}{\text{psi}} = \frac{\omega A^2}{\frac{F_d}{\hat{x}}}$$

But $\frac{\hat{F}_d}{\hat{x}} = \frac{F_d}{x}$ (a ratio)

Therefore,

$$\left[\frac{\text{cis}}{\text{psi}} = \frac{\omega A^2}{\left(\frac{F_d}{x} \right)} \right]$$

This relationship shows that the damping flow is function of frequency as well as the measured damping force-to-deflection magnitude.

Figure V-24 is a plot of the damping flow gains calculated from the response data presented in Figures V-21, V-22 and V-23. The reference value of 0.016 cis/psi at 12.3 Hz is exceeded with feedback gain potentiometer settings of both 0.4 and 0.8. The effect of increasing the feedback gain is to increase the damping flow gain at frequencies below 20 Hz. At 12.3 Hz, a damping flow gain of 0.034 cis/psi was achieved at the highest gain setting. Note that the damping flow gain versus frequency curve resembles a parabola. The effect of increasing the feedback gain is to shift the parabola to the right, resulting in an increased damping flow gain at low frequencies and decreased damping flow gain at higher frequencies. The parabolic effect may be associated with the phase characteristics of the pressure feedback filter and servovalve. The total measured phase shift of the bandpass filter and servovalve was the following:

Frequency (Hz)	Phase Angle (degrees)
10	+ 10.5
30	- 30.8
50	- 62.0

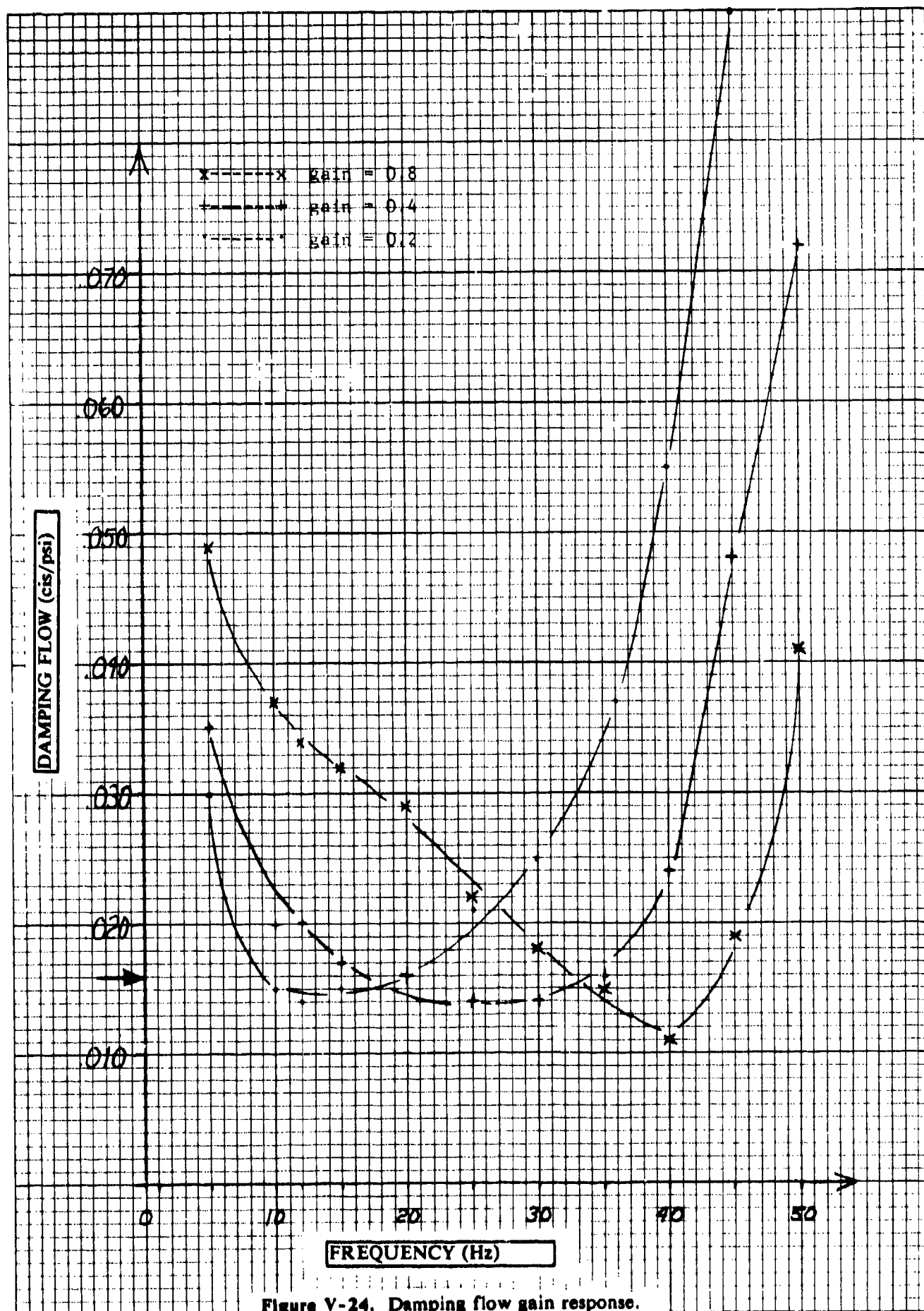


Figure V-24. Damping flow gain response.

Electrical compensation for these measured phase angles of the filter and servovalve could be used to reduce the phase shift to lower values (at the expense of the amplitude's flat response). This potentially could reduce the parabolic shape of the damping flow gain versus frequency curve.

V. CONCLUSIONS AND RECOMMENDATIONS

The use of electronically implemented load pressure feedback was successful in creating useful load damping flow characteristics over the frequency range of 0 to 25 Hz. The approach does offer flexibility in implementing load pressure feedback. The limitation in implementing the pressure feedback loop is the frequency response of the electrically operated servovalve which provides the damping flow control (and position control) for the actuator. The approach requires a high response servovalve with very little phase shift over the frequency regions in which the load pressure feedback is to be effective. This places a difficult requirement on the servovalve performance.

The effect of load pressure feedback is to reduce the dynamic spring rate or stiffness (displacement in phase with force) of the actuator over the region it is effective. This effect will have to be considered when damping resonant motions whose frequency is determined by the actuator stiffness.

Because electronic feedback offers considerable flexibility in incorporating compensation for the phase characteristics of the control valve, it is recommended that electronic compensation techniques be considered and evaluated as part of implementing load pressure feedback. This may allow using servovalves which have response determined by the position control requirements of the actuator, rather than requiring extended response for incorporating load pressure feedback.

SECTION VI DIRECT DRIVE F-16 ACTUATOR

I. INTRODUCTION AND SUMMARY

The objective of the F-16 Direct Drive Actuator investigation was to investigate the application of direct drive control technology to a current Fly-By-Wire (FBW) aircraft control actuator. The F-16 integrated servoactuator (ISA) was selected for the investigation since it is used in a current (still in production) FBW flight control system and an F-16 flaperon/horizontal tail ISA was available for use in the investigation. The design and test evaluation of the system was conducted from March 1985 to June 1987.

The failure mode and performance requirements for the normal F-16 ISA were used for design of the test system. The design of the test system was based upon using a pulse-width-driven, moving-coil, direct drive servovalve. This force motor design was successfully flight tested in an F-4E aircraft at Edwards Air Force during 1980 and 1981. The F-16 direct drive system used analog failure-detection in the control electronics. An alternative microprocessor-based failure-detection system to monitor the performance of the system (and reconfigure it upon component failure) was also designed and tested as part of the investigation. The system was unusual in using pulse width modulation (PWM) to control the direct drive servovalves and the use of a microprocessor for failure detection and ground checkout (self-test). The testing conducted on the system was a measurement of the input-to-output characteristics. The evaluation included operating the system in both the analog-controlled and microprocessor-controlled fault-detection modes.

The actuator section of the normal F-16 actuator was used with the direct drive valve. The secondary actuator of the normal F-16 actuator was replaced with the direct drive control package. The direct drive valve package was designed as a *bolt-in* replacement for the normal actuator's secondary actuator package. The normal F-16 ISA uses mechanical feedback for actuator position. This provides positive centering of the actuator as the last failure mode. To provide this same failure mode with the direct drive F-16 actuator, mechanical feedback was also used with the direct drive package, but only in the final failure mode. Electrical feedback was used for the electrical control modes of the direct drive actuator. No *inner loop* electrical feedback of the direct drive spool position and no gain changing with failures was used with F-16 direct drive actuator. The system was designed so that frequency response of the actuator after two electronic failures still met or exceeded the frequency response of the normal F-16 ISA.

The test system operated successfully and met or exceeded the performance requirements for the normal F-16 ISA. The microprocessor was able to identify failures and reconfigure the system successfully. The use of a microprocessor allowed duplicating the failure detection capability of the analog electronics and provided additional automatic test capability. The automatic pre-flight self-test operated properly. The parts count for the direct drive mechanization was less than 25 percent of normal ISA. The package size and weight for the direct drive actuator package was similar to that of the normal ISA. The use of mechanical feedback for the direct drive valve controlled actuators creates difficult design problems. The PWM drive for the direct drive valves worked well and minimized the heat sink requirements for the driving amplifiers.

II. TECHNICAL APPROACH

General

The direct drive F-16 investigation used an F-16 ISA (Horizontal Tail/Flaperon assembly 38330021, SN 0368). The secondary actuator was removed from the actuator barrel and a direct drive control package used to replace it on the actuator barrel. The direct drive control package was designed as a "bolt in" replacement for the normal secondary actuator. The performance characteristics of the normal F-16 ISA were used as design inputs for the direct drive system.

The control electronics for the direct drive actuator were designed with an option to use either analog failure detection and correction electronics or a plug in microprocessor unit for the same function. Pulse width modulation (PWM) was used for the servovalve driving electronics to reduce the heat sink requirements for the amplifiers. Four electronics units were constructed for the investigation. A power supply unit was used to convert 28 volts DC to six independent ± 15 volts DC supplies for the control channel electronics. The control electronics unit was used to mount the PWM servoamplifiers and the analog control and failure detection electronics. The control electronics unit incorporated connectors on the front panel to allow connection to the microprocessor failure detection unit. A pilot monitor unit was constructed and used with the analog control electronics unit to provide pre-flight test inputs and failure status monitoring. The microprocessor unit (logic processor) was constructed to connect to the control electronics unit and provide a substitute for the analog failure detection function of the control electronics.

F-16 ISA Description

Figure VI-1 is a photograph of the standard F-16 ISA. The actuator is used for controlling the horizontal tail, flaperons and rudder (in a shorter stroke version) for the F-16 aircraft. The actuator is designed to operate with 3,000 psi supply pressure. The actuator has a total force output capability of 36,000 lbs, a maximum slew rate of 5.5 inches/second and a nominal frequency response of 3 Hz (- 3 dB amplitude ratio relative to 0.1 Hz). The actuator is designed to accept two electrical failures and/or one hydromechanical failure and continue to operate. Upon detection of a third electrical failure or a second hydromechanical failure, the actuator will move to a centered position.

Figure VI-2 is a schematic of the standard F-16 ISA servoactuator. The standard F-16 ISA uses a secondary actuator to position the main control valve. The secondary actuator is controlled by three jet pipe servovalves. Failure detection and removal is accomplished hydromechanically using comparator spools to monitor the servovalve spool driving pressures. The comparator spools detect failures of the servovalves, hydraulic supply pressures and current inputs to the servovalves. A first failure of SV1 or SV2 will cause transfer of control to the standby servovalve SV3. A first failure of SV3 will lock the servoactuator on SV1 and SV2 control. Mechanical feedback loops are used for the the servovalves, main control valve and the actuator ram positions. Solenoid valves are used to remove/apply supply pressure to the servovalves and transfer to the fail center mode upon receipt of an electrical command from the actuator control electronics. Note that the servovalve torque motors are not included inside the mechanical feedback loops. This results in the actuator position being commanded by current input to the servovalve coils.

To provide the dual fail operational capability for the control electronics, each servovalve has two electrically separated windings. Either winding is capable of full servovalve control. These windings are driven by the flight control computer in an active-standby manner so that a servoamplifier first failure will be corrected within the flight control computer without activating the ISA voting logic. The control electronics also incorporates a mathematical model of the ISA's rate + position feedback position. This model is used (with the output of the position LVDT incorporated in the ISA) to determine that the actuator output is in error and transfer the ISA (after the pilot has armed the monitor) to the centering mode of operation. The actuator position in the centering mode is established by the centering spring attached to the feedback linkage from the actuator and the main control valve.



Figure VI-1. F-16 integrated servoactuator (ISA).

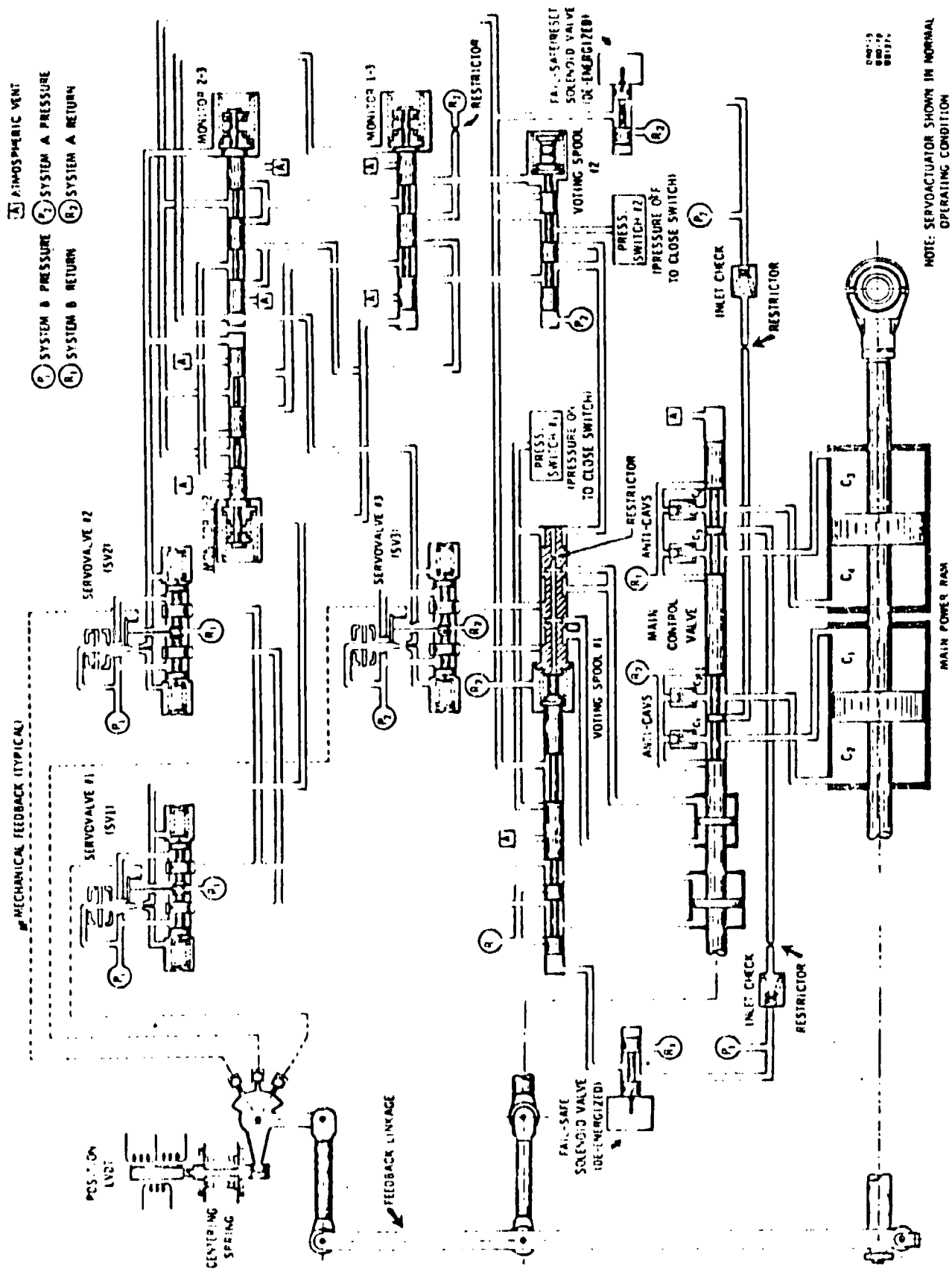


Figure VI-2. Integrated servoactuator schematic diagram.

Direct Drive System Description

General

The direct drive valve (DDV) concept investigated for the F-16 actuator eliminated the normal ISA's secondary actuator completely. Two force motors were used to drive the main control valve. The force motors were spring centered, requiring no inner loop feedback. Figure VI-3 illustrates the single fail-operate control mechanization used to control an F-4E aileron actuator. The actuator was successfully flight tested at Edwards Air Force Base in 1980 and 1981. The development of the F-4E direct drive aileron actuator is described in technical reports AFFDL-TR-77-91 and AFFDL-TR-79-3117 (Vol I). The results of the flight test are presented in technical report AFWAL-TR-82-3035. For the F-16 application, which requires two fail-operate control for electrical failures, a third channel of electronics was added to drive an additional coil in the force motors. Each channel was self-monitoring and completely independent of the others. Six feedback transducers were required in order to retain complete channel independence for the two fail-operate mechanization.

Figure VI-4 shows the F-4E direct drive aileron actuator along side of the standard F-16 ISA. The program objective was to incorporate the direct drive valve concept shown on the F-4 actuator as a replacement for the control valve package on the F-16 actuator. The implementation approach was the following:

- a. Mechanical feedback would be used for the fail-safe mode only.
- b. Electrical feedback would be used for the operate and fail-operate modes.
- c. Gain changing after channel failures would not be used.
- d. The valve package would be a *bolt-on* replacement for the normal F-16 ISA's secondary actuator section.
- e. Analog-failure detection would be used for the initial (Phase I) implementation.
- f. Microprocessor-failure detection would be used for the second (Phase II) implementation.
- g. The force motors would be driven by a pulse width modulation driving signal.

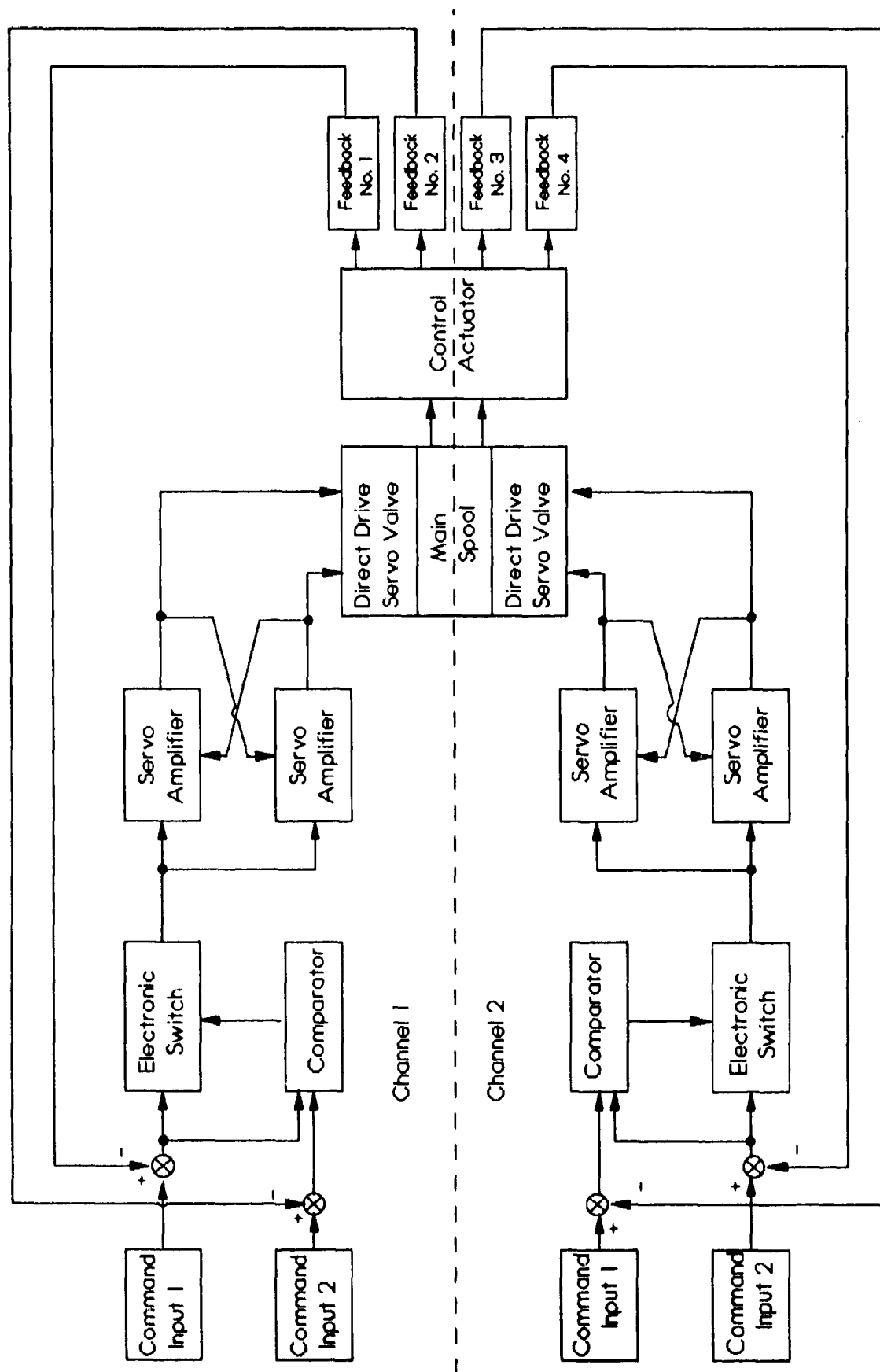


Figure VI-3. Single fail operate direct drive valve (DDV) system.

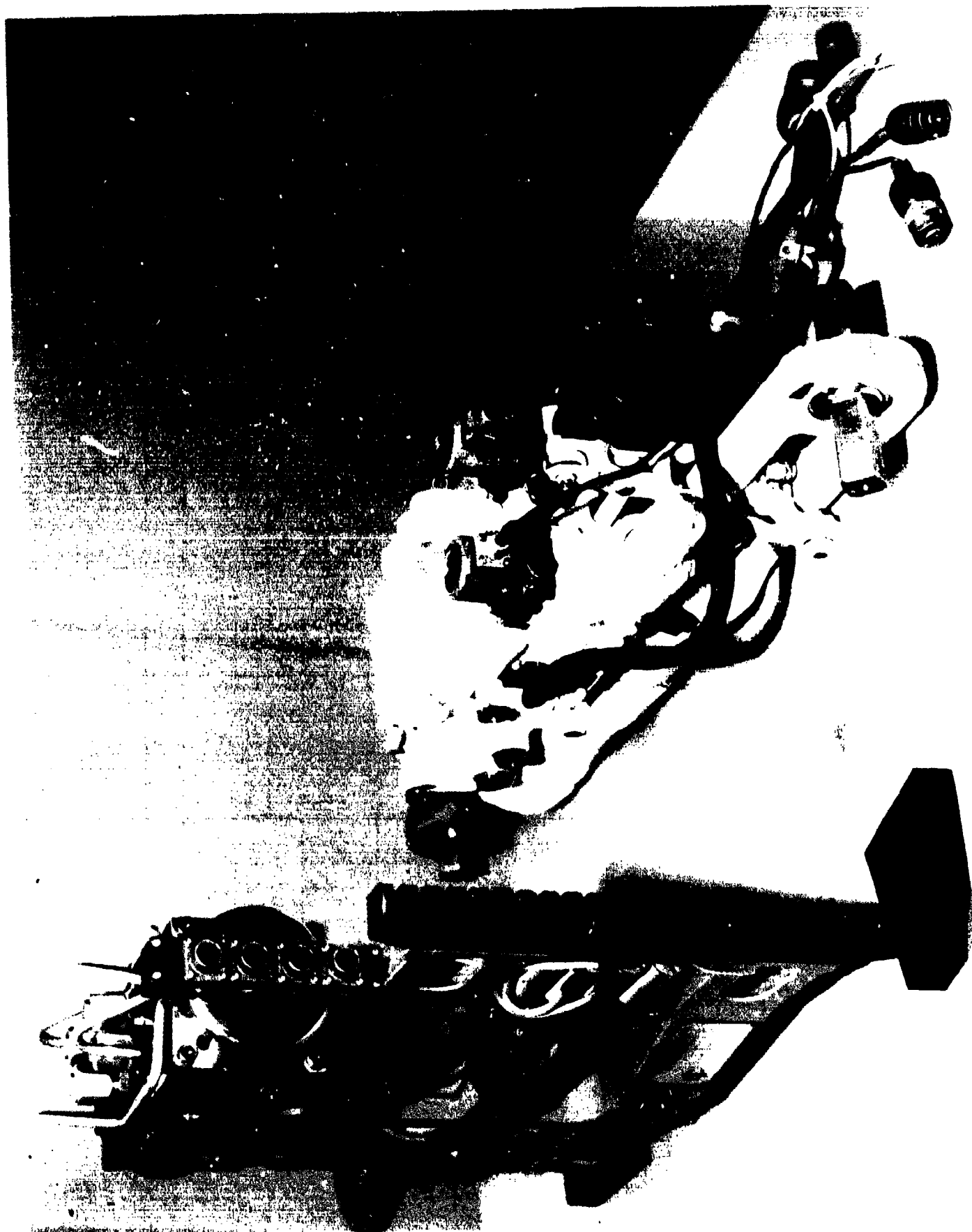


Figure VI-4. F-4 direct drive valve (DDV) aileron and F-16 integrated servoactuator (ISA).

The decision to use mechanical feedback only for the fail-safe mode was based upon the desirability of using the direct drive valve within an integrating feedback loop. This approach results in power to the direct drive valve being required only when motion of the actuator (and flow from the control valve) is commanded. If the direct drive valve is used outside the actuator feedback loop, power to the valve is required for any position of the actuator other than the centered position. To achieve maximum flow output, a direct drive valve requires more electrical power than a two-stage valve. (However, the two stage valve requires continuous hydraulic power for first stage quiescent flow while the direct drive valve does not.) The most efficient use of a direct drive valve is within an actuator's position feedback loop. Using the direct drive valve within an integrating feedback loop also relaxes the linearity requirements on the motion of the direct drive valve spool. With the use of integrating feedback, inner loop feedback of the direct drive valve position is not necessary to achieve good actuator output position linearity.

Using electrical feedback of the direct drive F-16 actuator motion allowed including the force motor and valve inside the actuator position loop for the operate and fail-operate modes. Upon failure of the three self-monitoring electrical control channels or both hydraulic supplies, transfer was made from the electrical-control mode to the fail-safe centering mode. The transfer was accomplished with solenoid valves (as on the normal F-16 ISA).

With a multiple coil direct drive valve, the force applied to move the valve spool is a direct function of the current in each coil. Direct drive valves use centering springs to achieve a high resonant frequency. The position of the valve is therefore a direct function of the force motor's output (which is directly proportional to the sum of the coil currents). The position gain (and hence flow gain) of the valve therefore changes with loss of control channels. Using inner loop feedback of the spool position will tend to keep the flow gain constant, at an increase in complexity and decrease in reliability. The use of gain changing after channel failure (with or without inner loop feedback) can be used to keep the frequency response of the direct drive actuator the same in all the *operate* modes. If one channel fails, the gain of the remaining good channels can be increased to compensate for the loss of a channel. However, gain changing requires coupling between control channels, which reduces control channel independence and introduces possible common failure modes. The approach used for the F-16 direct drive actuator was to not use gain changing or inner loop feedback. The frequency response of the actuator with a single control channel operating (after failure of the other two control channels) was sized to meet the frequency response requirements of the normal F-16 ISA. The frequency response with two and three channels operating was therefore greater than that of the normal F-16 ISA. For applications where extended actuator response is undesirable (such as where the actuator response roll-off is used as part of structural mode filter design) electrical filters can be used in series with the actuator system's inputs to reduce the actuator system's frequency response.

The failure detection used for the first phase of the F-16 direct drive was analog and similar to that used with the F-4E aileron actuator system described in the technical reports AFFDL-TR-77-91, AFFDL-TR-79-3117 and AFWAL-TR-82-3035. With that approach, the failure monitoring system is checked prior to flight. The system is designed so that failures of the monitoring system components appear as single channel failures and can not cause *hardover* channel output failures. As part of the configuration, a pilot monitor control box was used to inject initial *pre-flight* test signals and to display channel failures during normal system operation.

Microprocessor failure detection and correction was used for a second phase of the investigation in order to evaluate the approach. The microprocessor was not redundant or self-monitoring. The microprocessor was programmed to provide both pre-flight test and continuous-monitoring during operation. The microprocessor had the potential to add both flexibility and capability to the monitoring function of the F-16 direct drive actuation system.

Using pulse width modulation for the driving the force motors coils reduces the heat sink requirements for the driving amplifiers. This is because the driving amplifier is used in either a full *On* or *Off* current mode. This minimizes the internal heat generation of the driving amplifier. The potential disadvantage is the generation of electrical noise as a result of the current switching.

Control System Description

Figure VI-5 is a block diagram schematic of the F-16 direct drive control system for the operate modes of the actuator. The system is designed to operate with all three channels for normal operation, two channels for the fail-operate mode and one channel for the single fail-operate mode. Note that three channels are self-monitoring and no electrical mixing of the channels occurs. Each channel uses two command inputs (so that the failure logic can be used to detect input failures). These inputs are strapped together if input failures are detected and corrected ahead of the control actuator system. The six feedback transducers allow each channel to be self-monitoring. A failure of a feedback transducer, summing amplifier failures or and command input is detected by the channel comparator and the inputs to the servovamplifiers is grounded. Two servoamplifiers are used for each channel. The servoamplifiers are cross-strapped together so that if an amplifier fails hard-over, the other amplifier of the pair is driven in the opposite direction, cancelling the output force of the channel. If the amplifier fails to a *no-output* condition, the gain of the remaining amplifier increases, tending to keep the channel's force gain (but not total force contribution) constant.

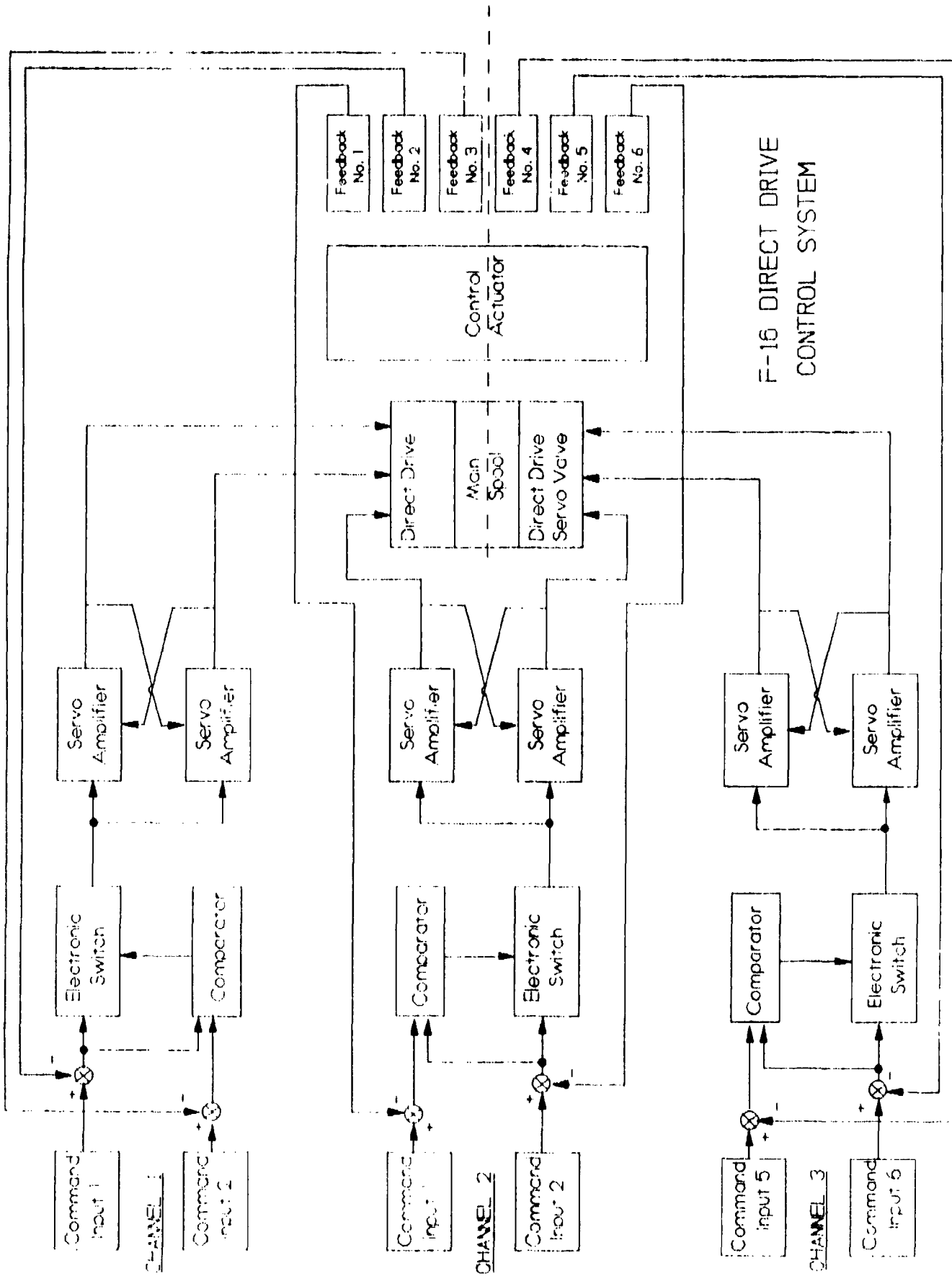


Figure VI-5. F-16 direct drive valve (DDV) actuator schematic.

Control Valve Description

The direct drive valve concept used by Dynamic Controls, Inc. is based upon a moving coil design (as opposed to moving magnet or moving iron). The coil assembly is suspended on a folded linkage which incorporates both the centering spring and Bendix flexures for pivot points. The coil assembly consisted of three individual coils, electrically isolated with each coil having four layers of wire. Figure VI-6 shows one of the two coil assemblies used for the F-16 direct drive valve. The coil assembly diameter is nominally 2.75 inches and the length is 0.62 inches.

The moving coils are used with a rare earth magnetic structure. Stainless 416 steel was used for the pole piece and the outside cup. Tascore 21 was used for the permanent magnet material. The force output of the force motor was 55 lbs with all coils energized with 1.2 amps. The resistance of each coil was nominally 4 ohms. The weight of the magnet structure, coil and housing was nominally 5 lbs. Figure VI-7 illustrates the magnet structure, coil, coil suspension and force motor housing. The force motor is a wet coil design, flooded with return oil through a filter disc with a 2 micron nominal rating. Using a wet coil design eliminates a dynamic seal, provides increased cooling for the coil and damping for the coil motion. Since the oil in the magnetic structure is fed through a filter disc from return and is circulated only locally, the problem of the magnetic structure acting as a magnetic filter for the oil in the hydraulic system does not occur.

Two force motors were used for the F-16 direct drive valve package, one on each end of the control valve. The force motors were connected together in the valve package with a large connecting passage so that the pressure balance between the magnetic structures was maintained. The return pressure of one hydraulic system was used for both magnetic structures.

The control valve which the force motors positioned was part of a three piece design. The control valve moved in a sleeve which was normally held stationary by a locking mechanism. Electrical feedback was normally used to control the actuator output position. When mechanical feedback was used in the fail safe mode, the sleeve was unlocked and driven by the mechanical feedback linkage. In the fail safe mode, the driving electronics for the center spool are turned off and the control spool is maintained in a centered position by the spring centering of the force motors. Figure VI-8 shows the control valve, the moveable sleeve used for the fail-safe mode, and the stationary sleeve in which the moveable sleeve ran.

The locking of the sleeve and the motion in the fail-safe mode was accomplished with a lever-mounted ball, a slot in the sleeve and a shaft with a taper. Figure VI-9 shows the linkage lever with the ball and the shaft with the taper. The linkage lever was prevented from engaging the tapered

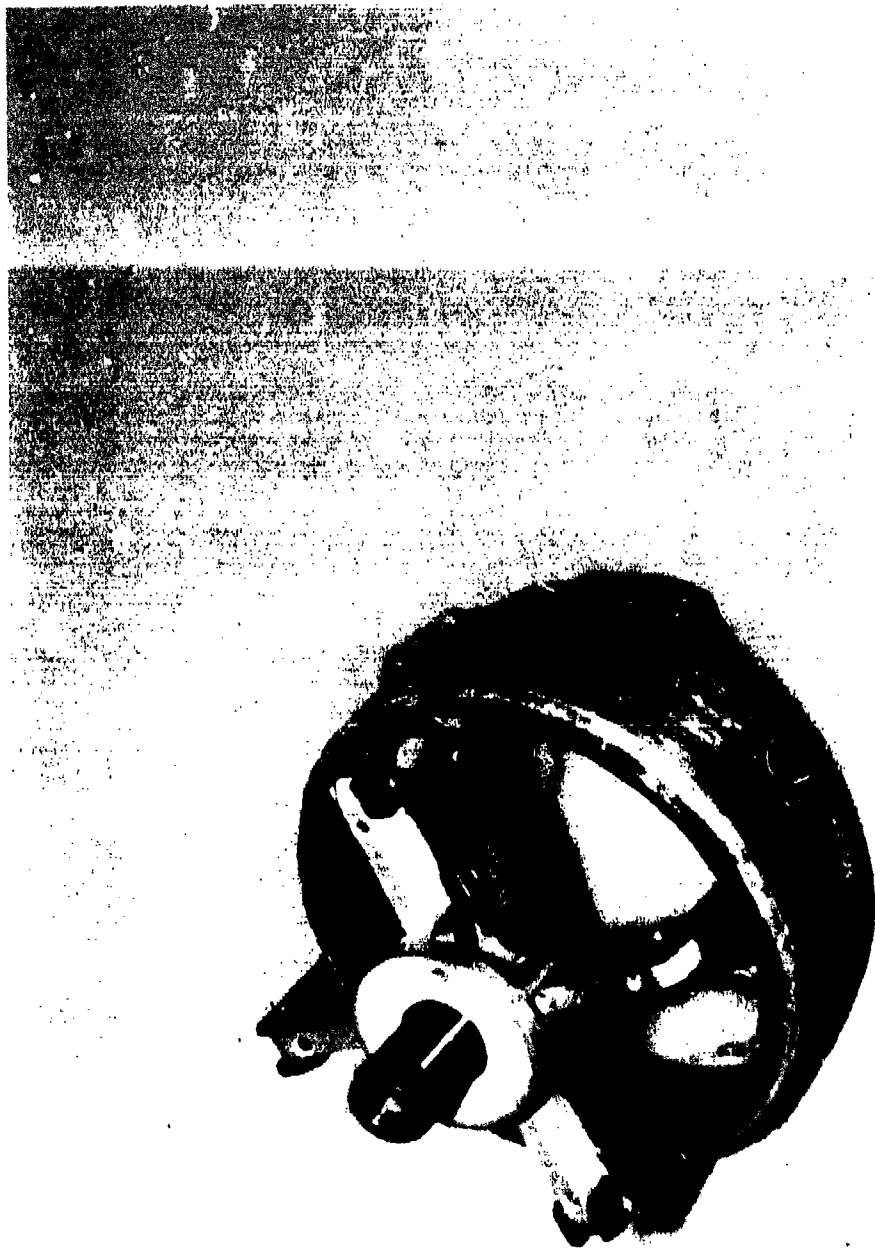


Figure VI-6. Direct drive valve (DDV) coil and suspension.





Figure VI-8. DDV control spool and sleeves.

ramp when the actuator operated with electrical feedback. The valve body, as shown in Figure VI-10, incorporated the locking lever and locking piston. The locking piston was controlled by two solenoid valves so that either three electrical failures or two hydraulic failures would release the locking lever, engaging the fail safe mode.

Feedback Design Description

Attached to the valve body was the mechanical feedback linkage and housing for the electrical feedback transducers. The linkage attached to existing mounting holes on the F-16 ISA's actuator body. Figure VI-11 shows the housing and one of the linear bearings used to guide the tapered shaft. The linkage was designed to provide a motion reduction ratio of 171 to 1. Figure VI-11 also shows one of the electrical feedback transducer housings used to mount three of the six feedback transducers used with the actuator. Precision film-potentiometers were used for the motion transducers. The film-transducers offer better linearity (at the expense of shorter component life) than LVDTs and have been used in several current aircraft for position feedback. The film-potentiometers also eliminate the modulation and demodulation electronics required if LVDTs had been used instead.

Figure VI-12 shows the manifold plate used to adapt the direct drive valve package to the standard F-16 ISA actuator barrel. The manifold plate provided the connections for hydraulic supply and return lines and mounting for the position feedback transducers housings.

Figure VI-13 shows the direct drive control package assembled prior to installation on the F-16 actuator barrel. Note the two solenoid valves at the left top of the valve package. These solenoids were used to transfer the actuator to the fail-safe centering mode.

Figure VI-14 shows the direct drive control package mounted on the actuator barrel. The three connectors used for the control channels are mounted on the side of the valve package. The wires from the position transducers, solenoid valves and force motors are terminated at the connectors. Thirty four wires were used to control the direct drive package. No pressure transducers to detect hydraulic system failures were incorporated into the valve package, since loss of both hydraulic pressures would release the locking lever and engage the fail-safe centering mode.

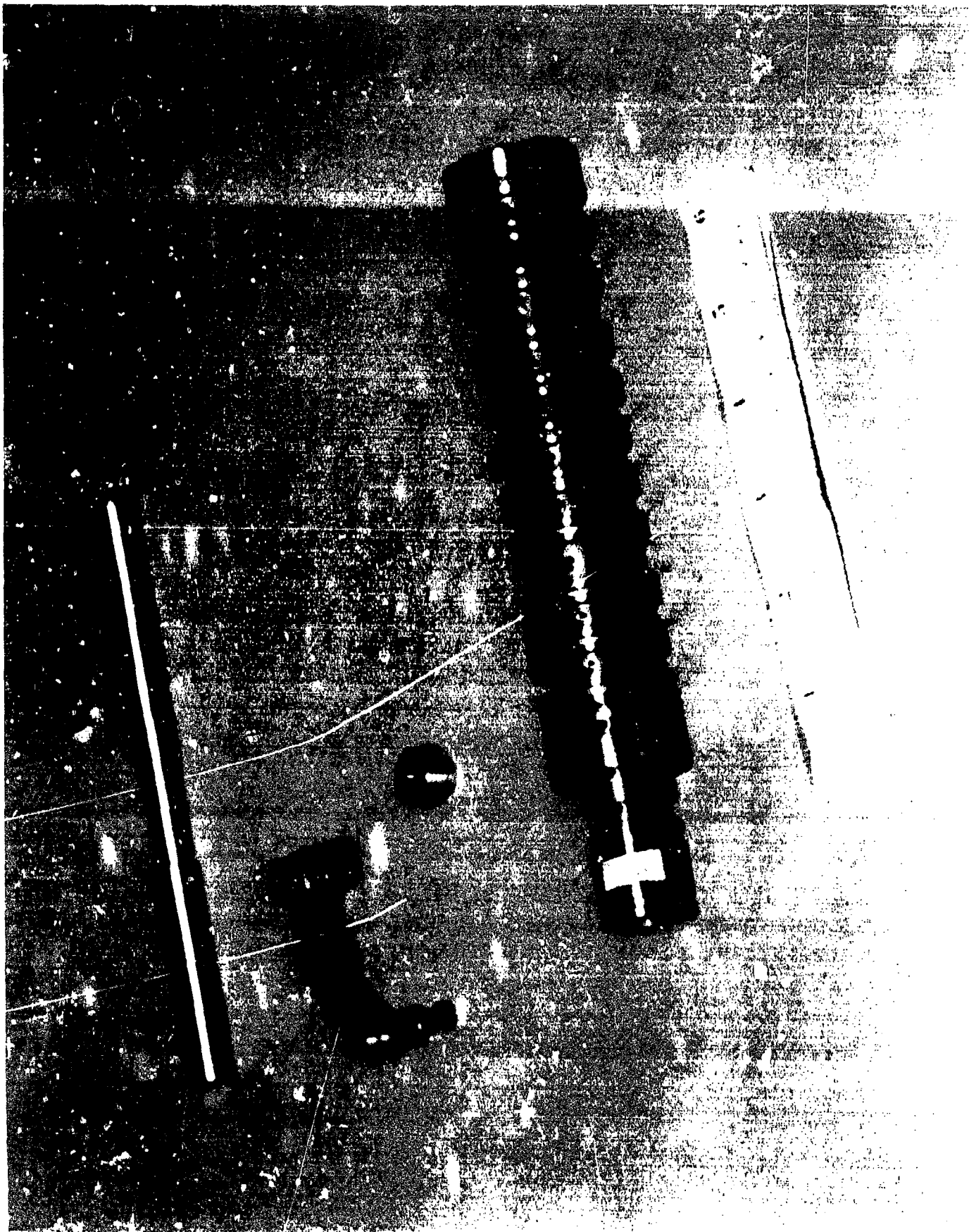


Figure VI-9. Centering sleeve, link, and shaft.

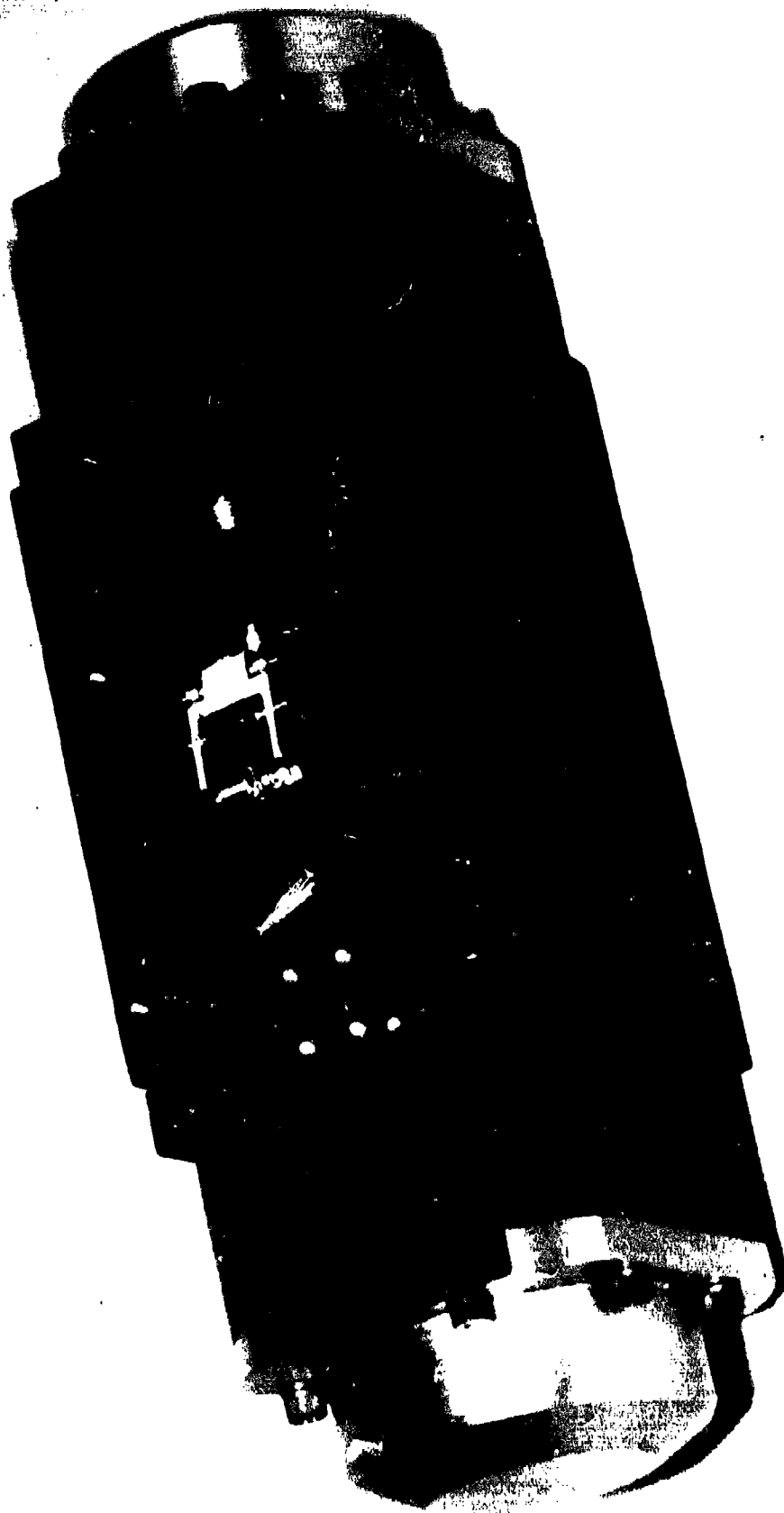


Figure VI-10. DDV body and force motors.

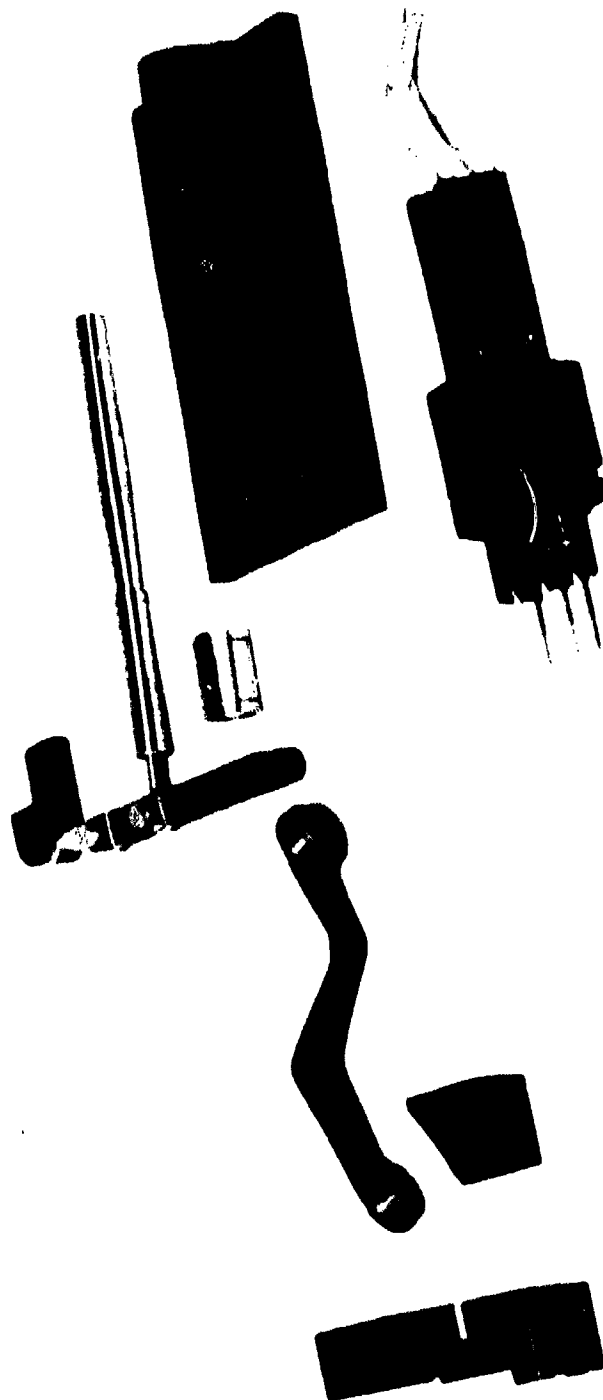


Figure VI-11. Feedback hardware.





Figure VI-13. Control package assembly.



Control Electronics Description

General

The electronics for the direct drive F-16 actuator consisted of a power supply unit, a pilot monitor box and a control electronics chassis. The power supply was designed to convert 28 volts DC to ± 15 volts DC. Six separate ± 15 volt outputs were provided by the power supply.

The control electronics for the direct drive valve were housed in the single control box shown in Figure VI-15. The front panel contained all the input and output connectors for the box, including the connection to the pilot's monitor box, direct drive F-16 actuator, power supply and the test inputs and output connections.

The pilot monitor box incorporated status lights and a failure input and reset switch for each of the three control channels of the actuator.

Control Electronic Circuits

Figure VI-16 shows the direct drive actuator control box internal construction. Three circuit cards were used for each control channel. Each circuit board was supplied by two separate ± 15 volt power supplies. Any failure of either one of the ± 15 volt supplies would caused the control channel to fail, eliminating the output current of that channel.

Figure VI-17 is a single channel schematic for the direct drive control box electronics. The circuitry shown within the dashed lines on Figure VI-17 was used in the pilot monitor box. The circuits including and to the left of SW-1 on Figure VI-17 are the implementation of the two command inputs, two feedback inputs, two summers, a comparator and electronic switch of one channel as shown previously in Figure VI-5. The circuitry to the right of SW-1 is the implementation of the PWM servoamplifiers. Jumpers (or breaks) J1 through J8 were used to connect to the Logic Processor for the Phase II part of the investigation. Each side of a break was brought out to one of the three front panel connectors used for connection to the Logic Processor during the Phase II investigation. For the Phase I investigation, the *breaks* were jumped by the wiring of the mating connectors. The component values for this and the following 4 schematics are included in Appendix A-2.

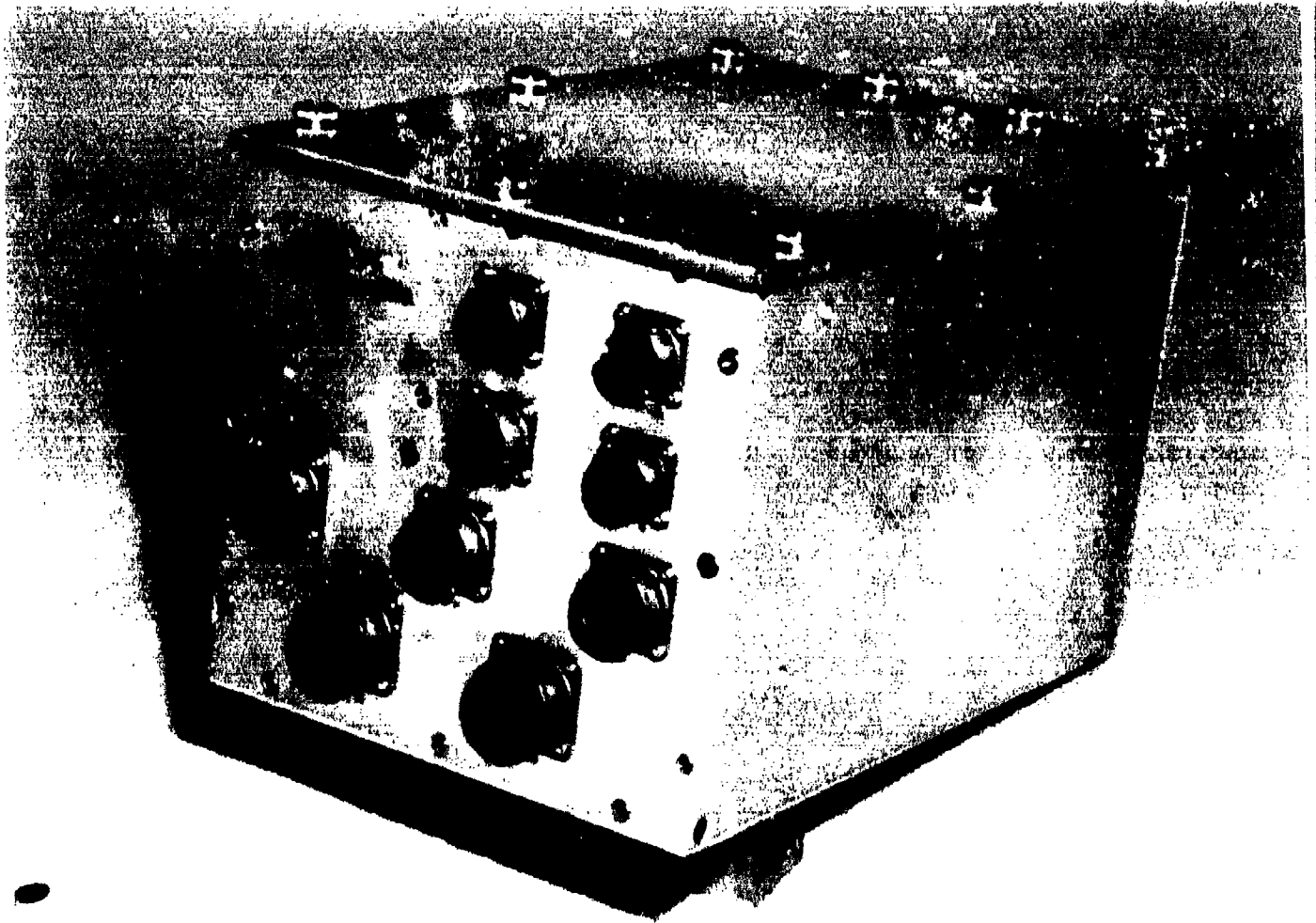


Figure IV-15. Control electronics chassis.

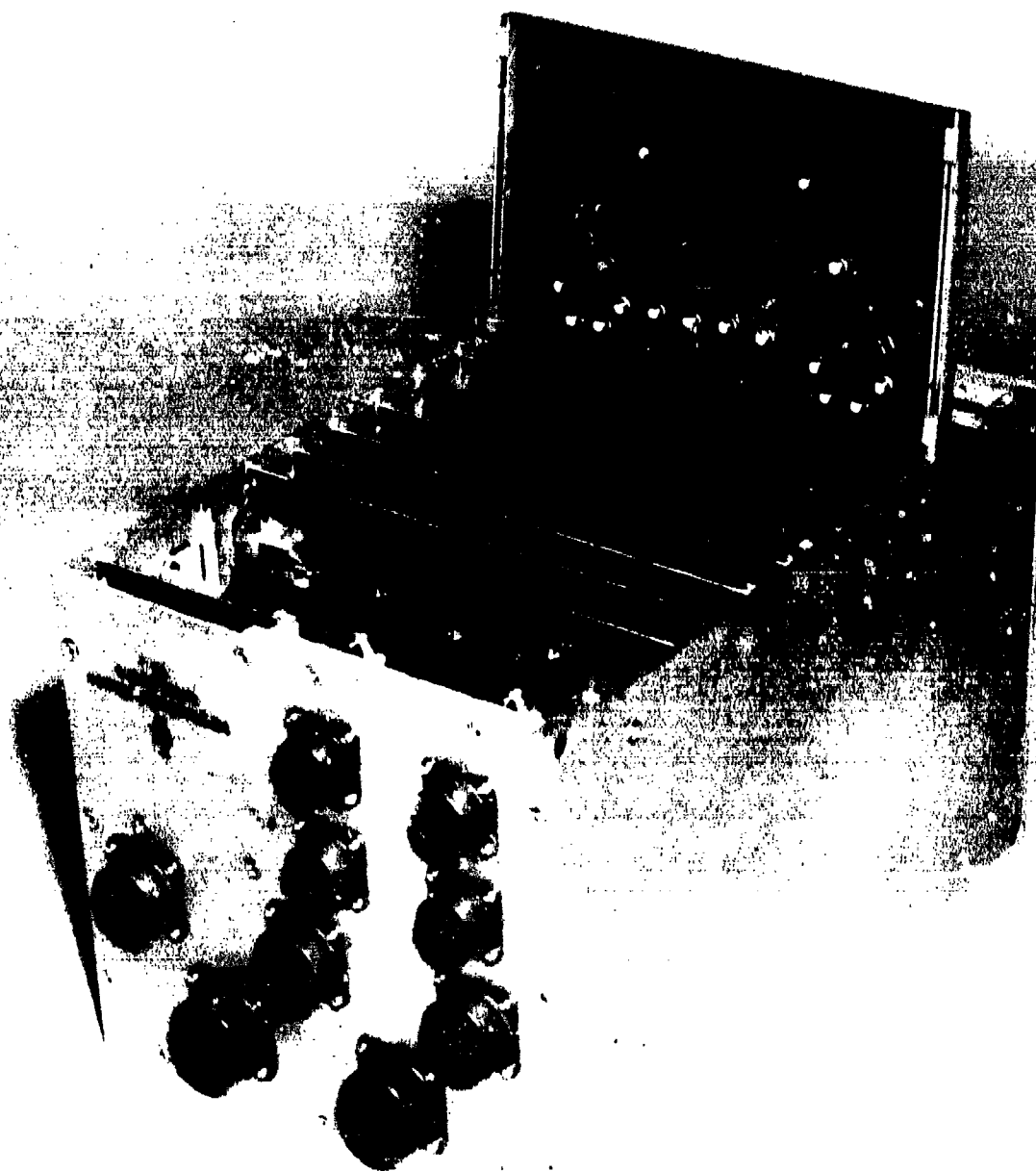


Figure IV-16. Open control chassis.

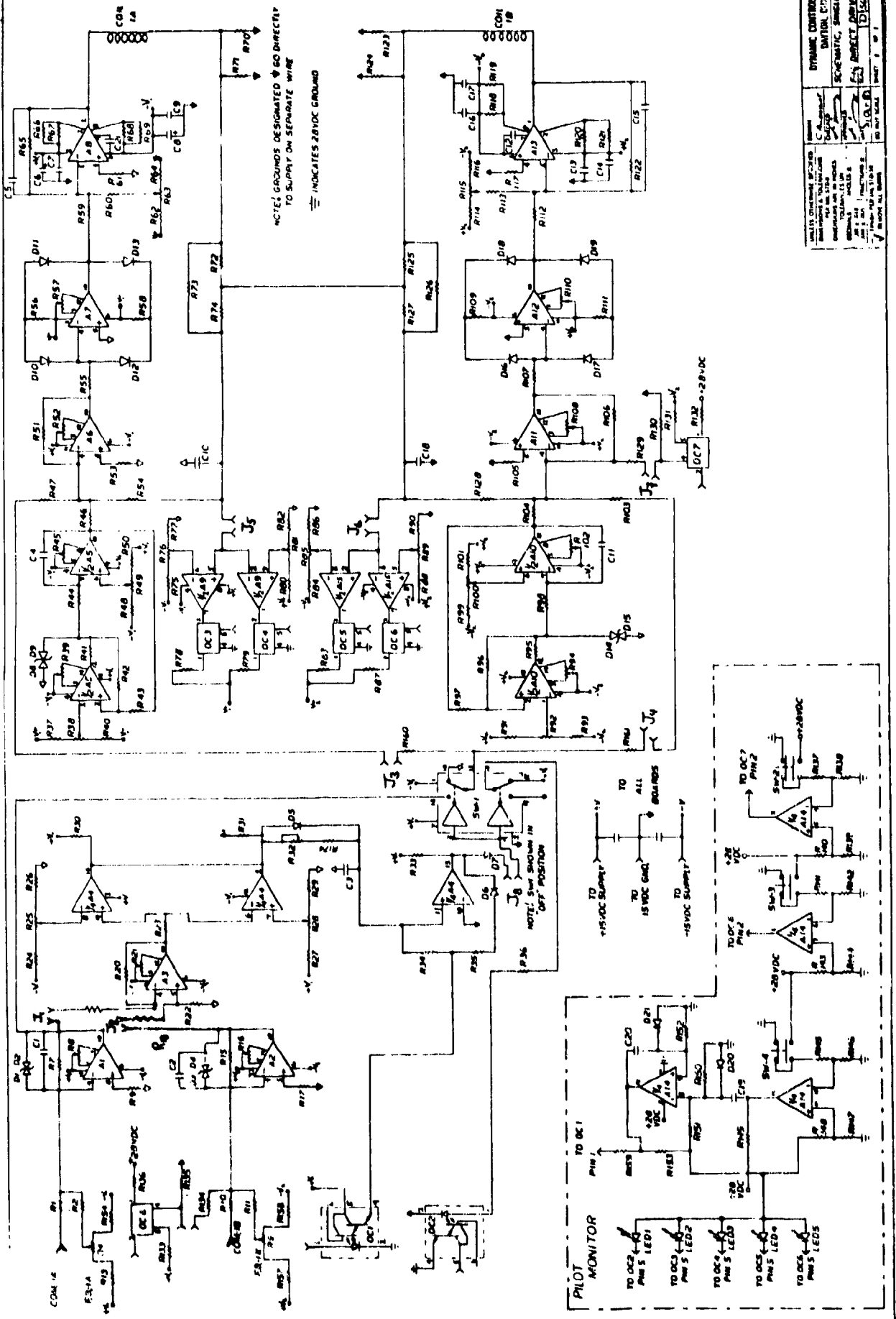


Figure VI-18 shows the PWM section of the single channel electronics in larger scale. Two identical PWM amplifiers are used, powered by two different power supplies. As shown on this figure, op amps A5 and A10 are used to create a 2000 Hz triangle waveform at their outputs. The triangle wave is summed with input and feedback signals by op amps A6 and A11. The difference between the input and feedback signals biases the triangle wave form off zero, causing the op amps A7 and A12 to create a 2000 Hz pulse train. The polarity is the same as the bias and the pulse duration is proportional to the amplitude of the bias. The circuit shown is three level pulse width modulated generator which produces zero output at zero input bias. The diodes D10 through D13 and D16 through D19 are biased by supply voltages through resistors to make the op amps A7 and A12 window comparators. With low comparator input current, the diode bridges around A7 and A12 provide low impedance feedback to hold the amplifier outputs to near zero. As the input signals raise the input current to the comparator above that supplied by the diode bias, the output is driven away from zero level. Capacitors C10 and C18 are used as low pass filters for the feedback signals (proportional to coil current). The resistor networks R72 through R74 and R125 through R127 are used to establish the cross-strap feedback signal gain and prevent shorts or opens of the cross-strap from causing hardover outputs from the amplifiers. The output of A7 and A12 drove the op amps A8 and A13 (reference Figure VI-17).

Five opto-couplers were used with the PWM sections of each channel. Four of the opto-couplers were used to provide four signals to the pilot monitor box when the current level of the PWM amplifiers reached a particular level. Comparators A9 and A15 were used to control the opto-coupler operation. The \pm current levels at which the comparators drove the opto-couplers to switch was established by R76, R81, R85 and R89. Opto-coupler OC7 was used to apply a test voltage to A11 for verification of the cross-strap operation during pre-flight test.

Two circuit boards were used for constructing the PWM amplifier section of each channel. One circuit card was used for the driving transistors for the force motor coils. The two power op amps (Burr Brown P3572) were mounted directly to the circuit boards with copper foil left largely intact as a heat sink surface. The wedge board retainers at the edge of the circuit board were used to load the circuit board against the chassis guide slots to provide a heat conduction path from the circuit board to the chassis. On the second board were mounted the components for the triangle waveform generator, summing amplifier, and opto-isolators of Figure VI-18.

The third board for each channel was used to mount the summing amplifiers for the command and monitor sections of each channel, a comparator, electronic switch and two opto-isolators. Figure VI-19 shows the summing circuit of Figure VI-17 in a larger scale. Op amps A1 and A2 are used as summing amplifiers for the control and monitor channel respectively. Op amp A3 is used as a difference amplifier to drive comparator A4. If differences between the control and monitor channel

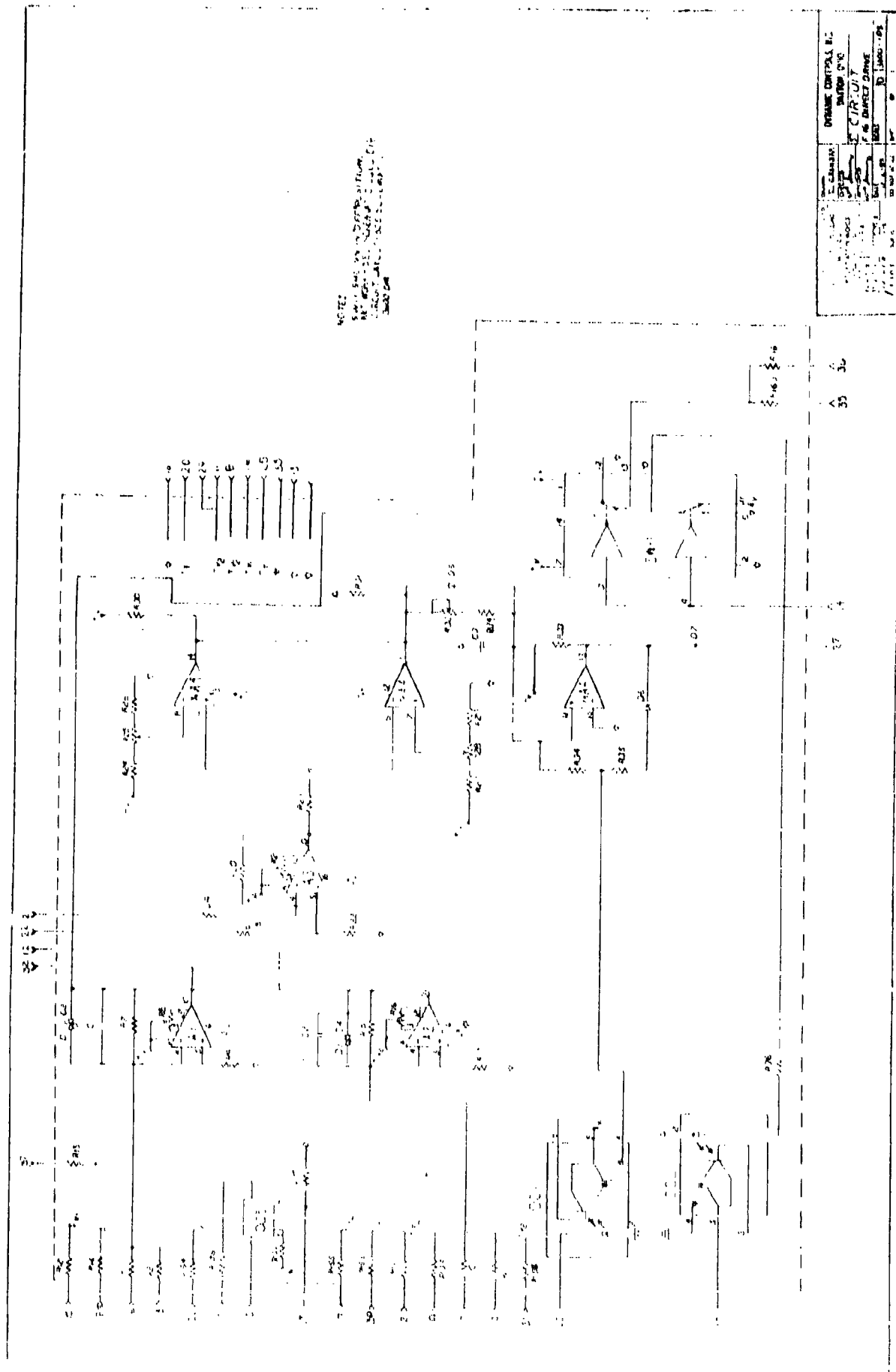
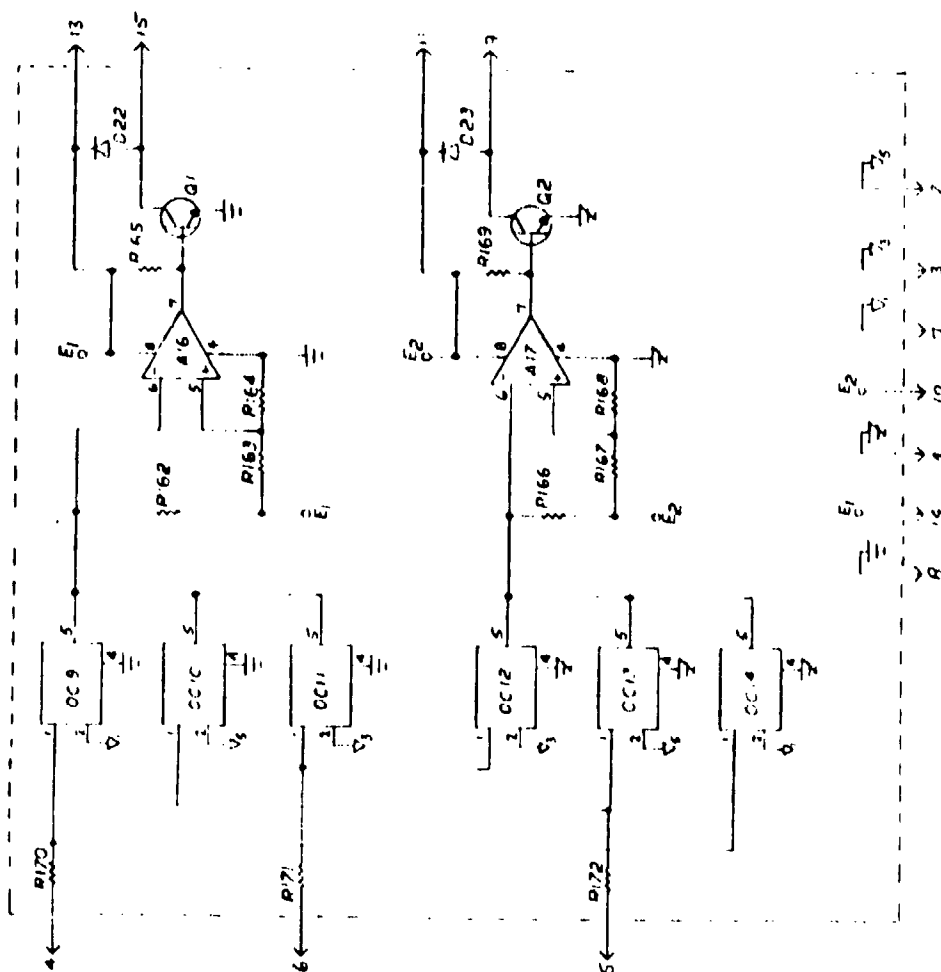


Figure VI-19. Summing circuit.

error signals exceed the \pm switching voltages of the comparator established by R25 and R28, SW-1 disconnects the input voltage to the servoamplifiers and connects the input lines of the amplifiers to ground. Resistors R160 and R161 are used to provide input line isolation between the two amplifiers to prevent a hardover input line voltage of one amplifier from driving the other to a hardover output. Opto-isolator OC1 is used to input a signal to reset SW-1. Opto-isolator OC2 is used to output a signal to the pilot monitor box when SW-1 turns the channel off.

The small circuit board at the front left of the control box (reference Figure VI-16) was used to mount six opto-isolators, two op amps and two driving transistors for the solenoid valves in the direct drive actuator. Figure VI-20 is the schematic for the board circuits. The opto-isolators are used in two AND gate circuits to drive the solenoid valves. The circuit is designed to operate with two separate 28 volt DC supplies. A failure of both 28 volt DC supplies is required to cause the solenoids to transfer the actuator to the fail centered mode.

PN 1 CC 9-14 Normally H.
 PN 5 CC 9-14 Normally LO
 PN 1 A-H 17 A/10-24 H.
 S. 5 32 Normally 40N



E₁ & E₂ ARE 28VDC SUPPLY POWER
 C₁, C₂ & C₃ ARE 15VDC CAPACITORS FROM C₁ 1.2, C₂ 3
 AND C₃ 4.7 VALUES TO 3101, 3103, 3107 RESPECTIVELY

[illegible]

Figure VI-20. Solenoid driver schematic.

Power Supply Description

Figure VI-21 shows the power supply constructed for the direct drive F-16 actuator. The power supply incorporated eight toggle switches, six for the ± 15 volt DC supply outputs and two for the 28 volt DC supply to the control electronics. The switches were used to simulate supply voltage failures to the control electronics. Output indicator lights mounted below the ± 15 volt DC switches were used to indicate failure of a power supply.

Figure VI-22 shows the power supply with the cover removed. Six Abbott converters were used to create the ± 15 volt DC output from the 28 volt DC input lines. These same converters were used in the F-4E direct drive flight test program (reference AFWAL-TR-82-3035). Each supply was capable of delivering 2.1 amperes at ± 15 volts DC over an input voltage range of 24 to 30 volts DC.

Pilot Monitor Box

Figure VI-23 shows the pilot monitor box front panel and the internal construction. Three circuit boards, light sets and switches were used, corresponding to the three control channels. Two momentary failure inject switches and a failure reset switch were used for each channel. The failure inject switches checked the operation of the failure-detection comparator and operation of the servoamplifier cross-strap wiring. One failure inject switch applied a voltage to the input of the monitor section of a channel, causing the failure monitor comparator to operate, shutting the channel off. The other failure inject switch caused an opto-isolator to apply a voltage in one servoamplifier input, causing the amplifier to drive hardover. The current polarity and amplitude indicator lights below the switches were used to verify that the servoamplifiers operated and that the amplifier outputs drove in opposite current directions as a result of the test input. The reset switch was used to reset a channel after the comparator detected a failure and latched the channel off.

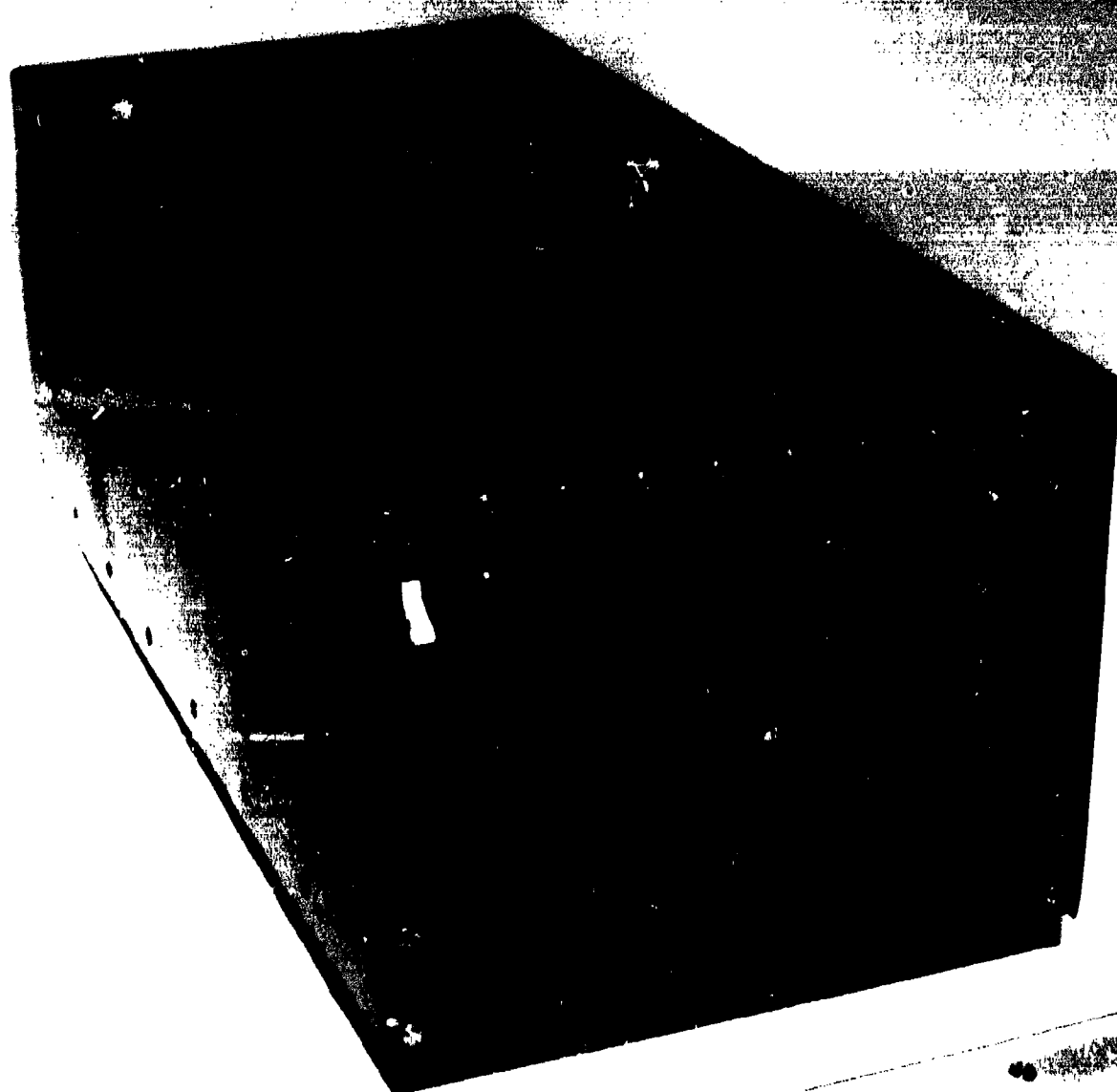


Figure VI-21. Power supply.



Figure VI-22. Power supply without cover.

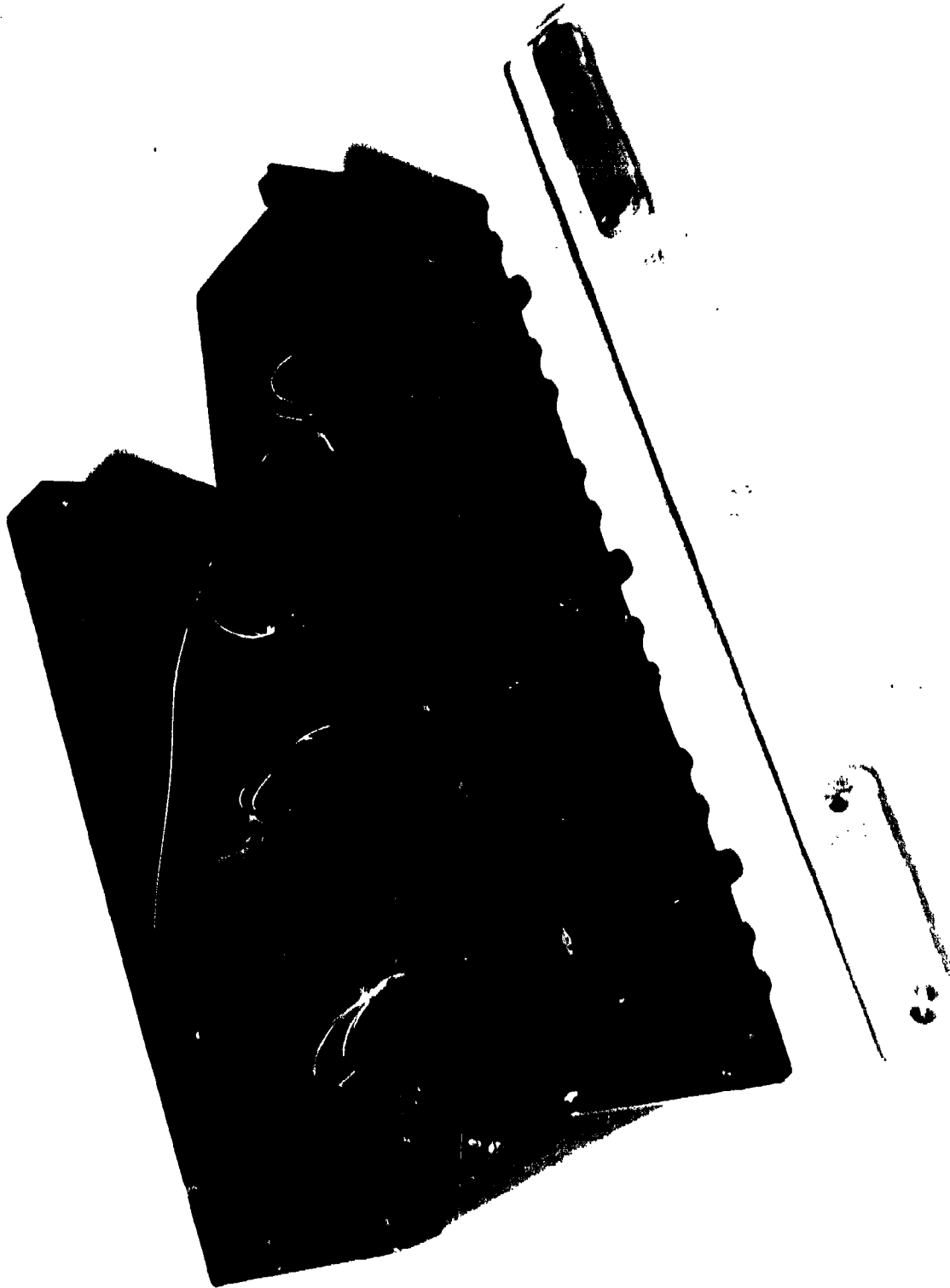


Figure VI-23. Pilot monitor.

Microprocessor Description

General

The microprocessor (Logic Processor) used for the Phase II investigation of the direct drive F-16 actuator was designed as a stand-alone unit. The Logic Processor chassis was connected by cable to the control electronics box (reference Figure VI-15) using three front panel connectors assigned for that purpose. The analog electronics were fabricated with *breaks* in the circuit lines. These *breaks* were brought out to three connectors used for coupling to the Logic Processor. For the Phase I analog operation, the breaks were *jumpered* by mating connectors. Figure VI-24 shows the Logic Processor unit used to evaluate the use of digital monitoring and failure detection on the operation of the system. The Logic Processor replaced the pilot's monitor box used in Phase I. The design of the F-16 Logic Processor was based on Z-80 standard bus hardware.

Two modes of operation were used with the Logic Processor, a self-test and continuous-monitor mode. The self-test mode duplicated the failure injection test capability of the pilot's monitor box while the continuous-monitor mode performed the monitoring function of the normal analog failure-detection electronics. As shown in Figure VI-24, the front panel of the F-16 Logic Processor contained nine light emitting diodes (LEDs) for *failure* identification and three LEDs for *channel-fail* notification. Six of the failure identification LEDs and the channel-fail LEDs were used for the continuous-monitor mode. The self-test performance used all of the failure identification LEDs, channel-fail notification LEDs and two additional *pass* and *fail* LEDs mounted to the right of the channel failure LEDs.

The self-test mode initiated hardover failures in the control electronics either with the internal opto-isolators of the control electronics or by buffered direct connection to the *break* lines provided for the Logic Processor. The self-test mode detected the associated failures and declared the monitoring function as working (pass) or not working (fail). A toggle switch provided for selecting the operating mode of the Logic Processor was located at the lower right of the front panel.

In the continuous-monitor mode, the Logic Processor polled voltages at two locations in each of three channels (a total of six test points in the drive electronics). These voltages were compared to each other or to a reference voltage for sign and amplitude. If the voltage resulting from the comparison exceeded a predetermined value, a failure was declared and the violating channel disconnected by a processor controlled analog switch. The failure-detection software was designed to require a test point to register a failure for a predetermined number of samples before the

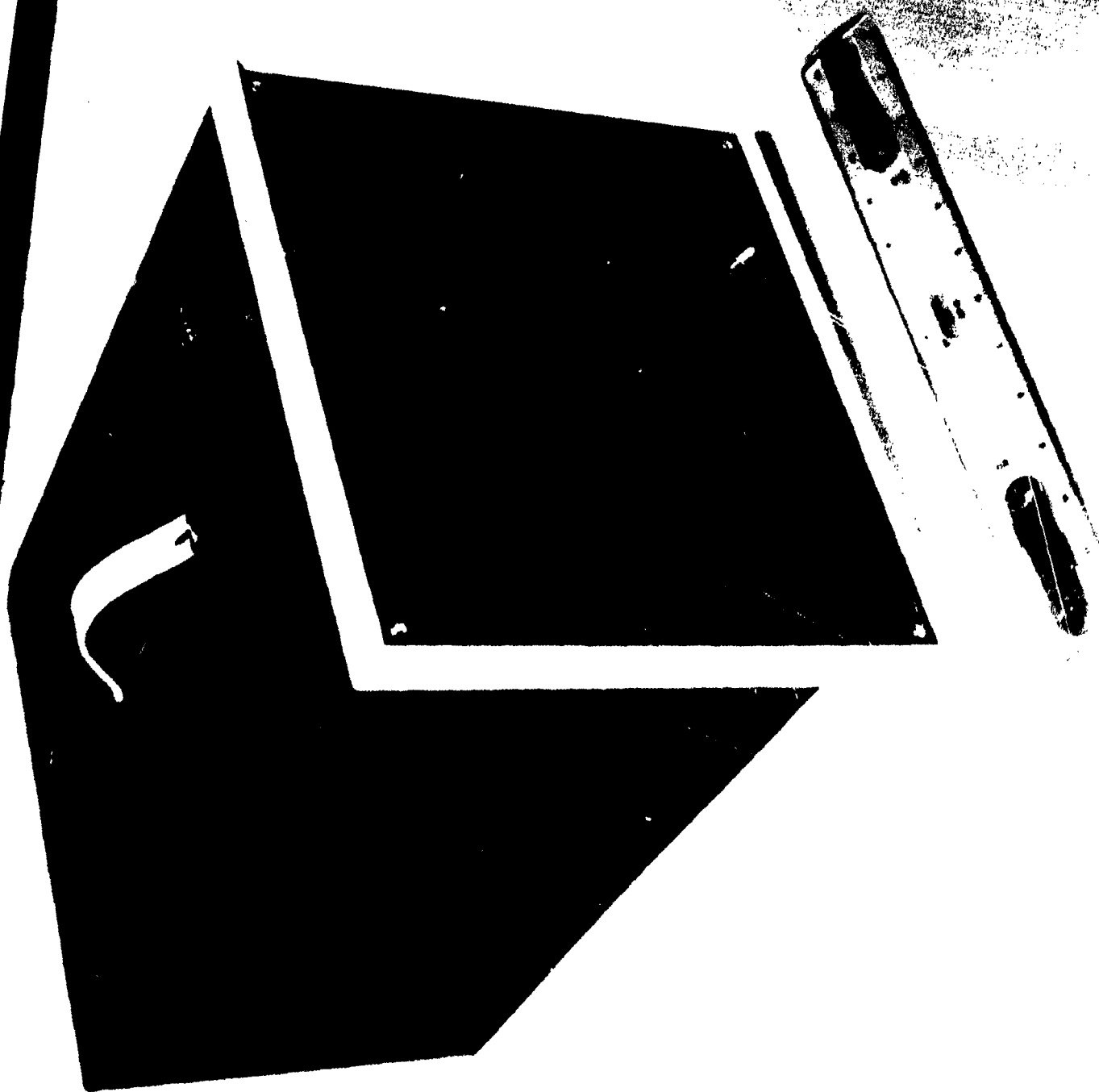


Figure VI-24. F-16 Logic Processor.

corresponding channel was voted out. In the continuous-mode, only the model and current failure-detection tests were used. The amplitude/gain failure test and identification lights were used only in the self-test mode.

In the self-test mode, the failure logic operation was tested by injecting failures (using the opto-isolators) into the control channels. The self-test checked both the failure-detection logic and the operation of the control channels in responding properly to the test inputs. For the self-test, a gain and sign test was used to check the operation of the servoamplifiers.

Analog System Modification

To interface the Logic Processor to the control electronics, the three *jumper* connectors were removed and replaced by the cable connectors of the Logic Processor. The control electronics were also modified by opening the cross-strapping between the servoamplifiers. This allowed the Logic Processor to read amplifier current differences and detect amplifier failures (the cross-strap used in the analog system prevented independent operation of the servoamplifiers).

Hardware

General. Figure VI-25 shows the internal construction of the Logic Processor. The system is packaged in a 10-slot Standard Bus card cage with a built in power supply and switch panel. The system CPU is a Z-80 based STD BUS processor card with a serial I/O port, up to 16K of RAM/PROM and built in diagnostic firmware (test and debug functions). A dual channel serial I/O board and a 64/256K memory board with battery backup were used to interface with a developmental system for assembling and debugging the software. Two modular I/O interface boards were used to drive the analog fail inject hardware (opto-isolators), the front panel LEDs and thumbwheel switches. Two prototype wire-wrapped boards were used to multiplex front panel signals and provide analog test voltages by using digital relays. A 16-differential/32-single-ended input 12-bit A/D converter provided the interface with the analog system electronics.

Components. As shown in Figure VI-25, the front panel contained binary-coded decimal thumbwheel switches to input data (3 digits plus sign) and address (2 digits) information to the microprocessor. The three LEDs for each of the three channels (9 LEDs total) represented the three function tests of the valve drive electronics; MODEL, GAIN/SIGN and CURRENT.



Figure VI-25. Logic Processor construction.

The function tests checked the operating sections of the drive electronics. There were three channel FAIL LEDs and two self-test LEDs (PASS and FAIL). Depressing the LOAD button placed the displayed data information at the displayed address location. The test mode switch selected the test mode; SELF TEST or CONTINUOUS MONITOR. The RESET button reset and initialized the microprocessor by placing the default data at the address locations. Seven boards were used in the card cage. Five were standard cards designed for operation with the standard bus. Two cards were prototype cards and were constructed for the processor using wire wrap circuitry. The cards used were a *Smart Card*, Memory Board, two I/O boards, an A/D board, and two prototype boards.

The Versallogic model STD Z80-1 Smart Card processor board combined a 4 MHz Z80A CPU chip with an on-board RS-232C serial port, RAM expandable to 16K bytes, and built-in diagnostic firm-ware for use with the STD BUS. This board operated the Logic Processor.

The Versallogic model VL-7709 64/256K Memory Board accepted 8K or 32K RAM/ROM devices. The memory board offered 4 to 10 year data retention with a on-board lithium battery backup. The memory board requires 220 microseconds to access RAM/ROM when used with the 4 MHz Z80 CPU. This board provided the additional memory required for developing and assembling the program.

Two I/O interface boards were used. The first board (#1), a Versallogic model STD MIO-24 Modular Interface was Z80 and Opto 22/Gordo compatible with 24 buffered I/O channels and two interrupt channels. The Logic Processor controlled the system failure injects and the Standard prototype board #1 inputs with this board. The second I/O interface board (#2) was identical to interface board #1. The Logic Processor used this board to retrieve the analog data lines and control the Standard prototype board #2 (a data/LED mux board).

The A/D input board, an Analog Devices model RT1-1260 Analog Input Card, provided data acquisition of analog signals from up to 32 single-ended or 16 differential voltage inputs. User configurable gains of 1 to 1000 allowed input ranges from .010 volts to 10.0 volts. A sample and hold amplifier and 12-bit converter provided throughput of up to 25,000 channels per second. The A/D conversion time was 25 microseconds. The Logic Processor accessed analog data (model and current) from the drive electronics using this board.

Two Standard Bus prototype boards were used. Board 1 was wire-wrapped by DCI and contained three TI SN74S139 Dual 2-to-4-Line Decoders and six Analog Devices AD7511D CMOS Analog Switches. The relays input \pm voltages and grounds to the channel drive

electronics as required by the CPU via I/O Interface Board #1 and the decoders. Board 2 was wire wrapped by DCI and contained three TI SN7438 open-collector positive NAND buffers and three Analog Devices AD7512D Analog switches. Pull up resistors were also mounted on this board to provide current to the LEDs. This board was used to mux data lines and LED lines as required and was controlled by I/O interface board #2.

The rear panel of the Logic Processor provided mounting locations for the 120 volt AC fuse, power cord and cable connectors. The cables connected the Logic Processor to the F-16 Direct Drive Control Electronics. Figure VI-26 is a schematic of the Logic Processor hardware and the interface to the analog electronics. The schematic shows the seven STD BUS boards, the three analog control channels, the Logic Processor's front panel and the connection between all the elements.

Logic Description

General. The valve drive electronics consists of three sections: the model compare section, the pulse-width modulation section and the current driver section. In the self-test mode the Logic Processor examines each of these sections in sequence for each of the three channels. In the continuous-monitor mode, the Logic Processor continuously examines the model and current driver sections of each channel.

While in the self-test mode, the system must detect induced failures and shut down the appropriate channel to pass. The inability to detect a failure will result in turning on the offending section LED with the Logic Processor continuing to test the remaining sections and turning on the FAIL LED after the completion of the self-test. The operator therefore, is alerted to the self-test failure and the section of the valve drive electronics where the failure occurred.

If a channel sustains a failure in one of the two monitored sections while in the continuous-monitor mode, the channel is shut down and the Logic Processor ignores the failed channel for the duration of the operation or flight. In the event of a second channel failure, the Logic Processor will monitor only the remaining operating channel. A third failure will cause the channel to be shut down and the actuator transfer to the centering mode.

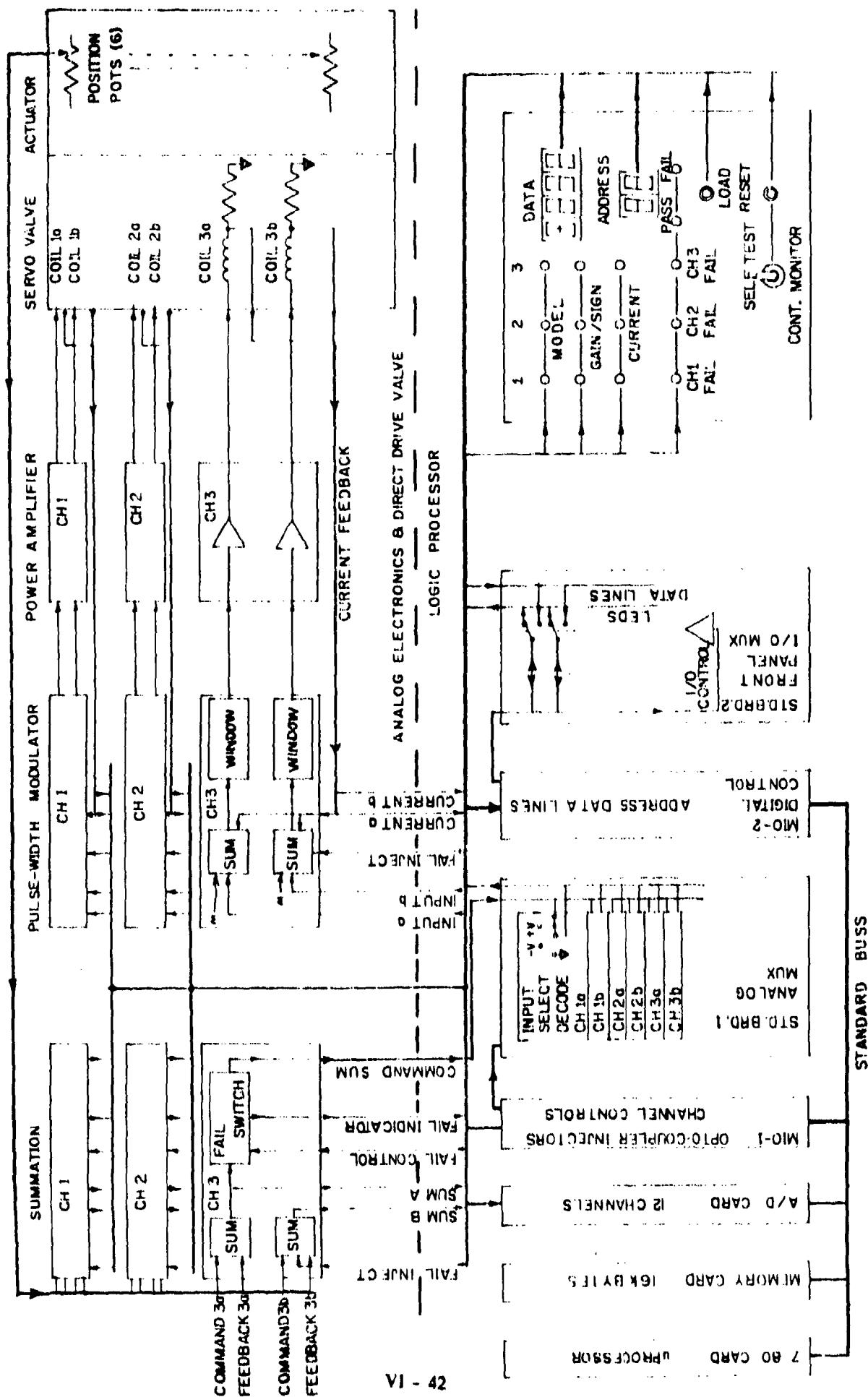


Figure VI-26. F-16 logic processor hardware and interface schematic.

The *MAIN* procedure of the Logic Processor initializes the entire program and continuously polls the mode select switch, calling either the self-test procedure or the continuous-monitor procedure when required. If the system is booted up in the self-test mode, the procedure will perform the model, gain/sign and zero current checks. The self-test procedure then polls the mode select switch and when the switch is placed in the continuous-monitor mode, calls the continuous-monitor procedure to perform the last self-test hardover current check. A system reset is then required to begin the actual continuous-monitor procedure. If the system is booted up in the continuous-monitor mode, the continuous-monitor procedure will begin immediately, without the last self-test hardover current check.

Self-Test. The self-test procedure begins by failing all three channels and turning on all nine section LEDs. Channel 1 is then activated with the other two channels remaining in the failed mode (with all the LEDs on). If any self-test failures (*failure to detect failures*) occur in the first channel, the section where the failure occurred will be indicated by an illuminated LED. The sequence is continued by activating the next channel and leaving channel three in the failed mode. This sequence is continued for all three channels. If self-test failures are detected, the FAIL LED will be turned on and the section LEDs associated with the failures will be turned on. If no *failures to detect failures* occur, the PASS LED will be turned on. In either case, the self-test mode switch will be polled for the next self-test check (the hardover current check). The self-test procedure is made up of the Hardover Input, Gain/Sign, Current and Hardover Current tests. A description of these tests with the subroutine labels in parenthesis is as follows:

Hardover Input Test. A hard-over input is compared (MTH1) to the model and since the difference should exceed the self-test model limit (STMODLIM), a failure is declared, the test is passed and the test sequence continued. If this procedure does not detect the hard-over failure, the self-test sequence will continue but will turn on the FAIL LED and the MODEL LED for the corresponding channel upon completion of the SELF TEST procedure.

Gain/Sign Test. This test compares the polarity and magnitude of the two coil output signals to the same parameters of the coil input signals. A negative voltage is input to one of the two coil driver circuits (A). The coil output current is checked for the proper polarity and compared to the input value (TESTVAL) and a test limit (TSTLIM) to determine if the current magnitude is consistent with the required gain values (MTH2). This test is repeated for the other coil driver (B). The test is then repeated with a positive input (MTH3) to both coil drivers (A&B).

Current Test. This procedure inputs zero voltage to the coil drivers and compares (MTH4) the coil outputs (A&B) to a test limit (TSTLIM). If the outputs do not exceed the limit, the test is passed and the self-test sequence is continued.

Hardover Current Test. This test is performed by the continuous-monitor procedure immediately after the self-test mode switch is placed in the continuous-monitor mode. All the LEDs are turned off and the channels that passed the self-test are reset. A hard-over voltage is input by the PWM opto-isolator (OC7 on Figure VI-18) to the active channels. The continuous-monitor current failure logic should detect the failure, turn on the channel fail LEDs and the self-test PASS LED, thus completing the self-test or *pre-flight check out*.

Continuous Monitor.

Failure Sampling. When the model compare value or the current compare value exceeds the pre-established limit, the failure is assigned a channel fail type (CH(n)FTYPE) and is counted (CH(n)CNTR). The fail-type count is compared to a preestablished value (CNTRMAX) and if this value is exceeded, the Continuous Monitor declares the hard failure by shutting down the offending channel and turning on the LED corresponding to the channel fail type. The counting logic drops a count every other sample; for example, if the value (5) is loaded in CNTRMAX and a continuous failure occurs, the hard failure will occur after the ninth consecutive, identical bad sample. This algorithm effectively screens nuisance failures. The count value CNTRMAX, is a variable and can be easily changed.

Model Compare. The Continuous Monitor compares the sum of the command signal and the feedback signal with an identically summed model signal (MTH5). If the voltage difference exceeds a predetermined limit (35 percent of full scale input voltage) for a predetermined number of samples (9), the Continuous Monitor declares a failure by shutting down the offending channel and turning on the corresponding failure-indicator LEDs. The values in parenthesis represent the processor default values for these two variables.

Current Compare. Each channel drives two opposing coils. The Continuous Monitor compares the drive currents through each coil (MTH5). If the current difference exceeds a predetermined value (0.5 amperes) for a predetermined number of samples (9), the Continuous Monitor will declare the failure by shutting down the offending channel and turning on the corresponding LEDs.

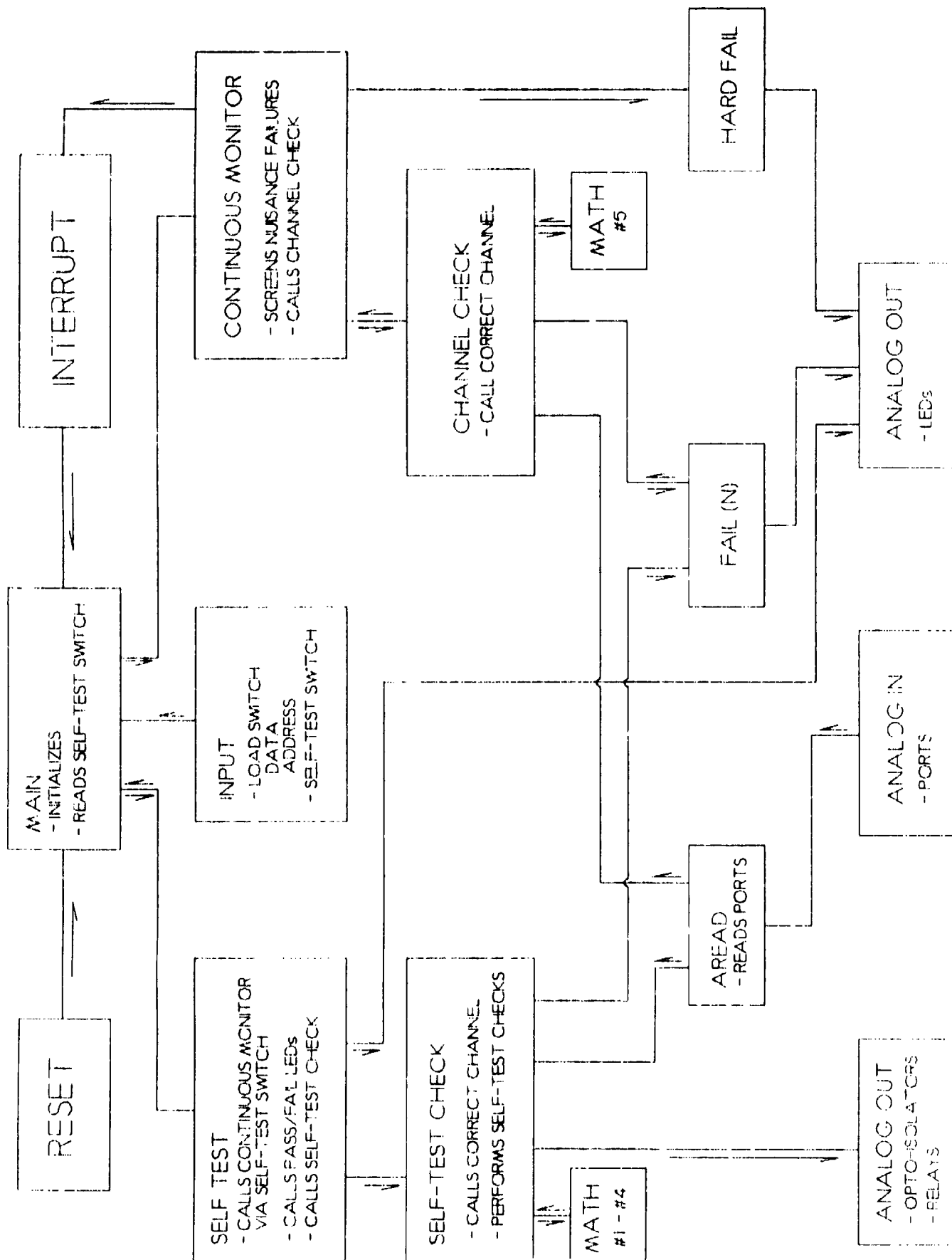


Figure VI-27. Structure chart.

Program. The program for the Logic Processor was written in 8085 assembly language and performed the functions as indicated in structure chart of Figure VI-27. The following is a table of contents for the program. The program itself appears in Appendix A-3.

Table VI-1. F-16 program descriptive table of contents.

START UP PROCEDURES

0E00	Auto Jump
F048	Z-Assist Monitor Routines
0001	Analog Access (address labels)
0040	Masks; Switch & Thumbwheel Switches; Fail Injects
0100	Jump Table (default data)
0200	Data Base (thumbwheel data)

INITIAL PROCEDURES

0300	ASCX	16 Bit Subtract (absolute value)
0309	AREAD	Analog channel in to accumulator (A) and out with value in (HL)
0319	MATH1 through	19 Math procedures (compares, subtracts and logicals)
0400	MATHFS	
0403	INITIALIZE	Stores counters, zeros accumulator and performs Z-80 block moves
0438	DELAY1	Fixed delay value
043B	DELAY	Decrementing loop
0444	STCHECK	Determines the correct channel and performs the self-test model, gain/sign and zero input current checks using the CH(n)ST, CH(n)TC, DELAY, AREAD, MATH(n) and FAIL(n) procedures
0648	CHCHECK	Determines the correct channel(CK(n)) in the continuous-monitor mode, moves in the analog data for each channel using AREAD, calls CK0 to do model current compares using MATH5, calls the FAIL(n) procedures and finally returns the fail count and type to the Continuous Monitor (CHK(nn))
06F2	FAILC	Current failures Ch3, Ch2 & Ch1
074A	FAILS	Gain/Sign failures Ch3, Ch2 & Ch1
07A2	FAILM	Model failures Ch3, Ch2 & Ch1

Table VI-1. F-16 program descriptive table of contents (continued).

MAIN PROGRAM

07FA	MAIN	Program beginning, calls INITIALIZE and sets up variables, etc
080A	LOOP 1	Reads the self-test switch and calls the SELF TEST or CONTINUOUS MONITOR procedures

SELF TEST PROCEDURE

081B	SELF TEST	Clears flags, moves and sets counters, turns LEDs off and turns off all channels and calls procedures STCHECK and DELAY
087F	ST7 thru ST40	Turns on the pass LED, polls the self-test switch, sets up channels 1-3 and performs the current self-08AC test using the monitor section and PWM fail inject (OC7)

CONTINUOUS MONITOR PROCEDURE

08AE	MONITOR	Counts failures using procedures CHKFLG, CNTR 0-3 and FLIP
0904	CHK1	Determines the correct channel, compares fail counts with the number of failures allowed and calls the hard fail procedures HF1M (model), HF1C (current) and HF1 (channel failure), else jumps to CHK11
095E	CHK11	Calls CHCHECK
0966	CHK2	Same as CHK1 for channel 2
09B4	CHK22	Calls CHCHECK
09BC	CHK3	Same as CHK1 for channel 3
0A0A	CHK33	Calls CHCHECK
0A12	CHKO	Calls interrupt HANDLER, resets system, turns off LEDs, resets failed flags, restores counters, compares data addresses and back to the continuous monitor if valid; else changes data (1s, 10s, & 100s), converts data from decimal to hex, stores data and jumps back to continuous monitor

Table VI-1. F-16 program descriptive table of contents (concluded).

FINAL PROCEDURES

0A96	HANDLER	Handles interrupts, saves present LED status and sets up to read the thumbwheel switches
0AD9	DUMP	Active for debug and channel determination for FAIL(n) procedures
0B0B	SPACE	Calls CONOUT (one of the Z-80 assist monitor routines)
0B11	END	

III. GENERAL TEST PROCEDURE

The following general test procedure was used for evaluating the demonstration system. This procedure defines the measured parameters and states the general method used in making the measurement. The procedure is divided into the following categories:

1. Performance Measurements
2. Failure Effect on Performance
3. Failure Transients
4. Failure Logic Detection Characteristics

Performance Measurements

Performance measurements are measurements of the output to input characteristics of a control device and can be defined in part by the following terms and procedures:

Static Threshold. *The minimum input change from zero level which causes a measurable output change.*

Procedure: Apply a slowly increasing + input until a measurable output change occurs. Repeat for - input. Threshold is indicated by the minimum input change for a measurable output change.

Dynamic Threshold. *The input level (at a particular frequency) required to cause a measurable output level.*

Procedure: A sinusoidal input at a selected frequency of 50 percent of the bandpass of the actuator is applied to the actuator. The amplitude of input to create a measurable output indicates the dynamic threshold. The bandpass of the actuator is defined as the frequency at which -3 dB amplitude or 90° phase shift occurs (whichever is lower in frequency).

Frequency Response *With a sinusoidal actuator input, the frequency response of the actuator is the relationship of the output to input expressed as an amplitude ratio and phase angle as a function of frequency.*

Procedure: Apply a sinusoidal input of an amplitude which is:

- a. large enough to minimize the nonlinearity distortions of threshold and hysteresis
- b. small enough to avoid velocity saturation in the frequency range of interest. The ratio of output amplitude to input amplitude and output phase angle relative to input is recorded.

The plot of the amplitude ratio and phase indicate the frequency response.

Linearity *The deviation of output versus input from a straight line relationship.*

Procedure: Apply an input from - to + maximum input while recording the corresponding output position. Linearity is indicated by the deviation of the plotted output versus input from a straight line drawn between zero and a point which minimizes the maximum deviation of the plotted curve from the straight line. Repeat for + input to - input.

Hysteresis *The non-coincidence of loading and unloading curves.*

Procedure: Apply a slowly varying input to the actuator at up to 1 percent of the maximum input in the following sequence while recording the actuator output position:

1. 0 to + direction input
2. + input to - direction input
3. - input to + input

Repeat for an input up to 10 percent of the maximum input. From the plot of output versus input, the hysteresis is indicated by the difference between + direction actuator output position and - direction output position for the same input level.

Time Response

Saturation Velocity. *The maximum velocity at which the actuator is capable of moving in each direction.*

Procedure: With the actuator at zero position, a maximum amplitude input is applied to the actuator while the actuator motion vovs time is recorded. The test is conducted for both directions of actuator motion. The slope of the position vovs time record indicates the saturation velocity.

Step Response. *The time response of the actuator output to an applied step input.*

Procedure: Apply a step input to the actuator and record the corresponding actuator motion. The amplitude of the step should be:

- a. large enough to minimize the nonlinearity distortion of threshold and hysteresis
- b. small enough to avoid velocity saturation.

Failure Effects On Performance

Failure Effect. *The change in the performance of a redundant actuator due to input failures or internal failures of actuator components.*

Procedure: Inject hydraulic or electrical input failures into the actuator under test to cause it to operate in its *failure operational* modes. For each mode, measure the performance by repeating the Performance Measurement tests. The input levels should be maintained at those used for the *no failure* performance tests, unless the performance changes dictate different levels in order to obtain reasonable test data.

Failure Transients

Electrical Failure Transients. *The change in actuator output during failure corrective action due to electronic input failures causing transfer from one operational mode to another.*

Procedure:

- a. Apply a slowly changing input to one control channel of the actuator. Record the actuator output change during the corrective action of actuator. Repeat the test for each control channel input and failure mode condition. Repeat for a hardover step input.
- b. Apply a sinusoidal input to all channels. Ground each input while recording actuator output.

Hydraulic Failure Transients. *The change in actuator output during failure removal corrective action due to hydraulic input failures causing transfer from one operational mode to another.*

Procedure:

- a. Apply a decreasing hydraulic input to one control channel of the actuator. Record the output change during the corrective action of the actuator. Repeat the test for all hydraulic inputs.
- b. Repeat the preceding test with a rapid decrease of hydraulic input pressure.

Failure Logic Detection Characteristics

Logic Detection Characteristics. *The difference in multiple input time histories which will cause failure logic to declare a failure.*

Procedure:

- a. Static Failure-Detection Level

Apply a slowly increasing ramp signal to all inputs. Ground one input as the input crosses zero and determine the input voltage difference that is present when a failure occurs. This voltage expressed as a percent of the input for maximum position and as a percent of the input for maximum rate is the failure-detection level.

b. Dynamic Failure-Detection Level

Apply a slowly increasing input to one channel of the system at frequencies from DC to a frequency at which the system response is attenuated by at least 15 dB. The other channel inputs are maintained at zero levels. The voltage at which the channel is declared failed, expressed as a percentage of the input for maximum position and a percentage of the input for maximum rate is the *dynamic failure-detection level*.

IV. SPECIFIC TEST PROCEDURES

System Setup

For all tests, each channel's failure-detection level for the model and control channel's error voltage comparator was set at voltage differences which corresponded the error voltage to produce a valve motion of 35 percent of the total servovalve stroke. The use of this value for the system operation was verified by performing one complete series of input testing to establish that nuisance disconnects did not occur. Note that for the F-16 direct drive actuator, the minimum error voltage detection level without nuisance disconnects is determined by the command and feedback voltage tracking between just two pairs of feedback and command voltages (not three or more required if cross channel voting had been used). The 35 percent of spool deflection (maximum rate of the actuator) had been successfully used previously for the F-4E direct drive flight test system.

For the Phase II testing with the microprocessor, the failure-detection level was also set at 35 percent of the spool stroke. The failure logic was set to declare a failure after 9 consecutive failures were detected (failures being error voltage differences which exceeded the 35 percent detection threshold). This value gave a failure-detection time delay of 12.6 milliseconds and a failure amplitude detection characteristic with error voltage frequency which was flat up to 10 Hz. The failure logic setting was established after a series of tests documenting the detection level vovs frequency characteristics for different failure declaration settings. The use of this value for the Phase II testing was also verified by performing one complete series of input testing to establish that nuisance disconnects did not occur.

Specific Test Conditions

The general test procedures listed in the previous section were used for the Phase I and Phase II tests. The application of these tests was as listed in the Table VI-2 following. Not all tests used for the Phase I testing were repeated for the Phase II portion of the evaluation (since the system changes for the Phase II could not affect the test results).

"A" suffix on test condition number - Analog Controller

"B" suffix on test condition number - Microprocessor Control

Test conditions 1 through 28 describe the operating conditions for the test system.

Test conditions 1 through 5 define the operating modes of the F-16 direct drive actuator, both for normal and after failure conditions. The entire series of performance measurements were run for each of these operating modes.

Test conditions 6 through 28 are the failure transient tests. These test conditions define the method of testing for output changes with specific input failures.

Table VI-2. Test conditions for the F-16 Direct Drive Actuator.

Condition Numbers	Test Conditions
<u>Operational Modes - Performance Tests</u>	
1	Channels 1, 2 and 3 active
2	Channel 1 failed, Channels 2 and 3 active
3	Channels 1 and 2 failed, Channel 3 active
4	Channels 1, 2 and 3 active - P1 failed, P2 active
5	Channels 1, 2 and 3 active - P1 active, P2 failed
<u>Hardover Failure Transients</u>	
6(A&B)	Apply a positive hardover voltage sequentially to Channels 1A, 2A and 3A with the system at null.
7(A)	Apply simultaneous positive then negative 3.0 volt steps to Channels 1A, 2A, and 3A with the system at null.
8(B)	Ground inputs to Channels 1B, 2B and 3B simultaneously with the system output at 75 percent extend.
9(B)	Ground inputs to Channels 1B, 2B and 3B simultaneously with the system output at 75 percent retract.
<u>Slowover Failure Transients</u>	
10(A)	Apply a 0.40 V peak, 0.3 Hz ramp input to all (6) channels and ground Channel 1A as the slope crosses zero.
11(A)	Apply a 0.40 V peak, 0.3 Hz ramp input to all (6) channels and ground Channel 2A as the slope crosses zero. (Ch. 1 failed)
12(A)	Apply a 0.40 V peak, 0.3 Hz ramp input to all (6) channels and ground Channel 3A as the slope crosses zero. (Ch. 1,2 failed)
13(B)	Apply a 0.30 V peak, 0.03 Hz ramp input to all (6) channels and ground Channel 1A as the slope crosses zero.
14(B)	Apply a 0.30 V peak, 0.03 Hz ramp input to all (6) channels and ground Channel 2A as the slope crosses zero. (Ch. 1 failed)

Table VI-2. Test conditions for the F-16 Direct Drive Actuator (continued).

- 15(B) Apply a 0.30 V peak, 0.03 Hz ramp input to all (6) channels and ground Channel 3A as the slope crosses zero. (Ch. 1,2 failed)

Dynamic Hardover Failure Transients

- 16(A&B) Apply a positive hardover voltage sequentially to Channels 1A, 2A and 3A with the system operating at 0.3 HZ with a 1.5 V peak input amplitude.
- 17(A&B) Apply a negative hardover voltage sequentially to Channels 1A, 2A and 3A with the system operating at 0.3 HZ with a 1.5 V peak input amplitude.
- 18(A&B) Ground Channels 1A, 2A and 3A sequentially with the system at 50 percent extend, operating at 0.3 HZ with a 0.8 V peak input amplitude.
- 19(A&B) Ground Channels 1A, 2A and 3A sequentially with the system at 50 percent retract, operating at 0.3 HZ with a 0.8 V peak input amplitude.

Pressure Failure Transients

- 20(A) Apply a 0.160 V peak, 0.1 HZ ramp input to all (6) channels and reduce P1 from 3000 psi to zero with P2 at 3000 psi. Then reduce P2 from 3000 psi to zero with P1 at 3000 psi.
- 21(B) Apply a 0.160 V peak, 0.1 HZ ramp input to all (6) channels and reduce P1 from 3000 psi to zero then reduce P2 from 3000 psi to zero. Restore P2 to 3000 psi then P1 to 3000 psi.
- 22(B) Apply a 0.160 V peak, 0.1 HZ ramp input to all (6) channels and reduce P2 from 3000 psi to zero then reduce P1 from 3000 psi to zero. Restore P1 to 3000 psi then P2 to 3000 psi.

Current Failure Transients

- 23(B) Apply a hardover to the servodriver (via OC-7) to Channels 1, 2 and 3 sequentially.
- 24(B) Apply a hardover to the servodriver (via OC-7) to Channels 1, 3 and 2 sequentially.
- 25(B) Apply a hardover to the servodriver (via OC-7) to Channels 2, 1 and 3 sequentially.
- 26(B) Apply a hardover to the servodriver (via OC-7) to Channels 2, 3 and 1 sequentially.
- 27(B) Apply a hardover to the servodriver (via OC-7) to Channels 3, 1 and 2 sequentially.
- 28(B) Apply a hardover to the servodriver (via OC-7) to Channels 3, 2 and 1 sequentially.

Deviations And/Or Additions To The General Test Procedure

Because the Logic Processor was not designed as a failure tolerant control device, no testing of the failure effects of the microprocessor itself was attempted. The intent of the Phase II evaluation was to determine the performance potential of the microprocessor as a failure monitoring and correcting device.

Measurement of the static threshold was accidentally omitted from the tests conducted on the nominal performance of the F-16 direct drive actuator. However, dynamic threshold tests (at input frequencies of 50 percent of the bandpass of the actuator) were run. Based upon previous tests of the general DDV configuration (as documented in technical report AFFDL-TR-77-91), the static threshold for the general configuration is no greater than the dynamic threshold.

Test Hardware Setup

Figure VI-28 is an overall view of the test hardware as installed for the performance testing. The F-16 direct drive actuator was mounted in the General Purpose Actuation Test Rig (GPATR) in the Actuation Laboratory, Building 145, WPAFB, Ohio. The control electronics were installed on a table in front of the actuator. The GPATR was used as holding fixture for the actuator testing and the GPATR's loading actuator was not connected to the F-16 direct drive actuator.

Figure VI-29 shows the mounting method of the F-16 direct drive actuator in the GPATR. The actuator was mounted as a moving body actuator with the rod end attached to a stationary slug. An additional position transducer to measure the actuator position was mounted below the control system feedback transducers. A 3000-psi hydraulic supply was connected through separate shutoff valves to each of the actuator's hydraulic system ports. As shown in this figure, the control cable from the electronics to the actuator is at the left of the figure. A cable of 34 individual wires (12 for the force motor, 18 for the potentiometers and 4 for the solenoid valves) was required for operation of the actuator.

Figure VI-30 shows the four electronic units of the F-16 direct drive actuator investigation as assembled on the table in front of the actuator. The pilot's monitor on top of the power supply is not connected to the control electronics box in this figure. The system had been setup for the Phase II investigation when the photograph was taken. Note that the power cables from the power supply are connected to the control electronics box on the front panel and are routed behind the control electronics box for the figure.



Figure VI-28. F-16 direct drive test installation.

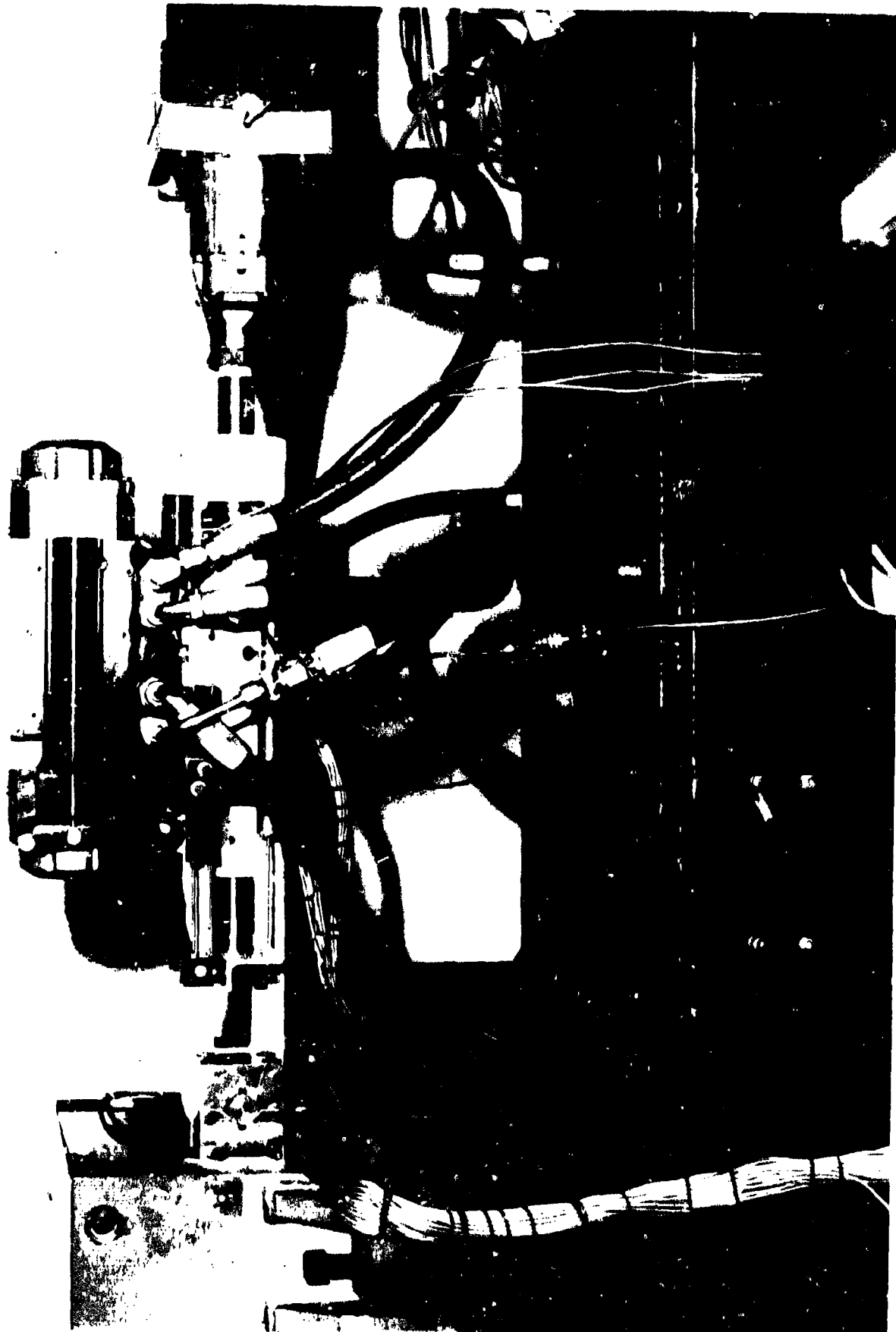


Figure VI-29. F-16 direct drive actuator.

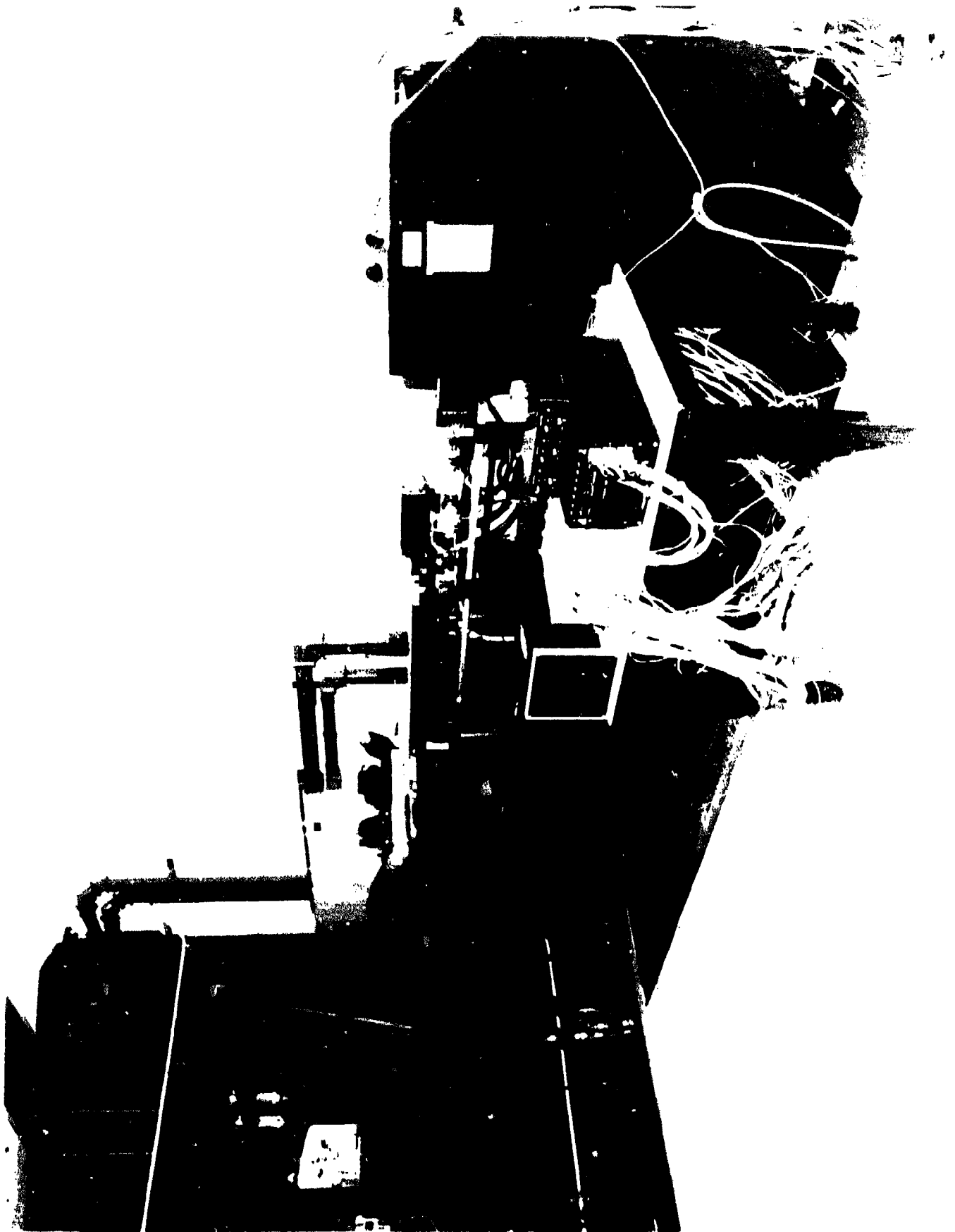


Figure VI-30. Direct drive test electronics.

V. TEST RESULTS

In order to reduce the volume of test data presented in this section, much of the performance measurement data has been reduced to tabulated form. The principal exceptions are the results for step response and failure transients. Since time response characteristics are not well defined by listing only one or two characteristic values, the step response measurements and the failure transient measurements are presented as recorded. Also presented in graphical form is the data taken for the measurement of input/output linearity. The results are presented in tabulated form for the following tests:

1. Dynamic Threshold
2. Hysteresis
3. Frequency Response

For the test results reduced to tabular form, a sample of representative recorded data is included for the test.

In presenting the measurements of threshold and hysteresis, the results are given both in percent of the input for full actuator stroke and percent of the input for full valve stroke. In terms of the full actuator stroke, the percentage value for a given amount of hysteresis decreases as the maximum stroke of the actuator increases. Presenting percentage in terms of the input for maximum control valve stroke shows the threshold and hysteresis characteristics better in terms of comparing different control valve driving mechanizations, independent of the stroke sizing of the power actuator.

The failure transient data is presented in the strip chart form as recorded. For each figure, the general arrangement of the data is from the top of each figure down:

- a. Channel Inputs 1 through 3 (E_{in})
- b. Channel Failure Indicators 1 through 3
- d. Actuator Position (X_{out})

The channel inputs are used as failure injection points for the test system. The actuator position trace shows the effect of the injected failure on the system output. The "failure indicate" time traces show the state of the voltages used to drive the failure indicators for the three actuator channels. Note that the failure indicate traces do show individual control channel status and are in series with the display lights on the front panel of the microprocessor. The test conditions 6 through 28 define both the initial operating status of the system and the input voltage changes used to cause the system to change

operating status. The "A" and "B" designations associated with the channels (1A, 2B, etc.) indicate the active or the monitor section inputs of a control channel. For example, a *failure input to 1A* indicates that the input controlling the servoamplifiers was failed. A *failure input to 1B* indicates that the input used for the monitor section of the channel was failed. The general order of the performance data presentation is:

a. Dynamic Threshold	Test Conditions 1 through 5
b. Hysteresis 1% Input	Test Conditions 1 through 5
c. Hysteresis 10% Input	Test Conditions 1 through 5
d. Linearity 110%	Test Conditions 1 through 5
e. Frequency Response	Test Conditions 1 through 5
f. Step Response	Test Conditions 1 through 5
g. Saturation Velocity	Test Conditions 1 through 5

Note, as listed previously, test conditions 1 through 5 were:

<u>Test Condition</u>	<u>Description</u>
1	Channels 1,2 and 3 active
2	Channels 1 failed, Channels 2 and 3 active
3	Channels 1 and 2 failed, Channel 3 active
4	Channels 1,2 and 3 active, P1 failed, P2 active
5	Channels 1,2 and 3 active, P1 active, P2 failed

Dynamic Threshold Results

Figure VI-31 shows the data recorded in establishing the dynamic threshold for test condition 1. The data shown is representative of the data recorded for test conditions 2 through 5. Note that on Figure VI-31, the start of motion and tracking of the input waveform is well defined. The frequency for the input signal is 13.5 Hz and is nominally half the frequency where the actuator exhibits a -3 dB amplitude ratio when operating in this test condition. Table VI-3 lists the measured threshold inputs for all the test conditions. Note that the threshold for all test conditions is under 0.35 percent of the maximum input. The threshold increases slightly from test condition 1 through 3, reflecting the lower force gain as fewer control channels are used. The threshold for conditions 4 and 5, with only one hydraulic supply operating, are the lowest of the five different operating conditions. This indicates that the spool breakout friction is a function of the hydraulic pressure applied to the control valve.

Dynamic threshold is not a specific performance measurement for the standard F-16 ISA. However, the specification for the F-16 ISA (General Dynamics specification No. 16ZH001F, 2 August 1978) uses an envelope of deviation for the output to input relationship. At zero input, the envelope allows a deviation of ± 1.25 percent (of maximum input). The 0.35 percent threshold measurement for the F-16 direct drive actuator is well below the 1.25 percent deviation limit. The static threshold was not measured for the F-16 direct drive actuator. However, based upon measurements of the F-4E control valve, the static threshold will not be greater than the dynamic threshold.

Hysteresis Test Results - 1 Percent Command

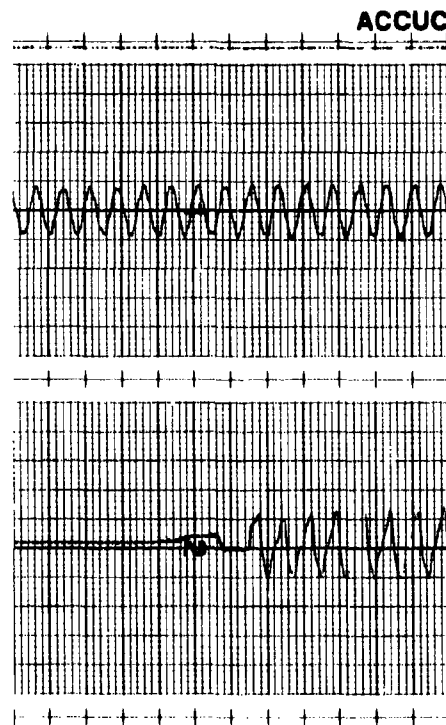
Figure VI-32 is a plot of the hysteresis performance of the F-16 direct drive actuator with a 1 percent command input and the actuator operating in Condition 1. This figure is representative of the data recorded for Conditions 2 through 4 with a relatively *open* hysteresis loop. Figure VI-33 is the data taken for Condition 5, with only PI pressure supply operating. The hysteresis value (the difference in the envelope between the extend and retract motions) is less than conditions 3 and 4. However, the actuator exhibits hunting within the hysteresis loop, a behavior not exhibited in the other four operating conditions. This hunting has been observed with other fly-by-wire actuators, including the normal F-16 ISA (specification No. 16ZH001F requires that in mode III, the periodic oscillation should not exceed 0.35 percent of the rated output stroke). The measured amplitude of .09 percent of the actuator stroke for the hunting of the F-16 direct drive actuator in condition 5 is significantly below the 0.35 percent of actuator stroke allowed for the normal F-16 ISA.

TEST DATA

TEST ITEM: F-16 Direct Drive Servoactuator

Date: 11-14-86

TEST: Dynamic Threshold - Condition 1



Scale

E_{in} = .002 v/div

X_{out} = .0011 in/div

t = 50 div/sec

Freq = 14.0 Hz

Figure VI-31. Dynamic threshold - condition 1.

Table VI-3. Dynamic threshold.

TEST ITEM: F-16 Direct Drive Actuator
TEST: Dynamic Threshold

Date: 3-26-86

Test Condition	Peak to Peak Input Volts	Dynamic Threshold	
		% of Max Input	% of Ev Max
1	0.017	0.21	3.53
2	0.020	0.25	4.15
3	0.025	0.31	5.19
4	0.005	0.06	1.04
5	0.011	0.14	2.28

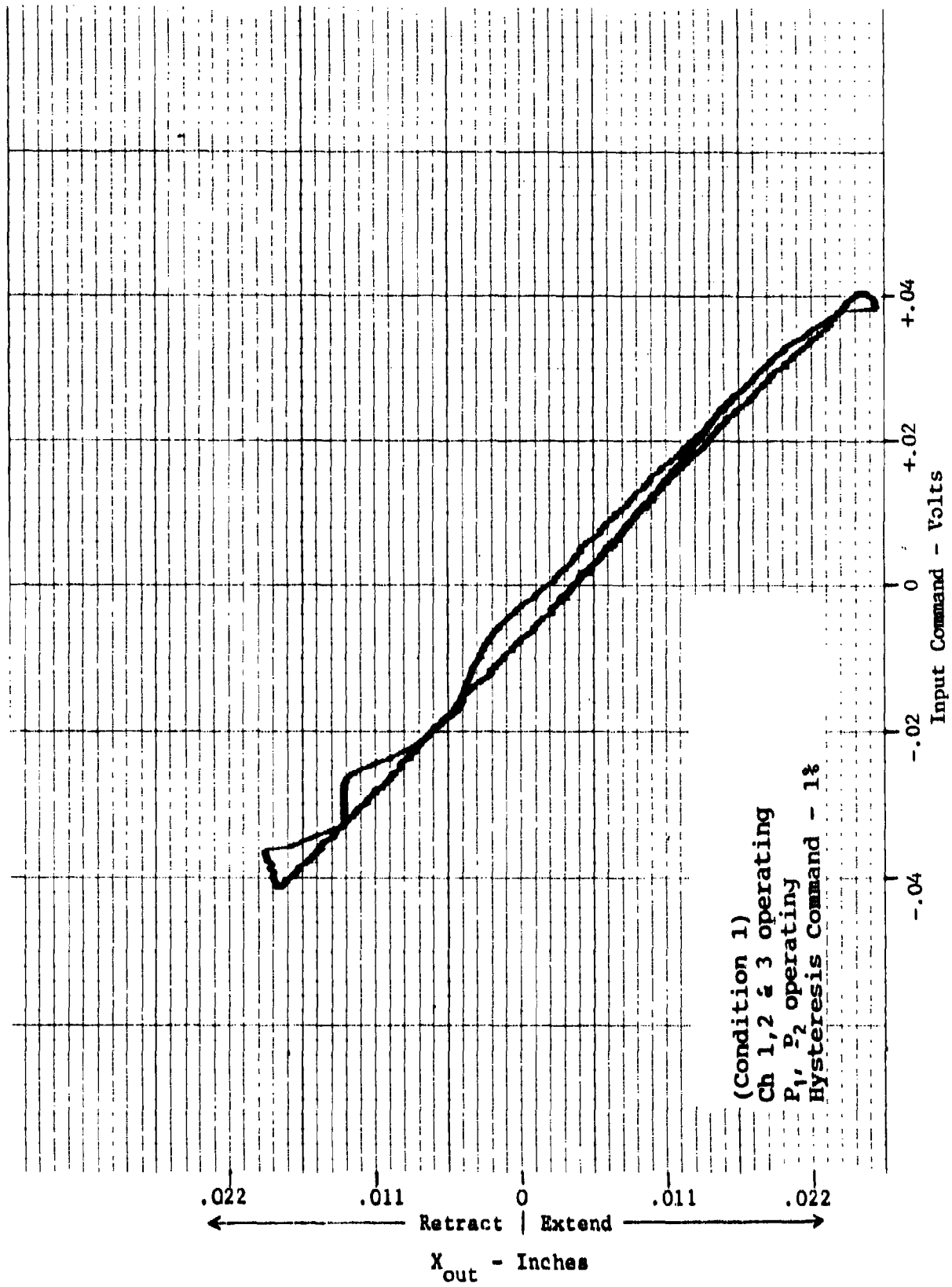


Figure VI-32. Hysteresis - 1 percent command - condition 1.

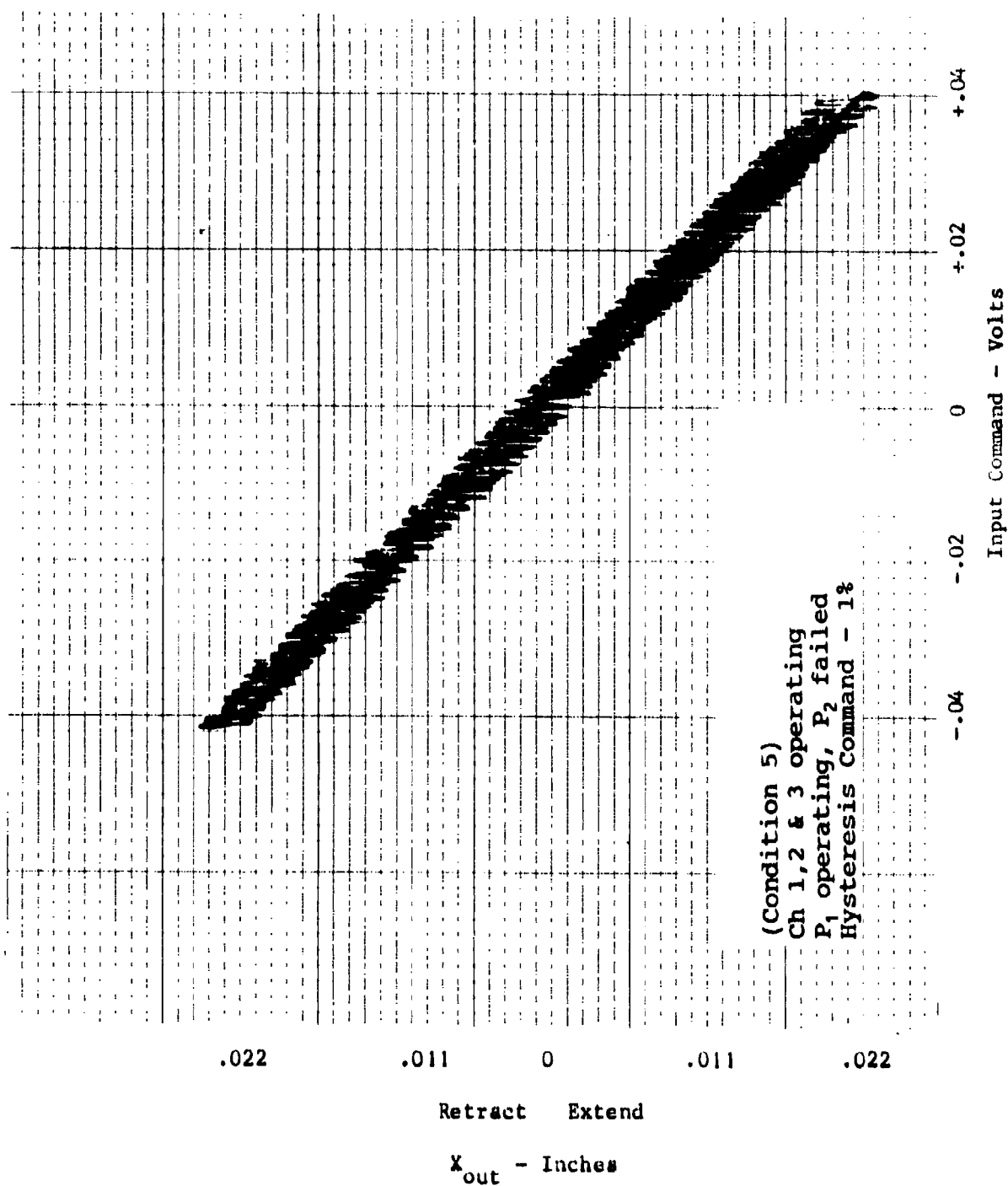


Figure VI-33. Hysteresis - 1 percent command - condition 5.

Table VI-4 lists the measured hysteresis for the 1 percent command input in terms of the actuator maximum input and the input to achieve maximum spool deflection in the normal operating (condition 1). Note that the hysteresis loop amplitude remains at or below 0.10 percent of the maximum actuator input (or output stroke) for all the operating conditions. In terms of the input for maximum spool stroke, the maximum hysteresis is 1.66 percent for any of the test conditions.

Hysteresis Test Results - 10 Percent Command

Figure VI-34 shows the hysteresis data for operating condition 1 with a 10 percent input. This data is representative data for conditions 2 through 5 with the same input. The hysteresis amplitudes as listed in Table VI-5 are slightly larger than with a 1 percent input command. However, the value in terms of maximum input is well within the ± 1.25 percent deviation limit for the F-16 ISA.

Linearity Test Results

Figure VI-35 is a linearity plot of the F-16 direct drive actuator to an input command of 110 percent. The actuator position linearity is determined by the feedback transducer linearity (which for the film potentiometers used for the F-16 direct drive actuator are better than 0.5 percent). Figure VI-35 does show some hysteresis during the retract stroke (nominally 0.9 percent of maximum stroke, well within the linearity deviation allowed for the F-16 ISA). The figure is representative of the data recorded for test conditions 2 through 5. However, although the linearity was unchanged for conditions 4 and 5, the hysteresis loop was eliminated, indicating a reduction in spool friction when operating with one supply pressure.

Frequency Response Test Results

Figures VI-36 and VI-37 show the amplitude ratio and phase response of the F-16 direct drive actuator operating in condition 1. The response is measured with a 3 percent input. The frequency response shown is representative of the measured response in operating conditions 2 and 3. The response has a flat amplitude response with no peaking to above 20 Hz. The amplitude response is attenuated by 3 dB at 28.7 Hz. As shown on Figure VI-36, the amplitude ratio slope below 0.5 Hz reflects a DC output component from the position transducer used to measure the actuator position. The slope does not reflect the frequency response of the actuator but the characteristic of the response analyzer which tries to measure frequency response to zero frequency. Note, because the F-16 direct drive actuator is a fly-by-wire actuator with electrical feedback, the frequency response is easily changed by changing the gain of the control electronics. The response shown was a result of adjusting the loop gains of the control channels to obtain the highest frequency response amplitude peaking in the normal operating condition. This response is significantly higher than the normal

Table VI-4. Hysteresis - 1 percent command.

Test Condition	Inches	Input Volts	% of Max Input	% of E_v Max
1	0.0033	0.0066	0.08	1.37
2	0.0026	0.0052	0.07	1.08
3	0.0040	0.0080	0.10	1.66
4	0.0040	0.0080	0.10	1.66
5	0.0035	0.0070	0.09	1.45

Table VI-5. Hysteresis - 10 percent command.

Test Condition	Inches	Input Volts	% of Max Input	% of E_v Max
1	0.0049	0.0098	0.12	2.03
2	0.0087	0.0174	0.22	3.61
3	0.0106	0.0212	0.27	4.40
4	0.0059	0.0118	0.15	2.45
5	0.0039	0.0078	0.10	1.62

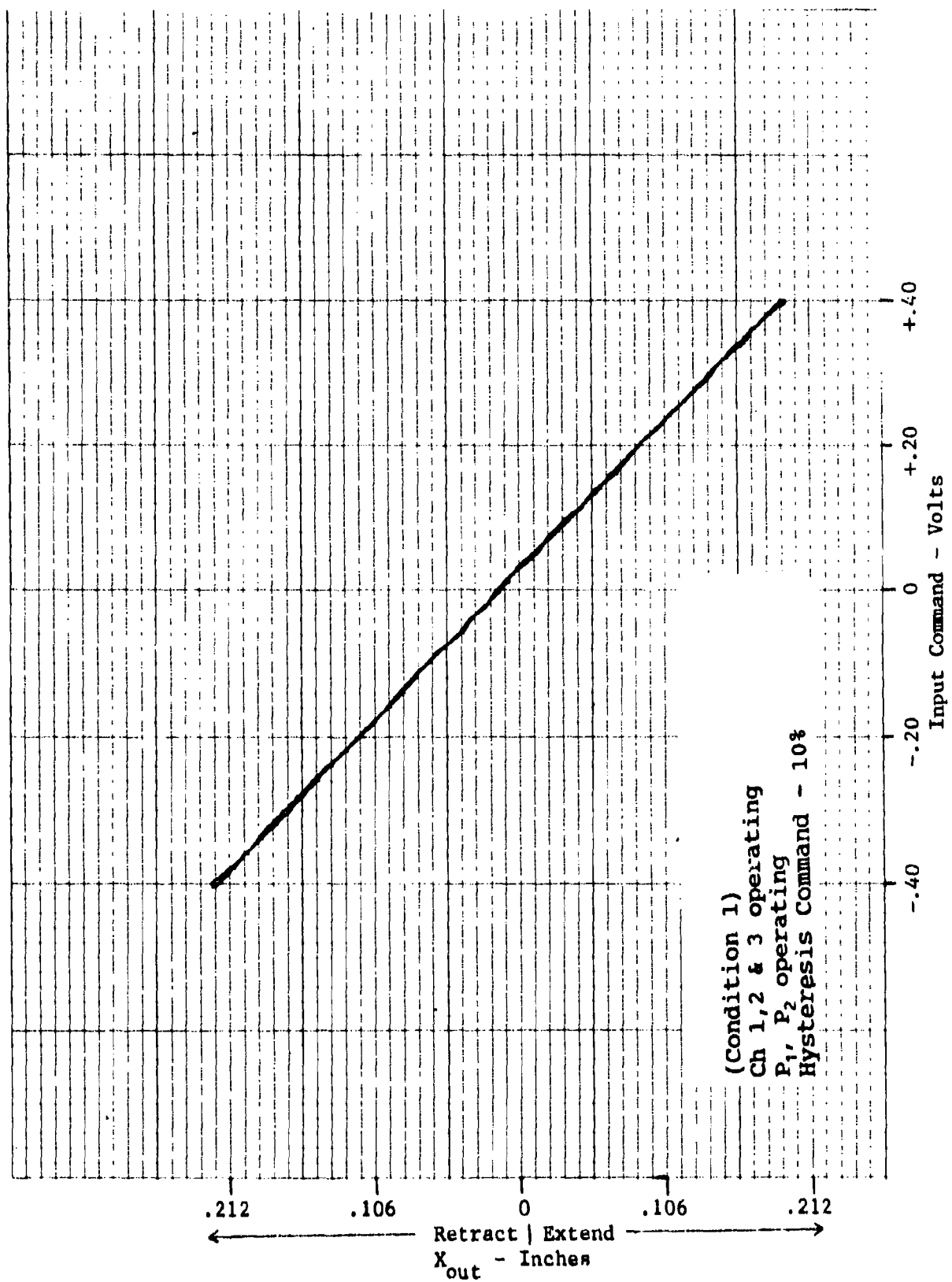


Figure VI-34. Hysteresis - 10 percent command - condition 1.

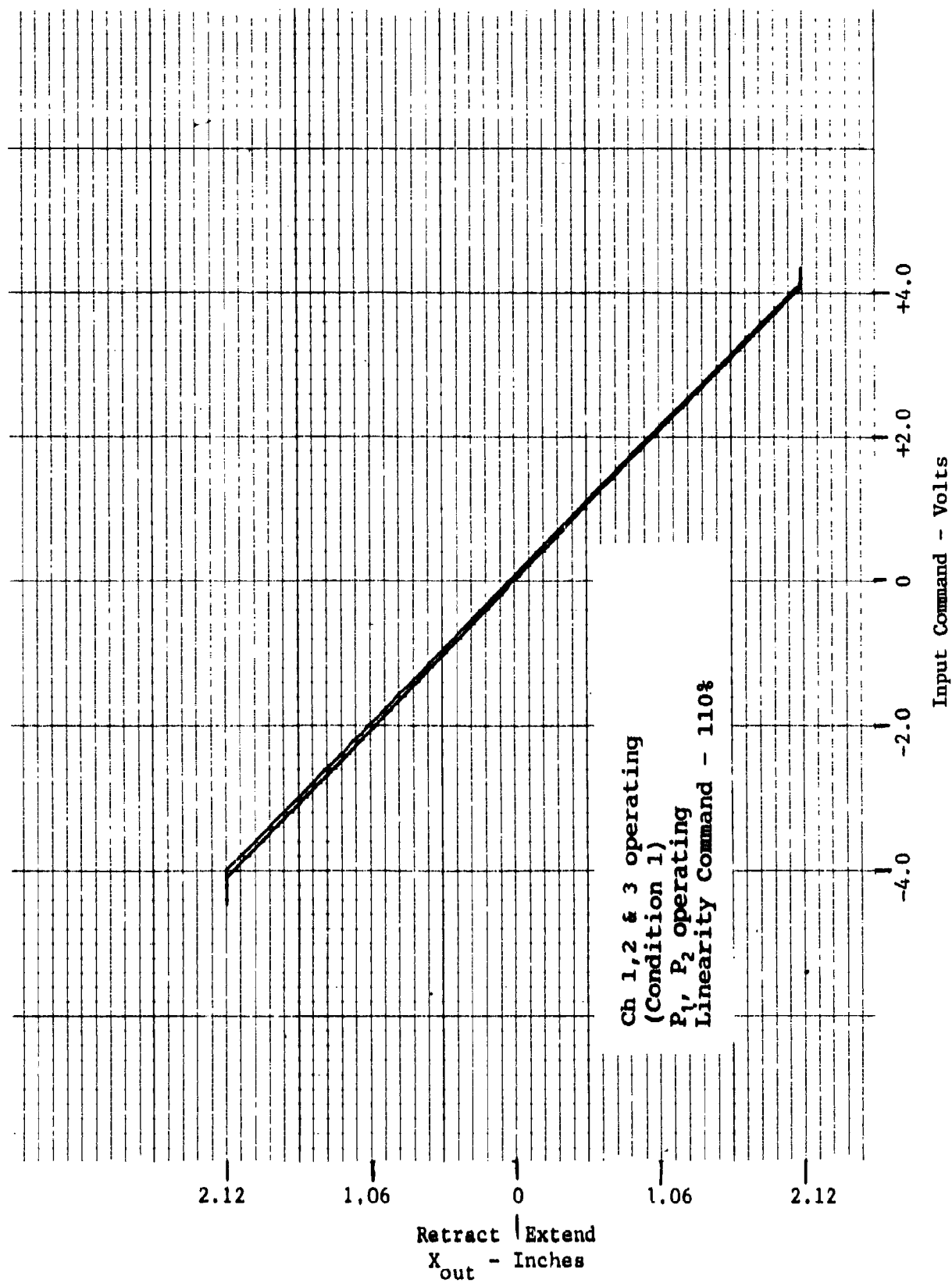


Figure VI-35. Linearity - 110 percent command - condition 1.

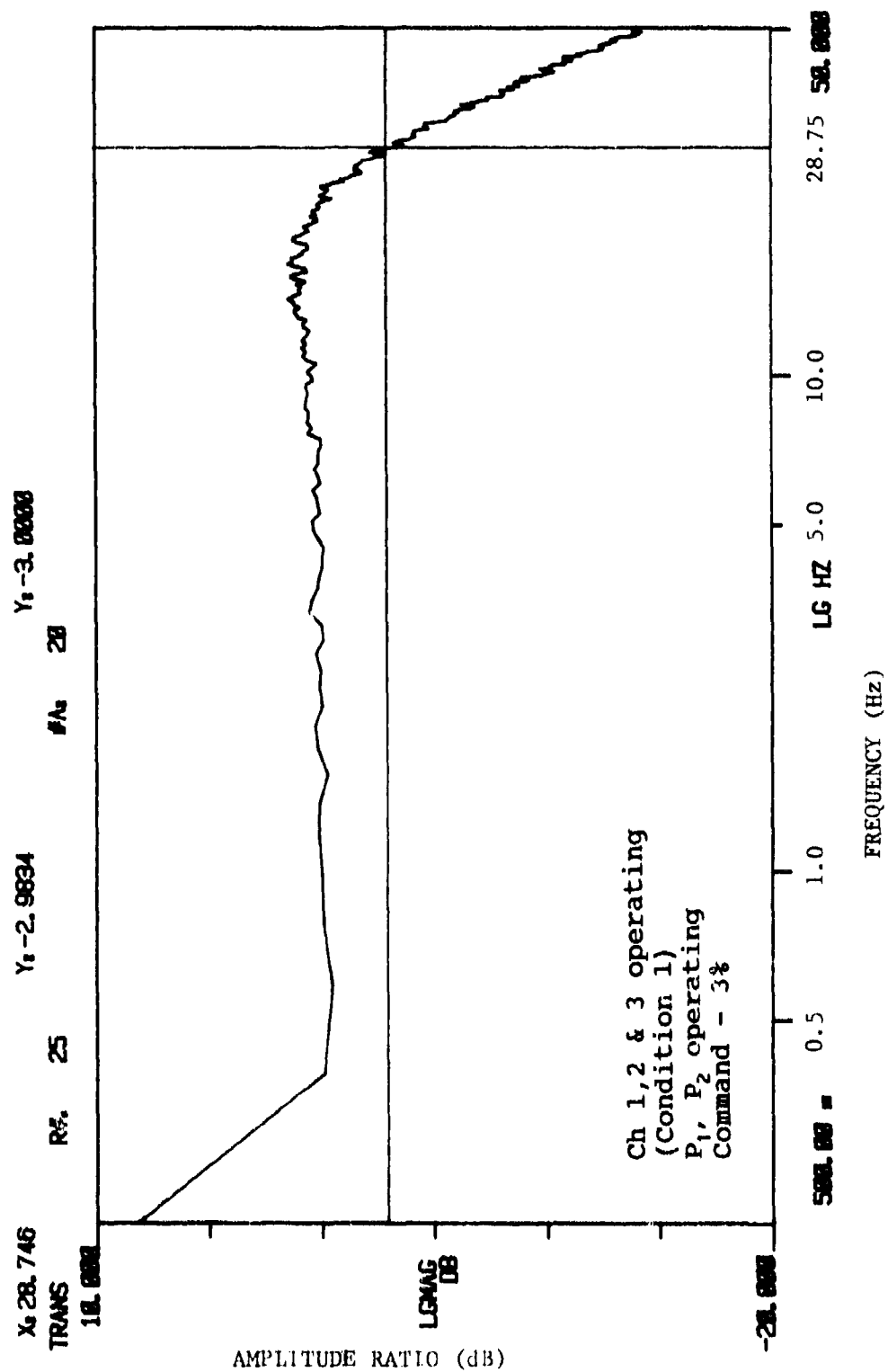


Figure VI-36. Amplitude ratio response - 3 percent input - condition 1.

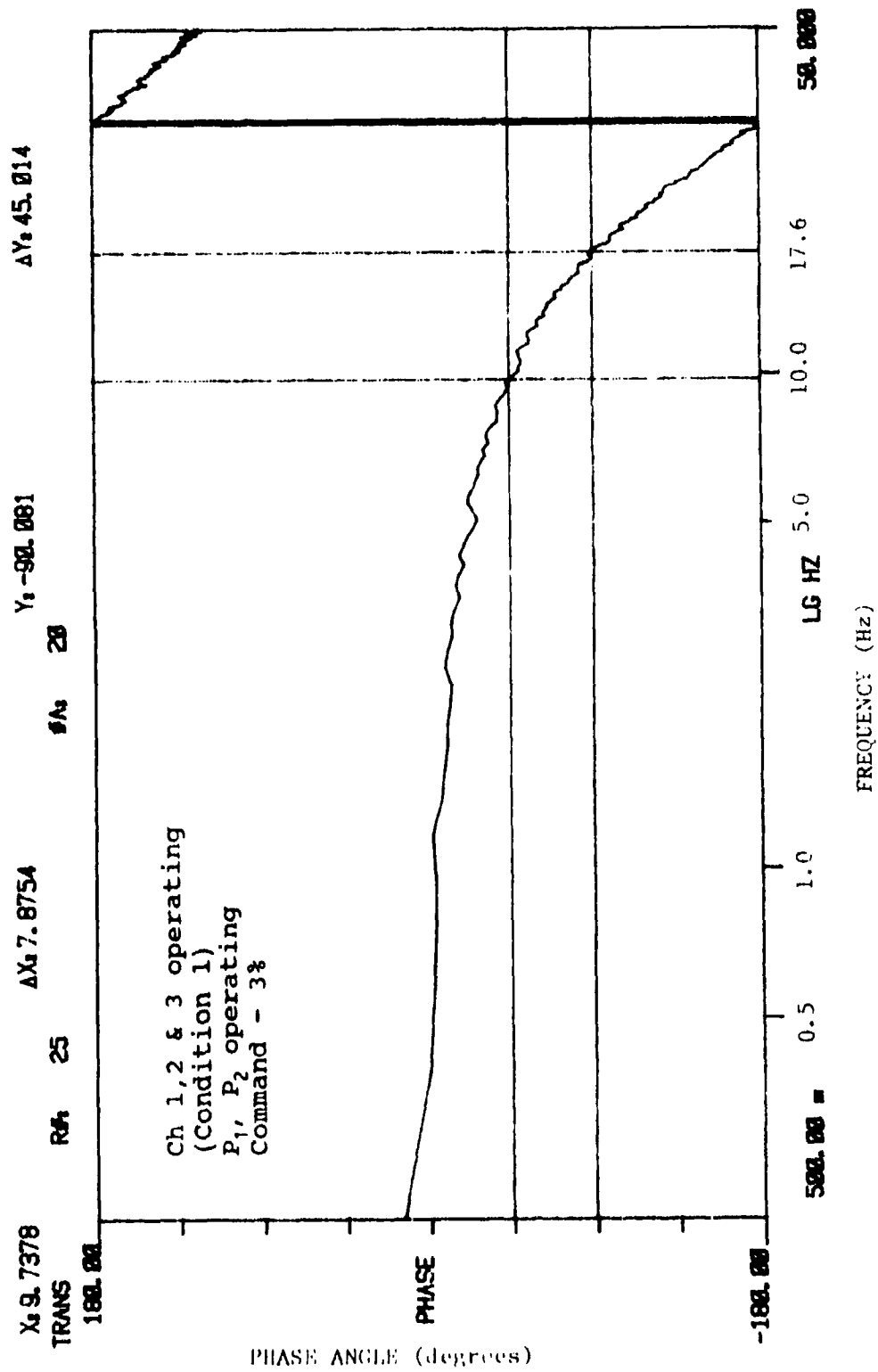


Figure VI-37. Phase response - 3 percent input - condition 1.

ISA's response at 2 percent input which exhibits an amplitude response which is - 3 dB at 3.7 Hz and a phase response which is - 90° at 3.5 Hz. Figures VI-38 and VI-39 show the amplitude ratio and phase response for condition 4 with one of the hydraulic supplies failed. For this condition with the 3 percent input, the amplitude response exhibits 6 dB of peaking at 20 Hz, indicating a reduction in damping with loss of a hydraulic pressure. The response resembles a second order system with a damping ratio of 0.2. The response for condition 5 is identical to the condition 4 response. The cause of the peaking is due to an increase in the flow gain of the control valve as a result of the hydraulic supply failure reducing the flow forces on the control valve. Since part of the force output from the force motors is used to overcome the flow forces, a reduction of the flow forces (to one half with a hydraulic supply failure) allows the valve to move farther with the same force input. The results in a flow gain increase for the remaining operating section of the actuator. Since the response was established with lower flow gain (P1 and P2 operating) for condition 1, the gain increase (with condition 4 and 5) results in a peaking of the frequency response.

Table VI-6 lists the frequency response for each test condition in terms of the frequency at which - 90° phase angle and - 3 dB amplitude ratio occur. Note that for conditions 1 through 3, the frequency response degrades as the control channels are failed. However, even for condition 3 with one channel operating, the frequency response is more than twice the normal F-16 ISA. The higher response for conditions 4 and 5 reflects the amplitude peaking corresponding to an apparent reduction in damping with those operating conditions. As previously mentioned in the mechanization approach, if a more constant response with channel failures is required, appropriate electronic roll-off filters can be used in series with the command inputs to establish a lower response for the actuator. The input filter response, being lower than the actuator response in all the operating modes, will determine the response of the actuator.

Figures VI-40 and VI-41 show the amplitude and phase response of the F-16 direct drive system with a 10 percent input and operating in condition 1. The amplitude response measurement starts at 0.5 Hz, eliminating the measurement of the DC output of the position potentiometer used to measure the actuator position. All of the response plots for conditions 2 through 5 resemble these figures with no peaking and a gradual roll off. The peaking associated with the 3 percent input and conditions 4 and 5 does not appear with the larger amplitude inputs. Figures VI-42 and VI-43 show the frequency response for condition 4. The frequency response of condition 5 is identical. The response is more extended than that of condition 1, as would be expected from the previous 3 percent input response measurements.

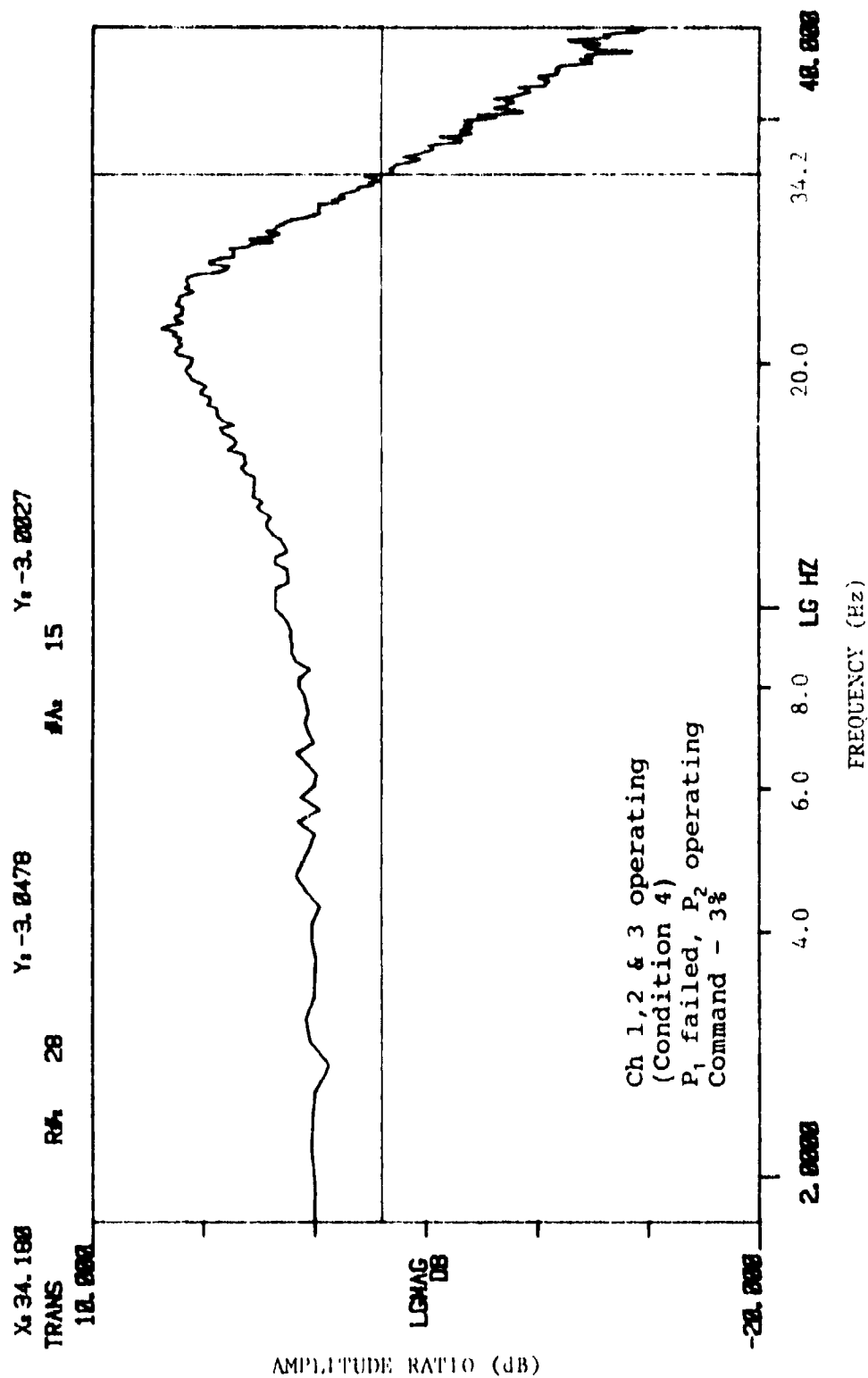


Figure VI-38. Amplitude ratio response - 3 percent input - condition 4.

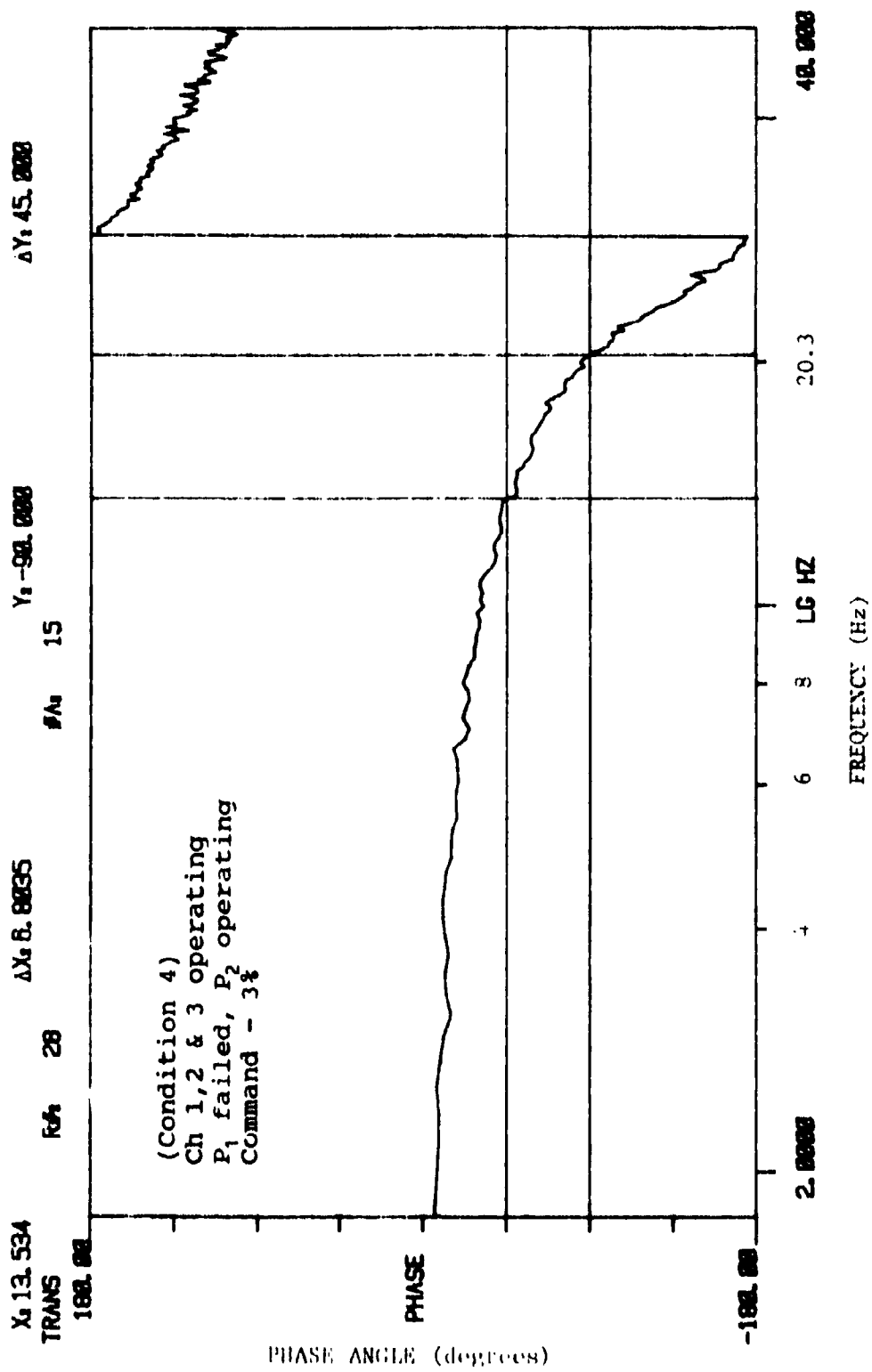


Figure VI-39. Phase response - 3 percent input - condition 4.

Table VI-6. Frequency response - 3 percent input.

Test Condition	Frequency for -3 dB Amplitude Ratio	Frequency for -90° Phase Angle
1	28.7	17.6
2	20.5	14.9
3	8.7	10.4
4	34.2	20.3
5	34.3	20.3

Table VI-7. Frequency response - 10 percent input.

Test Condition	Frequency for -3 dB Amplitude Ratio	Frequency for -90° Phase Angle
1	18.8	15.1
2	11.1	13.4
3	5.7	9.7
4	25.5	16.3
5	23.6	15.7

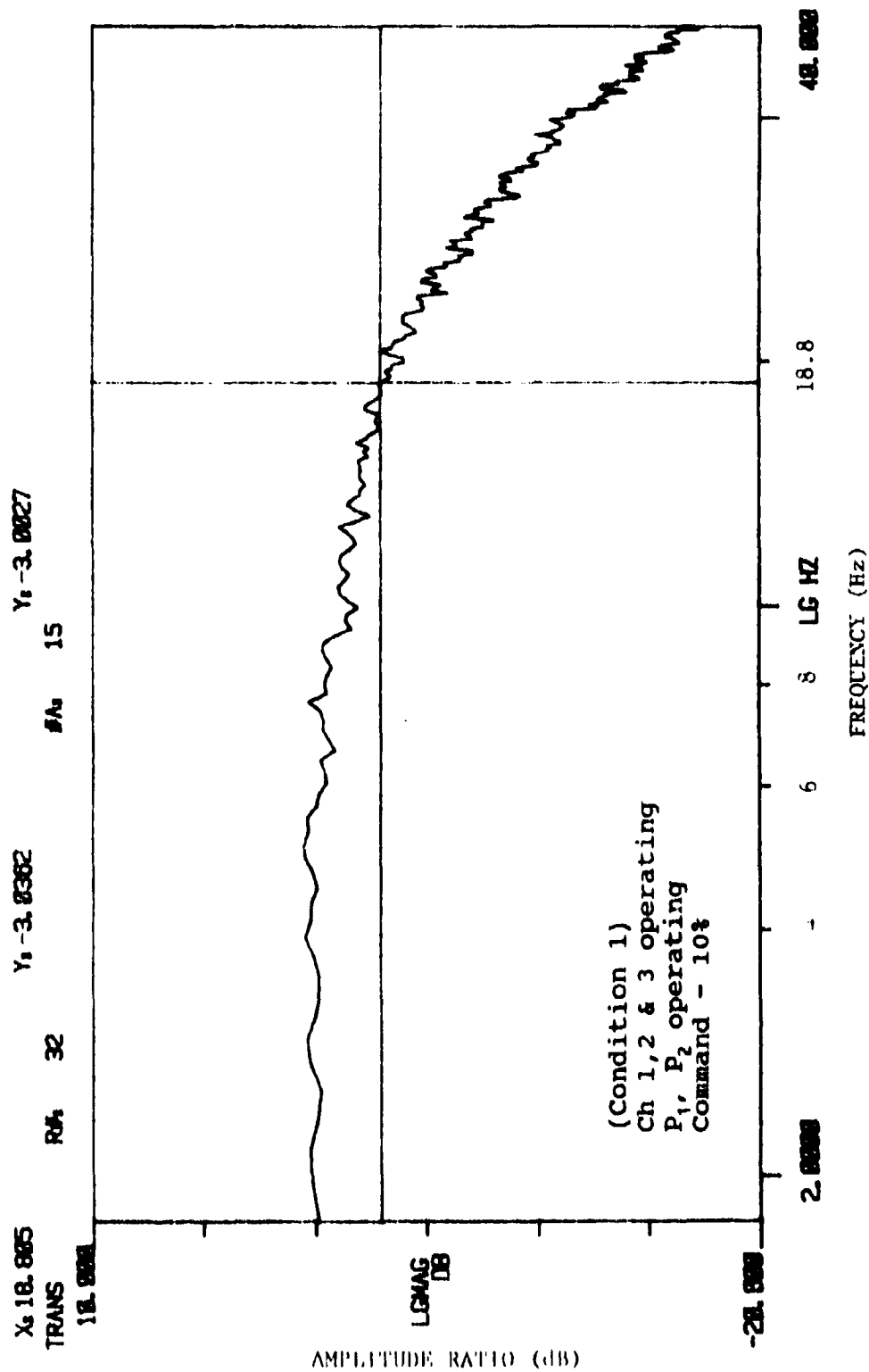


Figure VI-40. Amplitude response - 10 percent input - condition 1.

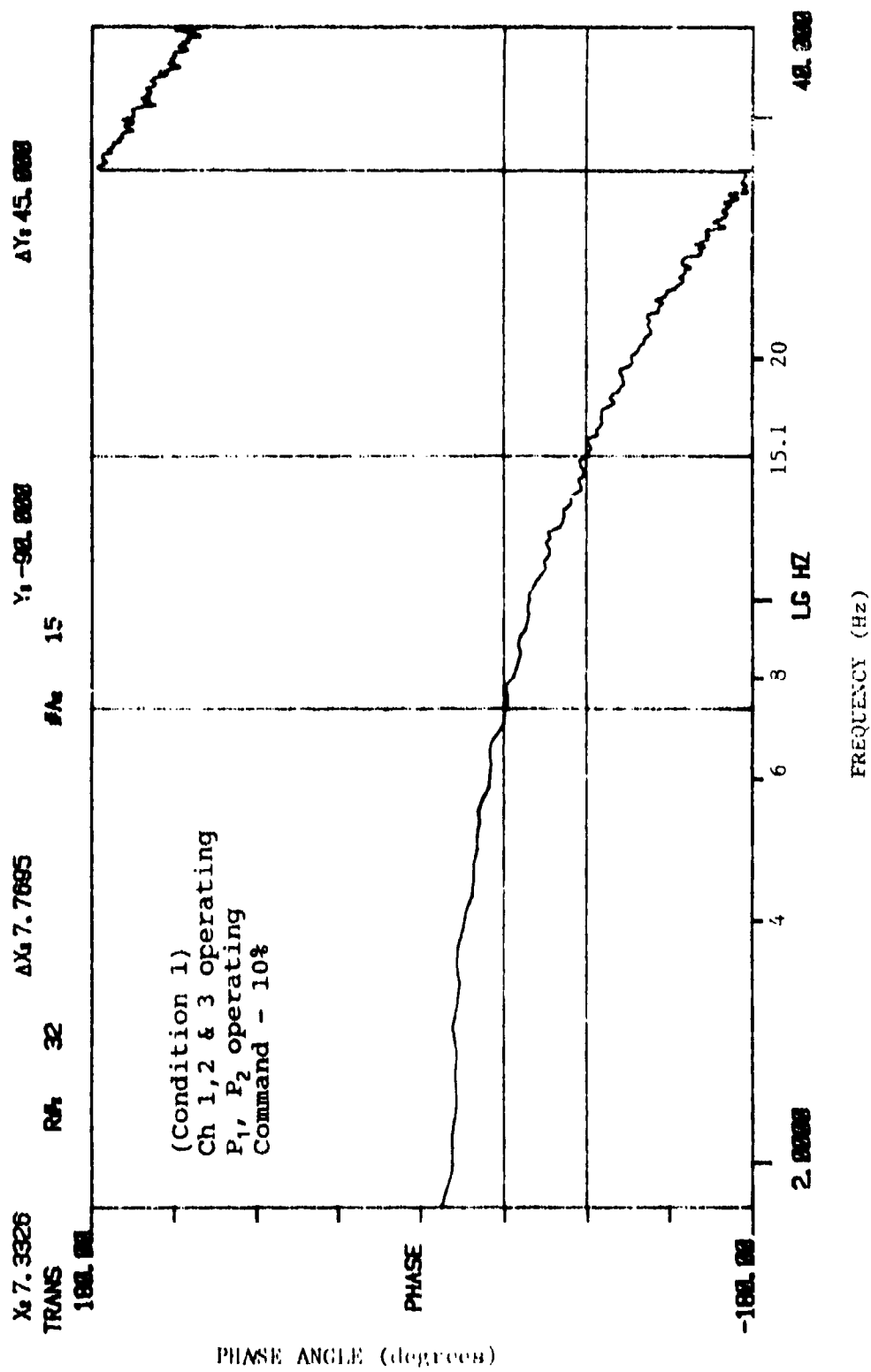


Figure VI-41. Phase response - 10 percent input - condition 1.

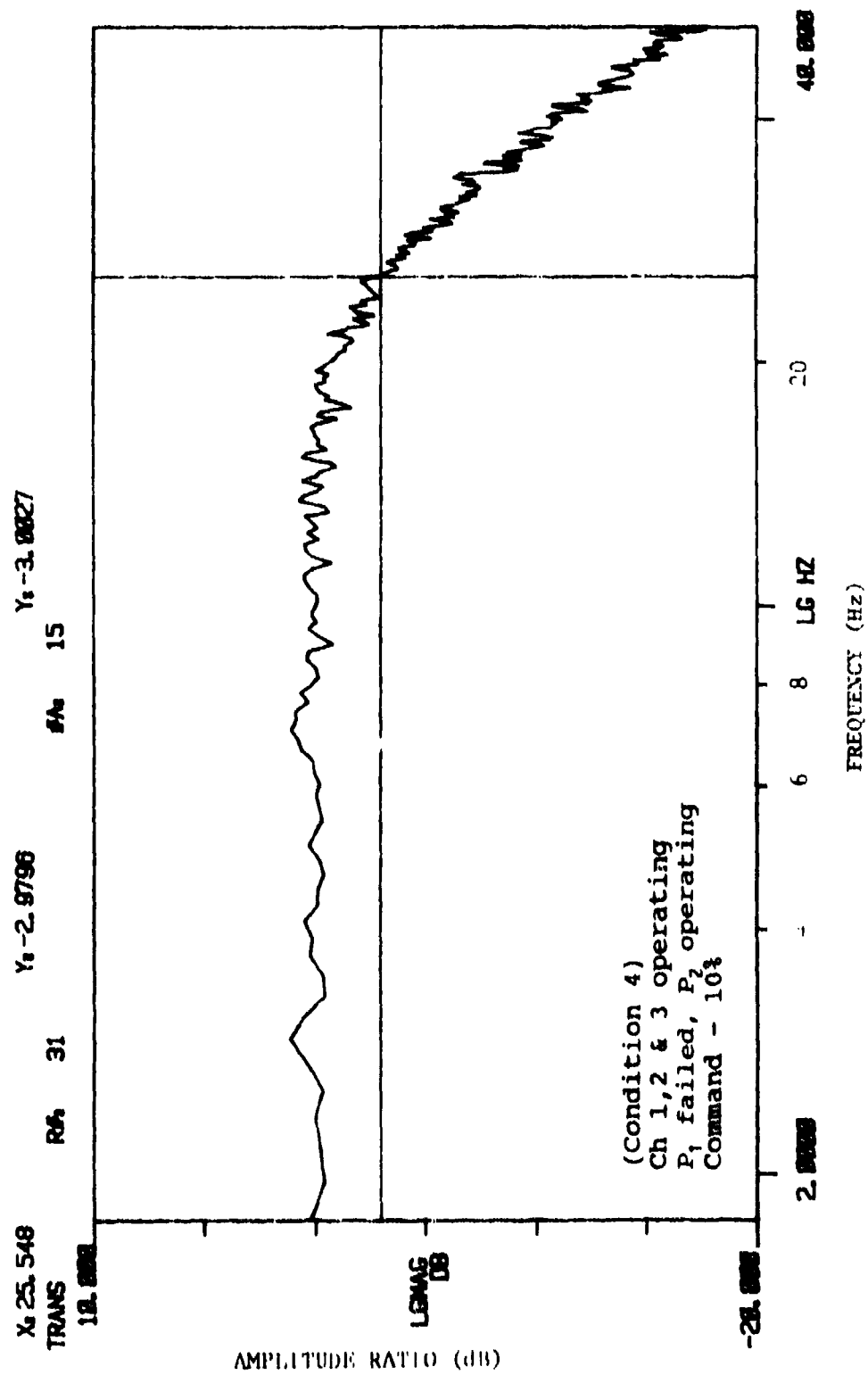


Figure VI-42. Amplitude ratio response - 10 percent input - condition 4.

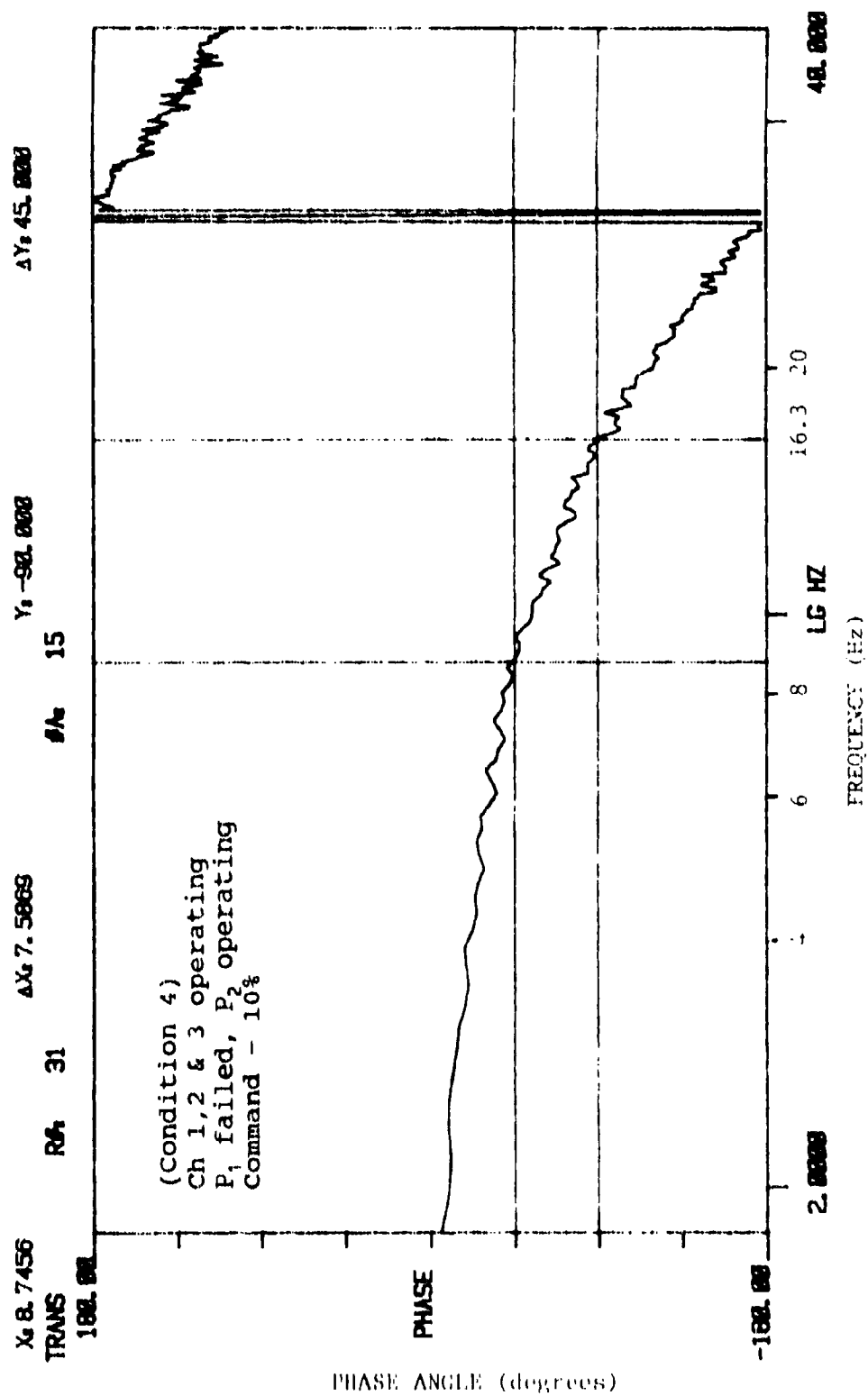


Figure VI-43. Amplitude response - 10 percent input - condition 4.

Table VI-7 lists the frequency response for each test condition in terms of the frequency at which - 90° phase angle and - 3 dB amplitude ratio occur. As for the 3 percent input, for conditions 1 through 3, the frequency response degrades as the control channels are failed. The response is lower than with the 3 percent input, but is still maintained well above that of the standard F-16 ISA.

Step Response

Figures VI-44 through VI-48 show the step response characteristics for the F-16 direct drive for operating conditions 1 through 5. The input amplitude of the step was 0.16 volts or 2 percent of the total command voltage of 8 volts. Both extend and retract direction step response is shown.

Figure VI-44 shows the step response when operating in condition 1. Note that there is a 1.5 millisecond time delay between the start of the application of the step and start of motion for both the extend and retract motions. The recording of the applied step shows a slight slope. This is due to the response limitations of the pen recorder used to document the step response. Including the 1.5 millisecond time delay, the time to reach 50 percent of the final output value is 5.1 milliseconds. The step response shows very little overshoot (nominally 2.5 percent) and no ringing. The time to reach 95 percent of the final value (including the initial time delay) is 9 milliseconds for the extend motion and 10 milliseconds for the retract motion.

Figure VI-45 shows the step response after channel 1 is turned off. The time response is similar to operating in condition 1. The initial time delay is still 1.5 milliseconds. The time to reach 50 percent of the final value is 5.5 milliseconds for the extend and retract motion. The time to reach 95 percent of the final value is 10 milliseconds for the extend and 12 milliseconds for the retract motion. The overshoot is nominally 2.5 percent and there is no ringing for either the retract or extend motions.

Figure VI-46 shows the step response in the two fail-operate mode of condition 3. The time delay is increased to 2 milliseconds. The time to reach 50 percent of the final value after application of the step is 8 milliseconds for the retract motion and 9 milliseconds for the extend motion. The overshoot for the extend motion is 1.5 percent with a corresponding 1 percent undershoot 50 milliseconds after the peak overshoot. The retract motion exhibits a 2.5 percent overshoot and no undershoot. The time to reach 95 percent of the final value is 15 milliseconds for the extend motion and 18 milliseconds for the retract motion. This slower response is consistent with the reduction in force gain as the control channels driving the actuator are failed.

Figure VI-47 shows the step response with one hydraulic system (PI failed). The response shows slight ringing with an amplitude of the ringing no greater than 2.5 percent of the step amplitude. The time to reach 50 percent of the final value is 5 milliseconds for the extend motion. The extend

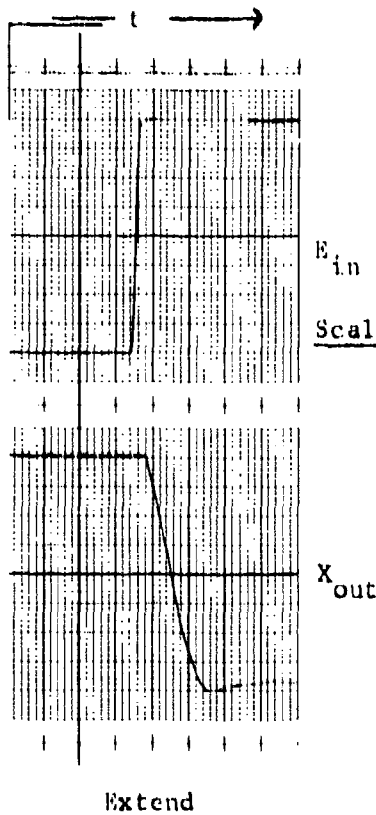
TEST DATA

Test Item - Dynamic Controls, Inc.
F-16 Direct Drive
Servoactuator

Date:
Prepared: 11-14-86

Test - Step response

- Channel 1,2,&3 Operating
P₁, P₂ Operating



Scale:

$E_{in} = 0.02 \text{ v/div}$
 $X_{out} = 0.011 \text{ in/div}$
 $t = 100 \text{ div/sec}$

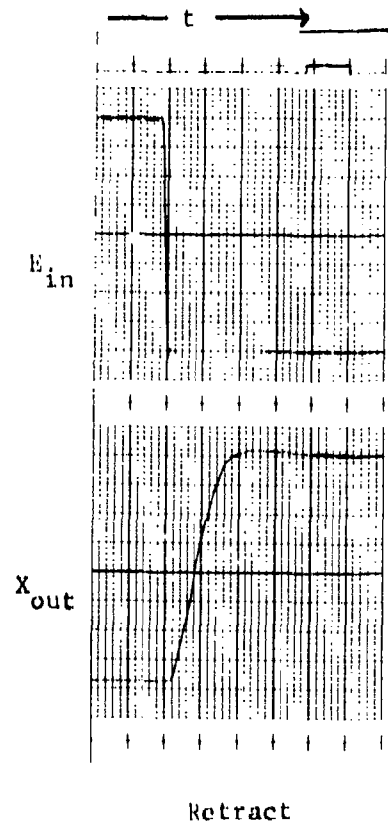


Figure VI-44. Step response - condition 1.

TEST DATA

Test Item - Dynamic Controls, Inc.
F-16 Direct Drive
Servoactuator

Date:
Prepared: 11-14-86

Test - Step response - Channel 1 Failed, Channels 2,3 Operating

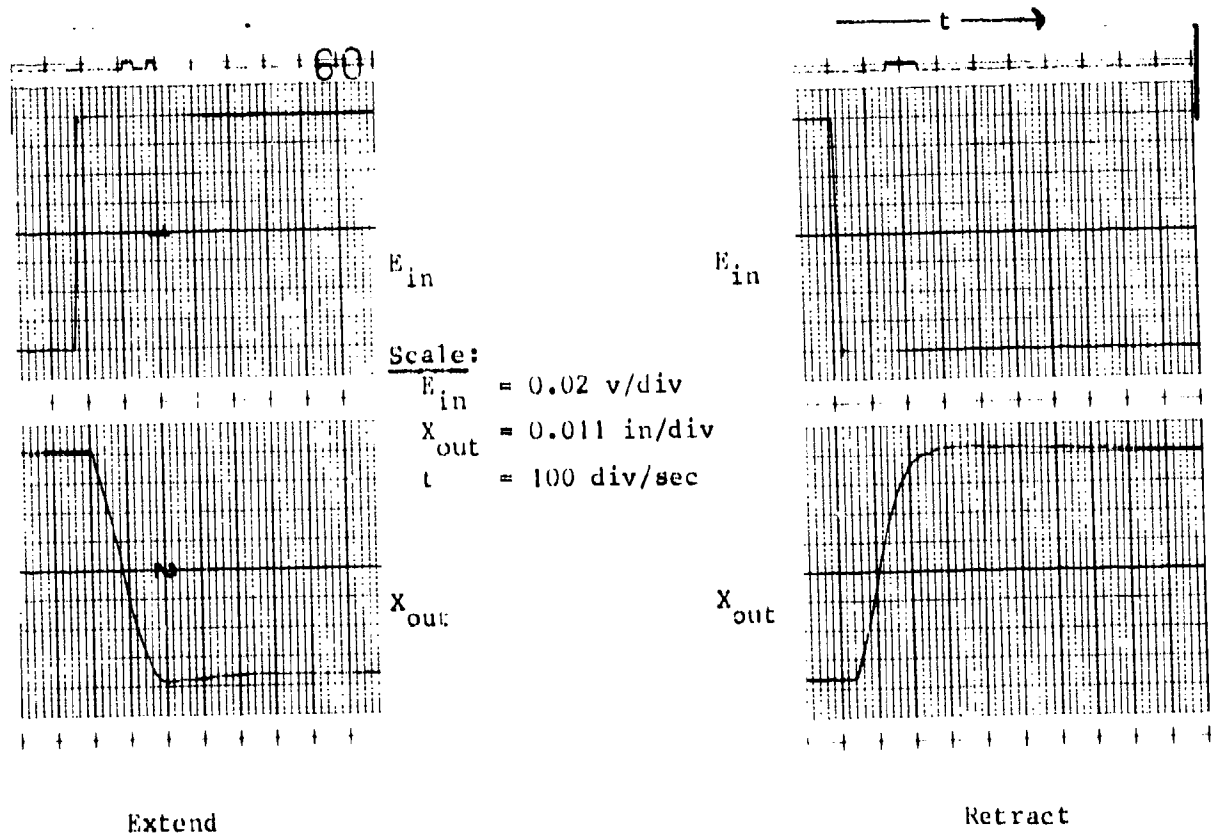


Figure VI-45. Step response - condition 2.

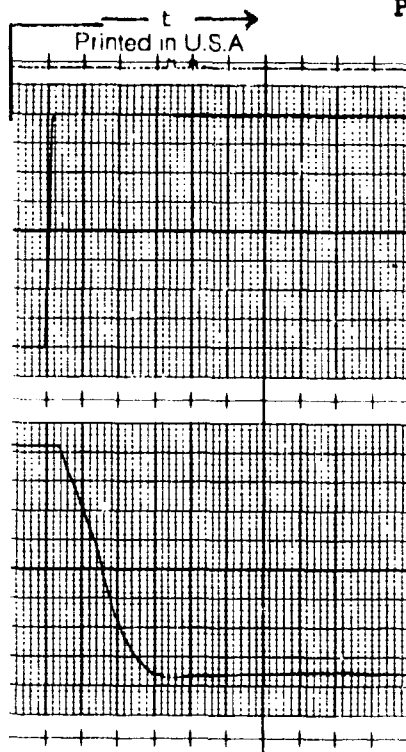
TEST DATA

Test Item - Dynamic Controls, Inc.
F-16 Direct Drive
Servoactuator

Date: _____
Prepared: 11-14-86

Test - Step response

- Channels - 1,2 Failed, Channel 3 Operating
 P_1, P_2 Operating



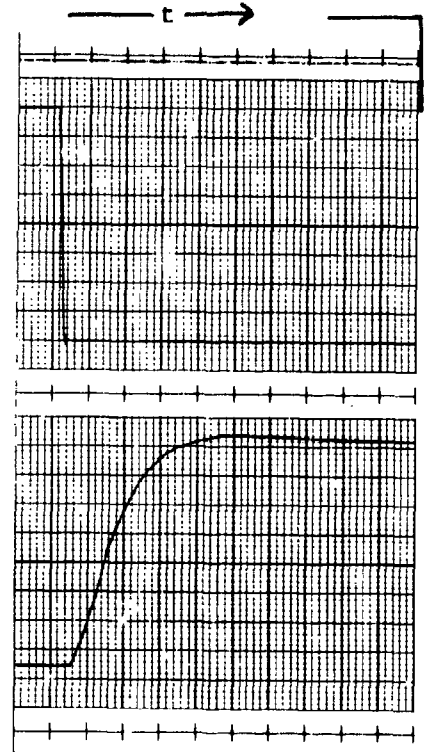
Extend

E_{in}

Scale:

$E_{in} = 0.02 \text{ v/div}$
 $X_{out} = 0.011 \text{ in/div}$
 $t = 100 \text{ div/sec}$

X_{out}



Retract

E_{in}

X_{out}

Figure VI-46. Step response - condition 3.

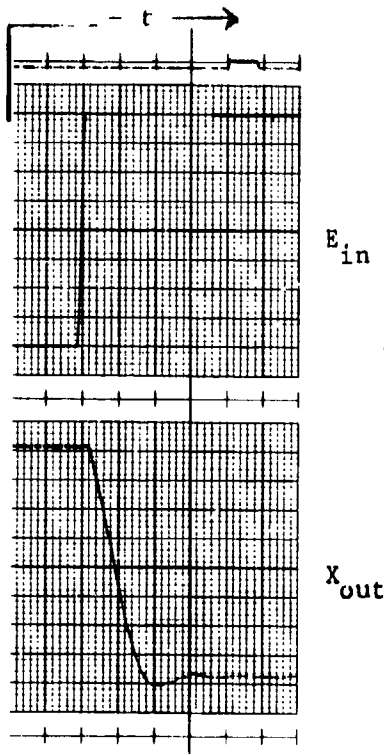
TEST DATA

Test Item - Dynamic Controls, Inc.
F-16 Direct Drive
Servoactuator

Date:
Prepared: 11-14-85

Test - Step response

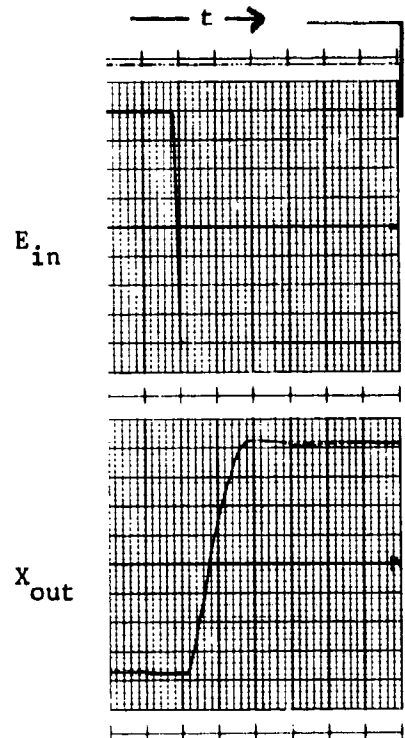
- Channels 1,2,3 Operating
P₁ Failed, P₂ operating



Extend

Scale:

$E_{in} = 0.02 \text{ v/div}$
 $X_{out} = 0.011 \text{ in/div}$
 $t = 100 \text{ div/sec}$



Retract

Figure VI-47. Step response - condition 4.

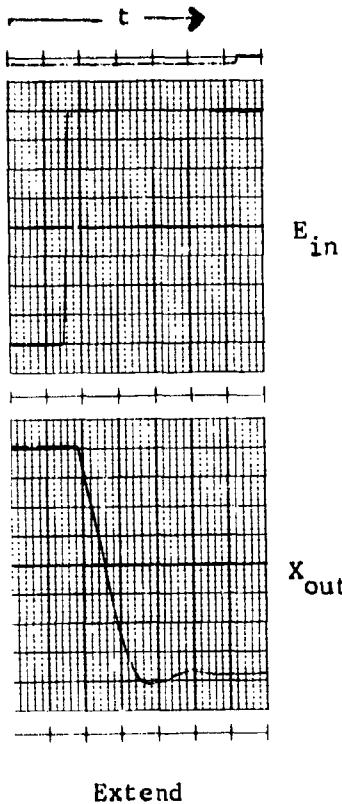
TEST DATA

Test Item - Dynamic Controls, Inc.
F-16 Direct Drive
Servoactuator

Date:
Prepared: 11-14-86

Test - Step response

- Channel 1,2&3 Operating
P₁ Operating, P₂ Failed



Scale:

$E_{in} = 0.02 \text{ v/div}$
 $X_{out} = 0.011 \text{ in/div}$
 $t = 100 \text{ div/sec}$

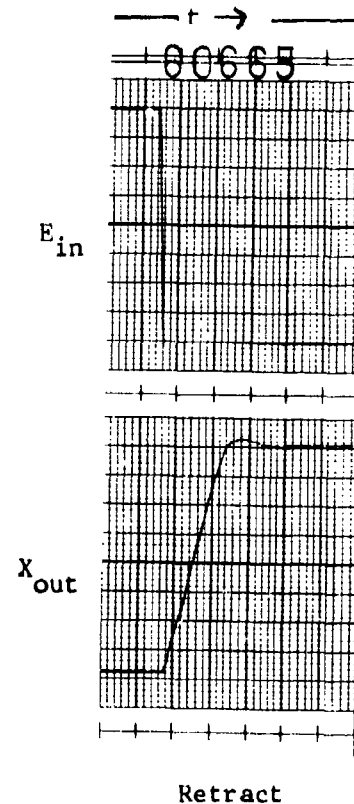


Figure VI-48. Step response - condition 5.

motion exhibits a 3.7 percent overshoot. The time to reach 95 percent of the final value for the extend motion is 9.5 milliseconds. The retract step response times are similar, being 4.5 milliseconds for 50 percent of the final value, 8.5 milliseconds for the time to achieve 95 percent of the final value. The slight ringing is consistent with the frequency response measurements for the same operating condition.

Figure VI-48 shows the step response with hydraulic system P2 failed. The response times are similar but not identical to operating condition 4 with P1 failed. The time to reach 50 percent of the final value is 6 millisecond for extend motion and 5 millisecond for retract motions (including the 1.5 millisecond time delay). The time to reach 95 percent of final value is 9 milliseconds. The extend and retract motions both exhibit slight overshoot (3.75 percent for extend motion, 2.5 percent for retract motion) and undershoot (2 percent for extend motion, 1.3 percent for retract motion).

All the step responses show a well-behaved control. The gradual increase in response times between conditions 1 through 3 is consistent with the reduction in flow gain with failure of the control channels.

Saturation Velocity

Figure VI-49 is the data recorded in order to establish the saturated rate for the F-16 direct drive actuator in condition 1. As shown on this figure, the actuator is positioned at one end of the stroke, either full retract or full extend. The input voltage changed to command the actuator to move to other extreme position. Note that the input voltage change is 8 volts and the actuator stroke change is 4.13 inches. This figure is representative of the data recorded for all operating conditions. As shown on this figure, there are two distinct slopes for the actuator rate. The change in slope was caused by the pumping system used to power the actuator. The pumping system used an accumulator to handle peak flow demands. The maximum rate of the F-16 actuator requires more flow than the hydraulic supply system could deliver continuously. After the accumulator is discharged (as the pressure output of the pump drops off with demand), the pump head continues to fall rapidly until the pump delivery volume and the flow demand of the actuator at that supply pressure are equal. This is the second slope of the rate curve and corresponds to a rate limiting of the actuator by the pumping system. Table VI-8 lists the extend and retract rates for each of the operating conditions. The values used are the initial slopes from the recorded data.

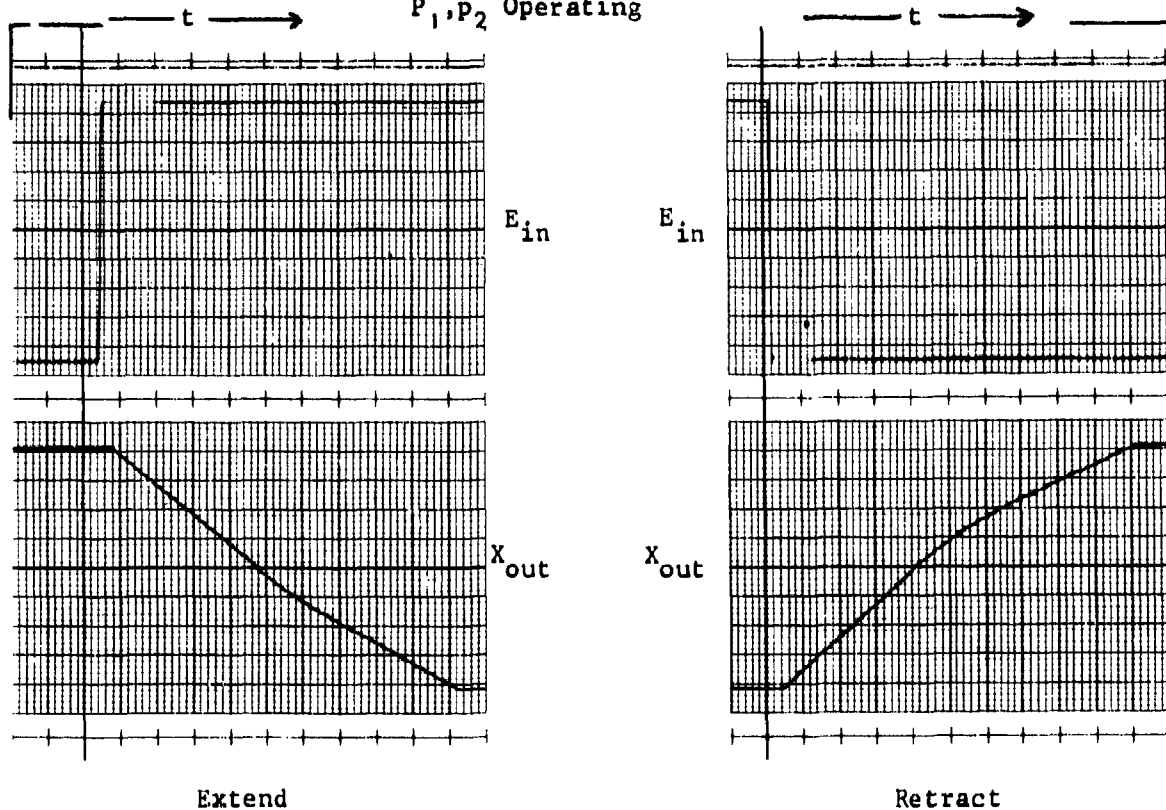
As shown in Table VI-8, the saturation or slew rate degrades between conditions 1 and 3, reflecting the loss of control channels. Conditions 1 and 2 meet the F-16 ISA design slew rates. Condition 3 does not meet the slew rate requirements (with the slew rate nominally 80 percent of the condition

TEST DATA

Test Item - Dynamic Controls, Inc.
F-16 Direct Drive
Servoactuator

Date
Prepared: 11-13-86

Test - Saturation Velocity - Channel 1,2&3 Operating
 P_1, P_2 Operating



Scale:

E_{in} = 0.20 v/div
 X_{out} = 0.106 in/div
 t = 50 div/sec

Figure VI-49. Saturation velocity - condition 1.

1 and 2). This indicates that the single channel force output is slightly low. This characteristic could be changed by decreasing the spring rate of the force motor suspension. However, the correction could be made easily without any mechanical modification by increasing the maximum current out of the servoamplifiers. The servoamplifiers are not voltage-limited and the force output can be increased by changing the external current-limiting resistors to increase the servoamp current limit by 20 percent. The power op amps and power supplies were used at less than 75 percent of their design rating for the F-16 direct drive actuator and could easily accept the change.

As assembled for test, the spool stops for the control valve were not adjusted to limit the stroke of the control valve to that necessary to achieve the 5.5 inch/second slew rate. For conditions 4 and 5, the slew rate is greater than that for condition 1. This is because part of the force motor's output is used to overcome the spring rate of the suspension and part to overcome the flow forces of the control valve. The system was designed with a 50-50 split between the centering spring force and the flow forces. With one hydraulic system failed, half the flow forces are eliminated (and the control valve can move farther with the same force input), increasing the control valve's open porting area and therefore the flow through the valve. This effect is also the reason for the peaking associated with the frequency response in operating conditions 4 and 5, as mentioned previously. Adjusting the spool stops to limit the valve stroke will cause the condition 4 and 5 slew rate to match condition 1.

Table VI-8. Saturation rates.

Test Condition	Extend Rate (in/sec)	Retract Rate (in/sec)
1	5.56	5.88
2	5.30	5.56
3	3.71	4.28
4	7.20	7.42
5	7.42	7.42

Hardover Failure Transients - Analog Monitor

The hardover failure transient allowed by specification No. 16ZH001F for the F-16 1A is a time-displacement curve with a area limitation of *0.700 percent-seconds* and a requirement for a *negative slope after 0.08 seconds*. One hundred (100) percent equals 2.125 inches for the F-16 horizontal tail actuator used for the direct drive system.

Figure VI-50 shows the effect on the output of sequentially applying a positive hardover input into channels 1, 2 and 3. The actuator is initially positioned at null with zero input. Positive 4-volt command inputs are applied to the active section (1A, 2A, and 3A) inputs for each channel. Since the monitor section's input of each channel remained at null, the hardover input appeared as a failure to the failure-detection logic, causing the electronic switch to disable the channel by grounding the input lines to the servoamplifiers for the *failed* channel. As shown on Figure VI-50, the output voltages to each channel's OC2 (reference Figure VI-17) have been connected to the chart recorder and show when the electronic switch disconnects the failed input. OC2s are used to drive the channel failure indicating lights in the pilot's monitor box. The actuator's output position is recorded on the bottom trace of the figure. This trace shows that there is very little change in the output position with the three channel failures. After the channel 1 failure, the actuator moves over a period of 2 seconds to a slight offset position 0.0053 inches from the initial position. This shift in position probably reflects a slight force-fight between the control channels. No change in the output position occurs after failure of channel 2. After the failure of channel three, the actuator transfers to the fail-centered mode and moves slightly towards the centered position.

Figures VI-51 through VI-53 show the effect of both positive and negative hardover inputs applied to each control channel. The time scale is expanded so that each division is .001 seconds. Figure VI-51 shows the effect of the positive and negative hardover inputs into channel 1. The time delay for the failure logic measures .002 seconds. Note that the actuator position trace at 0.106 inch per division is relatively coarse compared to Figure VI-50. However, no position change is indicated with either positive or negative hardover failures. Figure VI-52 shows the effect of the positive and negative hardover inputs into channel 2 (with channel 1 failed). The fail indicator trace for channel 1 shows that it has already been failed. Again the output shows no change upon the input failure. Figure VI-53 shows the same test applied to Channel 3, the only operating channel. No output change appears on the position trace for the actuator. These figures illustrate the effect of the rapid failure-detection time. The hardover input failures are detected and the input removed before the actuator can respond.

TEST DATA

Test Item - Dynamic Controls, Inc.
F-16 Direct Drive
Servoactuator

Date:
Prepared: 10-30-86

Test - Hardover Failures - condition 6

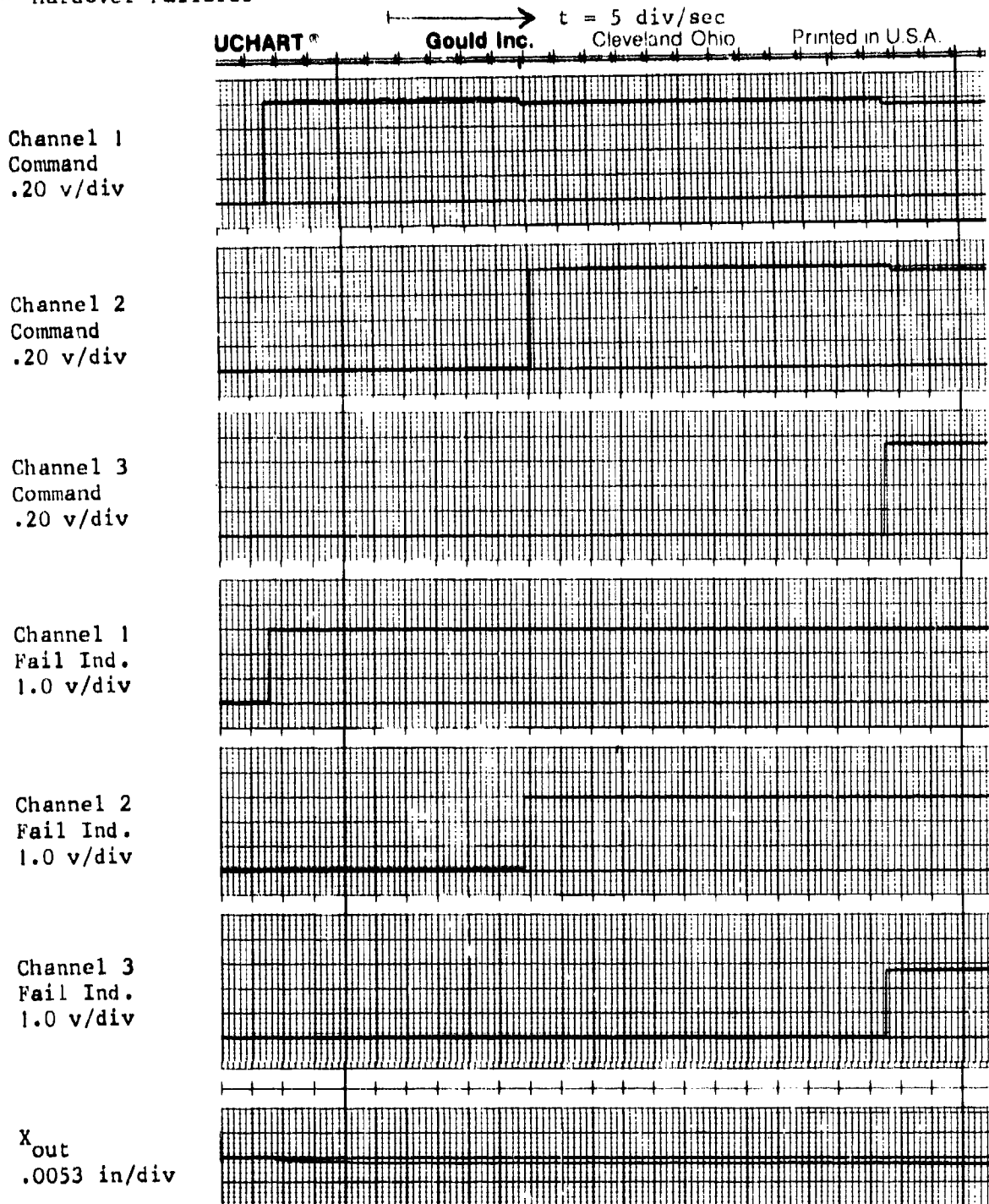


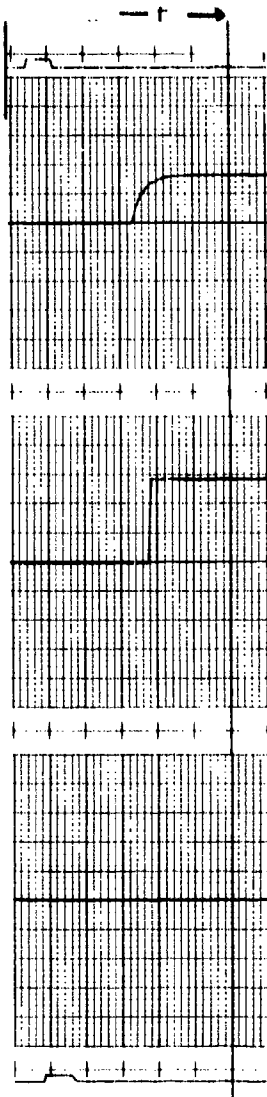
Figure VI-50. Hardover failures - condition 6.

TEST DATA

Test Item - Dynamic Controls, Inc.
F-16 Direct Drive
Servoactuator

Date: 11-12-86
Prepared: 11-12-86

Test - + & - haldovers into channel 1 - condition 7



$t = 100 \text{ div/sec}$

E_{in}

Input Command
Channel 1A - 0.5 v/div

Fail Indicator
Channel 1 - 1 v/div

X_{out}

$X_{out} = 0.106 \text{ in/div}$

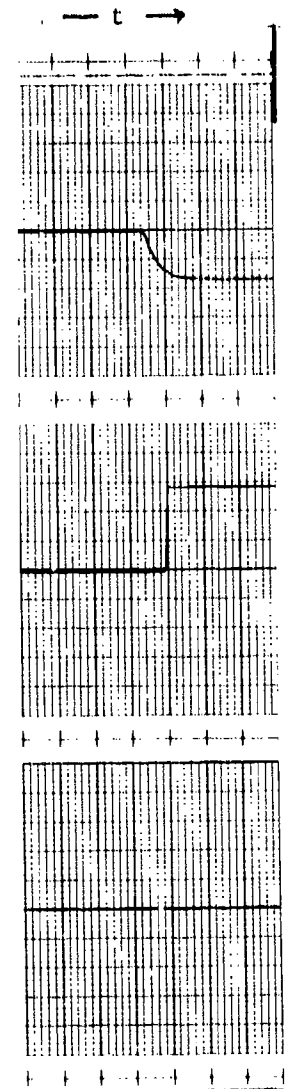


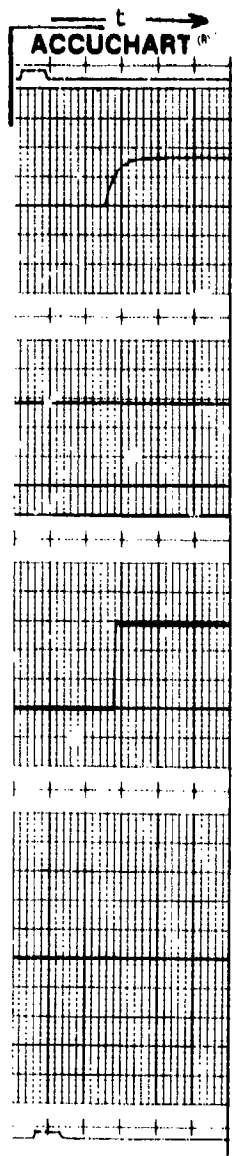
Figure VI-51. Halldover failures - condition 7 - channel 1

TEST DATA

Test Item - Dynamic Controls, Inc.
F-16 Direct Drive
Servoactuator

Date }
Prepared: 11-12-86

Test - + & - Hardovers into Channel 2, Channel 1 Failed - condition 7



E_{in}

$t = 100 \text{ div/sec}$

Input Command
Channel 2A - 0.5 v/div

Fail Indicator
Channel 1 - 1 v/div

Fail Indicator
Channel 2 - 1 v/div

X_{out}

$X_{out} = 0.106 \text{ in/div}$

E_{in}

X_{out}

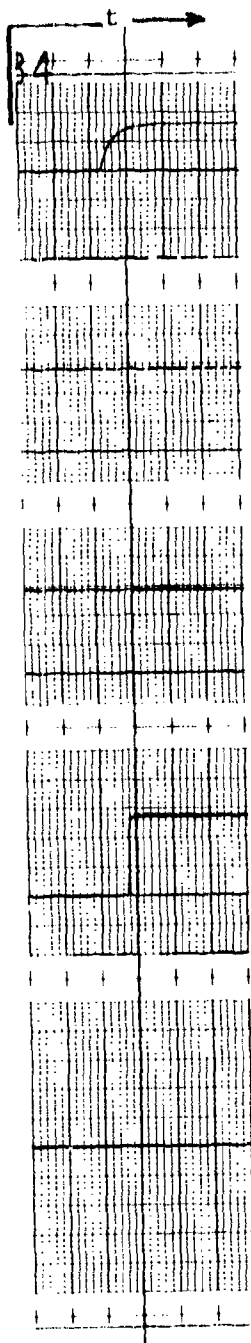
Figure VI-52. Hardover failures - condition 7 - channel 2.

TEST DATA

Test Item - Dynamic Controls, Inc.
F-16 Direct Drive
Servoactuator

Date:
Prepared: 11-12-86

Test - + & - Hardovers into Channel 3, Channels 1,2 Failed - condition 7



E_{in}

$t = 100 \text{ div/sec}$

Input Command
Channel 3A - 0.5 v/div

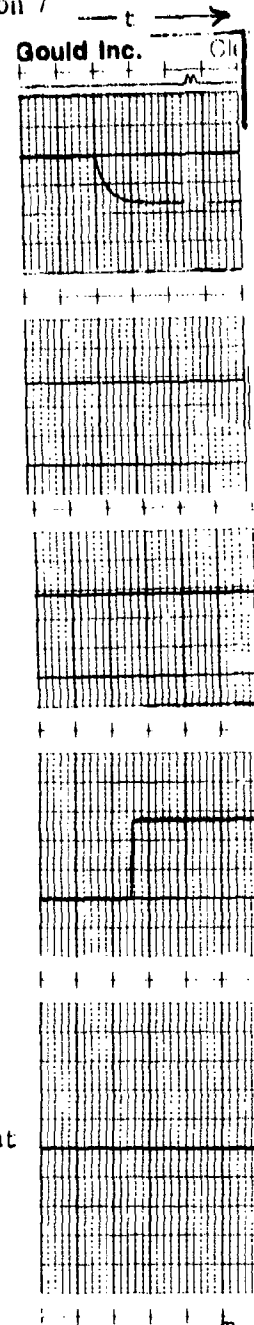
Fail Indicator
Channel 1 - 1 v/div

Fail Indicator
Channel 2 - 1 v/div

Fail Indicator
Channel 3 - 1 v/div

X_{out}

$X_{out} = 0.106 \text{ in/div}$



E_{in}

X_{out}

Figure VI-53. Hardover failures - condition 7 - channel 3.

The short time used for the failure detection was practical with the direct drive configuration without nuisance disconnects. This is because there are no inherent dynamic differences in feedback or input signals for the failure logic to detect. Had LVDTs been used for the position transducers, the demodulation and filter circuits would have to be closely matched to avoid nuisance disconnects. For some applications, a long failure-detection time is desirable. Inputs with transients riding on them could create problems with the nuisance disconnects. The F-16 allowable failure transient envelope will allow hardover failure-detection time delays of up to 60 milliseconds.

Slowover Failure Transients - Analog Monitor

Figures VI-54 through VI-56 show the data recorded to document the effect of applying slowover failures on the output of the actuator. Figure VI-54 shows the effect of applying a 0.4 peak volt 0.3 Hz triangle waveform to all three channels and then grounding the channel 1A's input when the ramp crosses zero. The actuator output shows no apparent waveform change with the input failure. Figure VI-55 shows the same test with channel 1 failed and channel 2A's input grounded. Again there is negligible change in the output motion. Figure VI-56 shows the effect of the third channel failure using the triangular input. After the failure is detected, the actuator moves slowly to the actuator position determined by the mechanical feedback linkage. Note that the input to channel 3B continues after the grounding of the channel 3A's input, allowing detection of the failure.

Static Failure Detection - Analog Monitor

Figures VI-54 through VI-56 were also used to measure the failure-detection level of the analog failure-detection logic. The change in the amplitude of the input voltage between grounding of the active input of a channel and detection of the failure is the *failure-detection level*. As shown on the figures (note that there is a small pen offset between channels), the measured failure-detection level of the inputs was nominally ± 0.170 volts.

Dynamic Hardover Failure Transient - Analog Monitor

Figures VI-57 and VI-58 show the effect on the actuator output of hardover failures occurring while the actuator is being commanded by a sinusoidal input at 0.3 Hz. Figure VI-57 show the effect of positive hardovers on the actuator output. There is no apparent change in the motion of the actuator until the third hardover is applied. As shown on Figure VI-57, the third hardover causes the system to transfer to the fail-center mode. The effect of negative hardovers as shown on Figure VI-58 is similar with no apparent change in the actuator output until the third failure.

TEST DATA

Test Item - Dynamic Controls, Inc.
F-16 Direct Drive
Servoactuator

Date 1
Prepared: 11-13-86

Test - + Slow over Failure

$t = 5 \text{ div/sec}$

Input Command
Channel 1 - 0.02 v/div

Input Command
Channel 2 & 3 - 0.02 v/div

Fail Indicator
Channel 1 - 1 v/div

Fail Indicator
Channel 2 - 1 v/div

Fail Indicator
Channel 3 - 1 v/div

$X_{out} = 0.0266 \text{ in/div}$

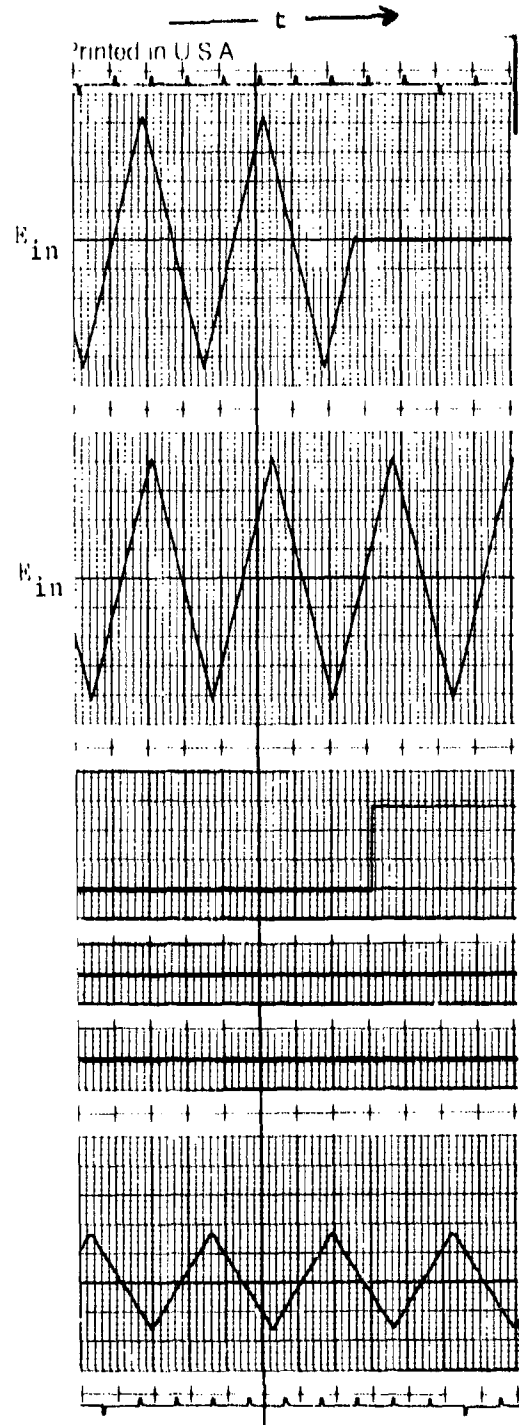


Figure VI-54. Slowover failure transients - condition 10.

TEST DATA

Test Item - Dynamic Controls, Inc.
F-16 Direct Drive
Servoactuator

Date:
Prepared: 11-13-86

Test - - Slowover Failure

t = 5 sec/div

Input Command
Channel 2 - 0.02 v/div

Input Command
Channel 3 - 0.02 v/div

Fail Indicator
Channel 1 - 1 v/div

Fail Indicator
Channel 2 - 1 v/div

Fail Indicator
Channel 3 - 1 v/div

$X_{out} = 0.0266$ in/div

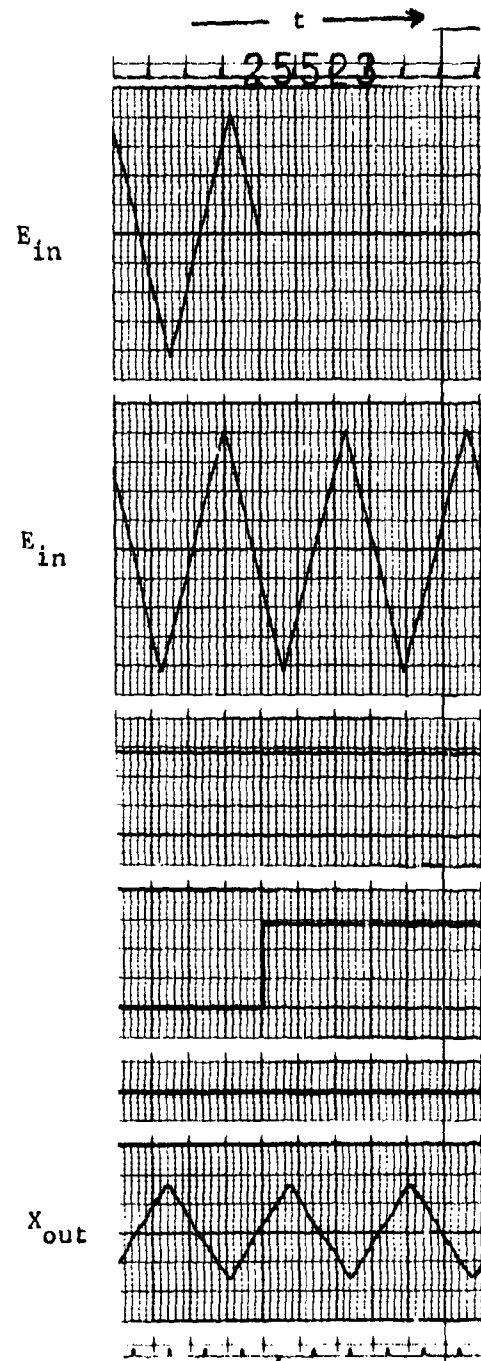


Figure VI-55. Slowover failure transients - condition 11.

TEST DATA

Test Item - Dynamic Controls, Inc.
F-16 Direct Drive
Servoactuator

Date:
Prepared: 11-13-86

Test - + Slowover Failure

$t = 5 \text{ div/sec}$

Input Command -- 0.02 v/div

Input Command
Channel 3 - 0.02 v/div

Fail Indicator
Channel 1 - 1 v/div

Fail Indicator
Channel 2 - 1 v/div

Fail Indicator
Channel 3 - 1 v/div

$X_{out} = 0.0266 \text{ in/div}$

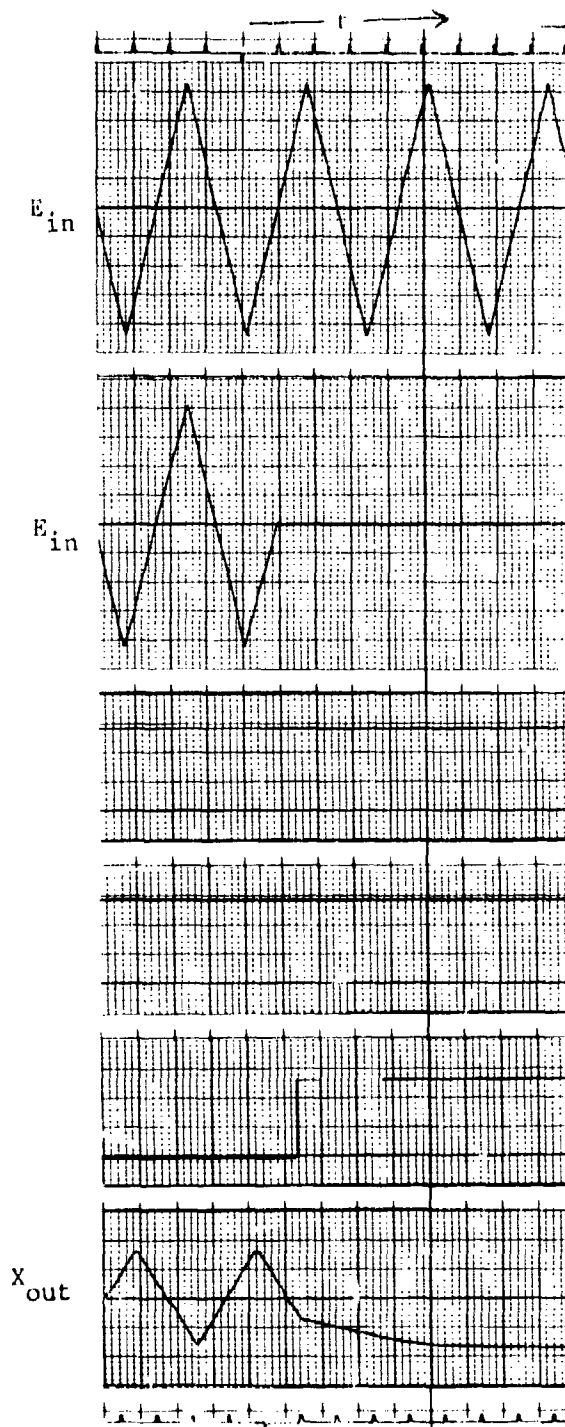


Figure VI-56. Slowover failure transients - condition 12.

TEST DATA

Test Item - Dynamic Controls, Inc.
F-16 Direct Drive
Servoactuator

Date
Prepared: 11-4-86

Test - Dynamic Failure Transient
Positive Hardovers

Channel 1
Command
.5 v/div

Channel 2
Command
.5 v/div

Channel 3
Command
.5 v/div

Channel 1 Fail
Indicate
1 v/div

Channel 2 Fail
Indicate
1 v/div

Channel 3 Fail
Indicate
1 v/div

X_{out}
.2 v/div

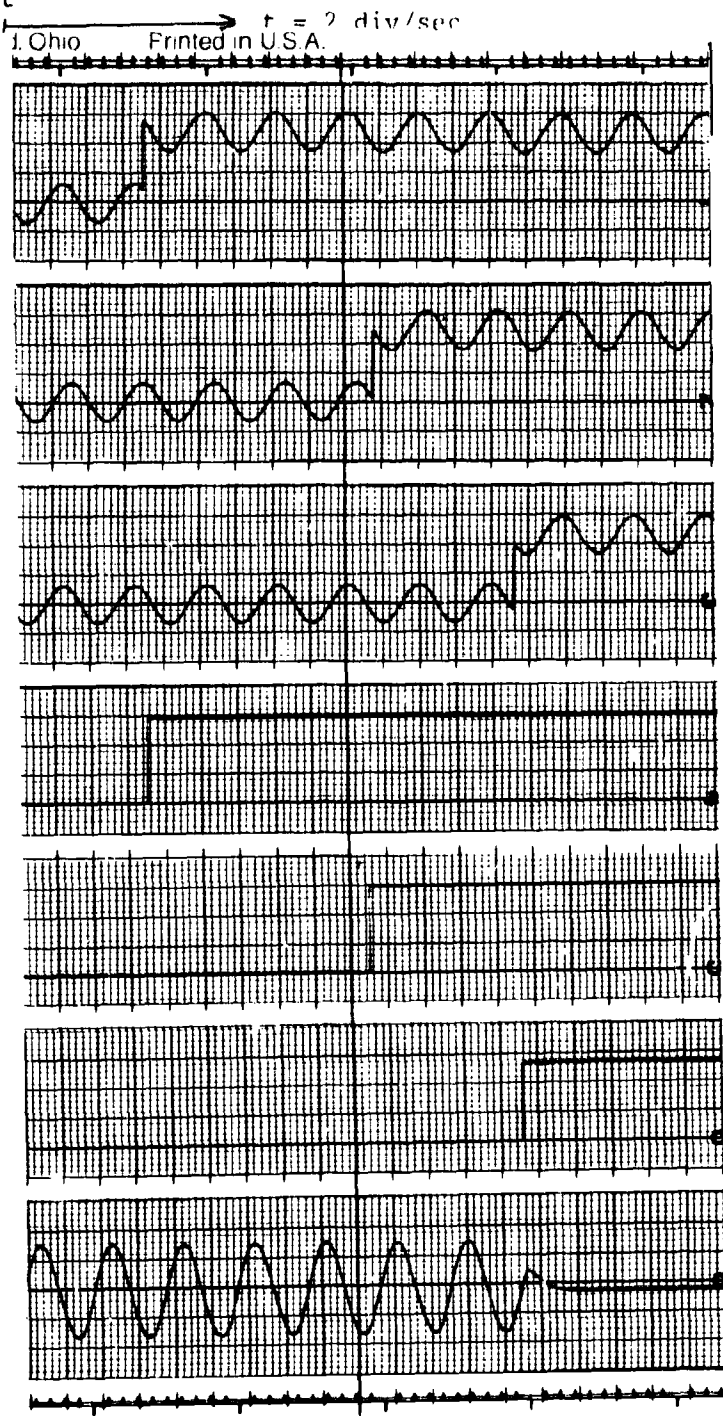


Figure VI-57. Slowover failure transients - condition 16.

TEST DATA

Test Item - Dynamic Controls, Inc.
F-16 Direct Drive
Servoactuator

Date
Prepared: 11-4-86

Test - Dynamic Failure Transient
Negative Hardovers

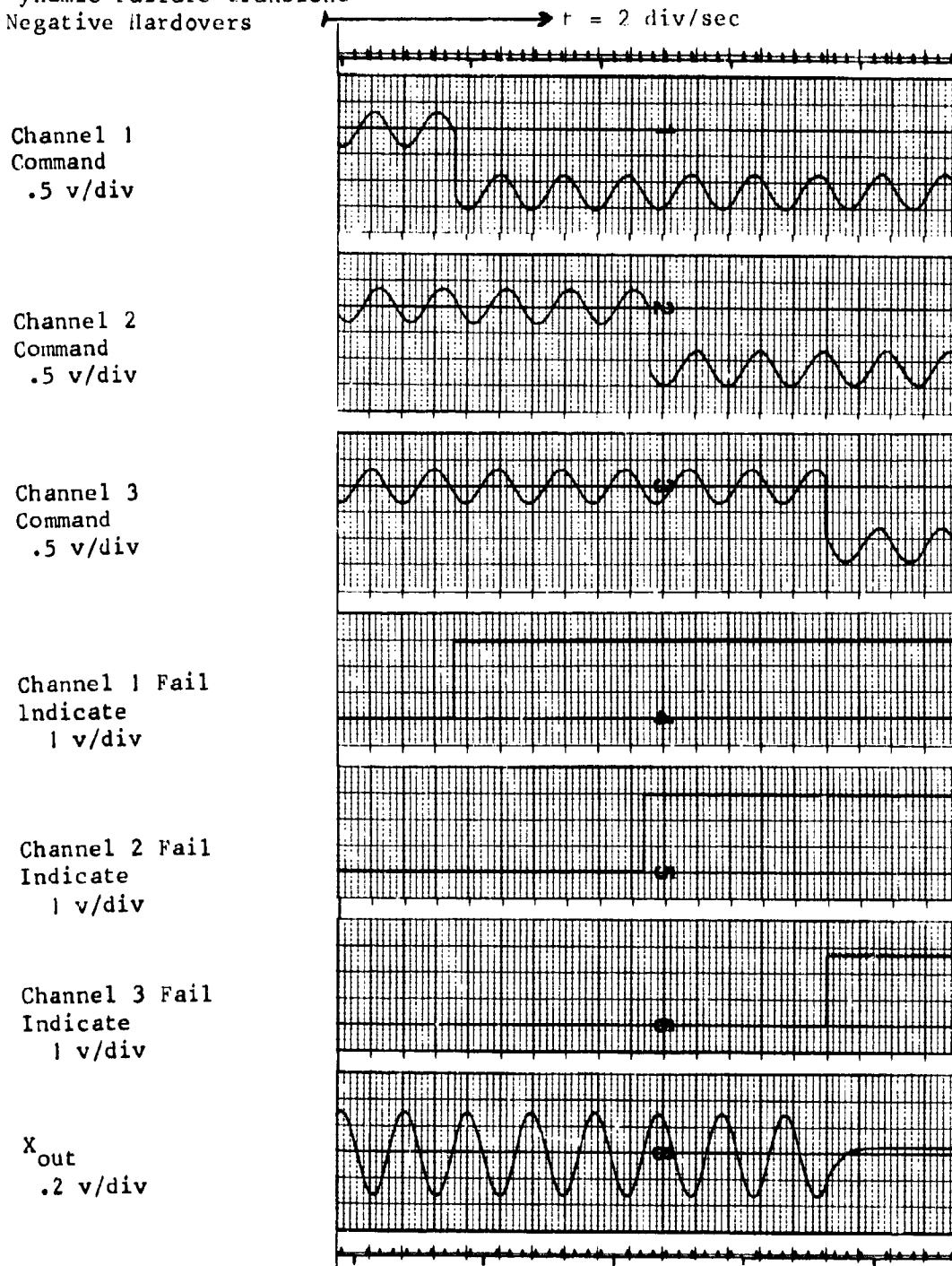


Figure VI-58. Slowover failure transients - condition 17.

Figures VI-59 and VI-60 show the effect of loss of a control input on the output of the actuator when the actuator is operating at a deflection of 1.13 inches (25 percent of the total stroke) from null position. Figure VI-59 shows the actuator motion with the actuator biased to + 50 percent of the extend motion. The output of the actuator is not affected by the channel failures until the third failure. Upon the third failure the actuator moves towards a centered position. Figure VI-60 presents similar data for the actuator operating in a 50 percent retract stroke position. No change in the actuator motion occurs until the third input failure when the actuator transfers to the fail-centered mode.

Pressure Failure Transients - Analog Monitor

Figure VI-61 shows the effect of supply pressure failures on the output of the actuator. The left hand data on the figure shows a failure of P1 supply pressure. The right hand data on the figure shows a failure of P2 supply pressure. For both of these tests, the actuator is being commanded with a 0.1 Hz triangular waveform. The output shows no change upon loss of hydraulic supply pressure.

TEST DATA

Test Item - Dynamic Controls, Inc.
F-16 Direct Drive
Servoactuator

Date:
Prepared: 11-13-86

Test - Grounded Input Failure at 50% Extend

$t = 2 \text{ div/sec}$

Input Command
Channel 1 - 0.20 v/div

Input Command
Channel 2 - 0.20 v/div

Input Command
Channel 3 - 0.20 v/div

Fail Indicator
Channel 1 - 1 v/div

Fail Indicator
Channel 2 - 1 v/div

Fail Indicator
Channel 3 - 1 v/div

$X_{out} = 0.106 \text{ in/div}$

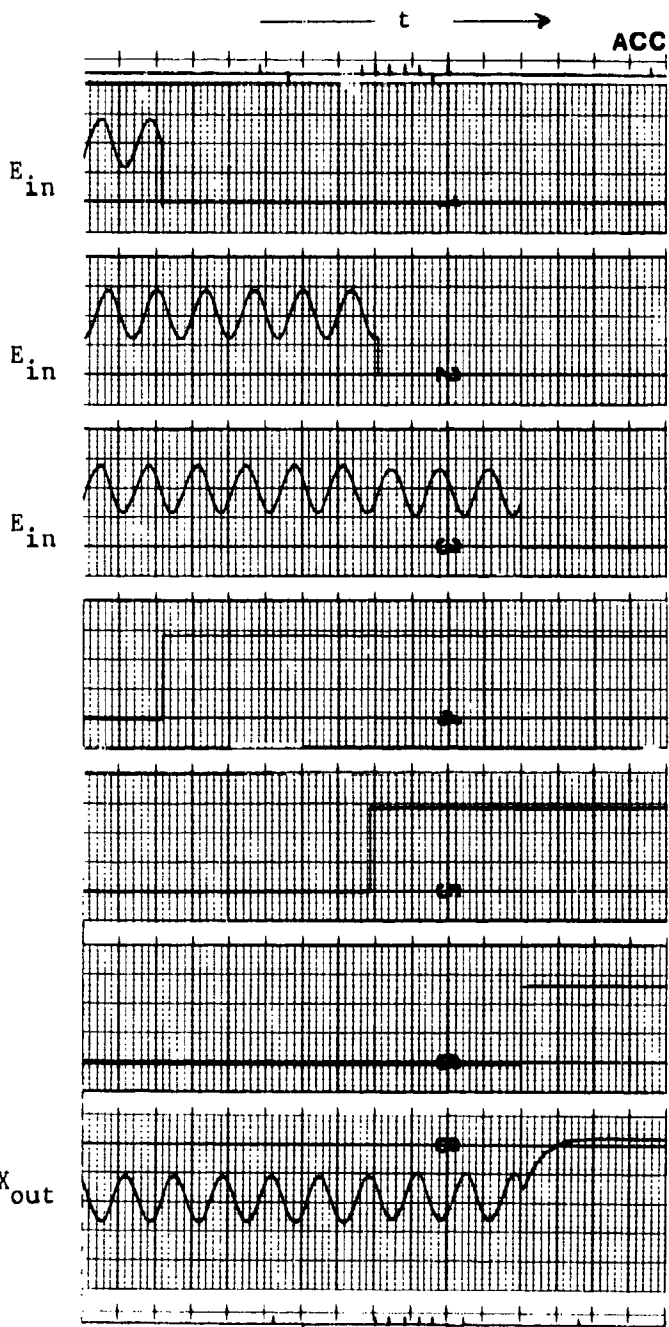


Figure VI-59. Slowover failure transients - condition 18.

TEST DATA

Test Item - Dynamic Controls, Inc.
F-16 Direct Drive
Servoactuator

Date:
Prepared: 1-13-86

Test - Grounded Input Failure at 50% retract

$t = 2 \text{ div/sec}$

Input Command
Channel 1 - 0.20 v/div

Input Command
Channel 2 - 0.20 v/div

Input Command
Channel 3 - 0.20 v/div

Fail Indicator
Channel 1 - 1 v/div

Fail Indicator
Channel 2 - 1 v/div

Fail Indicator
Channel 3 - 1 v/div

$x_{\text{out}} = 0.106 \text{ in/div}$

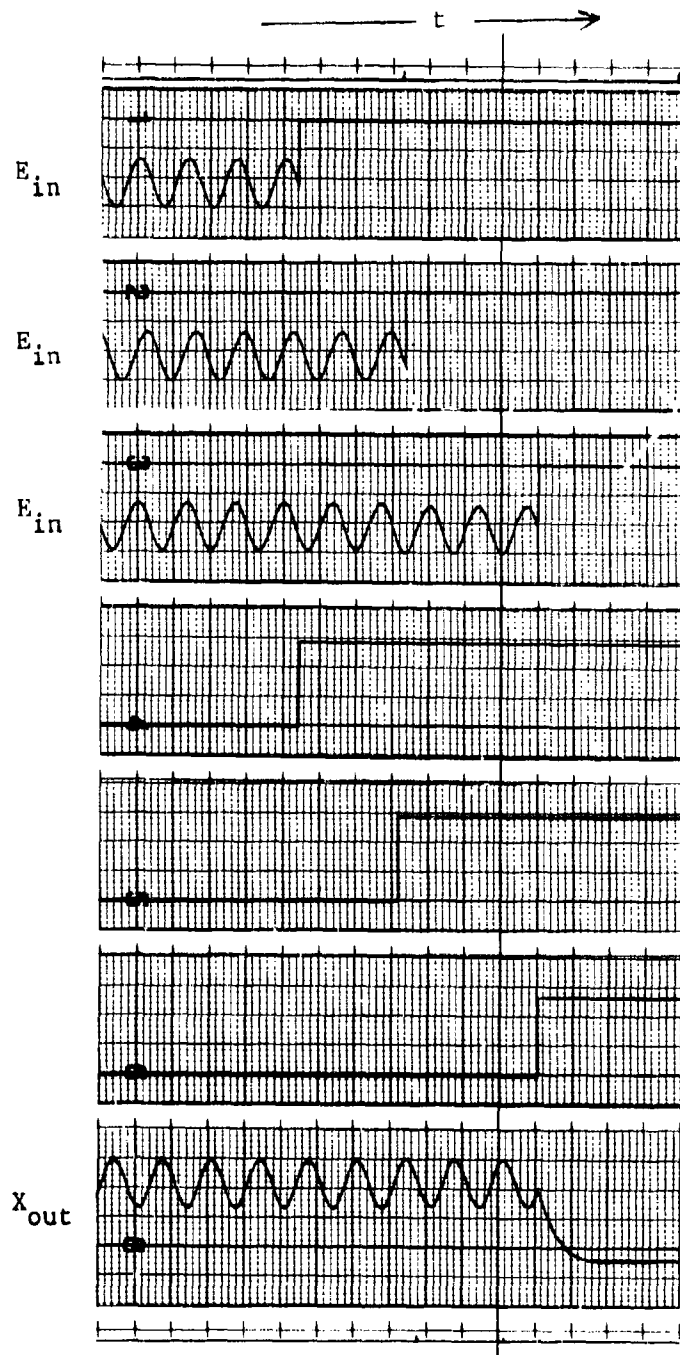


Figure VI-60. Slowover failure transients - condition 19.

TEST DATA

Test Item - Dynamic Controls, Inc.
F-16 Direct Drive
Servoactuator

Date:
Prepared: 10-30-86

Test - Pressure Failures (P_1 & P_2)

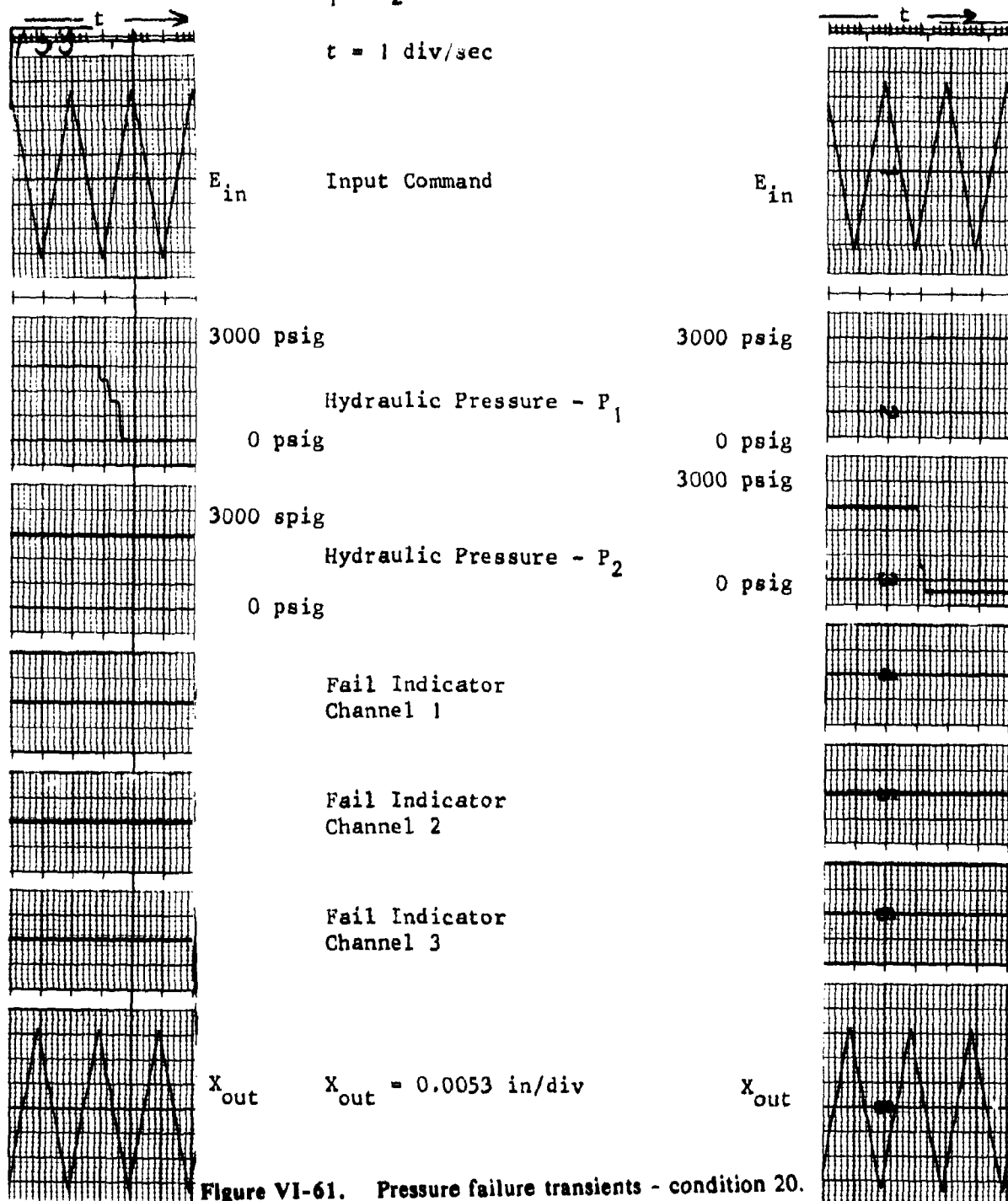


Figure VI-61. Pressure failure transients - condition 20.

Hardover Failure Transient - Logic Processor

Figure VI-62 shows the effect of applying a positive hardover voltage sequentially to channels 1A, 2A and 3A with the system at null. The Logic Processor was set to vote a failure after 9 consecutive failures (an error voltage greater than the 35 percent detection threshold). As recorded on this figure, the time base is 5 divisions per second or 200 milliseconds per division. The amplitude of the output change with the first failure is .06 inches. The duration of the transient is nominally 20 milliseconds. The area under the transient curve is nominally .06 percent-seconds (compared to the 0.700 percent-seconds allowed for the normal F-16 ISA). The amplitude of the transient with the second failure is .04 inches. This is consistent with having a slightly lower slew rate after failure of one channel. The time duration of the transient is consistent with the time duration for the first failure transient. After the second failure, the actuator slowly moves to a position .025 inches from the actuator position before the second failure. This indicates a slight null mismatch between the individual channels. The position change occurs over a five-second period. After the hardover input is applied to the active input of the third channel, the actuator transfer to the fail-centered mode and moves to the *centered* position. The Logic Processor, because of the multiple samples requirement for declaring failures, allowed slightly larger hardover failure transients than the analog system. The failure transient amplitude-time area is considerably less than that allowed for the F-16 ISA.

Figures VI-63 and VI-64 show the effect of a grounding the inputs to the monitor channels simultaneously with the actuator initially moved 1.60 inches from null. Since the channels are self-monitoring, the failure logic correctly detects the three simultaneous input failures. The response of the actuator in the fail-centered mode does show ringing of the actuator motion. The frequency of the ringing is very low (note that the time scale is 10 seconds per division). The ringing was not observed during the Phase I testing of the system. The change in the operation in the fail-centered mode indicated that a problem with the mechanical feedback linkage had developed during the testing. Due to time constraints, no attempt to eliminate the ringing was made as part of the Phase II investigation.

Slowover Failure Transients - Logic Processor

Figure VI-65 shows the effect of grounding the input to channel 1A with the actuator being commanded by a .03 Hz triangular waveform input. The failure is detected by the Logic Processor when the disagreement between channel 1A and 1B reaches the detection level. As shown in the actuator position trace at the bottom of the figure, the actuator position gain changes when the input to channel A is grounded. This is because until channel 1 is declared failed and disabled, there is a

TEST DATA

Date

Prepared: 3/31/87

Test Item - Dynamic Controls, Inc.
F-16 Direct Drive Servoactuator
Logic Processor

Test - Hardover Failure Transients - Condition 6
----- t ----->

t = 5 div/sec

Channel 1A
Command
0.5 v/div

Channel 2A
Command
0.5 v/div

Channel 3A
Command
0.5 v/div

Fail Indicate
Channel 1
2.0 v/div

Fail Indicate
Channel 2
2.0 v/div

Fail Indicate
Channel 3
2.0 v/div

X_{out}
.010 in/div

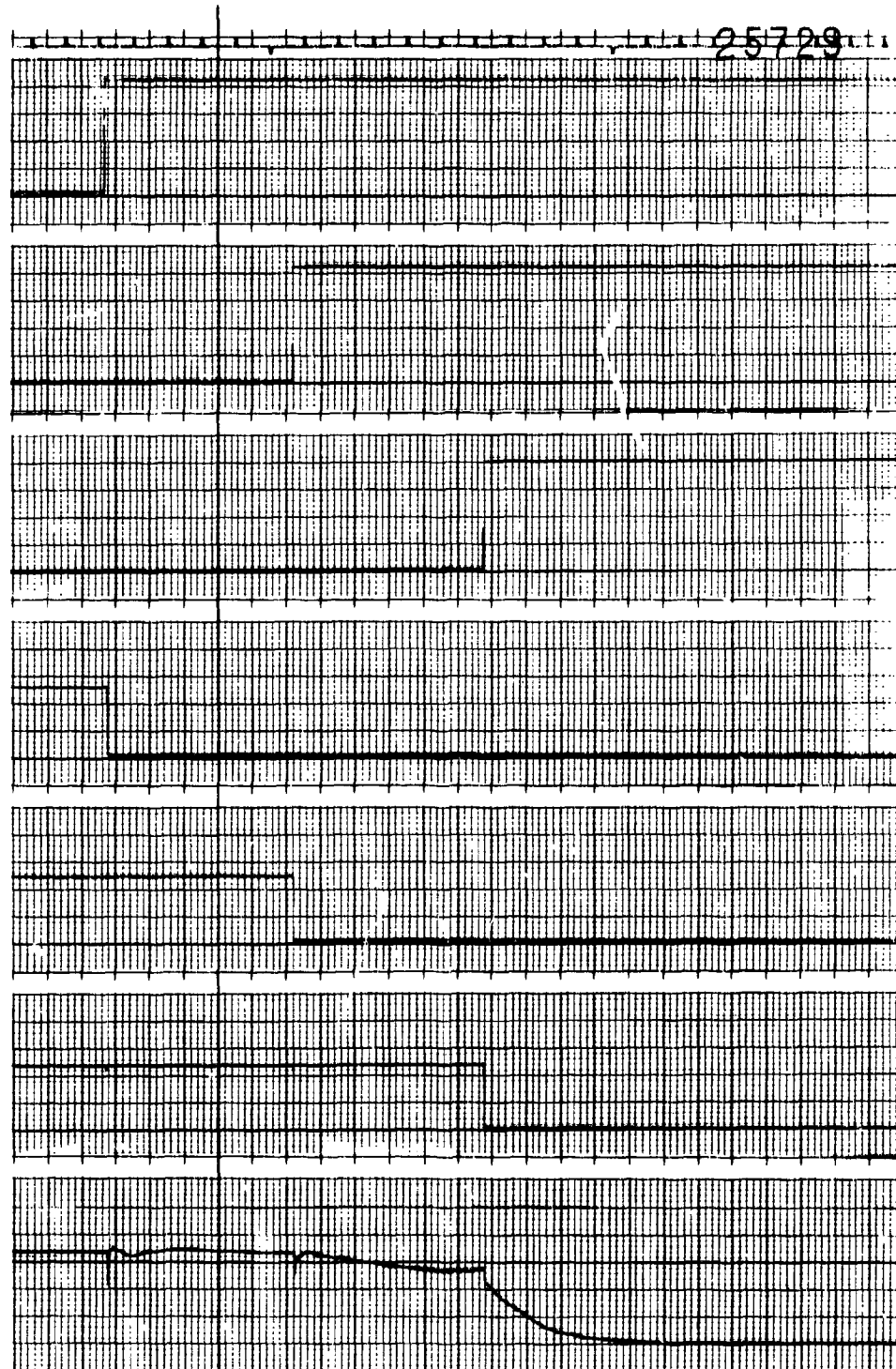


Figure VI-62. Hardover failure transients - condition 6.

TEST DATA

Date

Prepared: 4/10/87

Test Item - Dynamic Controls, Inc.
F-16 Direct Drive Servoactuator
Logic Processor

Test - Positive Voltage to Ground (75% extend)
----- t ----->

t = 0.1 div/sec

Channel 1B
Command
0.20 v/div

E_{in}

Channel 2B
Command
0.20 v/div

E_{in}

Channel 3B
Command
0.20 v/div

E_{in}

Fail Indicate
Channel 1 - 2.0 v/div

Fail Indicate
Channel 2 - 2.0 v/div

Fail Indicate
Channel 3 - 2.0 v/div

X_{out} = 0.100 in/div

X_{out}

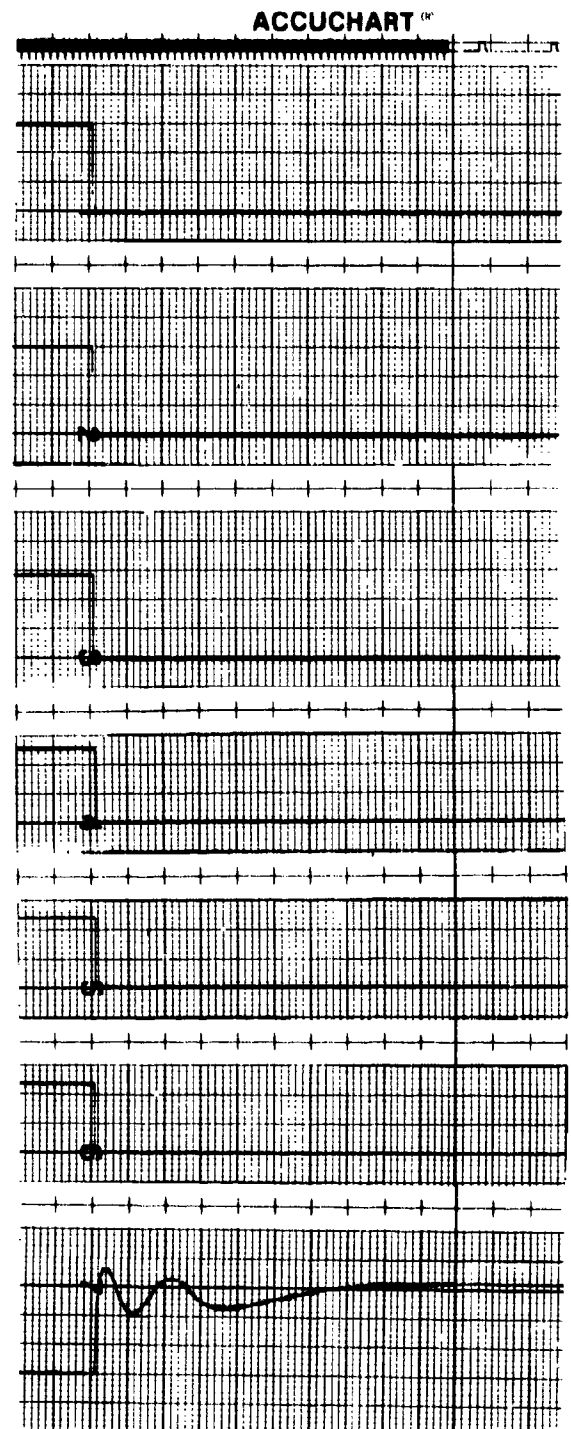


Figure VI-63. Hardover failure transients - condition 8.

TEST DATA

Test Item - Dynamic Controls, Inc.
F-16 Direct Drive Servoactuator
Logic Processor

Date

Prepared: 4/10/87

Test - Positive Voltage to Ground (75% extend)
----- t ----->

t = 0.1 div/sec

Channel 1B
Command
0.20 v/div

E_{in}

Channel 2B
Command
0.20 v/div

E_{in}

Channel 3B
Command
0.20 v/div

E_{in}

Fail Indicate
Channel 1 - 2.0 v/div

Fail Indicate
Channel 2 - 2.0 v/div

Fail Indicate
Channel 3 - 2.0 v/div

X_{out} = 0.100 in/div

X_{out}

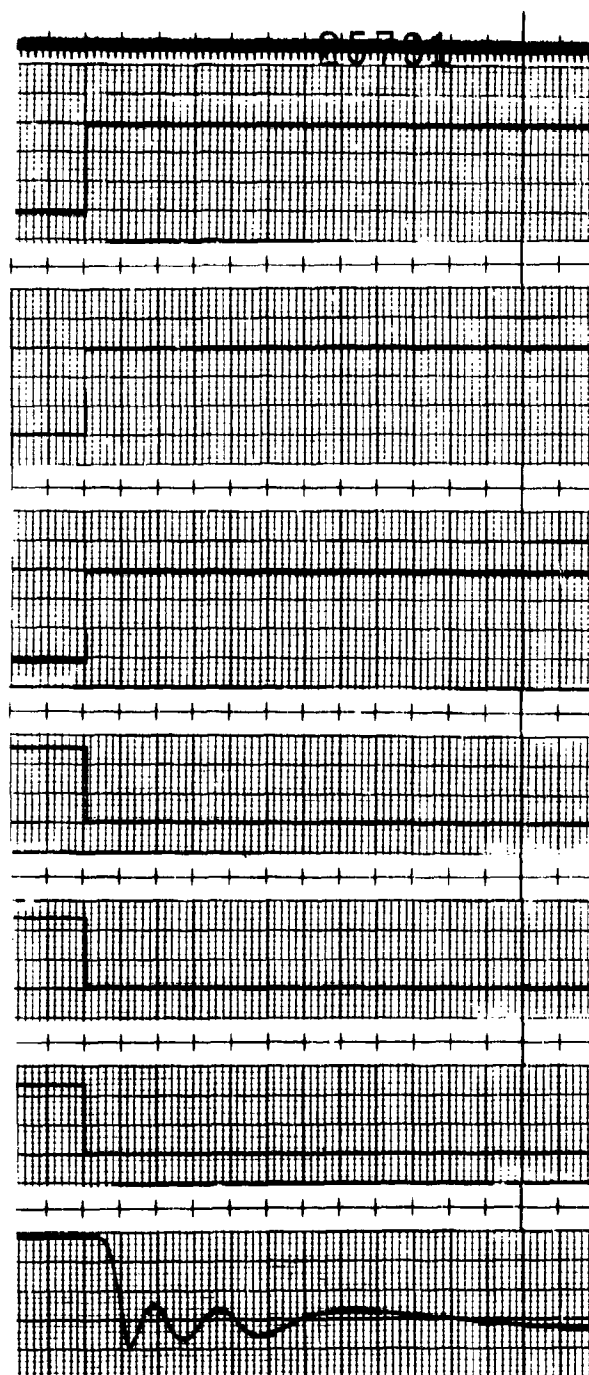


Figure VI-64. Hardover failure transients - condition 9.

TEST DATA

Test Item - Dynamic Controls, Inc.
F-16 Direct Drive Servoactuator
Logic Processor

Date
Prepared: 5/18/87

Test - Slower Failure Transients - Condition 13

$t = 2 \text{ div/sec}$

Channel 1A
Command
0.20 v/div

Channel 1B
Command
0.20 v/div

Channels 2A, 2B,
3A, and 3B
Command
0.20 v/div

Fail Indicate
Channel 1 -
2.0 v/div

Fail Indicate
Channel 2 -
2.0 v/div

Fail Indicate
Channel 3 -
2.0 v/div

$X_{out} = .025 \text{ in/div}$

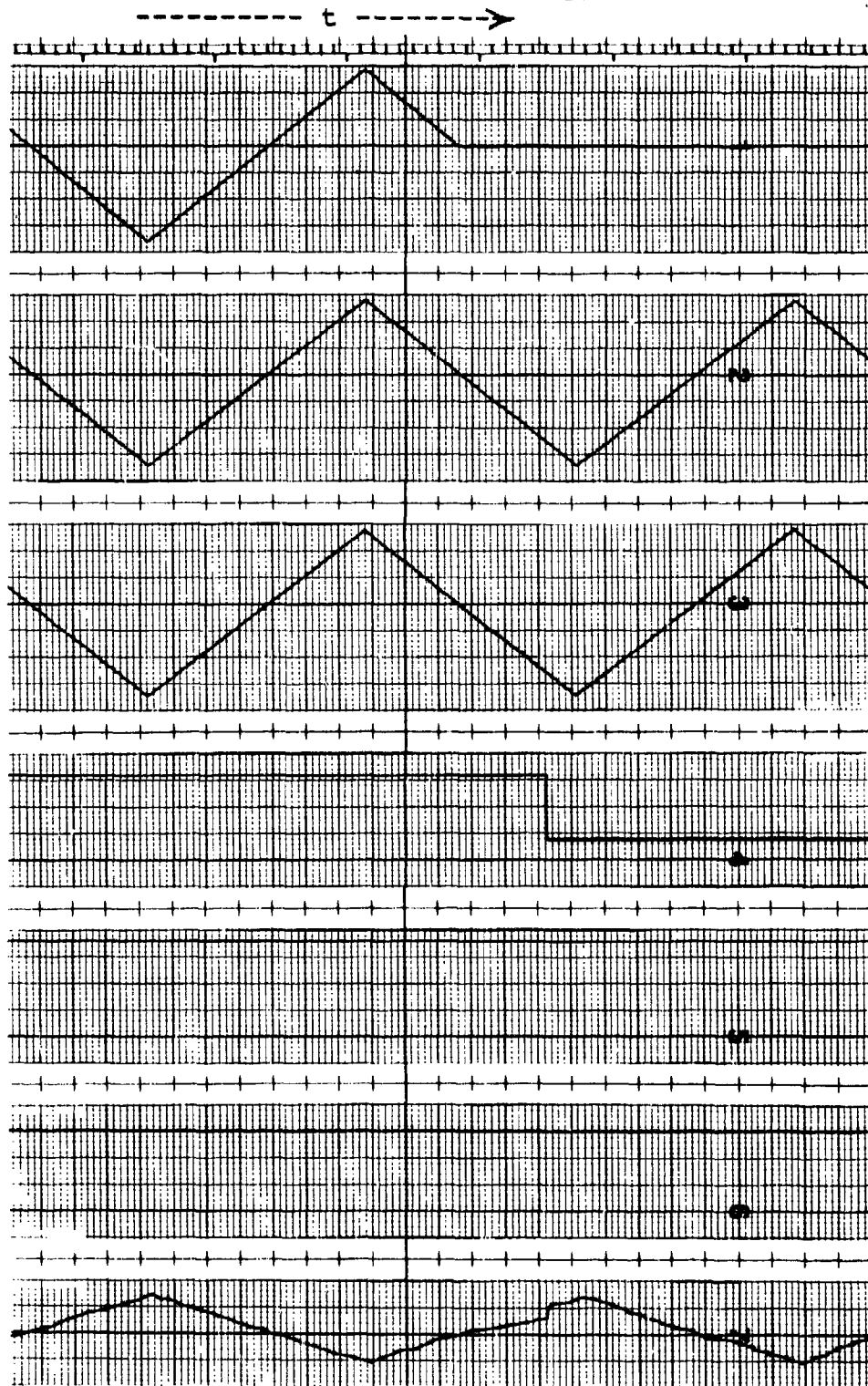


Figure VI-65. Slower failure transients - condition 13.

force-fight between the three channels, with channel 1 opposing actuator movement away from a position corresponding to a grounded input. After channel 1 is disabled, the actuator position gain is restored to the *pre-failure* position gain. The failure transient occurring upon failure of channel 1 has an amplitude of .07 inches.

Figure VI-66 shows the effect of grounding the input to channel 2A with the actuator being commanded by a .03 Hz triangular waveform input after channel 1 has already been failed. The top trace shows that channel 1A with no changing input since the channel was already failed. With the grounding of the input to channel 2A, the position gain of the actuator gradually becomes zero as channels 2 and 3 force-fight each other and cancel. Upon detection of the channel 2 failure and the disabling of the channel, the actuator is returned to the position commanded by the triangle waveform input into channel 3. The transient occurring with the disabling of channel 2 is .07 inches.

Figure VI-67 shows the effect of grounding the input to channel 3A with the actuator being commanded by a .03 Hz triangular waveform input after both channels 1 and 2 were failed. The failure causes transfer of the actuator to the fail-centered mode of operation. When the 3A channel input is grounded, actuator motion stopped (since that channel controlled the actuator output).

Figures VI-65 to VI-67 show that the Logic Processor detected the slowover failures correctly and that the failure transients with the slowover failures are less than 1.75 percent of the actuator stroke.

Static Failure Detection - Logic Processor

Figures VI-65 to VI-67 were also used to measure the failure-detection level loaded into the Logic Processor. The change in the input voltage between grounding of the active input of a channel and detection of the failure is the *failure-detection level*. From these figures, the failure-detection level used for the Phase II evaluation was nominally 0.240 volts. This is higher than the value (0.170 volts) used for the analog monitor. The higher detection level correlates with being able to observe failure transients with the Logic Processor where none were apparent with the analog monitor.

Dynamic Hardover Failure Transients - Logic Processor

Figure VI-68 shows the effect of sequentially applying positive hardover failure inputs into channels 1A, 2A and 3A with the system operating with a sinusoidal input of 0.3 Hz. The output waveform temporarily distorts with the first two channel failures. The failure of channel 3 causes the actuator

TEST DATA

Test Item - Dynamic Controls, Inc.
F-16 Direct Drive Servoactuator
Logic Processor

Date
Prepared: 5/18/87

Test - Slowover Failure Detection - Condition 14
----- t ----->

t = 2 div/sec

Channel 1A
Command
0.20 v/div

Channel 2A
Command
0.20 v/div

Channels 2B, 3A
and 3B
Command
0.20 v/div

Fail Indicate
Channel 1 -
2.0 v/div

Fail Indicate
Channel 2 -
2.0 v/div

Fail Indicate
Channel 3 -
2.0 v/div

X_{out} = .025 in/div

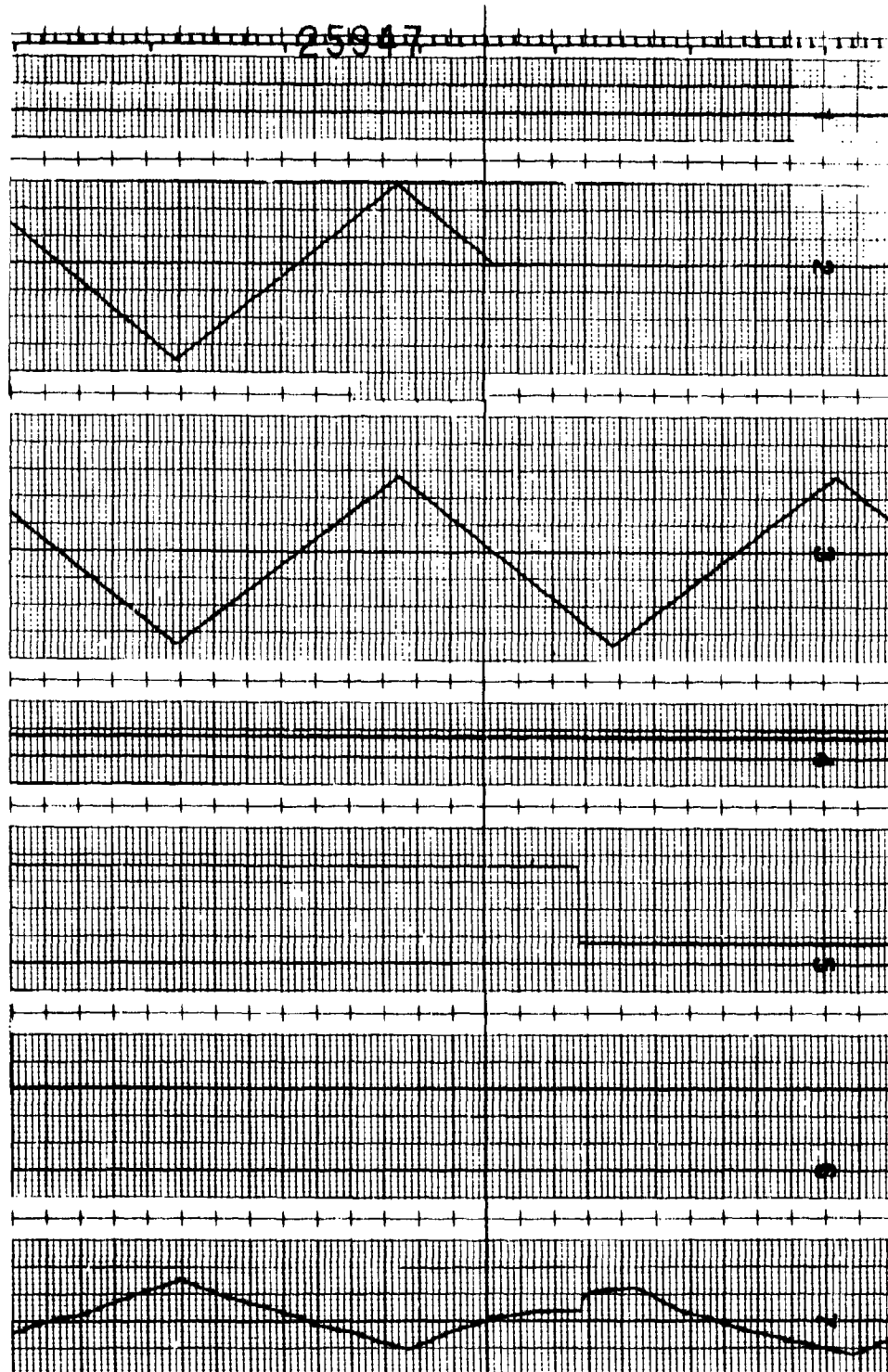


Figure VI-66. Slowover failure transients - condition 14.

TEST DATA

Test Item - Dynamic Controls, Inc.
F-16 Direct Drive Servoactuator
Logic Processor

Date
Prepared: 5/18/87

Test - Slowover Failure Transients - Condition 15
----- t ----->

t = 2 div/sec

Channels 1A, 2A
Command
.020 v/div

Channel 3A
Command
.020 v/div

Channels 3B
Command
.020 v/div

Fail Indicate
Channel 1 -
2.0 v/div

Fail Indicate
Channel 2 -
2.0 v/div

Fail Indicate
Channel 3 -
2.0 v/div

X_{out} = .025 in/div

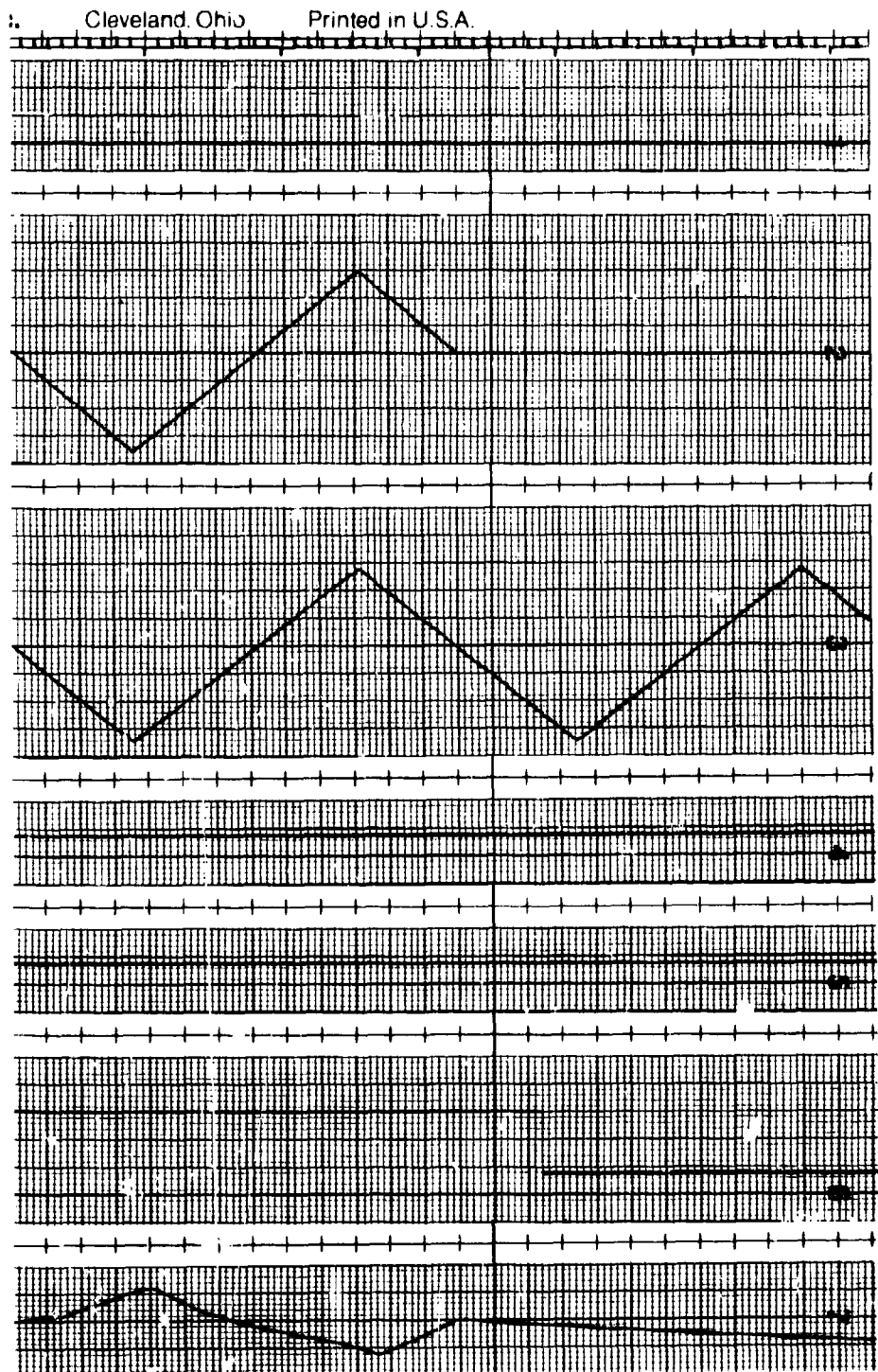


Figure VI-67. Slowover failure transients - condition 15.

TEST DATA

Test Item - Dynamic Controls, Inc.
F-16 Direct Drive Servoactuator
Logic Processor

Date

Prepared: 4/10/87

Test - Dynamic Failure Transient - Condition 16
Positive Hardovers

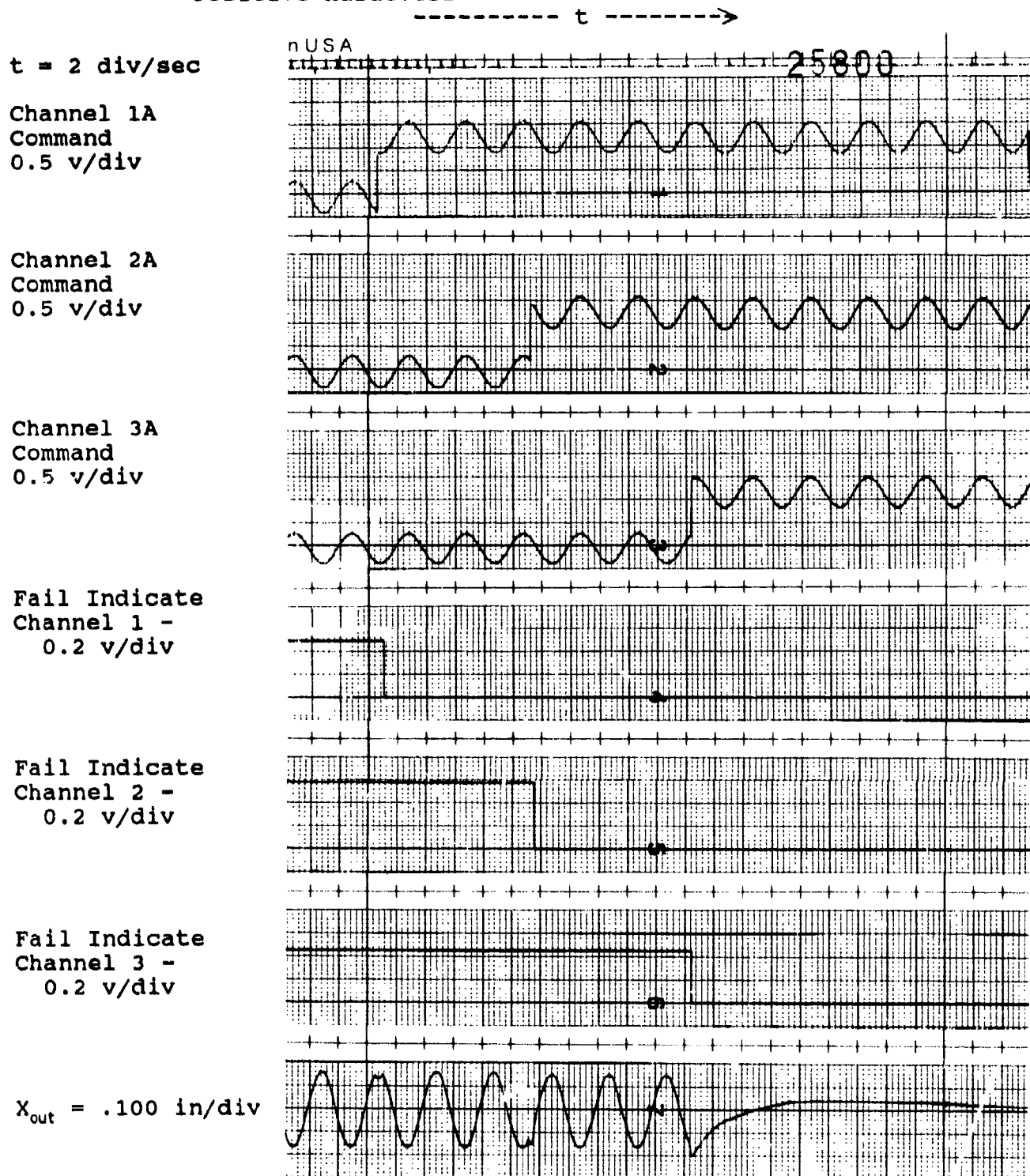


Figure VI-68. Dynamic failure transients - condition 16.

to transfer to the fail-center mode. The amplitude of the waveform distortion is less than 0.100 inches (2.35 percent of the actuator stroke). For the failures of channel 1 and 2, the actuator output is the same after the channel failure as before.

Figure VI-69 shows the effect of sequentially applying negative hardover failure inputs into channels 1A, 2A and 3A with the system operating with a sinusoidal input of 0.3 Hz. There is minor distortion of the output waveform with the first two channel failures and transfer to the fail-centered mode of operation with the third failure. As with the positive hardover failures, the waveform distortion is less than 2.35 percent of the actuator stroke.

Figure VI-70 shows the effect of sequentially grounding the input of channels 1A, 2A and 3A with the system biased to a 50-percent extend position and operating with a 0.3 Hz sinusoidal input. The Logic Processor correctly identifies each failure. The first two failures create a change in the output of one division on the data recording or 0.10 inch in amplitude. The distortion is 2.4 percent of the actuator stroke. After the third input failure, the actuator correctly transfers to the fail-centered mode. Note that the failure indication channel for Channel 1 does not indicate failure transfer until 0.5 seconds after the failure. This was due to a pen misalignment and not the operation of the Logic Processor.

Figure VI-71 shows the effect of sequentially grounding the input of channels 1A, 2A and 3A with the system biased to a 50-percent retract position and operating with a 0.3 Hz sinusoidal input. As with the extend bias failures, the failures cause a temporary distortion of the output of the actuator amounting to less than 2.5 percent of the actuator stroke. Upon the third failure, the actuator correctly transfers to the fail-centered mode.

Pressure Failure Transients

Figures VI-72 and VI-73 show the effect of hydraulic pressure failures on the output of the actuator. A 0.1 Hz triangular waveform is applied to all three channels. Figure VI-72 shows the failure of P1 and then P2. With the failure of P1 there is no output change in the actuator motion. With the failure of P2 (P1 already failed), the output motion of the actuator stops (the actuator has transferred to the fail-centered mode with loss of both hydraulic pressures). With the restoration of P2, the actuator motion resumes and does not change with the subsequent restoration of P1. Figure VI-73 indicates similar results for a different sequence of pressure failures and restoration. Note that the failure logic for the control channels does not detect hydraulic failures. The failure detection for hydraulic pressures is automatic for transferring to the fail-centered mode (since the transfer is controlled by the pressure output of the solenoid valves).

TEST DATA

Test Item - Dynamic Controls, Inc.
F-16 Direct Drive Servoactuator
Logic Processor

Date
Prepared: 4/10/87

Test - Dynamic Failure Transient - Condition 17
Negative Hardovers

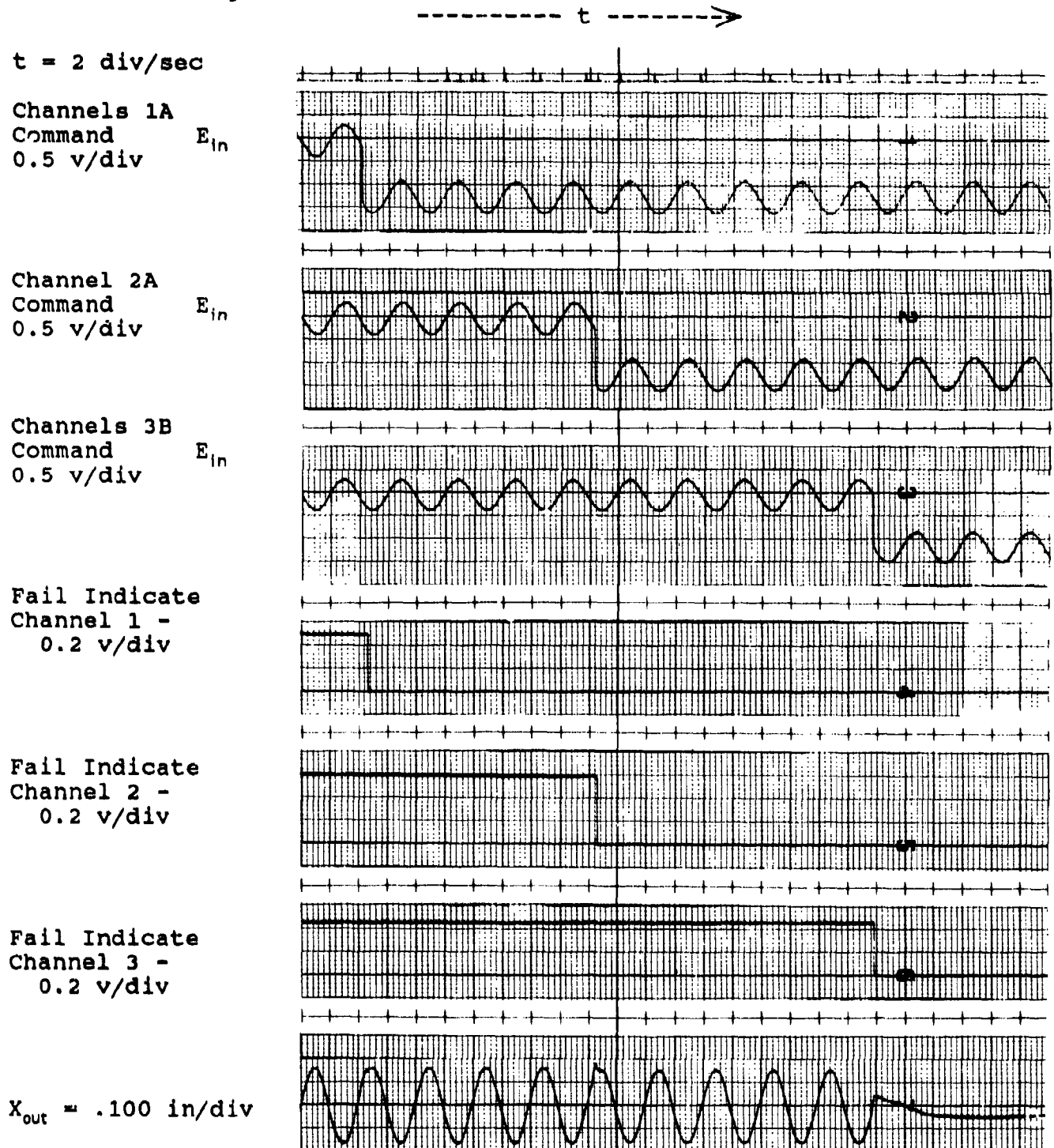


Figure VI-69. Dynamic failure transients - condition 17.

TEST DATA

Test Item - Dynamic Controls, Inc.
F-16 Direct Drive Servoactuator
Logic Processor

Date

Prepared: 4/10/87

Test - Grounded Input Failure at 50% Extend - Condition 18

----- t ----->

t = 2 div/sec

Channels 1A
Command
0.2 v/div

Channel 2A
Command
0.2 v/div

Channels 3A
Command
0.2 v/div

Fail Indicate
Channel 1 -
0.2 v/div

Fail Indicate
Channel 2 -
0.2 v/div

Fail Indicate
Channel 3 -
0.2 v/div

X_{out} = 0.10 in/div

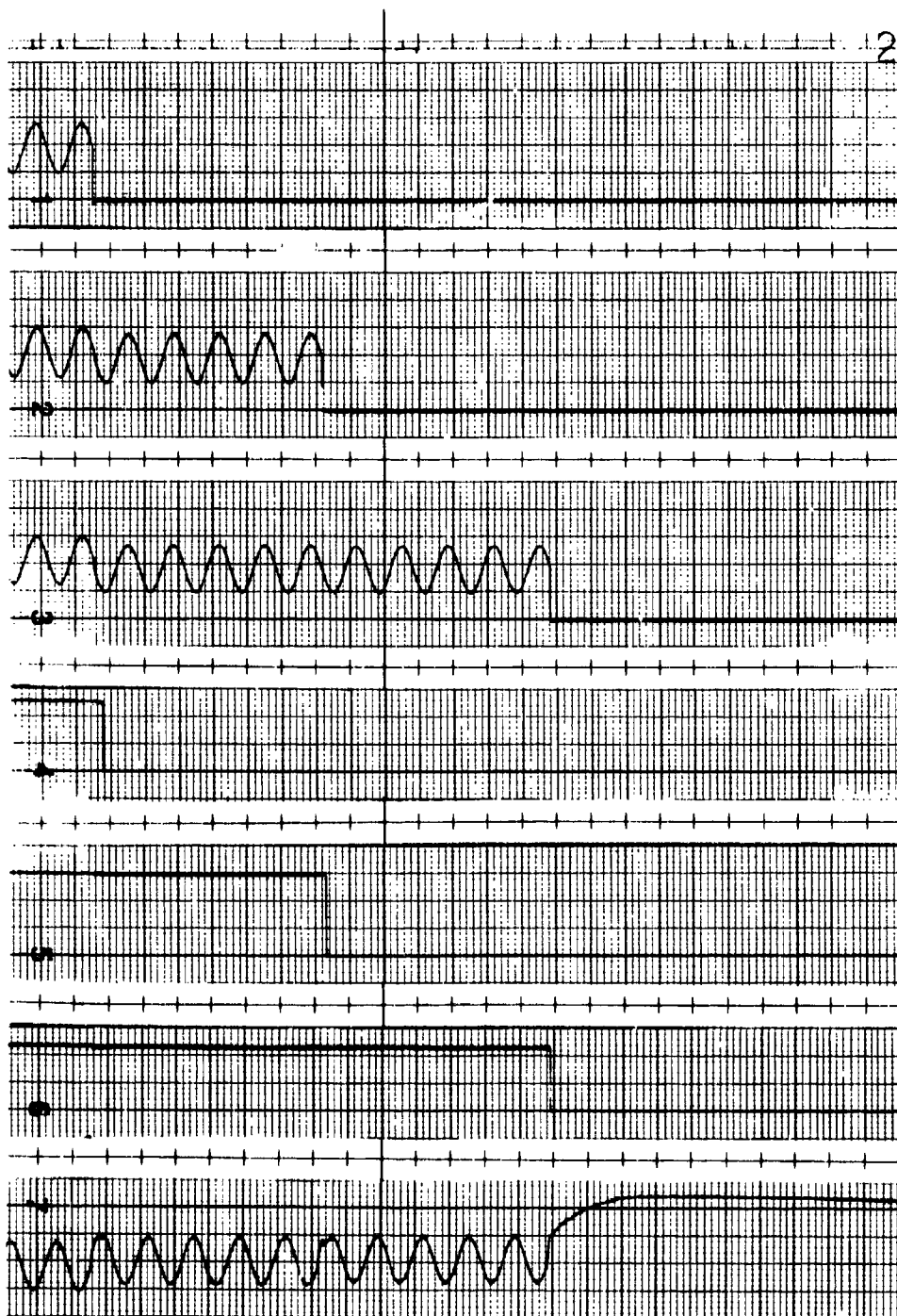


Figure VI-70. Dynamic failure transients - condition 18.

TEST DATA

Test Item - Dynamic Controls, Inc.
F-16 Direct Drive Servoactuator
Logic Processor

Date
Prepared: 4/10/87

Test - Grounded Input Failure at 50% Retract - Condition 19
----- t ----->

t = 2 div/sec

Channels 1A
Command
0.2 v/div

Channel 2A
Command
0.2 v/div

Channels 3A
Command
0.2 v/div

Fail Indicate
Channel 1 -
0.2 v/div

Fail Indicate
Channel 2 -
0.2 v/div

Fail Indicate
Channel 3 -
0.2 v/div

X_{out} = 0.100 in/div

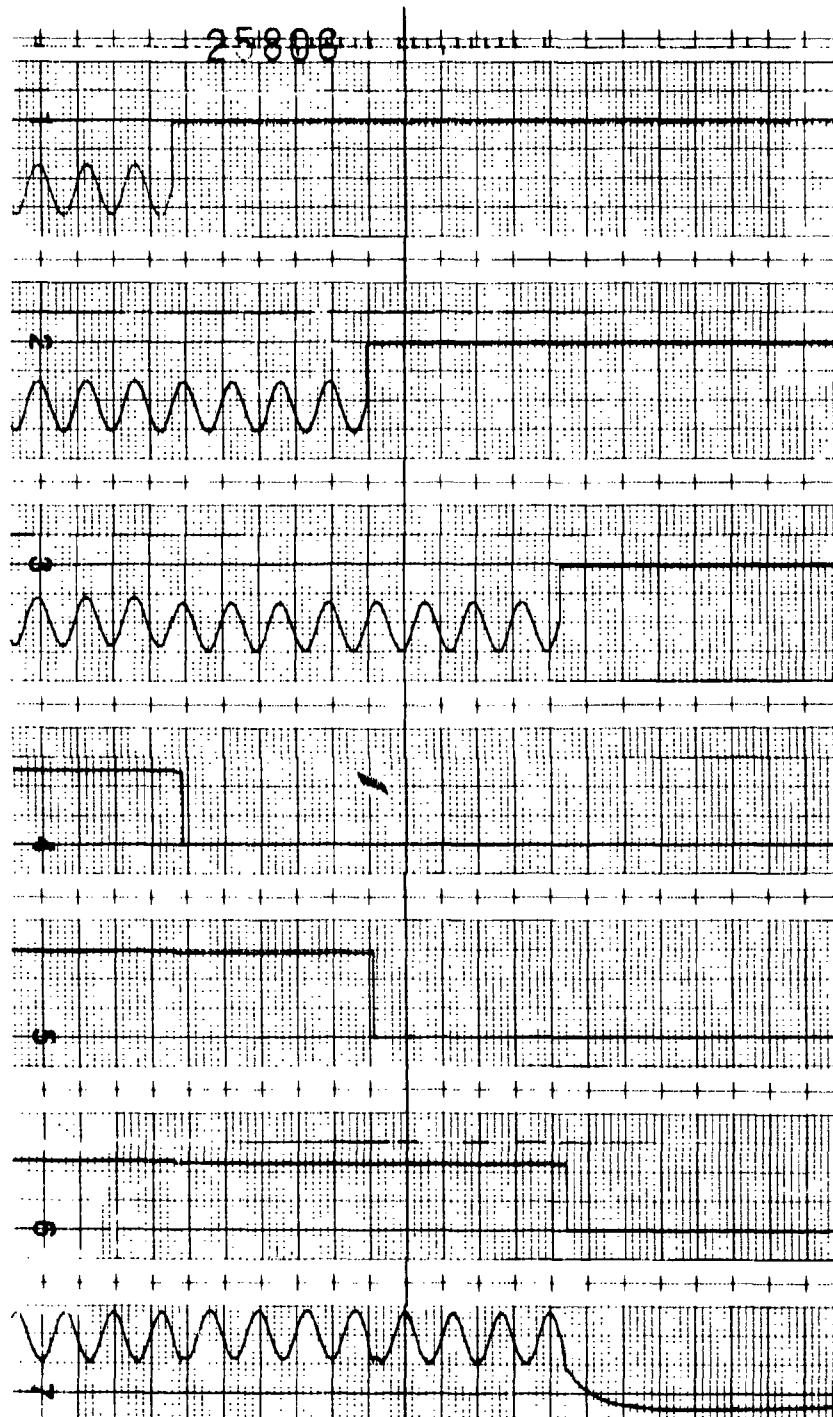


Figure VI-71. Dynamic failure transients - condition 19.

TEST DATA

Test Item - Dynamic Controls, Inc.
F-16 Direct Drive Servoactuator
Logic Processor

Date
Prepared: 4/6/87

Test - Pressure Failures (P_1 & P_2)

$t = 1 \text{ div/sec}$

Command
.010 v/div E_{in}

Hydraulic
Pressure

3000 psi
 P_1
0 psi

Hydraulic
Pressure

3000 psi
 P_2
0 psi

Fail Indicate
Channel 1 -
2.0 v/div

Fail Indicate
Channel 2 -
2.0 v/div

Fail Indicate
Channel 3 -
2.0 v/div

$X_{out} = .005 \text{ in/div}$

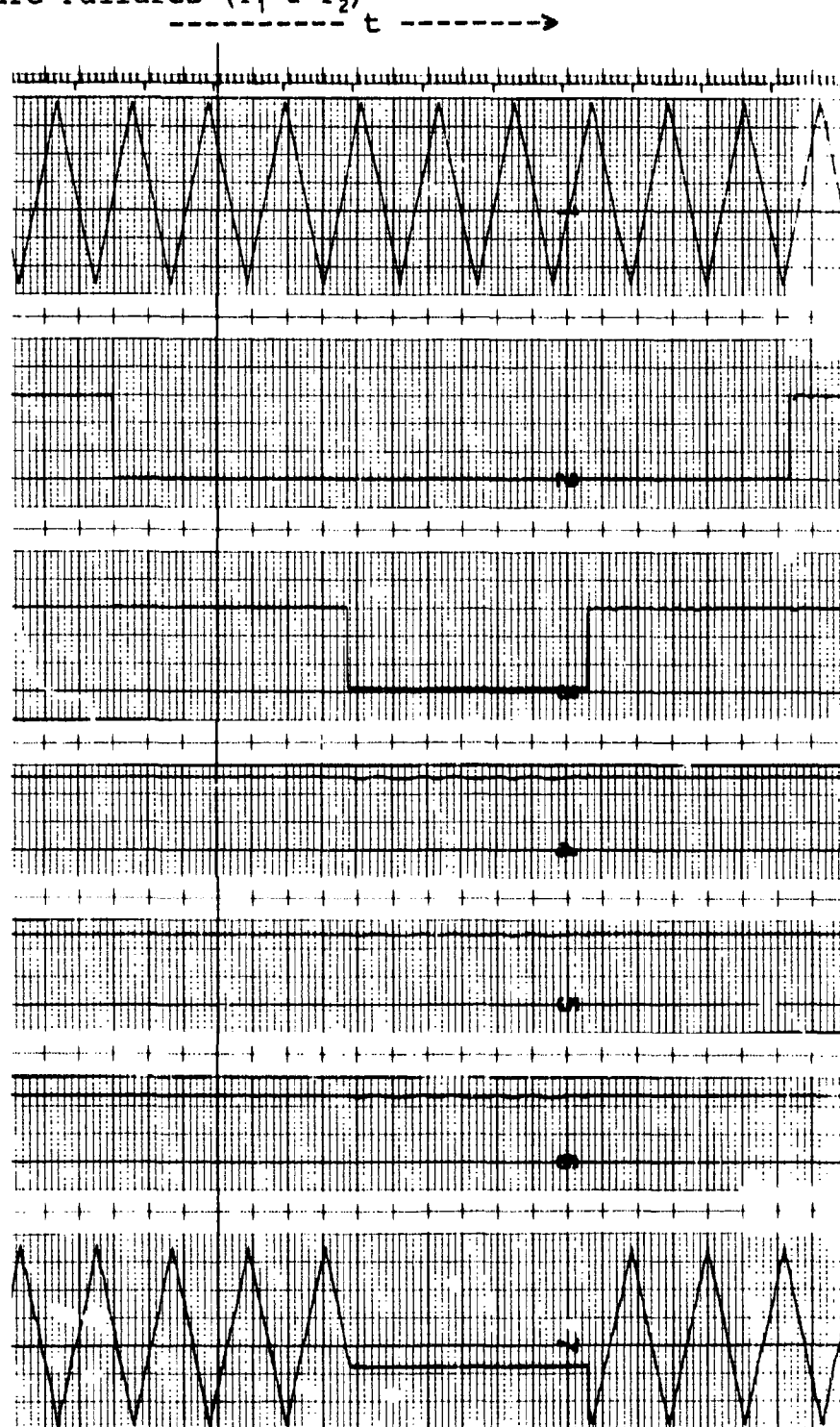


Figure VI-72. Slowover failure transients - condition 21.

TEST DATA

Test Item - Dynamic Controls, Inc.
F-16 Direct Drive Servoactuator
Logic Processor

Date
Prepared: 4/6/87

Test - Pressure Failures (P_1 & P_2)

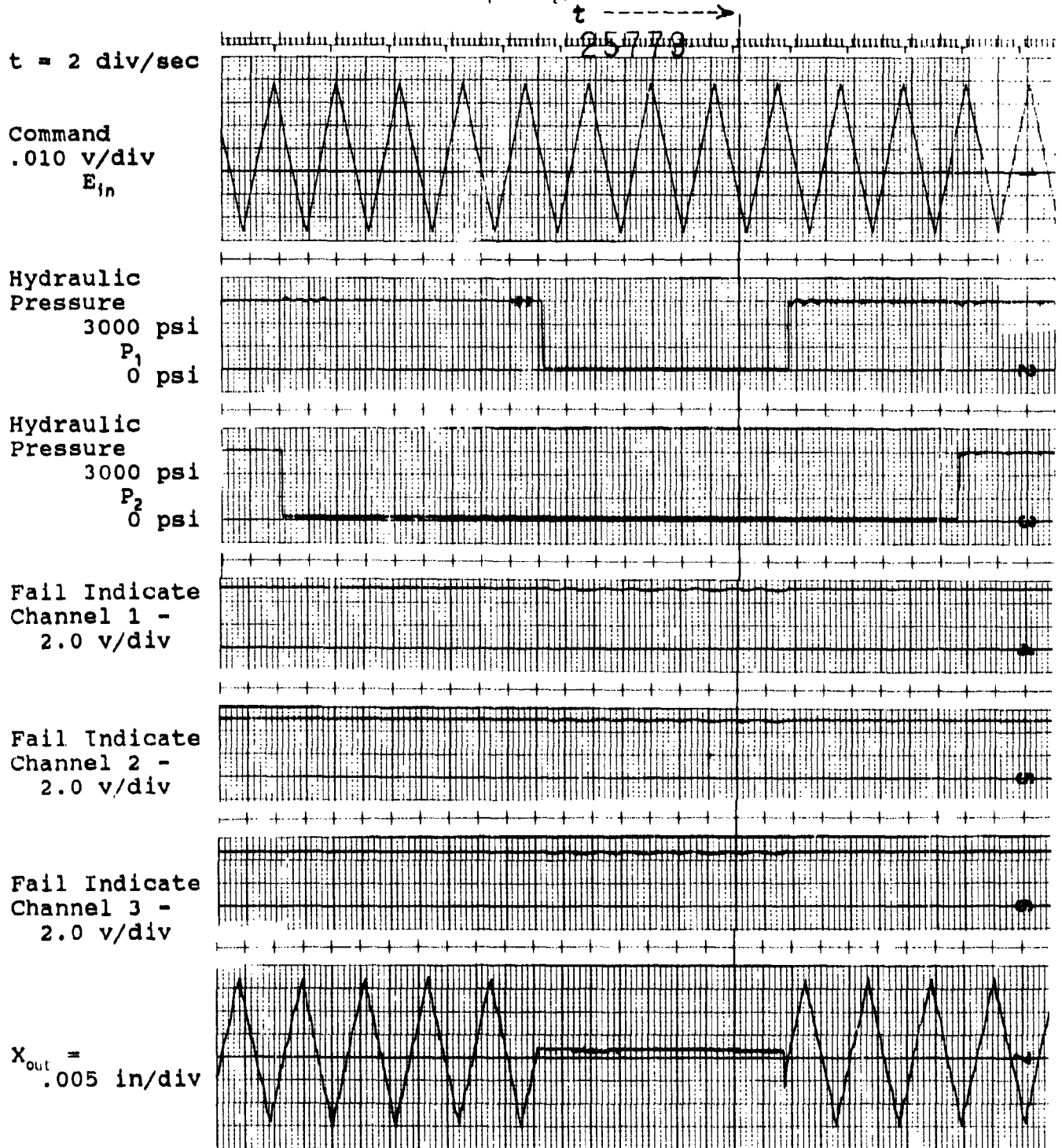


Figure VI-73. Slowover failure transients - condition 22.

Current Failure Transients - Logic Processor

The Logic Processor monitored the current output of the two servoamplifiers in a channel. Upon a current disagreement, the channel was failed. Channel failure was implemented by grounding the inputs to the servoamplifiers. The analog mechanization used a cross-strap so that failures of one of the two servoamplifiers of a channel was offset by the output of the remaining good servoamplifier, and grounding the servoamplifier inputs was effective in disabling the channel. With the Logic Processor, the cross-strap between the amplifiers of a channel was opened. For the Logic Processor the channel disconnect would normally be accomplished by disconnecting the servoamplifier from the force motor coils using solid-state switches.

Figures VI-74 and VI-75 are representative of the test results from test conditions 23 through 28. Figure VI-74 shows the test results of condition 23 with the sequential application of a hardover to one amplifier of the channels 1, 2 and 3 using the optical coupler OC7. The failure command was applied manually and held until the channel failure indication occurred. Note that the failure command to OC7 is a grounding of pin 2 of the opto-coupler, causing a 10 volt DC input into the servoamplifier. The actuator output for the hardover input for the first failure is .05 inches (or 1.17 percent of the actuator stroke). The actuator output change for the failure into channel 2 causes an actuator change of 0.10 inches or 2.34 percent of the actuator stroke. Upon the application of the third failure, the actuator moves off until the channel failure is declared and the actuator transfers to the fail-centered rnode. The small actuator change with the first two failures is a result of a force-fight between the control channels. Even without the cross-strap between amplifiers of a channel, there is a coupling between amplifiers via actuator motion. A failed servoamplifier causes an error signal which causes the other servoamplifiers to offset the failed amplifier. For the first (channel 1) failure, there are five other amplifiers to offset the hardover of the one amplifier (one in channel 1, two in channels 2 and 3).

Note that after the channel is declared failed, the failure input is removed, simulating the disconnect of the channel from the force motor coils. The larger failure transient after the third failure is due to not disconnecting the force motor coils upon the failure and having no offsetting amplifier in channel 3 after the failure is declared (the input to the remaining servoamplifier is grounded upon channel failure). The actuator moves off in response to the servoamplifier until the failure logic transfers (via the solenoid valves) the actuator to the fail-centered mode. With coil disconnecting (as would normally be used) the last transient would be much smaller. Figure VI-75 shows the results of test condition 25 with a different order of failures. The results are similar to test condition 23.

TEST DATA

Test Item -Dynamic Controls, Inc.
F-16 Direct Drive Servoactuator
Logic Processor

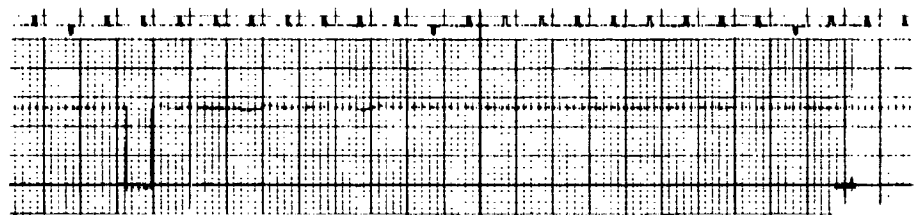
Date

Prepared: 5/18/87

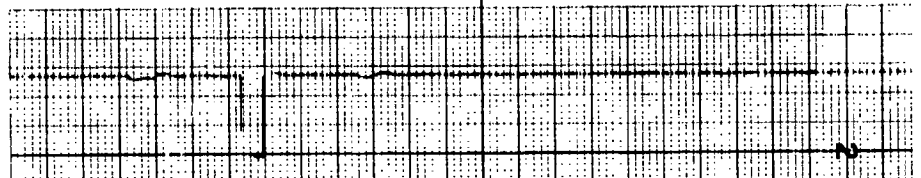
Test - Current Failures - Channels 1, 2, and 3
----- t ----->

t = 5 div/sec

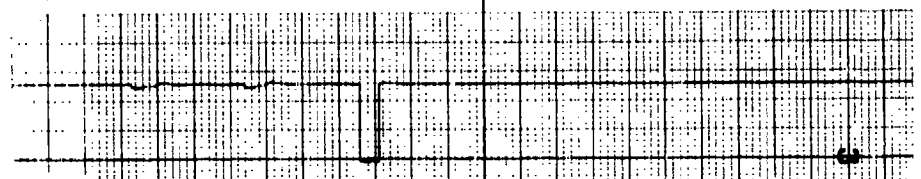
Channel 1
Command to OC7
2.0 v/div



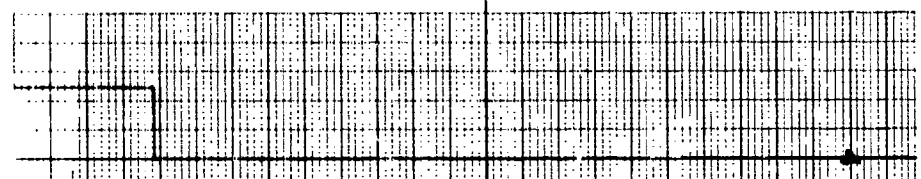
Channel 2
Command to OC7
2.0 v/div



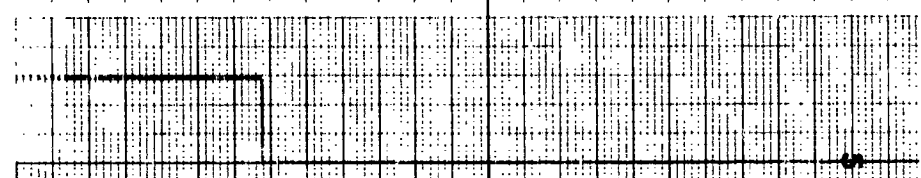
Channels 3
Command to OC7
2.0 v/div



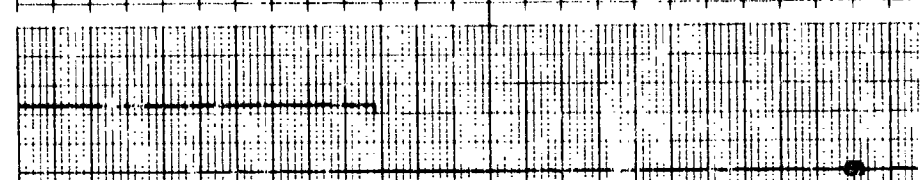
Fail Indicate
Channel 1 -
0.2 v/div



Fail Indicate
Channel 2 -
0.2 v/div



Fail Indicate
Channel 3 -
0.2 v/div



X_{out} = .050 in/div

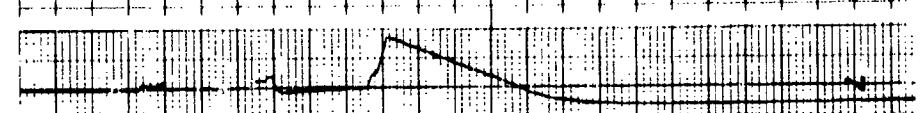


Figure VI-74. Current failure transients - condition 23.

TEST DATA

Test Item -Dynamic Controls, Inc.
F-16 Direct Drive Servoactuator
Logic Processor

Date
Prepared: 5/18/87

Test - Current Failures - Channels 1, 2, and 3
----- t ----->

t = 5 div/sec

Channel 1
Command to OC7
2.0 v/div

Channel 2
Command to OC7
2.0 v/div

Channels 3
Command to OC7
2.0 v/div

Fail Indicate
Channel 1 -
0.2 v/div

Fail Indicate
Channel 2 -
0.2 v/div

Fail Indicate
Channel 3 -
0.2 v/div

X_{out} = .050 in/div

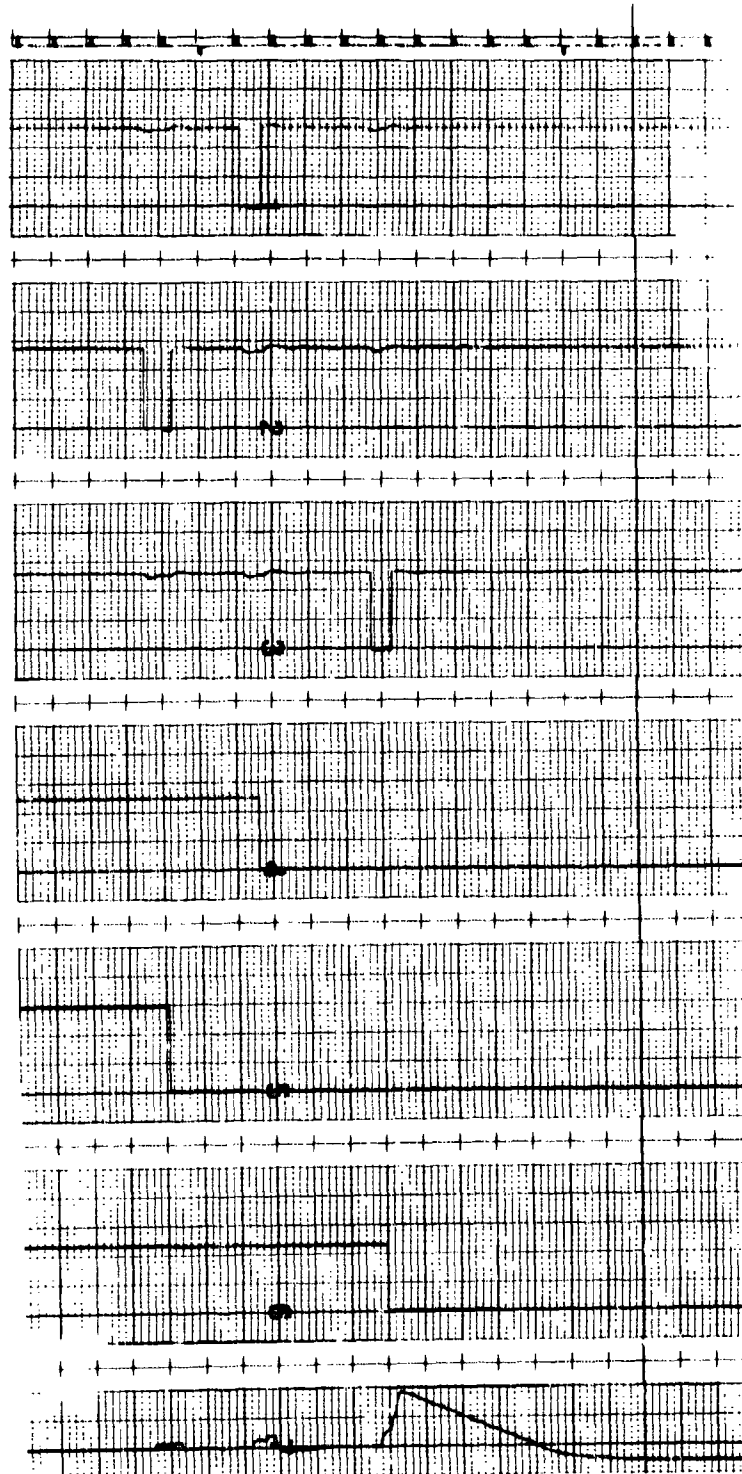


Figure VI-75. Current failure transients - condition 25.

Dynamic Failure Detection - Logic Processor

Figure VI-76 is a plot of the failure-detection amplitude of the Logic Processor for sinusoidal failure inputs. The figure shows that the failure-detection level is frequency and failure-count dependent. The inability of the detection logic to maintain a uniform detection level with sinusoidal inputs is a direct result of using a sampling system with a *failure count* requirement before a failure is declared. The number of samples before a failure is declared defines a time interval (or time delay). A sinusoidal input passes through zero amplitude at time intervals equal to one half the reciprocal of the input frequency. If the time for the sinusoid to pass through zero is less than the time interval to declare a failure, the failure is not detected. For a low frequency sinusoidal inputs, the time interval for the sinusoid passing through zero amplitude is much longer than the failure declaration time and the amplitude of the sinusoid for failure detection will be constant. Between the two preceding extremes is a range of input frequencies where detection of the failure requires increasing the input amplitude (to increase the amplitude of the sine wave either side of zero) so that more samples are counted as failures.

Figure VI-76 demonstrates the failure-detection characteristics of the Logic Processor set for 9, 19, 39 and 79 failure samples before a failure is declared. The sample time interval for the failure monitoring was .0014 seconds. As the number of failure counts required for failure declaration were increased from 9 to 79, the frequency up to which the detection level was constant decreased. The failure count setting of 9 was used for the Phase II evaluation. This setting gave a flat failure-detection amplitude up to 10 Hz. Having a failure-detection amplitude characteristic which increases with frequency is acceptable (perhaps desirable to exclude nuisance failure declarations) as long as the response is flat over the response band of the actuator being monitored.

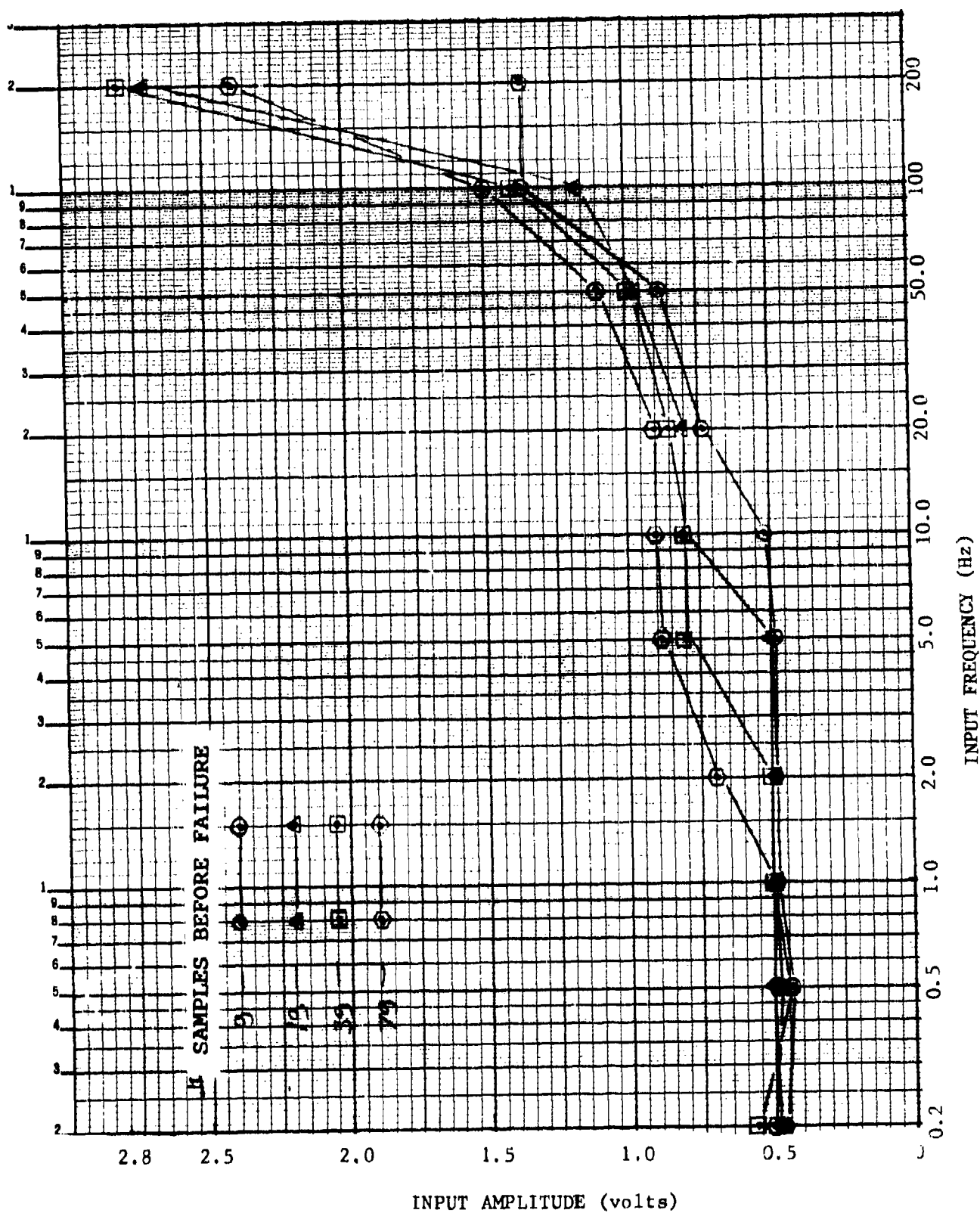


Figure VI-76. Dynamic failure detection - Logic Processor.

VI. CONCLUSIONS AND RECOMMENDATIONS

The F-16 direct drive actuator operated successfully and met or exceeded the performance requirements for the normal F-16 ISA. The frequency response capability of the direct drive actuator (in the normal operate mode) extended to nominally 5 times the normal F-16 actuator. The transients with hardover channel failures were considerably less than allowed for the normal F-16 ISA. The use of pulse width modulation to drive the direct drive force motors worked well and minimized the heat sink requirements for the driver amplifiers. The parts count for the direct drive mechanization was considerably less than that of the normal F-16 ISA.

Two performance characteristics which would require minor modification of the direct drive F-16 actuator were a low slew rate in the two-fail-operate mode and a light damping of the centering step response in the fail-centered mode. The low slew rate could easily be corrected by increasing the maximum current from the driving amplifiers without exceeding the operational rating of the driving electronics. The feedback linkage operated satisfactorily for most of the test series and then developed a "lightly-damped-response" characteristic. The cause of the change in the characteristic was not investigated because of time constraints.

The direct drive F-16 actuator was 0.5 lbs lighter than the normal F-16 actuator, an insignificant change. Although some improvement in the weight and volume of the actuator with the direct drive mechanization is still feasible, using mechanical feedback for the fail-centered mode creates a weight and volume penalty for the normal direct drive valve package valve which is difficult to overcome. The investigation indicated that direct drive valves do not inherently reduce the volume or weight of an actuator using conventional two stage servovalve control.

The use of electrical feedback for the operating modes of the direct drive actuator worked well. Including the direct drive force motors within the actuator's electrical feedback loop simplified the control system (no feedback around the spool position was required) and minimized the steady state power consumption of the force motors.

The F-16 ISA has a frequency response "gate" requirement, apparently because the actuator is used as part of structural mode filter design. The direct drive F-16 actuator electronics would require the addition of electronic input filters to meet the response gates. The electronic filters would dominate the actuator's frequency response. This approach is practical because of the extended response of the direct drive F-16 actuator in the operating modes. The alternative approach would be to gain change the control electronics upon control channel failure (with the normal operate response adjusted to meet the response gates).

The microprocessor monitoring of the control channel performance worked well and provided convenient changing of the failure detection characteristics. The failure transients with the particular settings of the processor were slightly larger than those measured with the analog monitoring, due to the time delay and detection level of the Logic Processor both being set slightly greater than the analog mechanization. The automatic pre-flight test checkout software worked well and provided a more convenient check of the control system operation than obtainable with the analog monitoring. It is recommended that the approach be investigated further with an emphasis in providing failure tolerance for the microprocessor.

APPENDIX A-2

PARTS LIST FOR F-16 DIRECT DRIVE

ITEM NO.	DWG. REF.	PART NO.	NAME	QTY REQD.	DESCRIPTION OF PART
1	R1	RN 55D	RESISTOR	1	50K
2	R2	RN 55D	RESISTOR	1	50K
3	R3	50LMF-149	LINEAR POT.	1	5.0K 5% MFGR: NEI.
4	R4	50LMF-149	LINEAR POT.	1	5.0K 5% MFGR: NEI.
5	R5	50LMF-149	LINEAR POT.	1	5.0K 5% MFGR: NEI.
6	R6	50LMF-149	LINEAR POT.	1	5.0K 5% MFGR: NEI.
7	R7	RN 55D	RESISTOR	1	499K
8	R8	62M20	POT.	1	20K
9	R9	RN 55D	RESISTOR	1	50K
10	R10	RN 55D	RESISTOR	1	50K
11	R11	RN 55D	RESISTOR	1	50K
12	R12	RN 60D	RESISTOR	1	500 OHM
13	R13	RN 60D	RESISTOR	1	500 OHM
14	R14	RN 60D	RESISTOR	1	500 OHM
15	R15	RN 55D	RESISTOR	1	499K
16	R16	62M20	POT.	1	20K
17	R17	RN 55D	RESISTOR	1	50K
18	R18	RN 55D	RESISTOR	1	100K
19	R19	RN 55D	RESISTOR	1	100K
20	R20	RN 55D	RESISTOR	1	100K
21	R21	62M20	POT.	1	20K

22	R22	RN55D	RESISTOR	1	100K
23	R23	RN55D	RESISTOR	1	20K
24	R24	RN55D	RESISTOR	1	24.3K
25	R25	62M5	POT.	1	5K
26	R26	RN55D	RESISTOR	1	1K
27	R27	RN55D	RESISTOR	1	24.3K
28	R28	62M5	POT.	1	5K
29	R29	RN55D	RESISTOR	1	1K
30	R30	RN55D	RESISTOR	1	10K
31	R31	RN55D	RESISTOR	1	5K
32	R32	62M200	POT.	1	200K
33	R33	RN60D	RESISTOR	1	2.4K
34	R34	RN55D	RESISTOR	1	12.5K
35	R35	RN55D	RESISTOR	1	4.99K
36	R36	RN55D	RESISTOR	1	1.87K
37	R37	RN55D	RESISTOR	1	6.98K
38	R38	62M1	POT.	1	1K
39	R39	62M10	POT.	1	10K
40	R40	RN55D	RESISTOR	1	6.98K
41	R41	RN55D	RESISTOR	1	50 OHM
42	R42	RN55D	RESISTOR	1	11K
43	R43	RN55D	RESISTOR	1	8.66K
44	R44	RN55D	RESISTOR	1	30K
45	R45	62M10	POT.	1	10K
46	R46	RN55D	RESISTOR	1	100K
47	R47	RN55D	RESISTOR	1	100K
48	R48	RN55D	RESISTOR	1	100K

49	R49	62M20	POT.	1	20K
50	R50	RN55D	RESISTOR	1	100K
51	R51	RN55D	RESISTOR	1	100K
52	R52	62M20	POT	1	20K
53	R53	RN55D	RESISTOR	1	50K
54	R54	RN55D	RESISTOR	1	12.1K
55	R55	RN55D	RESISTOR	1	20K
56	R56	RN55D	RESISTOR	1	100K
57	R57	62M20	POT.	1	20K
58	R58	RN55D	RESISTOR	1	100K
59	R59	RN55D	RESISTOR	1	90K
60	R60	RN55D	RESISTOR	1	90K
61	R61	RN55D	RESISTOR	1	100K
62	R62	RN55D	RESISTOR	1	100K
63	R63	62M10	POT.	1	10K
64	R64	RN55D	RESISTOR	1	100K
65	R65	RN55D	RESISTOR	1	100K
66	R66	RS-28	RESISTOR	1	1.5 OHM, 3 WATT
67	R67	RS-28	RESISTOR	1	1.5 OHM, 3 WATT
68	R68	RS-28	RESISTOR	1	2.0 OHM, 3 WATT
69	R69	RS-28	RESISTOR	1	1.5 OHM, 3 WATT
70	R70	RS-28	RESISTOR	1	1.0 OHM, 3 WATT
71	R71	RS-28	RESISTOR	1	1.0 OHM, 3 WATT
72	R72	RN55D	RESISTOR	1	2K
73	R73	RN55D	RESISTOR	1	10K
74	R74	RN55D	RESISTOR	1	8K
75	R75	RN55D	RESISTOR	1	69.7K

76	R76	62M2	POT.	1	2K
77	R77	RN55D	RESISTOR	1	887 OHM
78	R78	RN60D	RESISTOR	1	3.65K
79	R79	RN60D	RESISTOR	1	3.84K
80	R80	RN55D	RESISTOR	1	49.9K
81	R81	62M2	POT.	1	2K
82	R82	RN55D	RESISTOR	1	887 OHM
83	R83	RN60D	RESISTOR	1	3.84K
84	R84	RN55D	RESISTOR	1	49.9K
85	R85	62M2	POT.	1	2K
86	R86	RN55D	RESISTOR	1	887 OHM
87	R87	RN60D	RESISTOR	1	3.84K
88	R88	RN55D	RESISTOR	1	49.9K
89	R89	62M2	POT.	1	2K
90	R90	RN55D	RESISTOR	1	887 OHM
91	R91	RN55D	RESISTOR	1	6.98K
92	R92	62M1	POT.	1	1K
93	R93	RN55D	RESISTOR	1	6.98K
94	R94	62M10	POT.	1	10K
95	R95	RN55D	RESISTOR	1	50 OHM
96	R96	RN55D	RESISTOR	1	11K
97	R97	RN55D	RESISTOR	1	8.66K
98	R98	RN55D	RESISTOR	1	30.1K
99	R99	RN55D	RESISTOR	1	100K
100	R100	62F20	POT.	1	20K
101	R101	RN55D	RESISTOR	1	100K
102	R102	62M10	POT.	1	10K

103	R103	RN 55D	RESISTOR	1	100K
104	R104	RN 55D	RESISTOR	1	100K
105	R105	RN 55D	RESISTOR	1	50K
106	R106	RN 55D	RESISTOR	1	100K
107	R107	RN 55D	RESISTOR	1	20K
108	R108	62M20	POT.	1	20K
109	R109	RN 55D	RESISTOR	1	100K
110	R110	62M20	POT.	1	20K
111	R111	RN 55D	RESISTOR	1	100K
112	R112	RN 55D	RESISTOR	1	90K
113	R113	RN 55D	RESISTOR	1	90K
114	R114	RN 55D	RESISTOR	1	100K
115	R115	RN 55D	RESISTOR	1	10K
116	R116	RN 55D	RESISTOR	1	100K
117	R117	RN 55D	RESISTOR	1	10K
118	R118	RS-28	RESISTOR	1	2.0 OHM, 3 WATT
119	R119	RS-28	RESISTOR	1	1.5 OHM, 3 WATT
120	R120	RS-28	RESISTOR	1	1.5 OHM, 3 WATT
121	R121	RS-28	RESISTOR	1	1.5 OHM, 3 WATT
122	R122	RN 55D	RESISTOR	1	100K
123	R123	RS-28	RESISTOR	1	1.0 OHM, 3 WATT
124	R124	RS-28	RESISTOR	1	1.0 OHM, 3 WATT
125	R125	RN 55D	RESISTOR	1	2K
126	R126	RN 55D	RESISTOR	1	10K
127	R127	RN 55D	RESISTOR	1	8K
128	R128	RN 55D	RESISTOR	1	12.1K
129	R129	RN 55D	RESISTOR	1	100K

129	R129	RN55D	RESISTOR	1	100K
130	R131	RN55D	RESISTOR	1	10K
131	R131	RN55D	RESISTOR	1	4.3K
132	R132	RN60D	RESISTOR	1	3.84K
133	R133	RN55D	RESISTOR	1	10K
134	R134	RN55D	RESISTOR	1	100K
135	R135	RN55D	RESISTOR	1	5K
136	R136	RN55D	RESISTOR	1	7.5K
137	R137	RN55D	RESISTOR	1	46K
138	R138	RN55D	RESISTOR	1	10K
139	R139	RN55D	RESISTOR	1	4.99K
140	R140	RN55D	RESISTOR	1	49.9K
141	R141	RN55D	RESISTOR	1	46K
142	R142	RN55D	RESISTOR	1	10K
143	R143	RN55D	RESISTOR	1	49.9K
144	R144	RN55D	RESISTOR	1	4.99K
145	R145	RN55D	RESISTOR	1	46K
146	R146	RN55D	RESISTOR	1	10K
147	R147	RN55D	RESISTOR	1	4.99K
148	R148	RN55D	RESISTOR	1	49.9K
149	R149	RN55D	RESISTOR	1	49.9K
150	C1	V17246L	CAPACITOR	1	.0047 mf
151	C2	V17246L	CAPACITOR	1	.0047 mf
152	C3	86122G1	CAPACITOR	1	.5 mf
153	C4	CK05BX472K	CAPACITOR	1	.0047mf
154	C5	CK05BX221K	CAPACITOR	1	220pf
155	C6	B556KM	CAPACITOR	1	56mf

157	C8	B556KM	CAPACITOR	1	56mf
158	C9	CK06BX103K	CAPACITOR	1	.01mf
159	C10	CK05BX104K	CAPACITOR	1	.1mf
160	C11	CK05BX472K	CAPACITOR	1	.0047mf
161	C12	CK05BX472K	CAPACITOR	1	.0047mf
162	C13	B556KM	CAPACITOR	1	56mf
163	C14	CK05BX103K	CAPACITOR	1	.01mf
164	C15	CK05BX221K	CAPACITOR	1	220pf
165	C16	B556KM	CAPACITOR	1	56mf
166	C17	CK05BX103K	CAPACITOR	1	.01mf
167	C18	CK05BX104K	CAPACITOR	1	.1mf
168	C19	CK05BX101K	CAPACITOR	1	100pf
169	C20	CK05BX102K	CAPACITOR	1	.001mf
170	C21	CK05BX472K	CAPACITOR	1	4700pf
171	C22	CK06BX473K	CAPACITOR	1	.047mf
172	C23	CK06BX473K	CAPACITOR	1	.047mf
173	R150	RN55D	RESISTOR	1	1 MEG
174	R151	RN55D	RESISTOR	1	1 MEG
175	R152	RN55D	RESISTOR	1	1 MEG
176	D1	IN5530C	DIODE	1	10V @ 2% ZENER
177	D2	IN5530C	DIODE	1	10V @ 2% ZENER
178	D3	IN5530C	DIODE	1	10V @ 2% ZENER
179	D4	IN5530C	DIODE	1	10V @ 2% ZENER
180	D5	JAN IN914	DIODE	1	
181	D6	JAN IN914	DIODE	1	
182	D7	JAN IN914	DIODE	1	
183	D8	JAN IN5518B	DIODE	1	3.3V @ 2% ZENER

184	D9	JAN LN 5518B	DIODE	1	3.3V @ 2% ZENER
185	D10	JAN LN 914	DIODE	1	
186	D11	JAN LN 914	DIODE	1	
187	D12	JAN LN 914	DIODE	1	
188	D13	JAN LN 914	DIODE	1	
189	D14	JAN LN 5518B	DIODE	1	3.3V @ 2% ZENER
190	D15	JAN LN 5518B	DIODE	1	3.3V @ 2% ZENER
191	D16	JAN LN 914	DIODE	1	
192	D17	JAN LN 914	DIODE	1	
193	D18	JAN LN 914	DIODE	1	
194	D19	JAN LN 914	DIODE	1	
195	D20	JAN LN 914	DIODE	1	
196	D21	JAN LN 914	DIODE	1	
197	A1	OP-05 CY	OP. AMP.	1	MFGR: P.M.I.
198	A2	OP-05 CY	OP. AMP.	1	MFGR: P.M.I.
199	A3	OP-05 CY	OP. AMP.	1	MFGR: P.M.I.
200	A4	LM-339 N	OP. AMP.	1	COMPARATOR
201	A5	PM-747 CY	OP. AMP.	1	MFGR: P.M.I.
202	A6	OP-05 CY	OP. AMP.	1	MFGR: P.M.I.
203	A7	OP-05 CY	OP. AMP.	1	MFGR: P.M.I.
204	A8	BB-3572 A	PWR. AMP.	1	MFGR: BURR BROWN
205	A9	LM-2903N	OP. AMP.	1	COMPARATOR
206	A10	PM-747 CY	OP. AMP.	1	MFGR: P.M.I.
207	A11	OP-05 CY	OP. AMP.	1	MFGR: P.M.I.
208	A12	OP-05 CY	OP. AMP.	1	MFGR: P.M.I.
209	A13	BB-3572 A	PWR. AMP.	1	MFGR: BURR BROWN
210	A14	LM-339 N	OP. AMP.	1	COMPARATOR

211	OC-1	4N32	OPTO-COUPLER	1	MFGR: G.E.
212	OC-2	4N32	OPTO-COUPLER	1	MFGR: G.E.
213	OC-3	4N32	OPTO-COUPLER	1	MFGR: G.E.
214	OC-4	4N32	OPTO-COUPLER	1	MFGR: G.E.
215	OC-5	4N32	OPTO-COUPLER	1	MFGR: G.E.
216	OC-6	4N32	OPTO-COUPLER	1	MFGR: G.E.
217	OC-7	4N32	OPTO-COUPLER	1	MFGR: G.E.
218	OC-8	4N32	OPTO-COUPLER	1	MFGR: G.E.
219	R153	RN60D	RESISTOR	1	3.0K
220	R154	RN60D	RESISTOR	1	500 OHM
221	R155	RN60D	RESISTOR	1	500 OHM
222	R156	RN60D	RESISTOR	1	500 OHM
223	R157	RN60D	RESISTOR	1	500 OHM
224	R158	RN60D	RESISTOR	1	500 OHM
225	R159	RN60D	RESISTOR	1	1.0K
226	A15	LM-2903N	OP. AMP	1	COMPARATOR
227	OC-9	4N32	OPTO-COUPLER	1	MFGR: G.E.
228	OC-10	4N32	OPTO-COUPLER	1	MFGR: G.E.
229	OC-10	4N32	OPTO-COUPLER	1	MFGR: G.E.
230	OC-11	4N32	OPTO-COUPLER	1	MFGR: G.E.
231	OC-12	4N32	OPTO-COUPLER	1	MFGR: G.E.
232	OC-13	4N32	OPTO-COUPLER	1	MFGR: G.E.
233	OC-14	4N32	OPTO-COUPLER	1	MFGR: G.E.
234	R160	RN55D	RESISTOR	1	10K
235	R161	RN55D	RESISTOR	1	10K
236	A16	LM2903N	OP-AMP	1	COMPARATOR
237	A17	LM2903N	GP-AMP	1	COMPARATOR

238	R162	RN60D	RESISTOR	1	7K
239	R163	RN55D	RESISTOR	1	20K
240	R164	RN55D	RESISTOR	1	20K
241	R165	RN60D	RESISTOR	1	7K
242	R166	RN60D	RESISTOR	1	7K
243	R167	RN55D	RESISTOR	1	20K
244	R168	RN55D	RESISTOR	1	20K
245	R169	RN60D	RESISTOR	1	7K
246	R170	RN55D	RESISTOR	1	3.01K
247	R171	RN55D	RESISTOR	1	3.01K
248	R172	RN55D	RESISTOR	1	3.01K
249	R174	RN55D	RESISTOR	1	10K
250	D22	1N4002	DIODE	1	
251	D23	1N4002	DIODE	1	
252	J101	DCMF378	CONNECTOR	1	D SUB-MIN. CANNON
253	J102	DCMF378	CONNECTOR	1	D SUB-MIN. CANNON
254	J103	DCMF378	CONNECTOR	1	D SUB-MIN. CANNON
255	J104	DBMF258	CONNECTOR	1	D SUB-MIN. CANNON
256	J105	DBMF258	CONNECTOR	1	D SUB-MIN. CANNON
257	J106	DBMF258	CONNECTOR	1	D SUB-MIN. CANNON
258	J107	DBMF258	CONNECTOR	1	D SUB-MIN. CANNON
259	J108	DBMF258	CONNECTOR	1	D SUB-MIN. CANNON
260	J109	DBMF258	CONNECTOR	1	D SUB-MIN. CANNON
261	J110	DAMF158	CONNECTOR	1	D SUB-MIN. CANNON
262	J111	DAMF158	CONNECTOR	1	D SUB-MIN. CANNON
263	J112	DAMF158	CONNECTOR	1	D SUB-MIN. CANNON
264	J113	DAMF158	CONNECTOR	1	D SUB-MIN. CANNON

265	P 101	DCM37PG	CONNECTOR	1	D SUB-MIN. CANNON
266	P 102	DCM37PG	CONNECTOR	1	D SUB-MIN. CANNON
267	P 103	DCM37PG	CONNECTOR	1	D SUB-MIN. CANNON
268	P 104	DBM25PG	CONNECTOR	1	D SUB-MIN. CANNON
269	P 105	DBM25PG	CONNECTOR	1	D SUB-MIN. CANNON
270	P 106	DBM25PG	CONNECTOR	1	D SUB-MIN. CANNON
271	P 107	DBM25PG	CONNECTOR	1	D SUB-MIN. CANNON
272	P 108	DBM25PG	CONNECTOR	1	D SUB-MIN. CANNON
273	P 109	DBM25PG	CONNECTOR	1	D SUB-MIN. CANNON
274	P 110	DAM15PG	CONNECTOR	1	D SUB-MIN. CANNON
275	P 111	DAM15PG	CONNECTOR	1	D SUB-MIN. CANNON
276	P 112	DAM15PG	CONNECTOR	1	D SUB-MIN. CANNON
277	P 113	DAM15PG	CONNECTOR	1	D SUB-MIN. CANNON
278	P 1	KPT06F 14-5S	CONNECTOR	1	MIN.-CIRC. CANNON
279	P 2	KPT06F 14-5P	CONNECTOR	1	MIN.-CIRC. CANNON
280	P 3	KPT06F 14-58X	CONNECTOR	1	MIN.-CIRC. CANNON
281	P 4	KPT06F 20-16P	CONNECTOR	1	MIN.-CIRC. CANNON
282	P 5	KPT06F 20-16S	CONNECTOR	1	MIN.-CIRC. CANNON
283	P 6	KPT06F 18-11P	CONNECTOR	1	MIN.-CIRC. CANNON
284	P 7	KPT06F 18-11S	CONNECTOR	1	MIN.-CIRC. CANNON
285	P 8	KPT06F 20-39P	CONNECTOR	1	MIN.-CIRC. CANNON
286	P 9	KPT06F 18-32P	CONNECTOR	1	MIN.-CIRC. CANNON
287	P 10&A	KPT06F 14-18P	CONNECTOR	2	MIN.-CIRC. CANNON
288	P 11	KPT06F 18-32PX	CONNECTOR	1	MIN.-CIRC. CANNON
289	P 12&A	KPT06F 14-18PX	CONNECTOR	2	MIN.-CIRC. CANNON
290	P 13&A	KPT06F 14-18PY	CONNECTOR	2	MIN.-CIRC. CANNON
291	P 14	KPT06F 18-32S	CONNECTOR	1	MIN.-CIRC. CANNON

292	P 15	KPT06F 14-158	CONNECTOR	1	MIN.-CIRC. CANNON
293	P 16	KPT06F 14-158X	CONNECTOR	1	MIN.-CIRC. CANNON
294	P 17	KPT06F 14-158Y	CONNECTOR	1	MIN.-CIRC. CANNON
295	J1	KPT02P 14-5P	CONNECTOR	1	MIN.-CIRC. CANNON
296	J2	KPT02P 14-5S	CONNECTOR	1	MIN.-CIRC. CANNON
297	J3	KPT02P 14-5PX	CONNECTOR	1	MIN.-CIRC. CANNON
298	J4	KPT02P 20-16S	CONNECTOR	1	MIN.-CIRC. CANNON
299	J5	KPT02P 20-16P	CONNECTOR	1	MIN.-CIRC. CANNON
300	J6	KPT02P 18-11S	CONNECTOR	1	MIN.-CIRC. CANNON
301	J7	KPT02P 18-11P	CONNECTOR	1	MIN.-CIRC. CANNON
302	J8	KPT02P 20-39S	CONNECTOR	1	MIN.-CIRC. CANNON
304	J9	KPT02P 18-32S	CONNECTOR	1	MIN.-CIRC. CANNON
305	J10	KPT02P 14-18S	CONNECTOR	1	MIN.-CIRC. CANNON
306	J11	KPT02P 18-32SX	CONNECTOR	1	MIN.-CIRC. CANNON
307	J12	KPT02P 14-18SX	CONNECTOR	1	MIN.-CIRC. CANNON
308	J13	KPT02P 14-18SY	CONNECTOR	1	MIN.-CIRC. CANNON
309	J14	KPT02P 18-32P	CONNECTOR	1	MIN.-CIRC. CANNON
310	J15	KPT02P 14-15P	CONNECTOR	1	MIN.-CIRC. CANNON
311	J16	KPT02P 14-15PX	CONNECTOR	1	MIN.-CIRC. CANNON
312	J17	KPT02P 14-15PY	CONNECTOR	1	MIN.-CIRC. CANNON

APPENDIX A-3

(PASCII)

LOGIC PROCESSOR PROGRAM

```

;F16A.ASM1/29/86
;LAST CHANGE 6/19/87
; RE-ADDRESS TO USE AUTO JUMP XXXXX
; PUT DUMP BACK IN FOR MORE DEBUGGING
; PRINTS DATA ON FAILS WHEN BYTE AT DUMP (C9H)
; CHANGED TO 00
; CORRECT COUNTER STORAGE ADDRESS
;
; MACHINE CODE LOCATED AT 0E000H (2816 EEPROM)
; TO RUN AUTO JUMP
; 0E000 210080;LXI H,08000H (SOURCE )
; 0E003 110001;LXI D,0100H (DEST )
; 0E006 010010 ;LXI B,01000H (COUNT )
; 0E009 EDB0;Z80 BLOCK MOVE
; 0E00B C30001;JMP 0100H
; 0E00E END OF MACHINE CODE FOR AUTO JUMP
;
; MAIN CODE STORED AT 08000H IN 8K x 8 EEPROM
; IS DOWN LOADED TO 0100H TO RUN
;
F048 = CONINEQU 0F048H;Z-ASSIST MONITOR ROUTINES
F045 = CONOUT EQU 0F045H
F015 = HEX2EQU 0F015H
F018 = HEX4EQU 0F018H
F012 = MSOUTEQU 0F012H
F01E = CRLF EQU 0F01EH

;ANALOG ACCESS
0001 = C1CSAEQU 01H;CHANNEL 1 COMMAND SUM A
0000 = C1CSBEQU 00H;CHANNEL 1 COMMAND SUM B
0002 = C1CRAEQU 02H;CHANNEL 1 CURRENT A
0003 = C1CRBEQU 03H;CHANNEL 1 CURRENT B
000E = C2CSAEQU 0EH ;CHANNEL 2 COMMAND SUM A
000D = C2CSBEQU 0DH ;CHANNEL 2 COMMAND SUM B
000F = C2CRAEQU 0FH ;CHANNEL 2 CURRENT A
0018 = C2CRBEQU 18H ;CHANNEL 2 CURRENT B
0013 = C3CSAEQU 13H ;CHANNEL 3 COMMAND SUM A
0012 = C3CSBEQU 12H ;CHANNEL 3 COMMAND SUM B
0014 = C3CRAEQU 14H ;CHANNEL 3 CURRENT A
0015 = C3CRBEQU 15H ;CHANNEL 3 CURRENT B
;
;MASKS
0040 = MIO2AEQU 40H
0004 = SELFTEQU 00000100B;SELF TEST SWITCH
0010 = LSD1EQU 00010000B;TWS LSD 1 AND FAIL LED
0020 = LSD2EQU 00100000B;TWS LSD 2 AND PASS LED
0040 = LSD3EQU 01000000B;TWS LSD 4 AND CH3 CURR LED
0080 = LSD4EQU 10000000B;TWS LSD 8 AND CH3 G/S LED
0041 = MIO2BEQU 41H
0001 = ID1EQU 00000001B;TWS ID 1 AND CH3 MODEL LED
0002 = ID2EQU 00000010B;TWS ID 2 AND CH2 CURR LED o7 3
0004 = ID4EQU 00000100B;TWS ID 4 AND CH2 G/S LED
0008 = ID8EQU 00001000B;TWS ID 8 AND CH2 MODEL LED
0010 = MSD1EQU 00010000B;TWS MSD 1 AND CH1 CURR LED
70 3

```



```

0020 = MSD2EQU 00100000B;TWS MSD 2 AND CH1 G/S LED
0040 = MSD4EQU 01000000B;TWS MSD 4 & CH1 MODEL LED
0042 = MIO2CEQU 42H
004C = MIO1AEQU 4CH
000F = PWM3EQU 00001111B;PWM INJECT SELECT CH3
0020 = HDOV3EQU 00100000B;PWM FAIL INJECT CH3 (OC7-CURRENT)
0040 = FAILSW EQU 01000000B;FAIL SWITCH CH3
0080 = FINJ3EQU 10000000B;HARD OVER INJECT CH3 (OC8-MODEL)
004D = MIO1BEQU 4DH
000F = PWM2EQU 00001111B;PWM INJECT SELECT CH2
0020 = HDOV2EQU 00100000B;PWM FAIL INJECT CH2 (OC7)
0040 = FAILSW2 EQU 01000000B;FAIL SWITCH CH2
0080 = FINJ2EQU 10000000B;HARD OVER INJECT CH2 (OC8)
004E = MIO1CEQU 4EH
000F = PWM1EQU 00001111B;PWM INJECT SELECT CH1
0020 = HDOV1EQU 00100000B;PWM FAIL INJECT CH1 (OC7)
0040 = FAILSW1 EQU 01000000B;FAIL SWITCH CH1
0080 = FINJ1EQU 10000000B;HARD OVER INJECT CH1 (OC8)
008B = ANACHEQU 8BH;ANALOG CHANNEL TO CONVERT
008C = ANALEQU 8CH;PORT OF LOW 8 BITS A/D
008D = ANAEQU 8DH;UPPER 4 BITS A/D AND STAT
0080 = ANSTEQU 10000000B;ANALOG STATUS BIT MASK
; *****
; *****
; *****
; *****

```

```

0100          ORG 0100H

```

```

0100 C3FA07    JMP MAIN

```

```

0103 = INITABLE: EQU $;INITIATE TABLE (DEFAULT VALUES)
0103 0000000000 DB 0,0,0,0,0;DEC0-4
0108 0000000000 DW 0,0,0,0;COMSA-CURB
0110 010000      DB 1,0,0;CHANNEL SWITCH INTF
0113 6400        DW 100;HODLIM (.5V)
0115 3200        DW 50;CURLIM (.25V = .5AMP COIL)
0117 3C00        DW 60;TSTLIM
0119 6400        DW 100;TSTVAL
011B F401        DW 500;MAXCUR
011D 9001        DW 400;STMODLIMIT
011F 0500        DW 5;CNTMAX
0121 0000000000 DW 0,0,0;CHF1-3
0127 0000        DW 0;FLAGX
0129 000000      DB 0,0,0;CHFCNTRS
012C 000000      DB 0,0,0;CHFTYPES
012F =          INITENDEQU $

```

```

0200 = DSEEQU 0200H ;DATA BASE
0200 = DEC0EQU DSE;LSD OF DATA
0201 = DEC1EQU DSE+1;ID OF DATA o7 3
0202 = DEC2EQU DSE+2;MSD OF DATA
0203 = DEC3EQU DSE+3;LSD OF ADDR
0204 = DEC4EQU DSE+4;MSD OF ADDR
0205 = COMSUM EQU DSE+5

```



```

0207 = CONSUMB EQU DSE+7
0209 = CURAEQU DSE+9
020B = CURBEQU DSE+11
020D = CHANNEL EQU DSE+13
020E = SWITCHEQU DSE+14
020F = INTPEQU DSE+15
0210 = DATATABLE EQU DSE+16
0210 = MODELLIMIT EQU DSE+16;ADDR 0
0212 = CURLINEQU DSE+18;ADDR 1
0214 = TSTLINEQU DSE+20;ADDR 2
0216 = TESTVAL EQU DSE+22;ADDR 3
0218 = MAXCUREQU DSE+24;ADDR 4
021A = STMODLIM EQU DSE+26;ADDR 5
021C = CNTRMAX EQU DSE+28;ADDR 6
021E = CHF1EQU DSE+30;ADDR 7
0220 = CHF2EQU DSE+32;ADDR 8
0222 = CHF3EQU DSE+34;ADDR 9
0224 = FLAGXEQU DSE+36;ADDR 10
0226 = CH1CNTR EQU DSE+38;ADDR 11
0227 = CH2CNTR EQU DSE+39;ADDR 12
0228 = CH3CNTR EQU DSE+40;ADDR 13
022C = CH1FTYPE EQU DSE+44;ADDR 14
022D = CH2FTYPE EQU DSE+45;ADDR 15
022E = CH3FTYPE EQU DSE+46;ADDR 16
022F = STFLAG EQU DSE+47;ADDR 17
0232 = STATSAB EQU DSE+50;A PLACE TO SAVE
      ;STAT FOR PORT 40H
0234 = LOOPCEQU DSE+52;LOOP COUNTER

0300 CODEBEGINORG 0300H;BEGINNING OF SUBROUTINES
; *****
      ASCX;16 BIT ABSOLUTE SUBTRACT ((HL)-(DE))
0300 37 STC;SET THE CARRY FLAG
0301 3F CMC;COMPLIMENT CARRY
0302 7D MOV A,L
0303 93 SUB E
0304 6F MOV L,A
0305 7C MOV A,H
0306 9A SUB D
0307 67 MOV H,A
0308 C9 RET
; *****
      AREAD; ANALOG CH IS IN A LEAVES WITH VALUE IN HL
0309 D38B OUT 08EH
030B DB3D AWAIT;IN 08DH ;GET THE CONVERSION STAT
030D E680 ANI 080H ;LOGICAL AND (*),A=A*8
030F C20B03 JNZ AWAIT;WAIT TIL DONE
0312 DB8C IN 08CH;GET THE LOW BYTE
0314 6F MOV L,A;PUT IN L
0315 DB8D IN 08DH;GET THE HIGH NIBLE
0317 67 MOV H,A;SAVE A COPY IN H
      ; REMEMBER OFFSET BINARY INPUT 10V=FFF,0=800,-10V=0 o7 3
0318 C9 RET
; *****
      MTH1;FUNCTION - MODEL CHECK
      ;IF ABS(HL-DE)<=BC. THEN A=FFH ELSE A=0

```



```

0319 E5      PUSH H
031A D5      PUSH D
031B CD0003  CALL ASCX;SUBTRACT
031E D22803  JNC MTH1A;NO SO CARRY HL>DE
0321 E1      POP H;GET BACK IN REVERSE ORDER
0322 D1      POP D
0323 D5      PUSH D;COPY BACK ON STACK
0324 E5      PUSH H
0325 CD0003  CALL ASCX;SUBTRACT
              MTH1A;GOT ABS(HL-DE)
0328 D1      POP D;CLEAR THE COPIES
0329 D1      POP D
032A C5      PUSH B;MODEL LIMIT TO DE
032B D1      POP D
032C CD0003  CALL ASCX ;SHOULD BE CARRY FOR SELF TEST
032F DA3403  JC MTH1F
0332 AF      XRA A;SET A=0
0333 C9      RET
              MTH1F;FAILED
0334 AF      XRA A;SET A=0
0335 3D      DCR A;SET A=FF
0336 C9      RET
; *****
; IF (CUR+) OR
; MTH2;;FUNCTION - (+) GAIN CHECK
; (TV+TL) < ABS(CUR) < (TV-TL) THEN FAIL
; THEN A=FFH ELSE A=0
0337 7C      MOV A,H
0338 E608    ANI 08H;CHECK SIGN
033A C20004  JNZ MTHFS ;NOT A NEG SO SIGN FAIL
              ;HERE IF NEG CURRENT MAKE ABS
033D E5      PUSH H
033E D1      POP D
033F 210008  LXI H,0800H;CENTER OF SCALE
0342 CD0003  CALL ASCX;NORMALIZE CURRENT
0345 E5      PUSH H;SAVE ABS(CUR)
0346 2A1402  LHLD TSTLIM
0349 E5      PUSH H
034A D1      POP D
034B 2A1602  LHLD TESTVAL
034E 19      DAD D;X=TV+TL
034F D1      POP D;CURRENT TO DE,X TO HL
0350 D5      PUSH D ;SAVE A COPY FOR LATER
0351 CD0003  CALL ASCX;X-CUR
0354 DA6E03  JC MTHF1;IF C THEN CUR>TV+TL--FAILED
              ;MUST CLEAR 1 BEFORE LEAVING
              ;IF HERE PASS TV+TL<ABS(CUR)
              ;NOW CHECK TV-TL>ABS(CUR)
0357 2A1402  LHLD TSTLIM
035A E5      PUSH H
035B D1      POP D
035C 2A1602  LHLD TESTVAL
035F CD0003  CALL ASCX;TV-TL=Y
0362 D1      POP D;ABS(CUR) TO DE
0363 EB      XCHG;Y TO D,CUR TO HL
0364 CD0003  CALL ASCX;CUR-Y
0367 DA6F03  JC MTHF ;IF C THEN TV-TL>CUR--FAILED

```



```

036A AF      XRA A;SET A=0
036B C9      RET      ;STACK SOULD BE OK TO RETURN
              MTHF3: ;ENTER HERE TO CLEAR 3
036C D1      POP D
              MTHF2:;ENTER HERE TO CLEAR TWO FROM STACK
036D D1      POP D;CLEAR TL
036E E1      MTHF1:POP H;CLEAR TV
              MTHF:;ENTER HERE TO LEAVE FAILED
036F AF      XRA A;SET A=0
0370 3D      DCR A;SET A=FF
0371 C9      RET;RETURN FAILED
; *****
              MTH3:;FUNCTION - (-) GAIN CHACK
;IF (CURRENT-) OR
              ;(TV+TL) < ABS(CUR) < (TV-TL) THEN FAIL
              ;THEN A=FFH ELSE A=0
0372 7C      MOV A,H
0373 E608    ANI 08H;CHECK SIGN
0375 CA0004  JZ MTHF5 ;NOT A PLUS CURRENT SO FAIL
              ;HERE IF PLUS CURRENT MAKE ABS
0378 7C      MOV A,H
0379 E607    ANI 07H
037B 67      MOV H,A
037C E5      PUSH H;SAVE ABS(CUR)
037D 2A1602  LHLD TESTVAL
0380 E5      PUSH H
0381 D1      POP D
0382 2A1402  LHLD TSTLIM
0385 19      DAD D;TV+TL=X,,HL
0386 D1      POP D;GET ABS(CUR) TO DE
0387 D5      PUSH D ;NORMALIZED CURRENT ON STACK
0388 CD0003  CALL ASCX;X-CUR
038B DA6E03  JC MTHF1 ;IF C THEN CUR>TV+TL--FAILED
              ;MUST CLEAR 1 BEFORE LEAVING
              ;IF HERE PASS TV+TL<ABS(CUR)
              ;NOW CHECK TV-TL>ABS(CUR)
038E 2A1402  LHLD TSTLIM ;TL
0391 E5      PUSH H
0392 D1      POP D
0393 2A1602  LHLD TESTVAL;TV
0396 CD0003  CALL ASCX;TV-TL=Y
0399 D1      POP D
039A EB      XCHG;Y TO D,CUR TO HL
039B CD0003  CALL ASCX;CUR-Y
039E DA6F03  JC MTHF ;IF C THEN TV-TL>CUR--FAILED
03A1 AF      XRA A
03A2 C9      RET      ;STACK SHOULD BE OK TO RETURN
; *****
;
;
              MTH4:;FUNCTION - TEST OA
              ;IF ABS(HL)> TSTLIM THEN A=FFH ELSE A=0
              ;FORMAT      ABS(CUR)>TSTLIM
03A3 7C      MOV A,H
03A4 E608    ANI 08H
03A6 C2B303  JNZ MTH4A ;NOT CLEARED SO +CURRENT

```



```

03A9 EB      XCHG;CURRENT TO DE

03AA 210008   LXI H,0800H
03AD CD0003   CALL ASCX;NORMALIZE
03B0 C3B703   JMP MTH4B;GO CHECK
              MTH4A:; +CURRENT CLEAR MSB

03B3 7C      MOV A,H
03B4 E607    ANI 07H
03B6 67      MOV H,A
              MTH4B:;HERE TO CHECK AGAINST TESTLIMIT
03B7 EB      XCHG;ABS(CUR) TO DE
03B8 2A1402   LHLD TSTLIM;GET THE TEST LIMIT
03BB CD0003   CALL ASCX
03BE DA6F03   JC MTHF;IF C THEN ABS(CUR)>TSTLIM
03C1 AF      XRA A;SET A=0
03C2 C9      RET
; *****
MTH5:;FUNCTION ABS(HL-DE)>BC=FAIL
;FORMAT ABS(X)-(Y)>(LIMIT)
03C3 E5      PUSH H;SAVE COMSUMA
03C4 D5      PUSH D;SAVE COMSUMB
03C5 CD0003   CALL ASCX;COMSA-COMSB=Y
03C8 D2D303   JNC MTH5A;IF C THEN COMSUMA<COMSUMB
03CB E1      POP H ;SO DO THE OTHER WAY
03CC D1      POP D
03CD CD0003   CALL ASCX;COMSB-COMSA=X
03D0 C3D503   JMP MTH5B
MTH5A:;ALMOST READY TO CHECK
03D3 D1      POP D;CLEAR THE STACK
03D4 D1      POP D
MTH5B:;READY TO CHECK
03D5 EB      XCHG;X TO DE
03D6 C5      PUSH B
03D7 E1      POP H
03D8 CD0003   CALL ASCX;LIM-X
03DB DA6F03   JC MTHF;IF C THEN X>LIMIT
03DE AF      XRA A;ELSE PASSED, SET A=0
03DF C9      RET
; *****
MTH6:;FUNCTION
;ABS(DE)>MAXCUR=FAIL
;FORMAT ABS(CUR)>MAXCUR
03E0 7A      MOV A,D
03E1 E608    ANI 08H
03E3 C2F003   JNZ MTH6A;+VALUE
03E6 210008   LXI H,0800H
03E9 CD0003   CALL ASCX ;NORMALIZE NEG VALUE
03EC EB      XCHG;NORM TO DE
03ED C3F503   JMP MTH6B;GO CHECK
MTH6A:;PLUS VAL
03F0 7A      MOV A,D
03F1 E607    ANI 07H
03F3 57      MOV D,A
03F4 EB      XCHG;CURRENT TO DE
MTH6B:;CHECK LIMIT
03F5 2A1802   LHLD MAXCUR
03F8 CD0003   CALL ASCX;LIMIT-ABS(VALUE)

```



```

03FB DA6F03    JC MTHF ;IF C THEN ABS(VAL)> LIMIT
03FE AF        XRA A

```

```

03FF C9        RET
; *****
MTHFS:;SIGN FAIL
0400 3E80      MVI A,080H
0402 C9        RET
; *****

```

```

INITIALIZE:;
0403 3E01      MVI A,1
0405 320D02    STA CHANNEL
0408 3EAF      MVI A,0AFH;OPERATE CODE
040A D34C      OUT 4CH
040C D34D      OUT 4DH
040E D34E      OUT 4EH
0410 AF        XRA A
0411 321E02    STA CHF1
0414 322002    STA CHF2
0417 322202    STA CHF3
041A 322602    STA CH1CNTR
041D 322702    STA CH2CNTR
0420 322802    STA CH3CNTR
0423 D341      OUT 41H
0425 320F02    STA INTF
0428 3E04      MVI A,04H
042A D340      OUT 40H
042C 210301    LXI H,INITABLE
042F 110002    LXI D,DSE
0432 012C00    LXI B,INITEND-INITABLE
0435 EDB0      DB 0EDH,0B0H;280 LDIR BLOCK MOV
0437 C9        RET
; *****

```

```

DELAY1:;FIXED DELAY
0438 210010    LXI H,1000H
DELAY:;
043B 10FE      DB 10H,0FEH;DJNZ FOR 280
043D 2B        DCX H
043E 7C        MOV A,H
043F B5        ORA L
0440 C23B04    JNZ DELAY
0443 C9        RET
; *****

```

```

STCHECK: ; THIS IS THE SUBROUTINE WHICH HANDLES THE
; TESTING OF THE CURRENTLY LOGGED CHANNEL
; IN THE SELF TEST MODE

```

```

;CHANNEL SELECT
0444 3A0D02    LDA CHANNEL
0447 FE01      CPI 01
0449 CAA105    JZ CH1ST
044C FE02      CPI 02
044E CAFA04    JZ CH2ST
CH3ST:;SELFTEST CHANNEL 3

```

```

;CH 3 - MODEL CHECK
0451 3EAF      MVI A,0AFH ;MAKE THIS CHAN ACTIVE
0453 D34C      OUT 4CH

```


0455 CD3804	CALL DELAY1 ;DELAY SO ACTUATOR CATCHES UP
0458 3E2F	MVI A,02FH;OC8 FAIL
045A D34C	OUT 4CH
045C 210500	LXI H,5
045F CD3B04	CALL DELAY;DELAY FOR OC8 TO ENGAGE

0462 3E13	MVI A,C3CSA
0464 CD0903	CALL AREAD
0467 EB	XCH

BIBLIOGRAPHY

SECTION IV

Gilbert, W.W. Journal of Aircraft, Volume 18, No 7, July 1981, pp. 597-602.

SECTION V

No citations.

SECTION VI

Dynamic Controls, Inc. Research and Development of Aircraft Control Actuation Systems: The Development of a Direct Drive Fly-By-Wire Flight Control System and Evaluation of a Force Sharing Fly-By-Wire Actuator, AFFDL-TR-77-91, Air Force Flight Dynamics Laboratory, AFWAL-AFSC, Wright-Patterson AFB, Ohio, September 1977.

Dynamic Controls, Inc. Research and Development of Control Actuation Systems for Aircraft - Volume I, AFFDL-TR-79-3117, Air Force Flight Dynamics Laboratory, AFWAL-AFSC, Wright-Patterson AFB, Ohio, June 1979.

Dynamic Controls, Inc. Flight Test of A G.E. and DCI Direct Drive Fly-By-Wire Flight Control System, AFWAL-TR-82-3035, Air Force Flight Dynamics Laboratory, AFWAL-AFSC, Wright-Patterson AFB, Ohio, June 1982.

LIST OF ACRONYMS

A/D	analog-to-digital
AC	alternating current
AFCs	automatic flight control system
BHN	Brinell Hardness Number
C	capacitance
CAS	control augmentation system
cis	cubic inches per second
CTFE	chlorotrifluoroethelene
DCI	Dynamic Controls, Incorporated
DDV	direct drive valve
EMI	electromagnetic interference
FBW	fly-by-wire
GD	General Dynamics
GPATR	general purpose actuator test rig
gpm	gallons per minute
HUI	Hydraulic Units, Incorporated
I/O	input-output
IC	integrated circuit
ISA	integrated servomotor
kg	kilograms
ksi	kilograms per square inch
L	inductance
LED	light emitting diode
LVDT	linear variable differential transformer
MASTR	Multipurpose Actuation System Test Rig
MAW	Mission Adaptive Wing
psi	pounds per square inch
PTFE	polytrifluoroethelene
PWM	pulse width modulation
PZ	piezoelectric
R	resistance
RS	reset-set
SCR	silicon controlled rectifier
VAC	volts alternating current
VDC	volts direct current